Tribology of Hemiarthroplasty

Jia Lizhang (BEng)

Submitted in accordance with the requirements for the degree of

Doctor of Philosophy

The University of Leeds
School of Mechanical Engineering

September, 2010

The candidate confirms that the work submitted is her own and that appropriate credit has been given where reference has been made to the work of others.

Acknowledgements

Finally I have come to the stage of finishing my PhD and now, one of my biggest dreams is going to come true: to be a doctor. It was not an easy task to reposition myself in academics after 3 years working in Industry. Although my previous industrial experiences provided me with good organisation, management and analytical skills, it did mask my many flaws, i.e. super-carelessness, impatience, and a lackadaisical approach to deadlines. If it were not for my PhD experiences, I would not have been determined enough to change my ways and develop new skills. I thank God for this gift and for the blessing that gives me the spirits and strength in my heart throughout my way.

I would like to thank my supervisors: Dr. Sophie Williams, Prof. John Fisher, Prof. Zhongmin Jin, and Dr. Andrew Burton, for the great opportunity to study for my PhD and the patience they have demonstrated in guiding me to completion. I would also like to thank the generous funding from Engineering and Physical Sciences Research Council (EPSRC) and DePuy International Ltd.

I truly appreciate the excellent lab support led by Mr. Devon Darby and Dr. Louise Jennings, along with the lab team Phil, Amisha, Jane, Adrian, Irvin, Lee, and Keith, your understanding and hard work contributed to so much of my experimental work. Great thanks to our super IT staff Mags, Ted, and Graham, for sorting out the IT problems so effectively and always on time. Thanks to our IT-star Dr. Sainath Pawaskar, for being supportive in cartilage mechanics modelling, and all kinds of IT issues.

Many thanks to the academic support of Dr. Joanne Tipper, Dr. Ruth Wilcox, Dr. Alison Galvin, Dr. Jay Katta, Dr. Claire Brockett, Dr. Nagitha Wijayathunga, Dr. Laura McCann, and Dr. Adam Stops, for they have all provided significant help towards developing my methodologies, training my lab skills and correcting my written work. I would also like to thank my presentation advisor Mazen, Matlab advisor Manyi, SolidWorks consultant Mr. Simon Taylor, and our Cake organisers Ramon and Stewart. Cath, Debra, Cheryl, Jane, and Moyra, I would like to thank you for being so helpful and patient each time I came to you with problems.

I enjoyed my memorable PhD: the hard work, the stress, the talks in conferences, the medical technician experiences, the sub-warden duties, the dance performances, 10K races for charities, the iMBE sports days, the orienteering night... supervening with the spirited rhythmic songs from my dear friend – KSII (Knee Simulator – II)!

Huge thanks to my dearest mum, brother, sister-in-law, family and true friends all around the world for the love and trust. A special thanks to my husband William, you have offered the encouragement and support when I have needed it the most! Massive thanks to my dad who has passed away ten years ago; now he should be very proud of me in peace. I have faith in you all.

Abstract

Hip hemiarthroplasty (HA) is a conservative treatment for hip diseases (e.g. osteoporosis, femoral head necrosis) and injuries (e.g. femoral neck fractures) compared to total hip replacement (THR). HA is commonly used in elder patients who have low activity requirements and can be delivered with reduced blood loss, shorter operation time, and hospital stay. HA has been developed to unipolar and bipolar prostheses, and the range of motion has been improved with new designs of the bipolar prostheses. However, satisfaction of HA is not always positive due to the erosion, degradation of the acetabular cartilage, and the dislocation of femoral head which have reported in clinical studies. Hence, the mechanical factors which affect the tribological properties of articular cartilage in HA have been investigated experimentally in an *in-vitro* simulation of HA.

In a simple geometry HA model, the articular cartilage coefficient of friction, deformation, and wear have been examined in a cartilage pin on metal plate model. The loading time, contact stress levels, contact areas, stroke lengths and sliding velocities were set as the input variables, and it was found that: 1) coefficient of friction was time- and load- dependent in short-term (1 hour) testing; 2) wear was load-dependent in long-term (24 hours) testing; 3) contact area only affected the coefficient of friction when both fluid and solid phase of cartilage supported the load due to the different aspect ratio; 4) the stroke length and sliding velocity affected the coefficient of friction only under low level of contact stress (≤2 MPa), but affected the cartilage wear under all levels of contact stresses.

In an entire simulation of HA, the acetabular cartilage coefficient of friction, surface roughness, wear, and deformation have been studied with metal or ceramic heads articulating against acetabular cartilage in a pendulum friction simulator. The clearance between the head and acetabulum, loading types, and prosthesis design were set as the input variables, and it was demonstrated that: 1) a trend of decrease of the coefficient of friction was shown with increasing clearances under both constant and dynamic loading; 2) severe cartilage severe damage was observed when radial clearance was >1.8 mm under constant loading; 3) ceramic heads decreased the cartilage wear, and change of surface roughness compared to metal heads; 4) a novel bipolar design with a thin metal cup and metal head failed to reduce the coefficient of friction due to the cup locking in the acetabulum.

The methodologies and findings in this research can currently adopted for related future studies, additionally the anatomic pendulum friction natural joint simulation can be used for the pre-clinical studies in less invasive procedures in the future.

Table of Contents

List of Figures

List of Tables

Abbreviations

AC Articular Cartilage
AFM Atomic Force Microscopy
AVN Avascular Necrosis
BS Bovine Serum
BMD Bone Mineral Density
C400 with Constant 400N loading
CAT/CT Computed Tomography
CCD Angle Caput-Collum-Diaphyseal Angle
CMM Coordinate Measuring Machine
CoCr Cobalt Chrome
D800 with 800N peak load Dynamic loading
DHS Dynamic Hip Screws
DTI Dial Test Indicator
ECM Extracellular Matrix
EHL Elasto-hydrodynamic Lubrication
ESEM Environmental Scanning Electron Microscopy
FE/FEA/FEM Finite Element/Finite Element Analysis/Finite Element Method
GAG Glycosaminoglycan
HA Hemiarthroplasty
HDPE High Density Polyethylene
HR Hip Resurfacing
ICRS International Cartilage Repair Society
LVDT Linear Variable Differential Transformer
MHRA Medical Healthcare Related Device Agency
MRI Magnetic Resonance Imaging
μCT Micro Computed Topography
μMRI Micro Magnetic Resonance Imaging
OA Osteoarthritis
PAO Periacetabular Osteotomy
PBS Phosphate Buffered Saline
PGs Proteoglycans
PL Protein Lubricant
PMMA Polymethyl-methacrylate
PoP Pin-on-Plate
Ra Arithmetic mean of absolute departures of roughness profile from the mean line

RA Inflammatory Arthritis

RS Ringer's Solution

SAL Surface Amorphous Layer

SEM Scanning Electron Microscopy

SF Synovial Fluid

SoD Sphere-on-Disc

SS Frictional Shear Stress

STZ Superficial Tangential zone

TA Traumatic Arthritis

TEM Transmission Electron Microscopy

TJR Total Joint Replacements

THR Total Hip Replacement

4-4 Four mm stroke length with four mm per second sliding velocity

8-8 Eight mm stroke length with eight mm per second sliding velocity

Chapter 1 Introduction and Literature Review

Hip hemiarthroplasty is similar to a total hip replacement, but it involves only half of the hip replacement (hemi means half, and arthroplasty means joint replacement). Hip hemiarthroplasty is a common treatment for hip fracture and femoral head necrosis (also known osteonecrosis or avascular necrosis, AVN). Hip hemiarthroplasty replaces only the femoral head and hence it is a more conservative treatment compared to total hip replacement (THR). Between 1990 and 2000, there was a 25% increase in hip fractures worldwide (www.iofbonehealth.org). By 2050, the worldwide incidence of hip fracture in men is projected to increase by 310% and 240% in women (Gullberg *et al.*, 1997). Approximately 1.6 million hip fractures occur worldwide each year, by 2050 this number could reach between 4.5 million (Gullberg *et al.*, 1997) and 6.3 million (Cooper *et al.*, 1992). Prognosis following hip fracture is not entirely positive, for example, a 50 year old woman during her remaining lifetime, the risk of death related to hip fracture is 2.8%, which is equivalent to the risk of death from breast cancer (Cummings *et al.*, 1989). The incidence of AVN is approximately 15,000 cases per year in the United States, and the incidence of AVN is increasing owing to an increase in the use of exogenous steroids, and an increase in the incidence of trauma and of alcohol abuse (http://emedicine.medscape.com).

This thesis focuses on developing *in-vitro* methods for investigating the tribology of cartilage in hip hemiarthroplasty in a pre-clinical experimental simulation system. This simulation system will allow the *in-vitro* investigation of hemiarthroplasty on cartilage friction, surface roughness, surface deformation, and wear in both unconfined cartilage specimens and confined entire acetabulum samples. The novel methodologies developed in these studies are expected to be suitable to apply in the future to investigate other less invasive procedure in hip joints *in-vitro* studies as fundamental methods.

1.1 Hip Joint

1.1.1 Healthy Hip Joint Anatomy

The bones of hip region are the pelvis (which includes pubis, ilium, sacrum, ischium, and coccyx) and the femur. The hip joint (Figure 1.1) includes the femoral

head, acetabulum, and associated articular cartilage, synovial capsule, synovial fluid, ligaments and muscles.

The hip joint is the largest ball-and-socket synovial joint in the body, the round femoral head articulates with the cup-like acetabulum of the pelvis. The surface of the inside of the acetabulum and the femoral head are covered with articular cartilage. This articular cartilage, which is integrated with the bone, is a strong, compliant, slick, biphasic material which allows the surfaces to slide against one another smoothly and freely in all directions with minimal friction.

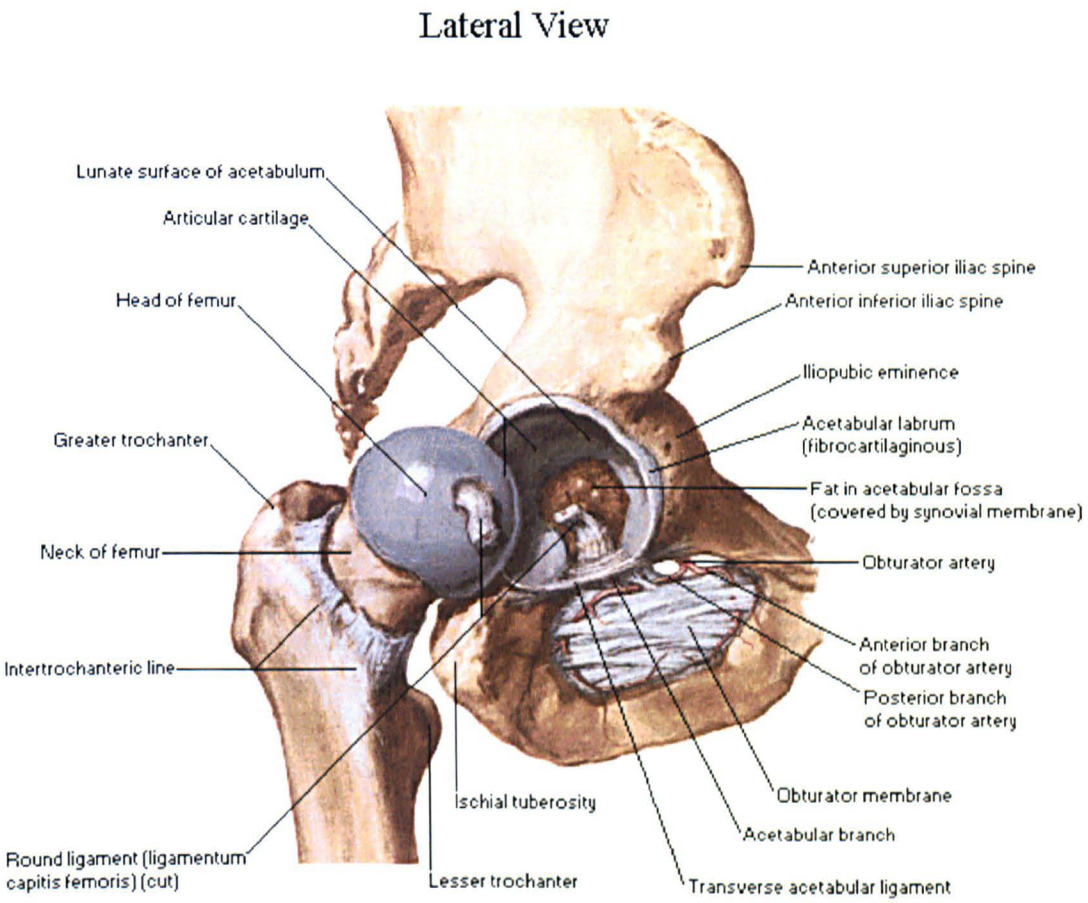

Figure 1.1 Hip joint (lateral view) (www.laboratorium.dist.unige.it)

The hip capsule attaches to the hip bone outside the acetabular labrum and projects into the capsular space, which permits the hip joint to have the second largest range of movement in the body (second to the shoulder) and support body weight. The nutritive synovial fluid inside the hip capsule acts as a lubricant reducing the friction between articular cartilage and other tissues in the hip during the movement. The hip joint is reinforced by five ligaments; four extracapsular ligaments (the iliofemoral, ischiofemoral, pubofemoral, and zona orbicularis ligaments) and one intracapsular ligament (the ligamentum teres), which are essential for stability and keeping the hip from moving outside of its normal range of

motion. Surrounding the hip are thick muscles of the thigh in the anterior direction and of the buttock at the posterior. The muscles work together to provide power for the hip to move in all directions, and stabilise the entire leg and foot (Callagha *et al.*, 2004).

The blood supply of the hip joint is mainly from the medial circumflex femoral and lateral circumflex femoral arteries, which are both branches of the deep artery of the thigh (profunda femoris).

The difference of bone geometry in hip joints (such as femoral neck angle, the wideness of the hip bone, etc) may lead to higher risk of hip fractures for individuals (Kanis and McCloskey, 1996). The femoral neck angle between the longitudinal axes of the femoral neck and shaft (known as caput-collum-diaphyseal [CCD] angle), and it is approximately 120-135° normally. An abnormally coxa vara (<120°) or coxa valga (>135°) is in result of changes in the stress applied on the hip joint which may be caused by a dislocation or changes the trabecular patterns inside the bones. The female hips are broader than male hips due to the wideness during puberty and the femurs are more widely spaced facilitate child birth.

1.1.2 Kinematics and Dynamics of the Hip Joint

In general the normal hip joint is expected to last over 70 years or over 100 million cycles, and it naturally has a wide range of motion which takes place in the sagittal, coronal, and transverse planes (Figure 1.2). Movements of the hip joint performs are summarised in Table 1.1 (Standard, 2002).

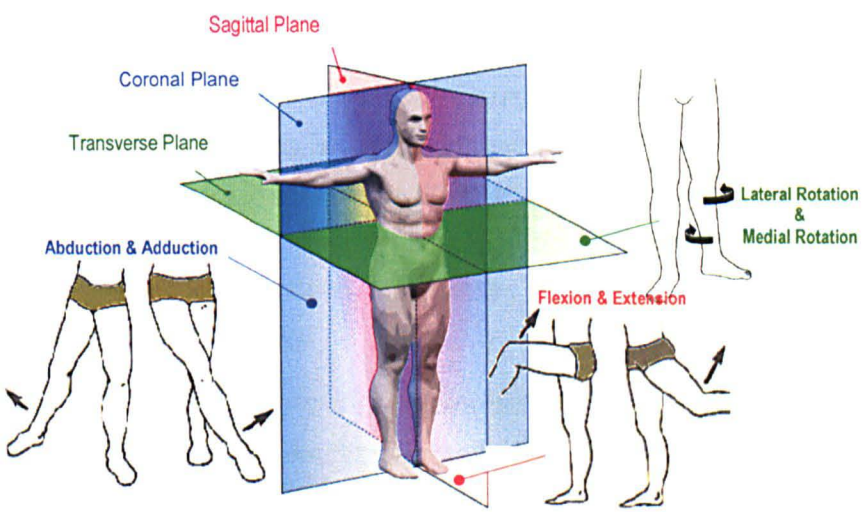

Figure 1.2 A wide range of hip movement in the sagittal, coronal, and transverse planes (image of three planes: www.itstactical.com; images of abduction & adduction, flexion & extension: www.brianmac.co.uk; image of lateral & medial rotation: http://completehealthacupuncture.com)

Table 1.1 Range of movement of the hip joint (Standard, 2002)

Direction	Planes	Range of Movement
Flexion and Extension	Sagittal	-18°~25°
Abduction and Adduction	Coronal	-7°~4°
Medial and Lateral	Transverse	-10°~2°

The gait cycle is a series of movements by the lower limbs during walking, and a gait diagram of one step of the right leg is shown in Figure 1.3.

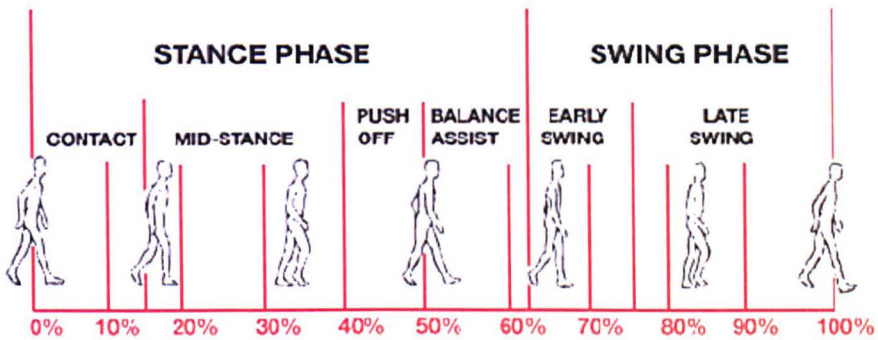

Figure 1.3 A hip gait includes stance phase 60% of per cycle, and swing phase 40% per cycle (www.orthopaedicsurgeries.co.uk).

A single normal gait cycle starts with the stance phase, and this is approximately 60% of each cycle, the right limb is in contact with the ground, and can be considered in three sections: contact (0-15%), mid-stance (15-40%), push off (40-50%), balance assist (50-60%). The two peaks of loading (Figure 1.3) occur in the stance phase: the first peak occurs when the heel fully contacts the ground (15%), and the second peak happens when the right leg becomes rigid and pushes off into the next step (45%). The final 40% of the cycle is the swing phase, when the load is supported by the opposing leg. This comprises of early swing (60-75%), and late swing (80-100%). Early swing is to clear the limb from the ground when it passes the other leg. Once past the standing leg, late swing occurs and the centre of gravity of the body moves forwards, the hip continues to flex (www.orthopaedicsurgeries.co.uk).

One of the earliest reports of hip forces acting during walking was by Paul (1966), it was examined though electrodes mounted over specific muscle groups to indicate the load carried by muscle at given phases of the gait cycle. It was found that the average peak hip joint force has 3-4 times of body weight, and two major peaks during each gait cycle during stance phase which corresponding with the heel-strike and toe-off, but much lower forces occurred during swing phase. Later

studies have investigated the hip forces during different activities: the range of peak loads was determined to be 1.8-6 times of body weight during single-legged stance (Williams and Svensson, 1968; McLeish and Charnley, 1970). Other studies (Svesnsson *et al.*, 1977; Röhrle *et al.*, 1984; Bergmann *et al.*, 1993; Bergmann *et al.*, 2001) have explored the loading pattern during normal gait and have reported results endorsing the findings of Paul (1966). A typical time dependent contact force of the hip during normal walking gait is shown in Figure 1.4.

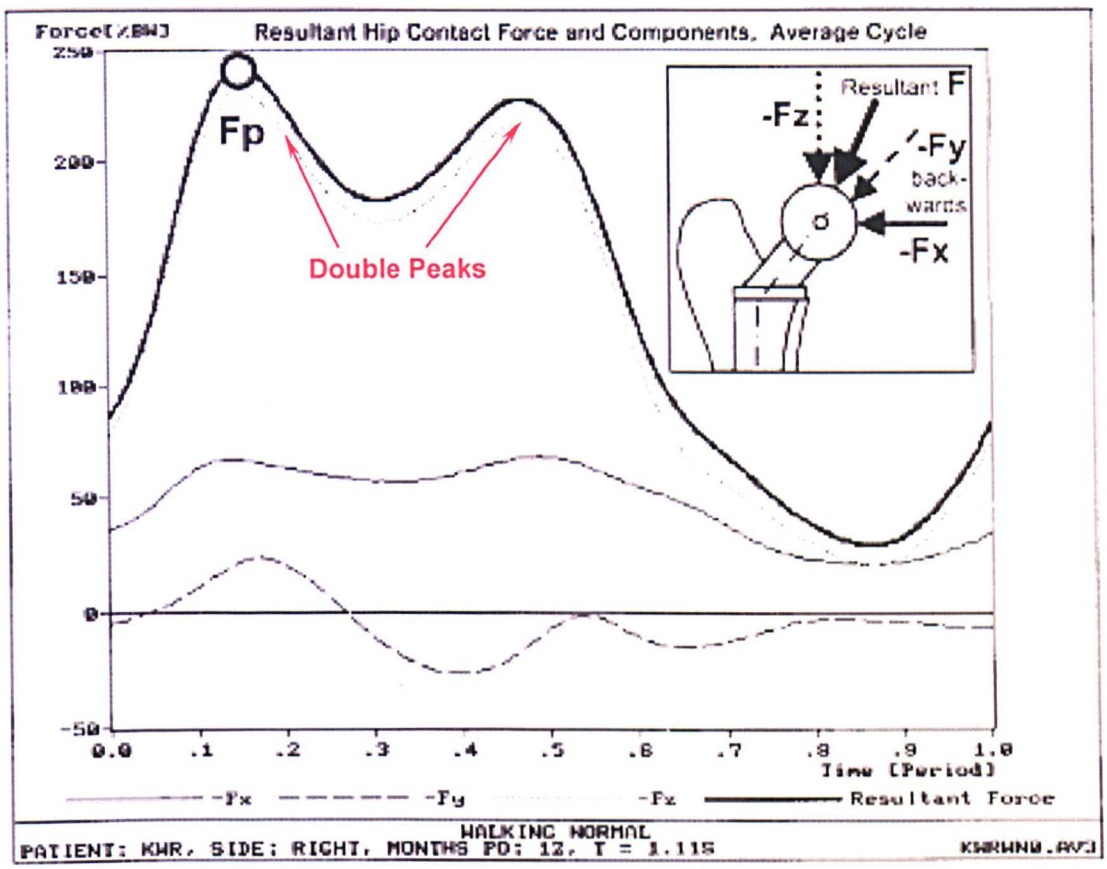

Figure 1.4 Average contact force F of patient during normal walking in x, y, and z directions *-Fx, -Fy, -Fz,* the highest value is the peak force *Fp* (Paul, 1966; Bergmann *et al.*, 2001).

1.1.3 Contact Stresses in Hip Joint

Peak contact stresses in the normal human hip joint have been investigated by many studies and have been reported to range from 2.1 MPa (Hipp *et al.*, 1999), 1.6-2.7 MPa (Ipavec *et al.*, 1999), 4.9-9.6 MPa (Adams and Swanson, 1985), and to 6-10 MPa (Maxian *et al.*, 1995). Cartilage in the hip joint is subjected to contact stresses of approximately 1-5 MPa (Hodge *et al.*, 1985) under normal conditions, however stresses of 18 MPa were measured for a patient standing up from a

seated position (Hodge *et al.*, 1985). Higher stress may be expected under conditions of strenuous exercise or extreme sports.

In the hip joint, the contact pressures have been studied and examined *in-vivo* in the past 20 years. In 1995, Fagerson (Fagerson *et al.*, 1995) studied the early phase hemiarthroplasty rehabilitation through an instrumented femoral head prosthesis implanted in a patient with a displaced left hip fracture. The acetabular contact pressures were measured and found to range from 1.2 MPa to 7.1 MPa during various functional activities: sit-to-stand, ambulation, and stair-climbing. The highest peak acetabular contact pressure was found during unassisted reciprocal gait on stairs at 15.5 MPa. Another case study of a unilateral hip hemiarthroplasty patient on the cartilage degeneration in relation to repetitive pressure by McGibbon (1999), demonstrated that the highest repetitive *in-vivo* contact pressures during gait were 4.5-6.5 MPa in the superior dome of the acetabulum.

1.2 Hip Joint Conditions

Generally the most common hip joint diseases include osteoarthritis, osteoporosis, and femoral head necrosis. Hip injuries include strains, bursitis, dislocations and fractures, which can be caused by doing sports, overusing or falling or accidents, and also certain diseases.

Several diagnostic procedures may be involved to arrive at the right diagnosis of the joint disease, and they include with radiation methods (e.g. X-ray roentgen picture, computer assisted axial tomography [CAT or CT]), and without radiation method (e.g. magnetic resonance imaging [MRI], and ultrasound).

1.2.1 Osteoarthritis (OA)

Osteoarthritis (known as degenerative arthritis, OA) is the most common form of arthritis, and it is a group of mechanical abnormalities involving degradation of joints which includes articular cartilage and subchondral bone. OA degenerates the cartilage that cushions the bones of the hip and eventually leads to the two opposing bones directly articulating. The symptoms of OA may include joint pain, tenderness, stiffness, locking and effusions. The first symptoms are usually minor pain and stiffness which begins as the cartilage starts to erode, and it worsens over time. More than 650,000 in the UK have painful osteoarthritis in one or both hips, 67% of whom are aged over 65.2 years (Odding *et al.*, 1998). There are a further

1.5 million people who may not have any symptoms of hip OA, but have X-ray evidence of hip OA (Lanyon *et al.*, 2003).

Surgical treatments are required when osteoarthritis in the hip joint becomes severe, such as severe loss of cartilage, damage of bone, causing pain and limited motion. The common hip surgeries for OA are total hip replacement (THR) and hip resurfacing (HR).

Another two common arthritis types are rheumatoid arthritis (inflammatory arthritis, RA), and traumatic arthritis (TA). RA is a disorder of the body's own immune system which attacks both joints and other parts of the body. It causes pain, joint inflammation, and cartilage degeneration. TA is caused by a serious hip injury or fracture which can lead to AVN where the blood supplies to the femoral head deteriorate and produce pain, death of tissue, and other symptoms.

1.2.2 Osteoporosis

Osteoporosis literally means porous bones, it is a progressive condition that affects bones and it becomes more common with aging which leads to an increased risk of fracture (Figure 1.5). Osteoporosis makes bones fragile by reducing the bone mineral density (BMD), and more prone to break easily due to the disrupted microarchitecture and the altered amount and variety of proteins in bone.

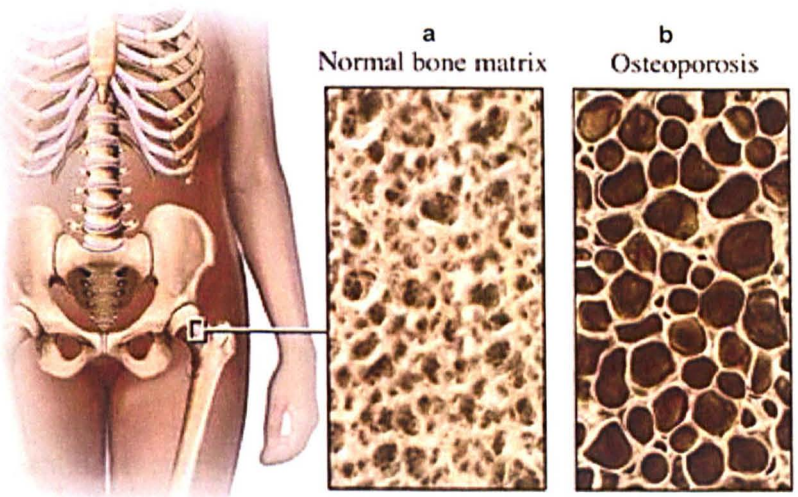

Figure 1.5 Femoral head with: a. normal bone matrix, and b. osteoporosis bone matrix (www.iraqimsi.com)

Osteoporosis is most common in women after menopause due to the hormonal changes which is known as postmenopausal osteoporosis, but may also develop in men. Osteoporosis may occur in anyone who has hormonal disorders, chronic diseases, or under medications such as glucocorticoids, it is often referred as the 'silence disease' because few people only know they have it when they break a bone. Almost 3 million people are estimated to have osteoporosis in the UK, and approximately 230,000 fractures caused because of osteoporosis every year in the UK (www.ageuk.org.uk).

1.2.3 Femoral Head Necrosis (AVN)

Femoral Head Necrosis (AVN) is a serious hip disease which results from an interruption in the blood supply to the femoral head, and it leads to the localised destruction of the bone in the subchondral femoral head. When the blood flow in the arteries which supplies the femoral head are disrupted, and the bone cell necrosis occurs along with failure to respond to continuously changing compressive loads. The trabeculae inside the femoral head bone are no longer renewed, and hence there is a lack of sufficient stability, this causes the necrotic bone to collapse. This creates a hole in the subchondral bone and can cause serious damage to the cartilage in the hip joint above the hole (Figure 1.6).

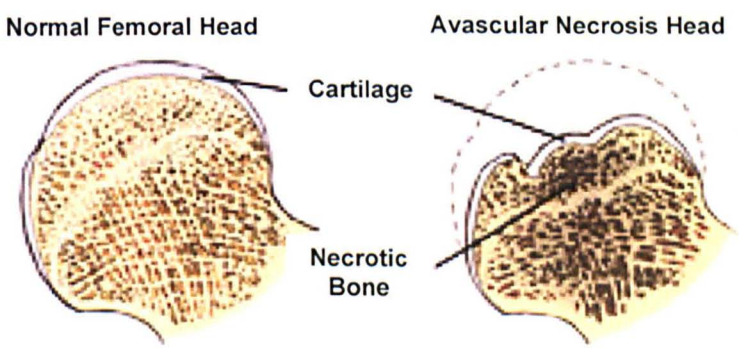

Figure 1.6 Femoral head necrosis (www.zimmer.com)

AVN is an increasingly common cause of musculoskeletal disability, and the incidence of AVN is higher in men than women and the most common age group is between 35 and 45-years-old. In 30-70% of all cases, the disease develops in both hips (www.gelenk-klinik.de). It is reported that the relative frequencies of the most common causes of AVN are 20-40% alcoholism and 35-40% steroid treatment, and 20-40% idiopathic (http://emedicine.medscape.com).

The treatments of AVN include hip replacement (HA or THR), physical therapy, hyperbaric oxygen therapy, autologous cartilage-bone transplantation, and osteotomy. The treatment mainly depends on the stage of AVN, and the patient health conditions. However, most cases of AVN are treated by HA or THR due to diagnosis is done in the late stage of AVN.

1.2.4 Hip Fractures

Hip fracture is a fracture in the proximal end of the femur, and it is commonly caused by osteoporosis, osteoarthritis, AVN, a fall or minor trauma in weakened osteoporotic bone, or high-energy trauma with normal bone for example car accidents. Hip fracture is a serious condition that has been found to increase morbidity and mortality in elderly people (Baudoin *et al.*, 1996), and approximately 75% of all hip fractures occur in women (Cooper *et al.*, 1992; Jordan and Cooper, 2002). Hip fractures are invariably associated with chronic pain, reduced mobility, disability, and an increasing degree of dependence (Keene *et al.*, 1993). It has been postulated that the etiologies of the two main hip fracture types (femoral neck fracture and trochanteric fracture) are different (Mautalen *et al.*, 1996).

Hip fracture has been classified based on the location of fracture as head, neck, intertrochanteric, trochanteric, and subtrochanteric fractures (Figure 1.7). Femoral neck fracture is an intra-capsular fracture, and intertrochanteric, trochanteric, and subtrochanteric factures are extra-capsular fractures. Femoral neck fractures (46-54% of all hip fractures) and trochanteric fractures (34-46%) are the most common types of hip fracture (Partanen *et al.*, 2003). Intertrochanteric fractures (2-8%) and subtrochanteric fractures (2-7%) are rare (Jalovaara *et al.*, 1992; Berglund-Rödén *et al.*, 1994).

1) Femoral head fracture (Figure 1.7.a): is a rare injury, which mainly caused by hip dislocation (http://emedicine.medscape.com);

2) Femoral neck fracture (Figure 1.7.b): is rare among younger patients but is commonly seen in older adults and most often secondary to osteoporosis or osteomalacia. The Garden classification of femoral neck fractures is the most widely used system as Grade 1~4 (Garden, 1964; Müller, 1990; Bartonícek, 2001);

3) Intertrochanteric fracture (Figure 1.7.c): is also called basicervical fracture which is extracapsular two-part fracture, with the fracture plane running along the line of capsular insertion, just proximal to the lesser and greater trochanter

(Parker *et al.*, 1997). It commonly happens in elder patients and women secondary to osteoporosis;

4) Trochanteric fracture (Figure 1.7.d): it usually results from avulsion injuries at the insertion of the gluteus medius, and is most common in children and young athletes (http://emedicine.medscape.com);

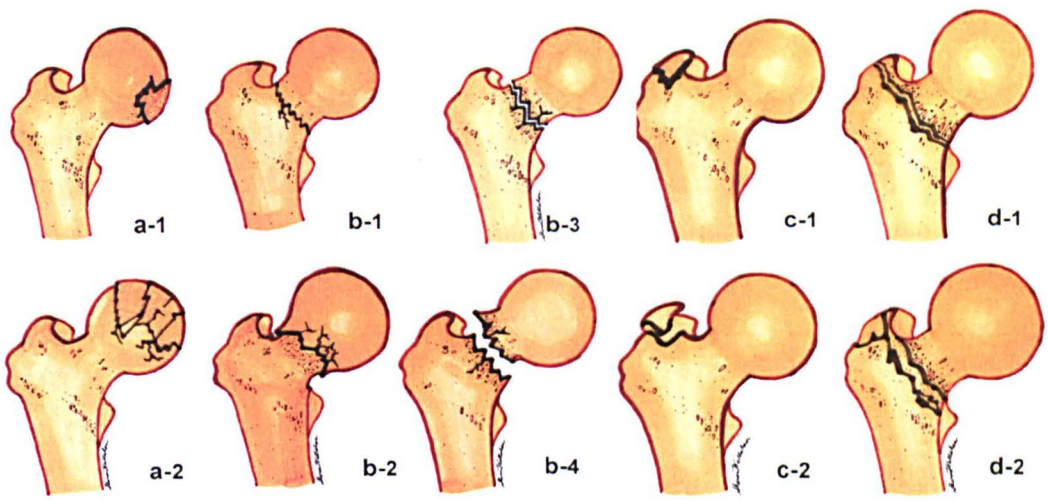

Figure 1.7 Hip fractures modes (http://emedicine.medscape.com): a. femoral head fractures, a-1) single-fragment fracture; a-2) comminuted fracture; b. femoral neck fractures, b-1) Grade 1, stress or incomplete fractures; b-2) Grade 2, impacted fracture; b-3) Grade 3, partially displaced fracture; b-4) Grade 4, completely displaced or comminuted fractures; c. intertrochanteric fractures, c-1) single fracture line without displacement; c-2) multiple fracture lines (comminution) with displacement, unstable; d. trochanteric fractures, d-1) non-displaced fractures; d-2) displaced fractures.

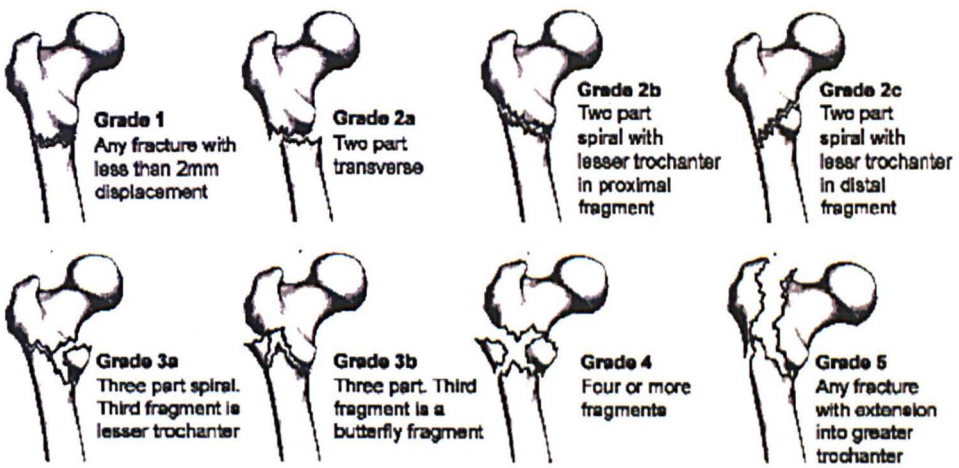

Figure 1.8 Seinsheimer classification of subtrochanteric fractures (Seinsheimer, 1978; Partanen *et al.*, 2003).

5) Subtrochanteric fracture (Figure 1.8): has a bimodal age distribution and is seen mostly in those aged 20-40 years in association with high-energy trauma

and in patients older than 60 years secondary to falls on osteoporotic bones (http://emedicine.medscape.com/). It is subdivided into undisplaced, two-part, and comminuted fractures as the Seinsheimer classification which is mostly used (Seinsheimer, 1978).

1.3 Treatments of Hip Joint Conditions

The treatments of hip joint diseases and injuries depend on the level of damage of the hip joint, and they include resting, medication, physical therapies, or surgery. For hip joint diseases and injuries the most common treatments are total hip joint replacement (THR), hip resurfacing (HR), hip hemiarthroplasty (HA, also called endoprosthesis). Other treatments also been used are: hip periacetabular osteotomy (PAO), arthroscopic surgery (also known as key-hole surgery), and tissue engineering.

1.3.1 Total Hip Replacement (THR)

A total hip replacement or total hip arthroplasty (THR) replaces the hip joint and eliminates the damaged cartilage and bone. This replaces the acetabulum with a cup, the femoral head, and a metal stem which connects the material head to the femoral neck.

The existing or potential material combinations of THR have been described by Dowson (2001) in six generations. and are summarised in Figure 1.9 and Table 1.2.

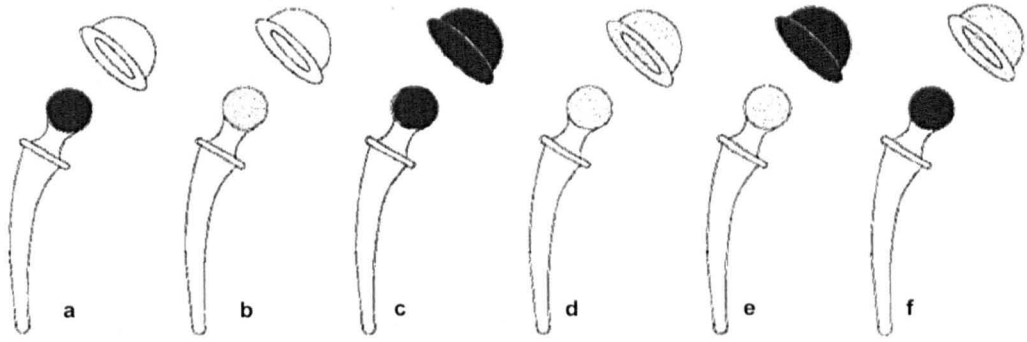

Figure 1.9 Existing and potential combinations for THR implants materials: a) metal-on-polymer; b) ceramic-on-polymer; c) metal-on-metal; d) ceramic-on-ceramic; e) ceramic-on-metal; f) metal-on-ceramic (Dowson, 2001)

Table 1.2 Comparison of friction and wear in six generations of THR (Dowson, 2001)

THR	Friction (*in-vitro*)	Wear
Metal-on-Polymer Figure 1.9.a	0.02-0.06 (Scholes and Unsworth, 2000),	40-380 μm/year (Dowson and Wallbridge, 1985; Livermore et al., 1990; DEVANE et al., 1997)
Ceramic-on-Polymer Figure 1.9.b	0.099 in dry conditions 0.015 in CMC lubricant (Unsworth et al., 1995).	0.5 (0.29-0.71) times compared to metal-on-polyethylene in a review of five clinical studies (Dowson, 1995).
Metal-on-Metal Figure 1.9.c	0.17 (three times of metal-on-polymer and ceramic-on-ceramic THR) (Scholes and Unsworth, 2000).	100-fold less than metal-on-polyethylene (Anissian *et al.*, 1999); 0.58-8.99 mm^3/million cycles (Williams *et al.*, 2008)
Ceramic-on-Ceramic Figure 1.9.d	0.4 (range 0.1-0.75, pin-on-disc) (Wallbridge et al., 1983); 0.6 (rang 0.5-0.7, dry conditions) (Sliney and DellaCorte, 1993); 0.07 (in distilled water) (Miller et al., 1996).	0.05 mm^3/million cycles (Nevelos et al., 2001), and penetration rates of 2-20 mm/year from retrieval studies (Dowson, 2001).
Ceramic-on-Metal Figure 1.9.e	0.04-0.06 (0.11-0.13 in metal-on-metal; 0.04-0.06 in ceramic-on-ceramic; hip simulator; in 25% bovine serum) (Williams *et al.*, 2007).	0.01 mm^3 (1.23 mm^3 in metal-on-metal; 0.08 mm^3 in ceramic-on-ceramic) every million cycles in similar prostheses (Dowson, 2001; Firkins *et al.*, 2001; Williams *et al.*, 2007).
Metal-on-Ceramic Figure 1.9.f	N/A (not be commonly used)	Aseptic loosening, catastrophic metal wear after 6 months implantation (Valentí et al., 2007).

1.3.2 Hip Resurfacing (HR)

Hip resurfacing (HR, Figure 1.10) is an intervention alternative of THR, which is considered by some to be a more bone preservation option and has a potentially lower number of hip dislocations due to the relatively larger femoral head size. HR only reshapes and resurfaces the femoral head, and exchanges the damaged hip socket with a metal prosthesis. For young patients, it gives them more time before a THR becomes necessary, but it may cause potential femoral neck fractures (rate of 0.4%), aseptic loosening, and metal wear (Mont *et al.*, 2008). The same concerns have been revised about adverse biological reactions by the Medical and Healthcare Related Devices Agency (MHRA) on 22nd April, 2010.

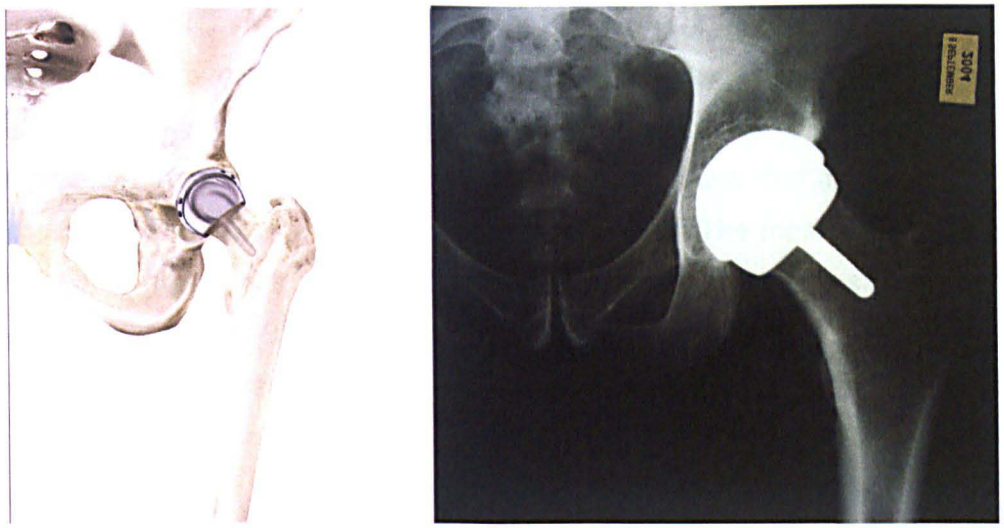

Figure 1.10 a) The Birmingham hip resurfacing device (www.medicalmoment.org); b) radiographic image of hip resurfacing (www.hrorthopaedics.co.uk)

1.3.3 Hip Hemiarthroplasty (HA)

Hip hemiarthroplasty (HA) is a conservative treatment to some hip diseases and injuries, when the acetabulum maintains a good healthy condition. HA is a surgical procedure which replaces one half of the joint with an artificial surface and leaves the other part in its natural (pre-operative) state. This class of procedure is most commonly performed on the hip after fracturing the neck of the femur (a hip fracture) and involves removing the fractured head of the femur and replacing it with a metal or composite prosthesis. HA is commonly used as the treatment of displaced intracapsular fractures of the proximal femur in old patients with low functional demands.

Hemiarthroplasty prostheses can be unipolar or bipolar, which are used clinically in the recent 40 years. The most commonly used prosthesis designs of this type are the Austin Moore prosthesis and the Thompson Prosthesis (unipolar endoprosthesis, Figure 1.11.a). More recently a composite of metal and HDPE (High-Density Polyethylene) which forms two articulating interfaces (Bipolar Prosthesis, Figure 1.11.b) has also been used.

There are two methods in hip hemiarthroplasty to set the femoral head stem into the femur: uncemented prostheses (Figure 1.12.a) or cemented prostheses (Figure 1.12.b). The methods of in hip hemiarthroplasty in both unipolar and bipolar hemiarthroplasties have been reported as: cemented prostheses provided better stability and lower dislocation rate compared to uncemented prostheses (Kenzora *et al.*, 1998; Khan *et al.*, 2002; Foster *et al.*, 2005; Parker *et al.*, 2010), but the higher risk of hypotension and fat embolism was associated with the cemented

hemiarthroplasty (Christie *et al.*, 1994; Ozturkmen *et al.*, 2008). It has been reported that the average operating room times and blood loss volumes were 95 minutes and 467 mL for the cemented HA, and respectively, 80 minutes and 338 mL for the uncemented HA cohorts, but the postoperative mortality rates, overall complications, and pain were similar (Ahn *et al.*, 2008). The most recent studies of HA to treat femoral neck fractures has demonstrated 12.4 minutes shorter of the surgery duration and 89 mL less of the intraoperative blood loss in uncemented method compared to cemented method, but complications and mortality rates, and hence the authors concluded that both uncemented and cemented HA may be used with good results after displaced femoral neck fractures (Figved *et al.*, 2009).

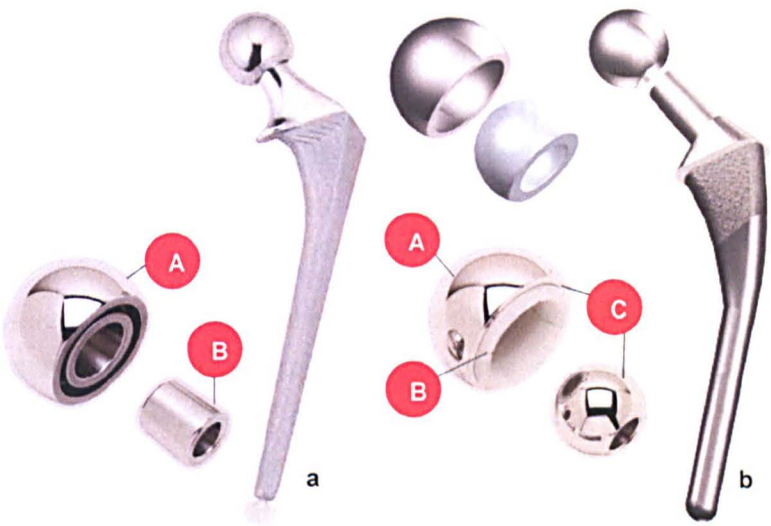

Figure 1.11 Two types of hip hemiarthroplasty: a) unipolar prosthesis A. Fully machined wrought cobalt chrome shell for an accurate fit and minimised wear, B. Modular design with five neck length options, and restores patients' normal femoral offset; (www.med.wayne.edu, and www.exac.com); b) bipolar prosthesis A. Bipolar design allows for easy assembly with hand pressure, B. Designed to maximize polyethylene durability with optimal positive eccentricity throughout the range of sizes, C. Precision-machined forged cobalt chrome shell for accurate fit and minimised wear) (www.eorthopod.com, and www.exac.com).

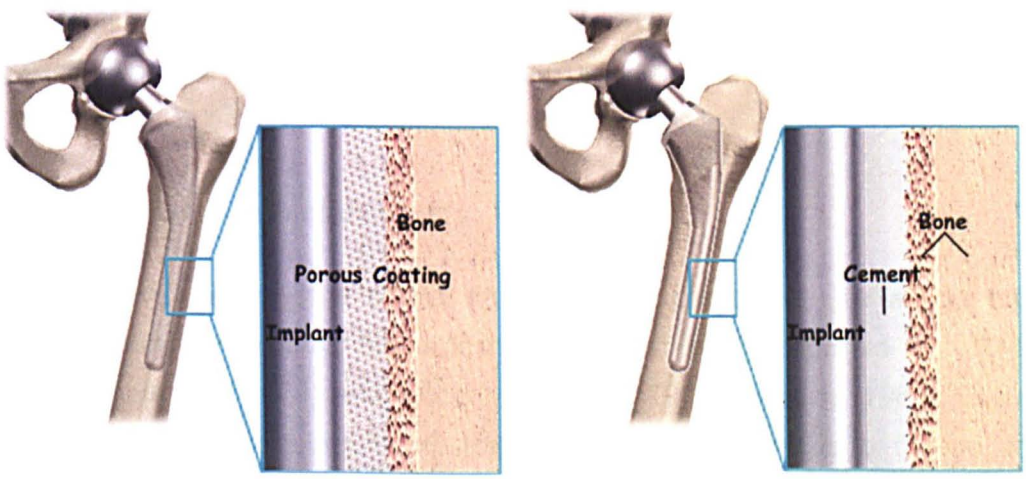

Figure 1.12 a) uncemented hip hemiarthroplasty; b) cemented hip hemiarthroplasty (http://www.eorthopod.com)

1.3.3.1 Unipolar Hemiarthroplasty

Unipolar hemiarthroplasty (known as unipolar endoprosthesis, or unipolar replacement) was the forerunner of hip hemiarthroplasty which was used in the 1940's by Judet and Judet (Anderson and Milgram, 1978). The Vitallium unipolar prosthetic femoral head was introduced in the early 1950's by Moore, and bears his name (Moore, 1952). The Moore unipolar prosthesis and others such as the Thompson unipolar replacement of the femoral head were frequently used for the treatment of displaced and un-united femoral head fractures and avascular necrosis (Bochner *et al.*, 1988). Clinical studies have reported acceptable results using Moore (Moore, 1957) and Thompson (Thompson, 1954) designs of unipolar endoprostheses. Although treatment of THR is a common procedure for elderly patients who have a displaced intracapsular fracture, it presents a high risk of dislocation in femoral neck fractures up to 20% (Sim, 1983; Ravikumar and Marsh, 2000). It has been concluded that the unipolar hemiarthroplasty is an efficacious and cost-effective treatment option for femoral neck fractures for the elder patients (Harjeet *et al.*, 2009).

However, residual hip pain, acetabular erosion or protrusion, and femoral stem loosening have been reported associated with unipolar prostheses (Hinchey and Day, 1964; Whittaker *et al.*, 1972; Salvati and Wilson, 1973; Hunter, 1974; D'Arcy and Devas, 1976; Beckenbaugh *et al.*, 1977). It has been postulated that there are several reasons for the unipolar prostheses failure including high frictional forces between the metallic head and acetabular cartilage, abnormal frictional shear stresses within the cartilage, lack of shock absorption, and uneven subchondral bone loading patterns because of mismatching the metallic head size to the acetabulum in early studies (Anderson *et al.*, 1964; Bateman, 1977; Giliberty, 1977; Simon, 1977; West and Mann, 1979). It has also been reported in a meta-analysis that 6~18% of patients required a second surgery after unipolar hemiarthroplasty (Lu-Yao *et al.*, 1994), and that protrusion was a complication of unipolar hemiarthroplasty in 54% of cases in long-term studies (Söreide *et al.*, 1980).

1.3.3.2 Bipolar Hemiarthroplasty

The development of a bipolar femoral head prosthesis (known as bipolar endoprosthesis, or bipolar hemiarthroplasty) was firstly reported in 1974 by Bateman (Bateman, 1974) and Giliberty (Gilberty, 1974; Giliberty, 1983). Bateman (1974) described that the bipolar prosthesis provides two surfaces for motion, which transfer the motion of the metal head in the acetabulum to the low friction inner

bearing of the prosthesis. Later, further bipolar prostheses have been developed: the Hastings Hip (Devas and Hinves, 1983), the Variokopf (Verberne, 1983), and Bi-articular hip prostheses (Franklin and Gallannaugh, 1983), which all comprise a femoral component with a spherical head that articulates with a high-density polyethylene acetabular insert, enclosed by an outer steel shell. Other design such as the Monk prosthesis (Monk, 1976) which was originally made of polyethylene alone was subsequently modified to be covered with an outer metal shell (Chen *et al.*, 1980). The trunnion-bearing Christiansen prosthesis (Christiansen, 1969) was similar to the Monk prosthesis which comprised a polyethylene acetabular component at its inception, and later was reinforced by an outer metal shell (Søreide *et al.*, 1975). A comparison study of three different designs of two-component bipolar prostheses (Brueton *et al.*, 1993) has classified the movements difference with particular reference to the relevance of the size of the femoral head to the self-centring mechanism of the Hasting hip (Brueton *et al.*, 1987). The movement of the three design prostheses have shown different percentage of intraprosthetic, extraprosthetic, and both intra- and extraprosthetic movements which indicated that the design of bipolar prosthesis is essential to where the motions occur on the bearing surfaces.

Compared to unipolar hemiarthroplasty, no protrusion was found in 4 years experience of bipolar prostheses (Devas and Hinves, 1983; Bochner *et al.*, 1988). In a short-term retrospective nonrandomised study, the authors concluded that bipolar endoprosthesis not only produced good functional outcomes with minimal complications for displaced intracapsular femoral neck fractures but also has several advantages compared to unipolar prostheses (Krishnan *et al.*, 2010).

Although HA is the main treatment method of hip fractures and femoral head necrosis (Lu-Yao *et al.*, 1994), different studies have reported that HA delivered better mobilisation (Söreide *et al.*, 1979; Sikorski and Barrington, 1981) and lower re-operation rate 0~13% compared to OS 17.6~44% during 1 to 3 years follow-up (Söreide *et al.*, 1979; Söreide *et al.*, 1980; Sikorski and Barrington, 1981; Parker, 1992; Parker and Pryor, 2000; Puolakka *et al.*, 2001).

1.3.4 Dynamic Hip Screw (DHS)

Dynamic hip screw (known as Sliding Screw Fixation, DHS, as Figure 1.13) is an orthopaedic prosthesis for internal fixation of femoral neck, intertrochanteric and subtrochanteric fractures which controls the dynamic sliding of the femora head along the construct. It consists of a large cancellous lag screw and a side plate with a few fixation screws. The lag screw is inserted into the femoral head, and it glides

freely in a metal sleeve. The sleeve is attached to a side plate fixed to the lateral femoral cortex with screws. The side plate is fixed on the side of the femur by the fixation screws inserting into the femoral diaphysis. The weight bearing leads to femoral head to be impacted onto the femoral neck which produces dynamic compression of the fracture. The lag screw shaft slides down to the sleeve to maintain the reduction of fracture when compression happens.

DHS fixation is a straightforward and quick procedure, and facilitates healing due to the utilisation of controlled impaction during weight-bearing to stabilise the fracture (Jensen *et al.*, 1978; Müller *et al.*, 2003). However, DHS has been reported unsatisfactory due to failure of the fixation or to re-establish acceptable hip biomechanics from the functional results (Jensen *et al.*, 1978; Moroni *et al.*, 2005). Some studies have shown that DHS is also less likely to cut out if put into the lower half of the femoral head (Mainds and Newman, 1989). Technical failure of fixation can cause prolonged bed rest and follow-up, or complete failure of the fixation (Heyse-Moore *et al.*, 1983; Moller *et al.*, 1984).

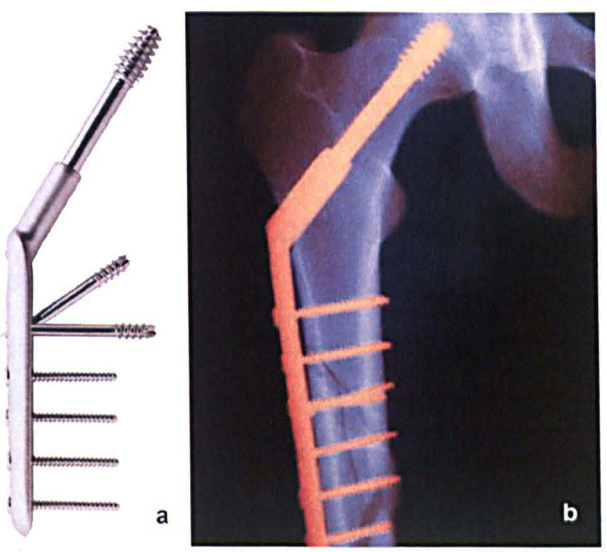

Figure 1.13 Dynamic hip screws a. DHS implants (www.med.wayne.edu); b. X-ray image of a DHS prosthesis (www.gettyimages.co.uk)

Compared to uncemented HA, DHS has been reported to provide no advantage in functional outcome for elderly patients with an unstable intertrochanteric femoral fracture (Kim *et al.*, 2005). DHS was suggested to be handled with care due to its significantly higher dislocation rate compared with HA, especially in unstable fractures (Geiger *et al.*, 2007). A comparison study of outcomes following (minimum 3 years) uncemented HA and DHS in treating displaced sub-capital hip fractures in patients (over 70 years) has demonstrated better results in DHS group, but no significant difference of revision surgery existed (EL-ABED *et al.*, 2005). The use of radiographs in the postoperative period has

been recommended following DHS and CS fixation, but a check radiograph following hip hemiarthroplasty is only requested if it is to have a bearing on the clinical management of the patient (Chakravarthy *et al.*, 2007).

1.3.5 Biomaterials

1.3.5.1 Biomaterials Used in Orthopaedic Implants

Highly developed biomaterials are used in orthopaedic implants to provide high standards of mechanical properties and meet high functional expectations. Many different biomaterials used in orthopaedic implants include cobalt chrome, stainless steel, titanium alloys, titanium, tantalum, ceramic, and polyethylene, composite materials, *Trabecula Metal*, bio-absorbable materials, and silicone etc. However, there is no single biomaterial that is best for all orthopaedic implants and all patients due to the different requirements of implants. These specific requirements vary depending on how the implants are designed to be used. Biomaterials can possibly produce side effects, such as microscopic debris, increased ion levels in the blood or urine, or inflammation though these effects are rare.

Biomaterials used in the orthopaedic implants require high physical characteristics in terms of:

1. Strength to withstand the accumulated effect of repeating high levels of mechanical stresses on bones and joints without breaking or permanently changing shapes in everyday activities;
2. Flexibility to avoid shielding of bones from stress (known as stress-shielding) so some of the stress passes through the flexible implant to the surrounding bone.
3. Resistance to wear to reduce the risk of inflammation by reducing the wear particles of the biomaterial released into the surrounding tissues.
4. Resistance to corrosion of the biomaterial to the chemicals in body fluid.
5. Biocompatibility to avoid harmful interact of biomaterial to the body, such as irritation or allergic reaction. All biomaterials used in medical devices must be extensively tested for biocompatibility before they are approved for use.

Generally, high strength, flexibility, hardness (more resistant to wear), resistance to corrosion, and biocompatibility are the essential requirements for the articulating surfaces of the implants.

1.3.5.2 Cobalt Chromium Alloys

Cobalt chromium alloys (known as cobalt chrome, CoCr) contain mostly cobalt and chromium, and also include other metals, such as molybdenum (to increase the material strength). CoCr alloys are widely used for medical prosthetic implant devices especially where high stiffness of a highly polished and extremely wear-resistant material is required. The high hardness of the material and the excellent material qualities allow polishing components to optical or mirror-like finishes, which ensures long life of the implants (Arcam, 2007). CoCr alloys are strong, hard (hardness: 37-49 HRC), biocompatible, and corrosion resistant biomaterials, and are used in a variety of joint replacement implants and some fracture repair implants which require a long service life, for example knee implants, metal on metal hip joints, and dental prosthetics. The corrosion resistance in chloride environments of CoCr alloy is related to its bulk composition and the surface oxide (nominally Cr_2O_3) (Ratner *et al.*, 2004). Studies had shown that the passive layer created in the electropolishing and chemical passivation process improves the corrosion resistance of the CoCr alloy (Walke *et al.*, 2006) All elements of the passive-carbon layer presented mainly in the oxides compounds which have higher biotolerance in environment of human physiological liquids (such as synovial fluid), and hence increased the biocompatibility (Kaczmarek *et al.*, 2007; Walke *et al.*, 2007; Paszenda *et al.*, 2008).

1.3.5.3 Ceramic

Ceramic materials are normally made by pressing and heating metal oxides (especially aluminium oxide and zirconium oxide). Ceramic materials are inorganic, non-metallic solids which have a crystalline or partly crystalline structure, or may be amorphous such as glasses. Ceramic materials are strong, resistant to wear and corrosion, and biocompatible which are used widely on implant surfaces without high requirement of flexibility.

Developed ceramic materials for example Biolox Delta Ceramic, not only maintain the high strength, high resistance to wear and corrosion, and good biocompatibility, but provide improved flexibility. Ceramic fracture rarely happens in

new generations of ceramic materials (such as Biolox Delta) (Knahr *et al.*, 1981; Cameron, 1991; Nizard *et al.*, 1992; Krikler and Schatzker, 1995; BIOLOX, 2008).

1.4 Articular Cartilage

Cartilage is a type of dense connective tissue, which is composed of collagenous fibres and elastin fibres, and cells called chondrocytes. All these are embedded in a firm gel-like substance called the matrix. There are few blood-vessels found in the deepest regions adjacent to the bone. However, articular cartilage is devoid of nerves and is generally considered to be avascular.

Cartilage is found in many places in the body including the joints, the rib cage, the ear, the nose, the bronchial tubes, and between intervertebral discs. The thickness of cartilage in large human joints, such as the hip and knee, is 2-4mm, and it varies from area to area within the joint, from joint to joint in the same species, and from species to species (Mow *et al.*, 1989). Provided that the surface remains locally intact, the thickness of human articular cartilage often remains unchanged during adult life (Meachim 1971). Cartilage thickness also varies locally within a particular joint based on the load experienced. The thickness can range from 0.1 mm to 0.5 mm in rabbit knees to up to 6 mm in major load bearing joints like bovine knee joints and human knee and hip joints.

Articular cartilage is crucial to the normal function of synovial joints since its presence enables the articulating bones to transmit high loads whilst maintaining contact stresses at an acceptably low level, and to move on each other with little frictional resistance (Freeman and Meachim 1979). During embryological development and early growth, cartilage is the formation of bone.

1.4.1 Types of Cartilage

There are three main different types of cartilage: hyaline cartilage, elastic cartilage and fibrocartilage, each with special characteristics adapted to local needs:

1. **Avascular Hyaline cartilage** (Figure 1.14.a and d)

This is a glassy smooth, bluish white tissue and the most abundant type of cartilage, and is made predominantly of type II collagen. It is found lining bones in joints (e.g. articular cartilage, gristle) and inside bones, serving as a centre of ossification or bone growth which forms most of the embryonic skeleton.

2. Elastic cartilage (also called yellow cartilage, Figure 1.14.b)

This is mostly made of elastin fibres and highly flexible, and it contains elastic bundles (elastin) scattered throughout the matrix. It is found in the pinna of the ear and several tubes, such as the walls of the auditory and eustachian canals and larynx and especially in the epiglottis.

3. **Fibrocartilage** (also called white cartilage, Figure 1.14.c)

This is specialised cartilage found in areas requiring tough support or huge tensile strength, the pubic and other symphyses, and at sites connecting tendons or ligaments to bones. There is rarely any clear line of demarcation between fibrocartilage and the neighbouring hyaline cartilage or connective tissue. The fibrocartilage in intervertebral disks contains more collagen compared to hyaline cartilage, which means it can withstand high compressive loads. When the hyaline cartilage at the end of long bones such as the femur is damaged, it is often replaced with fibrocartilage, which does not withstand weight-bearing forces as well as articular cartilage.

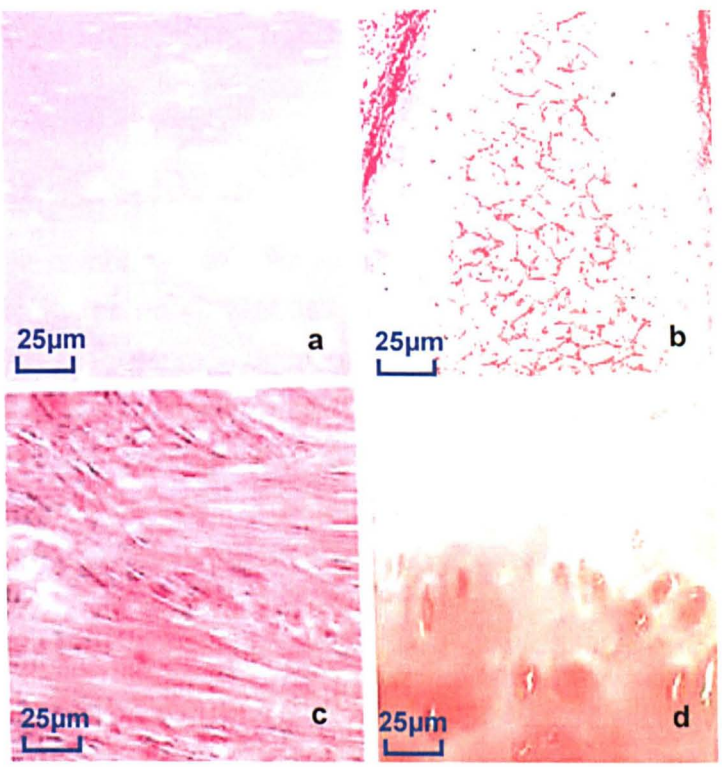

Figure 1.14 Histology of three types of cartilage (Orig.mag.×400): a. Normal hyaline cartilage, stained for connective tissue fibers (van Gieson's stain); b. Normal elastic cartilage: chondrocytes surrounded by ring-like collagen fibers and tiny elastic fibers (van Gieson's stain); c. Fibrocatilage of the meniscus (van Gieson's stain); d. Safranin O stain of osteoarthritic hyaline cartilage (Yuehuei H. An and Martin, 2003).

1.4.2 Compositions of Articular Cartilage

Much like other connective tissue, cartilage is composed of cells, fibres and a matrix; it is enclosed in a dense connective tissue called the perichondrium. Articular cartilage is mainly composed of interstitial water (65 to 85% wet weight), collagen (10% to 20% of wet weight), proteoglycans (5% to 10% of wet weight), glycoproteins and chondrocytes, and various ions such as sodium, potassium, and calcium etc (Freeman 1979).

1.4.2.1 Cells - Chondrocytes

Chondrocytes and their precursors, known as chondroblasts, are the only cells found in cartilage. These are responsible for maintenance and remodelling of the extracellular matrix. Chondrocytes occur singly or in groups (called "cell nests") within spaces called lacunae, and their morphology varies with depth in the tissue. Chondrocytes receive their nutrients through synovial fluid and they are encapsulated in a bag surrounded by the viscoelastic extracellular matrix – chondron (Freeman 1979).

1.4.2.2 Fibres - Collagen

Cartilage is composed of collagen and elastic fibres. In articular cartilage, Type II collagen makes up 40% of its dry weight and the collagen is arranged in cross-striated fibres, 15-45nm in diameter that do not assemble into large bundles. Elastic cartilage also contains elastic fibres and fibrocartilage contains more collagen than articular cartilage. Collagen is responsible for tensile stiffness and strength of cartilage; it also helps resist the swelling pressure due to proteoglycans (PGs). Orientation of collagen fibres varies with depth of the tissue (Freeman 1979).

1.4.2.3 Matrix - Proteoglycans and Glycosaminoglycan (GAG)

The matrix is mainly composed of proteoglycans, which are large molecules with a protein backbone and glycosaminoglycan (GAG) side chains. The most common types of GAGs in cartilage are chondroitin sulfate and keratan sulfate; the other types are dermatan sulfate and hyaluronic acid. GAGs are responsible for the swelling pressure in cartilage due to their large number of negatively charged

sulfate and carboxyl groups. The matrix immediately surrounding the chondrocytes is referred to as the territorial matrix, or capsule (Freeman 1979).

The matrix contains a large amount of water, a meshwork of collagen fibres, and a non-fibrous filler substance. Together these form stiff gel gristle. The filler substance is principally composed of carbohydrate and non-collagenous proteins; if it is removed by experimental procedures or through pathological causes, cartilage loses its rigidity although it may keep its form (Freeman 1979).

1.4.2.4 Interstitial Water

The major component of articular cartilage is interstitial water, and most of it is trapped in the proteoglycan domain while 30% exists in the intrafibrillar space in the collagen and a very small percentage in the intracellular space (Freeman, 1979). The amount of interstitial water depends on proteoglycan swelling pressure along with other ions in the interstitial fluid, and the organisation, strength and stiffness of the collagen network. In diseased conditions e.g. osteoarthritis, the water content is known to increase due to damage to the collagen network (Freeman 1979).

1.4.3 Micro and Macro Structure of Cartilage

The simple homogeneous appearance of cartilage hides its highly ordered complex structure. This structure apparently remains unchanged unless affected by disease or injury.

From the material standpoint, the extracellular matrix (ECM) of cartilage is a fibre-reinforced composite solid consisting of a dense stable network of collagen fibres embedded in a very high concentration of proteoglycan gel, which itself is also a viscoelastic network. The composition and structure of articular cartilage are inhomogeneous within the tissue and vary with depth. Along with the differences in collagen fibre and proteoglycan network, water content also changes. Chondrocyte shape and size also vary with the depth. This gives the tissue a layered appearance under electron microscopy (Mow and Huiskes 2005).

The zones of articular cartilage can be described as follows (Figure 1.15):

1. Superficial zone

This represents 10% to 20% of the total thickness of articular cartilage and the lowest aggrecan (a modular proteoglycan with multiple functional domains) level compared with the other zones. There is the highest content of water (75% to 80%)

and the highest content of collagen (85% dry weight) in this zone. Fine collagen fibrils are densely organised in parallel to the articular surface which may also help to resist shear forces generated during joint use. This is a region where tissue is exposed to the highest tensile and compressive stresses, and also tensile strength has been shown to be the highest in this zone (Mow and Huiskes 2005).

2. Transitional Zone (Middle Zone)

This comprises 40% to 60% of the total thickness and the aggrecan level increases to its maximum in this zone. Collagen content decreases from the superficial zone to the middle zone and remains relatively constant in the deeper zones. Water content generally decreases with depth. The collagen fibrils in the middle zone have a larger diameter that is less tightly packed with random orientation (Mow and Huiskes 2005).

3. Radial (Deep) zone

This accounts for about 30% of the total thickness, the fibres appear to be woven together to form large fibre bundles organised perpendicular to the surface. These bundles cross the 'tidemark' to insert into the calcified cartilage and subchondral bone, thus securely anchoring the uncalcified tissue onto the bone ends. The inhomogeneous distribution of collagen and PG produces pronounced variations in the tensile stiffness and swelling behaviours of various zones of the cartilage, and causes swelling and curling when the tissue is removed from the bone (Mow and Huiskes 2005).

4. Tide mark

This is the junction between cartilage and bone, which reduces stress concentration at this interface. It is an important differentiating landmark, and below it the calcified cartilage zone is anchored to subchondral bone (Mow and Huiskes 2005). Lesions of cartilage that do not violate the time mark result in minimal or no bleeding and have poor capacity for repair (Mankin, 1974).

5. Calcified Zone

This is where collagen fibres anchor into the bone.

Recent evidence indicates the presence of a boundary layer (also called Surface Amorphous Layer) on top of the superficial Zone. It is 200 to 500 nm in thickness and devoid of any cells or collagen, and also it protects the underlying bulk cartilage from the full effect of load in dynamic loading conditions, especially shock loads and aids in effective load transfer (Mow and Huiskes 2005).

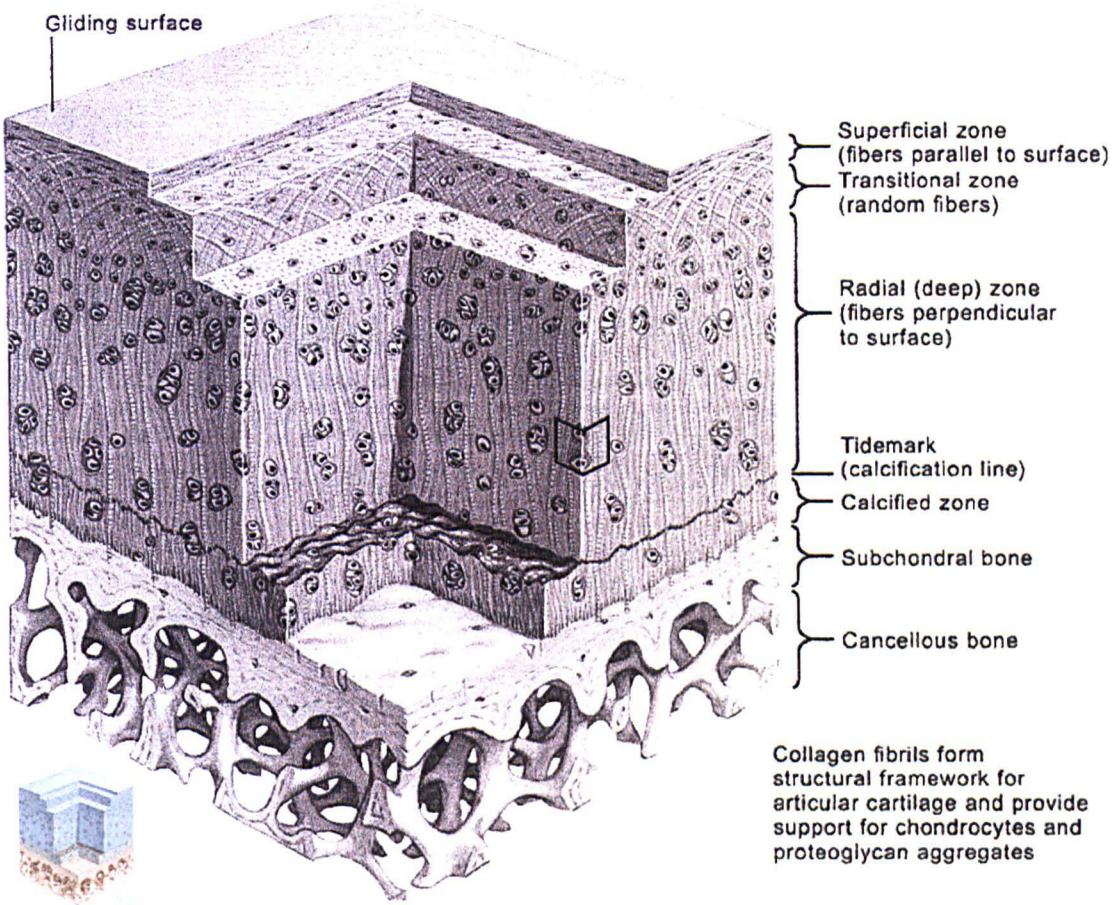

Figure 1.15 Zones of articular cartilage (Carey-Beth and Timothy, 2001)

1.4.4 Synovial Fluid

Synovial fluid is a clear, or sometimes slightly yellowish, highly viscous liquid secreted into the joint cavity by the synovium. It is a dialysate of blood plasma without clotting factors, erythrocytes, or hemoglobin, but containing hyaluronate, an extended glycosaminoglycan chain (Balazs and Gibbs 1970), and a lubricating glycoprotein (Swann and Radin 1972), which aids friction reduction. However, only small amounts of this fluid are contained in various human and animal joints, e.g. approximately 1 to 5 ml of fluid is contained in a healthy human knee joint.

Synovial fluid contains two major components: high molecular weight hyaluronan (also called hyaluronic acid) and lubricin. Hyaluronan creates the viscous and elastic properties of synovial fluid, and a lubricating glycoprotein. Lubricin is mainly responsible for boundary-layer lubrication by reducing friction between opposing surfaces of cartilage during joint articulation (Swann *et al.*, 1981; Swann *et al.*, 1985; Jay *et al.*, 1998; Benya *et al.*, 2002) and also it helps regulate synovial cell growth (Warman, 2003). Studies have shown that lubricin is composed of carbohydrates (≈ 50% w/w), amino acids (≈ 40% w/w), and phospholipids (≈ 10% w/w) (Swann *et al.*, 1985; Schwarz and Hills, 1998).

Synovial fluid exhibits non-Newtonian flow properties, which include a shear thinning effect (Balazs and Gibbs 1970), a normal stress effect (Caygill and West 1969), and an elastic effect. It not only aids in lubrication, but also provides the necessary nutrients for cartilage. Furthermore, synovial fluid acts as a medium for osmosis between the joint and the blood supply, and as protection for cartilage against enzyme activity (Davies 1966).

Very low friction appears to exist within diarthrodial joints regardless of the presence of synovial fluid or hyaluronate. Furthermore, dynamically applied loads, oscillations of sliding, tend to lower the coefficient of friction, whereas static loads act to increase frictional resistance (Mow and Hayes 1991).

1.5 Tribology of Articular Joint

Tribology is the science and technology of interacting surfaces in relative motion and of related subjects and practices (Bharat 2001), and it is defined as the science that deals with the friction, lubrication, and wear of interacting surfaces in relative motion, and is an interdisciplinary science involving physics and chemistry of the bearing surfaces and fluid and solid mechanics. Articular cartilage bears load and slides relative to an apposing tissue surface with remarkable tribological properties: low friction, low wear, and multiple modes of lubrication acting to lower friction and/or wear.

The basic purpose of articular cartilage is to provide a suitable functional covering material for the articular ends of bones at synovial joints (Freeman and Meachim 1979). The physiological and mechanical properties of cartilage depend upon the physical properties of its matrix, and the matrix in turn is dependent for its existence and composition upon the chondrocytes. The fluid flow through the tissue is crucial to its ability to carry load and possibly to the low friction between cartilage surfaces.

The functions of articular cartilage are to distribute the load, minimise peak stresses on subchondral bone, and provide a friction-reducing, weight-bearing surface. Articular cartilage has remarkable elastic mechanical properties; it can be deformed and regain its original shape.

1.5.1 Friction

Friction is the resistance to the sliding of one solid body over or along another (Bharat 2001), and it is the force that opposes the relative motion or tendency of

such motion of two surfaces in contact. There are two types of friction: surface friction and bulk friction. Surface friction comes either from adhesion of one surface to another because of roughness on the two surfaces or from the viscosity of the sheared lubricant film between the two surfaces (Mow and Huiskes 2005). Bulk friction occurs from the internal energy dissipation mechanisms within the bulk material or within the lubricant (Mow and Hayes 1991).

For cartilage, an internal friction is produced by the viscous drag caused when interstitial fluid flows through the porous-permeable solid matrix (Kwan, Lai et al. 1984). Ploughing friction is a specific form of internal friction and occurs in diarthrodial joints when a load moves across a joint surface causing interstitial fluid flow (Linn 1967). In the natural joints, increased levels of friction increase wear, surface damage, causing fibrillation, and also cause subsurface damage at the interface with the subchondral bone (Fisher, 2001).

1.5.1.1 Friction Measurements

The coefficient of friction (also known as the frictional coefficient) is a dimensionless scalar value which describes the ratio of the force of friction between two bodies and the force pressing them together. The coefficient of friction is an empirical measurement; it has to be measured experimentally, and cannot be found through calculations.

The coefficient of friction, when multiplied by the reaction force on the object by the contact surface, will give the maximum frictional force opposing sliding on the object. However, if the force pulling on the object is less than the maximum force of friction then the force of friction will be equal to the force pulling on the object. The coefficient of friction is calculated as Equation 1-1.

$$\mu = \frac{F}{N}$$ **Equation 1-1**

Where, μ is the friction coefficient between two solid surfaces and defined as the ratio of F (the tangential friction force, N) required producing sliding divided by N (the normal force, N) between the surfaces.

1.5.1.2 Comparison of Cartilage Friction

Many studies have tested the coefficient of friction of both entire joints and small specimens. If Tables 1.3 and 1.4 are compared: the coefficient of friction is lower in the whole natural joints (Table 1.3) than the small cartilage specimens on glass or metal (Table 1.4).

Table 1.3 The coefficient of friction in the entire joints *in-vitro*

Authors	Joint Type	Lubricant	Friction Coefficient
Jones, 1934	Horsy stifle	Synovial fluid	0.02
Linn, 1968	Canine ankle	Synovial fluid	0.0044±0.0003
Little *et al.*, 1969	Human hip	Synovial fluid	0.003
Unsworth *et al.*, 1975	Human hip	Synovial fluid	0.021-0.039
Clarke *et al.*, 1975	Human hip	Saline	0.0095-0.018
O'Kelly and McNulty, 1978	Human hip	Bovine Synovial	0.01-0.022
Roberts *et al.*, 1982	Human hip	Synovial fluid + Hyaluronic acid solution	0.033-0.07
Mabuchi *et al.*, 1994	Canine hip	Synovial fluid	0.007±0.004
Murakami *et al.*, 1995	Porcine shoulder	Hyaluronic acid solution	0.008

Table 1.4 The coefficient of friction in unconfined cartilage specimens *in-vitro*

Author	Bearing	Lubricant	Friction Coefficient
McCutchen, 1962	Cartilage/glass	Synovial fluid	0.003-0.15
Walker *et al.*, 1970	Cartilage/glass	Synovial fluid	0.006-0.048
Chappius *et al.*, 1983	Cartilage/glass	Synovial fluid	0.01-0.1
Ikeuchi *et al.*, 1994	Cartilage/PMMA	Saline	0.0-0.28
	Cartilage/cartilage	Saline	0.016-0.028
Stachowiak *et al.*, 1994	Cartilage/glass	Synovial fluid	0.02-0.065
Forster *et al.*, 1995	Cartilage/glass	Synovial fluid	0.010-0.27
Northwood and Fisher, 2007	Cartilage/metal	Synovial fluid	0.015-0.88
Katta *et al.*, 2007b	Cartilage/cartilage	PBS	0.04-0.35
McCann *et al.*, 2009	Cartilage/metal	25% BS	0.02-0.13

1.5.2 Surface Roughness

The cartilage surface roughness plays an important role in the lubrication regime and it may offer clues towards any pathological changes taking place in the cartilage tissue. Currently techniques include contact and non-contact profilometry and microscopy techniques (AFM, TEM, SEM), as shown in Table 1.5.

Table 1.5 Comparison of cartilage surface roughness

Authors	Tissue Type	Technique(s) Applied	Surface Roughness
Chiang *et al.*, 1997	Human	Ultrasonic imaging, confocal microscopy techniques	5.4-15 μm
Forster and Fisher, 1999	Bovine	SEM, TEM, Stylus and Laser profilometry, ESEM	0.24-1.6 μm
Saarakkala, Toyras et al. 2004	Bovine	Ultrasonic Characterisation	6.8-12.3 μm
Kobayashi *et al.*, 2001	Bovine	Atomic Force Microscopy	0.38 μm
Park *et al.*, 2004	Bovine	Atomic Force Microscopy	0.46 μm
Graindorge, 2006	Bovine	White light interferometry	0.6 μm

1.5.3 Wear

Wear is created when surface asperities of materials contact and reciprocate. There are two conventional types of wear: fatigue wear and interfacial wear. Fatigue wear is independent of the lubrication phenomenon occurring at the surfaces of bearings because of the cyclic stresses and strains generated within the cartilage due to the application of repetitive loads caused by joint motion. Thus, *in-vivo* wear is a balance of mechanical attrition and biological synthesis. Interfacial wear occurs due to solid-solid contact at the surface of the bearing materials, and includes adhesive wear and abrasive wear. Adhesive wear is the most common and occurs when a junction is formed between the two opposing surfaces as they come into contact, and if this junction is stronger than the cohesive strength of the individual materials, fragments of the weaker material may be torn off and may adhere to the stronger material (Dowson, Unsworth et al. 1981).

Although diarthrodial joints are subjected to an enormous range of loading conditions, the cartilage surfaces undergo little wear under normal circumstances. Under high-speed motion, such as during the swing phase of walking or running, loads of more than body weight are sustained. However, heel-strike and toe-off may generate forces three to five times body weight across the hip joints. During prolonged standing, or when a joint is held in a fixed loaded position, moderate

fixed loads are also generated. However, for biological materials, little or no quantitative information exists on wear mechanisms or wear rates.

1.5.3.1 Cartilage Wear Types and Grades

The wear of articular cartilage is defined as the removal of material from the surface due to mechanical or chemical action between the contact surfaces. However, the wear of cartilage is very difficult to measure due to the variable water content of the articular cartilage and its biphasic properties. The water content affects both gravimetric and geometric measurements of both wear and permanent deformation. Even when cartilage is allowed to re-stabilise after a period of time, it is difficult to distinguish wear from permanent deformation or permanent loss of water from the cartilage (Northwood and Fisher, 2007). It is possible to use changes in surface topography as an indication of surface damage caused by wear (Katta *et al.*, 2007b; Northwood and Fisher, 2007; Katta *et al.*, 2008a).

1.5.3.2 Quantification Measurements of Cartilage Wear

The most commonly used clinical classification system to distinguish between various damage levels of articular cartilage is the International Cartilage Repair Society (ICRS) cartilage wear grades system, and this is described as:

International Cartilage Repair Society (ICRS) Classification (Figure 1.16):

- ICRS Grade 0 – Normal tissue
- ICRS Grade 1 – Nearly Normal: Superficial lesions. Soft indentation (A) and/or superficial fissures and cracks (B)
- ICRS Grade 2 – Abnormal: Lesions extending down to <50% of cartilage depth
- ICRS Grade 3 – Severely Abnormal: Cartilage defects extending down >50% of cartilage depth (A) as well as down to calcified layer (B) and down to but not through the subchondral bone (C). Blisters are included in this Grade (D)
- ICRS Grade 4 – Severely Abnormal: Defects extending down into the subchondral bone.

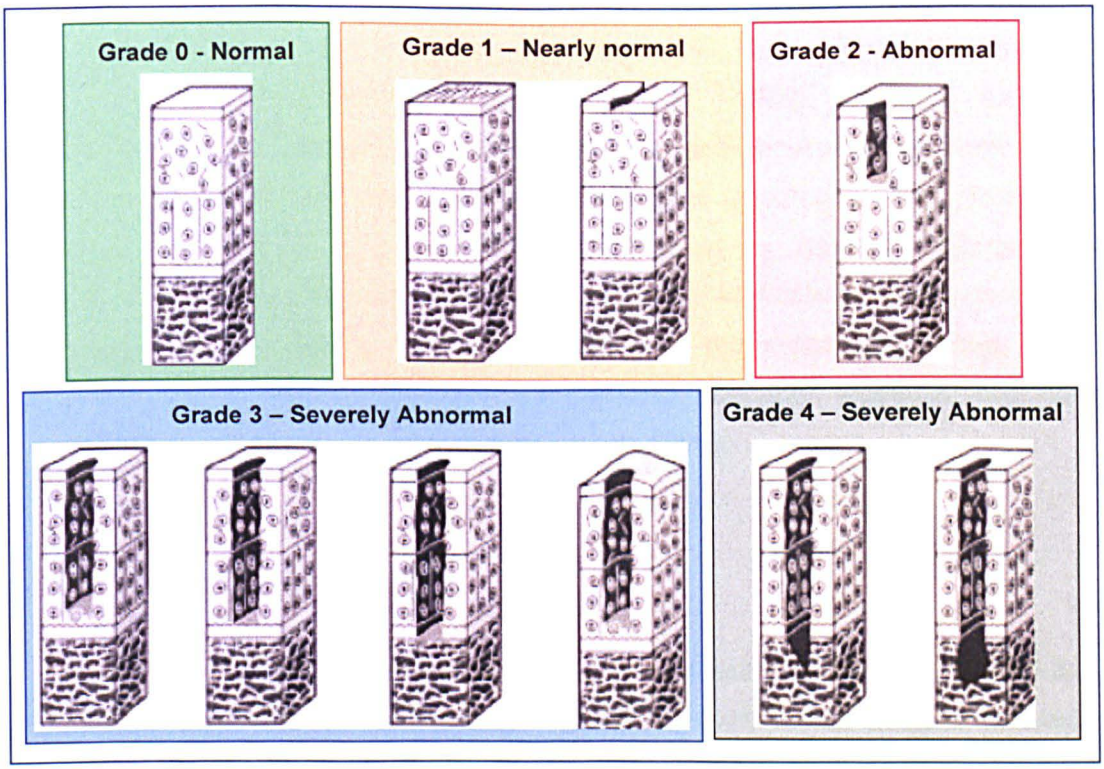

Figure 1.16 ICRS classification of cartilage macroscopic damage (Mats *et al.*, 2000)

1.5.4 Lubrication Mechanisms

When the applied load is carried by pressure generated within the fluid, the frictional resistance to motion arises entirely from the shearing of the viscous fluid. Lubrication acts to keep wear of articular cartilage in diarthrodial joints to a minimum, and under normal circumstances, with proper lubrication and repair responses by chondrocytes in the tissue, diarthrodial joints can function normally for many decades. However, in pathological cases, or under conditions of abnormally severe loading, both fatigue and interfacial wear become evident. Because the wear process initiates, the tissue becomes more susceptible to both surfaces and interior damage, thus leading to a progressive degeneration process. Failure of cartilage as a bearing surface results from the loss of balance between the wear rate and the ability of chondrocytes to repair the micro-damage (Lai *et al.*, 1991).

Articular cartilage in synovial joints withstand complex, varied and often-harsh loading regimes, which are subjected to both dynamic and static loads that occur from sliding and rolling of the two articulating surfaces. The mechanical features of cartilage enable large bearing loads by providing a surface with minimal friction, wear and excellent lubrication. The low friction and wear characteristics are due to the various mechanisms of lubrication (MacConaill, 1932): elastohydrodynamic lubrication (Dowson *et al.*, 1969), micro-elastohydrodynamic lubrication (Dowson

and Jin, 1986), boundary lubrication (Charnley, 1959; Radin *et al.*, 1970; Swann *et al.*, 1981), boosted lubrication (Walker *et al.*, 1968), weeping lubrication (McCutchen, 1959; McCutchen, 1962), biphasic self-generating lubrication (Mow and Lai, 1980), and biphasic boundary lubrication (Ateshian, 1997; Forster and Fisher, 1999; Ateshian *et al.*, 2003a; Graindorge *et al.*, 2004; Graindorge *et al.*, 2005). It is proposed that when mixed or boundary lubrication occurs (under high load and / or low sliding speed), the biphasic properties of cartilage play a significant role in reducing friction and enhancing lubrication (Ateshian and Wang, 1995; Ateshian *et al.*, 1998; Forster and Fisher, 1999).

1.5.4.1 Fluid-film Lubrication

Fluid-film lubrication occurs when opposing surfaces are separated by a lubricant film, and it is a lubricating regime in which a film of fluid completely separates the opposing surfaces. The film developed between the surfaces can be achieved in different ways depending on the properties of the fluid and the surface motion, and the load acting on the surfaces is supported by the pressure in the fluid film.

Hydrodynamic Lubrication

Hydrodynamic lubrication is the classical model of fluid film lubrication which occurs when two bearings surfaces move relative to one another, and this relative motion draws fluid into the space between them. The two surfaces are kept completely separated by a film thickness, which decreases in the direction of the motion by mechanism. This lubrication regime requires continuous motion in one direction to maintain the fluid film. It is generally accepted today that fluid film lubrication is likely to exist only under certain conditions of loading that are optimal for this mode of lubrication (high speed and low loads). Fluid-film mechanisms and multiple modes of lubrication were suggested to coexist in diarthrodial joints by Dowson 1967.

Self-generating Mechanism

The proposal by Mow and Lai (1979) proposed a "self-generating mechanism" in which fluid was observed to exude under the leading and trailing edges of the load distribution, while it was reabsorbed into the tissue near the centre. The exuded fluid at the leading edge could potentially provide a continuous supply of lubricant to maintain a fluid film between the surfaces, thus reducing the friction

coefficient. This self-generating mechanism may not only contribute significantly to fluid-film lubrication, but may also create a mechanically generated circulation system required for the nutrition of chondrocytes in the tissue *(Levick, 1979)*.

Squeeze-film Lubrication (Figure1.17.a)

When two surfaces approach one another under a load, a pressure is generated in the fluid film, which separates them. This fluid is squeezed out of the area of impending contact and the resulting fluid pressure keeps the two surfaces apart. In squeeze-film lubrication, two bearing surfaces simply approach each other along a normal direction. As a viscous lubricant cannot be instantaneously squeezed out from the gap between the surfaces, a time-varying pressure field is built up as a result of the viscous resistance offered by the lubricant as it is being squeezed from the gap. The pressure field in the fluid film formed in this manner is capable of supporting large loads. On account of the bearing surfaces being deformable layers of articular cartilage, the large pressure generated may cause localised depressions where the lubricant film can be trapped *(Kobayashi et al., 2001)*.

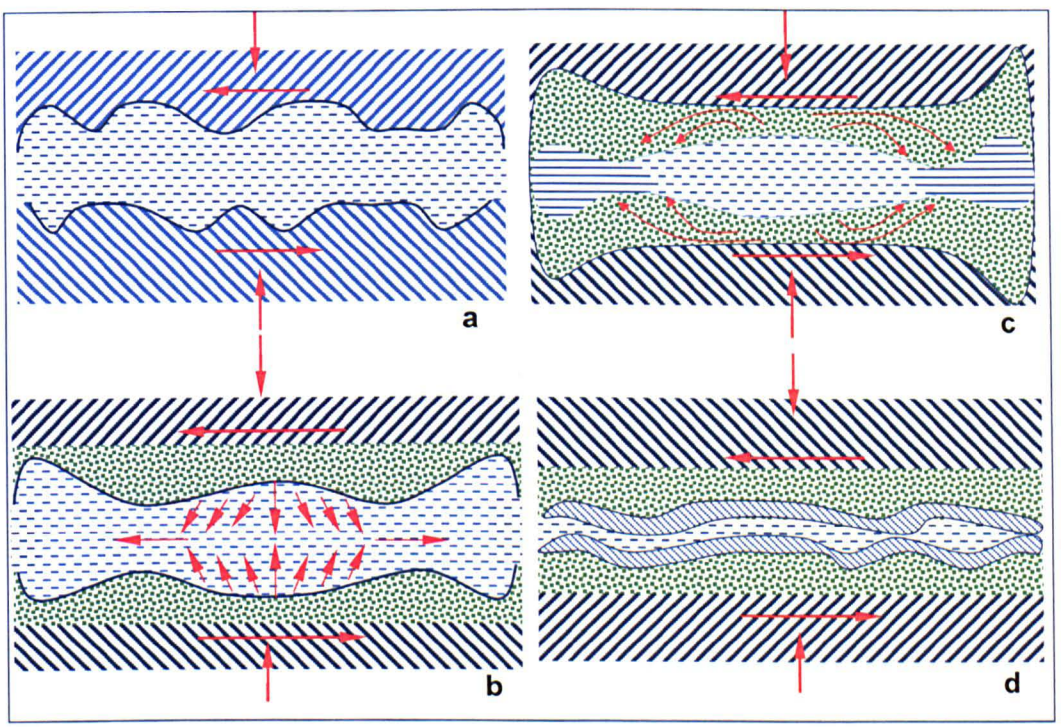

Figure 1.17 a) Pure fluid film lubrication: the fluid film between the surfaces can be maintained by three mechanisms – hydrostatic; squeeze film; hydrodynamic; b) Self-pressurised hydrostatic or "weeping" lubrication – as the load is increased, fluid is squeezed from the cartilage to provide the lubricating layer (McCutchen, CW 1967); c) Boosted lubrication: filtering of water through cartilage concentrates the lubricant in the contact area (Walker *et al.*, 1968); d) Boundary lubrication: lubricant molecules sick to the surfaces, keeping them apart.

Self-pressurised hydrostatic (or weeping) lubrication (Figure1.17.b)

A classical engineering lubrication theory, hydrostatic lubrication, exists in which a pressurised fluid film is maintained between two bearing surfaces via an external pump. Lewis and McCutchen (Lewis and McCutchen, 1959) introduced this lubricating theory which involves pressurized fluid being supplied from within the articular cartilage to the loaded region. According to this theory, compressing together the two layers of articular cartilage generates lubricant fluid film between the two articulating surfaces.

Boosted lubrication (or Ultrafiltration) (Figure 1.17.c),

Another theory proposed that as the articulating surfaces approach each other, the solvent component of synovial fluid, i.e., water, passes into the articular cartilage over the contact region during squeeze-film conditions, thus leaving a concentrated pool of hyaluronic acid protein complex behind to lubricate the surfaces *(Walker et al., 1968).* Boosted lubrication is a mechanism in which the fluid that is separating two cartilage surfaces is a highly viscous solution of hyaluronic acid. Under load the fluid between the cartilage surfaces is pressurised and the smaller molecules of the synovial fluid escape through the pores of the cartilage surface into the cartilage matrix. The hyaluronic acid molecules are too big to pass though these pores, so those molecules are left between the contacting surfaces. This leaves a high concentration of hyaluronic acid in the joint space which is considered to aid the lubrication of the joint.

In general, the fluid lubricant is forced into the cartilage at the high-pressure central region and out of the cartilage in the peripheral region of the squeeze-film gap within the load support area. Synovial fluid viscosity and cartilage permeability are the two dominant parameters governing the behaviour of joints when operating under squeeze-film action.

1.5.4.2 Boundary Lubrication

Boundary lubrication (Figure 1.17.d) is a mechanism in which the friction and wear between the surfaces in relative motion are determined by the properties of the surface and by the properties of the lubricant other than bulk viscosity. A fluid film is present in the boundary lubrication regime, which is not sufficiently thick enough to prevent contact between the asperities on the opposing surfaces.

1.5.4.3 Mixed Lubrication

In many bearings a combination of both boundary and fluid film lubrication exists this is called mixed lubrication. Under some conditions the boundary lubricating film may break down and dry contact may occur, and this regime generally occurs with intermittent motions where there is a continual change from boundary to fluid film regimes.

1.5.4.4 Biphasic / Triphasic Lubrication

Based on the biotribology of cartilage and diarthrodial joints, it appears that a dominant mechanism for regulating the frictional response of articular layers is interstitial fluid pressurisation (Ateshian and Wang, 1995). There is strong support of this mode of lubrication in terms of experimental and theoretical evidence, which explain fundamental experimental findings, particularly the time dependence of the friction coefficient, and the ability to produce low friction at high loads and at any sliding velocity, including quasi-stationary loading. It is compatible with fluid-film lubrication, mixed lubrication, and boundary lubrication, to the extent that all of these modes of lubrication may serve to enhance the role of interstitial fluid pressurisation (Ateshian *et al.*, 1998). It intimately ties the frictional response at the articular surfaces to the mechanics of cartilage because interstitial fluid pressurisation is primarily regulated by the porous-permeable nature and intrinsic properties of the tissue (Mow and Huiskes, 2005).

The overall friction and friction coefficient has been simply expressed by Forster and Fisher (1996), as Equation 1-2

$$F_T = \mu_T \times L = \mu_f \times L_f + \mu_s \times L_s \qquad \textbf{Equation 1-2}$$

Where F_T is the total (overall) friction force, μ_T is the total (aggregate) coefficient of friction, L is the total load, μ_f is the effective coefficient of friction attributed to the fluid phase, L_f is the load carried by the fluid phase, μ_s is the effective coefficient of friction attributed to the solid phase, and L_s is the load carried by the solid phase (Forster and Fisher, 1996).

Triphasic lubrication theory was first introduced as an extension of the biphasic theory (Lai *et al.*, 1991): negatively charged Proteoglycans were modelled to fix to the solid matrix, and monovalent ions in the interstitial fluid were modelled as an additional phase to the solid and fluid phases. Swelling of articular cartilage depends on both its fixed charge density and distribution, the stiffness of cartilage

collagen-proteoglycan matrix, and the ion concentrations in the interstitial fluid (Lai *et al.*, 1991). The triphasic model assumed the fixed charge groups to remain unchanged, and that the counter-ions are the cations of a single salt of the bathing solution. The momentum equation for the neutral salt and for the interstitial water is expressed in terms of their chemical potentials whose gradients are the driving forces for their movements. The ions phase plays an important role in the way cartilage physically behaves - attracting fluid in the matrix. Continuous triphasic studies have been show that the additional third ionic phase increased the accuracy of model predictions of cartilage deformational response, although it was determined to play a small role compared to the solid and fluid phases of cartilage (Gu *et al.*, 1997; Gu *et al.*, 1998; Narmoneva *et al.*, 1999; Sun *et al.*, 1999; Ateshian *et al.*, 2004).

Gu *et al* (1997) reported that when the fixed charge density within the tissue (or membrane) separating the two electrolyte (NaCl) solutions was lower than a critical value; solvent would flow from the high NaCl concentration side to the low concentration side (i.e. negative osmosis). Based on a linear version of the triphasic theory, this negative osmosis condition was derived and due to the friction between ions and water since they could flow through the tissues at different rates and different directions. (Gu *et al.*, 1997). Ateshian *et al* (2004) presented closed-form expressions which relate biphasic and triphasic material properties in tension, compression and shear. Compared to experimental findings, these expressions provided greater insight into the measured properties of articular cartilage (e.g. coefficient of friction, cartilage deformation, etc) as a function of bathing solutions salt concentrations and proteoglycan fixed-charge density (Ateshian *et al.*, 2004).

1.5.5 Tribology of Hemiarthroplasty

Tribology of hemiarthroplasty involves natural human or animal cartilage tissue, and biomaterial replacement (prosthetic) devices to replace diseased / injured tissues or organs. The study of hemiarthroplasty tribology includes the friction, wear, deformation, and lubrication when unconfined or confined cartilage specimens articulate against a biomaterial (e.g. metal, ceramic) *in-vitro* under cycling loading reciprocation. The tribology properties of articular cartilage are influenced by different factors such as contact stress, contact area, sliding velocity and distance, loading types, biomaterial types, geometry differences, etc, when the mechanism condition changes.

The mechanical response of articular cartilage is highly non-linear and both time- and load-dependent (Graindorge *et al.*, 2004). Previous experimental studies have found that under static loading followed by sliding reciprocation, the friction coefficient increases due to the biphasic properties of cartilage (Forster and Fisher, 1999; Ferrandez *et al.*, 2004; Graindorge *et al.*, 2005; Katta *et al.*, 2007b). The friction of cartilage in short-term tests (e.g. one hour) under low and medium contact stresses has been discussed in previous studies (Jin *et al.*, 2000; Katta *et al.*, 2008a). However, the cartilage frictional properties and deformational behaviour have not been previously investigated under longer-term prolonged static loading.

Table 1.6 Comparison of Friction Study in Pin-on-Plate Model.

Groups	Cartilage Friction Properties				Authors	Comments
	Time	Contact Stress (Mpa)	Coefficient of Friction (μ_{eff})	Lubricant / Load (N) / Pin Ø(mm)		
Cartilage Pin on Metal Plate	5 s – 45 min	0.5	0.001-0.27	SF 25 9	Forster *et al.*, 1995	1. Short-term (≤2 h), the μ_{eff} varied between 0.5-4 MPa, this might be due to the different lubricants and stroke lengths. 2. The μ_{eff} was found to be statistically lower in SF compared to in RS lubricant. 3. The μ_{eff} showed no significant difference from 2 h to 8 h constant loading. 4. Long-term (>8 h) higher contact stress (>4 MPa) friction studies have not been investigated.
	5 s – 45 min	0.5 and 4	0.001-0.32	SF or RS 25 9 / 3	Forster and Fisher, 1996	
	45 min	0.5	0.48	25% BS 25 9 / 3	(Pickard *et al.*, 1998a	
		4	0.32			
	5 s – 2 h	0.6	0.001-0.52	SF / 30 9 mm	Forster and Fisher, 1999	
			0.001-0.61	RS / 30 9		
	2 h	0.5	0.42 (±0.02)	RS / 25 9	Northwood *et al.*, 2007	
	8 h	0.5	0.45 (±0.02)	RS+16 g/l PL / 25 9		
Cartilage Pin on Cartilage Plate	2 h	0.5	0.03 (±0.01)	RS / 25 9		The μ_{eff} was reduced significantly with an increase of contact stress from 0.2 to 0.4 MPa in 1 h, but it was increased significantly with an increase of contact stress from 0.5 to 3.15 MPa in 2-7 h loading.
	8 h	0.5	0.03 (±0.01)	RS+16 g/l PL / 25 9		
	60 min	0.2	0.047	PBS/13/9	Katta *et al.*, 2007b	
		0.3	0.035	PBS/19/9		
		0.4	0.030	PBS/25/9		
	7 h	0.5	0.025	PBS/32/9	Katta *et al.*, 2008b	
		2	0.044	PBS/127/9		
		3.15	0.062	PBS/200/9		
Metal Pin on Cartilage Plate	45 min	0.24-0.3	0.025 – 0.30	SF and RS	Forster and Fisher, 1996	Short-term study have shown the μ_{eff} to be similar to cartilage on cartilage model.

Previous *in-vitro* studies have investigated the frictional properties of articular cartilage in a simple unconfined pin-on-plate model to mimic hemiarthroplasty: cartilage-on-metal, and metal-on-cartilage configurations (Forster *et al.*, 1995; Forster and Fisher, 1996; Pickard *et al.*, 1998a; Pickard *et al.*, 1998b; Northwood *et al.*, 2007) (Table 1.6). In all cases the coefficient of friction was dependent on loading time. Different lubricants: Synovial Fluid (noted as SF), Ringer's Solution (noted as RS), Protein Lubricant (noted as PL), Bovine Serum (noted as BS), Phosphate buffered saline (noted as PBS).

Cartilage wear studies are limited because it is difficult to quantify either the mass loss or volume loss in hydrated tissues because of the phenomenon of swelling. A previous study by Lipshitz and Glimcher (Lipshitz *et al.*, 1975) concluded that cartilage wear rates increased with increasing normal load and relative speed of the surfaces, but decreased with time, attaining an equilibrium value and may decrease 10 times if synovial fluid was used as the lubricant compared to phosphate buffer saline (0.03 molar; pH7.4). During reciprocating motion, wear was attributed to the interaction between two contacting surfaces and accumulation of microscopic damage, described as interfacial and fatigue (Armstrong and Mow, 1982). In other studies in the knee it has been shown that permanent deformation and wear increased with both increased friction and increased contact stress, these factors typically increased the frictional shear stress and the extent of cartilage wear and degradation (McCann *et al.*, 2009).

1.6 Research Scope and Goals

Hip hemiarthroplasty is used effectively for the treatment of femoral neck fracture or femoral head necrosis in old patients. This is a more conservative option to prevent removal of healthy tissue and provide the mechanical functions to the hip. For elder patients who have relatively low activity requirements, hip hemiarthroplasty delivers a shorter operation time, a shorter hospital stay, and quicker recovery compared to THR. The success of hip hemiarthroplasty has been reported to vary *in-vivo* clinical studies, and cartilage erosion (wear) is the main issue of this prosthesis in long-term follow up. There are many factors that will affect the tribological and mechanical properties of acetabular cartilage, which have only reviewed limited investigation *in-vitro* studies. *In-vitro* studies may provide information to improve or develop the design of hip hemiarthroplasty clinically.

1.6.1 Aims

The aim of this thesis was to investigate cartilage tribological properties: friction, deformation and wear, in both unconfined and confined models to mimic hip hemiarthroplasty *in-vitro*.

1.6.2 Objectives

Specifically this thesis has assessed the mechanical and tribological factors that affect hip hemiarthroplasty by developing new methods to assess cartilage friction, deformation, and wear in a range of conditions by applying a simplified physiological load and motion in a clinically relevant configuration. The specific objectives were:

1. To understand the mechanical factors (e.g. contact stress, contact areas, sliding velocities and sliding distance) which affect the tribological properties of cartilage in an unconfined pin-on-plate model *in-vitro*;
2. To investigate the mechanical factors (e.g. clearances, loading, materials, and prosthesis design) that affect the tribological properties of cartilage in a confined hip joint model *in-vitro*;
3. To link the findings of this *in-vitro* study to *in-vivo* clinical results to provide practical information that could be applied to improve the outcome of hemiarthroplasty prostheses.

Additionally, the methodologies in this thesis were developed with a view to their use in the future to assess less invasive procedures (for example, development of a whole hip model to assess chrondroplasty materials).

Chapter 2 General Materials and Methodology

2.1 Introduction

The tribological studies of hemiarthroplasty that have been undertaken have focused on the friction, cartilage deformation, and cartilage wear using two mechanical models: a simple geometry hemiarthroplasty pin on plate model and a hemiarthroplasty hip joint model. Both models included control tests with standard materials to ensure the methodology provided similar data to the previous similar studies / control data for the pin on plate study (Forster and Fisher, 1996; Katta, 2007; Northwood, 2007). Additionally study tests were conducted to investigate a matrix of variables. The hemiarthroplasty hip pendulum model was developed specifically part of this thesis. An overview of the models and methodologies is shown in Figure 2.1.

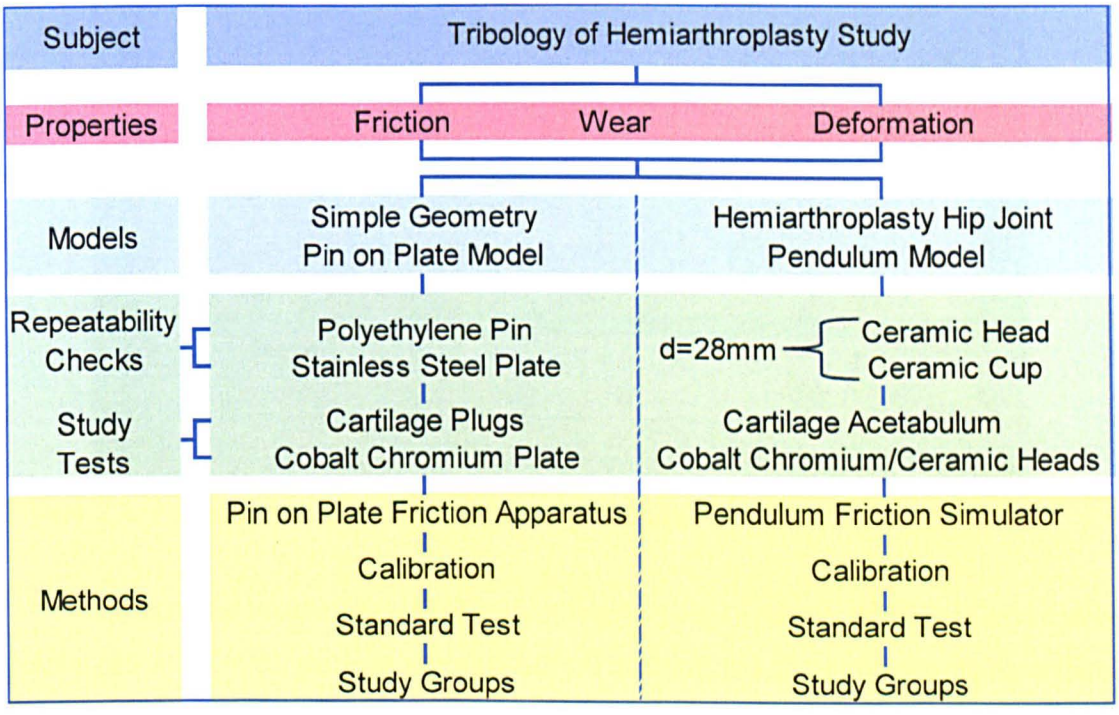

Figure 2.1 Summary of overall methods used in the study of tribology of hemiarthroplasty

2.2 Simple Geometry Pin on Plate Model

2.2.1 General Materials

Pin on plate studies used a reciprocating pin on plate rig manufactured at the University of Leeds (Forster and Fisher, 1996; Katta, 2007; Northwood, 2007). This section describes samples used in testing.

2.2.1.1 Standard Materials – Polyethylene Pin and Stainless Steel Plate

Polyethylene pins (grade 1120) and stainless steel plates (Figure 2.2) were used for the control test pin on plate friction study. Control tests were undertaken to validate the friction apparatus operation and to compare the results to previous tests by different users (Forster and Fisher, 1996; Katta, 2007; Northwood, 2007).

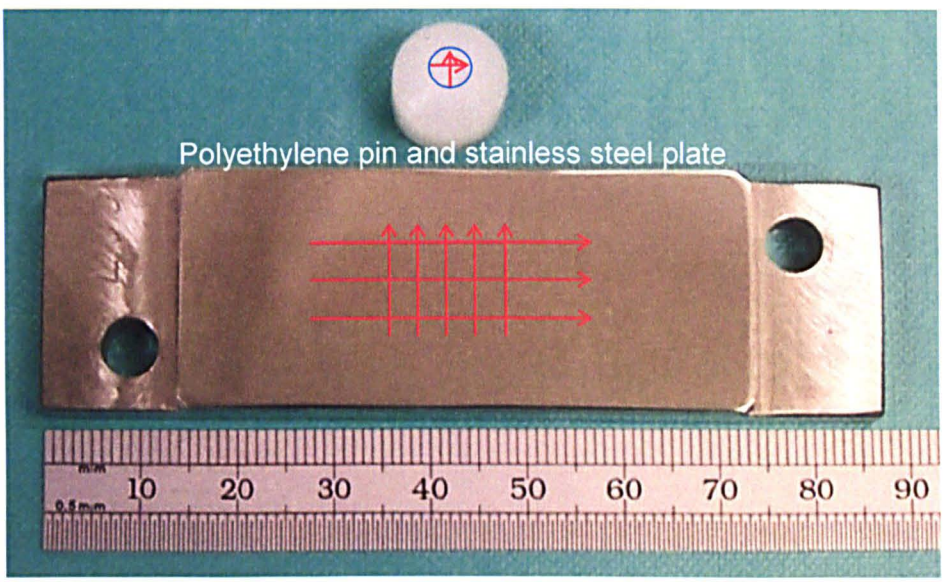

Figure 2.2. Polyethylene pin and stainless steel plate

The surface roughness of the polyethylene pins (5 mm in diameter) and metal plates (60 x 35 mm) were measured before starting the friction tests using a two-dimensional profilometer (Form Talysurf, Taylor Hobson, Leicester, UK). Prior to measurement it was ensured that the pin and plate surfaces were free from contamination. The Polyethylene pin was measured with two uniform traces across the middle perpendicular to each other. Metal plates were measured with three uniform traces length 10 mm in five positions across the middle of the wear surface, and R_a, R_v, R_p, R_t, (Figure 2.3), and R_{Sm} (Figure 2.4) were recorded at 5 x 0.8 mm cut-off.

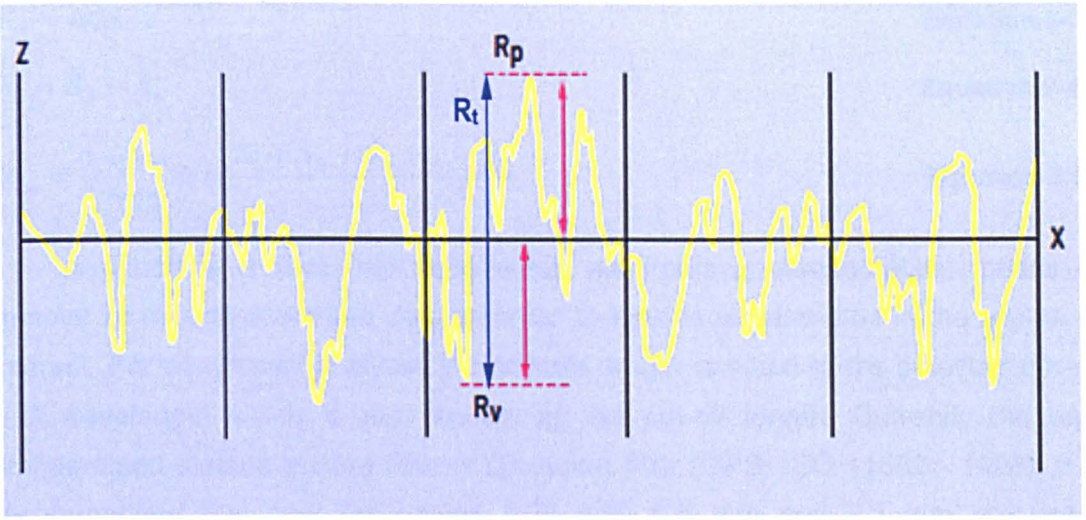

Figure 2.3 Definition of Rv, Rp, and Rt. (Talyor-Hobson, 2005)

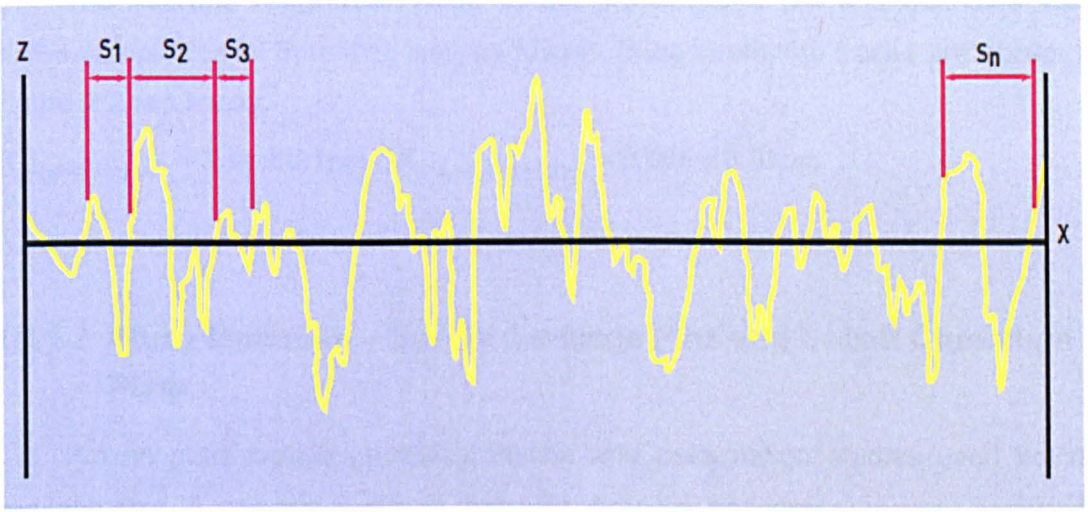

Figure 2.4 Definition of Si (Talyor-Hobson, 2005)

R_a is the universally recognised, and most used, international parameter of roughness. It is the arithmetic mean of the absolute departures of the roughness profile from the mean line (Equation 2-1). R_v is the maximum depth of the profile below the mean line within the sampling length (Equation 2-2). R_p is the maximum height of the profile above the mean line within the sampling length (Equation 2-3). R_t is the maximum peak to valley height of the profile in the assessment length (Equation 2-4). R_{sm} is the mean spacing between profile peaks at the mean line, measured within the sampling length (Equation 2-5, where n is number of peak spacing). (A profile peak is the highest point of the profile between an upwards and downwards crossing of the mean line).

$$R_a = \frac{1}{l}\int_0^l |z(x)|dx \qquad \textbf{Equation 2-1}$$

$$R_v = \min_i z_i \qquad \textbf{Equation 2-2}$$

$$R_p = \max_i z_i$$ **Equation 2-3**

$$R_t = R_p - R_v$$ **Equation 2-4**

$$R_{sm} = \frac{1}{n}\sum_{i=1}^{i=n} Si = \frac{S_1 + S_2 + S_3 + ... + S_n}{n}$$ **Equation 2-5**

A cut-off is a filter that uses either electronic or mathematical means to remove or reduce unwanted data in order to look at wavelengths in the region of interest. For roughness analysis, the sample length is equal to the selected cut-off (*Lc*) wavelength which is also known as the cut-off length. Currently the only standardised surface texture filter is Gaussian filter (GPS, ISO 11562 - 1996). It is recommended that only the values 0.25 mm; 0.8 mm and 2.5 mm are used, depending on the sample roughness and measurements required.

The average roughness value of the polyethylene pin and stainless steel plates samples used in testing was as follows (measurements traces are shown in Figure 2.2 red lines):

$R_{a-Polyethylene\ pin} = 3.16 \pm 0.1 \mu m$; $R_{a-stainless\ steel\ plate} = 0.006 \pm 0.01 \mu m$

2.2.1.2 Study Materials – Bovine Cartilage Pins and Cobalt Chromium Plate

Pin on plate simple geometry friction and deformation studies used bovine cartilage pins, 4 mm and 9 mm in diameter. Articular cartilage pins were harvested from the patella femoral groove of bovine femoral knee joints (12~24 months old) from the supplier (John Penny and Son of Rawdon, Leeds). The patello-femoral groove was used to harvest pins, used in these studies rather than the acetabulum. This was due to the acetabular irregular concave geometry, which would make controlling variables such as contact area and stress challenging. Bovine knee joints were taken from an abattoir within 36~48 hours of the animals being slaughtered and kept in cold storage with the knee and ankle joints skinned but fully intact. The collected cartilage pins were of a healthy, normal appearance, from the middle part of the patello-femoral groove, which is the contact area of the knee (the main load carrying area). The superior part of the groove is very soft and the inferior part is very hard; no specimens were collected from these two areas.

The procedure of harvesting the cartilage plugs is shown in Figure 2.5. Firstly, the locations where the cartilage plugs were to be drilled from were marked using a hand held surgical corer (Figure 2.5.a). Secondly, the cartilage was drilled from a direction orthogonal to the surface to a depth of over 12mm using an electric drill

(Figure 2.5.b) with a corer of the required size (Figure 2.5.c). The drilling speed was slow in order to avoid increasing the temperature of the bone, and PBS was sprayed onto the cartilage surface frequently throughout the dissection to keep the cartilage hydrated. Figure 2.5.d shows where a 4 mm in diameter bovine cartilage pin was taken, and Figure 2.5.e is shown a 9 mm in diameter bovine cartilage pin was taken. Thirdly, a long hand held corer was then inserted into the already drilled groove, and the pin was extracted by simply snapping it from the bone. Finally, the bone end of the cartilage plugs were filed parallel to the cartilage surfaces, and stored (for up to 30 days due to the degradation of cartilage – previous studies by Foster 1996 demonstrated that the cartilage mechanical properties did not significantly change during less than 30 days frozen storage) in a moist condition at -20°C (with 0.1% Aprotinin [Trasylol, Bayer]), used to slow down the fibrinolysis of cartilage during storage and testing). The pins had a cartilage thickness of 1-2mm (Figure 2.6) and were fully defrosted prior to use.

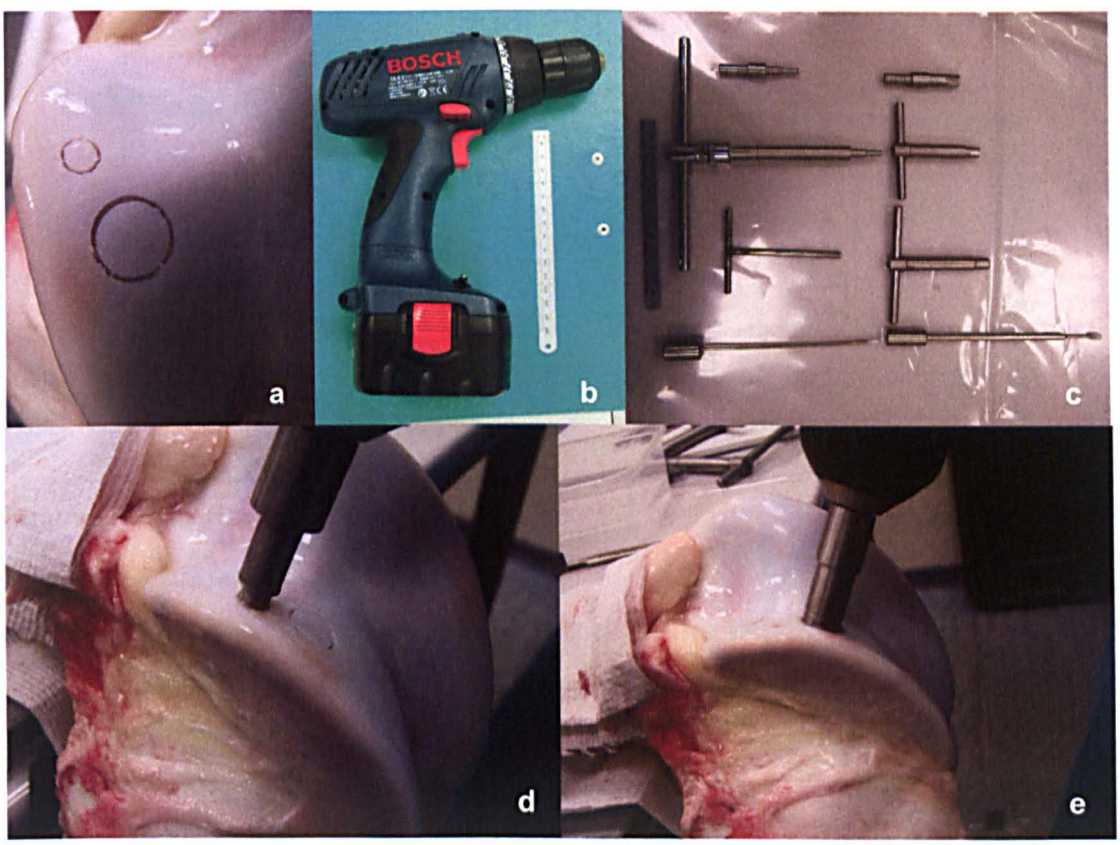

Figure 2.5. The process of harvesting bovine cartilage plugs a. the markings for pin extraction; b. electric drill; c. metal corer, plug driller, cuter, and plug pusher; d. extracting 4mm diameter cartilage pin; e. extracting 9mm diameter cartilage pin

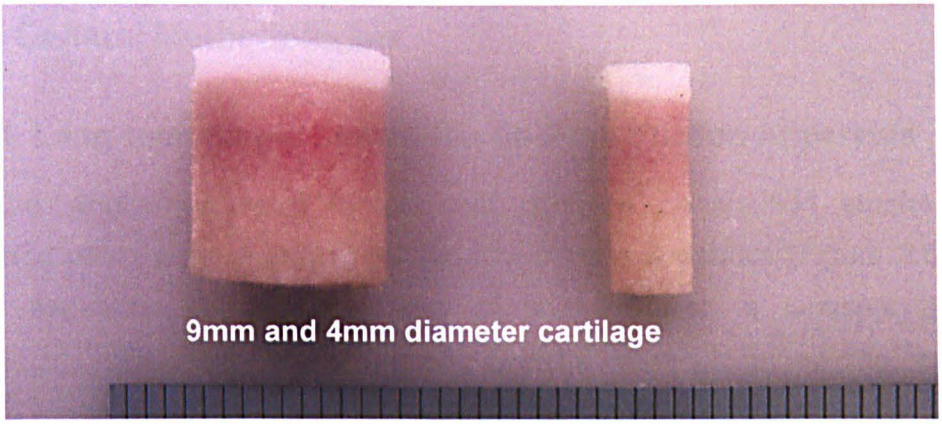

Figure 2.6. Bovine cartilage plugs 9 and 4mm diameter

Cobalt chromium alloy plates (Figure 2.7) were used as the counterfaces in the pin on plate friction studies to replicate the metallic femoral head in hemiarthroplasty, reciprocated against the bovine cartilage pins under constant loading. The roughness was measured (as described in Section 2.2.1.1) and found to be: $Ra(CoCrplate) = 0.005 \pm 0.001 \mu m$

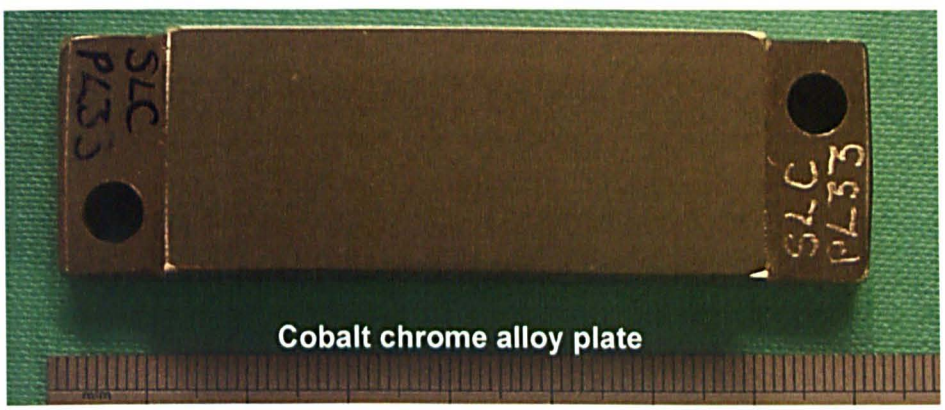

Figure 2.7. Cobalt chrome alloy plate

2.2.1.3 Lubricant - Phosphate Buffered Saline (PBS)

Phosphate buffered saline (PBS) was made up as per the manufacture's recommendation (MPBio; Catalogue Number: 2810305), by dissolving one PBS tablet per 100ml of sterile distilled water, to gain a composition shown in Table2.1.

Table 2.1 Composition of PBS

Component Name	mg/Liter
Potassium Chloride [KCl]	200
Potassium Phosphate Monobasic [KH_2PO_4]	200
Sodium Chloride [NaCl]	8000
Sodium Phosphate Dibasic [Na_2HPO_4]	1150

2.2.2 General Methodologies

2.2.2.1 Long-term Single Station Pin on Plate Friction Apparatus

The simple geometry friction and cartilage deformation studies were conducted using a reciprocating motion pin-on-plate apparatus (Figure 2.8). This friction apparatus primarily consisted of a pin holder, a lubricant bath, a piezoelectric sensor (force transducer), a linear bearing, an electric motor, a variable speed motor drive, a charge amplifier, and load (weights).

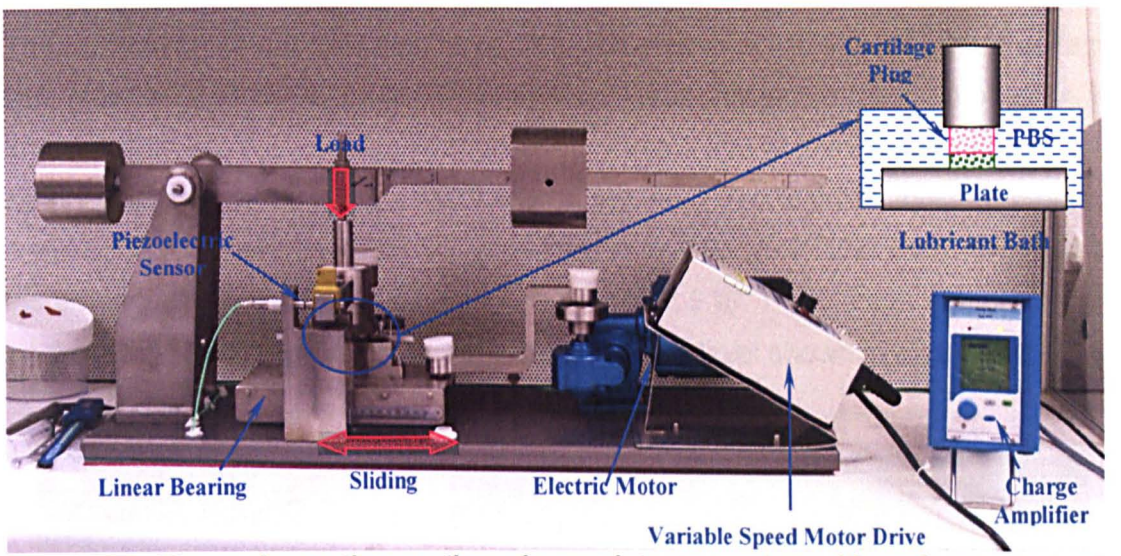

Figure 2.8. The reciprocating motion pin-on-plate apparatus with main components labeled

The friction apparatus was designed to accurately measure the cartilage friction at a range of loads from 5N to 230N during long-term *in-vitro* friction studies (Katta, 2007; Northwood, 2007). The cartilage pin was held in a pin holder which slides through a bearing in the load bearing arm that allows free movement in the vertical axis. The load was applied along the loading arm and masses placed at calibrated positions to produce different loads applied to the cartilage pin. The loading bearing arm was pivoted on one end and the opposing end was free to move over a piezoelectric sensor (Kistler Type 9207). Cobalt chrome plates were fixed inside a bath mounted on a linear bearing, and the sliding speed and stroke length was controlled by a motor (Model: 240505, CJ Controls Ltd, UK). During friction tests, a constant load was applied to the cartilage pin and the motor drove the CoCr plate to provide a linear reciprocal motion. The friction force between the articular cartilage pin and CoCr plate was transmitted through the pin holder to the load bearing arm, and detected by the piezoelectric force sensor. The voltage

generated by the piezoelectric force sensor was transferred through a charge amplifier (Kistler Type 5015) and logged using software and a data acquisition system.

2.2.2.1.1 Calibration

A calibration curve was used to calculate friction coefficient in experiments. Calibration of the friction apparatus was needed to ensure correct conversion of the piezoelectric force sensor output to friction force. This was completed every 4~5 weeks and reduced errors that may have occurred due to sensor drift over time. The calculation of the frictional force from the piezoelectric sensor output voltage was measured as a response to incremental loads applied to the pin holder at its lower end, where the articulating counterfaces came into contact (Figure 2.9.a). The weights were attached using a silk thread suspended over a pulley system. Weights were added in increments of 50 gms from 0 to 650 gms, and then removed in increments of 50 gms from 650 gms to 0 (Figure 2.9.b). The voltage output reading on the computer screen was recorded for each load level shown in Figure 2.9.c.

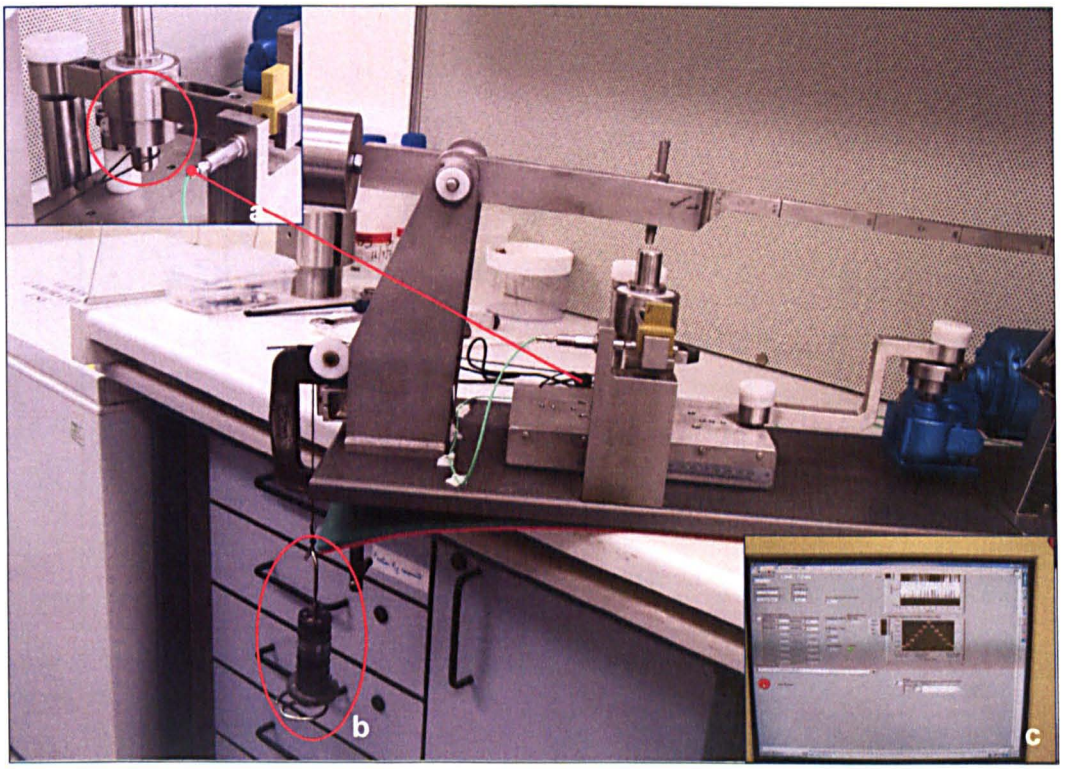

Figure 2.9. Calibration of the pin-on-plate friction apparatus, a. the silk thread was attached the lower end of the pin holder; b. the load was applied; c. the PC recorded the result.

The coefficient of friction between the two articulating surfaces was calculated from equation 2-6 below.

$$F_r = \mu \times F_n$$ **Equation 2-6**

Where, F_r is the calculated frictional force, μ is the coefficient of friction, and F_n is the normal force or the load applied on the pin.

A typical calibration result is shown in Figure 2.10.

The calibration result is show as Equation 2-7. 2-8, and 2-9:

$$F_r = W \times 9.8$$ **Equation 2-7**

$$V = 0.1092 \times F_r + 0.00008$$ **Equation 2-8**

$$F_r = \frac{V - 0.00008}{0.1092} + 0.0065$$ **Equation 2-9**

Where, *W* is the mass weight placed at the calibrated position (kg), *V* is the voltage examined by the amplifier, 0.0065 is the linear bearing modulus.

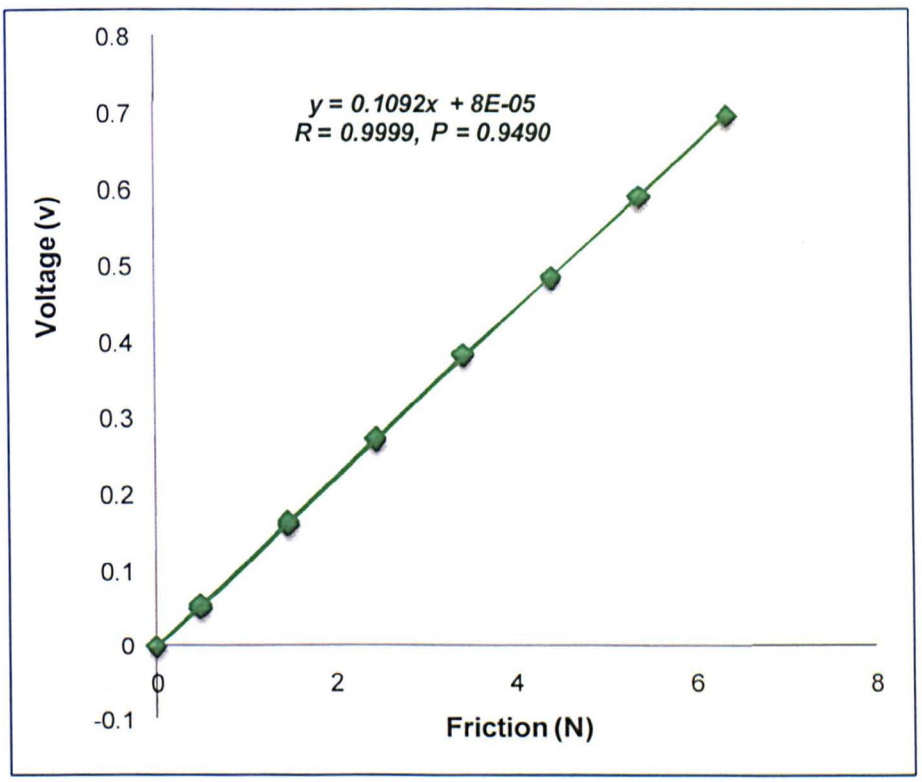

Figure 2.10 A typical example of a calibration factor for the pin-on-plate friction apparatus

2.2.2.1.2 Calculation of Friction Coefficient

To calculate the coefficient of friction (μ_{eff}) and frictional shear stress (SS), Equations 2-10 and 2-11 were used (where *r* is the radius of the cartilage pin).

$$\mu_{eff} = \frac{F_r}{L}$$ **Equation 2-10**

$$SS = \mu_{eff} \times P = \mu_{eff} \times \frac{L}{\pi \times r^2}$$ **Equation 2-11**

Where, F is the friction (N), L is the Load (N), P is the contact pressure (MPa), which average value is equal to the Load divided by the contact area (mm^2) at constant loading condition.

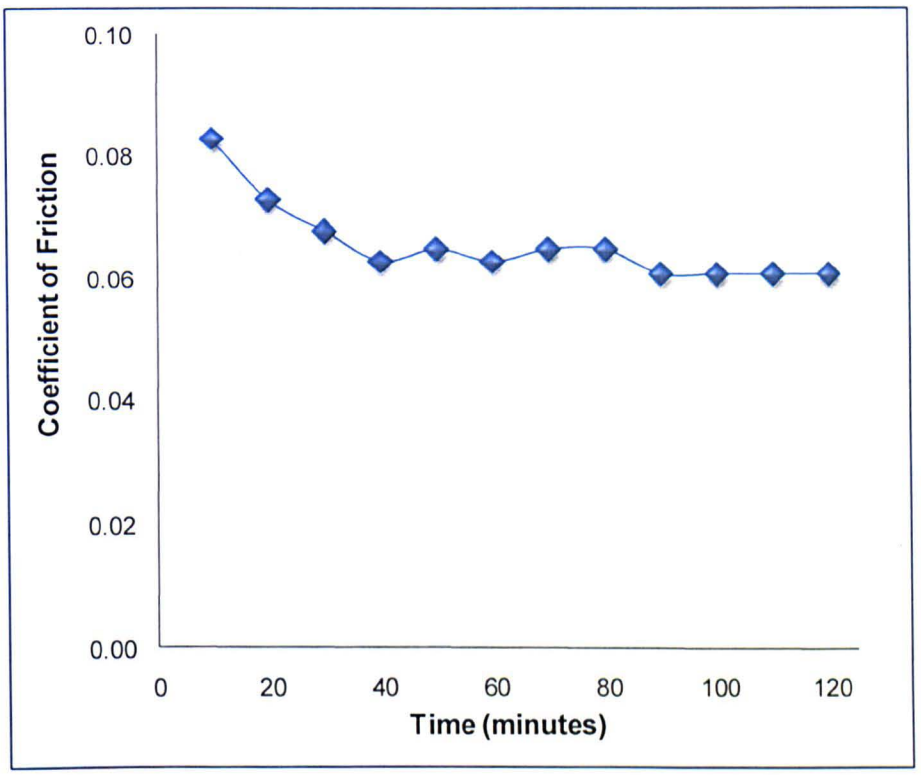

Figure 2.11 One sample of the coefficient of friction of a polyethylene pin on stainless steel plate in PBS lubricant during 2 hours with a constant load of 25N.

2.2.2.1.3 Standard Test Friction Result

The friction coefficient of a polyethylene pin against stainless steel plate in PBS lubricant in 2 hours is shown in Figure 2.11. This result of average coefficient of friction was found to be similar, within a 2% error from 30 minutes to 120 minutes from the previous studies (Forster and Fisher, 1996; Katta, 2007; Northwood, 2007).

2.2.2.1.4 Repeatability

Three different material combination groups of tests (n=6 per group) were tested to determine the repeatability of the coefficient of friction data generated. These tests were performed for 60 minutes with a constant load of 25N. The

material combinations were bovine cartilage pin on bovine cartilage plate; cobalt chrome pin on bovine cartilage plate; and bovine cartilage pin on cobalt chrome plate. All tests were performed in PBS lubricant, and the results are shown in Figure 2.12.

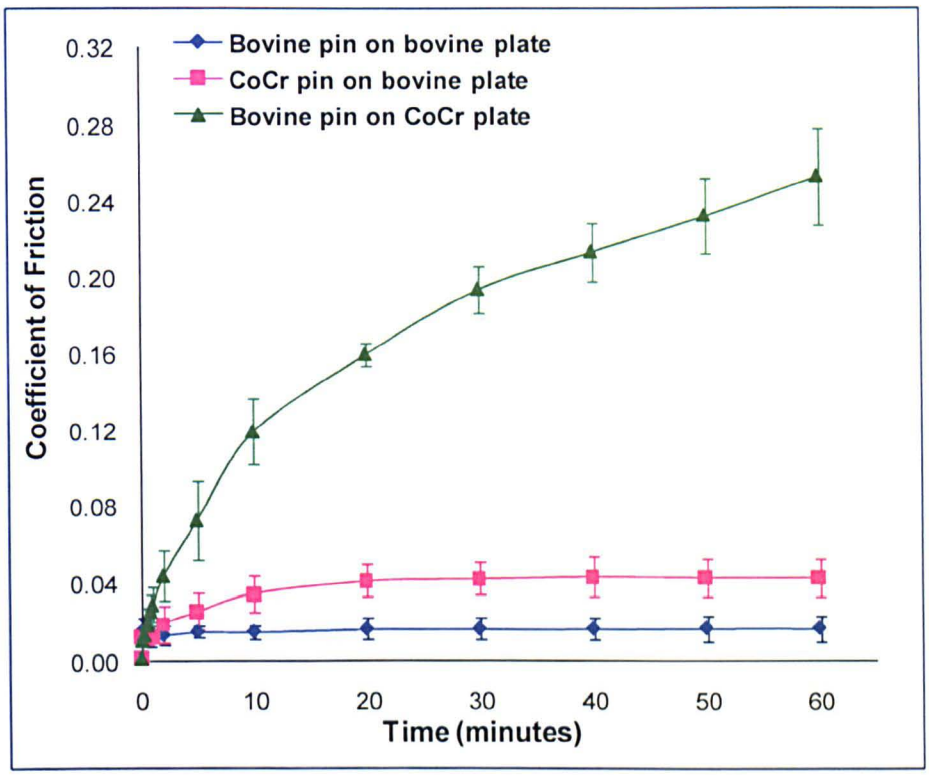

Figure 2.12 Friction coefficient of 25N constant loading in PBS for 60 minutes for different material combinations, stroke length 4mm, sliding velocity 4mm/sec (n=6 Mean±95% confidence limits)

The results are shown that the coefficient of friction kept increasing during the 60 minutes low constant loading in the group with bovine cartilage pin on cobalt chrome plate due to the supporting phase of cartilage pin was been transferring from a fluid phase into solid and fluid phase in equilibrium. However, the coefficient of friction increased only in the first 20 minutes loading then remained constant in both bovine cartilage pin on bovine cartilage plate group and cobalt chrome pin on cartilage plate group. This was due to the rehydration of the cartilage bovine plate when the pin reciprocated on it. Reciprocating on the bovine cartilage plate, the counterfaces of bovine cartilage pin created significantly lower coefficient of friction compared to cobalt chrome pin. This was due to the fluid phase of cartilage played an important role supporting the load between the articular cartilage on cartilage counterfaces. Significant difference of the coefficient of friction after 5 minutes loading is shown in the three groups: the coefficient of friction between bovine articular cartilage and bovine articular cartilage was significantly lower compared to

the coefficient of friction between metal (cobalt chrome) and bovine articular cartilage counterfaces (n=6, ANOVA, $p<0.05$). $\mu_{eff-BC-BC} < \mu_{eff-CoCr-BC} < \mu_{eff-BC-CoCr}$ (BC: bovine cartilage, CoCr: cobalt chrome)

2.2.2.2 Cartilage Thickness Measurement - Nikon Profile Projector

The cartilage thickness of the pins was measured by a Nikon profile projector (Nikon V-16 D, resolution 1 μm) at 10 times magnification (Figure 2.13.a). An average of six measurements from the cartilage superficial surface to the tide mark at the central point of the cartilage pin was taken as the cartilage thickness (T) shown in Figure 2.13.b.

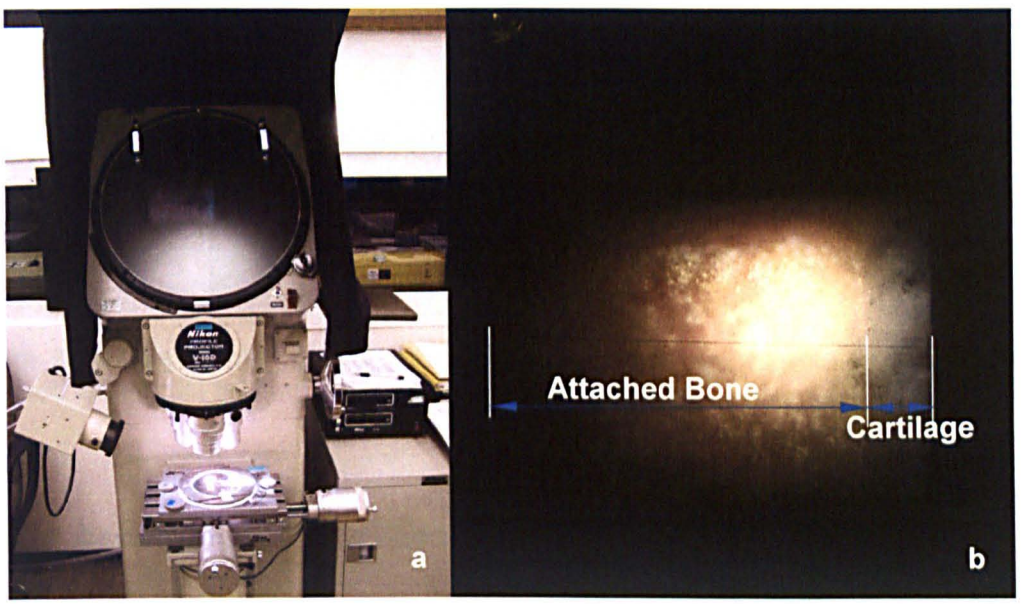

Figure 2.13. a. Nikon profile projector, b. the 10 times imagine of cartilage pin

2.2.2.3 Cartilage Deformation Measurement - Digital Height Gauge

The cartilage deformation was not able to be measured precisely by the Nikon profile projector after the loading or friction test due to the deformation of the cartilage and the spread of the edge of the cartilage under high contact stresses affected the image of the cartilage thickness. Hence the cartilage thickness changes were calculated through a indirect method – by measuring and calculating the cartilage pin height change. It was assumed that the attached bone height had no change during the loading or friction tests. The pin height was measured by the central point on the cartilage pin surface before and immediately after removing the

test load (in air, to avoid dehydration of the cartilage affecting the result) using a digital height gauge (TRIMOS height vernier scale, resolution; 1μm) with an attached dial test indicator (DTI, resolution: 10μm, Figure 2.14) which had a spring loaded arm. Due to the cartilage thickness difference of each individual cartilage pin specimen, the wear and deformation measurements were presented as the percentage of the articular cartilage thickness changes.

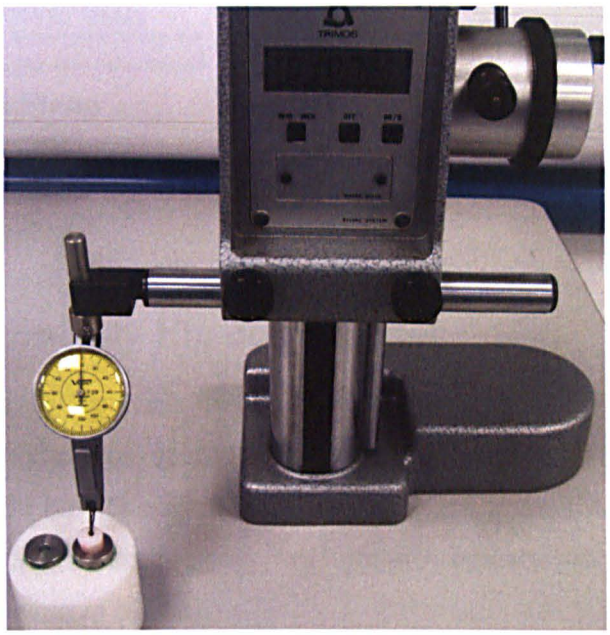

Figure 2.14. The height measurement of cartilage pin used a digital height gauge attached with a dial test indicator

2.2.2.4 Assessment of Pin Deformation with Loading Only

The six-station pin-on-plate rig (Figure 2.15) was used for the study of cartilage deformation with short-term and long-term loading with no motion. This six station pin-on-plate rig (Figure 2.15) was similar to the single station pin-on-plate friction apparatus in terms of how pins were loaded and enabled concurrent testing of six samples. Cartilage pins were immersed in PBS baths against cobalt chrome plate in each station. The required load was applied via the loading arm onto the cartilage pin in each station. The application of loads to each station was staggered by 10 minutes to allow the deformation measurements to be performed at the precise time intervals. Pins were loaded for the required time period and height was measured as described in Section 2.2.3.3.

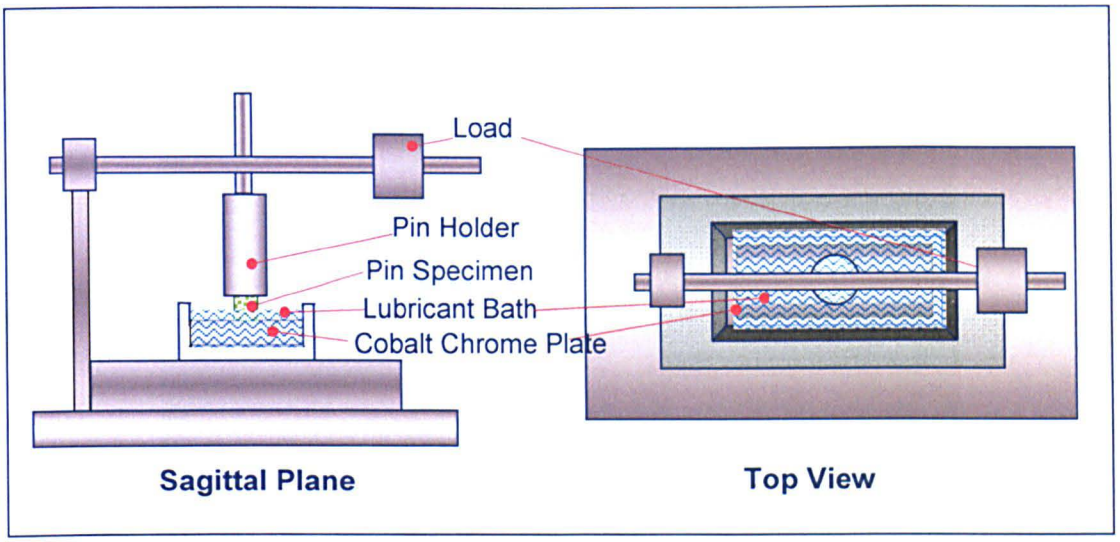

Figure 2.15. One station of the six-station pin on plate friction simulator

2.3 Hemiarthroplasty Hip Joint Model

Hemiarthroplasty hip joint friction and surface deformation studies used a pendulum friction simulator at the University of Leeds. (Brockett, 2007). The methods for artificial hip (Brockett, 2007) and nature knee (McCann, 2009) were adapted as part of this thesis to study the hemiarthroplasty hip model. This section describes samples used in testing.

2.3.1 General Materials

2.3.1.1 Standard Materials - Ceramic Components

Standard tests used artificial control components – ceramic head and cup 28mm diameter (Figure 2.16) to verify the operation of the pendulum friction simulator working conditions, ensure the correct calibration of the machine, and to compare operation to previous published work (Brockett, 2007).

Prior to testing the ceramic components were measured by two-dimensional profilometer (Form Talysurf, Taylor Hobson, Leicester, UK), and had a surface roughness (R_a) of 0.02±0.002μm. The radial clearance of the standard components was approximate 0.03mm.

$$R_{a-ceramic} = 0.02 \pm 0.002 \mu m$$

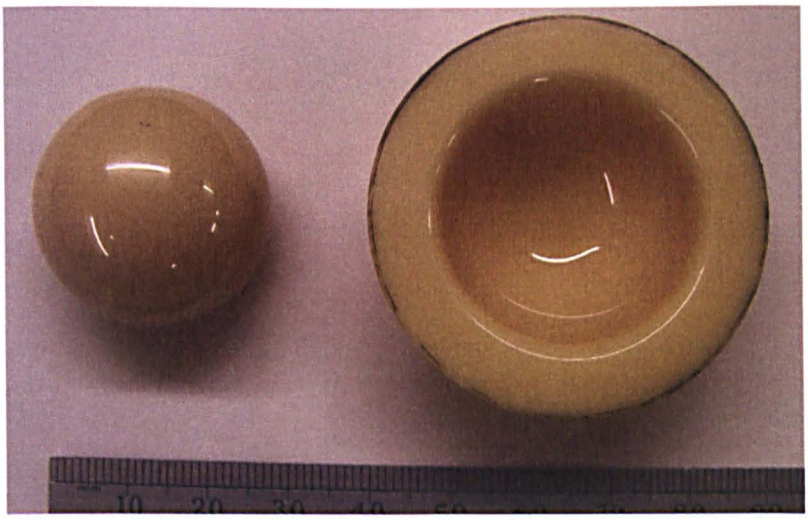

Figure 2.16. 28 mm diameter ceramic head and ceramic cup with a radial clearance of 0.03mm

2.3.1.2 Study Materials - Cobalt Chromium and Ceramic Heads

Different sizes of Cobalt Chromium heads (32, 34, 35, 36, 37mm in diameter, supplied by DePuy International Ltd., Leeds, UK, Figure 2.17) were used in this study. The different diameters enabled different clearances (small, medium, large, and extra large) to be provided as required, this was necessary due to the limited size range of available porcine acetabula. The surface roughness was measured before starting the pendulum friction tests using a two-dimensional profilometer (Form Talysurf, Taylor Hobson, Leicester, UK). A Gaussian cut-off filter equal to 0.8mm was used for assessing the variety of surface form within this study. Prior to measurement it was ensured that the heads surfaces were free from contamination. The cobalt chrome heads had a surface roughness (R_a) 0.006±0.001μm.

Biolox Delta ceramic heads (36mm in diameter, supplied by DePuy International Ltd., Leeds, UK, Figure 2.18) were also used in testing. These were used to compare the effect of head materials (between metal cobalt chrome and ceramic) on the friction and wear in hemiarthroplasty studies. The ceramic heads have the highest degree of biocompatibility, excellent wettability and superior surface smoothness. The surface roughness was measured using a 0.8mm cut-off filter before starting the pendulum friction tests using a two-dimensional profilometer (Form Talysurf, Taylor Hobson, Leicester, UK). Prior to measurement it was ensured that the head surfaces were free from contamination. The ceramic heads had a surface roughness (R_a) 0.004 ±0.001μm.

$$R_{a-BioloxDelta-ceramic} = 0.004 \pm 0.001 \mu m$$

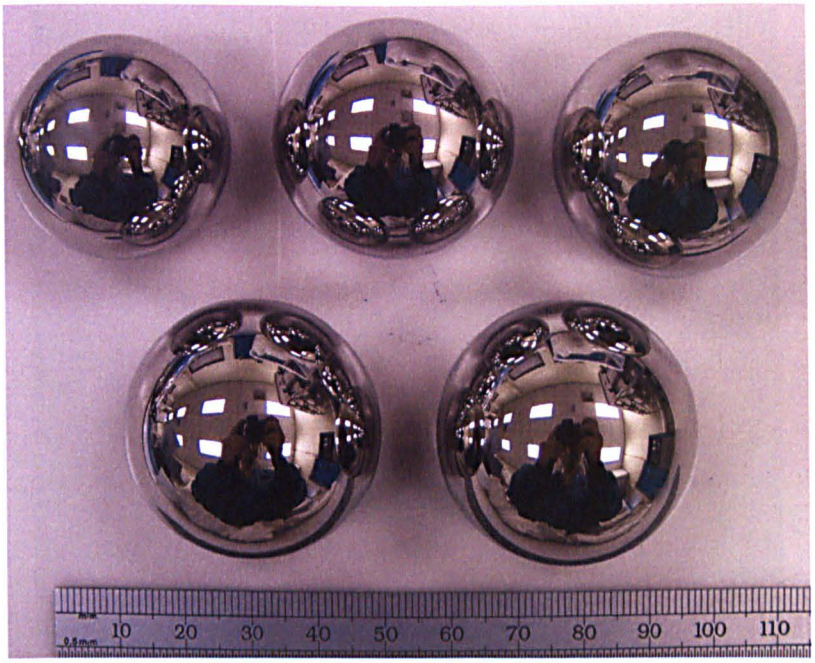

Figure 2.17. Cobalt chromium heads size 32, 34, 35, 36, and 37mm diameter

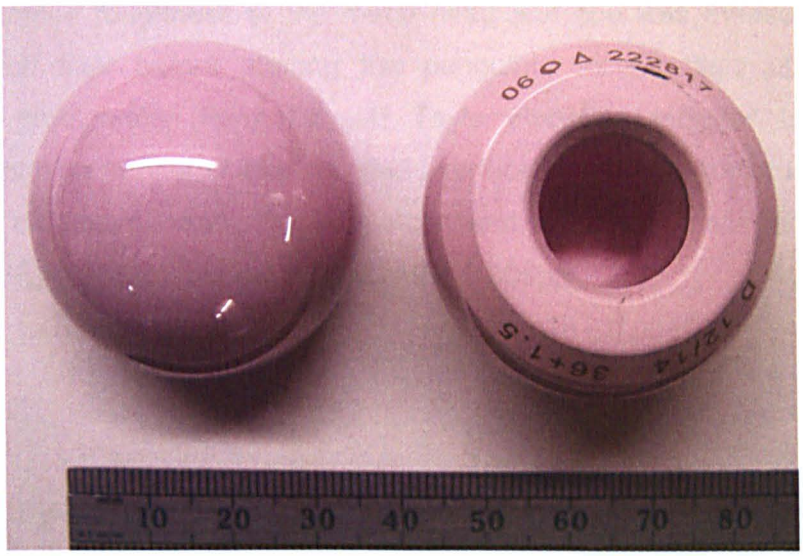

Figure 2.18. Ceramic heads size 36mm diameter

2.3.1.3 Study Materials - Bipolar Cobalt Chrome Components

The bipolar prosthesis is a two-component hemiarthroplasty, which consists of a femoral spherical head and a metallic cup. It produces two bearing surfaces, the inner bearing interface between the metallic head and the metallic insert (cup), and the outer bearing interface between the insert and the cartilage acetabulum. The bipolar components used in the hemiarthroplasty studies were a cobalt chrome head (28mm in diameter) and a cobalt chrome shell (inner surface 28mm and outer surface 36mm in diameter), both were supplied by DePuy International Ltd., Leeds, UK (Figure 2.19).

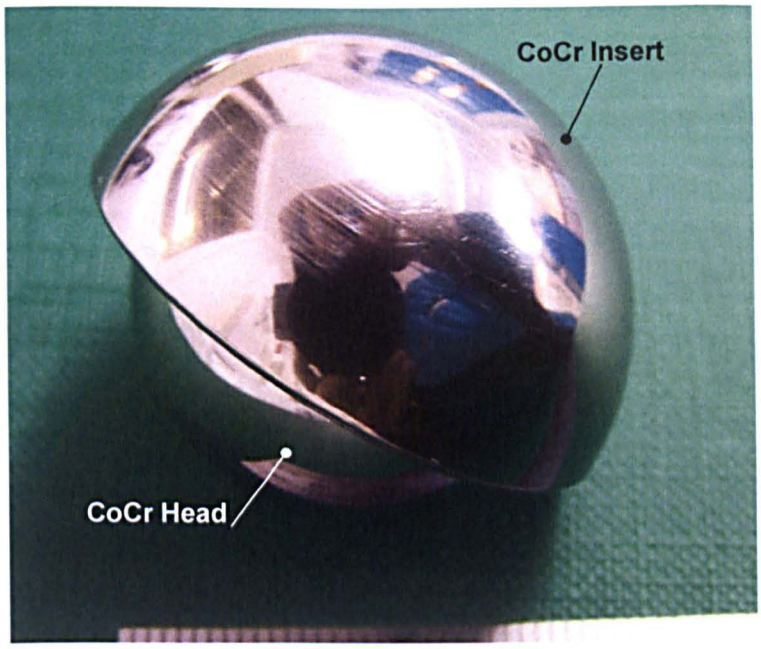

Figure 2.19 Cobalt chrome bipolar prosthesis includes a head and a cup

The surface roughness of the metal head and cup was measured using a 0.8mm cut-off filter before starting the pendulum friction tests using a two-dimensional profilometer (Form Talysurf, Taylor Hobson, Leicester, UK). Prior to measurement it was ensured that the heads surfaces were free from contamination. The cobalt chromium head, the cup inner and outer surfaces had a surface roughness (R_a) 0.008 ± 0.005μm, and 0.010 ± 0.005μm.

$$R_{a-CoCr\,cup-inner} = 0.008 \pm 0.005\,\mu m\,;\; R_{a-CoCr\,cup-outer} = 0.010 \pm 0.005\,\mu m$$

2.3.1.4 Study Materials - Porcine Acetabula

Porcine hip joints were collected from 6-month old porcine carcasses within 48~72 hours of commercial slaughter. Prior to dissection of the porcine legs, they were kept less than 24 hours in a cold storage area fully intact. Dissection began with the separation of the femoral head from the acetabulum with a scalpel. The following process was then used to prepare the acetabulum for testing:

The soft tissue behind the pelvis was removed, and dissected from the iliofemoral, ischiofemoral, and pubofemoral ligaments around the acetabulum. The synovial fluid oozed immediately when the hip joint socket was dissected. The round ligament which connects the acetabulum and the femoral head was dissected from the fovea area with care not to damage the lunate surface of the acetabular cartilage. When the acetabulum with attached pelvis was dissected from the porcine leg, the rest of the soft tissue (from the acetabulum) must be removed

for further dissection (Figure 2.20.a, b). The acetabulum and attached hip bone was protected using a piece of paper then the bone part was set into vice clips (Figure 2.20.c, d). The acetabulum was separated from the pelvis using a saw, front top, sides, and back as shown in Figure 2.20.e, f, g. Then the acetabulum was dissected.

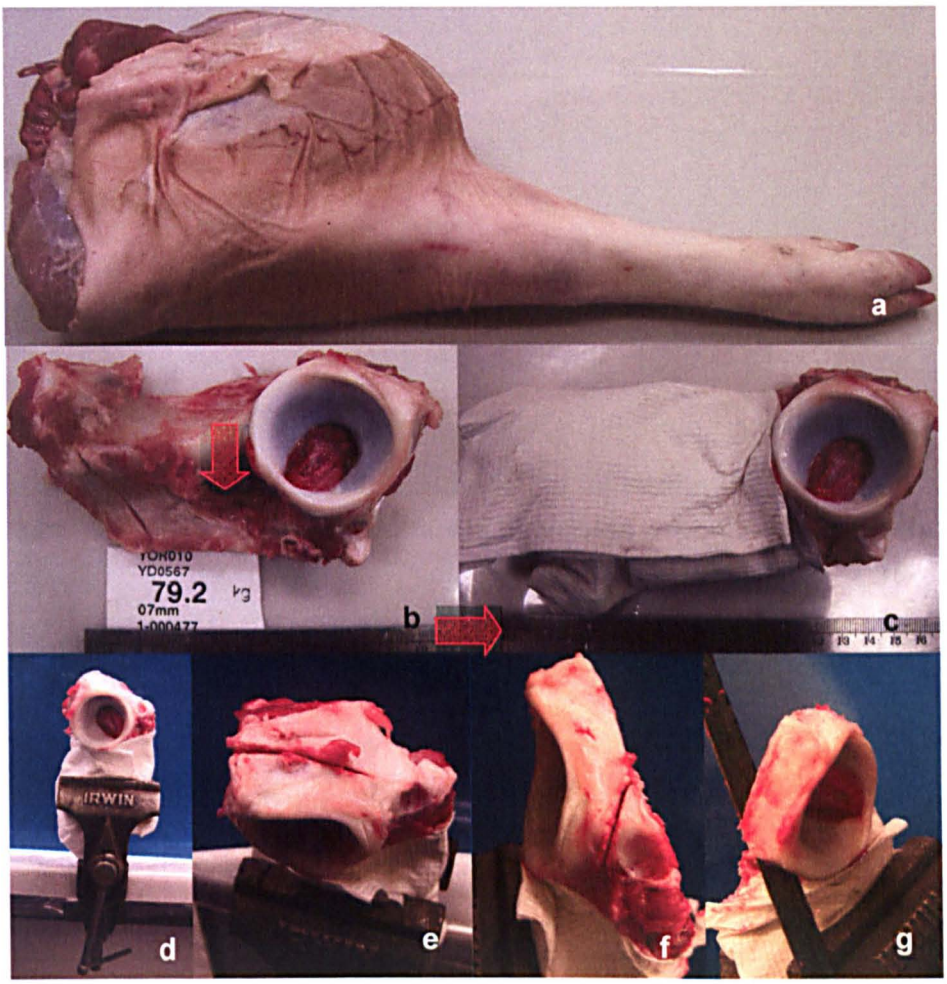

Figure 2.20. The process of harvesting porcine acetabulum: a. whole porcine left leg; b. soft tissue was removed from porcine acetabulum and attached hip bone; c. acetabulum and attached hip bone was protected with tissue paper; d. specimen was set into the vice clips tightly for further dissection; e. top cut; f. side cut; g. back cut.

The dimension of flexion-extension (FE) and medial-lateral (ML) directions of the acetabulum cup were measured by a vernier calliper (Figure 2.21). The acetabulum surface was covered by a piece of filter tissue wet in PBS, and kept into a small zip plastic bag with the dissection date, name, weight, FE and ML dimensions details labelled. The porcine acetabulum specimens were frozen (for up to 30 days) at -20°C until use.

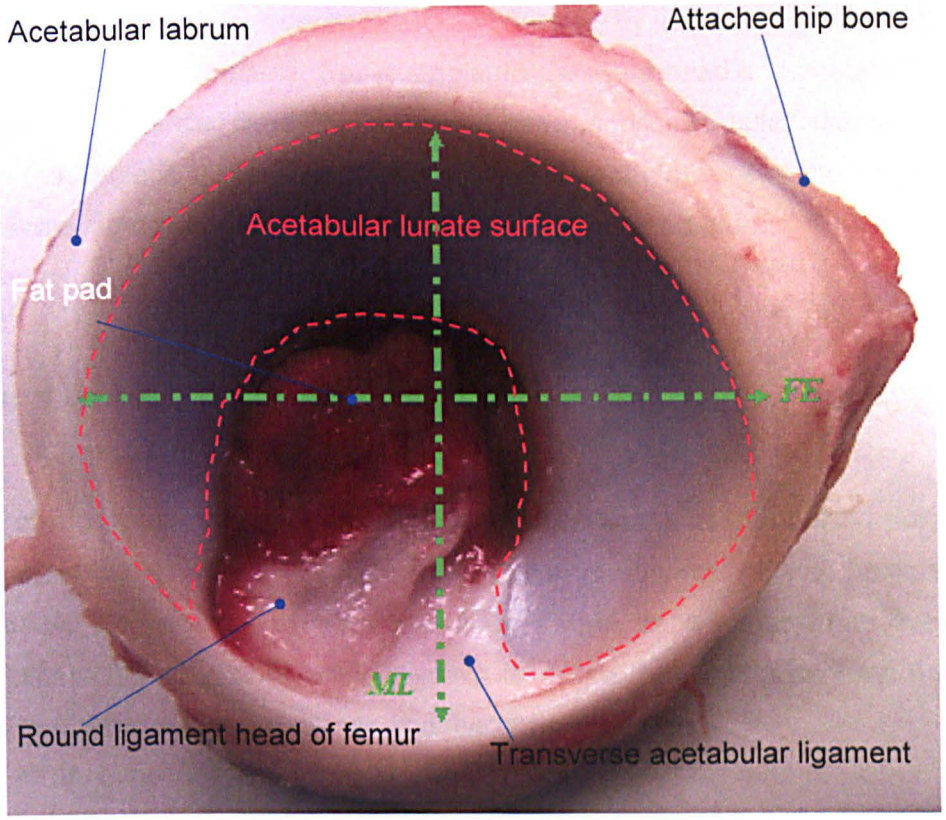

Figure 2.21. The measurement of FE and ML dimension of porcine acetabulum

2.3.1.5 Radial Clearance Definition

The radial clearances for the different groups were defined as shown in Table 2.2 in the flexion-extension direction.

Table 2.2 Radial clearance definition

Definition	Small	Medium	Large	Extra Large
Clearance x (mm)	x<0.6	0.6≤x<1.2	1.2≤x<1.8	1.8≤x

Table 2.3 Options of femoral head size and acetabulum FE dimension to create small clearance level

Options	Femoral Head Size (mm)	Acetabulum FE Dimension(mm)
Small-1	32	32.01-33.19
Small-2	34	34.01-34.19
Small-3	36	36.01-37.19
Small-4	37	37.01-38.19
Small-5	38	38.01-39.19

The same level of clearance was assessed by choosing different sizes of femoral heads and acetabula. For example, to assess a head and acetabular pair in the "small" clearance category, different head and acetabular diameters were chosen (as Table 2.3). However, most porcine acetabula were at the middle range of this scale, so options small-1 and small-2 were not used often.

2.3.1.6 Test Set-up Materials - Polymethylmethacrylate (PMMA) Bone Cement

Polymethylmethacrylate (PMMA) bone cement was used for fixing porcine hip joint acetabulum specimens in the Delrin (polyoxymethylene plastic) holders which located into the pendulum friction simulator. PMMA bone cement has been used very successfully to anchor artificial joints for more than half a century; it fills the free space between the prosthesis and the bone.

PMMA bone cement (W.H.W. Plastic, Southport, UK) was provided as two-component materials, which consisted of a powder and a liquid. The two components were mixed with a powder to liquid ratio of 2:1 by weight. The cement viscosity changed over time due to the exothermic reaction. When in a dough-like state it was workable before hardening into a solid material. The working time was around 8 minutes which allowed the porcine acetabulum specimen to be positioned as required.

2.3.1.7 Media Materials - Microset Silicon Polymer Compounds

Microset 101 silicon polymer compounds (Nuneaton, Warwickshire, UK) are formulated as mixtures of Siloxanes, organic and inorganic compounds. The product included a silicon gun, silicon refill, and a nozzle, and when assembled the gun pushed two tubes of black and grey viscous liquid to mix inside the nozzle. This was applied to surfaces to be moulded, and hardened to create a replica which had resolution of 0.1μm (Microset 101 silicon polymer compounds product introduction).

2.3.1.8 Lubricant - Bovine Serum Lubricant

Although PBS is highly convenient for tribological studies, it does not mimic fully the physiological conditions, hence bovine and porcine serums were considered to use in this study. Compared to PBS, bovine serum has low

haemoglobin, low endotoxin levels and excellent growth-simulating properties. Sterile filtered swine serum was considered due to the consistency with using porcine acetabula. It has similar components to bovine serum (Table 2.3). Bovine serum (from Harlan Bioproducts for Science, BT-9501-500) was chosen as the test lubricant because of it reduced cost and ease of procuring, its constituents are similar to swine serum as shown in Table 2.3.

Table 2.4. Datasheet Comparison of sterile filtered bovine serum and swine serum

Parameter	Newborn calf serum	Swine serum
Haemoglobin	<0.2mg/ml	<0.3mg/ml
Endotoxin	<6ng/ml	
Sterility	No microbial growth detected.	
Mycoplasma	None Detected.	
Filtration	0.1μm	
pH	6.8-8.1	6.5-8.0
Osmolality Osm/KgH_2O	274-362m	274-362m
Appearance	Clear, light straw to dark amber.	
Total Protein	45-80mg/ml	60-89mg/ml

For the pendulum friction study 25% (v/v) bovine serum (Table 2.4) in PBS was used as the lubricant because of the similar protein concentration (16~18 mg/ml) to the normal synovial fluid (around 20 mg/ml).

Table 2.5. Composition of Newborn Calf Serum

Name	Portion
pH	7.2
Osmolality	294 mOsm/kgH_2O
Hemoglobin	10.1 mg/dl
Total Protein	6.0 g/dl
Albumin	4.0 g/dl
α-globulin	0.9 g/dl
β-globulin	0.6 g/dl
γ-globulin	0.1 g/dl

2.3.2 General Methodologies

2.3.2.1 Pendulum Friction Simulator

A pendulum Friction Simulator (Simulation Solutions, Stockport, UK) was used in the hemiarthroplasty hip joint model friction testing. This is a single-station servo-hydraulic machine, controlled by personal computer via a graphic user interface (Figure 2.22). The pendulum friction simulator can apply a constant and dynamic loading cycle, similar to that experienced by the hip joint *in-vivo*.

The ProSim friction simulator mainly consists of seven parts: fixed frame, motion arm, femoral head, lubricant seat (acetabular cup located within), piezoelectric transducer, charge amplifier, and a computer as shown in the schematic in Figure 2.23.

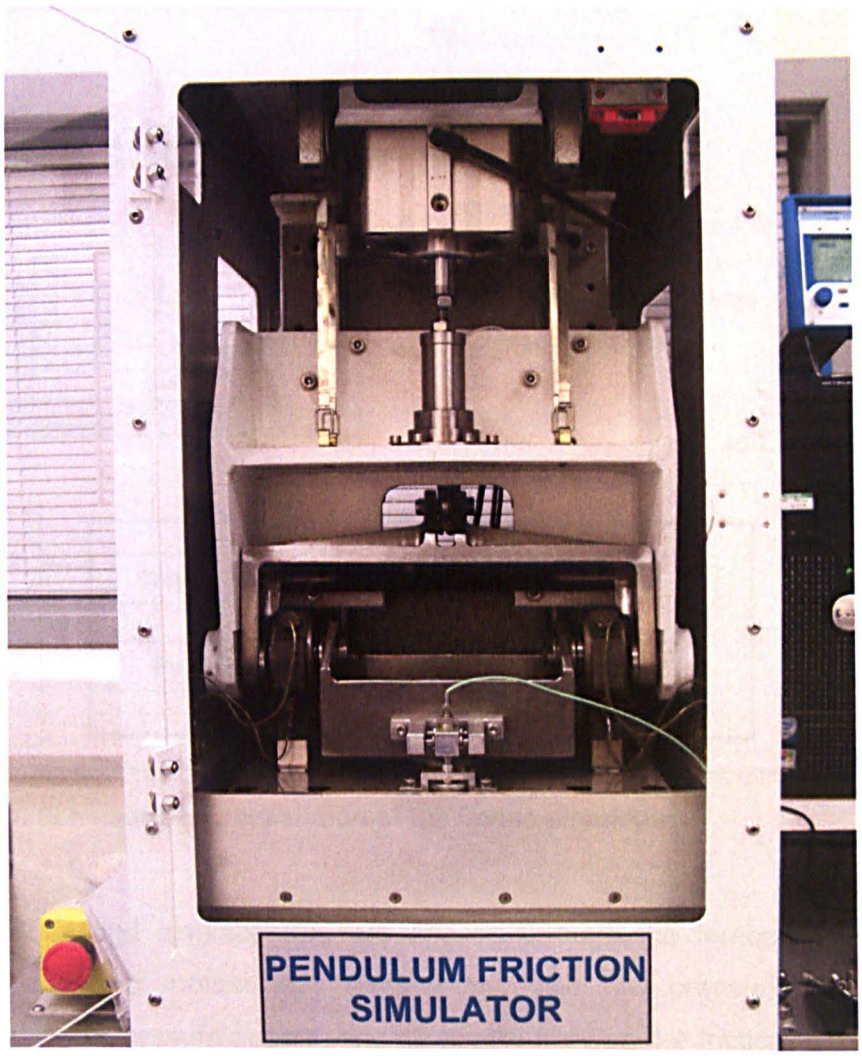

Figure 2.22. Pendulum Friction Simulator (Simulation Solutions, Stockport, UK)

The fixed frame consists of a friction measuring carriage, which sits on two externally pressurized hydrostatic bearings and a loading frame. The motion arm moves forward and backward with a maximum of ±30°, and the femoral head is attached to the loading frame via the motion arm. In the measuring carriage is the lubricant seat which holds the acetabular cup, this is mounted in the centre of the friction carriage. A piezoelectric transducer connected to the front of friction carriage and determines the frictional torque within the system, by measuring the forces transferred between the fixed frame and the carriage. The charge amplifier collects the signal from the piezoelectric transducer and transfers it to the computer. The computer records the data and calculates the friction torque and friction coefficient. Further to the definition in Section 2.3.2.1.1 is given in the load and motion.

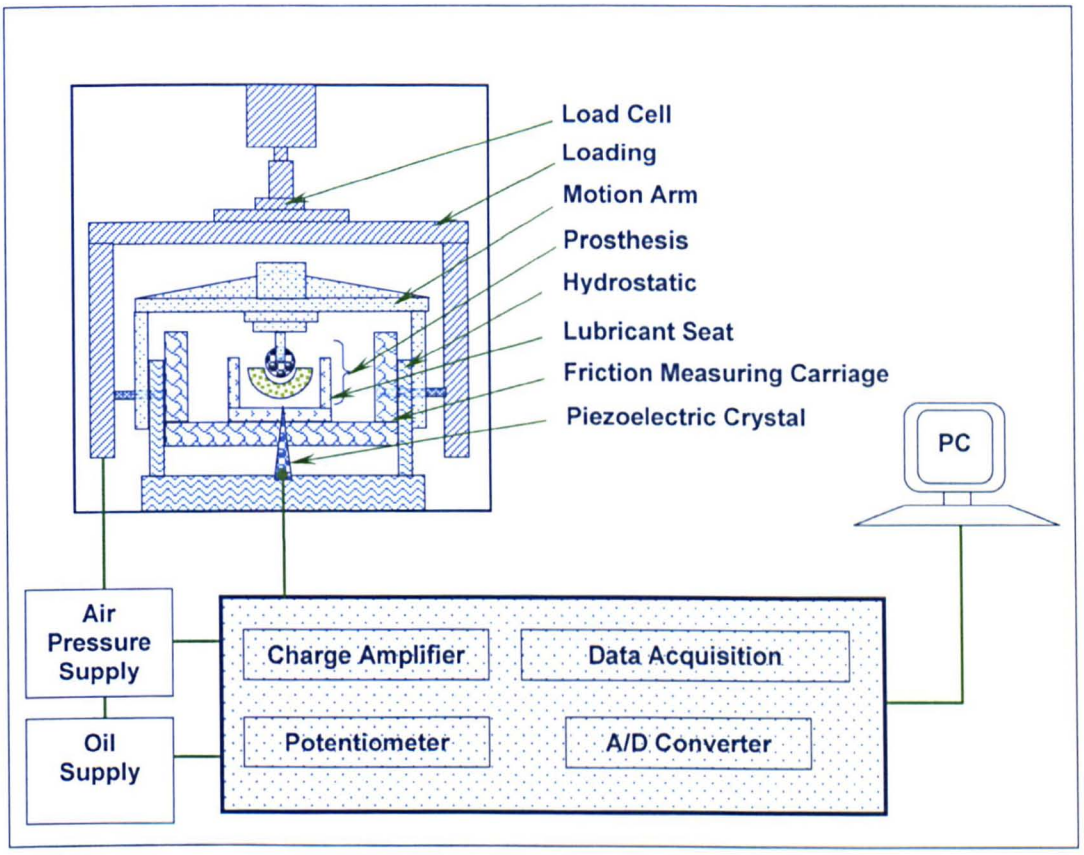

Figure 2.23. Schematic representation of the fiction simulator

The load and displacement are applied through the femoral head via the loading frame and motion arm respectively. The two pressurised hydrostatic bearings, the air pressure supply, and oil supply allowed the friction in the carriage to be considered negligible (as it is two orders of magnitude smaller than the friction in the implant), hence all measured frictional torque can be assumed to be between the bearing surfaces of the biomaterial head and the porcine acetabular cartilage.

The friction measuring carriage transfers all the friction movement and this is captured by the piezoelectric crystal and transmitted to the charge meter. The data processing system (A/D converter, potentiometer, charge amplifier and data acquisition software) analysed and processed the data and a computer displayed the output.

2.3.2.1.1 Friction Factor of Constant and Dynamic Loading

Both hemiarthroplasty hip joint constant and dynamic loading studies were performed with a FE displacement applied via the motion arm of the loading frame. Tests were conducted with FE angles ±15°, at a frequency of 1 Hz in 2 hours.

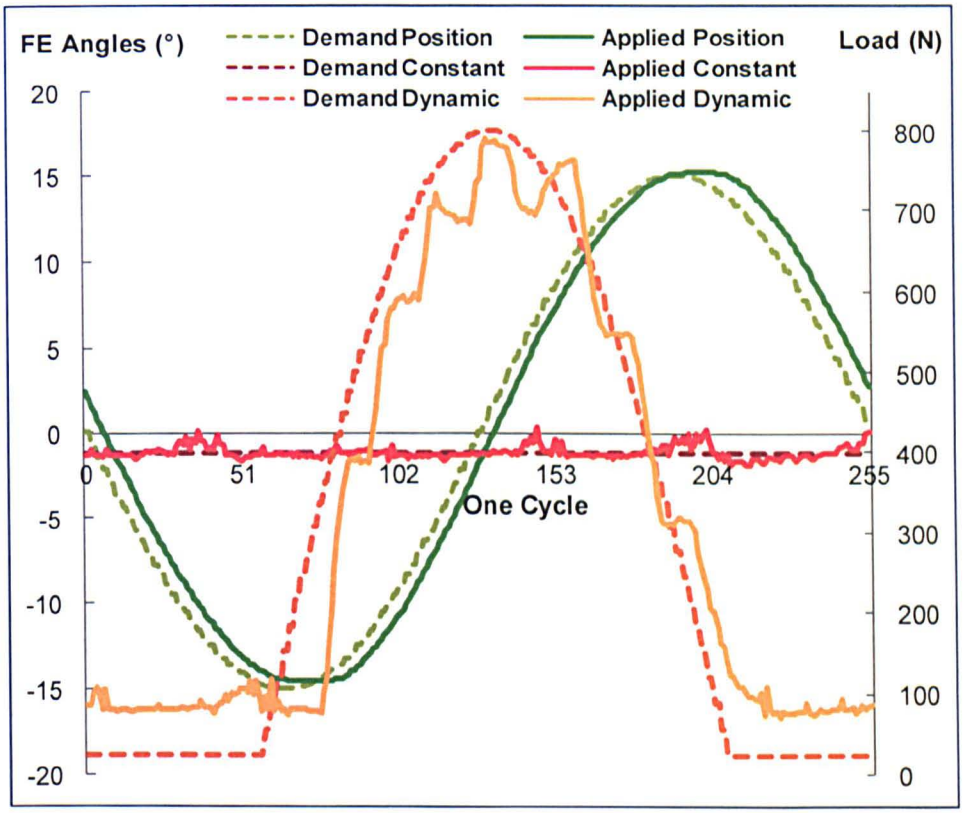

Figure 2.24 A example loading and motion profile of 400N constant load and 800N peak load dynamic load, dashed lines are the demand position and load, and the lines are real applied position and load.

The average 6-month old porcine weight is approximately 80 kg, and on average each leg supports 20 kg when pig is standing. Pig is an ungulate (hooved animals) and it walks with the weight of the body borne on the tips of the digits (unguligrade locomotion). During walking the pig's body weight is supported by two pairs of legs in turn (front left with rear right, and front right with rear left) as the diagonal gait. Hence the lowest average load on each leg that contacts the ground

is half of the pig's body weight (40kg). The highest load applied on the pig's leg can be approximate to its whole body weight (80kg) i.e. when there is only one leg is contacting the ground. In this study, half the body weight approximate 400N was chosen as constant load, and the whole body weight approximate 800N was chosen as the dynamic peak load.

Two types of loading cycle were applied via a hydraulic pressure system through the loading frame; 400N constant loading, and 75~800N dynamic loading. An example loading profile of constant and dynamic loading cycle is shown in Figure 2.24.

The friction factor was calculated by:

$$f = \frac{T_t}{R_h \times L} \qquad \textbf{Equation 2-12}$$

Where, f is the friction factor, T_t is the true friction torque, R_h is the head radius (m), and L is the load (N).

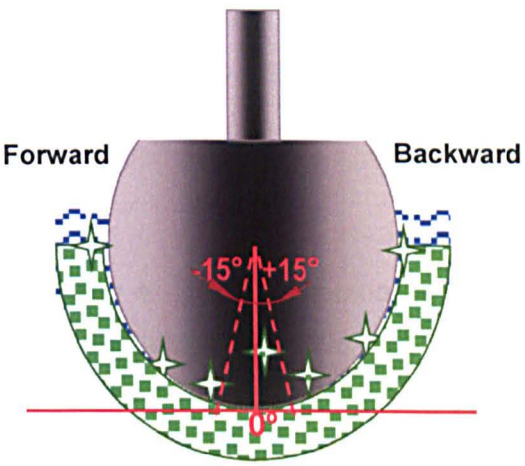

Figure 2.25. The sagittal plane of the femoral head on the articular acetabulum at 0 degree position, the friction factor was calculated at 0 degree position under constant loading.

The true friction torque was measured by the piezoelectric crystal and transmitted to the charge meter (described in Section 2.3.2.1).

Constant Load Tests

The friction factor was analysed at the 0 degree position where the head was vertically loaded and in contact with the lowest position of the cup as shown in Figure 2.25. The friction factor was calculated using Equation 2-12.

The constant load and motion profiles used in the studies were to investigate the friction factor calculation methods in hemiarthroplasty (material head and

acetabular cartilage) condition. The off-set and transducer drift was considered in the 2 hours pendulum friction test.

In the constant loading studies, the friction factor when the motion position was at 0° was used to calculate the true friction factor (Equation 2-13). The friction factor under constant loading was given by:

$$f_c = \frac{\left| f_{0,p1} - f_{0,p2} \right|}{2} \qquad \textbf{Equation 2-13}$$

Where, f_c is the friction factor at constant loading cycle, $f_{0,p1}$ is the friction factor at the first 0° motion position, and $f_{0,p2}$ is the friction factor at the second 0° motion position in one loading cycle. Both $f_{0,p1}$ and $f_{0,p2}$ were calculated followed Equation 2-12.

The friction factor deviation included both off-set and transducer drift, and it was given by Equation 2-14:

$$f_{de} = \frac{f_{0,p1} + f_{0,p2}}{2} \qquad \textbf{Equation 2-14}$$

Where, f_{de} is the friction factor deviation. Both $f_{0,p1}$ and $f_{0,p2}$ were calculated followed Equation 2-12.

Dynamic Load Tests

The dynamic loading was a simple sinusoidal waveform, which was applied through 60% of each cycle, to provide a dynamic load with a peak load of 800N and a swing phase load of 75N. The dynamic loading and motion profiles used in this study were simplified with respect to the standard gait cycle. Each test was run in a forward direction for 2 hours to examine the effect of clearance on cartilage friction and wear. The dynamic loading tests were run in a forward direction with 800N constant loading for 2 minutes before and after the 2 hours dynamic loading to eliminate any effect that may occur due to the loading offset and transducer drift by time.

In the dynamic loading studies, the friction factor when the motion position was at the second 0° was used to calculate the true friction factor (Figure 2.25). As the test was run for 2 hours, the off-set and transducer drift needed to be considered and given by the average value of the friction factor off-set and transducer drift of the 2 minutes 800N constant loading friction test (Equation 2-15). The friction factor under dynamic loading was given by:

$$f_d = f_p - \frac{f_{de,-2m} + f_{de,+2m}}{2} \qquad \textbf{Equation 2-15}$$

Where, f_d is the friction factor at dynamic loading cycle, f_p is the friction factor at peak load 800N, $f_{de,-2m}$ is the friction factor deviation of 2 minutes 800N constant loading test before the 2 hours dynamic loading, and $f_{de,+2m}$ is the friction factor of 2 minutes 800N constant loading test after the 2 hours dynamic loading. Both $f_{de,-2m}$ and $f_{de,+2m}$ were calculated following Equation 2-12.

2.3.2.1.2 Bipolar Prosthesis

Bipolar prosthesis remains in native the acetabulum, and allows for two articular sites which reduce stress to native acetabulum. The critical analysis of the friction factor at two bearing surfaces of bipolar prosthesis was carried out, and detailed analysis is described in Section 6.3.1.

2.3.2.1.3 Calibration and Repeatability

The calibrations include load cell calibration and the friction torque calibration, and the measurements should be carried out on a monthly basis or before a new test set. The repeatability of friction measurements was monitored and the load cell was calibrated.

Load cell calibration

The load transmitted through a standard head-cup bearing arrangement (ceramic-on-ceramic, Figure 2.16) was measured by the load cell mounted in the loading frame. The load system was calibrated via the automatic load calibration option in the ProSim Friction Simulator Software, which enables calibration constants to be calculated. During the calibration, the air pressure valve in the friction simulator was opened through five positions, from fully closed (zero) to fully open (250), causing the simulator to apply a pressure through the load cell. A test load cell was used to record the actual force measured five times, and this value entered into the calibration program, value 1 to 5 was manually entered as 20, 30, 40,... 100, and the other blanks were calculated automatically. The calibration constant calculated by the program would be used in the test system to correct the demand load applied by the simulator, hence ensuring the load applied in the test was the load specified.

Friction Torque Calibration

The frictional torque measurement was calibrated using an automatic calibration option in the software. Calibrated test weights were applied to a loading arm which sat on the friction carriage of known length (as Figure 2.26). At each weight interval, the frictional torque was measured and entered into the software to calculate the calibration constant. The calibration method was performed with the weights applied at the front and rear of the machine, corresponding with the forward and reverse directions of the test. The calibration constant calculated for each orientation was compared to ensure they were sismilar in magnitude and the value was entered in the software to ensure correct measurement.

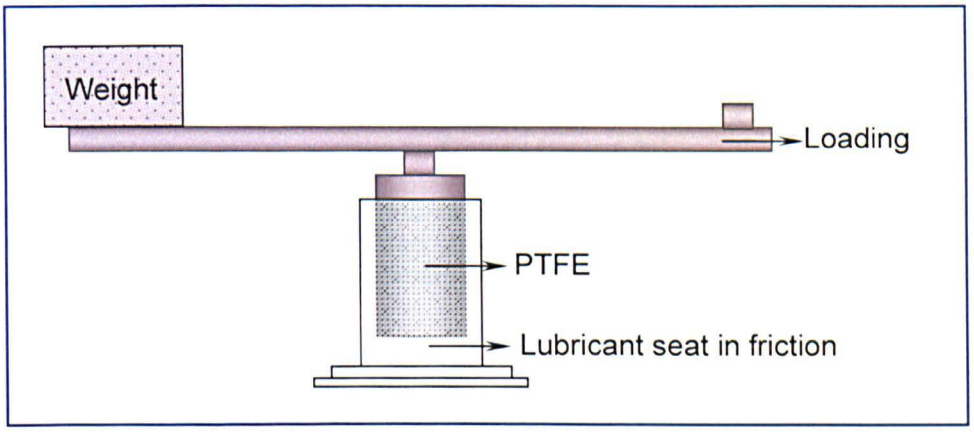

Figure 2.26 Schematic diagram of frictional torque calibration

Repeatability Check

The standard head-cup (ceramic on ceramic) bearing was used to determine the repeatability of the frictional factor data generated. The standard head-cup pendulum friction tests were performed in every 4~5 weeks, with the consideration of an acceptable error levels less than 0.025. The standard tests were performed for 300 cycles (300 seconds) with a constant load of 400N, and a dynamic load of 75~800N, ±15 degrees, a frequency of 1 Hz, in the lubricant of 25% (v/v) bovine serum. The typical results are shown as Figure 2.27.

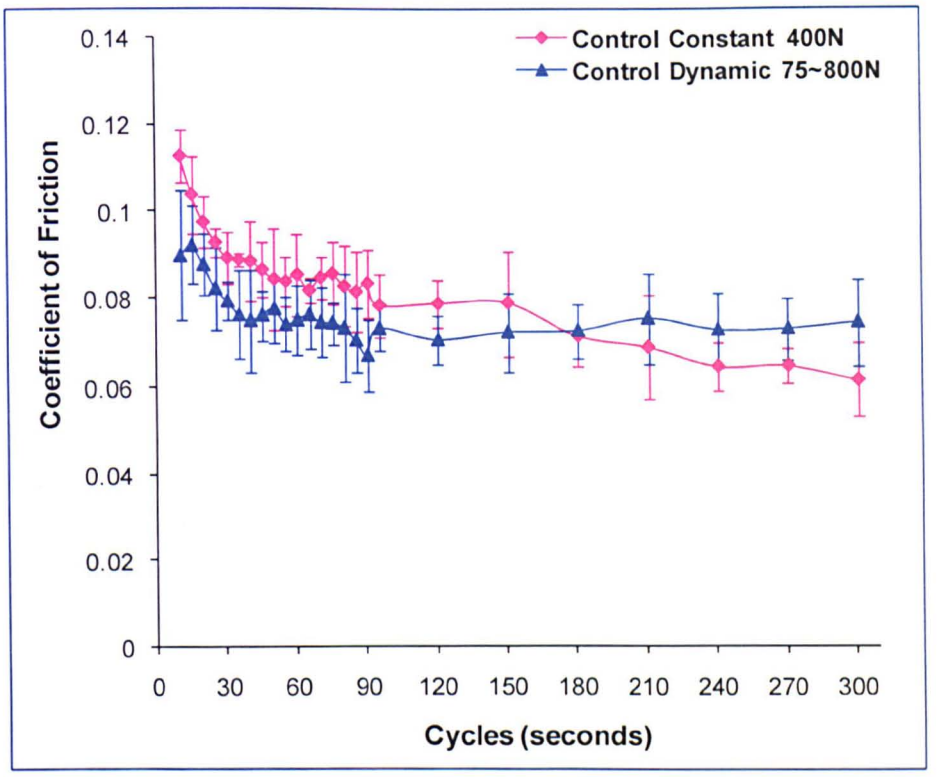

Figure 2.27 Friction coefficient of standard test (ceramic head against ceramic cup D=28mm) under 400N constant load and 25~800N dynamic load (±15°) over 300 cycles. Results are presented as mean (n=6) ± 95% confidence limits when the head loaded at 0°.

Porcine Acetabulum Specimen Setting Method

The cobalt chromium head and the porcine acetabulum cup needed to be set at the same centre for the friction test at a position that matched the centre of rotation in the pendulum friction simulator, and the dimension required are shown in Figure 2.28. The head and cup positions were set as in Table 2.6.

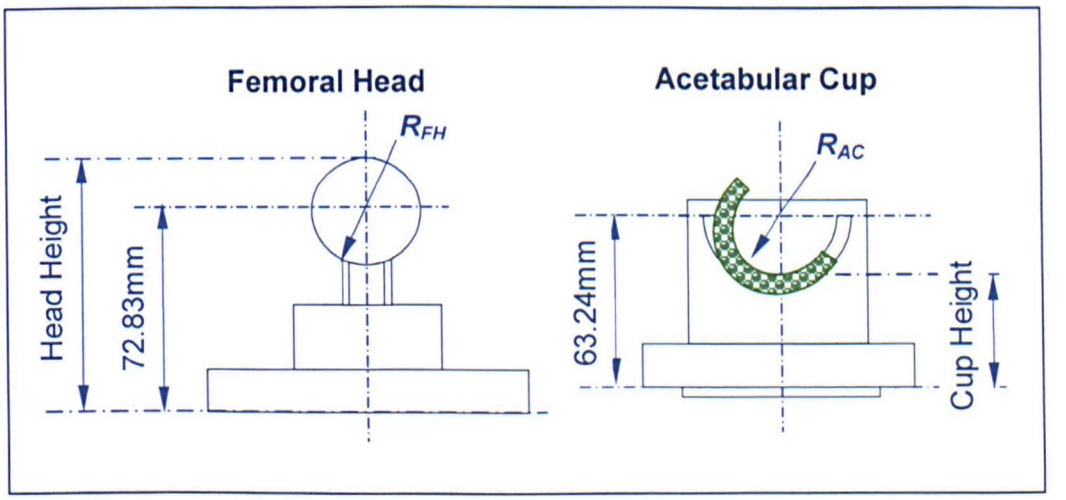

Figure 2.28. The setting requirement of the head and cup fixed in the pendulum friction simulator.

Table 2.6 Head and cup height dimension (mm) positions

Head Size	Head Height	Cup Height
32	88.83	49.74
35	90.33	48.24
36	90.83	47.74
37	91.33	47.24
38	91.83	46.74
Bipolar 28	86.83	47.74

The cobalt chromium head was set onto the top of the head base and its total height was measured by the digital height gauge and adjusted via a screw as required. The porcine acetabulum was set as an angle of 45 degrees in PMMA bone cements (Figure 2.29) used the device in Figure 2.28, design drawing details are shown in Appendix 1.

When the head and cup parts were prepared they were fixed into the pendulum friction simulator as Figure 2.29.a, the coronal plane is shown in Figure 2.29.b.

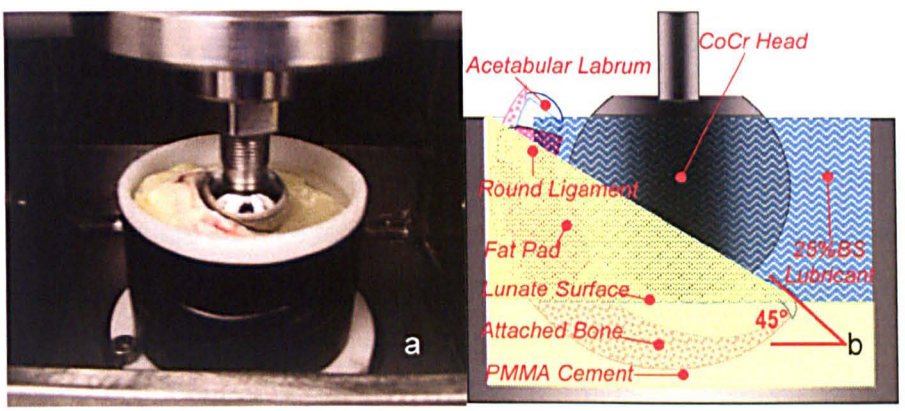

Figure 2.29. a. The cobalt chromium head and porcine acetabulum were fixed in the pendulum friction simulator, b. coronal plane of the porcine acetabulum set inside the Delrin holder.

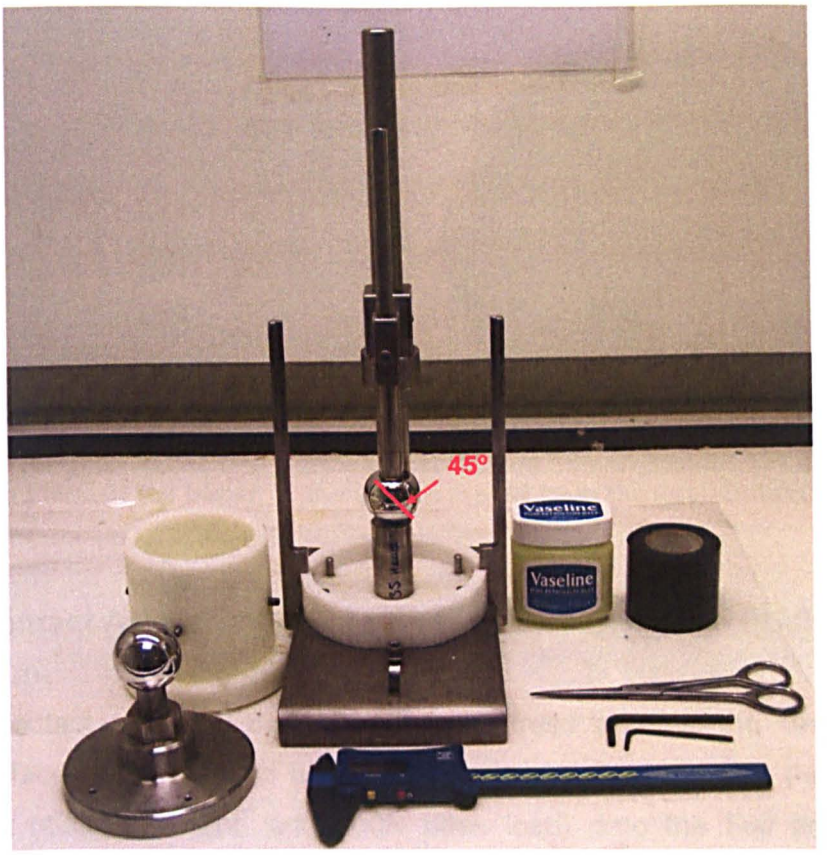

Figure 2.30. Device and tools for porcine acetabulum setting

2.3.2.2 Producing Moulds of Porcine Acetabulum

Porcine acetabulum silicon moulds were used to study the acetabular geometry cartilage wear and degradation after the friction test. The moulds replicated the cartilage surface texture and deviations of the porcine acetabula. The silicon moulds were taken of each porcine acetabulum immediately after the pendulum friction test. This was done using Microset 101 silicon polymer compounds (Nuneaton, Warwickshire, UK).

The porcine acetabulum was cleaned and dried with soft paper tissue, and the soft tissue (fat pad and round ligament) part was covered by a piece of aluminium foil (so only the cartilage lunate surface was moulded) (Figure 2.31.a). The acetabulum was filled with Microset slowly (to avoid creating any air bubbles) until it was filled to the edge of the acetabulum. The silicon mould was removed following setting (about 5 minutes) (Figure 2.31.b).

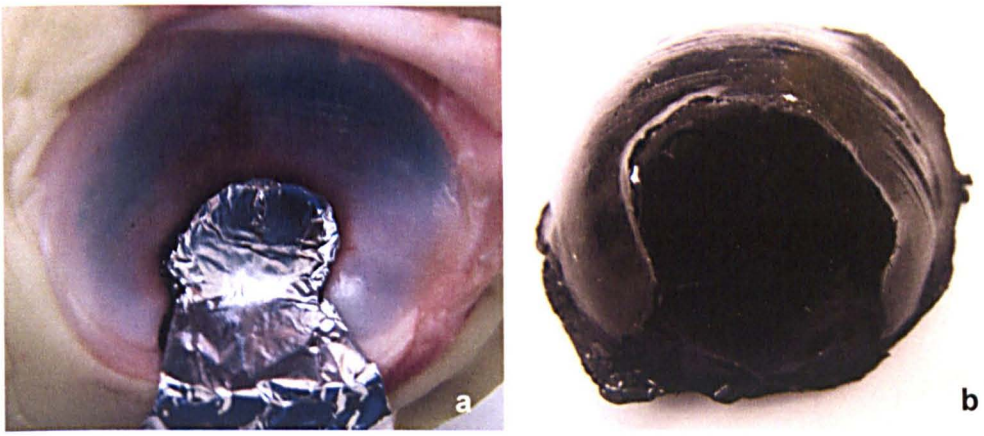

Figure 2.31. Process of making porcine acetabulum silicon mould: a. cover the soft tissue with a piece of foil paper, b. the silicon mould from the acetabulum.

2.3.2.3 Contact Area and Contact Stress Measurement – FUJI Pressure Film

The contact area and the peak contact stress between the head and cup bearing surfaces was recorded by applying the same load used for the pendulum friction test (400N constant, and 800N peak load) onto the Fuji pressure film (PressureX film, from Sensor Products LLC, USA) sealed with one sheet of cling film (to prevent wetting the Fuji film). When the metal head and porcine acetabular cartilage cup was set in the pendulum friction simulator, the Fuji film was put between the metal head and cartilage acetabulum cup contact surfaces and applied the required load for 30 seconds (a previous study showed that there is no difference in results using the FUJI film if between 30 seconds and 2 minutes loading was applied) (McCann, 2009). The Fuji film was placed into a Spectrodensitometer (X-Rite, UK, Figure 2.32.a), and a reading based on the density of colour (pink to red) on the film given (Figure 2.32.b). This was entered into the PointScan software (Sensor Products Inc., USA), and the contact pressure was calculated in megapascals. Before reading each measured Fuji film, the Spectrodensitymometer was calibrated by using a built-in automatic calibration option and measuring a standard white test patch.

The contact area at 0 ° position was measured through super-low pressure FUJI film, and calculated by Image Pro Plus software. The peak contact stress was measured through low pressure or medium pressure FUJI film. The average contact stress can be calculated by the load divided by the contact area as Equation 2-16.

$$\overline{S} = \frac{L}{A_m}$$ **Equation 2-16**

Where, $\overline{S}$ is the average contact stress (MPa), L is the applied load (N), and A_m is the measured contact area (mm^2).

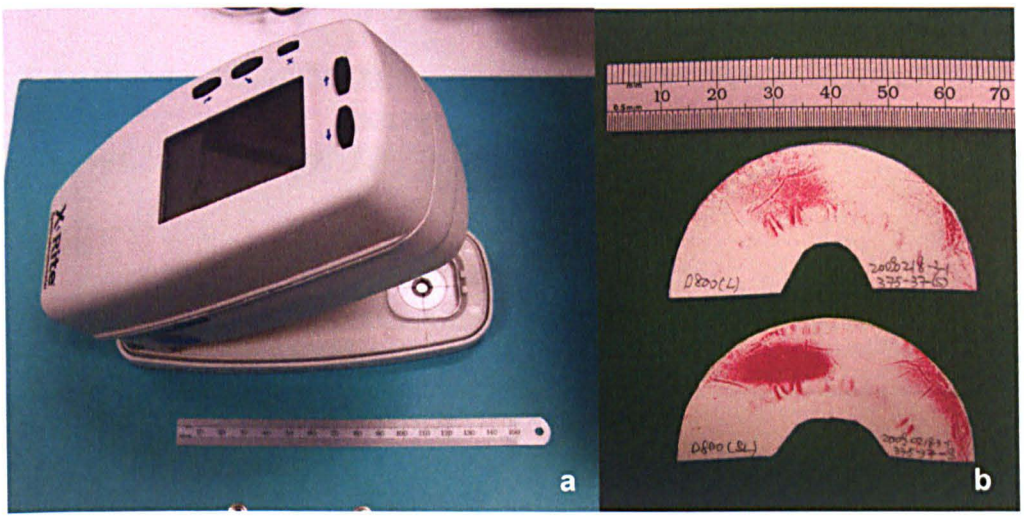

Figure 2.32. a. FUJI film Spectrodensitometer, b. tested FUJI film

2.3.2.4 Average and Peak Frictional Shear Stress

The average frictional shear stress was calculated following Equation 2-17.

$$\overline{SS} = \frac{f \times Load}{A_m} \qquad \textbf{Equation 2-17}$$

Where, $\overline{SS}$ is the average frictional shear stress (MPa), f is the friction factor, $Load$ is the applied load (N), and A_m is the measured contact area (mm^2).

The peak frictional shear stress was calculated by Equation 2-18.

$$SS_{peak} = f \times \overline{S_m} \qquad \textbf{Equation 2-18}$$

Where, SS_{peak} is the peak frictional shear stress (MPa), f is the friction factor, and $\overline{S_m}$ is the average measured contact stress (the highest 6 points per specimen) (as described in Section 2.3.2.4).

2.3.2.5 Wear Grades and Area Measurement and Calculation

The cartilage wear grades and area was traced onto flexible film and the area of different cartilage damage grades followed the ICRS (International Cartilage Repair Society) articular cartilage injury classification wear grading system (explained in 1.3.2.2.2) measured. Cartilage wear grade 0, 1, 2, 3, and 4 were applied to the acetabular cartilage damage scale shown in Figure 2.33.

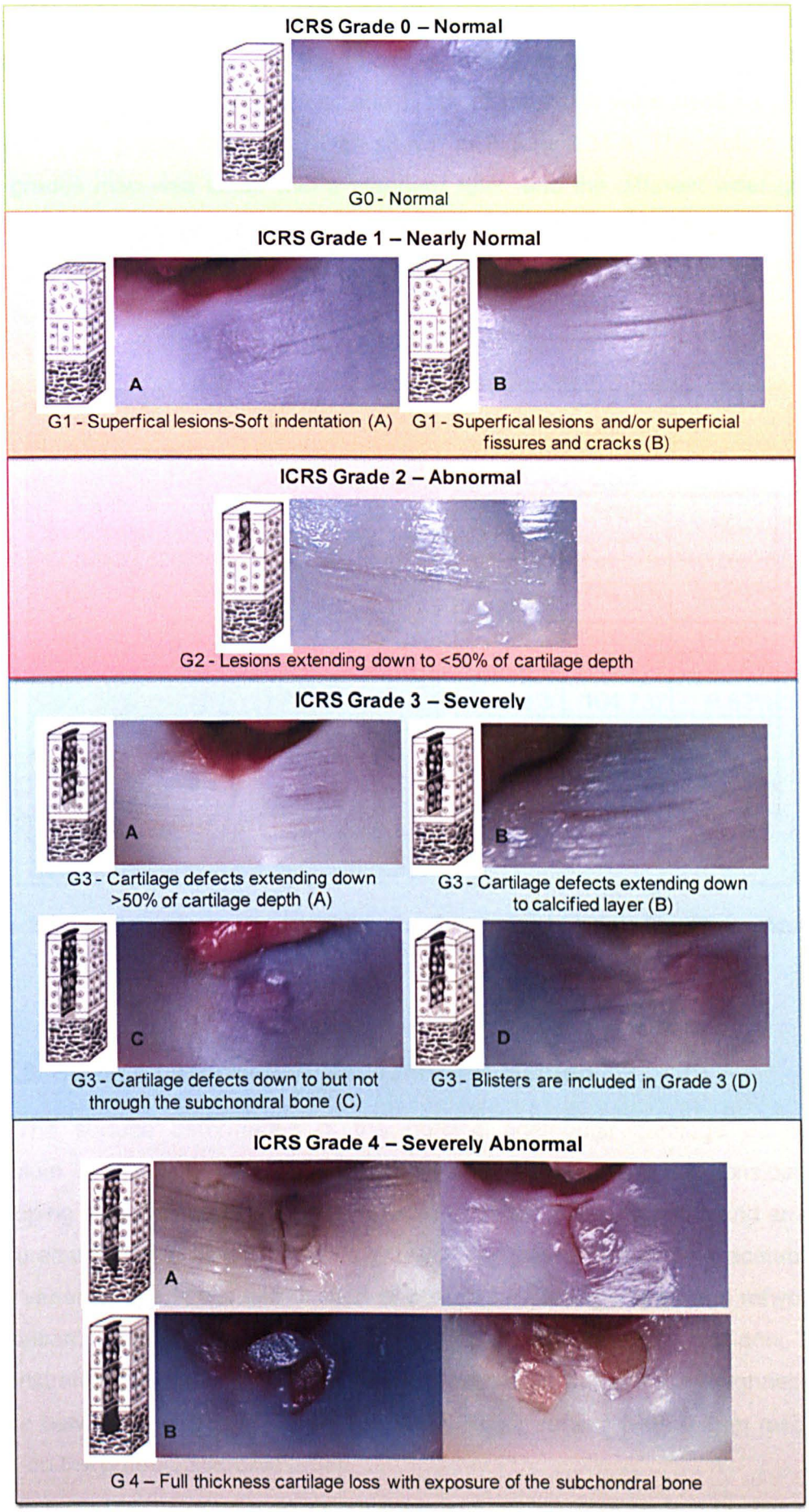

Figure 2.33 ICRS wear grades applied on acetabular cartilage damage scale

The area of the different wear grades were measured through marking a transparent cling film covering the microset replica of the acetabulum. Different colours – green, orange, red, blue, and black of markings were used to present cartilage wear grades from 0 to 4 as shown in Figure 2.34.a. The picture of the wear grades map was taken with a standard ruler, and the different wear grades areas were calculated using Image Pro Plus program, and the results were presented as the percentage of the lunate acetabular cartilage surface (Figure 2.34.b).

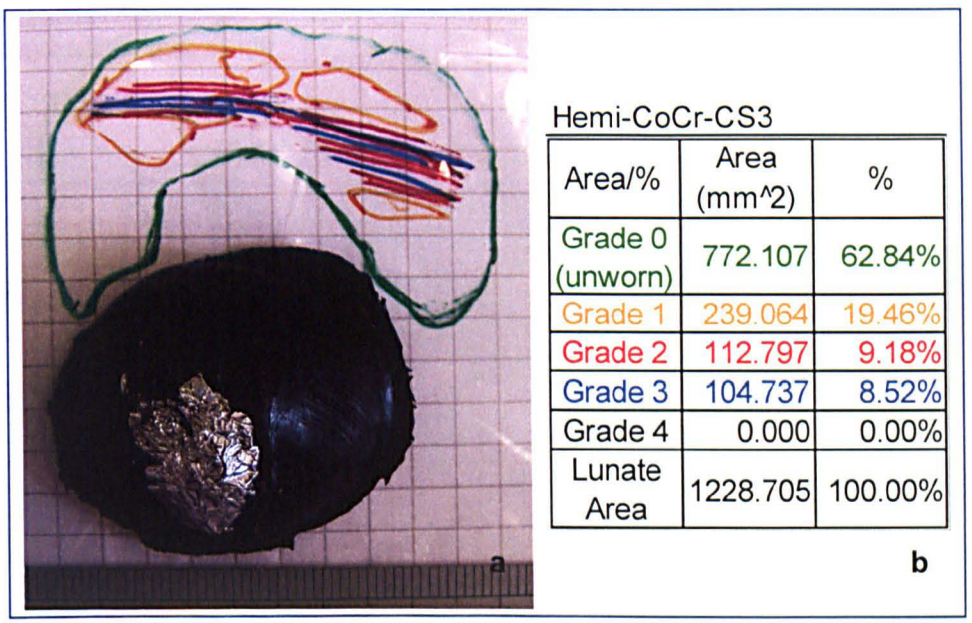

Figure 2.34 a. Wear grades image with a standard ruler, b. Image Pro Plus calculation result.

2.3.2.6 Surface Deformation Measurement Method

The surface deformation of the porcine acetabular cartilage during the pendulum friction test was studied. Different methodologies were considered in developing a final protocol for the surface deformation measurements and analysis. Measurements were conducted on the silicon replicas of the porcine acetabula to avoid variation due to the dehydration of acetabular cartilage in air and rehydration in lubricant. Previous studies (Katta, 2007; Northwood, 2007; McCann, 2009) demonstrated that there is no significant difference of the surface roughness and texture between the articular cartilage and its silicon replica (with 0.1μm resolution noted on the product Microset tube).

2.3.2.6.1 Surface Deformation Measurement and Calculation – Talysurf

Talysurf stylus profilometry is a common two-dimensional / three-dimensional method of quantifying the surface topography of engineering materials. A stylus traverses across the surface converting its vertical movement to an electrical signal, which through suitable processing, filtering and calibration can be used to build a trace of the surface profile. Modern profilometry is capable of high accuracy and reproducibility within resolution limits of approximately 0.001 to 0.002μm. The stylus profilometer used within this study was a Talysurf 5 model (Taylor-Hobson, UK) (Figure 2.35.a) connected to a standard computer. A 0.8mm Gaussian cut-off filter was used within this study.

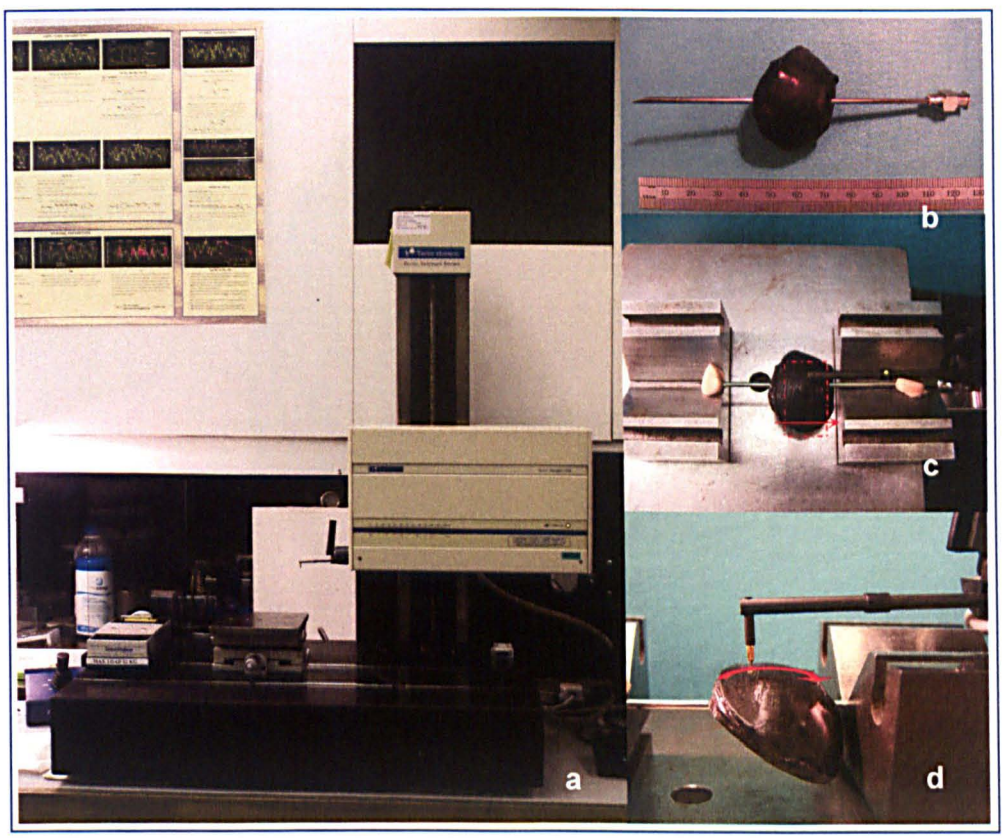

Figure 2.35. a. Talysurf stylus profilometry, b. a clinical needle was pushed through a Microset silicon replica, c. the Microset silicon replica was set onto the stainless steel stands, d. the stylus was measuring the replica surface – vertically to the wear scar direction.

Changes in the volume of the acetabulum replica were studied using Talysurf Stylus profilometry, and the measurements were conducted by a trained technician. A clinical needle was pushed through the Microset silicon replica (Figure 2.35.b) to locate the position on the stainless steel stand (Figure 2.35.c) during the measurement. When the position of the specimen was fixed the stylus started to measure the surface – vertically to the wear scar direction (Figure 2.35.d).

The replica surface was measured by the stylus across the wear area with approximately 20 traces with 0.5mm trace gap. The measured traces of one sample (silicon replica) are shown in Figure 2.36 as the red arrows. The replica wear surface was set still as Figure 2.36.a, and then a stylus travelled several parallel traces on the replica wear area in Figure 2.36.b. Each trace measurement result was shown on the PC (Figure 2.36.c) when the measurement had been completed. The form removal analysis of each trace can only be conducted correctly using Talymap software when the trace is recorded with the virgin surface on both sides of the deformation area. Hence, a full record of the original lunate surface of the acetabular replica on both sides of the wear / deformation scar was required (in Figure 2.36.b).

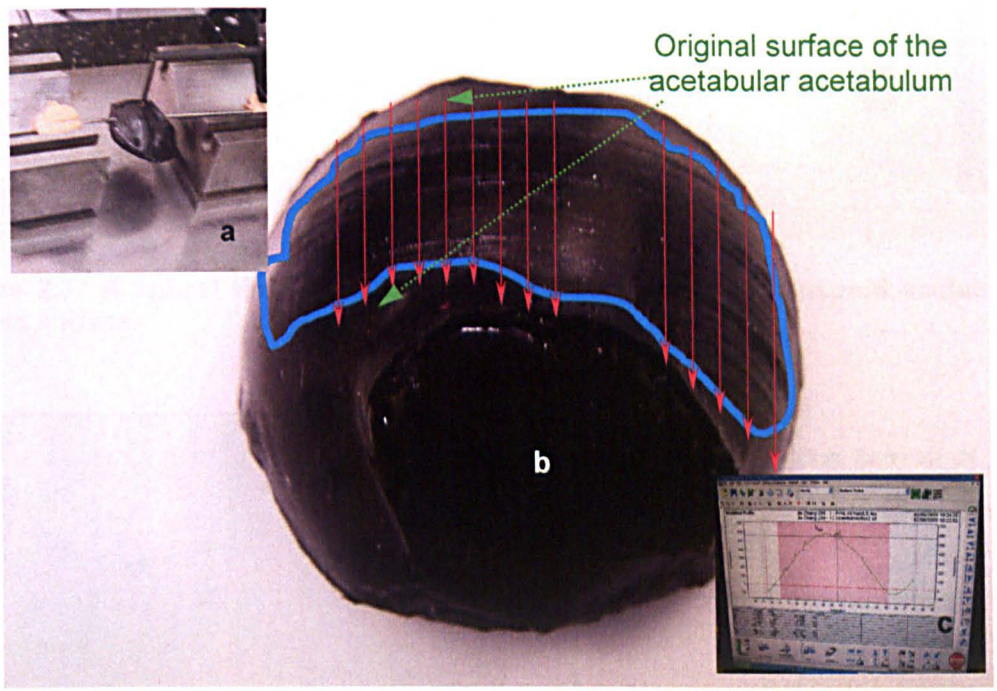

Figure 2.36 A sample of replica surface measurement, a. a replica was set still; b. a stylus traveled across the wear area – measured traces are shown as red arrows; c. each trace measurement result was shown on the PC when the measurement had been completed.

Three-dimensional measurement was available and was considered for a surface with a height less than 5mm and it took approximate 2 hours to complete a separated small area 150 mm^2 surface measurements. A typical three-dimensional image example of a piece of surface measurement is shown as Figure 2.37. The two-dimensional image of a sample line (in Figure 2.38.a) is shown as Figure 2.38.b. Three-dimensional measurements were not chosen as a measurement method of cartilage deformation because the limitation of the surface area and height was far less than the replica specimens, and also the long processing time.

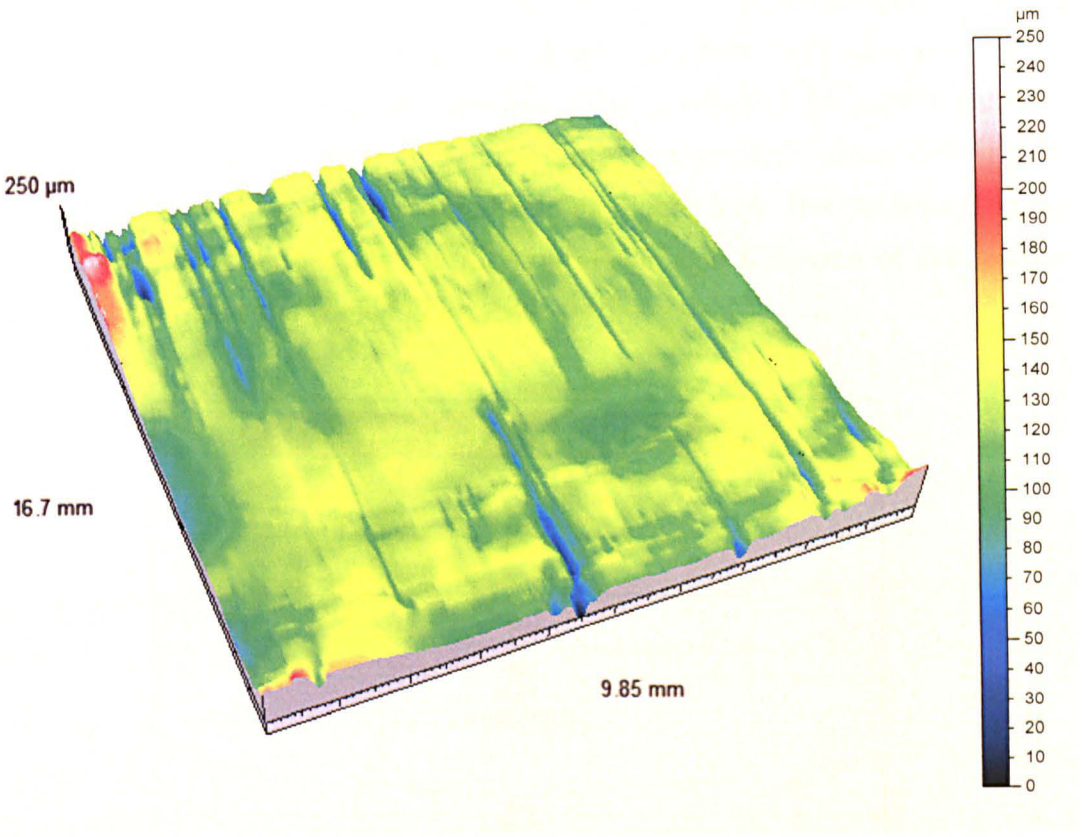

Figure 2.37 A typical three-dimensional image of a piece of measured acetabulum replica surface

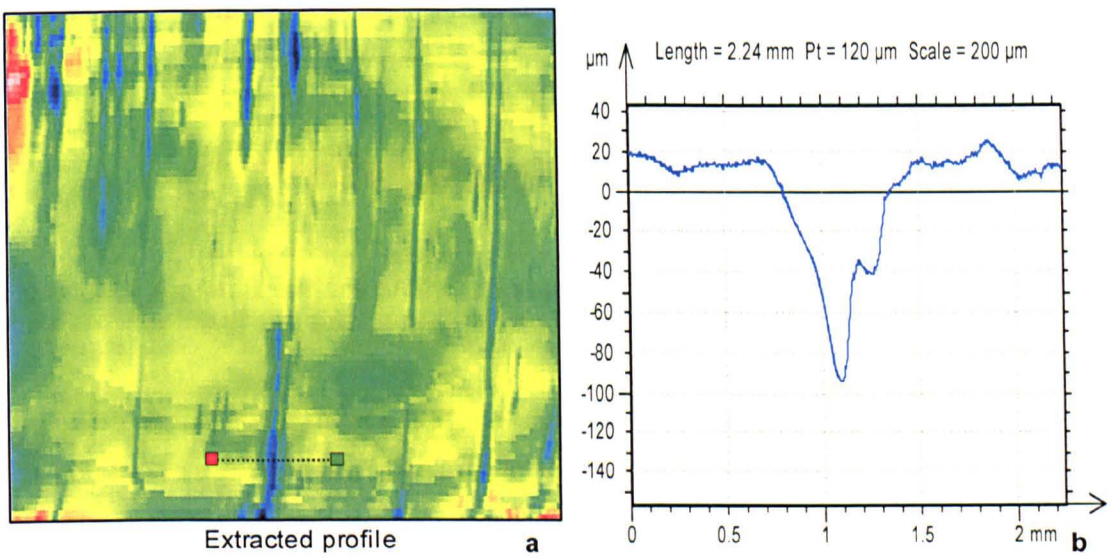

Figure 2.38 a. A 2D image transverse plane of a piece of measured acetabulum replica surface, b. the 2D coronal plane image of the analysed trace

Two-dimensional measurements were taken in a similar way to the three-dimensional measurements, and this method was chosen to measure the replicas surface. The two-dimensional measurements were operated on a larger area with longer surface height in a shorter time, e.g. approximately 40 minutes for one

replica specimen measurements in an area of 250 mm^2. Approximately 20 traces with 0.5mm trace gap were measured per sample, and each trace was analysed by TalyMap software. The analysis process was conducted through symmetry, leveling, form removal, zoom, and final profile deformation area. One typical example of of trace analysis graphs is shown as Figure 2.39. The deformation area of each trace was multiplied by the trace gap to provide a volume of deformation area in the blue block shown as Figure 2.40.

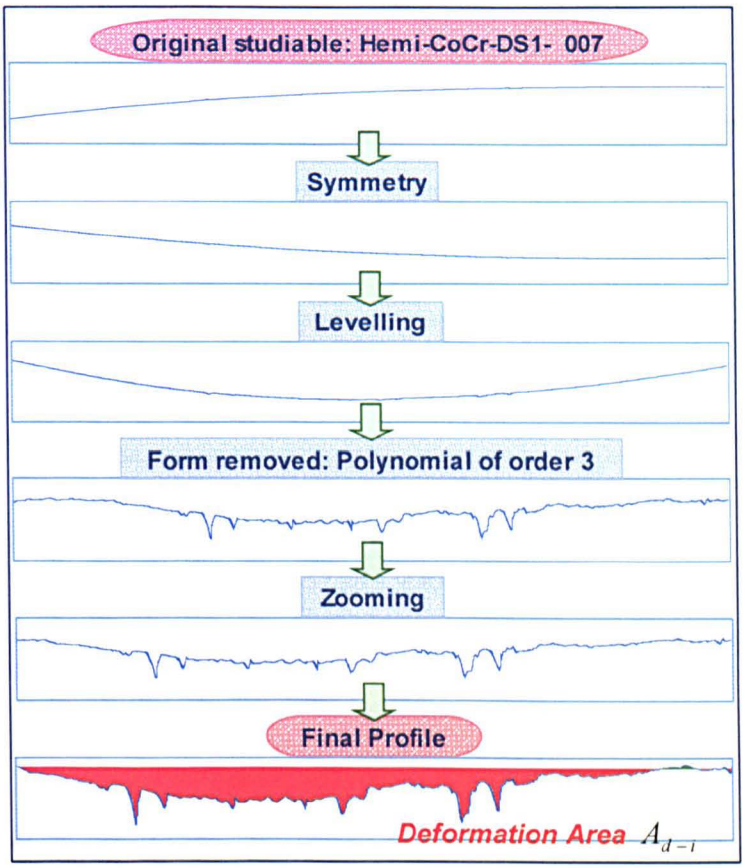

Figure 2.39 A typical surface analysis process of each trace: symmetry, leveling, form removed, zooming, and final profile peak and hole (deformation) areas.

The acetabular cartilage surface roughness was measured and the roughness (Ra) of each trace was calculated by software following Equation 2-19.

$$Ra = \frac{1}{n}\sum_{i=1}^{n}|y_i| \qquad \textbf{Equation 2-19}$$

Where, R_a is the arithmetic average of absolute values of the surface roughness profile (μm), n is the number of valley and peak on the trace, and y_i is the height of the absolute height of the valley or peak to the reference line.

Here the deformation area of the trace in the trace gap was estimated equal. One replica specimen (11 traces) analysed measurements graphs is shown in Figure 2.40. Hence the total surface deformation of each acetabulum replica was

the summation of all the individual volume (Equation 2-20). The average deformation depth in the studied area is calculated by Equation 2-21.

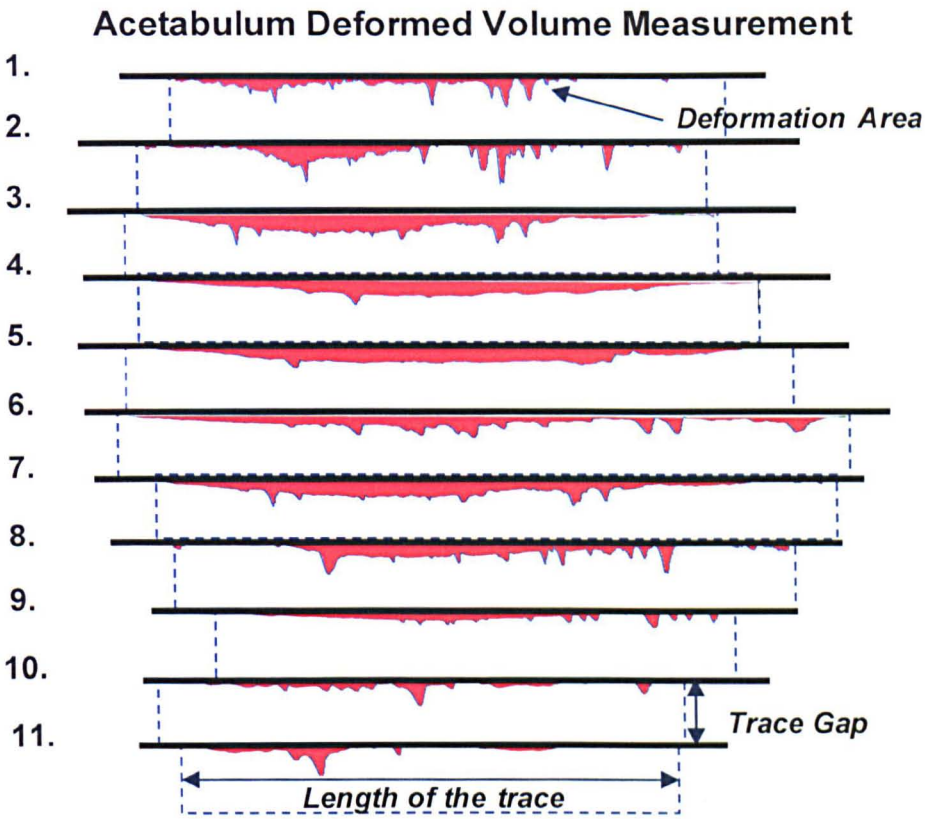

Figure 2.40 One replica specimen (11 traces) surface measurement results – red area is the deformation area of each trace.

$$V_d = \sum_{i=1}^{n} (A_{d-i} \times G_{trace}) \qquad \textbf{Equation 2-20}$$

Where, V_d is the volume of the surface deformation (mm^3), $A_{deformation\text{-}i}$ is the deformation area of each trace (mm^2), and G_{trace} is the average gap distance between each trace (mm).

$$\overline{D_d} = \frac{\sum_{i=1}^{n} A_{d-i}}{\sum_{i=1}^{n} L_{trace}} \qquad \textbf{Equation 2-21}$$

Where, $\overline{D_d}$ is the average deformation depth (mm), $A_{deformation\text{-}i}$ is the deformation area of each trace (mm^2), and L_{trace} is the studied length of each trace (mm).

2.3.2.6.2 Surface Deformation Validation – Pycnometer

To examine the accuracy of the two-dimensional profilometer measurements and surface deformation calculation methodology, surface deformation validation was completed before the measurements of the groups of silicon replicas were started.

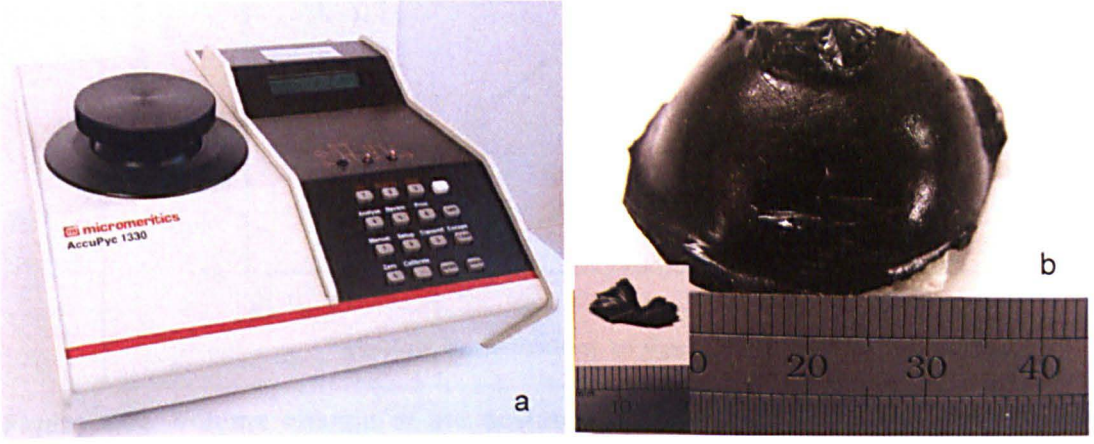

Figure 2.41. a. ACCUPyc 1330 Pycnometer, b. a piece of microset silicon from an acetabulum replica

The ACCUPyc 1330 Pycnometer (Figure 2.41.a) was used to measure the volume of a piece of microset silicon rubber (Figure 2.41.b) removed from an acetabulum replica to validate the two-dimensional profilometry measurement. The ACCUPyc 1330 pycnometer is a fast, fully automatic density analyser that provides high-speed, high-precision volume and density measurements on a wide variety of materials. It works by measuring the amount of displaced gas (helium). The pressures observed upon filling the sample (cell) chamber and then discharging it into a second empty chamber (expansion chamber) allow computation of the sample volume. Air volume difference in the small container with and without the specimen then the difference of volume of the air should be equal to the volume of the specimen.

Direct measurement using the ACCUPyc 1330 Pycnometer to measure the piece of Microset silicon volume, and indirect measurement using the two-dimensional profilemeter to measure the acetabular replica surface and calculated the piece of Microset volume were used. Five measurements of each method were taken, and the volume was calculated and compared (Figure 2.42). Good agreement (no significant difference, $p<0.1$) of the piece of Microset volume result was shown between the two different methods.

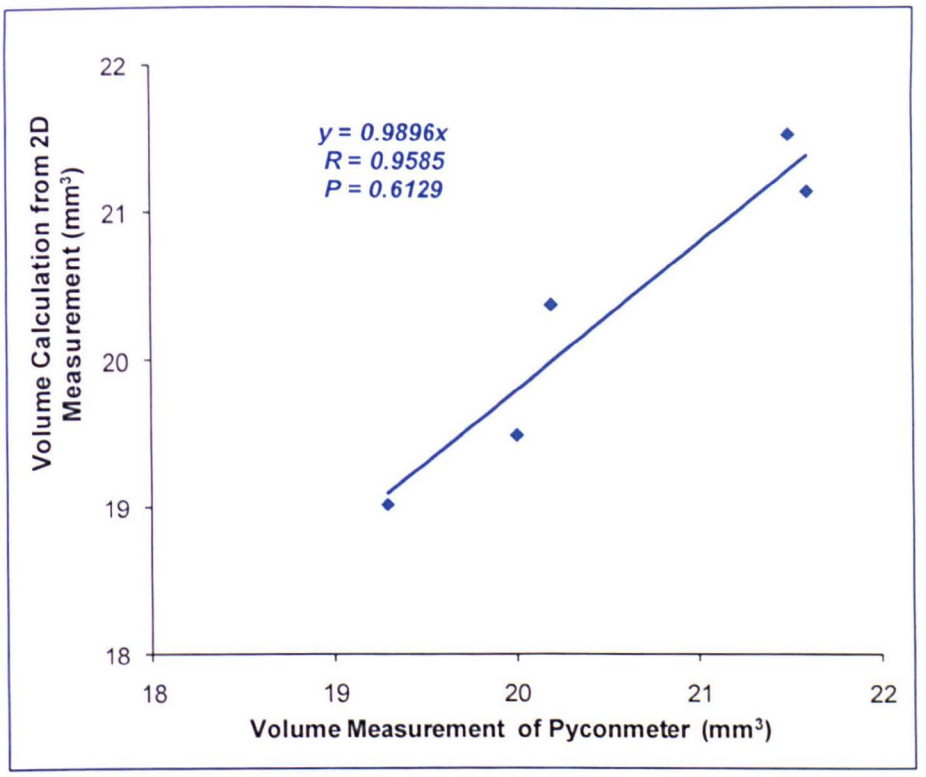

Figure 2.42. Volume change of the acetabular replica measured using 2D Talysurf profilemeter was compared to the volume measurements of the removed piece of replica using the AccuPyc gas displacement pycnometer. R and P values were obtained using a regression analysis in Microsoft Excel 2007 (Microsoft Corporation, Redmond, USA).

2.3.2.6.3 Other Methods – µ80 Micro CT Scanner

Wear assessment of the acetabular cartilage is complex because of the cartilage volume changes in water content. Accurate wear cannot be assessed by simple method such as measuring the weight changes then divided by cartilage density, or scanning the acetabulum before and after the friction test. Therefore several methods of indirect measurements were investigated of the porcine acetabulum wear studies. Two of the main compatible and most accurate methods were using computed tomography scanner to measure and calculate the wear volume (surface deformation). These are described in more detail as method A and method B.

In developing the two-dimensional profilemeter method for assessment of acetabulum deformation (the acetabular cartilage wear volume, and depth) other methods were also investigated.

The Scanco µ80 Micro Computed Tomography Scanner (SCANCO Medical AG, Switzerland) was used to measure fresh acetabular cartilage specimens, and acetabular replicas. The two-dimensional (noted as 2D) and three-dimensional

(noted as 3D) images of the fresh acetabular cartilage were used to study the geometry of acetabulum and cartilage thickness of the lunate surface. The 2D and 3D images of the replicas were used to analyse and calculate acetabular wear volume (surface deformation).

This scanning condition might affect the biomechanical properties of cartilage and lead to significant errors of the cartilage volume calculation from the scanned images. Hence the acetabular cartilage wear volume cannot be calculated by scanning the porcine acetabulum before and after the pendulum friction test.

Previous studies demonstrated that the boundaries between the lubricant and articular cartilage cannot be clearly recognised when the cartilage is scanned in contact with the lubricant because of the lack of density difference between the superficial zone of the cartilage and the lubricant. Therefore the cartilage was scanned without lubricant in the scanner, this meant that the dehydration of articular cartilage for 45 minutes or longer could not be avoided. One porcine acetabulum μ80 MicroCT image slices in 2D is shown in Figure 2.43. After scanning its 3D image was built up, this could be set as any angle and direction for the analysis (Figure 2.44).

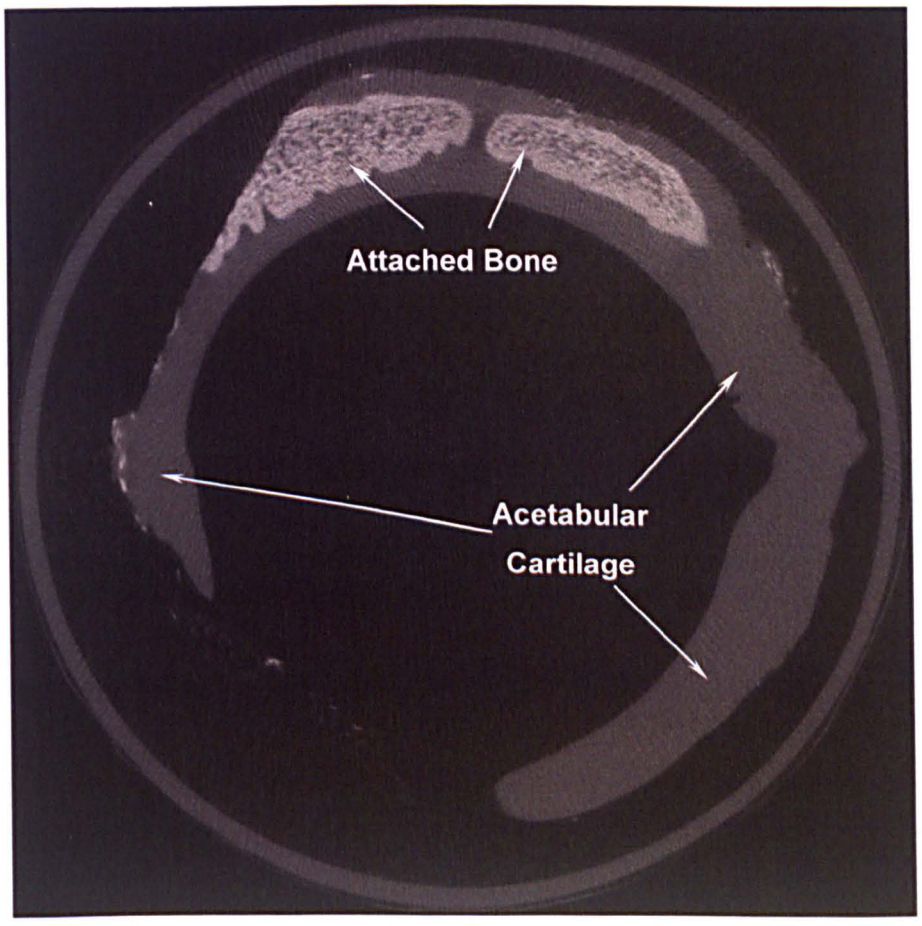

Figure 2.43. One typical two-dimensional image of a porcine acetabulum (resolution 0.2μm) by μ80 MicroCT scanner.

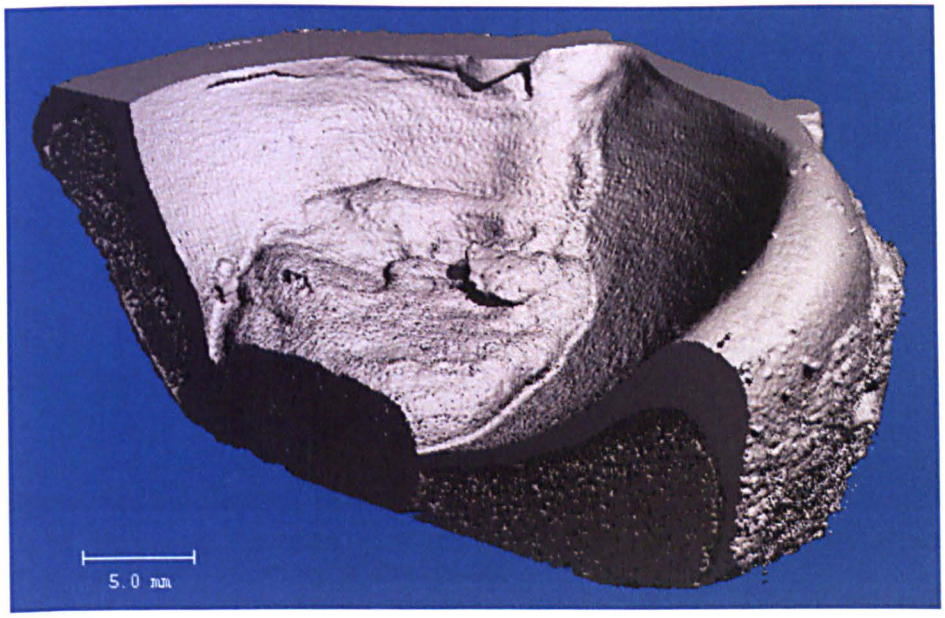

Figure 2.44. A transferred three-dimensional image of the porcine acetabulum from the scanning results (resolution 0.2μm) by μ80 MicroCT scanner.

Method A

A simple introduction of method A is shown in Figure 2.45. The wear volume result was calculated as the volume difference between the two marked planes of the two replicas of the acetabulum (before and after the friction test). To scan the acetabular two directions of scanning are available shown in Figure 2.46. The replica specimen can be scanned horizontal transverse planes (Figure 2.46.a) approximate 400 slices in 45 minutes, or vertical to the wear scar (Figure2.46.b) approximate 700 slices in 80 minutes with the same resolution. The information was assessed from both scanning methods, and the horizontal transverse plane scanning was chosen due to the shorter operation time (and no advantages when scanning vertically to the wear scar were observed).

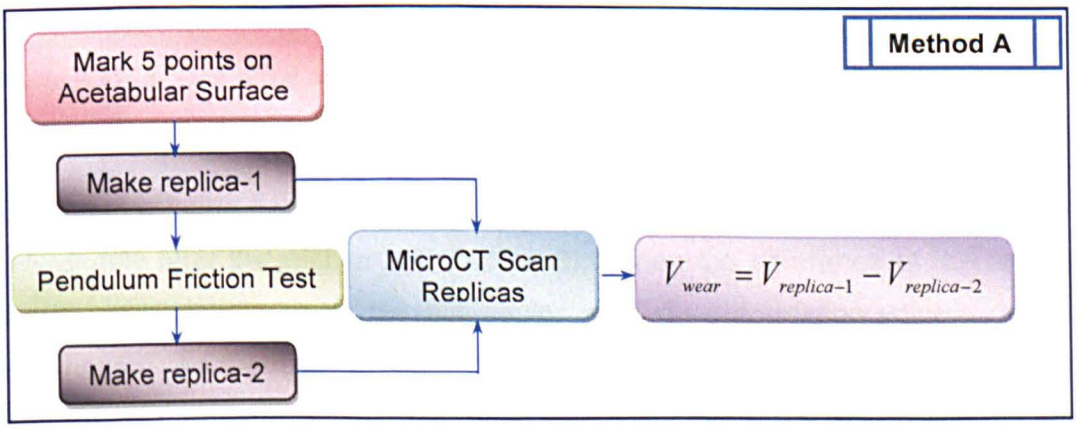

Figure 2.45 Introduction of method A to measure and calculate the acetabular cartilage wear

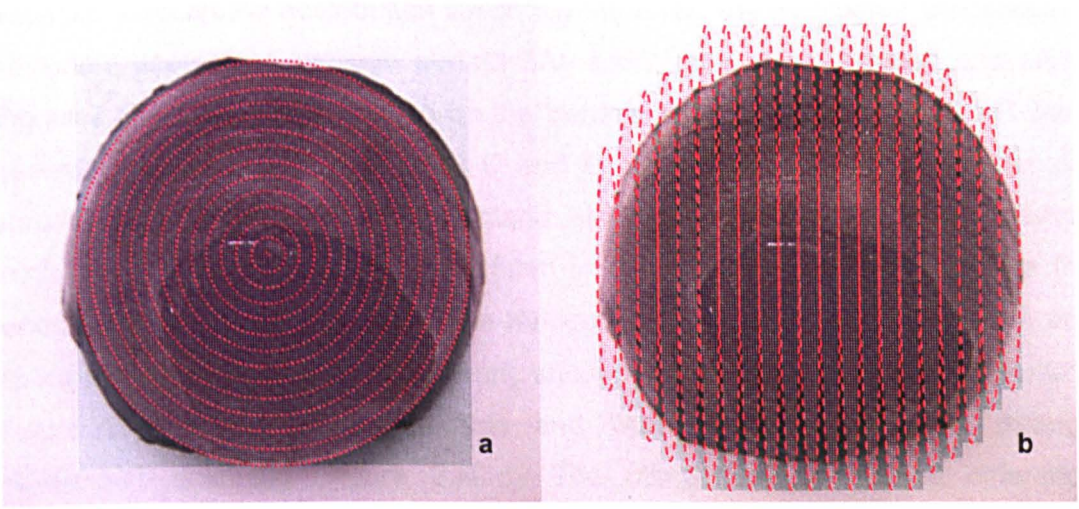

Figure 2.46. Scanning methods in high definition: a. horizontally 400 slices in 45 minutes; b. vertically 700 slices in 80 minutes

One typical 2D scan image of one slice is shown in Figure 2.47.a, and the built up 3D image of the replica is shown in Figure 2.47.b. However, the surface cartilage damage volume cannot be calculated straight away due to the missing information of the original surface images.

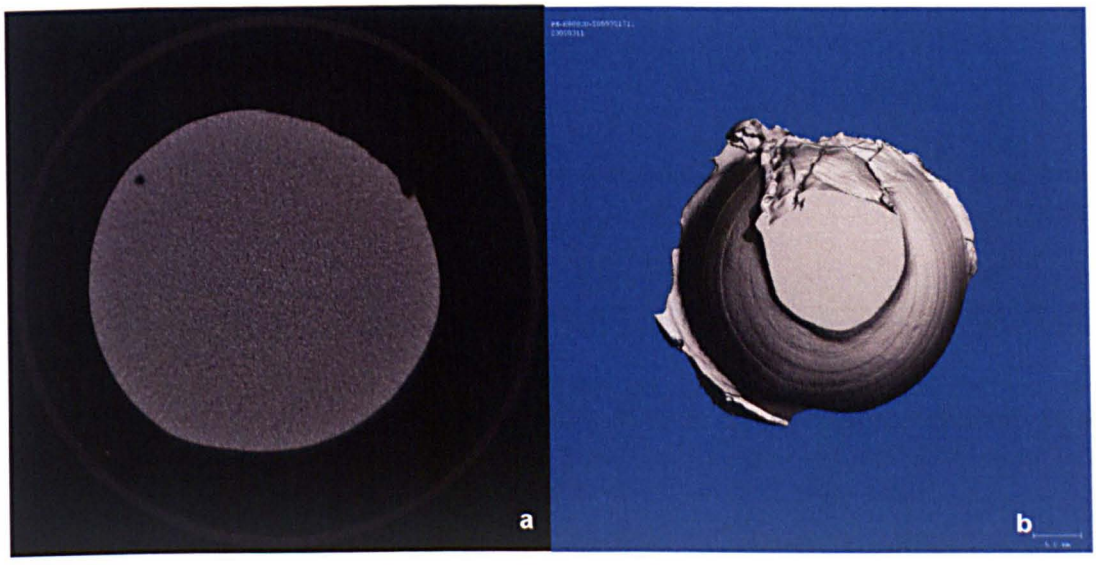

Figure 2.47. a. One slice scan image of a replica; b. built-up three-dimensional image of a replica

For the same porcine acetabulum, replicas were taken before (replica-1) and immediately after the friction test (replica-2); hence the difference of the replicas' volume was considered as the acetabular cartilage deformation volume (surface deformation). As the main difficulty of this method was moulding of the soft tissue parts (fat pad, round ligament, and transverse ligament) of the replica and the open acetabulum surface level of the replica was not able to be controlled equally. A method was developed by marking five points, and these marks were chosen at an

unloaded area on the acetabulum which did not affect the tribological properties of the lunate acetabular cartilage surface. As each three points created one plane (Figure 2.48: point A was marked on the transverse ligament, point B and C were marked close by the fat pad, point D and E were marked under the acetabular labrum), two planes were created (plane ABC, and plane ADE). These marked points were made by a hand drill 0.5mm in diameter (Figure 2.49.a) before the pendulum friction test, hence the five marks were mirrored on both replica-o and replica-a. These five marks were clearly shown on the acetabular cartilage surface (Figure 2.49.b), the replica surface and were highly recognisable through μ80MicroCT scanning (Figure 2.49.c). The comparison of volume difference between these two planes of both replicas was considered as the acetabular cartilage deformation, which includes the wear and surface deformation.

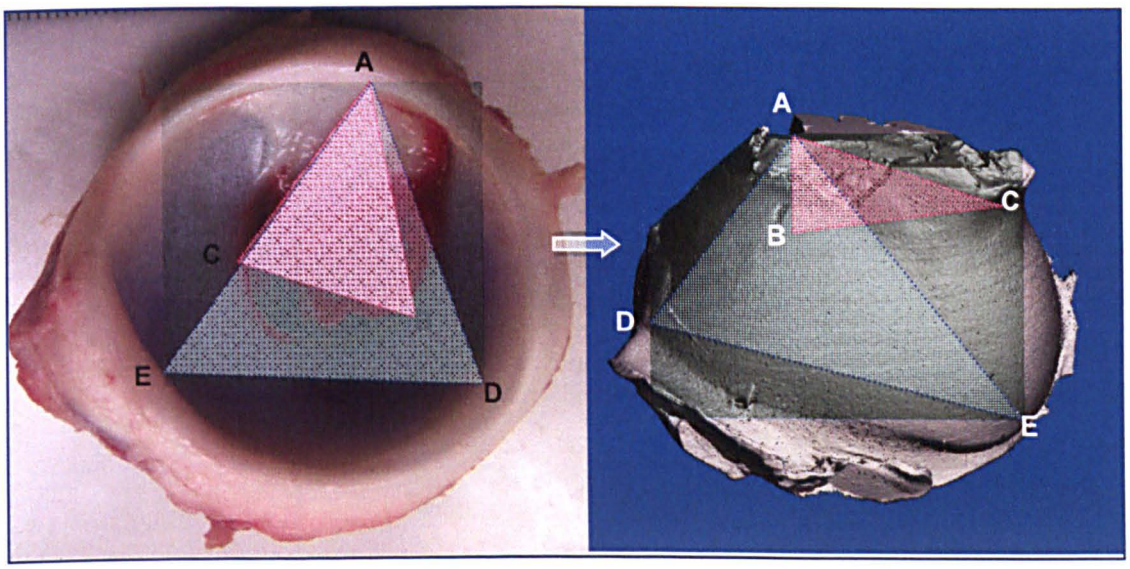

Figure 2.48 Five marked points were made on the porcine acetabulum surface, two planes were created as plane-ABC, and plane-ADE. a. on porcine acetabulum; b. on CT scanned three-dimensional image.

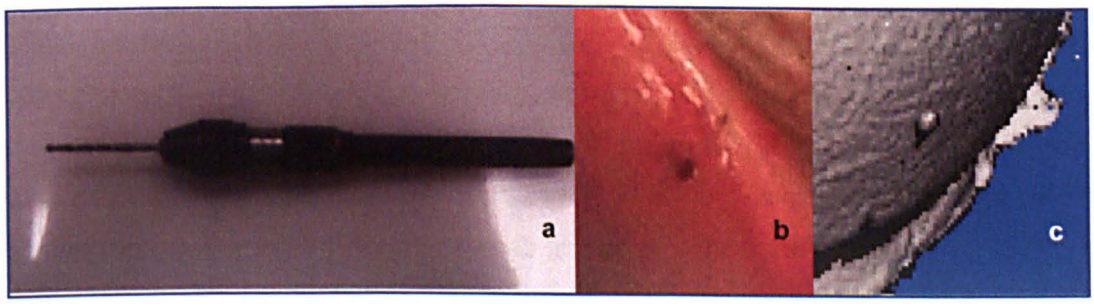

Figure 2.49. a. Marks drill with a 0.5mm diameter core; b. marked point on acetabular cartilage besides the labrum; c. the marked point was recognised clearly on the three-dimensional image through CT scan

The limitation of this method was its time-consuming process - for each individual porcine acetabulum two replicas required scanning at high definition; hence it suits to individual case studies. For groups with large amount of specimens, this method was not chosen for the clearance effect to friction and surface deformation studies under both constant and dynamic loading.

Method B

A simple introduction of method B is shown in Figure 2.50.

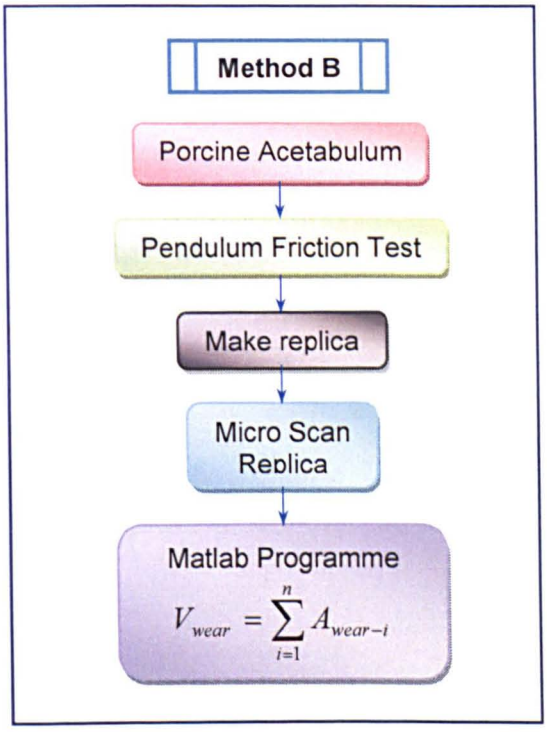

Figure 2.50 Introduction of method B to measure and calculate the acetabular cartilage wear

One replica of the acetabulum was made after the friction test, and the wear volume was calculated by Matlab 7.5 (Mathworks, Natick, USA) programme which manually recovered the original unworn surface. Method B had been practised to analyse the acetabular wear from the CT scan 2D images. The image was transferred into sagittal plane slices (Figure 2.51.a) and analysed using Matlab 7.5 (Mathworks, Natick, USA) programme as shown in Figure 2.51.b.

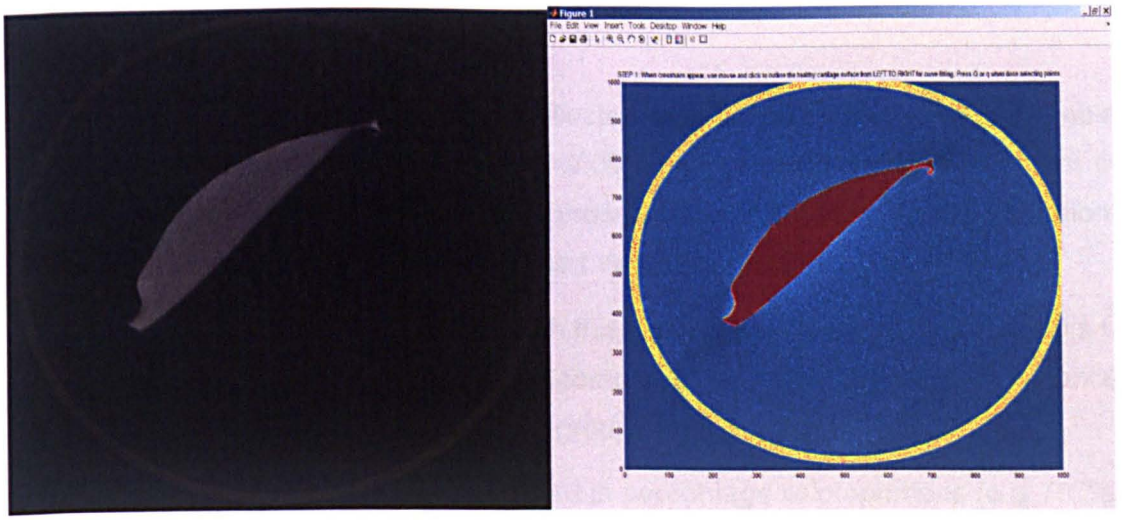

Figure 2.51 Acetabulum replica 2D scan image transferred in Matlab 7.5 (Mathworks, Natick, USA)

However, the pixel size was similar to the missing surface area size, and it was impossible to recover the original surface manually with high definition (Figure 2.52). Hence the high definition MicroCT scan method was not chosen for the acetabular surface deformation studies.

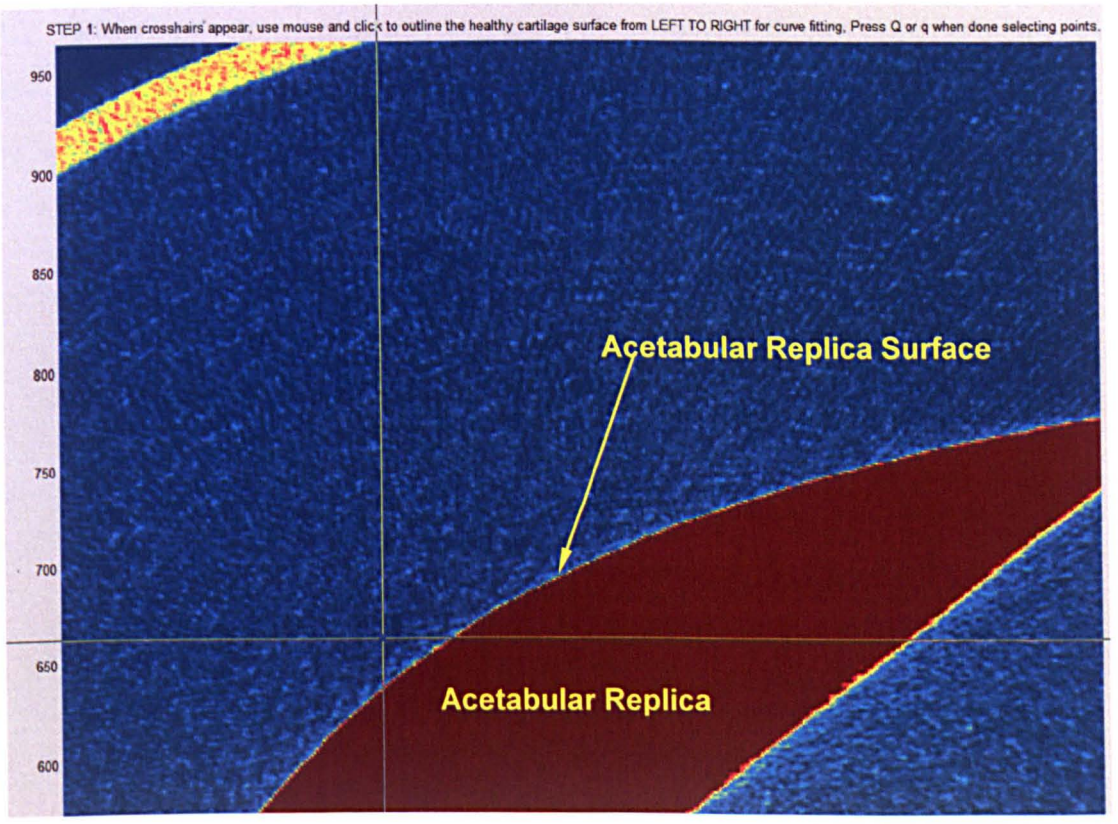

Figure 2.52 The 2D image of acetabulum replica slice in Matlab 7.5 (Mathworks, Natick, USA) was too small pixel to be analysed

2.4 Statistical analysis

Different statistical values were collected and calculated as shown in Table 2.7. 95% confidence limits (intervals) (α=0.05) were calculated with a minimum of three replicates. Statistical analysis on Microsoft Excel 2007 (Microsoft Corporation, Redmond, USA) was used to calculate the t value and p-value.

The statistical analysis used through this study for comparison: the student's t-test was used when two means were compared, one-way analysis of variance (ANOVA) was used when more than two groups was analysed.

When calculated data was expressed in percentage or proportions (e.g. *HC%*, W_{linear}%, A_{WG}%), the data was transformed to arcsine (Inverse sine) values to all accurate generation of 95% confidence limits. The arsine values were used to calculate 95% confidence intervals following the conversion. Then data was transformed back to the percentage or proportional values.

Linear regression analysis was performed on standard curves when interpolation / correlation results were required.

Table 2.7 Statistical sign, definition and equation

Sign	Definition and Equation
X	Individual value
N	Sample number
$\sum x$	Sum of = $\sum_{1}^{n} x_i$
$\bar{x}$	Mean value = $\frac{\sum_{1}^{n} x_i}{n}$
SD	Standard deviation = $\frac{\sqrt{\sum_{1}^{n}(x_i - \bar{x})^2}}{n-1}$
SE	Standard error = $\frac{SD}{\sqrt{n}}$
95%CL	95% confidence limits = $SE \times t - value$
t-value	Probability level = 0.05 or 0.01
p-value	Probability of obtaining a test statistic at least as extreme as the one that was actually observed (0.05)
Γ	Degrees of freedom = n-1

2.5 Summary

To conclude, different methodologies had been developed and used in the tribology of hemiarthroplasty study focusing on the articular cartilage friction, deformation, wear, and degradation applied on two different hemiarthroplasty models. The most effective and practical methodologies were chosen for the tribology study of each model. Simple geometry pin on plate hemiarthroplasty model was conducted on bovine knee articular cartilage pin on cobalt chrome plate tested by single station pin on plate apparatus. Hemiarthroplasty hip model was undertaken on porcine articular acetabulum on cobalt chrome / ceramic head tested by the pendulum friction simulator. Both hemiarthroplasty models, the friction was examined by the piezoelectric sensor, but calculated through different methods. However, the articular cartilage deformation and cartilage wear was measured and calculated completely different in both models. In simple geometry pin on plate hemiarthroplasty model, the cartilage deformation was measured directly from the specimen by digital height gauge, but the linear wear was calculated by comparing with the control groups using a new developed method. In the hemiarthroplasty hip joint model, the acetabular cartilage deformation was measured on the replicas of the specimens by two-dimensional profilemeter, and analysed by Talymap software. The articular cartilage deformation volume and average deformed depth were calculated using a new developed method.

Chapter 3 The Effect of Contact Stress on Cartilage Friction Deformation and Wear

3.1 Introduction

Following hemiarthroplasty implantation, acetabular cartilage can degenerate in response to articulation with the metallic component; however, the factors that affect the rate of cartilage erosion and degeneration of the acetabulum have not been fully investigated. Hence, the understanding of the tribological behaviour of artilcular cartilage following hemiarthroplasty is limited.

Articular cartilage in synovial joints withstand complex, varied and often-harsh loading regimes, and its mechanical features enable the transmission of large loads by providing a surface with minimal friction, wear and excellent lubrication. The mechanical response of articular cartilage is highly non-linear and both time- and load-dependent (Graindorge *et al.*, 2004). The friction coefficient of cartilage is a very useful measurement in the study of joint tribology, and it has been found to be 0.2-0.4 upon constant loading for durations of several hours (Forster and Fisher, 1996; Krishnan *et al.*, 2004b). The frictional response is primarily controlled by the biphasic condition of the cartilage, and load carriage by the fluid phase (Forster and Fisher, 1996; Forster and Fisher, 1999).

In hip hemiarthroplasty, the contact pressures have been studied and examined *in-vivo* in the past 20 years. The acetabular contact pressures were measured (Fagerson *et al.*, 1995) and found to range from 1.21 MPa to 7.09 MPa during various functional activities: sit-to-stand, ambulation, and stair-climbing. The highest peak acetabular contact pressure were found during unassisted reciprocal gait on stairs at 15.52 MPa. Hence, it is necessary to study the tribology of articular cartilage under a range of stress conditions.

The wear of articular cartilage is defined as the removal of material from the surface due to mechanical or chemical action between the contact surfaces. However, the wear of cartilage is very difficult to measure in an *in-vitro* experiment due to the variable water content of the articular cartilage and its biphasic properties. The water content affects both gravimetric and geometric measurements of both wear and permanent deformation, hence, it is difficult to differentiate wear from permanent deformation or permanent loss of water from the cartilage (Northwood and Fisher, 2007). However, it is possible to use changes in surface topography as an indication of surface damage caused by wear (Katta *et al.*, 2007b; Northwood

and Fisher, 2007; Katta *et al.*, 2008a). A previous study by Lipshitz and Glimcher (Lipshitz *et al.*, 1975), concluded that cartilage wear rates increased with increasing normal load and relative speed of the surfaces, but decreased with time, attaining an equilibrium value. During reciprocating motion, wear was attributed to the interaction between two contacting surfaces and accumulation of microscopic damage, described as interfacial and fatigue by Armstrong and Mow (1982). In the knee hemiarthroplasty study, it has been found the permanent deformation and wear increased with both increased friction and increased contact stress (McCann *et al.*, 2009), these typically occurred at high levels of contact stress.

This summarised literature review has led to the development of series of research questions:

1. How does contact stress affect cartilage friction, deformation and wear?
   - Does the coefficient of friction, cartilage deformation, and cartilage wear increase proportionally to the increasing contact stress?
   - What level of contact stress can cartilage withstand – without damaging the matrix of cartilage, in a hemiarthroplasty configuration?
2. How does the loading time affect the cartilage friction, deformation and wear?
   - Is cartilage thickness influenced by fluid uptake (and no loading)?
   - Does loading of cartilage (with no reciprocating motion) of different contact stresses cause permanent deformation of cartilage?
   - How does loading time (short-term and long-term) affect articular cartilage deformation (with no reciprocating motion)?
   - How does cartilage wear vary under short-term and long-term loading and reciprocating motion?
3. How does the sliding distance and sliding velocity affect the cartilage friction, deformation, and wear?
   - What is the different effect of the sliding distance and sliding velocity on the coefficient of friction, cartilage deformation, and cartilage wear under different contact stress levels?
   - What is the different effect of the sliding distance and sliding velocity on the coefficient of friction, cartilage deformation, and cartilage wear under different loading times?
4. How does the contact area affect on the cartilage friction?
5. How does frictional shear stress relate to the contact stress and coefficient of friction, the cartilage matrix damage, permanent deformation and wear?

3.2 Objectives

The objectives of this study were to use a simple geometry model of cartilage pins reciprocating against metal plates to consider a range of variables. These variables were contact stresses (from 0.5 MPa to 16 MPa for short-term one hour tests, and from 0.5 MPa to 8 MPa for long-term 24 hours tests), stroke lengths (4 and 8mm), and sliding velocities (4mm/sec and 8mm/sec). Variables were controlled independently to assess the short-term and long-term the effect of (1) contact stress levels and loading time; (2) stroke length and sliding velocity; (3) contact area and load; on the coefficient of friction, and cartilage wear.

The overall aim was to define the conditions (in terms of loading time, contact stress, contact area, stroke length, and sliding velocity) that affect the tribological properties of cartilage and cause unrecoverable levels of cartilage wear. Different loading conditions were applied to this simplified model of hemiarthroplasty, and used to consider the cartilage tribology of the hip hemiarthroplasty. An overview of this study is shown in Figure 3.1.

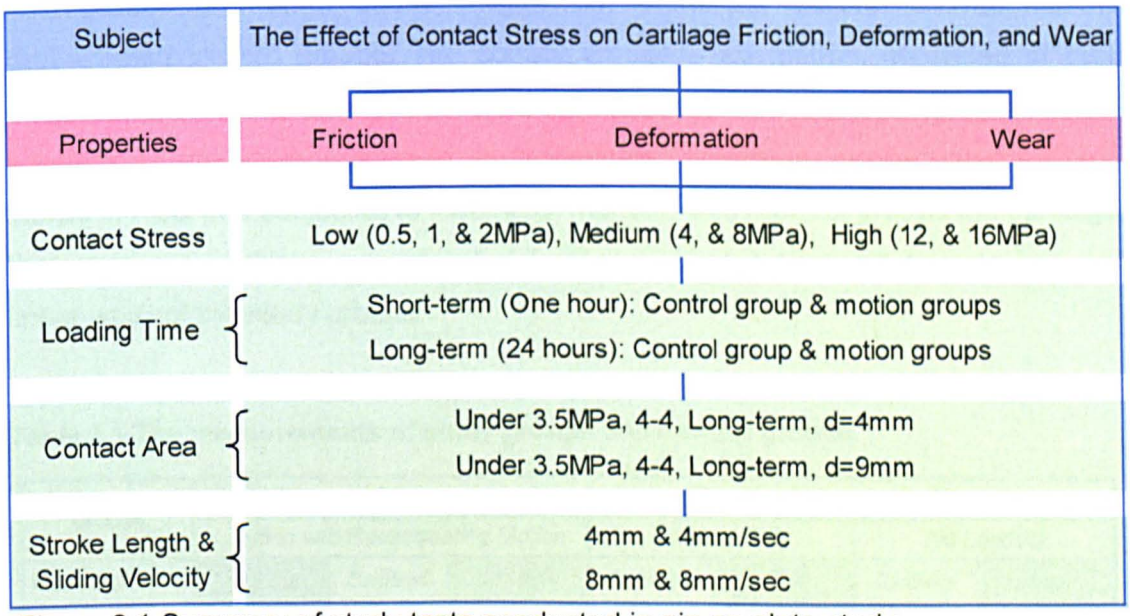

Figure 3.1 Summary of study tests conducted in pin on plate study

3.3 Materials and Methods

3.3.1 Materials

All studies used Cobalt Chromium (CoCr) alloy plates (surface roughness (Ra) of 0.005±0.001 microns) and bovine cartilage pins, as described in Section 2.2.12. and 2.2.3.1. Cartilage pins were harvested from the bovine patello-femoral

groove and used in these studies rather than the acetabulum, due to the acetabulum's irregular concave geometry, that would make controlling variables such as contact area and stress challenging. PBS with 0.1% Aprotinin (Trasylol, Bayer, which used to slow down the fibrinolysis of cartilage during storage and testing) was used as lubricant.

3.3.2 Methods

Simple geometry friction and cartilage deformation studies were conducted using a reciprocating motion pin-on-plate apparatus, as described in Section 2.3.1.1.

This study included study groups and control groups, measurements conducted are shown in Table 3.1. The study groups – pins loaded (under a range of contact stresses in short-term and long-term) with reciprocating motion were measured for cartilage thickness, friction coefficient, and cartilage permanent deformation (height change). The study groups were tested under the following conditions: 4mm stroke length with 4mm per second sliding velocity (abbreviated to 4-4) groups and 8mm stroke length with 8mm per second sliding velocity (abbreviated to 8-8) groups. The control groups – no motion, consisted of pins subjected to loading only group (pins loaded under the same range of contact stresses as the study groups in short-term and long-term) and a group of pins stored in PBS (not subjected to loading or motion). Both control groups the cartilage thickness and cartilage permanent deformation were measured, to calculate the linear wear of the study groups.

Table 3.1 The measurements of study groups and control groups.

Groups	**Study Groups - Motion & Loading**			**Control Groups - No Motion**			
	Loading with Reciprocating Motion			*Loading Only*		*No Loading*	
Measurements (n=6)	*Friction Coefficient*	*Cartilage Thickness*	*Cartilage Deformation*	*Cartilage Thickness*	*Cartilage Deformation*	*Cartilage Thickness*	*Cartilage Deformation*
			Cartilage Wear				

Seven groups in total were tested in this study and the definition of each group is given in Table 3.2.

Friction data was collected in the following way:

1. Short-term friction studies: data was recorded once every 15 seconds during the first 5 minutes, and then once every 5 minutes to one hour.

2. Long-term friction studies: after the initial first hour friction test, data was collected once every 15 minutes.

Table 3.2 Definition of seven tested groups

No	Group Name	Definition
1	Control UL	Control unloaded group
2	Control L	Control loaded group
3	4-4 1hour	4mm stroke length with 4mm/sec sliding velocity short-term study
4	4-4 24hours	4mm stroke length with 4mm/sec sliding velocity long-term study
5	8-8 1hour	8mm stroke length with 8mm/sec sliding velocity short-term study
6	8-8 24hrs	8mm stroke length with 8mm/sec sliding velocity long-term study
7	4-4 3.5MPa 24hrs	4mm stroke length with 4mm/sec sliding velocity under 3.5MPa contact stress long-term study

The mean coefficient of friction (±95% confidence limits, n=6) was calculated for each condition throughout the test, and statistical comparison was carried out using p value ($p < 0.05$) and minimum significant difference 95% confidence limits at selected time points. The coefficient of friction (μ_{eff}) and frictional shear stress (SS) were calculated, as described in Section 2.2.2.1.2.

The cartilage thickness of the osteochrondral pins was measured using a Nikon profile projector (Nikon V-16 D, resolution 1 μm) at 10 times magnification, as described in Section 2.2.2.2. Additionally, the pin height was measured at the central point on the pin surface before and 24 hours after friction test or control loading test (this was done in air) using a digital height gauge, as described in Section 2.2.2.3. It was assumed that there was no permanent change in the bone height during the test and recovery. Both the cartilage thickness and cartilage pin height were measured three times per specimen, and the mean value of the measurements was used. The cartilage pin height change percentage to the cartilage thickness was calculated using Equation 3-1.

$$\%HC = \frac{H_{before} - H_{24hrs-after}}{CT} \times 100 \qquad \text{Equation 3-1}$$

Where, $\%HC$ is the cartilage pin height change percentage, CT is the cartilage thickness, H_{before} is the cartilage pin height before the friction test or control loading test, and $H_{24hrs-after}$ is the cartilage pin height 24 hours after the friction test or control loading test (during the 24 hours the cartilage pins were recovered in PBS lubricant).

During reciprocating friction tests, the cartilage pin height change would be due to linear wear (material loss) and also the permanent deformation of cartilage due to the loading. Any changes in the height of the control loading pins were considered to be the permanent deformation therefore the height change difference between the control loading pins and study pins was considered to represent linear wear. The cartilage linear wear percentage to the cartilage thickness ($\%W_{Linear}$) was calculated from the height change percentage difference between the study groups and control groups, as given in Equation 3-2 (Figure 3.2).

$$\%W_{Linear} = \%HC_{reciprocating} - \%HC_{control} \qquad \text{Equation 3-2}$$

Where, $\%W_{Linear}$ is the linear wear percentage to the original cartilage thickness, $\%HC_{reciprocating}$ is the cartilage height change percentage to the original cartilage thickness due to the reciprocating motion, and $\%HC_{control}$ is the cartilage permanent height change percentage to the original cartilage thickness due to loading only.

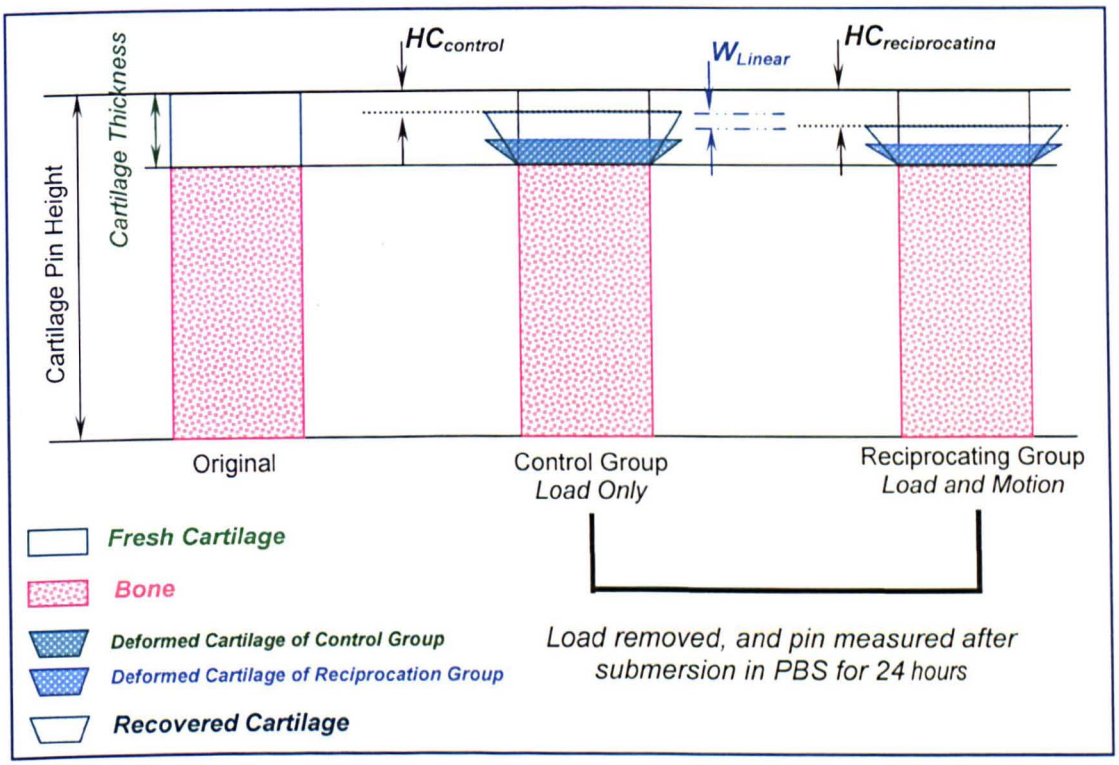

Figure 3.2 Cartilage pin height change (permanent deformation) and linear wear

The mean cartilage pin height change percentage and cartilage linear wear percentage (±95% confidence limits, n=6) were calculated for each test condition throughout the test, and statistical comparison was carried out using Arcsine ANOVA and minimum significant difference at each test conditions.

Studies were conducted at room temperature (20±2°C) under a variety of contact conditions under constant loading (Table 3.3, 3.4, and 3.5).

The study groups were cartilage pins 9mm and 4mm in diameter which were used to provide contact stress conditions from 0.5 to 16MPa. The load was applied for one hour and 24 hours and friction determined as a function of time. Pins were studied under 4-4 (4mm stroke length with 4mm/sec sliding velocity), and 8-8 (8mm stroke length with 8mm/sec sliding velocity). The friction coefficient was analysed as a function of loading time for different contact stresses and different sliding conditions (Table 3.3).

Table 3.3 Loading, contact stress, and sliding conditions for the study to assess the contact stress effect on friction (group: 4-4-1hour, 4-4-24hours, 8-8-1hour, and 8-8-24hours, explained in Table 3.2)

Cartilage Pin Diameter (mm)		9			4			
Applied Load (N)		35	64	127	50	100	150	200
Contact Stress	level	Low			Medium		High	
	(MPa)	0.5	1	2	4	8	12	16
N		6						
Reciprocating Condition		4-4 and 8-8						

The control groups were cartilage pins with no motion and with the same range of contact stress levels from 0.5 to 8 MPa applied (Table 3.4).

Table 3.4 Loading and contact stress conditions of the control group for the deformation study (Control no loading, and control loading groups)

Cartilage Pin Diameter (mm)	9				4				
Applied Load (N)	0	35	64	127	0	50	100	150	200
Contact Stress (MPa)	0	0.5	1	2	0	4	8	12	16
N	6								
Reciprocating Condition	None								

Due to the loading limit of the pin-on-plate apparatus, smaller diameter cartilage pins (4mm) were used to attain the medium and high contact stress levels. Hence the effect of contact area on the coefficient of friction was also considered in comparing the coefficient of friction results of the different contact stress levels. Different diameters of cartilage pins (9mm and 4mm; n=9) were tested at the same contact stress (by applying different loads; Table 3.5) to investigate the effect of contact area on the friction. The coefficient of friction was analysed as a function of

loading time (24 hours) for different contact areas with different loading under the same contact stress level.

Table 3.5 Loading, contact stress, and sliding conditions for the contact area effect to the friction study (4-4-3.5MPa 24 hours group, explained in Table 3.2)

Cartilage Pin Diameter (mm)	9	4
Applied Load (N)	220	44
Contact Stress (MPa)	3.5	
N	9	
Reciprocating Condition	4-4	

3.4 Results

3.4.1 Effect of Contact Stress on Cartilage Friction Deformation and Wear

3.4.1.1 Cartilage Deformation in PBS – Control No Loading Study

In the control unloaded groups, two groups of 12 cartilage pins (diameters 4mm and 9mm, n=6 per group) were kept in PBS at 20±2°C for 48 hours. The height changes were measured at 1 hour, 24, and 48hours. It was found that: there was no significant cartilage deformation (i.e. cartilage pin height change) when measured at 1 hour, 24, and 48 hours time period in each group (n=6, Arcsine ANOVA, $p<0.05$). The cartilage thickness was not influenced by being immersed in PBS fluid in 48 hours at room temperature.

3.4.1.2 Cartilage Deformation in Control Loading Study

Control loaded groups with no motion were studied in both short-term (1 hour) and long-term (24 hours) loading under a range of contact stress levels (from 0.5 to 16MPa). After loading the cartilage pins were immersed in PBS for 24 hours to allow recovery the elastic deformation, the cartilage permanent deformation (i.e. cartilage height change $HC_{control}$) was calculated through the cartilage pin height change, and results are presented as the percentage of cartilage thickness ($\%HC_{control}$) shown in Figure 3.3.

It is shown that there was no significant permanent cartilage height change after loading following all (low, medium, and high) contact stress levels for both short-term (one hour) and long-term (24 hours) loading (n=6, ANOVA Arcsine, $p<0.05$).

3.4.1.3 Reciprocating Study – Short-term

Group 4-4 (4mm stroke length with 4mm/sec sliding velocity) was studied, to investigate the effect of contact stress and loading time on cartilage friction, deformation, and wear. Contact stresses ranging from 0.5 to 16 MPa were applied in short-term (1 hour) and long-term (24 hours) loaded reciprocating tests.

3.4.1.3.1 Coefficient of Friction

In 4-4 short-term studies, the coefficient of friction when cartilage pins reciprocated on metal plates under different contact stresses from 0.5 to 16 MPa is shown in Figure 3.4 for the first five minutes of testing, and in Figure 3.5 for the first one hour of testing.

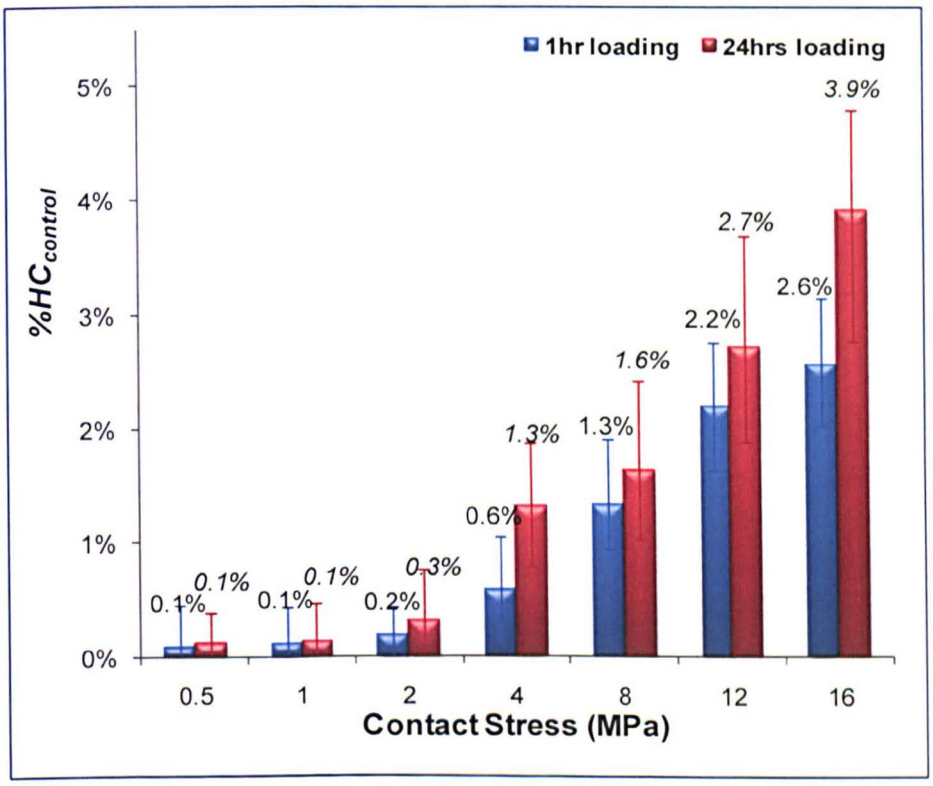

Figure 3.3 The cartilage height change in 1 hour and 24 hours loading control groups, n=6, mean±95% confidence limits.

The coefficient of friction increased rapidly in the first 20 minutes loading, then increased gradually as shown in Figure 3.5. The coefficient of friction was significantly lower under contact stresses of 1 and 2 MPa compared to under contact stresses of 0.5, 4, 8, 12, and 16MPa in the first 40 minutes loading (n=6, ANOVA, $p<0.05$). There was no significant difference in the coefficient of friction among tests carried out with contact stresses of 0.5, 4, 8, 12, and 16MPa during

one hour loading, and between contact stresses of 1 and 2 MPa (n=6, ANOVA, $p<0.05$).

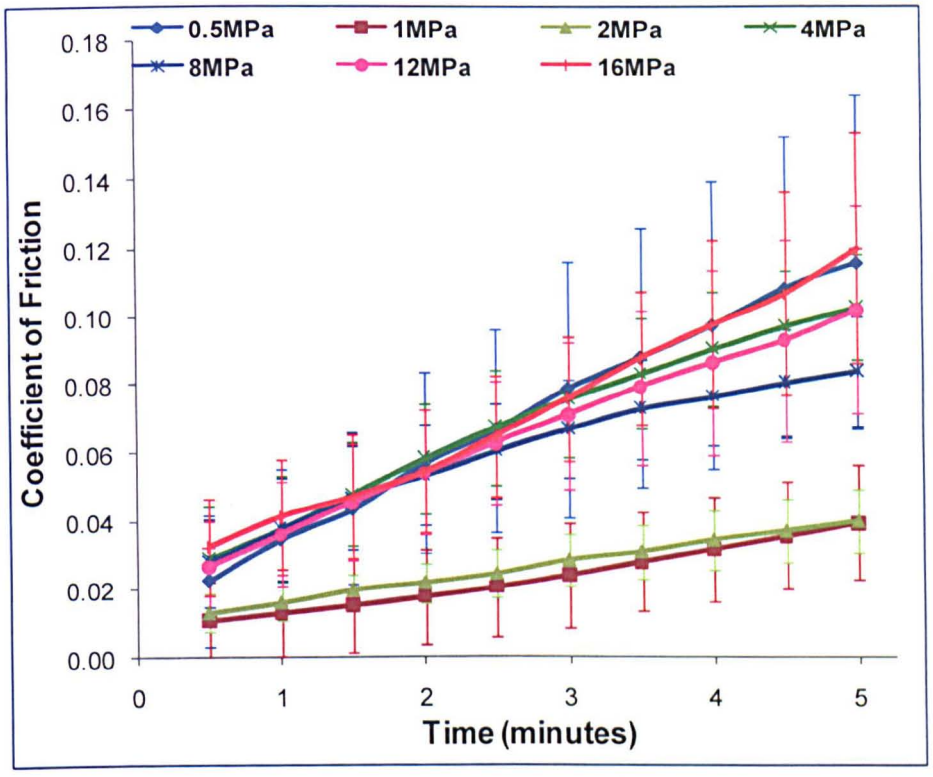

Figure 3.4. The coefficient of friction in the first 5 minutes loading (from 0.5 to 16 MPa) in 4-4, n=6, mean ± 95% confidence limits.

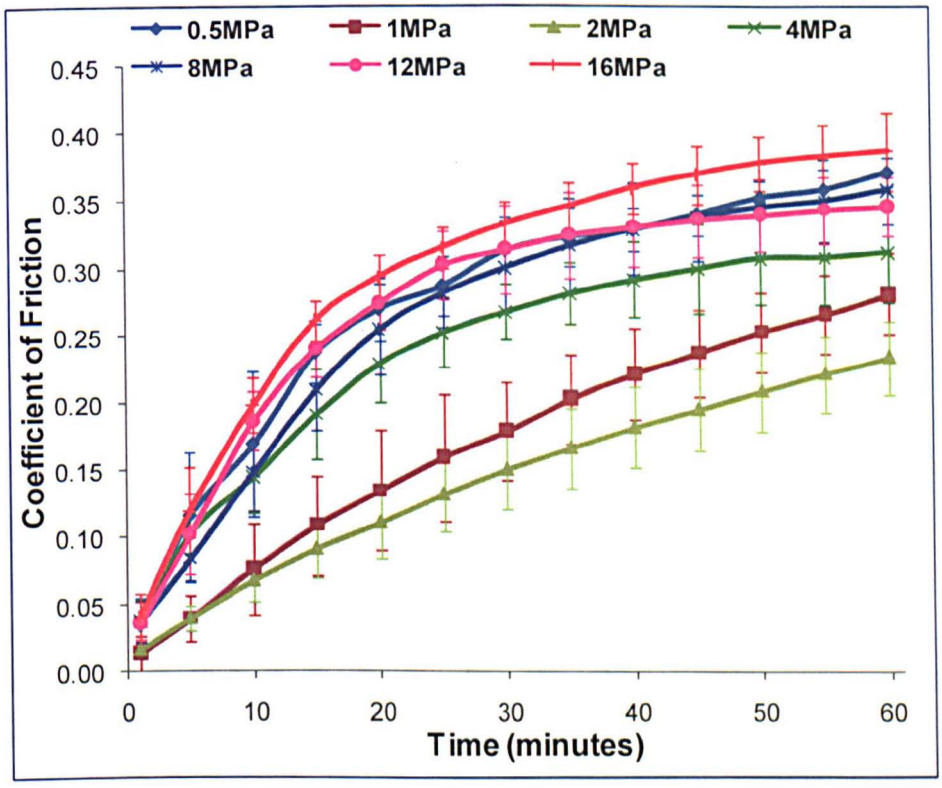

Figure 3.5. The coefficient of friction in one hour loading (from 0.5 to 16 MPa) in 4-4 group, n=6, mean ± 95% confidence limits.

3.4.1.3.2 Frictional Shear Stress

The frictional shear stress was calculated to investigate the correlation to the contact stress levels and time. The frictional shear stress result in group 4-4 short-term reciprocating study is shown in Figure 3.6. After 5 minutes loading, the frictional shear stress increased significantly when contact stress increased from 4 MPa to 16MPa (n=6, mean).

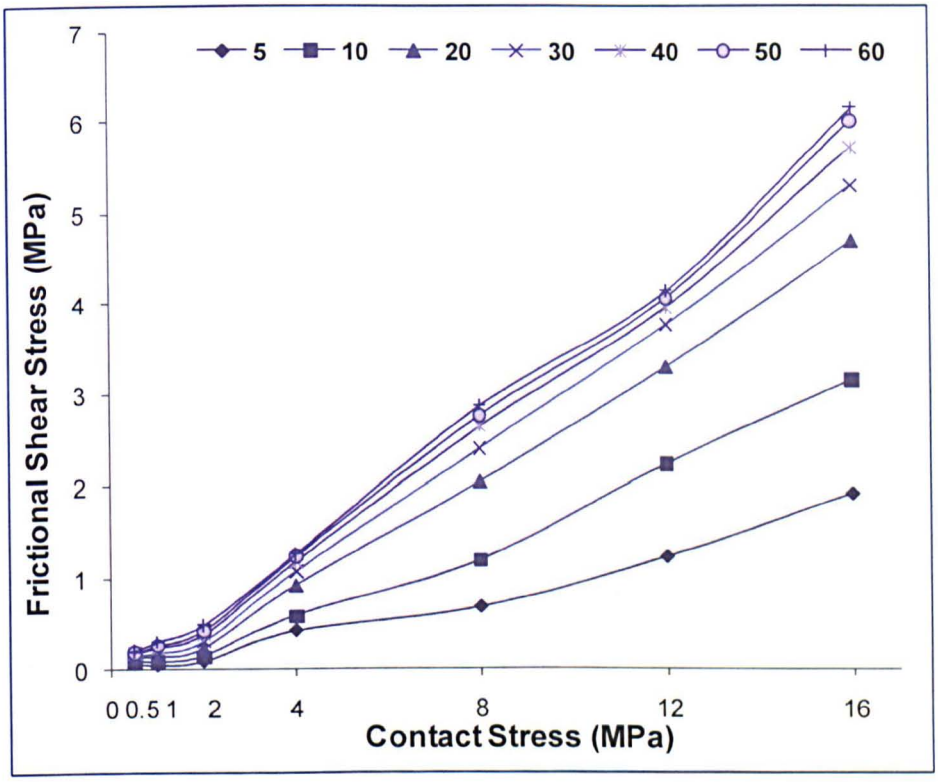

Figure 3.6. The average frictional shear stress vs. contact stress in one hour reciprocating loading group 4-4, mean, n=6.

3.4.1.4 Reciprocating Study – Long-term

3.4.1.4.1 Coefficient of Friction

In long-term (24 hours) friction study, with 4-4 reciprocating motion the coefficient of friction under different contact stress levels (from 0.5 to 16MPa) was measured and it is shown in Figure 3.7. The coefficient of friction kept increasing until approximately 4 hours of loading under all contact stress levels. Then:

Under low contact stress levels (0.5, 1, and 2 MPa), the coefficient of friction remained at approximately 0.4 from 4 hours loading until 24 hours loading. The coefficient of friction was not significantly different between contact stresses of 0.5

and 1 MPa from 4 to 24 hours loading, but it was significantly higher than under 2 MPa contact stress (n=6, ANOVA, $p<0.05$).

Under medium contact stress levels (4, and 8MPa), the coefficient of friction kept increasing after 4 hours until 24 hours loading. Under contact stress of 8 MPa, the coefficient of friction was significantly higher than contact stress of 0.5, 1, 2, and 4 MPa from 14 to 24 hours loading, and severe cartilage damage was observed when 24 hours testing completed. After 24 hours loading, the coefficient of friction for stress levels of between 0.5 to 4 MPa converged to a similar value of approximately 0.4 (n=6, ANOVA, $p<0.05$).

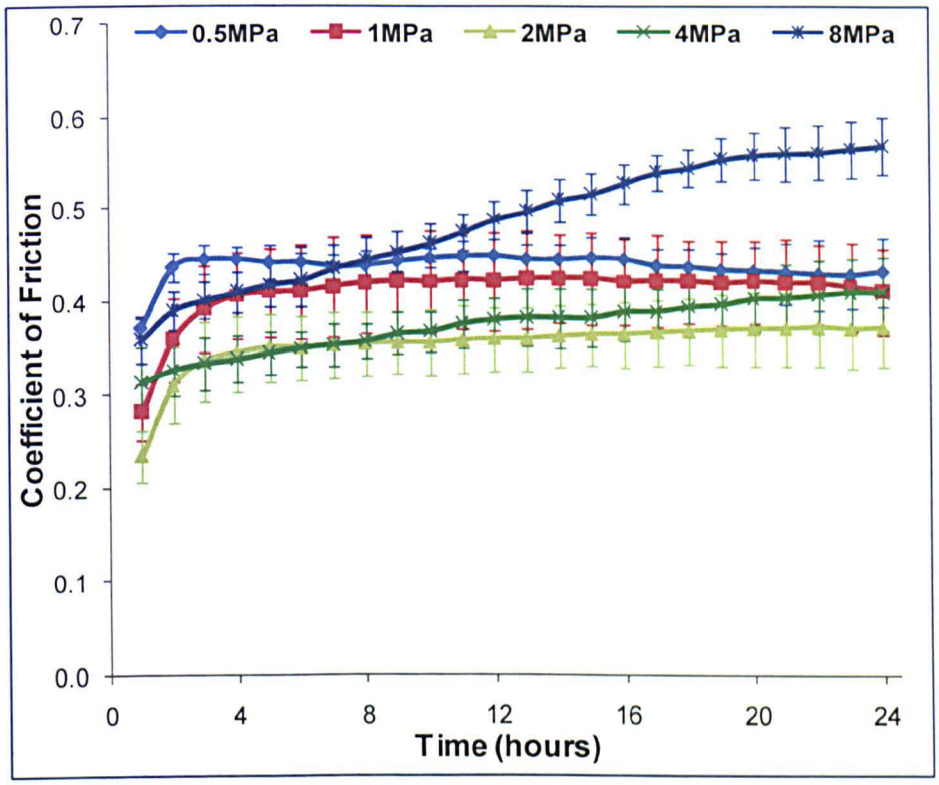

Figure 3.7. The coefficient of friction in 24 hours reciprocating loading 4-4 group from 0.5 to 16, n=6, mean ± 95% confidence limits.

3.4.1.4.2 Frictional Shear Stress

Catastrophic wear and damage to cartilage occurred after over one hour continuous loading and sliding with 12 MPa contact stress which corresponded to a peak frictional shear stress of 4.14 MPa and loading time of over one hour (Figure 3.8) (n=6, mean).

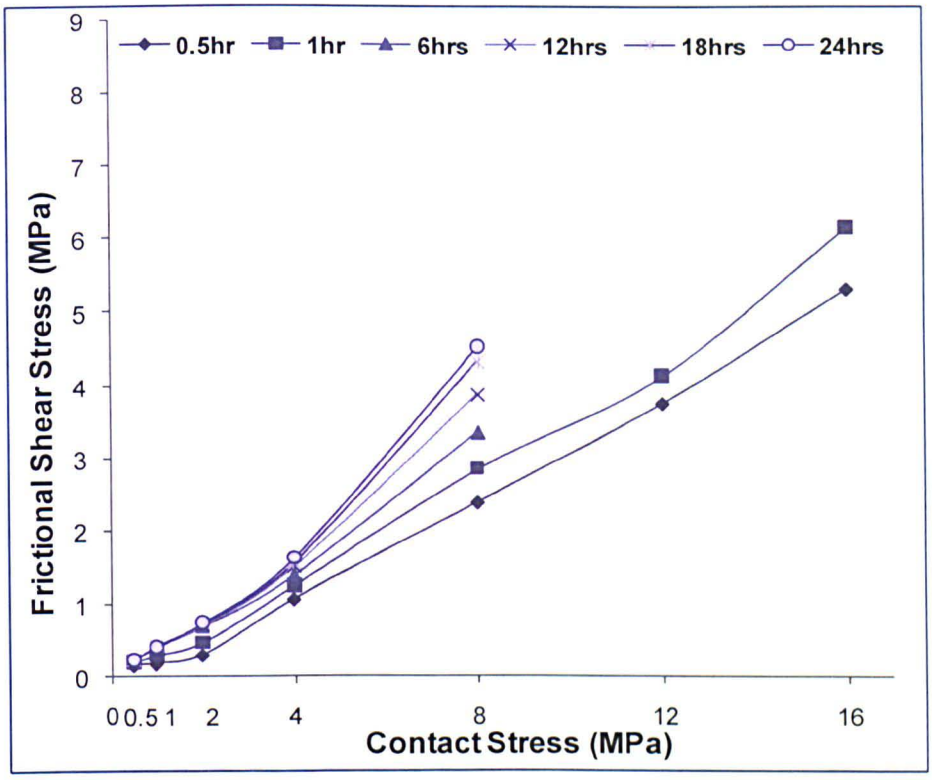

Figure 3.8. Comparison of the frictional shear stress and contact stress at 0.5, 1, 6, 12, 18, and 24 hours time points in 4-4 reciprocating group.

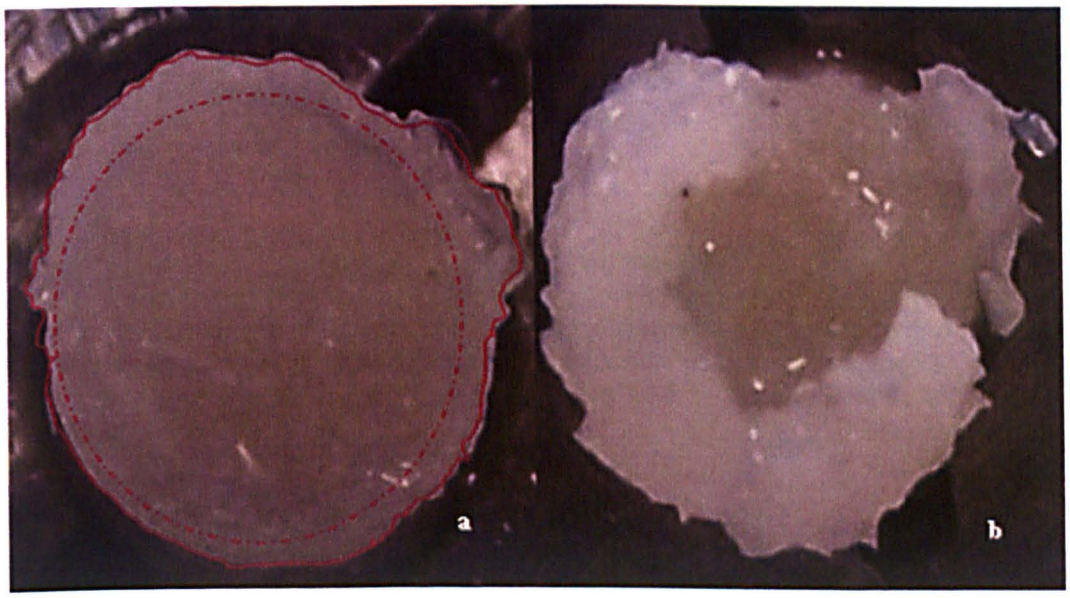

Figure 3.9 a. a typical deformed cartilage after long-term reciprocation and loading; b. "mushroom effect" of cartilage damage - a typical catastrophic damage

The catastrophic wear and damage to cartilage occurred when a threshold for frictional shear stress and time was reached, above this level and over continued loading time, the cartilage matrix becomes increasingly damaged. At these limits, a "mushroom effect" where the cartilage was "spread" about the end of the pin was observed as it was compressed and increasingly damaged. The images of typical deformed cartilage and "mushroom effect" of cartilage are shown in Figure 3.9.

3.4.1.4.3 Cartilage Height Change

The cartilage height change following 24 hours of reciprocating motion study under low and medium contact stress levels is shown in Figure 3.10. It was found that there was no significant difference in height change of cartilage when pins subjected to 0.5 and 1 MPa were compared; however, pins subjected to 2, 4, and 8 MPa showed a significant increase height change at each increment (n=6, ANOVA, $p<0.05$).

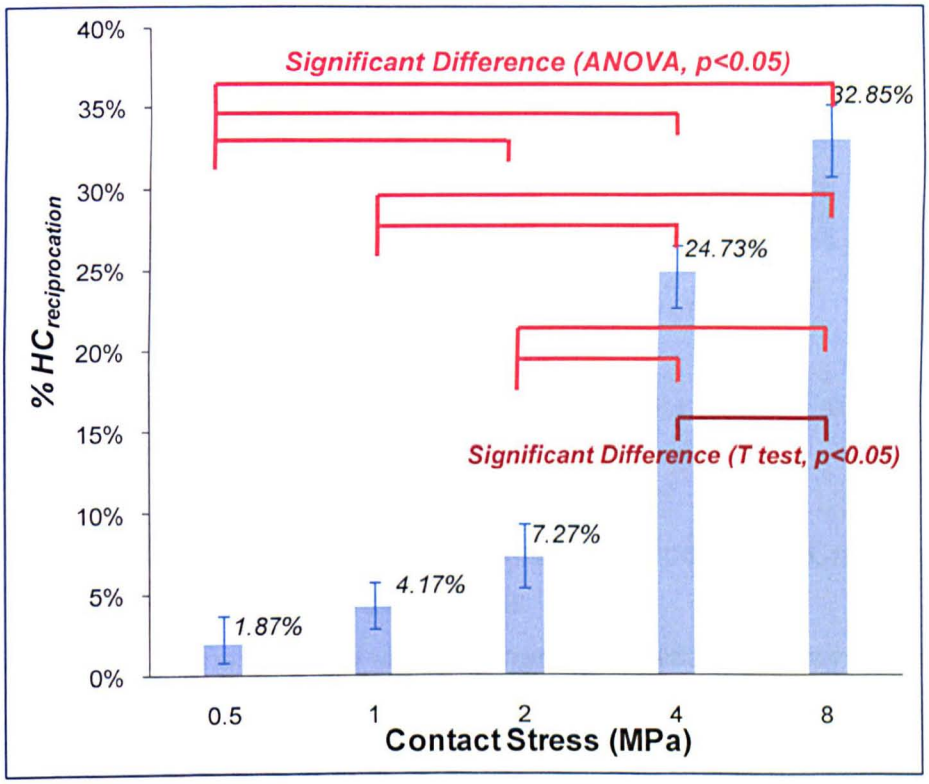

Figure 3.10 Cartilage permanent height change percentage (permanent deformation percentage) in control 24 hours loading group and reciprocating motion 24 hours loading group under different contact stresses (0.5 ~ 16 MPa), n=6, mean ± 95% confidence limits.

3.4.1.4.4 Cartilage Linear Wear

The cartilage linear wear following reciprocating motion is shown in Figure 3.11. It was found that cartilage linear wear increased significantly when pins tested at 0.5 and 2 MPa were compared. Significant increases in wear were noted at each increment above 2 MPa (n=6, ANOVA, $p<0.05$).

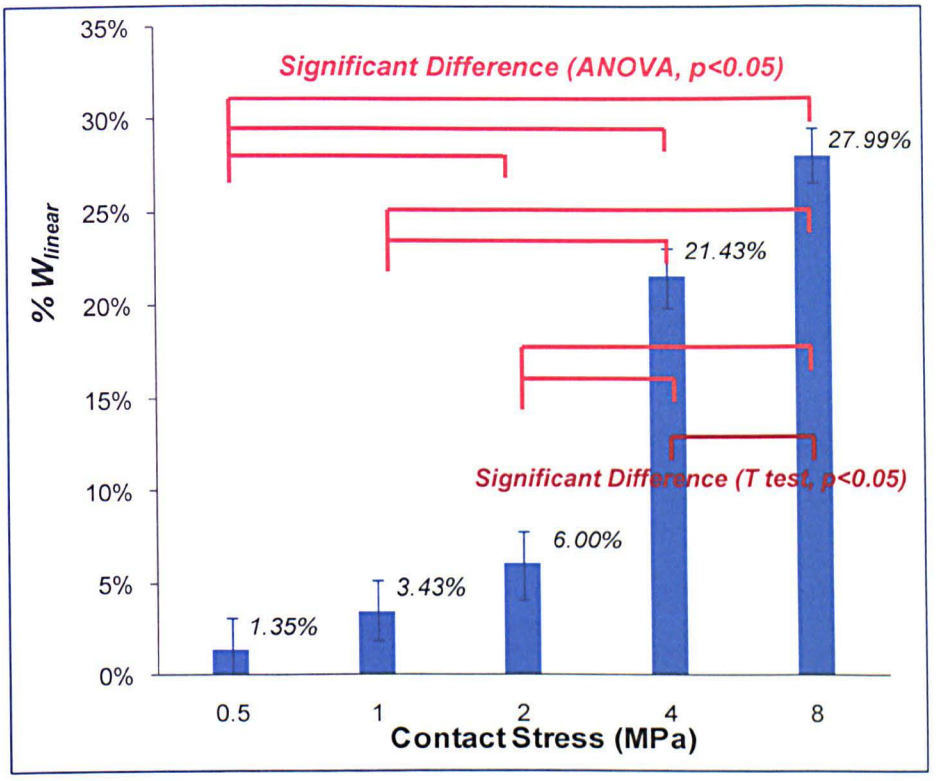

Figure 3.11 Cartilage linear wear percentage following 24 hours loading and reciprocating motion study group under different contact stresses (0.5 ~ 16 MPa), n=6, mean ± 95% confidence limits.

3.4.2 Effect of Stroke Length and Sliding Velocity on Cartilage Friction Deformation and Wear

To investigate the effect of stroke length and sliding velocity on cartilage friction, deformation, and wear another group of tests were compared with an 8mm stroke length and 8mm/sec sliding velocity (termed 8-8). In 8-8 group, contact stress ranging from 0.5 to 16 MPa were applied in short-term (1 hour) and long-term (24 hours) reciprocating tests to compare to the result of 4-4 (4mm stroke length with 4mm/sec sliding velocity as described in Section 3.4.1).

3.4.2.1 Short-term Study Comparison

3.4.2.1.1 Coefficient of Friction

Comparisons of the coefficient of friction in short-term tests under different levels of contact stress (low, medium, and high) in both 4-4 and 8-8 reciprocating groups are shown in Figure 3.12, 3.13, and 3.14 respectively.

Under low levels of contact stresses (0.5, 1, and 2 MPa, Figure 3.12) between different motion reciprocating groups, it was found that there was no significant difference in the coefficient of friction between 4-4 and 8-8 groups under the same low levels of contact stress (n=6, ANOVA, $p<0.05$).

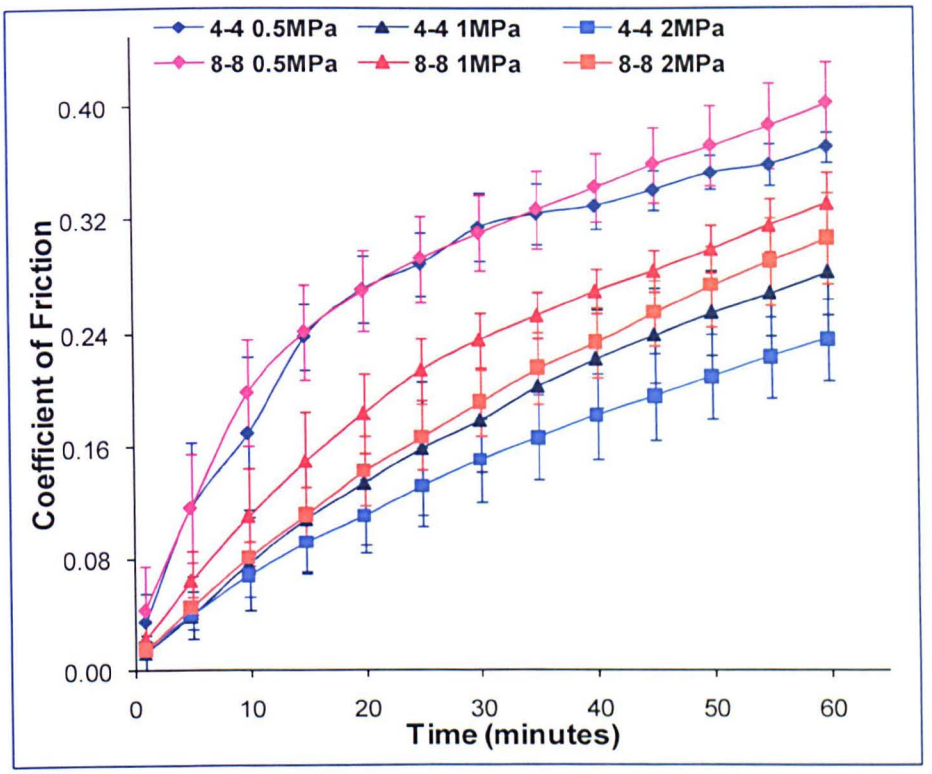

Figure 3.12. Comparison of the coefficient of friction under low contact stress levels (0.5, 1, and 2 MPa) in the short-term study for 4-4 and 8-8 reciprocating groups, n=6, mean ± 95% confidence limits.

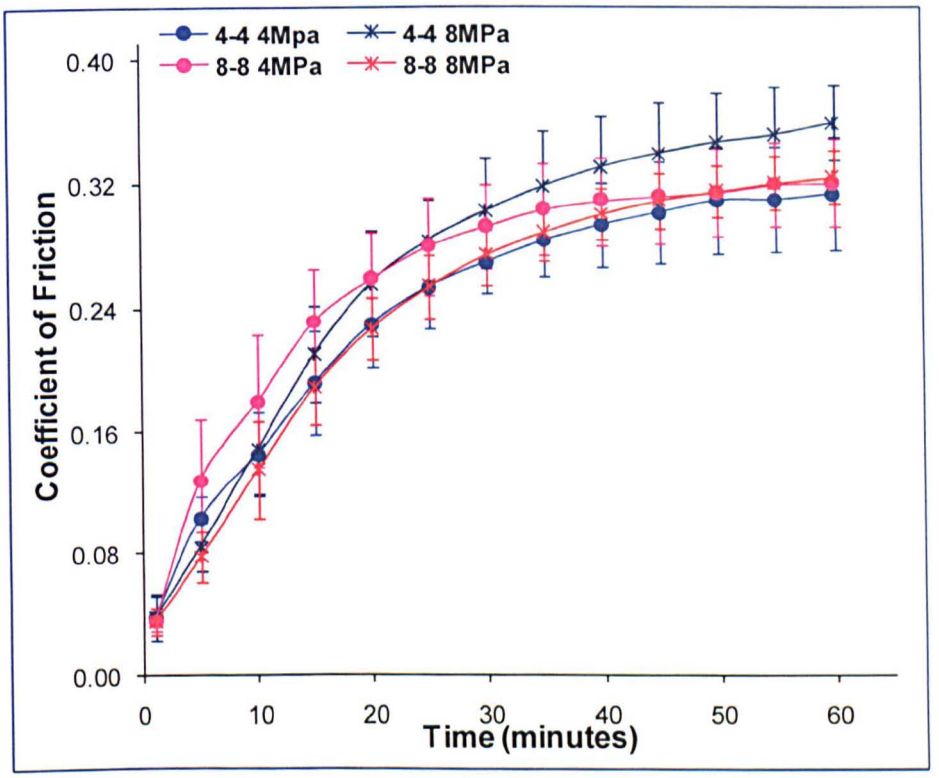

Figure 3.13. Comparison of the coefficient of friction under medium contact stress levels 4, and 8 MPa) in the short-term study for 4-4 and 8-8 reciprocating groups, n=6, mean ± 95% confidence limits.

Under medium levels of contact stresses (4, and 8 MPa, Figure 3.13), between different motion reciprocating groups, no significant difference in the coefficient of friction between 4-4 and 8-8 groups was observed (n=6, ANOVA, $p<0.05$).

Under high levels of contact stresses (12, and 16 MPa, Figure 3.14), between different motion reciprocating groups, there was no significant difference of the coefficient of friction between 4-4 and 8-8 groups (n=6, ANOVA, $p<0.05$).

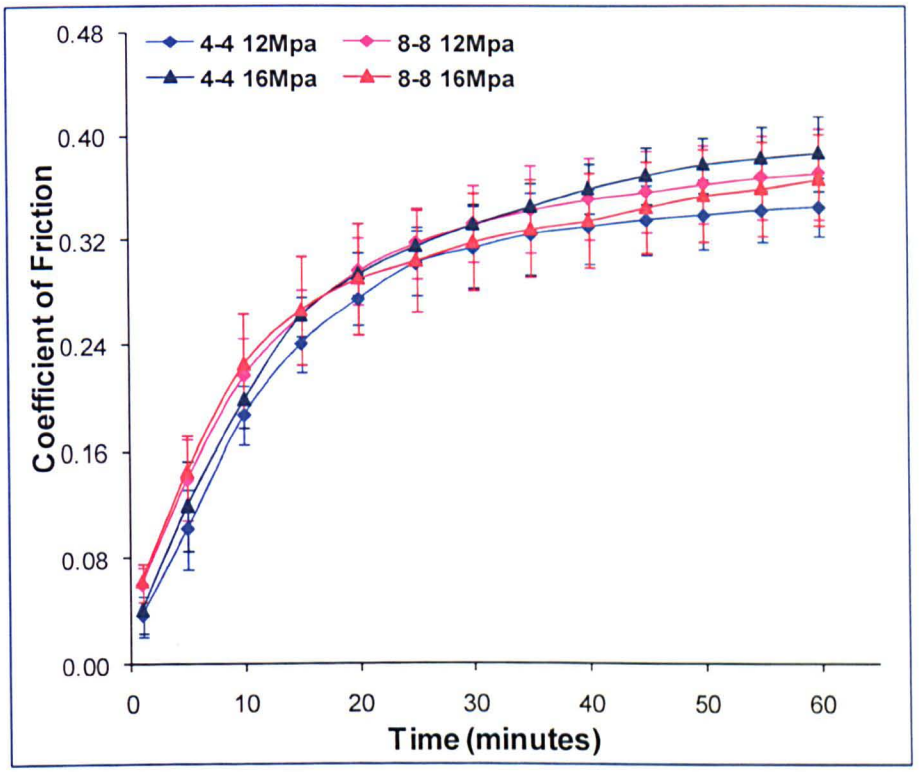

Figure 3.14. Comparison of the coefficient of friction under high contact stress levels (12, and 16 MPa) in the short-term study for 4-4 and 8-8 reciprocating groups, n=6, mean ± 95% confidence limits.

3.4.2.1.2 Frictional Shear Stress

No significant difference of frictional shear stress was observed in the reciprocating groups of 4-4 and 8-8 under the same level of contact stresses at a range from 0.5 to 16 MPa in short-term study.

3.4.2.2 Long-term Study Comparison

3.4.2.2.1 Coefficient of Friction

The comparisons of the coefficient of friction in long-term study under low and medium levels of contact stresses in both 4-4 and 8-8 reciprocating groups are shown in Figure 3.15, and 3.16 respectively.

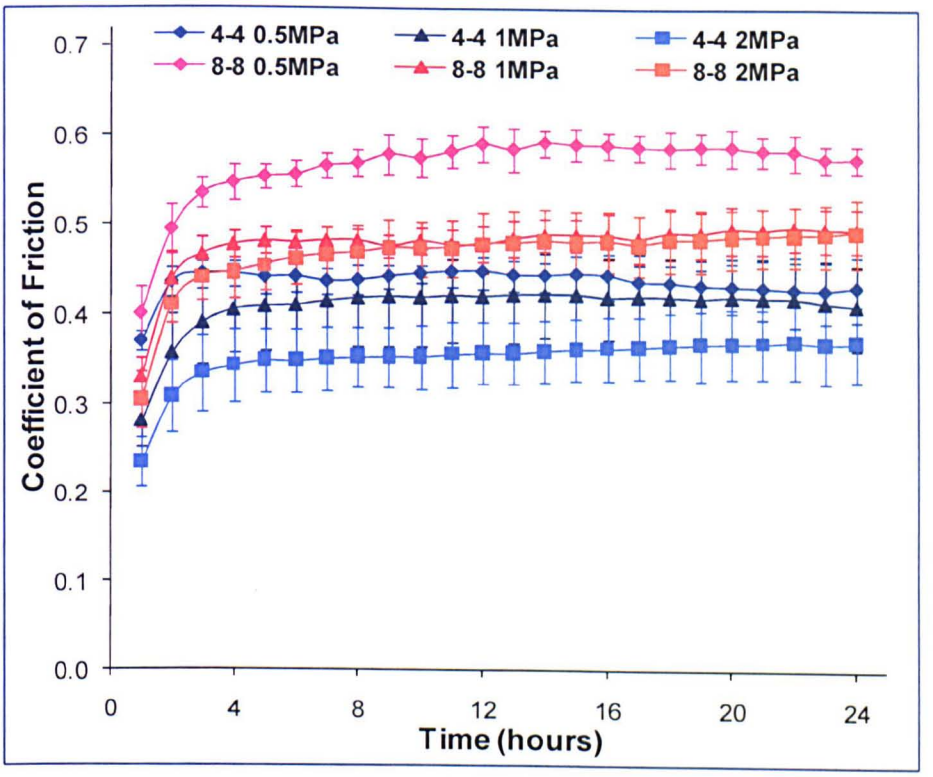

Figure 3.15 Comparison of the coefficient of friction in 24 hours under low contact stress levels between 4-4 and 8-8 reciprocating groups, n=6, mean ± 95% confidence limits.

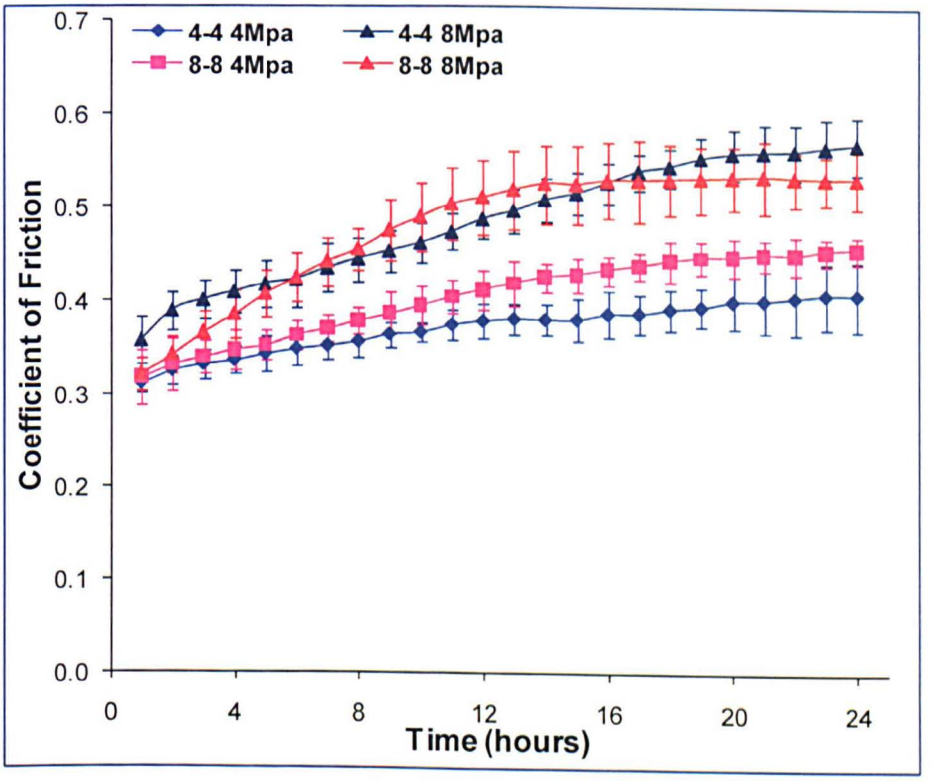

Figure 3.16 Comparison of the coefficient of friction in 24 hours under medium contact stress levels between 4-4 and 8-8 reciprocating groups, n=6, mean ± 95% confidence limits.

Under low level of contact stresses (0.5, 1, and 2 MPa, shown in Figure 3.15) between different reciprocating motion groups, it was found that there was significantly higher coefficient of friction in the group with longer stroke length and sliding velocity (8-8 group) (n=6, ANOVA, $p<0.05$).

Under medium levels of contact stresses (4, and 8 MPa, shown in Figure 3.16) between different reciprocating motion groups, no significant difference of the coefficient of friction between 4-4 and 8-8 groups was observed (n=6, ANOVA, $p<0.05$).

At 24 hours loading and reciprocating time point, the coefficient of friction under low and medium contact stresses of both 4-4 and 8-8 groups is shown in Figure 3.17. It was found significantly higher coefficient of friction in 8-8 group under low level of contact stresses compared to 4-4 group, but no significant difference under medium contact stresses between these two groups.

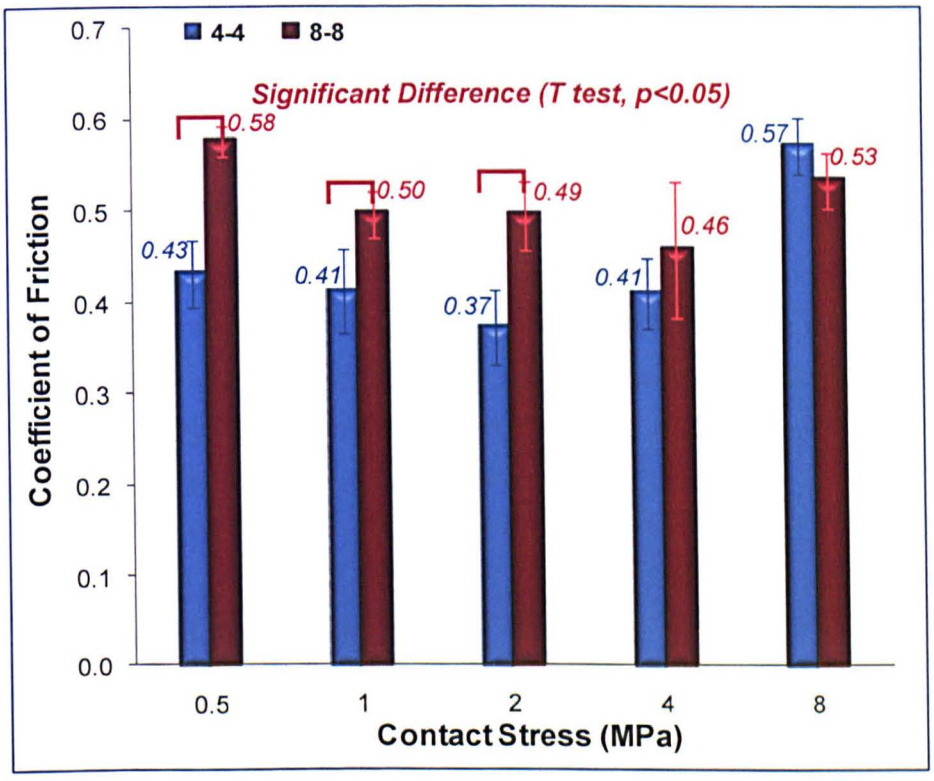

Figure 3.17 Comparison of coefficient of friction at 24 hours loading time point between two 4-4 and 8-8 reciprocating groups, n=6, mean ± 95% confidence limits.

3.4.2.2.2 Frictional Shear Stress

No significant difference of frictional shear stress was observed in the reciprocating groups of 4-4 and 8-8 under the same level of contact stresses at a range from 0.5 to 8 MPa in long-term study comparing Figure 3.18 (8-8 group), and Figure 3.10 (4-4 group).

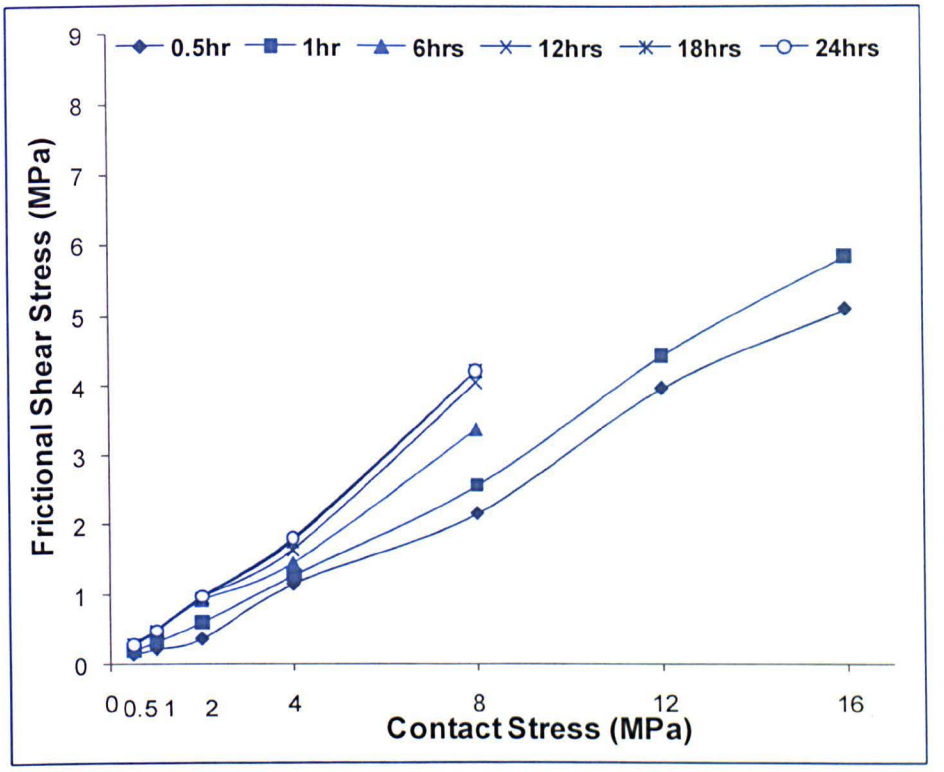

Figure 3.18. Comparison of the frictional shear stress and contact stress at 0.5, 1, 6, 12, 18, and 24 hours time points in 8-8 reciprocating group.

3.4.2.2.3 Cartilage Height Change

When the cartilage height change in 4-4 and 8-8 groups in long-term study was compared (Figure 3.19), it was found that under low and medium contact stresses, levels, the longer stroke length with increased sliding velocity (8-8 group) produced significantly higher cartilage height change at the same contact stress level than group 4-4 at 0.5, 1, 2, 4, and 8 MPa.

3.4.2.2.4 Cartilage Linear Wear

The cartilage linear wear in the reciprocating groups of 4-4 and 8-8 in long-term study was compared (Figure 3.20). It was found that the longer stroke length with increased sliding velocity (group 8-8) produced significantly higher linear wear than group 4-4.

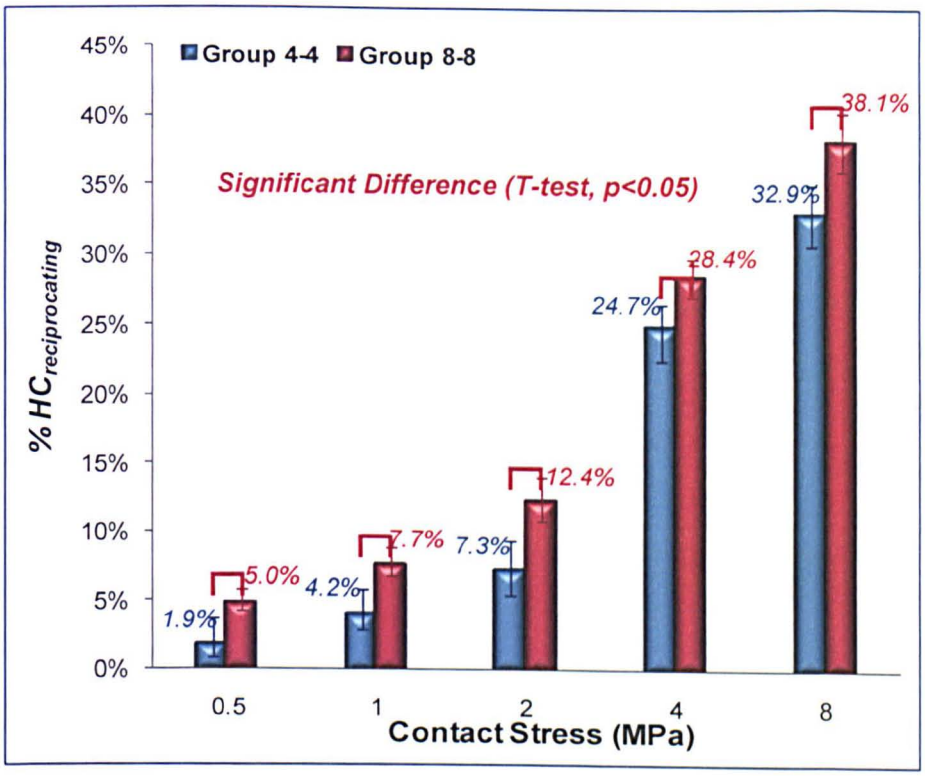

Figure 3.19 Comparison of the cartilage permanent height change in long-term study between 4-4 and 8-8 groups under a range of contact stresses (from 0.5 to 8 MPa), n=6, mean ± 95% confidence limits.

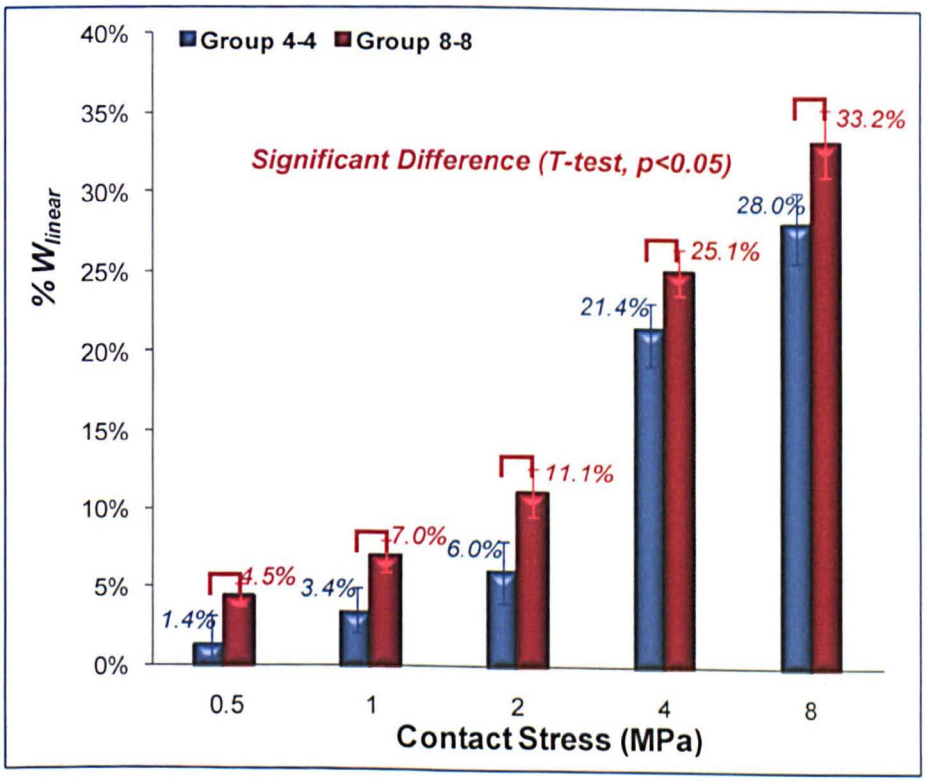

Figure 3.20 Comparison of the cartilage linear wear in long-term study between two reciprocating 4-4 and 8-8 groups under different contact stresses (0.5 ~ 8 MPa), n=6, mean ± 95% confidence limits

3.4.3 Effect of Contact Area and Load on Cartilage Friction

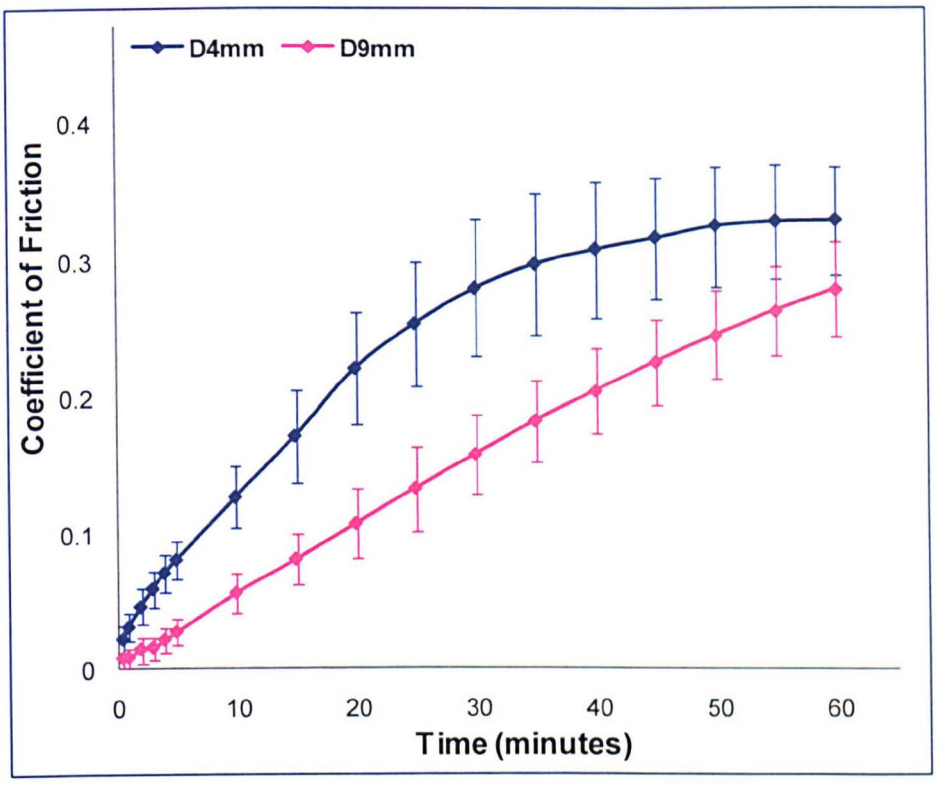

Figure 3.21. Comparison of the coefficient of friction under the same contact stress of 3.5 MPa in one hour reciprocating and loading, with diameter 4mm, and 9mm cartilage pins, n=6, mean ± 95% confidence limits.

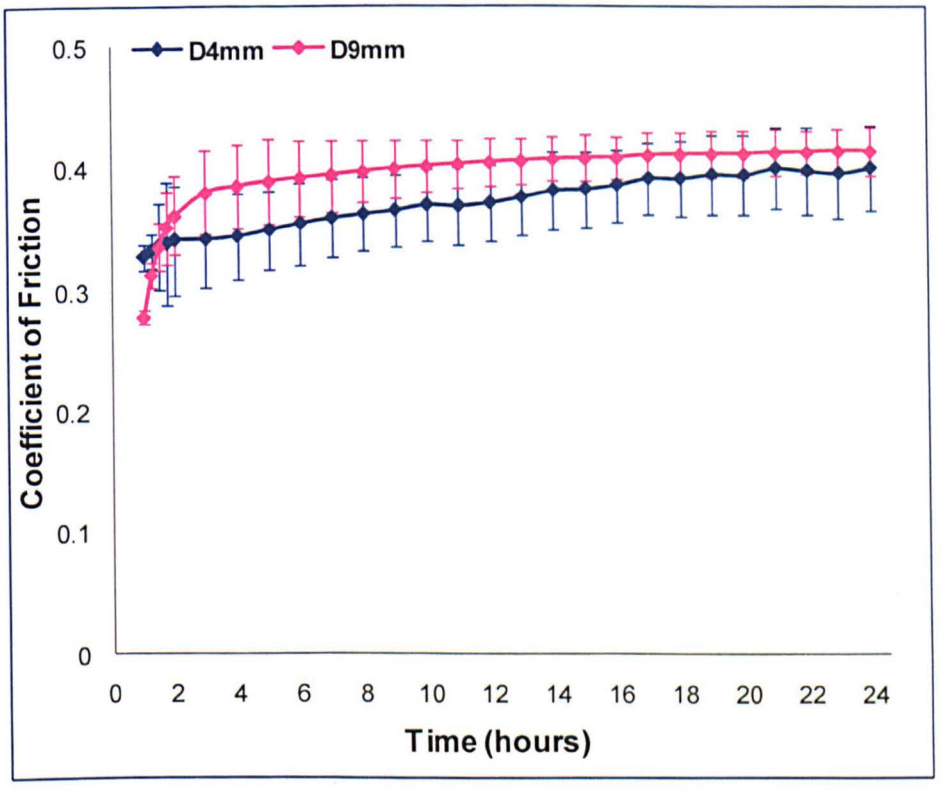

Figure 3.22. Comparison of the coefficient of friction under the same contact stress of 3.5 MPa from 1 hour to 24 hours reciprocating and loading, with diameter 4mm, and 9mm cartilage pins, n=6, mean ± 95% confidence limits.

Under the same contact stress (3.5MPa), the smaller contact area with lower load (4mm diameter cartilage pin with 44N loading) generated a significantly higher coefficient of friction in the first one hour of loading compared to 9mm diameter cartilage pins with 220N loading (n=9, ANOVA $p<0.05$) (Figure 3.21). Between 2 and 24 hours the coefficient of friction for the different diameters was not significantly different (n=9, ANOVA $p<0.05$) (Figure 3.22).

3.5 Discussion

Hip hemiarthroplasty has been queried as a procedure that may lead to cartilage degeneration. However, it has been clinically used for many decades and provides relatively good outcomes. The contact problem between cartilage and metals is very complex when addressed from a bioengineering perspective. In this case, the mechanobiology of the tissue and cell response also play an important role on the mechanism and cartilage tribology properties especially in the long-term study. However, this study mimicked simple hemiarthroplasty condition *in-vitro* to focus on the examination of the effects of mechanical factors on cartilage friction and wear. Results were compared with the main mechanical factors effects. However, this study did not consider the additional mixed effects of biological factors and cartilage degeneration in PBS at 20±2°C. This study has demonstrated under medium and high contact stress (4, 8, 12 and 16 MPa) in short-term (1 hour), and under contact stress from 0.5 to 8 MPa in the long-term (24 hours) cartilage tribological properties studies in a simple hemiarthroplasty set-up *in-vitro*, which others have not done in this area.

This study has used cartilage pins reciprocating against metal plates to assess the long-term effect of (1) contact stress levels and loading time; (2) contact area and load; (3) stroke length and sliding velocity; on the coefficient of friction, cartilage wear, degradation and cartilage recovery following reciprocal motion under load.

3.5.1 Effect of Contact Stress and Loading Time on Cartilage Friction Deformation and Wear

The coefficient of friction of cartilage on metal counterfaces is strongly affected by the contact stress and the loading time;

- The coefficient of friction, cartilage deformation, and cartilage wear did not increase proportionally with the increasing contact stress (Figure 3.4, 3.5, 3.9, and 3.11).
- The cartilage in a hemiarthroplasty pin on plate configuration was fully recovered under low contact stress levels (≤2 MPa) in both short-term and long-term (24 hours) constant loading with no motion (Figure 3.3).
- Loading only (with no motion) affected the cartilage permanent deformation under medium and high contact stress levels (>2 MPa) in both short-term and long-term loading. Under 16 MPa in 24 hours loading caused less than 5% permanent deformation of articular cartilage (Figure 3.3).
- Cartilage linear wear increased significantly under medium level of contact stresses (4 and 8 MPa) in long-term reciprocating loading (Figure 3.11).

The coefficient of friction increased with loading time during the first one to two hours loading for all contact conditions. This is in agreement with data previously reported (Forster and Fisher, 1996) and reflects the biphasic nature of cartilage. When the load is applied, initially the fluid phase of the cartilage is able to provide support, as the fluid is increasingly exuded from the cartilage; the load is transferred to the solid and fluid phase in equilibrium of the cartilage. After approximately one or two hours of loading and reciprocating motion most of the applied load is supported by the cartilage in its equilibrium state (solid and fluid phase). The increase in friction is then due to the solid phase interactions and the shearing between the contact surfaces.

For the short-term loading (Figure 3.5), the coefficient of friction reduced as the contact stress increased up to a value of 2 MPa and then subsequently increased as the contact stress increased to 16 MPa. The same trends of coefficient of friction changes have been reported in the previous studies in both experimental work (Pickard *et al.*, 1998a) (Figure 2.23) and computer modelling work on articular cartilage (Krishnan *et al.*, 2004b). This is due to the biphasic properties of cartilage; the load is transferred from the fluid phase of the cartilage to the equilibrium state of solid and fluid phase. Ateshian et al. (2003) have speculated the reduced friction in this case could be the flattening of surface roughness of articulating cartilage samples under load or the forces present between molecules on the cartilage surface (Ateshian *et al.*, 2003b). The drop of friction with increasing contact stress is generally known in compliant materials (Bowden, 1964; Gong and Osada, 2002; Katta *et al.*, 2008a). Hence, this decrease of friction could also be due to the boundary lubricant molecules with beneficial friction properties inherent

to cartilage, which are exuded into the contact zone between the articulating surfaces under loading. During this process, when low contact stresses 0.5, 1, and 2 MPa were applied with the same cartilage contact area (9mm diameter), the contact stress level contributed substantially to the deformation of effective lubricating surface between the cartilage surface and the metal plate. However, when the contact stress increased above 2 MPa (e.g. 4, 8, 12, and 16 MPa with the same contact area 4 mm diameter cartilage pins), due to the increasing contact stress the cartilage solid and fluid phase in equilibrium was carrying the load in all cases of the coefficient of friction increased with increasing contact stress. The contact stress range (0.5 – 2 MPa) for decreasing friction has been explored in this study, but from 2 MPa to 4 MPa the change of friction is not clearly identified in short-term loading due to the difference of sample sizes.

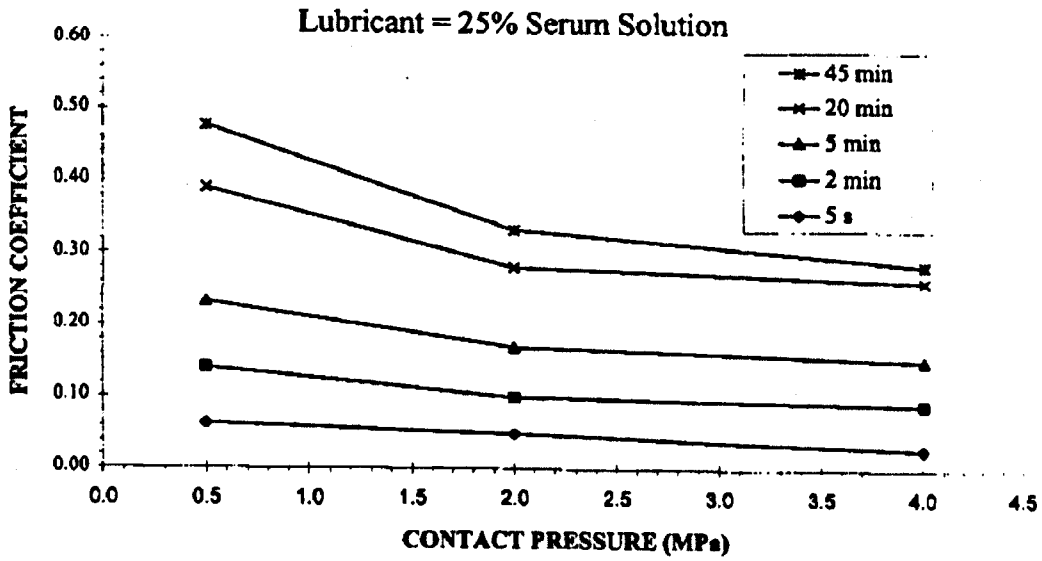

Figure 3.23. Coefficient of friction of bovine articular cartilage at different contact pressures plotted against loading time (Pickard *et al.*, 1998a).

In short-term reciprocation during the transmission of load support from a fully fluid phase into a solid and fluid phase in equilibrium, the cartilage friction was affected strongly by the contact stress at low levels. When the contact stress remained low (not more than 2 MPa), the velocity of fluid exuded from the cartilage increased with the increasing contact stress from 0.5 MPa to 1MPa till 2 MPa, hence reducing the friction. However, when the contact stress reached the medium level (4 and 8 MPa) and high level (12 and 16 MPa), the velocity of fluid exuded from the cartilage reached its limit, hence the friction of cartilage increased similarly with time under medium and high levels of contact stress.

For the long-term loading, the coefficient of friction reached a high terminal value of between 0.35 and 0.4 for stress levels of 0.5 to 4 MPa (Figure 3.7), however, for 8 MPa contact stress the coefficient of friction continued to rise and the cartilage was catastrophically damaged (Figure 3.9). When the contact stress was less and equal to 4 MPa, the cartilage linear wear remained less than 30% of the cartilage original thickness, we postulate that at this level the cartilage matrix was not damaged and that the frictional shear stress on the cartilage surface remained below a "damage threshold". When the higher contact stress 8 MPa was applied, the linear wear increased significantly (up to 38%), we postulate the increased frictional shear stress led to increased damage of the cartilage matrix hence the coefficient of friction continued to increase with time.

When the contact stress increased, the change in cartilage height of the reciprocating pins increased, attributed to increased linear wear. The control pins that were not subject to motion showed that when loaded at low contact stress levels approximately all deformation was recovered. At medium and high stress levels approximately 95% of deformation was recovered. This slight difference is thought to be due to increased cartilage matrix damage under medium contact stress levels. However, when pins were subjected to reciprocating motion, an increase in contact stress affected the cartilage height change significantly more due to the linear wear in addition to deformation. When sliding distance and velocity were greater (8-8 compared to 4-4) the amount of cartilage height change increased significantly, this was attributed to the linear wear.

Cartilage permanent deformation increased with the increasing contact stress, attributed to increased linear wear. The control pins that were not subject to motion showed that when loaded at low contact stress levels approximately all deformation was recovered. At medium and high stress levels approximately 95% of deformation was recovered. This slight difference is thought to be due to increased cartilage matrix damage under medium contact stress levels. However, when pins were subjected to reciprocating motion, an increase in contact stress affected the cartilage height change significantly more due to the linear wear in addition to deformation.

Catastrophic wear and damage to cartilage occurred after one hour continuous loading and sliding with 12 MPa contact stress which corresponded to a peak frictional shear stress of 4 MPa and loading time of over one hour. The catastrophic wear and damage to cartilage occurred when a threshold for frictional shear stress and time was reached, above this level and over continued loading time, the cartilage matrix became increasingly damaged. At these limits, a

"mushroom effect" where the cartilage was "spread" about the end of the pin as it was compressed and increasingly damaged was observed.

An interesting finding is there was no clear relationship between the cartilage friction and cartilage linear wear in these long-term reciprocating motion studies when the contact stress was not more than 4 MPa. This was due to the biphasic properties of cartilage mainly influencing the friction, whereas the contact stress levels strongly affected to the cartilage linear wear. However, under 8 MPa the coefficient of friction continued increasing with time and this may be due to the catastrophic damage of the articular cartilage during 24 hours reciprocating motion.

Physiologically the "mushroom effect" type of cartilage damage observed on the size of 4mm diameter cartilage pins in medium and high levels of contact stresses may not be entirely relevant. When the high contact stress was applied onto the cartilage plug (small surface), the cartilage tissue was "squeezed" to the edge area due to a lack of support from the surrounding tissue. However, in the human hip joint hemiarthroplasty is preformed, this is not the case. The whole acetabular cartilage would be fully supported by the surrounding bone and other tissue when high contact stress, cartilage would be deformed or broken. When high contact stresses cause a level of frictional shear stress which is above the "damage threshold", the cartilage might be "torn" or "broken" in the contact area instead responding in this "mushroom effect". Therefore, the size and shape of the cartilage plugs have influenced the catastrophic damage phenomenon of the articular cartilage. However, understanding the damage threshold of biological tissues is very complex and cannot be solely addressed from such a mechanical perspective. Biological degradation of the cartilage will also play an important role in such a threshold. However, investigation of this was beyond the scope of this study.

3.5.2 Effect of Stroke Length and Sliding Velocity on Cartilage Friction Deformation and Wear

The coefficient of friction, cartilage deformation and linear wear on metal counterfaces is affected by the stroke length and sliding velocity differently;

- For contact stresses between 2 MPa and 16 MPa applied for over one hour loading on cartilage (with no reciprocating motion) less than 5% permanent deformation of cartilage was observed.
- Loading time (short-term and long-term) does not affect articular cartilage permanent deformation (with no reciprocating motion) significantly.

- Longer stroke length and quicker sliding velocity produced significantly higher cartilage linear wear under low, medium and high contact stresses within long-term loading (Figure 3.20).

Increased stroke length and sliding velocity increased the coefficient of friction for stress levels between 0.5 and 2MPa and below, but made no difference at 4 and 8 MPa. Under low contact stress levels, the linear wear of the cartilage was significantly higher under greater stroke length and higher sliding velocities (8-8 compared to 4-4). However, under medium contact stress levels the cartilage linear wear increased to over 25% which means increased damage to the cartilage matrix. This could be caused by the different size of the cartilage plugs used under low and medium level of contact stress due to the loading limits of the reciprocating motion pin-on-plate apparatus. The area of the metal plates covered by the reciprocation of the cartilage pins (4mm and 8mm stroke lengths) is shown in Figure 3.24. Under low contact stresses (Figure 3.24.a and b.) 9mm in diameter cartilage pins were used, the repeated contact area was 28.84 mm^2 with 4mm stroke length and 2.78 mm^2 with 8mm stroke length. More repeated area was observed with the 4mm stroke length and this might decrease the surface roughness of the cartilage plug, hence it may produce lower coefficient of friction. However, under medium contact stresses (Figure 3.24.c and d) 4mm in diameter cartilage pins were used, there was no repeated contact area at 4mm or 8mm stroke length, and no difference on friction under the same contact stress with different motion conditions. Even though there were significant differences of the cartilage linear wear under the same contact stress (at 0.5, 1, 2, 4, and 8 MPa) between the two different motion conditions, it did not affect the cartilage friction as the cartilage linear wear did not relate to the friction.

The linear wear of the cartilage was significantly higher under greater stroke length and higher sliding velocity group (8-8 compared to 4-4). However, under medium contact stress levels the cartilage linear wear increased to over 25% which means increasing damage to the cartilage matrix was occurred. Damage was such that further increases to stroke length and sliding velocity did not further increase this.

When sliding distance and velocity were greater (8-8 compared to 4-4) the amount of cartilage permanent deformation (height change) increased significantly, this was attributed to the linear wear. Cartilage linear wear increased significantly at longer sliding distance with quicker sliding velocity under the same contact stress levels, and this was due to the longer contacting counterfaces on the metal plate increased the material loss.

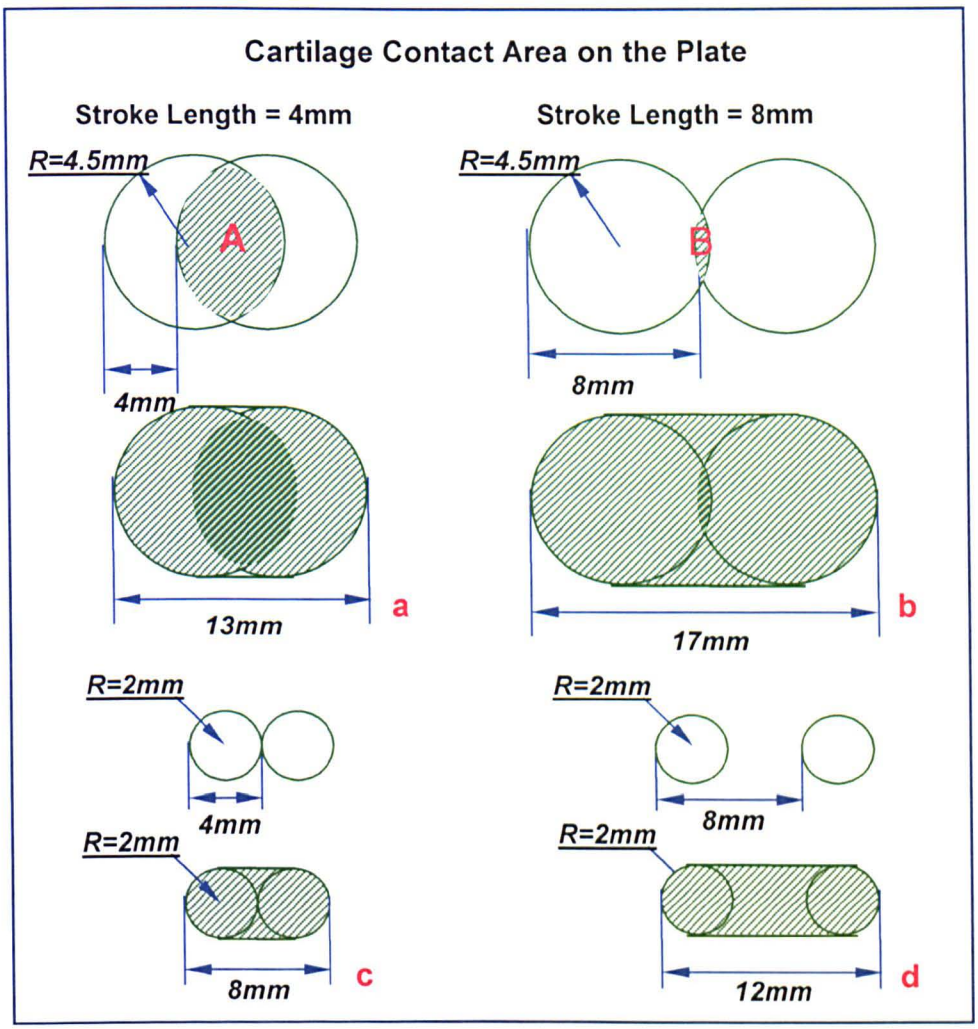

Figure 3.24 Cartilage contact areas on the plate with different stroke length and cartilage diameters.

3.5.3 Effect of Contact Area and Load on Cartilage Friction

The contact area and load affected the coefficient of friction by time;

- The contact area and load affected on the coefficient of friction significantly in the first two hours loading under the same contact stress level.
- In the long-term friction study after 2 hours loading, under the same contact stress level, the coefficient of friction was not significantly different with different contact areas and loads.

Under the same contact stress, the effect of contact area and load was demonstrated in short-term reciprocating study on friction. When the load was applied, the fluid started to flow out until equilibrium state (a solid and fluid phase in equilibrium) was reached in which the applied forces balance the internal pressure (i.e. 'swelling pressure'). During this period, the smaller diameter cartilage pin with the higher aspect radio reduced the fluid support with a through the side of the

cartilage, hence the coefficient of friction increased more quickly and more significantly compared to the larger diameter cartilage pin. However, when this transferred from the fluid phase to the solid and fluid phase in equilibrium supporting the load was completed; the coefficient of friction was comparable. The contact area and load did not affect the coefficient of friction in long-term reciprocating studies due to the cartilage load support through the equilibrium state of solid and fluid phase.

- The frictional shear stress level increased with both contact stress and the coefficient of friction.
- When the frictional shear stress arrived at 6 MPa over one hour static loading, or when the frictional shear stress reached over 4 MPa over 24 hours static loading, it caused the severe cartilage matrix damage, and visible linear wear.

Frictional shear stress is a factor that affects the degeneration process in articular cartilage, when it reaches a certain level the cartilage severe damage and increasing linear wear.

The results from this study demonstrated that in the simple geometry hemiarthroplasty model, the contact stress over 4 MPa for long-term reciprocating motion (over 1 hour) could lead to high friction and severe damage of the articular cartilage. Longer reciprocating distance and higher sliding velocity could increase the friction under low level contact stress, but it could cause significant increase of the cartilage linear wear under a range of contact stress from 0.5 to 8 MPa. When the contact stress is in low level (≤2 MPa) in the long-term reciprocating motion the cartilage linear wear could be less than 10% of the cartilage thickness. Hence long-term reciprocating motion with more than 4 MPa contact stress, and long distance with fast velocity motion should be avoided for patients who have received a hip hemiarthroplasty to reduce the possibility of cartilage severe damage and degradation. It may be useful to recommend to patients who recover from hip hemiarthroplasty to maintain low level of contact stress for long-term activities or medium and high level of contact stress for short-term activities in hip joint to reduce the deformation, linear wear and degradation of acetabular cartilage. However, high speed and long joint movement activities should be avoided after hip hemiarthroplasty.

3.6 Conclusion

A series of studies using a hemiarthroplasty simple geometry model where cartilage pins reciprocated against metal plates under different conditions were conducted, it was demonstrated that:

1. In short-term studies, the friction coefficient decreased with changes in the contact stress from 0.5 to 2 MPa, but increased from 2 to 16 MPa.
2. In long-term studies, the friction coefficient reached 0.35 with contact stress ≤4 MPa, but severe damage occurred with contact stresses of 8 MPa which significantly increased the friction coefficient after 12 hours. When a contact stress of ≥12 MPa was applied for more than one hour, catastrophic wear of cartilage occurred.
3. When pins with different contact areas were subjected to the same contact stress, in the long term studies there was no significant difference in the friction coefficient
4. Sliding distance and velocity only affected the friction coefficient under low contact stress (0.5 to 2 MPa).
5. Cartilage linear wear increased significantly with contact stress, sliding distance and sliding velocity.

Chapter 4 The Effect of Clearance on Cartilage in Hemiarthroplasty under Constant Load

4.1 Introduction

The current chapter focuses on the study of the friction and wear of cartilage in a hemiarthroplasty hip simulation with a constant loading regime applied. It extends the understanding of cartilage tribological properties in the hemiarthroplasty condition beyond that of the previous simple geometry model study. The tribological response of the acetabulum in hemiarthroplasty has not been previously studied in an *in-vitro* articulating hip joint due to the technical difficulties associated with central setting of the acetabulum and the complex calculations of friction and wear. Hence the whole hip joint tribology study *in-vitro* began with a study under constant loading and application of a pendulum motion; this was a precursor to the more complex application of dynamic loading.

Clinically, following hemiarthroplasty (for example, Austin Moore), the acute, repetitive impact and torsional joint loads have been speculated as causing damage to articular surfaces causing pain (either groin or thigh), joint dysfunction, and effusions. The pain is usually due to the pathological processes: acetabular cartilage degeneration or loosening of the prosthesis in the proximal femur, or infection and impingement (Amstutz and Smith, 1979; Sharkey *et al.*, 1998; Bilgen *et al.*, 2000; Cossey and Goodwin, 2002). Furthermore, inappropriate choice of head size, inadequate calcar seating, subsidence and rotational instability of the prosthesis (uncemented) may also cause pain (Sharif and Parker, 2002; Yau and Chiu, 2004). This articular surface damage can lead to progressive joint degeneration in some cases. Many factors are considered to exacerbate these pathological processes (Anderson *et al.*, 1964; Hinchey and Day, 1964; Gingras *et al.*, 1980; Cruess *et al.*, 1984; Kaltsas and Klugman, 1986; Cook *et al.*, 1989; Cossey and Goodwin, 2002) such as incongruencies between the femoral head and the acetabulum, the use of cement, excessive neck length, impaction at the time of injury, active patients, and more importantly the shear forces between the prosthesis and the articular cartilage.

Cartilage degeneration is one of the most important clinical issues following hip hemiarthroplasty, and the migration of the prosthesis head through the acetabular cartilage is a primary mode of failure (Anderson *et al.*, 1964; Salvati and Wilson, 1973; Kofoed and Kofod, 1983). This may be attributed to the excessive

pressure caused by inappropriate fit between the metallic prosthesis head and the natural articular acetabulum referred to as mismatched head size (Harris *et al.*, 1975; Devas and Hinves, 1983; Yamagata *et al.*, 1987; van der Meulen *et al.*, 2002; Krishnan *et al.*, 2004b).

Little is known clinically about the prevalence, and severity of acetabular erosion (Timour, 1999) secondary to the hip hemiarthroplasty (Figure 4.1). The level of physical activity and the duration of follow-up are the factors that have the highest correlation with the severity of the erosion of acetabular cartilage (Phillips, 1989; McGibbon *et al.*, 1999). In Philips and McGibbon's studies, it was found that the erosion through acetabular cartilage into the bone developed in 90% (34 of 38) of active patients, and 0% (0 of 34) of inactive patients. In active patients, the severity of the erosion increased with time (at an average rate of 3% per year) and was associated with pain and disability during walking. However, late acetabular erosion did not develop in all active patients, one patient still had high acetabular score (Harries Hip Score: 98 points) at the 11 year follow-up. It has been demonstrated in operative findings that loosening of the prosthesis and acetabular cartilage degeneration were the main pathological processes leading to failure of the hemiarthroplasty (Cossey and Goodwin, 2002). Hence, hemiarthroplasty can achieve a good long-term result for treating the femoral neck fractures for elder patients when these pathological processes and appropriate choices i.e. head size, adequate calcar seating, stable subsidence and rotation etc are applied.

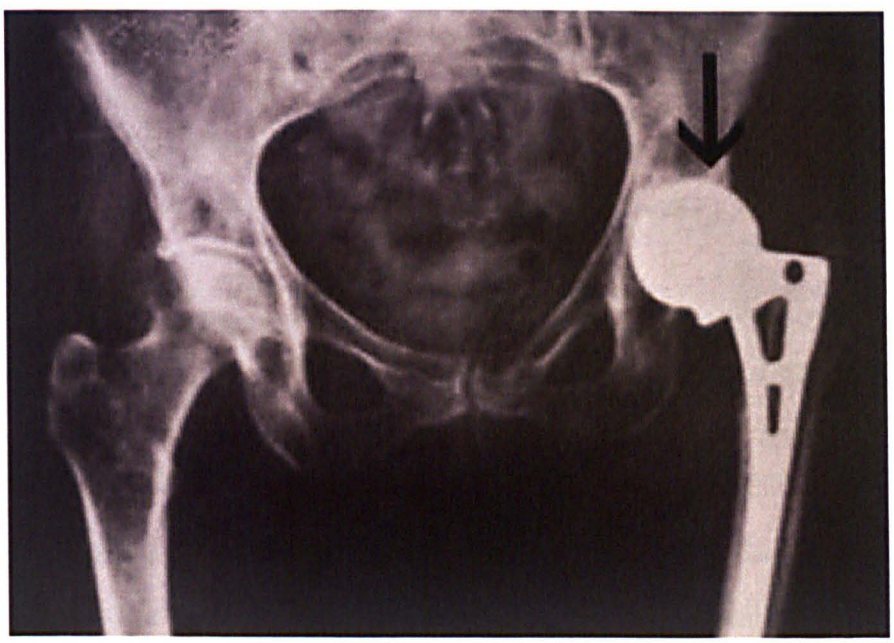

Figure 4.1 Painful Moore prosthesis, with apparent peripheral acetabular erosion (Timour, 1999).

The mechanogenesis of cartilage degeneration and erosion is largely unknown. Although the mechanical and biochemical properties of degenerated articular cartilage had been analysed previously (Roberts *et al.*, 1986a; Roberts *et al.*, 1986b; Guilak *et al.*, 1994; Wei *et al.*, 1997), the primary cause remains elusive. Previous fundamental studies (Forster and Fisher, 1996; Forster and Fisher, 1999; Krishnan *et al.*, 2004a; Krishnan *et al.*, 2004b; Bell *et al.*, 2006b; Carter *et al.*, 2007; Katta *et al.*, 2007a; Northwood and Fisher, 2007; Northwood *et al.*, 2007; McCann *et al.*, 2009) of the tribology of articular cartilage have indicated the complex relationships among the coefficient of friction, frictional shear stress, contact stress levels, cartilage deformation, and cartilage wear were due to the biphasic nature (Mow *et al.*, 1984) of articular cartilage and the time dependency of the tribological responses.

These studies suggested that the contact area, contact pressure, frictional shear stress, and loading time were the main factors that influenced the tribological properties of the acetabular cartilage in hemiarthroplasty. Furthermore, the clearance between the femoral head and the acetabulum motion direction (FE direction) not only affects the incongruencies between the femoral head and the acetabulum, but also is a key factor that influences the contact stress, contact area, and frictional shear stress in hip hemiarthroplasty. The effect of clearance on the tribological properties is very important to investigate and understand. It was hypothesised that increasing the clearance between the femoral head and the articular acetabulum would increase the contact stress and friction factor. This is because for the same articular acetabulum, decreasing the femoral head size increases the clearance; hence the contact stress increases by the decreasing contact area (as shown in Figure 4.2). For example, for the same porcine acetabulum, increased the clearance (reduce the metal head size) from small, medium, large, and to extra large, the contact area decreased as pink, red, green, to blue area.

This summarised literature review has led to the development of a series of research questions, which will be investigated under constant loading initially:

1. How does the clearance between the femoral head and the articular acetabulum (measured in the FE direction) affect cartilage friction?
   - What is the effect of clearance on contact area and contact stress?
   - What is the relationship between the variation of clearance and the contact area and the contact stress?
   - What is the effect of clearance on the friction factor?

- What is the effect of clearance on frictional shear stress?

2. How does the clearance (FE direction) affect the cartilage deformation, degradation and wear?
   - What is the effect of clearance on the acetabular cartilage surface roughness?
   - What is the effect of clearance on the cartilage wear grades and area?
   - What is the relationship between the variation of clearance and the cartilage deformation volume value of different clearances?

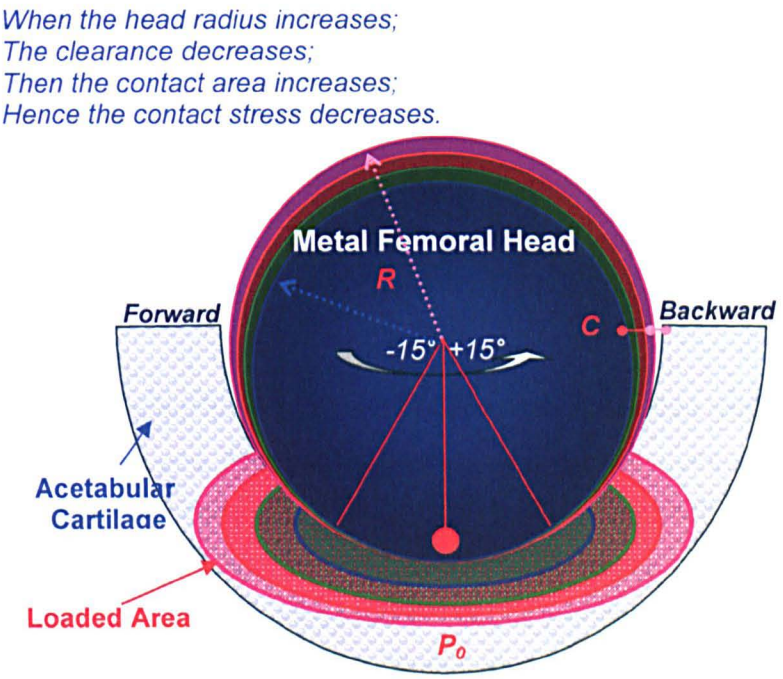

Figure 4.2 Contact stress increases when reducing the femoral head size due to the decreased contact area, and smaller head size – larger clearance causes higher contact stress

4.2 Objectives

The objectives of this study were to use a simulated hip joint model of the acetabular cartilage cup reciprocating against a metal head to consider the effect of clearance on the cartilage tribology. The clearance was considered in the flexion-extension direction and ranged from small, medium, large to extra large (as described in Section 2.3.1.5).

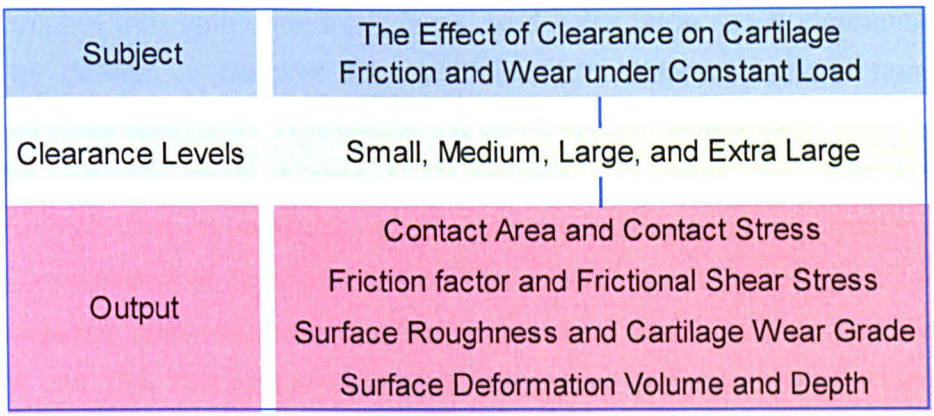

Figure 4.3 Summary of studied tribological properties in pendulum constant loading study in hip joint

Tribological properties studied were: (1) contact area and contact stress, (2) friction factor, (3) surface roughness, (4) cartilage wear grade, and (5) surface deformation after the 2 hours 400N constant loading in a pendulum friction study. An overview of this study is shown in Figure 4.3.

4.3 Materials

Tests materials used were six-month old porcine acetabula and cobalt chrome heads (32, 34, 35, 36, and 37mm in diameter), and the lubricant was 25% bovine serum, as described in Sections 2.3.1.2, 4, 5, and 8 respectively. The porcine acetabulum was set in PMMA cement at 45 degrees as described in Section 2.3.2.2, and friction tests were conducted using a pendulum friction simulator as described in Section 2.3.2.1. Microset silicon replicas of the porcine acetabulum after the friction test were taken, to study wear, as described in Section 2.3.2.3. Contact areas and stresses were measured using the FUJI pressure film as described in Section 2.3.2.4. The cartilage wear grade measurements were completed as described in Section 2.3.2.5, and the surface deformation measurements were taken as described in Section 2.3.2.6.

4.4 Methods

The constant load chosen was selected as half of the porcine body weight approximate 400N with a loading time of 2 hours (explained in Section 2.3.2.1.1). The **constant loading profile** was set as shown in Figure 2.24.

Samples with small, medium, large, and extra large radial clearances were tested as defined in Section 2.3.1.5, Table 2.2. Different femoral heads and acetabula sizes were chosen to create the same level of clearance.

The **average contact area** at 0° position was measured using super-low pressure FUJI film by applying 400N constant loading with no motion for 30 seconds, described in Section 2.3.2.4. The contact areas of six specimens with each clearance were measured and the mean value was calculated and compared (ANOVA, $p<0.05$). The **average contact stress** was calculated by the load divided by the average contact area using Equation 2-16. The **peak contact stress** was measured using low pressure FUJI film and selecting the six highest points at the 0 degree position of each specimen and the mean value of six specimens of each clearance were calculated and compared (ANOVA, $p<0.05$).

The **friction factor** was analysed as the coefficient of friction at the 0 degree position where the head was vertically loaded and in contact with the lowest position of the cup as shown in Figure 2.25. The friction factor (coefficient of friction) was calculated using Equation 2-13, as described in Section 2.3.2.1.1.1.

The **average frictional shear stress** and **the peak frictional shear stress** were calculated following Equations 2-17, and 2-18 in Section 2.3.2.5. The mean value of six specimens of each clearance group was calculated and compared (ANOVA, $p<0.05$).

The acetabular cartilage **surface roughness** was measured using microset replica and a two-dimensional profilometer. The roughness (Ra) of each trace was calculated using software following Equation 2-19.

The cartilage **wear grade area** was examined visually using an adaption of the International Cartilage Repair Wear Grading System (Section 2.3.2.6). The area of the different wear grades were measured through marking a transparent cling film covering the microset replica of the acetabulum, as described in Section 2.3.2.6. Then the wear area of the different wear grades and the whole acetabular lunate surface area were calculated using Image Pro Plus, and presented as the percentage of the acetabular lunate surface area. The mean value of each wear grade area percentage (six specimens) in each clearance group were calculated and compared (ANOVA arcsine, $p<0.05$).

The acetabular replicas ($n=3$) were selected depending on their suitability for measurements. Intact original surface on both sides of the wear scar on the replicas was required for two-dimensional profilometer measurements (as described in Section 2.3.2.6.1, Figure 2.40). The acetabular surface **deformation volume** and the **average deformation depth** were calculated using Equations 2-20, and 2-21.

The mean deformation volume and average deformation depth of each clearance group was calculated and compared (ANOVA, $p<0.05$, $n=3$).

4.5 Results

4.5.1 Effect of Clearance on Contact Area and Contact Stress

4.5.1.1 Contact Areas

Images of typical contact areas in each clearance group measured by super-low pressure FUJI film are shown in Figure 4.4, and detailed measurements are shown in Appendix 2.

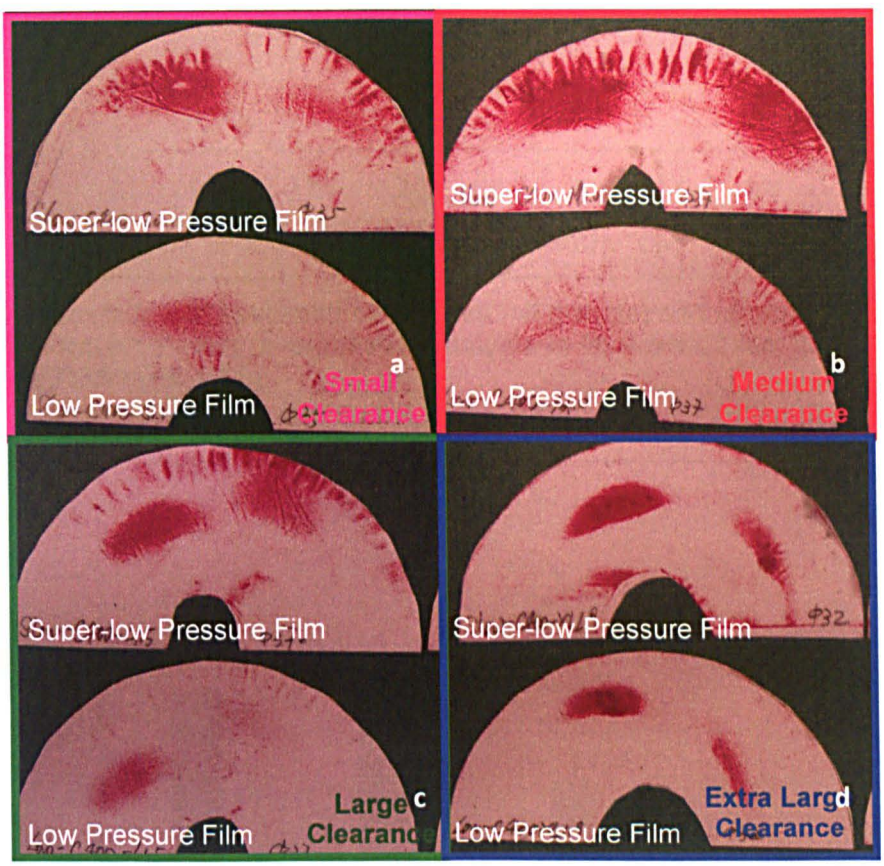

Figure 4.4 Contact area was measured by super-low pressure film and contact stress was measured by low pressure film loading at 0° position with a 400N constant load for a) small, b) medium, c) large, and d) extra large clearances between a cobalt chrome head and the porcine acetabula.

The contact area of six specimens of each clearance group was calculated by Image Pro Plus, and a correlation ($R=0.80$) between the contact area and the FE radial clearance was observed (Figure 4.5). The mean contact area of each clearance group decreased from 85 mm^2 to 169 mm^2 as the clearance increased from small to extra large (Figure 4.6). With extra large clearance, the contact area

was significantly smaller compared to with small, medium, and large clearances (n=6, ANOVA, $p<0.05$).

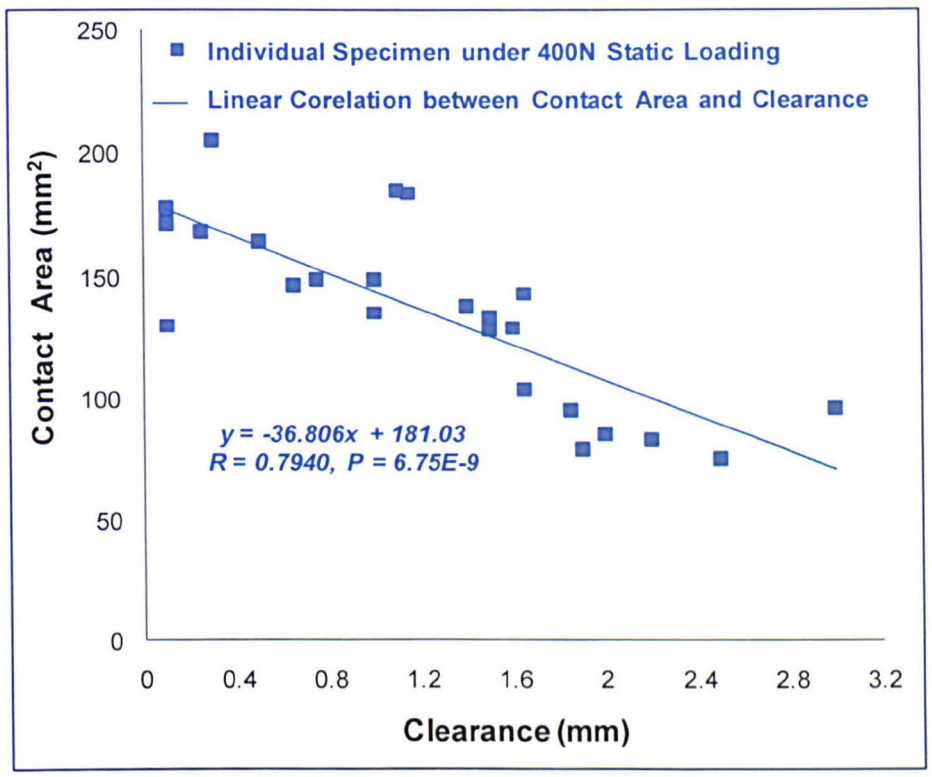

Figure 4.5 Correlation of specimen clearances (all groups) and contact area. R and P values were obtained using a regression analysis in Microsoft Excel 2007 (Microsoft Corporation, Redmond, USA).

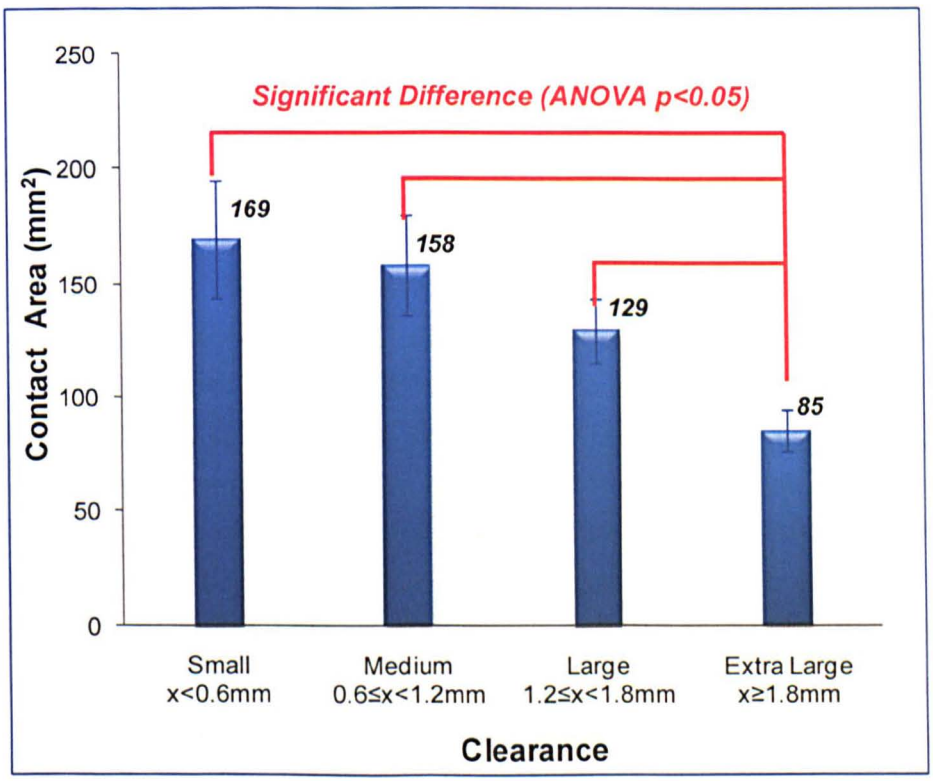

Figure 4.6 Contact area (mm^2) in specimens with different clearance levels (n=6, mean ± 95% confidence limits).

4.5.1.2 Contact Stress

The calculated average contact stresses and the measured peak contact stresses with different clearances under 400N static load for 30 seconds are shown in Figure 4.7. Both the calculated average contact stress and the measured peak contact stress increased with the increasing clearances with correlations of R=0.79 and R=0.87 respectively.

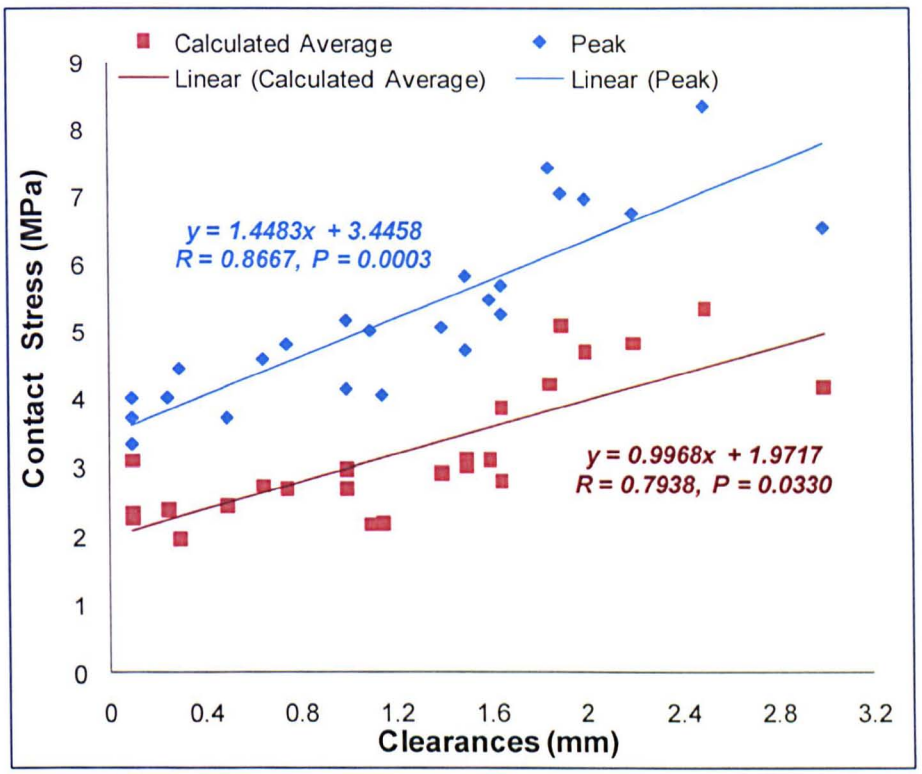

Figure 4.7 Correlations of calculated average contact stress / measured peak contact stress and specimen clearance. R and P values were obtained using a regression analysis in Microsoft Excel 2007 (Microsoft Corporation, Redmond, USA).

The calculated contact stress and measured peak contact stress of specimens in each clearance group is shown in Figure 4.8. The calculated average contact stress increased from 2.4 MPa to 4.7 MPa as the clearance of specimens increased from small to extra large. The average contact stress was significantly higher in specimens with extra large clearance compared to the average contact stress for specimens with small, medium, and large clearances (n=6, ANOVA, $p<0.05$). The measured peak contact stress increased from 3.9 MPa to 7.2 MPa with increasing clearance of specimens from small, medium, large to extra large. The measured contact stress in specimens with extra large clearances was found to be significantly higher compared to specimens with small and medium clearances and significantly higher contact stress was observed with large clearance specimens compared with specimens with small clearance (n=6, ANOVA,

p<0.05). The measured peak contact stress is shown 1.625~1.71 times greater than the calculated average contact stress in specimens at each clearance level, a parabolic form relationship is assumed (n=6, T test, p<0.05).

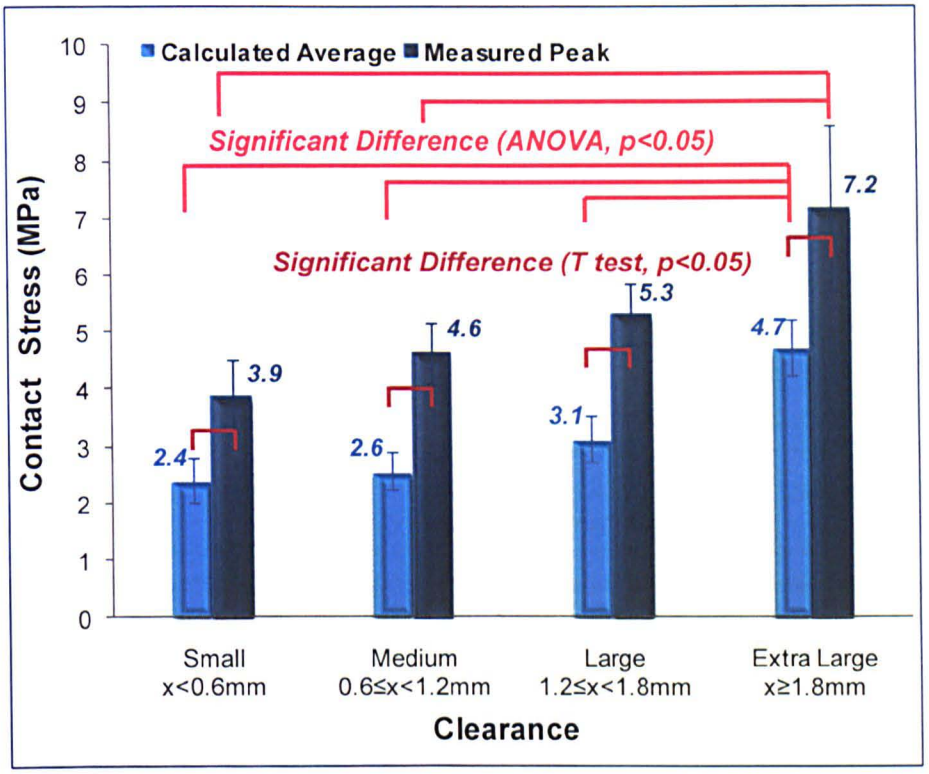

Figure 4.8 Calculated average contact stress and measured peak contact stress (MPa) with different clearances (peak contact stress is shown 1.625~1.7 times greater than the average contact stress, n=6, mean ± 95% confidence limits).

4.5.2 Effect of Clearance on Friction and Frictional Shear Stress

4.5.2.1 Friction Factor (Coefficient of Friction)

The coefficient of friction measured under a constant 400N load with ±15° pendulum motion of specimens with small, medium, large, and extra large clearances were analysed at the 0 degree position through a 2-hour friction test, and the results are shown in Figure 4.9-12 for the specimens with different clearances.

The coefficients of friction of six specimens with small clearances (from 0.15 to 0.55 mm) are shown in Figure 4.9. The mean coefficient of friction increased to a value of 0.3±0.05 during the first 2700 cycles (45 minutes) of pendulum friction loading. The coefficient of friction then remained at a similar value of 0.33±0.01 after 45 minutes to the end of the test.

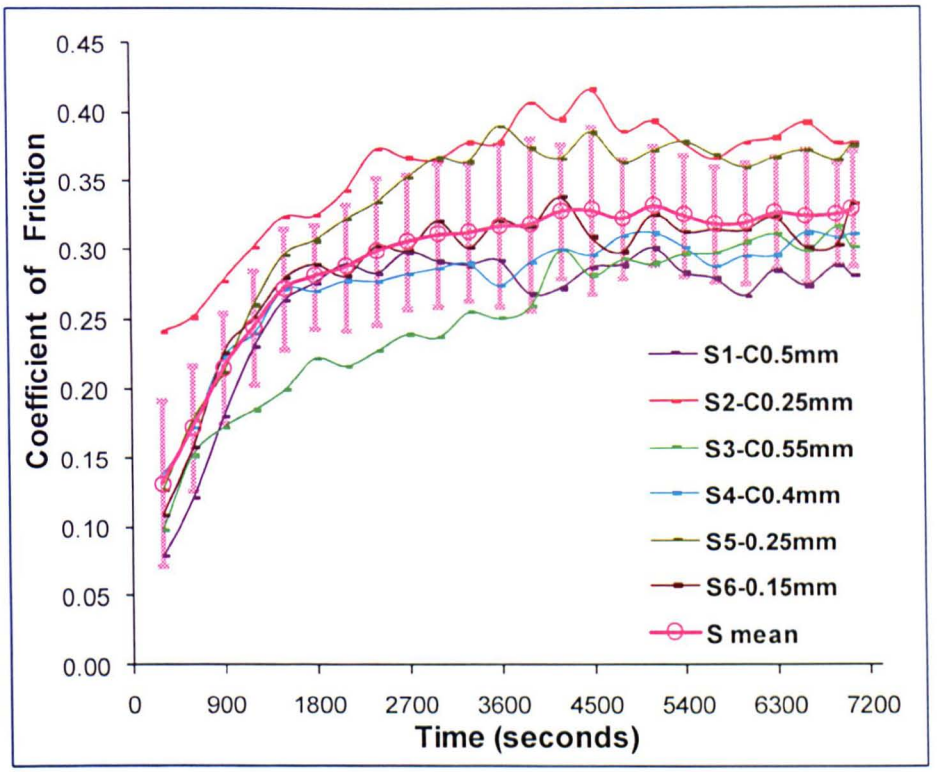

Figure 4.9 The coefficient of friction for specimens with small clearances (FE radial clearance < 0.6mm) under constant loading (n=6, mean ± 95% confidence limits) ***(S_n-x.xx: S-Small clearance, n-specimen number, x.xx-FE radial clearance).***

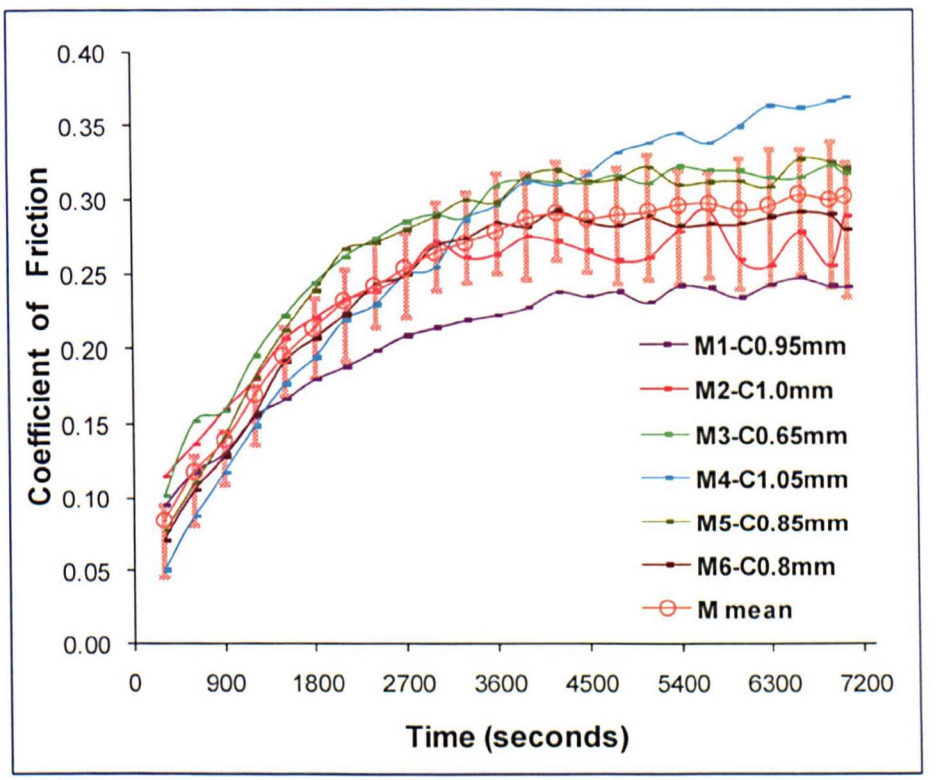

Figure 4.10 The coefficient of friction for specimens with medium clearances (0.6mm ≤ FE radial clearance < 1.2 mm) under constant loading (n=6, mean ± 95% confidence limits) ***(Mn-x.xx: M-Medium clearance, n-specimen number, x.xx-FE radial clearance).***

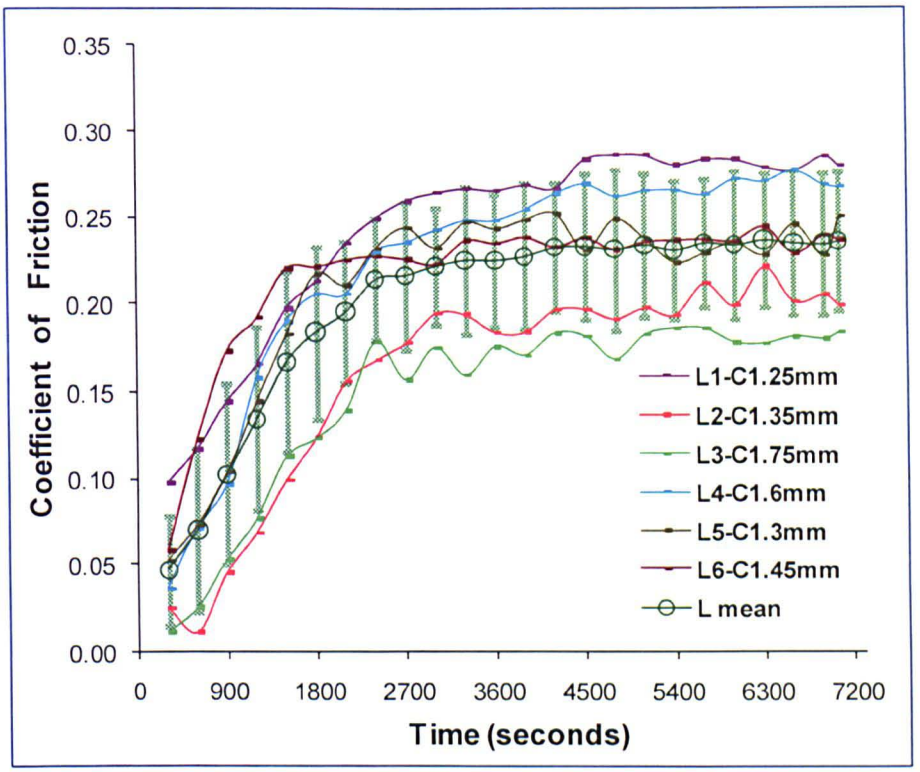

Figure 4.11 The coefficient of friction for specimens with large clearances (1.2mm ≤ FE radial clearance < 1.8 mm) under constant loading (n=6, mean ± 95% confidence limits) (*Ln-x.xx: L-Large clearance, n-specimen number, x.xx-FE radial clearance)*

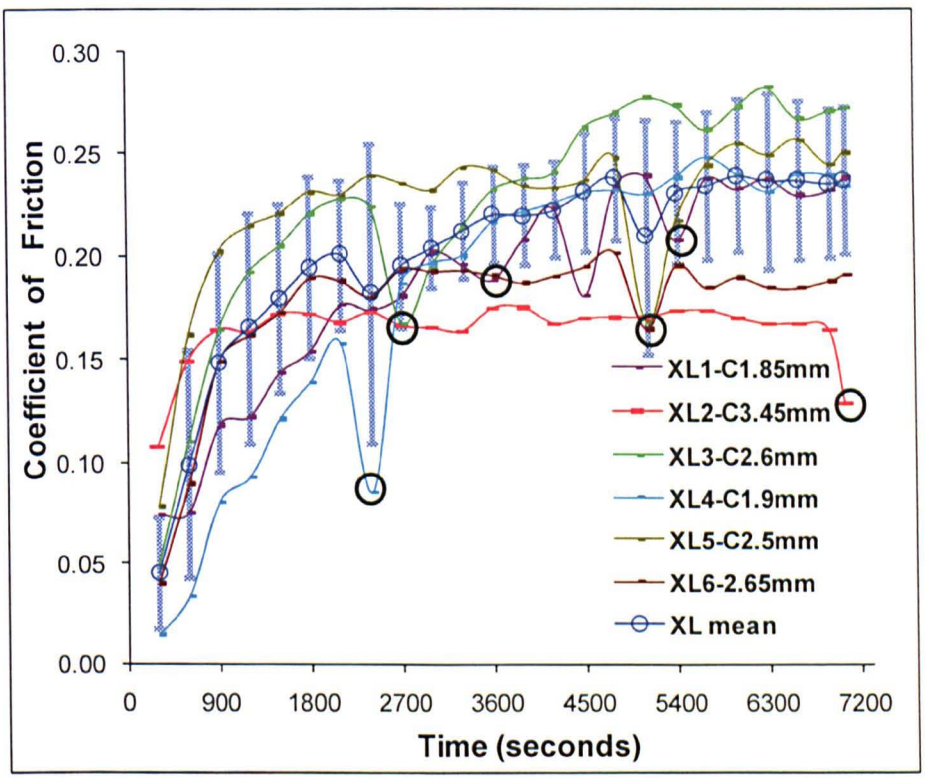

Figure 4.12 The coefficient of friction for specimens with extra large clearances (1.8mm ≤ FE radial clearance < 2.4 mm) under constant loading (n=6, mean ± 95% confidence limits) *(XLn-x.xx: XL-Extra large clearance, n-specimen number, x.xx-FE radial clearance).*

Six specimens with medium clearances (from 0.65 to 1.05 mm), the coefficients of friction are shown in Figure 4.10. During the first 3600 cycles (60 minutes) of pendulum friction loading, the mean coefficient of friction increased to a value of 0.25±0.04. After then to the end of the test, the coefficient of friction remained at a similar value of 0.29±0.02.

With large clearances (from 1.25 to 1.75 mm), the six specimens coefficients of friction are shown in Figure 4.11. From the beginning of the test till 2700 cycles (45 minutes) of pendulum friction loading, the coefficient of friction increased to a value of 0.2±0.04. From 45 minutes to the end of the test, the coefficient of friction remained at a similar value of 0.24±0.03.45.

Six specimens with extra large clearances (from 1.85 to 3.45 mm) the coefficients of friction are shown in Figure 4.12. During the first 3600 cycles (60 minutes) of pendulum friction loading, the mean coefficient of friction increased from a value of 0.05±0.03 to 0.23±0.03. The coefficient of friction then remained at a similar value of 0.23±0.03 from 60 minutes to the end of the test. However, a rapid decreasing coefficient of friction was observed in each specimen during the two hour pendulum constant loading (circled in Figure 4.12). It is postulated that this is a measurement artefact when the cartilage surface changed (i.e. became damaged).

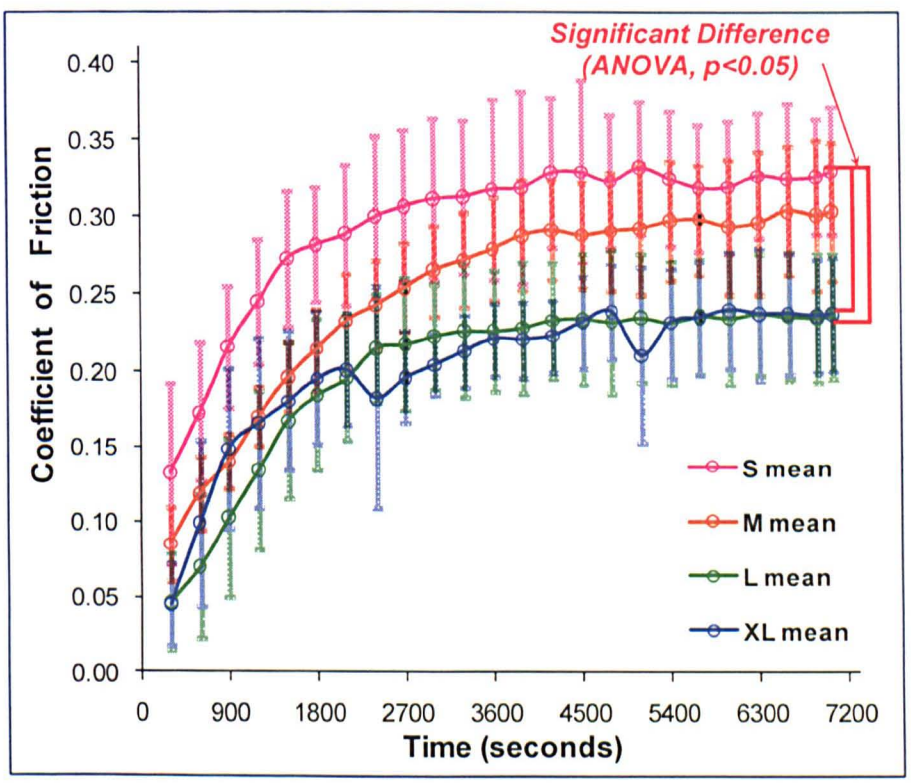

Figure 4.13 The coefficient of friction for specimens with small, medium, large, and extra large clearances under constant loading (n=6, mean ± 95% confidence limits) (*S: small, M: medium, L: large, and XL: extra large clearance).*

The mean value of the coefficient of friction for specimens tested with different clearances is compared in Figure 4.13. A trend of decreasing coefficient of friction with an increasing clearance (from small to large) is shown. The coefficient of friction was significantly higher in small clearance specimens compared to large and extra large clearances specimens (ANOVA, $p<0.05$), but no significant difference in the coefficient of friction between large and extra large clearance specimens was observed (ANOVA, $p>0.05$).

The correlation of coefficient of friction at 2 hours time point and the FE radial clearance under ±15 degree 400N static load is shown in Figure 4.14. The coefficient of friction decreased with the increasing clearances with a correlation of R=0.78.

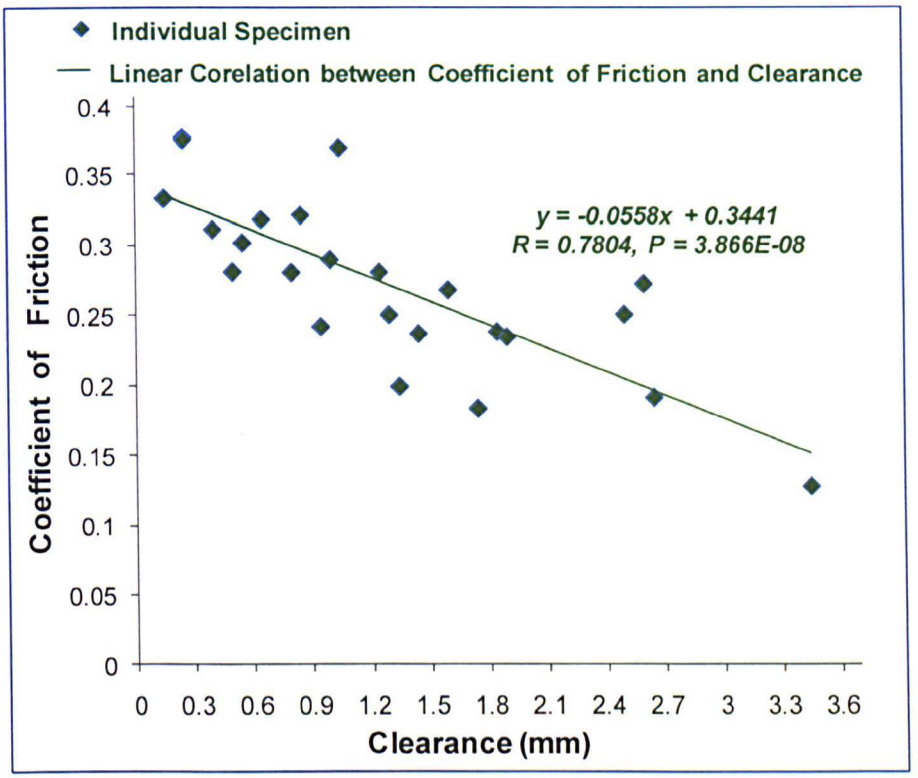

Figure 4.14 Correlation (R=0.78) between the coefficient of friction and FE radial clearance following 2 hours of constant load testing. R and P values were obtained using a regression analysis in Microsoft Excel 2007 (Microsoft Corporation, Redmond, USA).

4.5.2.2 Frictional Shear Stress

The calculated average frictional shear stress and the calculated peak frictional shear stress in specimens with different clearance groups are shown in Figure 4.15 and 4.16. The average frictional shear stress was lower compared to the peak frictional shear stress in specimens for each clearance level.

The average frictional shear stress increased with time during the first hour of loading, and then remained at constant with small, medium, and large clearance specimens. After one hour of pendulum 400N constant load testing, the average frictional shear stress increased to 0.7±0.02 MPa for specimens with small, medium, and large clearances. However, for extra large clearances specimens, the average frictional shear stress increased to 0.7 MPa in the first 15 minutes of loading, and then continued increasing to 1.07 MPa at the end of the test (2-hour time point).

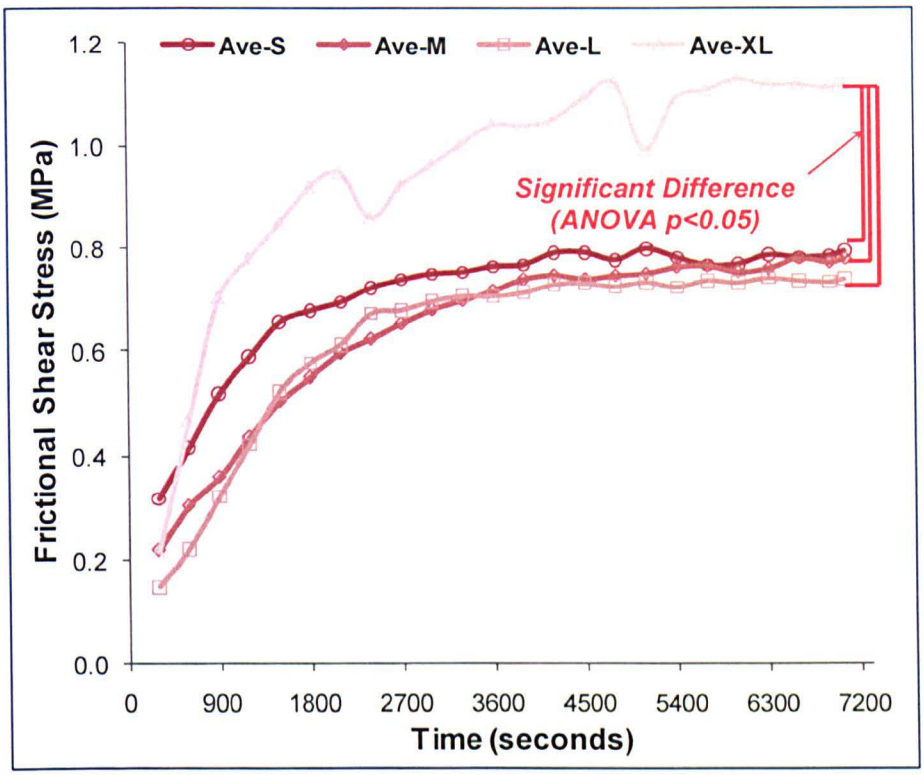

Figure 4.15. Comparison of calculated average frictional shear stress for specimens with small, medium, large, and extra large clearances under constant loading (mean, n=6) *(Ave: average value, S: small, M: medium, L: large, and XL: extra large).*

The peak frictional shear stress increased with time during the first hour of loading, and then remained at similar levels for specimens with small, medium, and large clearances. After one hour of pendulum constant loading, the peak frictional shear stress reached 1.3±0.5 MPa for specimens with small, medium, and large clearances, for specimens with extra large clearance it was approximately 1.65 MPa. Both average and peak frictional shear stress for specimens with extra large clearance were found to be significantly higher compared to specimens with small, medium, and large clearances from 1800 to 7200 cycles (n=6, ANOVA, $p<0.05$).

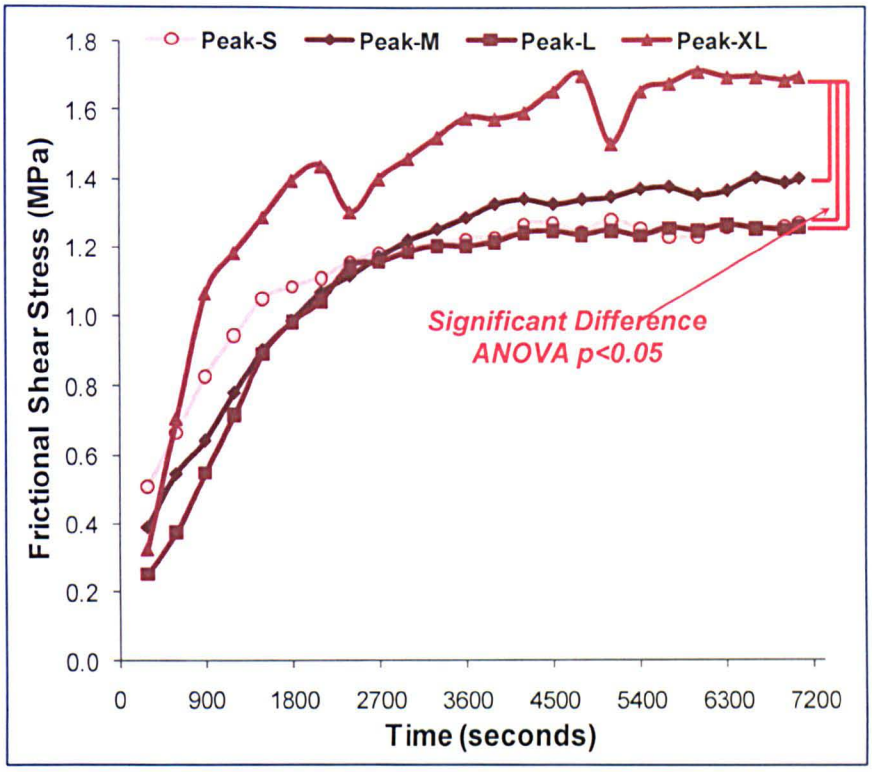

Figure 4.16. Comparison of calculated peak frictional shear stress for specimens with small, medium, large, and extra large clearances under constant loading (mean, n=6) ***(Peak: peak value, S: small, M: medium, L: large, and XL: extra large).***

4.5.3 Effect of Clearance on Cartilage Surface Roughness and Wear

4.5.3.1 Surface Roughness

Comparison of the surface roughness (R_a) of cartilage in samples with different clearances is shown in Figure 4.17. The surface roughness of the replicas in different clearances groups was 5.59 (± 0.49) – 7.85 (±1.48) μm. It is shown that there was no significant difference in the surface roughness in specimens among the four clearances groups (n=3, ANOVA, $p<0.05$).

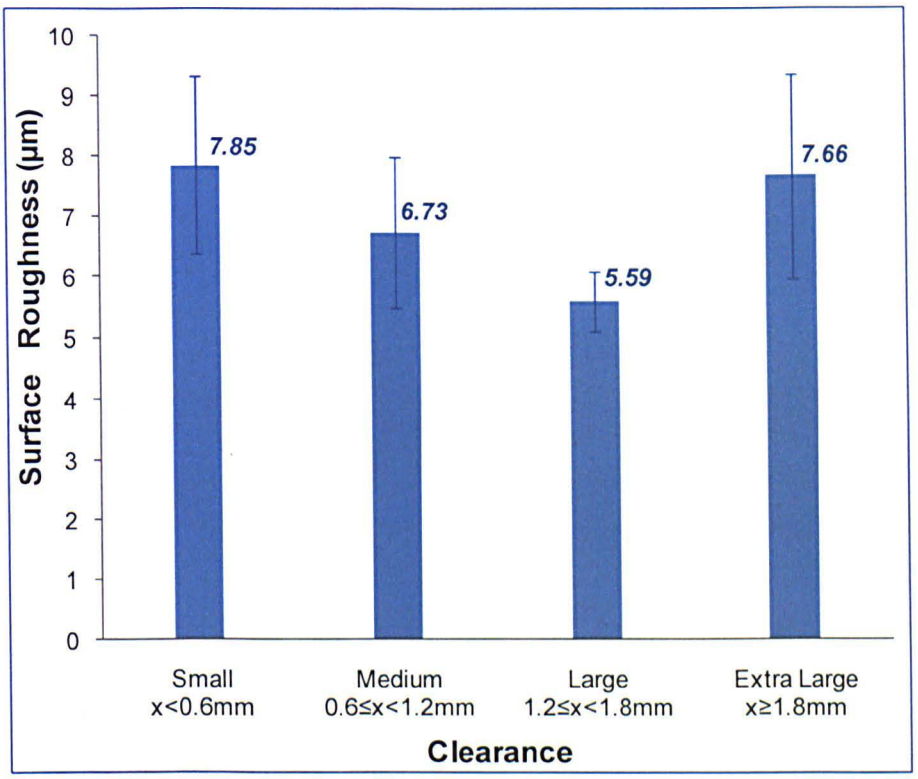

Figure 4.17. The acetabular replica surface roughness with small, medium, large, and extra large clearances following testing with constant load testing for 2 hours (n=3, mean ± 95% confidence limits).

4.5.3.2 Cartilage Wear Grade

Wear grades 1, 2, and 3 were observed on all the acetabular cartilage specimens used in tests with different clearances. However, wear grade 4 was only observed in specimens used in extra large clearances tests. The six specimens used in extra large clearances tests after two hours of 400 N constant loading in the pendulum friction test are shown in Figure 4.18.

Three types of cartilage damage were found in these six specimens:

a) Specimen 1, 3, and 5, the acetabular cartilage was delaminated, specimens 1 and 5 a small piece of delaminated cartilage was repositioned, and the cartilage was still attached to the specimen 3;

b) Severe cartilage wear and the damage was down to the cartilage Tide Mark (shown as pink colour in Figure 4.18), this was also observed in specimen 2;

c) In specimens 4 and 6, the acetabular cartilage was fractured in the middle of the lunate surface.

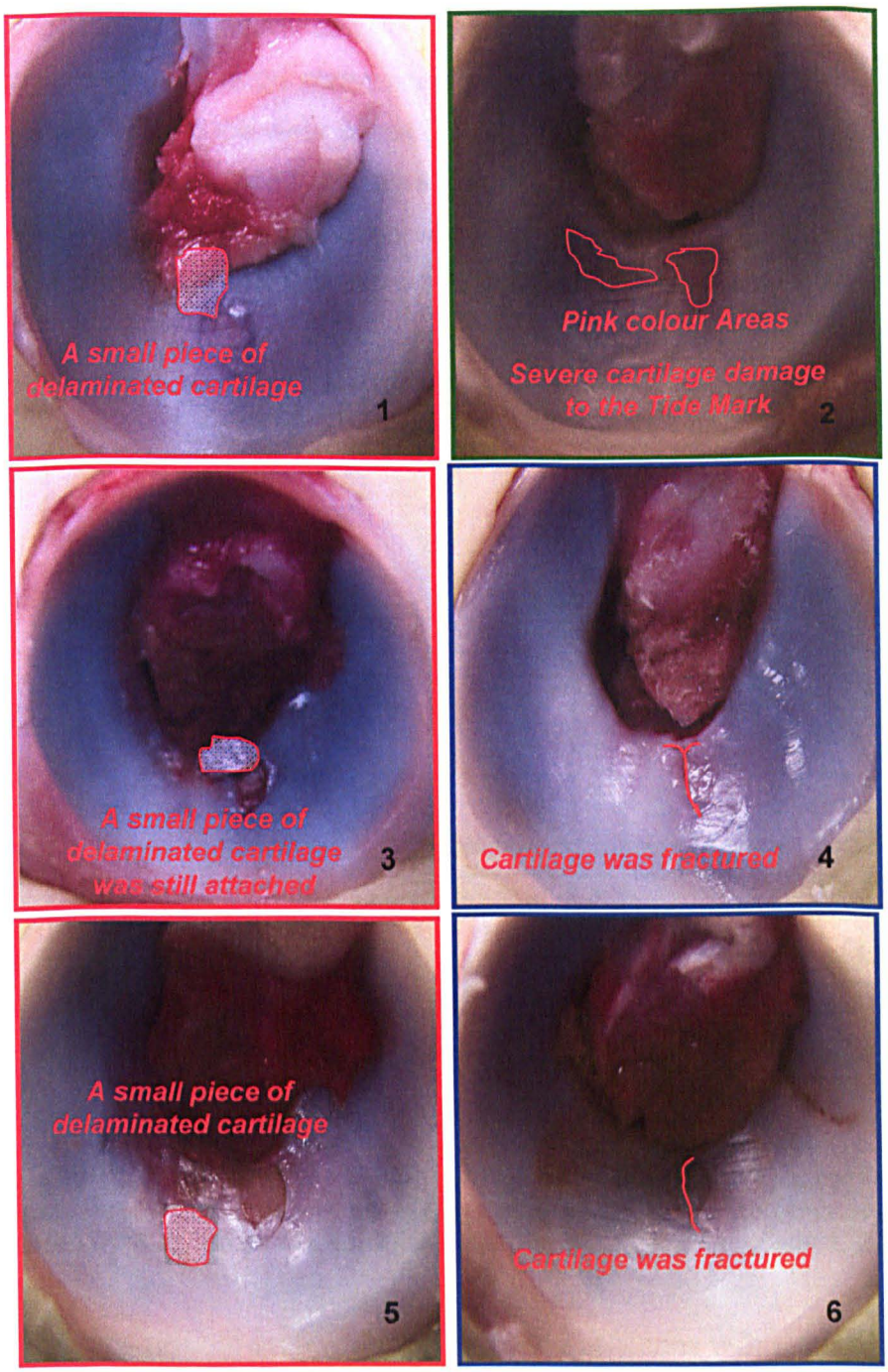

Figure 4.18. Acetabular cartilage damage types in extra large clearance specimens under 400N constant loading: specimens 1, 3, and 5, the acetabular cartilage was delaminated; severe cartilage wear and the damage was down to the cartilage Tide Mark was observed in specimen 2; in specimens 4 and 6, the acetabular cartilage was fractured in the middle of the lunate surface.

The percentages of the different wear grade areas are shown in Figure 4.19. In specimens with extra large clearances wear grade 4 was observed and this was up to 1.7% area of the acetabular lunate surface, which was significantly higher compared to the grade 4 damage in specimens with small, medium, and large clearances (ANOVA arsine, $p<0.05$, $n=6$). A significant increase in the size of wear grade 3 areas was found in specimens with medium compared to specimens with

large and extra large clearances (ANOVA arsine, $p<0.05$, $n=6$). In specimens tested with large and extra large clearances wear areas graded as 2 were significantly smaller compared to the wear areas graded as 2 in specimens with small, medium, and large clearances (ANOVA arsine, $p<0.05$, $n=6$). No significant difference in the area of wear graded as 1 was observed among specimens with small, medium, and large clearances (ANOVA arsine, $p>0.05$, $n=6$).

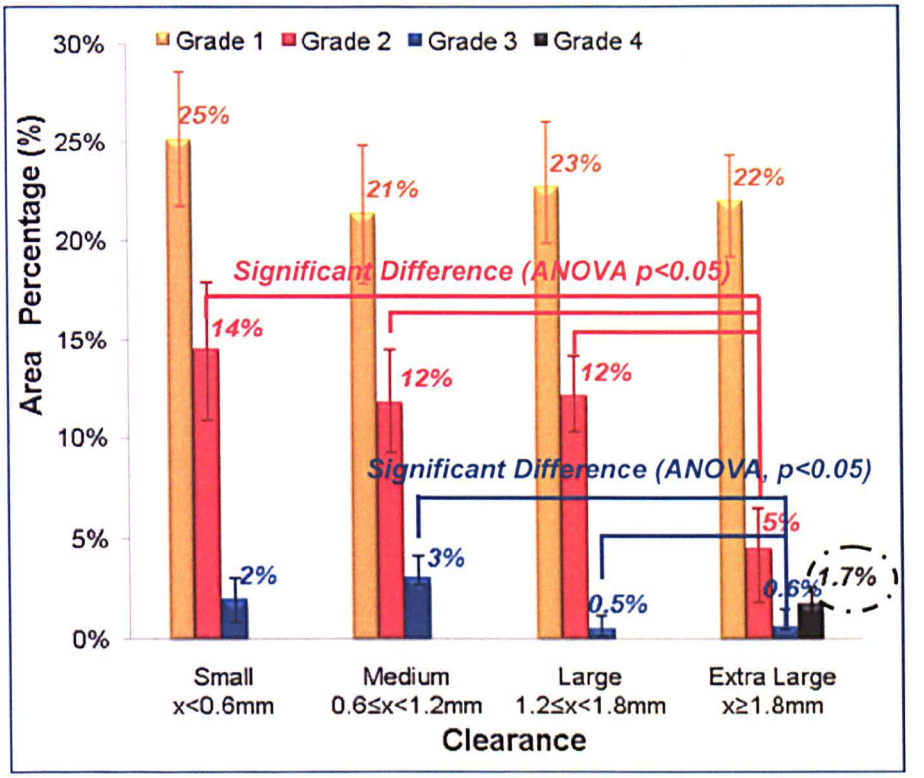

Figure 4.19 The acetabular replica surface wear grade area percentage for specimens with small, medium, large, and extra large clearances following constant load testing for 2 hours (n=6, mean ± 95% confidence limits, G1, 2, 3: wear grade 1, 2, 3).

The total unworn area (wear grade 0) in specimens with small, medium, large and extra large clearances is shown in Figure 4.20. The unworn area in specimens with extra large clearances was significantly higher compared to specimens with small, medium, and large clearances (ANOVA arsine, $p<0.05$, $n=6$).

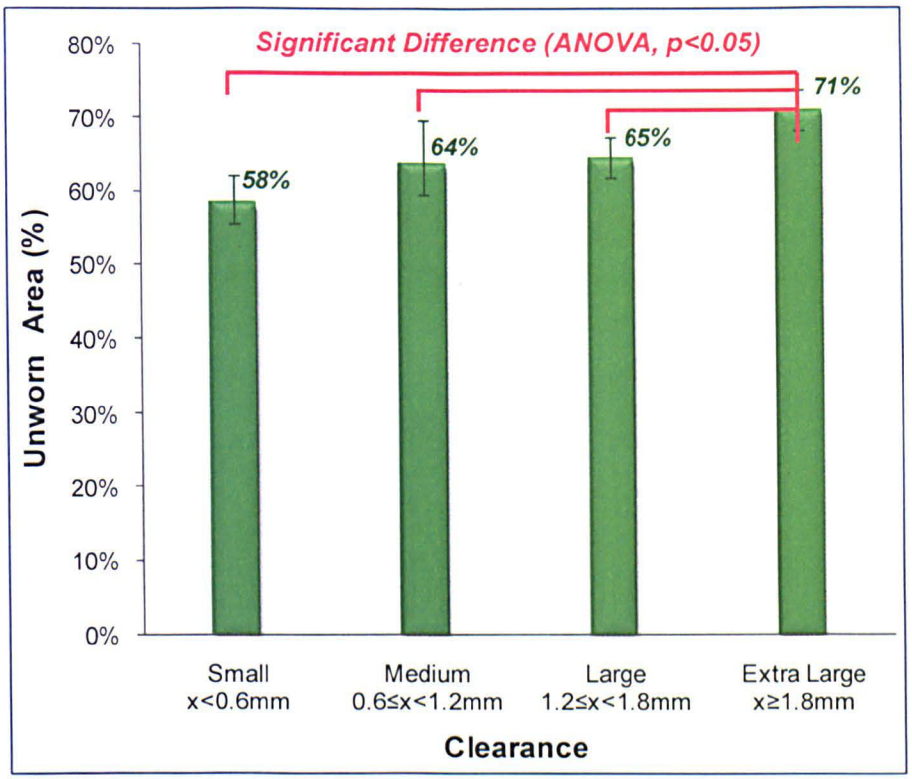

Figure 4.20. Unworn area (wear grade 0 area) percentage in specimens with small, medium, large, and extra large clearances following 2 hours of constant load testing (n=6, mean ± 95% confidence limits).

4.5.4 Effect of Clearance on Cartilage Surface Deformation

4.5.4.1 Cartilage Deformation Volume

The acetabular surface deformation volume was affected by both the average deformation area and the trace gap. For example, a small deformed surface area with a deep deformation depth can result as the same deformation volume with a large deformed surface area with a shallow deformation depth. The deformation volume is compared for specimens with small, medium, large and extra large clearances in Figure 4.21. It was found that the deformation volume in specimens with small clearances was significantly higher compared to with medium and large clearances (ANOVA, $p<0.05$, $n=3$). For specimens with medium clearances the deformation volume was significantly lower compared to specimens with extra large clearances (T-test, $p<0.05$, $n=3$).

No significant difference of the deformation volume in specimens with small and extra large clearances, and with medium and large clearances (ANOVA, $p>0.05$, $n=3$).

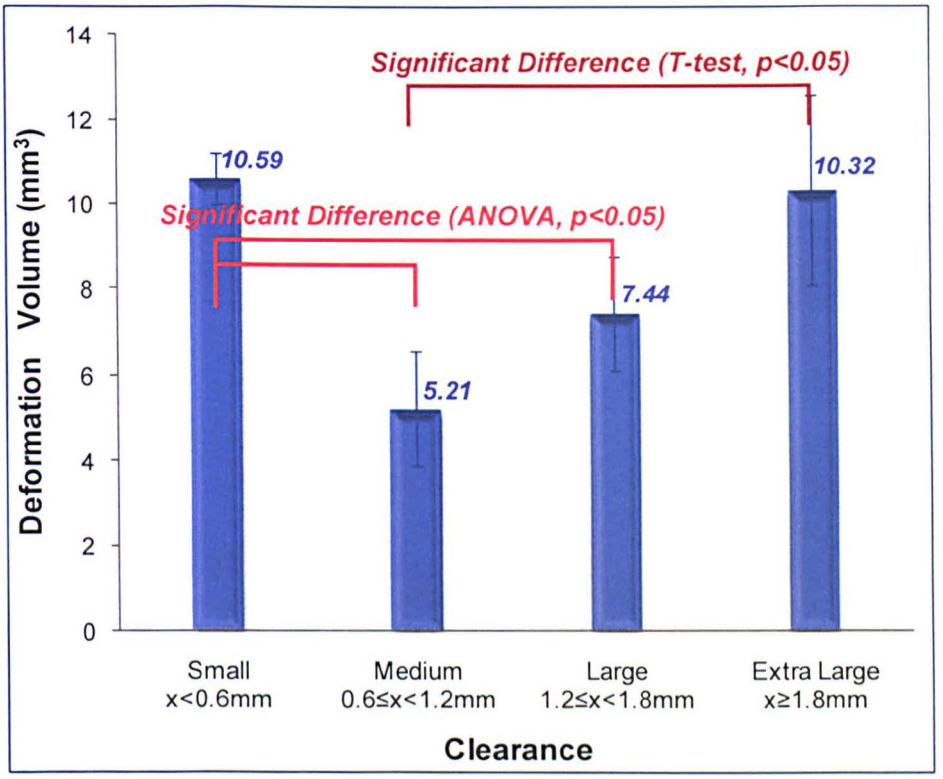

Figure 4.21. Comparison of acetabular deformation volume of acetabular cartilage in specimens with small, medium, large, and extra large clearances under 400N constant loading (n=3, mean ± 95% confidence limits).

4.5.4.2 Cartilage Deformation Depth

The average deformed depth in the studied area is compared in specimens with small, medium, large and extra large clearances in Figure 4.22. It was found that the average deformed depth was significantly higher in specimens with extra large clearances compared with the specimens with small, medium, and large clearances (ANOVA, $p<0.05$, $n=3$). The average deformation depth was significantly higher in specimens with small clearances compared to specimens with medium and large clearances (ANOVA, $p<0.05$, $n=3$). No significant difference of the average deformation depth between specimens with medium and large clearances (ANOVA, $p>0.05$, $n=3$).

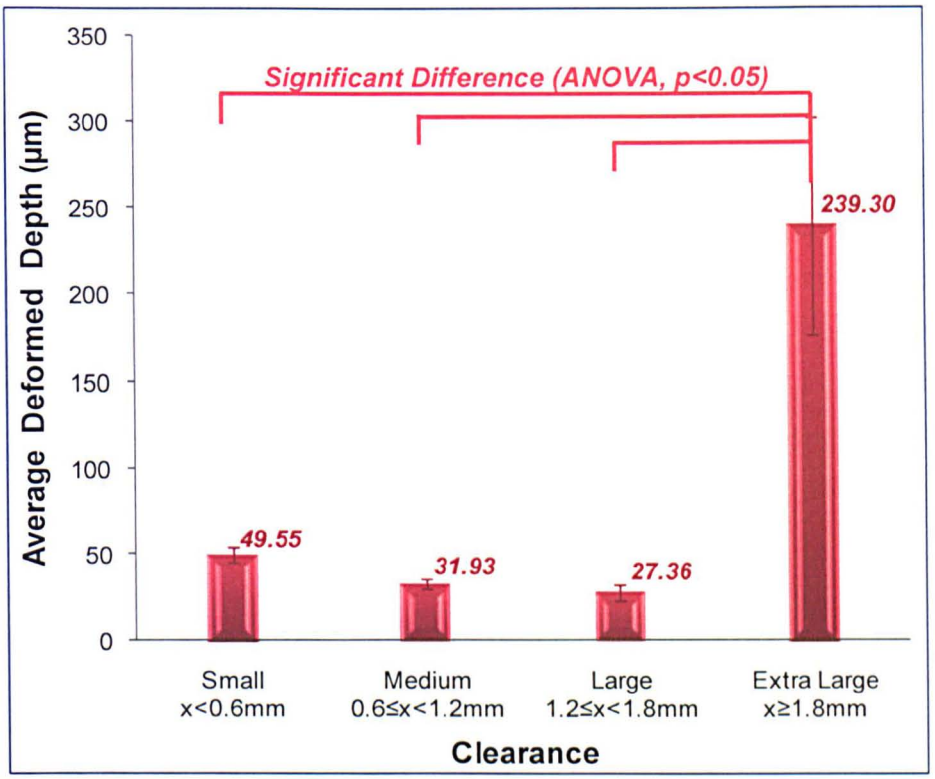

Figure 4.22. Comparison of average deformation depth of acetabular cartilage in the studied area in specimens with small, medium, large, and extra large clearances following 2 hours of constant load testing (n=3, mean ± 95% confidence limits).

4.6 Discussion

4.6.1 Effect of Clearance on Contact Stress and Contact Area

The hip contact stress is considered as one of the major most important factors influencing the development of articular cartilage in the hip joint. When half of the porcine body weight was applied constantly to acetabulum with a range of FE radial clearances 0.05~3.45mm, the average contact stress on the acetabulum was found to be approximately 2.4~4.7 MPa, and the peak contact stress was approximately 3.9~7.2 MPa. This peak contact stress range is close to values in the literature of the hip peak contact stress measured by *in-vitro* pressure-sensitive film; these are cited as approximately 2.90~9 MPa in human hip joint: 2.9~8.6 MPa (Afoke *et al.*, 1987), 4.0~6.0 MPa (Bay *et al.*, 1997), 7.5~9.0 (Hak *et al.*, 1998), and 7.7 MPa (von Eisenhart *et al.*, 1999).

In this hemiarthroplasty hip model, the contact stress increased in specimens with increasing clearance due to the decreasing contact area in specimens. With extra large clearances the contact stress was significantly higher compared to specimens with small, medium, and large clearances (ANOVA, $p<0.05$, $n=6$). This was due to the significantly reduced contact area in specimens with extra large

clearances (ANOVA, $p<0.05$, $n=6$). However, the contact area measurements taken using the super-low pressure FUJI film appeared to contain errors in some specimen measurements due to the sensitivity of super-low pressure film. When the load was applied to acetabulum, we postulate that the metal head slid and then fitted (located) inside the acetabulum, during this process all the contact area was marked on the super-low FUJI film. Hence there appeared to be "extra" unexpected regions of contact that were considered in the measurement of the contact area. This may be due to the geometry of the individual acetabulum. For example, as shown in Figure 4.23 as the white circled area. The contact stress in the circled area is significantly higher compared to the loaded contact area average contact stress.

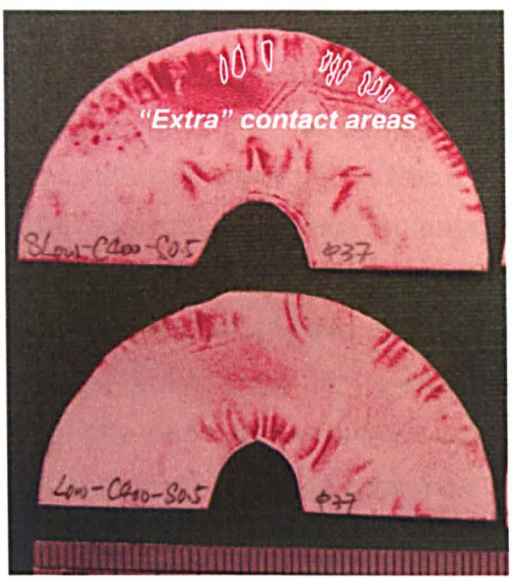

Figure 4.23. "Extra" contact areas marked on the super-low FUJI film when the metal head loaded (slid and then fit red) into the acetabulum due to the geometry of the individual acetabulum.

From the results of the FUJI film testing, it is concluded that the small clearances in the acetabula may reduce both the average and peak contact stress by enlarging the contact areas. Although the smaller clearances may also cause high local contact stress in some "extra" unexpected contact areas which might be harmful to the deformation and degeneration of articular cartilage in this *in-vitro* study. However, when the femoral head implant is placed in the natural acetabulum clinically, this "extra" unexpected contact areas would not occur during the patients daily life. In specimens with extra large clearances, both average and peak contact stresses are significantly higher, which might cause severe damage of the articular cartilage when it articulates against a metal counterface. In this case, extra large

clearances between the acetabulum and the implant metal head should not be recommended for hip hemiarthroplasty.

4.6.2 Effect of Clearance on Friction and Frictional Shear Stress

In this hemiarthroplasty hip model, the coefficient of friction increased with time in the first hour loading, and then remained at a relatively constant level till 2 hours with all different clearances. This was due to the biphasic property of cartilage, when load was applied, the biphasic support phases of articular cartilage was transferred from full fluid phase into a combined fluid and solid phase in equilibrium. When the supporting phase reached the equilibrium value the coefficient of friction remained at that level. The loading area and fluid movements in acetabular cartilage under constant loading is shown in Figure 4.24. Under constant loading, the fluid moved from the centre of the acetabular cartilage loading area to the edge, a small amount of fluid moved from the unloaded area to the loading area edge when the contact area migration was occurred.

It is hypothesed that when the clearance increased between the orbicular head and the regular orbicular shape of cup, there is a decrease of the contact area, hence the contact stress increase and this leads to increase of coefficient of friction. However, in this hemiarthroplasty hip model, the friction findings are contrary to the hypothesis. The coefficient of friction was found decreased (from 0.33 to 0.23 at the 2-hour time point) when the clearance increased (from small, to medium, to large, till extra large) under constant loading, and this was due to two factors: the geometry of the cup (porcine acetabulum), and the biphasic property of articular cartilage counterface. Firstly, the geometry of porcine acetabulum is irregular and it is varying from specimens to specimens. Hence, the contact area between the metal head and the acetabular cartilage was not regular or even from area to area. Secondly, the contact surface was articular cartilage, and the biphasic property of cartilage transferred the load from fluid phase to a solid and fluid phase in equilibrium. Hence, when there was increased translation and fluid support during the contact area migration in the cartilage, hence, the increase of fluid support led to the coefficient of friction to decrease.

In Figure 4.25, for example, for the same porcine acetabulum, increased the clearance (reduce the metal head size) from small, medium, large, and to extra large, the contact area decreased as pink, red, green, to blue area. When the pendulum reciprocation motion was applied the contact area migration was created, smaller contact area had more fluid support phase following the migration of contact

area, and the coefficient of friction decreased. Previous friction studies on the "unconfined" cartilage pin on metal plate simple geometry model by Pickard et al, (1998) have reported increased contact stress decreased the coefficient of friction with the range of contact stress of 0.5~4 MPa. After 45 minutes reciprocation in 25% bovine serum solution the coefficient of friction was: 0.48 under 0.5 MPa, 0.32 under 2 MPa, 0.28 under 4 MPa (Pickard *et al.*, 1998b).

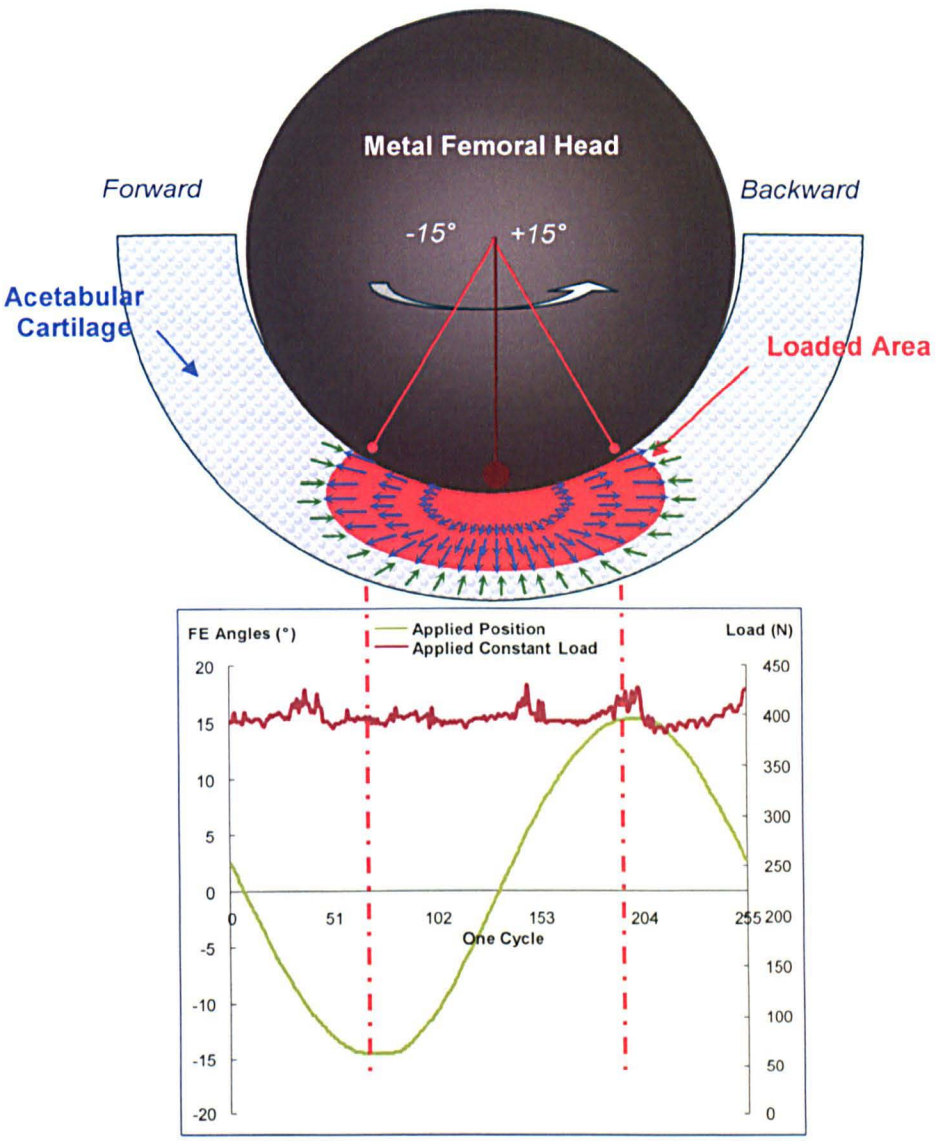

Figure 4.24 Loading area and fluid movements of the acetabular cartilage during the pendulum motion under constant loading.

However, in specimens with extra large clearances under constant loading, an increased contact pressure and frictional shear stress was observed and this exceeded the durability limit of the cartilage. For specimens with extra large clearance, after one hour of pendulum reciprocation, the average frictional shear stress reached 1.1 MPa, and the peak frictional shear stress was approximately 1.7

MPa. Both the average and the peak frictional shear stress were significantly higher compared to other clearance groups (small, medium and large) (ANOVA, $p<0.05$, $n=6$). The combined effects may cause the cartilage surface fibres and collagen to fracture, and delaminate / separate the cartilage from the attached bone. When this damage occurred, the damaged acetabular area deformed and then reduced the contact area between the metal head and the cartilage with (over) time, until a piece of cartilage was delaminated from the bone. This delaminated cartilage my remain in the same position, or it may be removed from the bone and repositioned (Figure 4.18 specimens 1, 3, and 5 may be related to this). The artifact in the coefficient of friction that was observed when the cartilage damage was being occurred (Figure 4.12). However, the damaged cartilage surface did not cause the coefficient of friction to increase significantly further. It is postulated that the coefficient of friction artifact was caused when (as) the cartilage surface was changing: either being broken or removed. It is speculated that after the damage, a new biphasic load support phases was built and the coefficient of friction remained. The damaged cartilage area lost GAGs and when the molecules were forced out from the matrix a gel-like lubricant was formed between the metal and cartilage articulating surface, hence, the coefficient of friction was remained or even reduced.

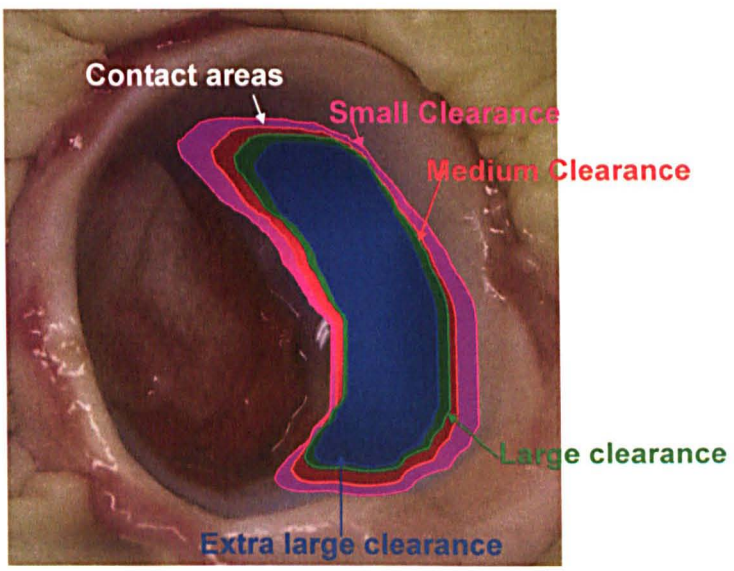

Figure 4.25 Contact are on the acetabular cartilage with small (pink), medium (red), large (green), and extra large (blue) clearances.

Similar observations of damaged cartilage have been reported in previous studies: A study on survival of articular cartilage after controlled impact showed that, structural damage of cartilage occurred at the surface of cartilage if the stress levels on impact exceeded 25 MPa (Repo and Finlay, 1977). In a knee

hemiarthroplasty friction test that mimicked meniscectomy, it was shown that contact stress was an important factor influencing friction and wear (Figure 4.26.d) (McCann *et al.*, 2008). For articular cartilage and stainless steel counterfaces, the average contact stress at low load (16.7~259N) was 8.93MPa and at high load (66.6~1036N) it was 31.3 MPa. However, in this hemiarthroplasty hip model the measured peak contact stress with extra large clearance was found to be approximately 7.2 MPa, which led to the catastrophic cartilage damage. Hence, the porcine hip acetabular cartilage presented lower limitation of contact stress compared to human knee and bovine knee cartilage.

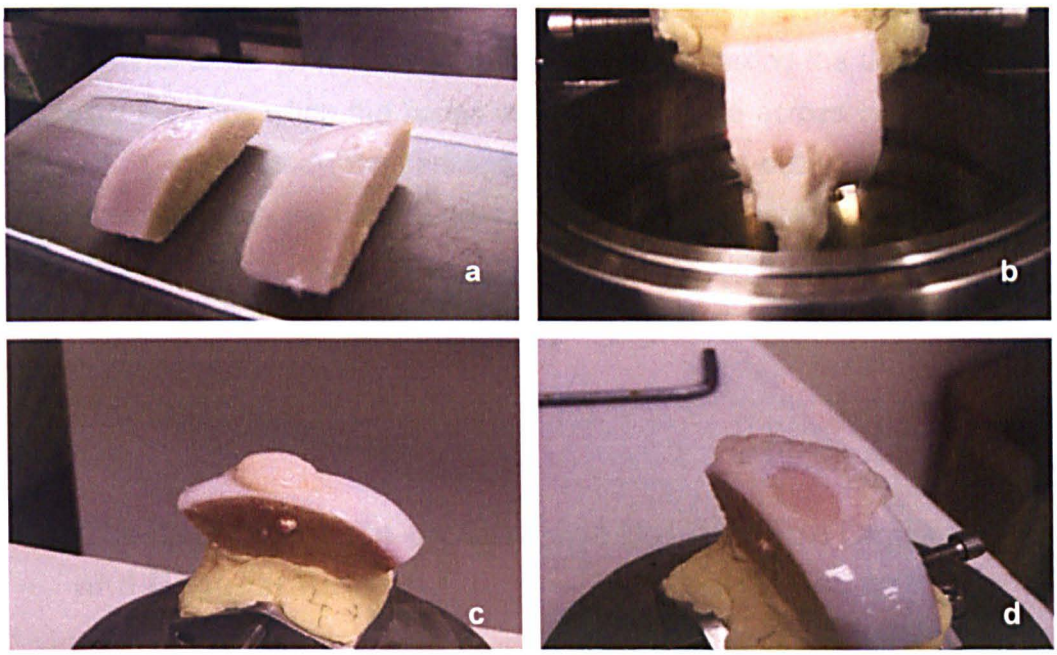

Figure 4.26 Wear of femoral surfaces articulating against stainless steel (a) surface fibrillation at low load (b), (c) and (d) catastrophic wear of cartilage through to underlying bone (McCann *et al.*, 2008).

4.6.3 Effect of Clearance on Cartilage Surface Roughness and Wear

A solid surface has a complex structure and complex properties depending on the nature of the solids. Properties of articular surfaces are crucial to surface interaction due to the surface properties affect the real area of contact, friction, wear and lubrication. Although the coefficient of friction was observed to decrease with the increasing clearance in this hemiarthroplasty hip model with 2 hours constant pendulum reciprocation, no significant difference of surface roughness was observed among the specimens in different clearance levels (an R_a value between 5.59 μm to 7.85 μm) (ANOVA, $p>0.05$, $n=3$). The surface roughness of the replica

only presented the texture of cartilage surface, but the roughness value does not provide information about the cartilage wear and deformation level.

Different cartilage wear grades 1, 2, and 3 were seen in specimens with small, medium, large, and extra large clearances, but wear grade 4 (full thickness cartilage loss with exposure of the subchondral bone) was only observed in specimens with extra large clearances. It is postulated that the constant loading with high local contact stress in specimens with extra large clearance produced frictional shear stress that was beyond the damage threshold of the acetabular cartilage. Hence, the pieces of cartilage were delaminated and repositioned. It was also found that the examined percentage of unworn cartilage area increased, when clearance increased. Clinically, an articular cartilage chondral fracture occurs when there is trauma to the joint articular surface without breaking the underlying bone. This mostly happens when the bones are forced to slide across one another with marked force. In this study, the cartilage chondral fracture occurred (wear grade 4) in the hemiarthroplasty hip model under constant load in specimens with extra large clearances, where the metal head and the articular acetabular met, and may be caused by the high friction force and frictional shear stress within 2-hour loading time with the pendulum reciprocation.

4.6.4 Effect of Clearance on Cartilage Deformation Degradation and Degeneration

In addition to tribological functions, surface deformation is important at providing information about the damage level of the articular cartilage. It is postulated that the cartilage damage (deformation, degradation, and wear) was occurred mostly due to the failure mechanisms of collagen fibres in the articular cartilage. In this hemiarthroplasty hip model, cartilage deformation included both permanent deformation (due to the loading which damaged the extracellular matrix) and cartilage wear (material loss of cartilage). It was shown that the deformation volume and the average deformation depth were affected by clearance.

Specimens with small and extra large radial clearances produced higher deformation volume and average deformation depth compared to specimens with medium and large clearances. When the clearance was small (<0.6mm), the metal head contacted a greater cartilage area during the pendulum reciprocation, and due to the geometry of porcine acetabulum the metal head caused squeezing of some acetabular cartilage areas to fit in. The porcine acetabulum specimens geometry had been studied before the friction test, and it was found that the dimension on the

FE (flexion-extension) direction was mostly a few millimetres greater than the dimension on the ML (Medial-lateral) direction (Figure 2.21). Hence, during the fit in process it caused deeper deformation, and then with the larger cartilage contact surface higher deformation volume was created. When specimens with extra large clearance (≥2.4mm) were tested, the contact area between the metal head and the acetabulum reduced and this caused an increase in contact stress. Previous pin on plate hemiarthroplasty studies demonstrated higher contact stress increased both cartage permanent deformation and linear wear. Hence, in this hemiarthroplasty hip model in specimens with extra large clearances the increased contact stress led to deeper deformations. Furthermore, the increased frictional shear stress caused chondral fracture of cartilage hence the deformation depth reached the full cartilage thickness.

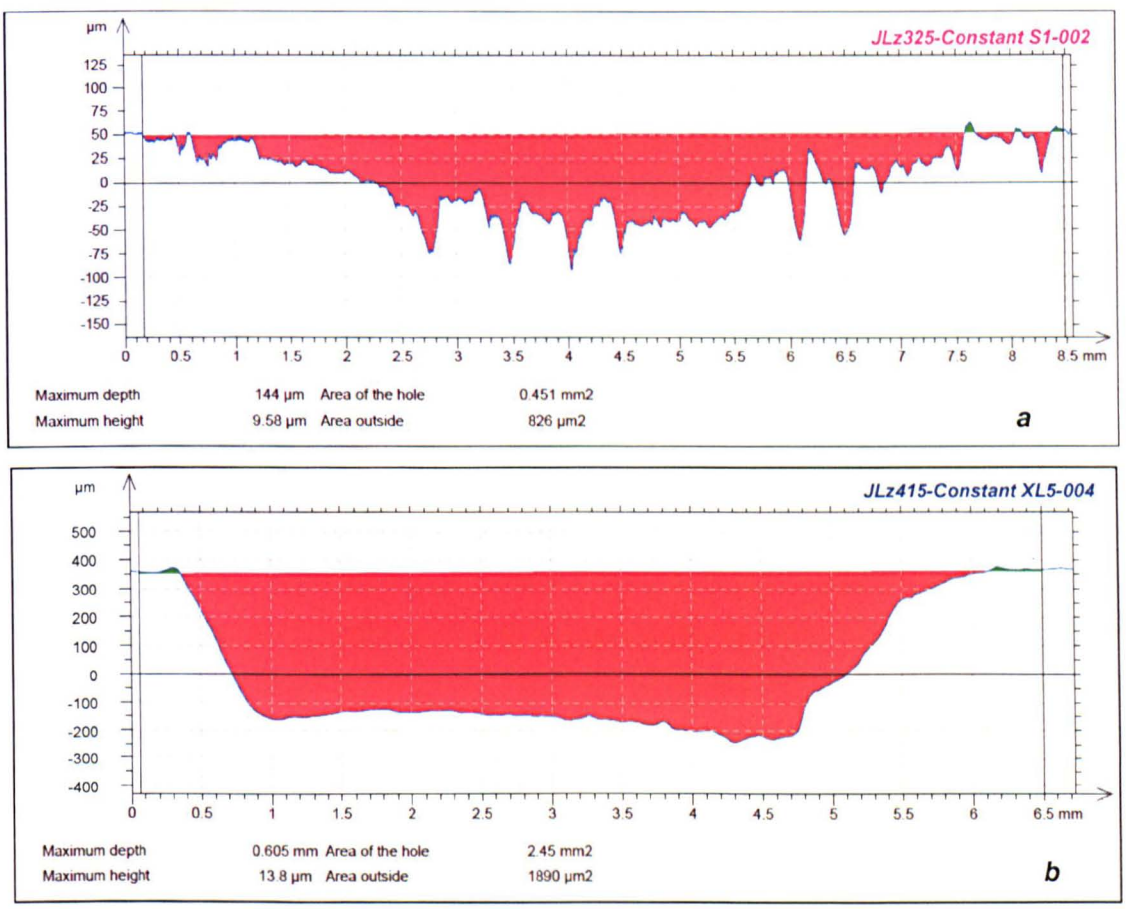

Figure 4.27 a. A typical trace analysis result of the specimen with small clearance; b. A typical trace analysis result of the specimen with extra large clearance.

Although no significant differences in deformation volumes between specimens with small and extra large clearances were observed (ANOVA, $p>0.05$, $n=3$), the cartilage wear grades and the deformation area were significantly

different. Typical traces analysis result on small and extra large clearances specimens is shown in Figure 4.27. The trace in a specimen with small clearance (Figure 4.27.a) the maximum deformation depth was approximate 150 μm, and the deformation depth was not even - it was deeper in the middle and shallow on both sides. However, in the specimen with extra large clearance (Figure 4.27.b) the trace deformation depth was approximate 600 μm (equal to the deformed cartilage thickness) and spread evenly.

4.6.5 Clearance Recommendation in Clinical Practice

In this hip joint hemiarthroplasty constant loading model, four categories of clearances were chosen. The clearance was calculated from two parameters (femoral head size and acetabulum size). This type of categorisation was selected because clinically, patients have different sizes of acetabula, and it is realistic for different femoral head sizes to be selected to provide a specific clearance. The results have shown that small clearance limited the space between the femoral head and acetabular cartilage especially in the ML direction as in general the dimension in FE direction was greater than the dimension in ML direction. When the clearance was small, more cartilage wear was caused during the pendulum motion, and the metal head caused deeper levels of deformation into the cartilage. in acetabula tested with heads to produce extra large clearance, severe damage to the acetabular cartilage was observed, this was due to the increased frictional shear stress. The greater space between the head and acetabulum caused the head motion to delaminated the cartilage, it then became fully removed and this cartilage segment could be repositioned. These findings suggest that the patient's acetabulum size in FE direction should be measured after removing the natural femoral head during the surgery. From the 2 hours constant loading cartilage friction and deformation results small clearance (0.1-0.6 mm) and extra large clearance (>1.8 mm) should be avoided clinically.

4.7 Conclusion

Good correlations of contact area (R^2=0.63), contact stress (average and peak, R^2=0.63 and R^2=0.75), and coefficient of friction (R^2=0.61) with the FE radial clearance were observed under constant pendulum reciprocation in this hemiarthroplasty hip model. The effect of clearance on cartilage friction, deformation, degradation, and degeneration was as follows:

1. With increasing clearance, the contact area decreased, and both average contact stress and peak contact stress increased.
2. A trend of decreasing coefficient of friction with increasing clearance under constant loading conditions was observed.
3. Low levels of friction (less than 0.35) and short term (2 hours) durability were seen for a range of clearances (up to 1.8mm) under constant loading.
4. There is some evidence that extra large clearances (>1.8mm) may cause the frictional shear stress limits of the cartilage to be exceeded and severe damage / degradation of the acetabular cartilage to occur. This was due to the combined effects of higher frictional average and peak shear stress above the critical threshold.
5. The wear area decreased and the wear grade increased with the increasing clearance.
6. The deformation area and average wear depth was significantly high in specimens with extra large clearances due to the increase in frictional shear stress.
7. Cartilage deformation volumes were similar in specimens with small and extra large clearances, and in specimens with medium and large clearances, this was due to the clearance effects to the deformation area and deformed surface area.

Chapter 5 The Effect of Clearance on Cartilage in Hemiarthroplasty under Dynamic Loading

5.1 Introduction

This chapter focuses on studying the effect of clearance on acetabular cartilage friction and deformation in a hemiarthroplasty hip simulation when a dynamic loading regime is applied. It continues on from the previous study, when a constant loading regime was applied (Chapter 4) and extends the understanding of cartilage tribological properties under a simplified walking cycle in a hemiarthroplasty hip model.

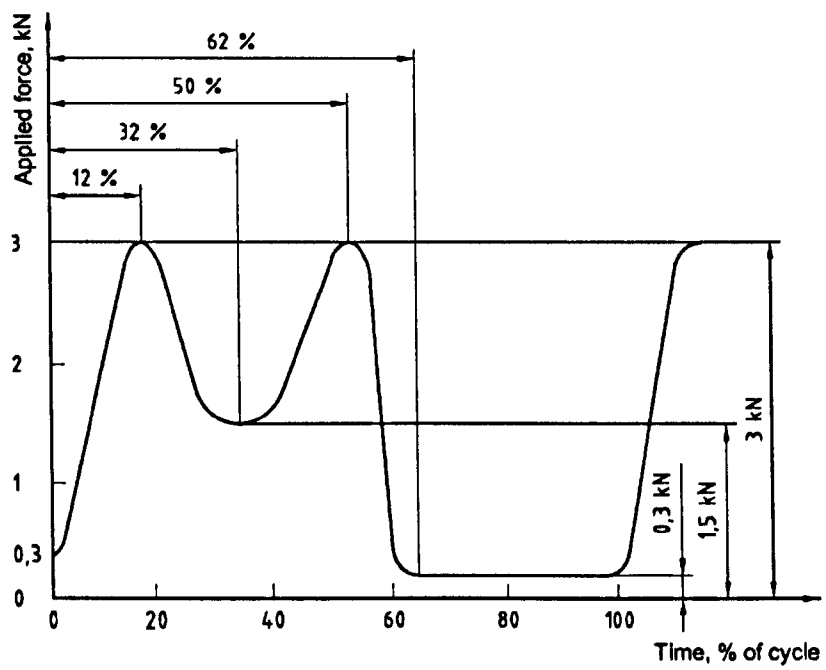

Time, % of cycle (± 3 %)	0	12	32	50	62	100
Applied force, kN (± 90 N)	0,3	3,0	1,5	3,0	0,3	0,3

Figure 5.1 Variation with time of force in a simplified walking cycle as defined by ISO standard 14242-1 (Standard, 2002)

The human walking gait in the natural hip joint has been examined in the last twenty years in both experimental studies and modelling studies (Paul, 1999; Bergmann *et al.*, 2001; Standard, 2002; Yoshida *et al.*, 2006). The British Standard Implants for surgery wear of total hip-joint prostheses (BS ISO 14242-1: 2002)

recommendation has been widely used to provide (Figure 5.1) loading and displacement parameters for hip simulator wear-testing machines.

Friction studies (Broom *et al.*, 1996; Graindorge *et al.*, 2004; Krishnan *et al.*, 2005; Graindorge *et al.*, 2006) that apply dynamic loading and reciprocation between cartilage and metal or glass counterfaces have mostly used a simple geometry model, such as a pin on plate configuration. Experimental studies of cartilage plugs have found that the repetitive loading disrupted the tissue and the severity of the damage increased with increasing load and increasing number of loading cycles (Zimmerman et al., 1988). Three main effects of repetitive loading were concluded from Zimmerman's experiments: (1) propagation of vertical cartilage fissures from the joint surface to calcified cartilage; (2) extension of the damage of oblique fissures into areas of intact cartilage; (3) creation of cartilage flaps and free fragments.

However, few studies have investigated the frictional characteristics of articular cartilage under physiological activities conditions such as walking and running in the entire acetabulum specimens. For example, animal experiments *in-vivo* on hip hemiarthroplasty replacement have been reported mainly in canine hip joints (Cruess *et al.*, 1984; Cook *et al.*, 1989; Maistrelli *et al.*, 1991). However, under dynamic loading the tribological properties of confined cartilage samples *in-vitro* remain largely unknown. In the previous chapter under constant loading the coefficient of friction was found to decrease with the increasing FE radial clearance, which was contrary to the hypothesis. When specimens had extra large clearances and were subjected to constant loading, severe acetabular cartilage damage was observed due to the smaller contact area which increased the frictional shear stress to a threshold limit. It is interesting to know how the FE radial clearance affects the friction and cartilage damage under dynamic loading because this more closely implicates the clinical situation mimics the human walking gait motions.

This summarised literature review has led to the development of a series of research questions, which will be investigated under dynamic loading:

- Will the coefficient of friction increase with the increasing clearances as has been hypothesis?
- Will severe cartilage damage be observed with extra large clearance under dynamic loading as under constant loading?
- How does dynamic loading affect the acetabular cartilage tribological properties compared to constant loading?

5.2 Objectives

The objectives of this study were to use a hip joint model of the acetabular cartilage cup reciprocating against a metal head to consider the effect of clearance on cartilage tribological properties under a dynamic loading regime. The clearance was considered in the flexion-extension direction and ranged from small, medium, large to extra large (as described in Section 2.3.1.5). Properties studied were: (1) contact area and contact stress, (2) coefficient of friction and frictional shear stress, (3) surface roughness, (4) cartilage wear grade, and (5) surface deformation volume and depth after the 2 hours ±15° (FE direction) 25~800 N dynamic loading pendulum friction study. An overview of this study is shown in Figure 5.2.

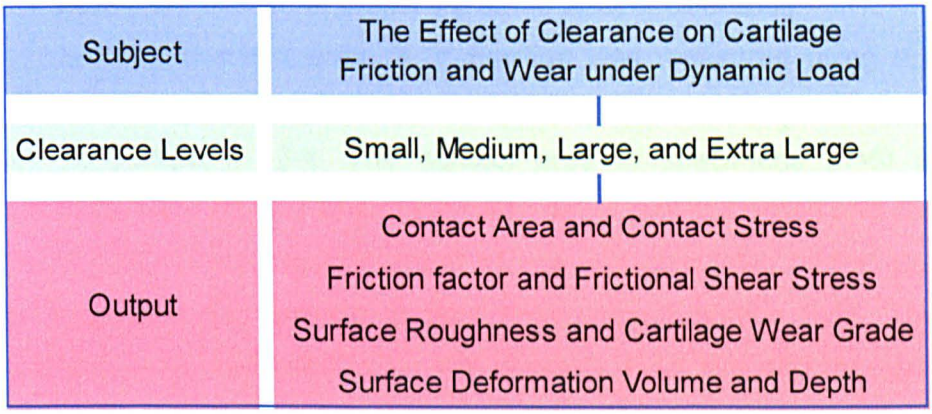

Figure 5.2 Summary of studied tribological properties in pendulum dynamic loading study in hip joint

5.3 Materials

Test materials used were six-month old porcine acetabula and cobalt chrome heads (32, 34, 35, 36, and 37mm in diameter), and the lubricant was 25% bovine serum, as described in Sections 2.3.1.2, 4, 5, and 8 respectively. The porcine acetabulum was set in PMMA cement at 45 degrees as described in Section 2.3.2.2, and friction tests were conducted using a pendulum friction simulator as described in Section 2.3.2.1. Microset silicon replicas of the porcine acetabulum after the friction test were taken, to study wear, as described in Section 2.3.2.3. Contact areas and stresses were measured using the FUJI pressure film as described in Section 2.3.2.4. The cartilage wear grade measurements were completed as described in Section 2.3.2.5, and the surface deformation measurements were taken as described in Section 2.3.2.6.

5.4 Methods

The peak load of dynamic loading was chosen as the whole porcine body weight approximate 800 N with a loading time of 2 hours (explained in Section 2.3.2.1.1.) The **dynamic loading profile** was set as shown in Figure 2.24, and is a single sinusoidal peak load (800 N) over 60% of the cycle. This dynamic loading profile provides a simplified cycle representing the two peaks walking cycle, and avoids the difficulties and instabilities a twin peak cycle would cause in the pendulum friction simulator. The friction study was focused on peak loading point of each cycle and the coefficient of friction changes with time during a 2-hour test.

Samples with small, medium, large, and extra large radial clearances were tested as defined in Section 2.3.1.5, Table 2.2. Different femoral heads and acetabula sizes were chosen to create the same level of clearance.

The **average contact area** at 0° position was measured using super-low pressure FUJI film by applying 800 N static loading with no motion for 30 seconds, described in Section 2.3.2.4. The contact area of specimens (n=6) in each clearance range were measured and the mean value was calculated and compared (ANOVA, $p<0.05$). The **average contact stress** was calculated by the static load (800 N) divided by the average contact area using Equation 2-16. The **peak contact stress** was measured using low pressure FUJI film and the six highest measurements of stress at the 0 degree position of each specimen were selected and the mean value specimens (n=6) of each clearance were calculated and compared (ANOVA, $p<0.05$).

The **friction factor** was analysed as the coefficient of friction at the 0 degree position where the head was vertically loaded and in contact with the lowest position of the cup as shown in Figure 2.25. The coefficient of friction was calculated using Equation 2-15, as described in Section 2.3.2.1.1.2.

The **average frictional shear stress** and **the peak frictional shear stress** were calculated following Equations 2-17, and 2-18 in Section 2.3.2.5. The mean value of six specimens of each clearance group was calculated and compared (ANOVA, $p<0.05$).

The acetabular cartilage **surface roughness** was measured using microset replica and a two-dimensional profilometer. The roughness (Ra) of each trace was calculated using software following Equation 2-19.

The cartilage **wear grade area** was examined visually using an adaptation of the International Cartilage Repair Wear Grading System (Section 2.3.2.6). The area of the different wear grades were measured through marking a transparent cling film covering the microset replica of the acetabulum, as described in Section 2.3.2.6.

Then the area of the different wear grades and the whole acetabular lunate surface area were measured using Image Pro Plus, and presented as the percentage of the acetabular lunate surface area. The mean percentage of each wear grade area (n=6) in each clearance group was calculated and compared (ANOVA arcsine, $p<0.05$).

The acetabular replicas (n=3) were selected depending on their suitability for measurements. Intact original surface on both sides of the wear scar on the replicas was required for two-dimensional profilometer measurements (as described in Section 2.3.2.6.1, Figure 2.40). The acetabular surface **deformation volume** and the **average deformation depth** were calculated using Equations 2-20, and 2-21. The mean deformation volume and average deformation depth of each clearance group was calculated and compared (ANOVA, $p<0.05$, n=3).

5.5 Results

5.5.1 Effect of Clearance on Contact Area and Contact Stress

5.5.1.1 Contact Areas

Images of typical contact areas in each clearance group measured by super-low pressure FUJI film are shown in Figure 5.3, and Appendix 2.

The contact area of six specimens within each clearance group from the FUJI film was measured by Image Pro Plus, and inverse correlation between the clearance and the contact area of R=0.86 was observed (Figure 5.4). The mean contact area of specimens in each clearance group ranged from 129 mm^2 to 239 mm^2 as the clearance decreased from extra large to small (Figure 5.5). Specimens with extra large clearance had significantly smaller contact areas compared to specimens with small, medium, and large clearances (n=6, ANOVA, $p<0.05$). No other significant difference of contact areas among different clearance groups existed.

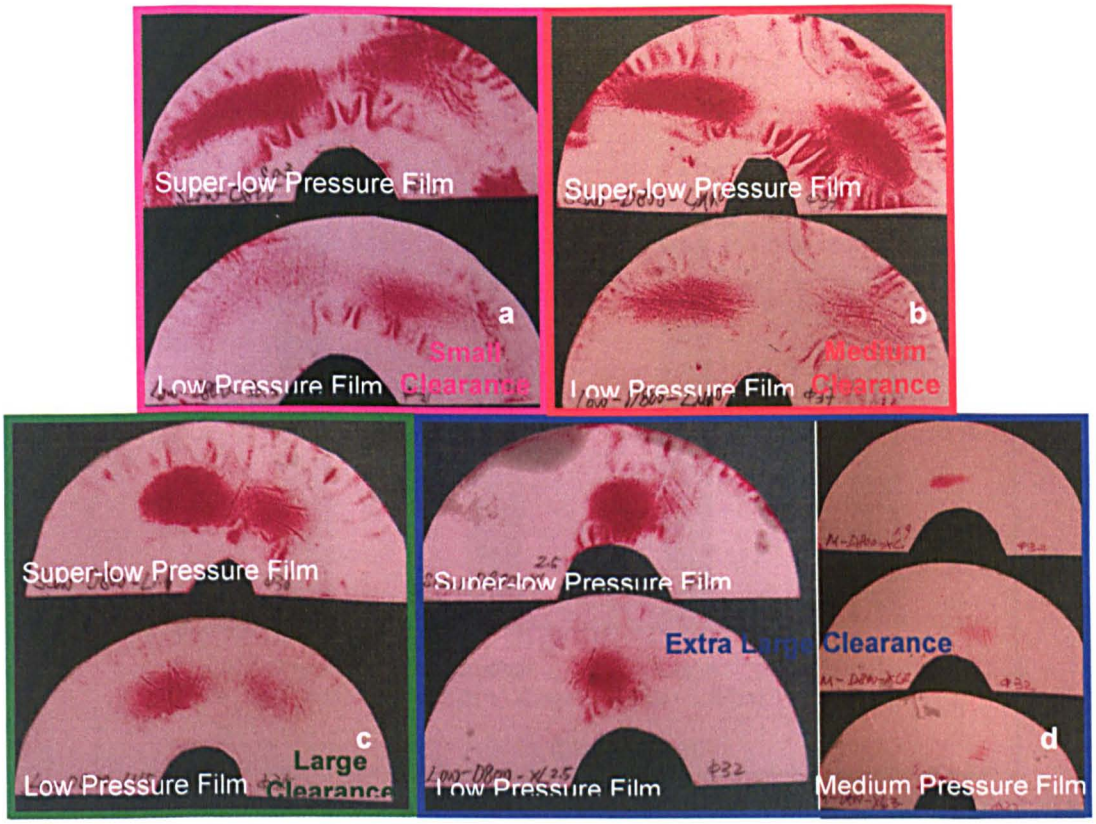

Figure 5.3 Contact area as measured by super-low pressure FUJI film and contact stress as measured by low pressure FUJI film in specimens with a) small, b) medium, c) large, and d) extra large clearances. Medium pressure FUJI film was used to measure the peak contact stress specimens with extra large clearance.

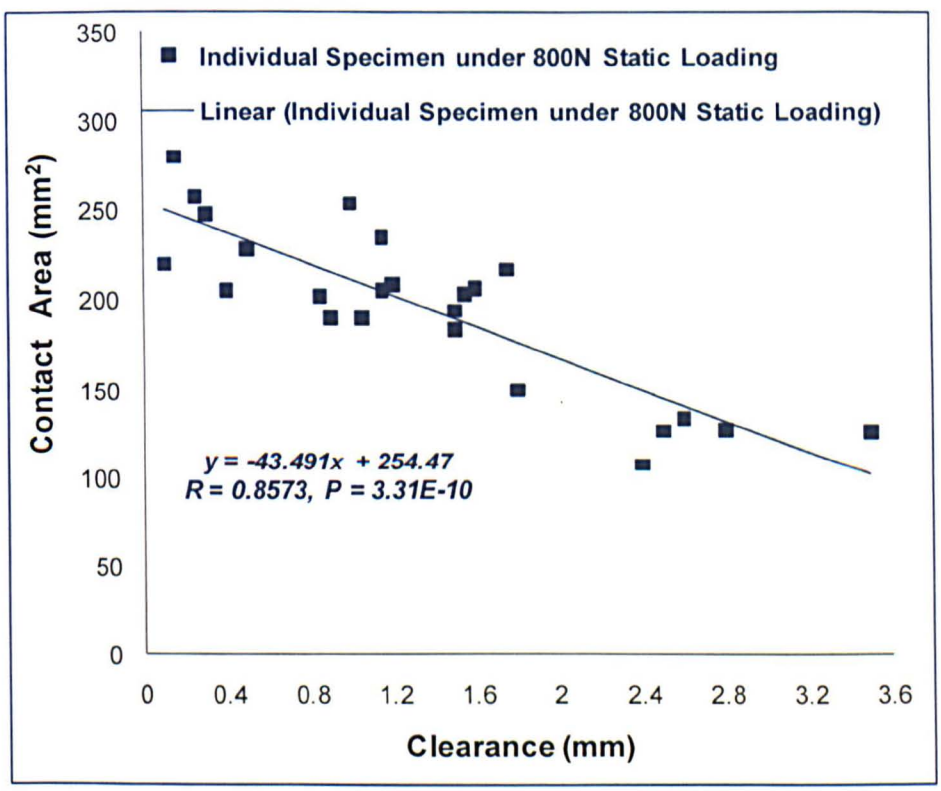

Figure 5.4 Correlation of specimen clearances (all groups) and contact area. R and P values were obtained using a regression analysis in Microsoft Excel 2007 (Microsoft Corporation, Redmond, USA).

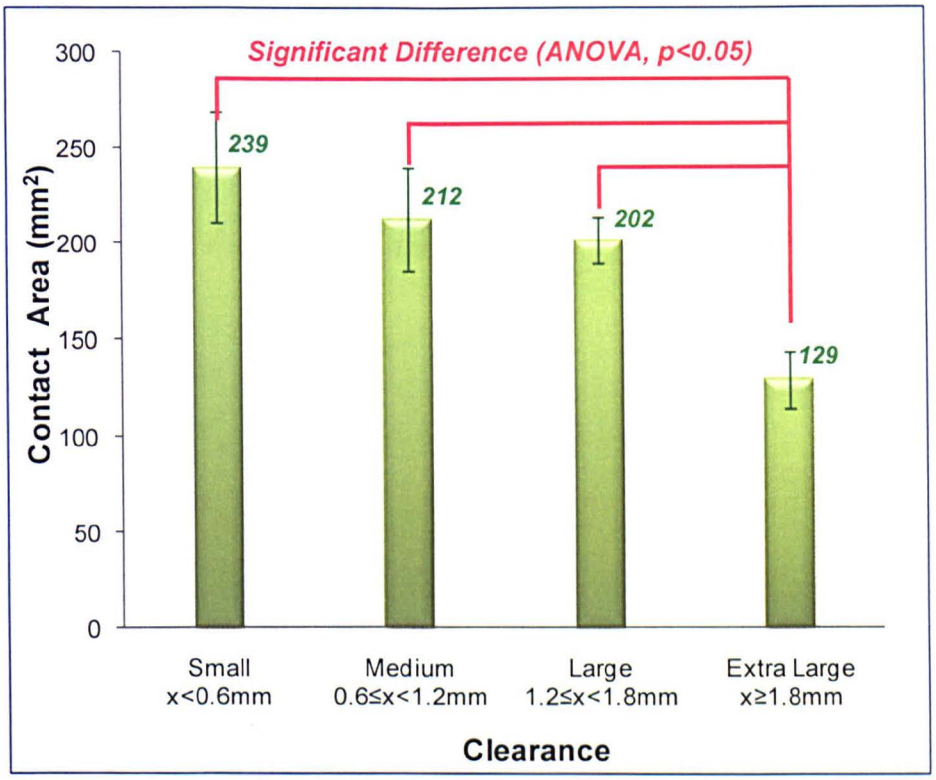

Figure 5.5 Contact area (mm^2) in specimens with different clearance levels (n=6, mean ± 95% confidence limits).

5.5.1.2 Contact Stress

The calculated average contact stress and measured peak contact stress in specimens with different clearances under 800 N static load applied for 30 seconds are shown in Figure 5.6.

Both the calculated average contact stress and the measured peak contact stress increased in specimens with increasing clearances. Correlations of R=0.85 and R=0.88 for the average contact stress and peak contact stress to the FE radial clearance were observed respectively.

Both the calculated contact stress and measured peak contact stress of specimens in each clearance group is shown in Figure 5.7.

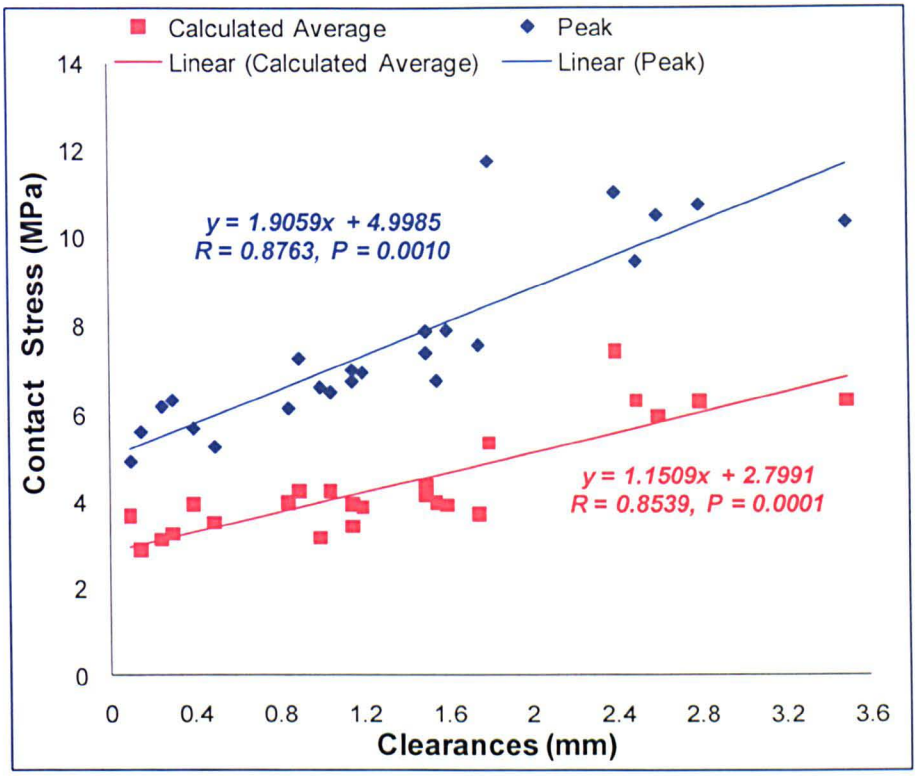

Figure 5.6 Correlations of calculated average contact stress / measured peak contact stress and specimen clearance. R and P values were obtained using a regression analysis in Microsoft Excel 2007 (Microsoft Corporation, Redmond, USA).

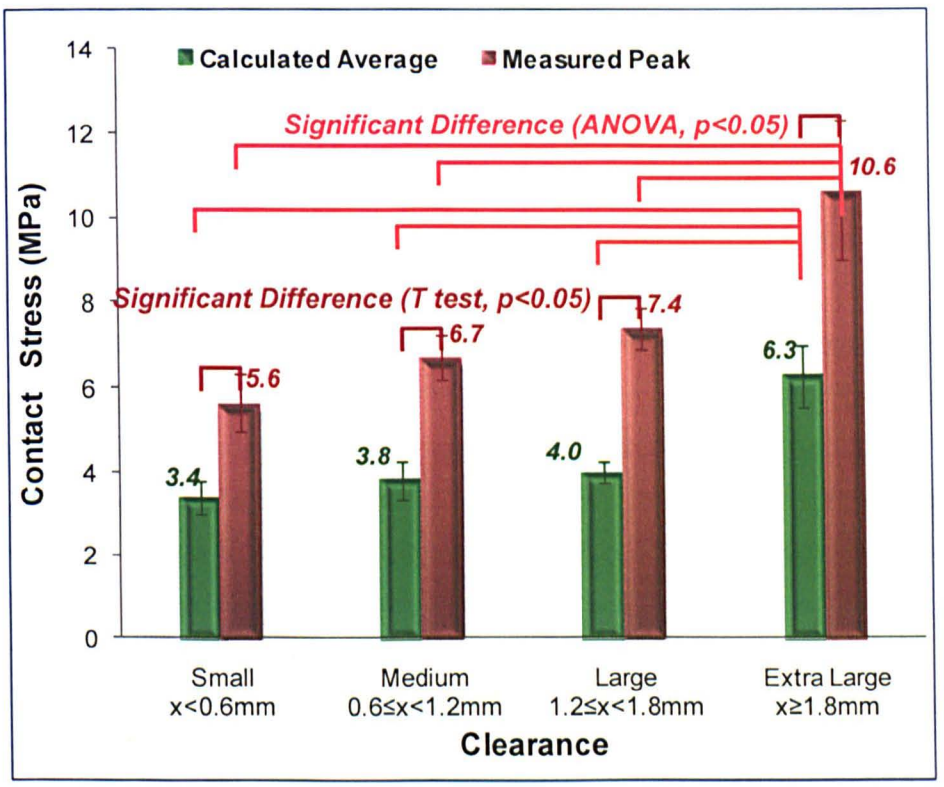

Figure 5.7 Calculated average contact stress and measured peak contact stress (MPa) in specimens with different clearances (n=6, mean ± 95% confidence limits).

The calculated average contact stress was significantly lower compared to the measured peak contact stress in specimens at each clearance level (n=6, T test,

$p<0.05$). The calculated average contact stress increased from 3.4 MPa to 6.3 MPa as the specimen clearance increased from small to extra large. The average contact stress was significantly higher in specimens with extra large clearances compared to the average contact stress in specimens with small, medium, and large clearances (n=6, ANOVA, $p<0.05$). The measured peak contact stress increased from 5.6 MPa to 10.6 MPa in specimens with increasing clearance from small, medium, large to extra large. The measured contact stress in specimens with extra large clearances was significantly higher compared to specimens with small and medium clearances (n=6, ANOVA, $p<0.05$). Significantly higher contact stress was observed in specimens with large clearances compared to specimens with small clearances (n=6, ANOVA, $p<0.05$). The measured peak contact stress was 1.65 to 1.85 times greater than the calculated average contact stress in specimens at each clearance level, a parabolic form relationship is assumed (n=6, T test, $p<0.05$).

5.5.2 Effect of Clearance of Friction and Frictional Shear Stress

5.5.2.1 Friction Factor (Coefficient of Friction)

The coefficients of friction measured under dynamic loading of specimens with different clearances during 2-hour friction tests are shown in Figures 5.8-11 for specimens with different clearances.

The coefficients of friction of specimens (n=6) with small clearances (from 0.1 to 0.5 mm) are shown in Figure 5.8. The mean coefficient of friction continued to increase from 0.07±0.03 to 0.16±0.03 during the 2-hour test.

In Figure 5.9, it is shown the coefficients of friction of specimens (n=6) with medium clearances (from 0.85 to 1.15 mm). During the 2-hour test, the mean coefficient of friction continued to increase from 0.06±0.02 to 0.15±0.02.

With large clearances (from 1.2 to 1.75 mm, n=6), the coefficients of friction are shown in Figure 5.10. The coefficient of friction kept increasing from 0.04±0.02 to 0.12±0.02 during the 2-hour test.

Specimens with extra large clearances (from 1.8 to 3.5 mm, n=6) had the coefficients of friction as shown in Figure 5.11. The coefficient of friction, during the 2-hour test, increased from 0.04±0.01 to 0.08±0.02.

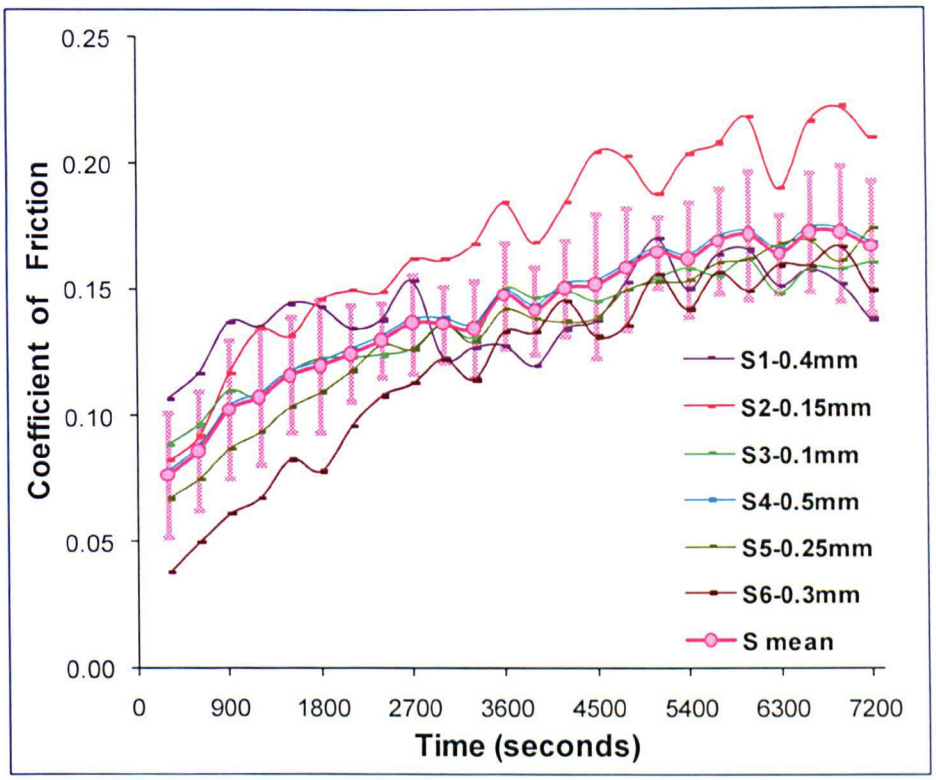

Figure 5.8 The coefficient of friction for specimens with small clearances (FE radial clearance < 0.6mm) under dynamic loading (n=6, mean ± 95% confidence limits), (*S_n-x.xx: S-Small clearance, n-specimen number, x.xx-FE radial clearance*).

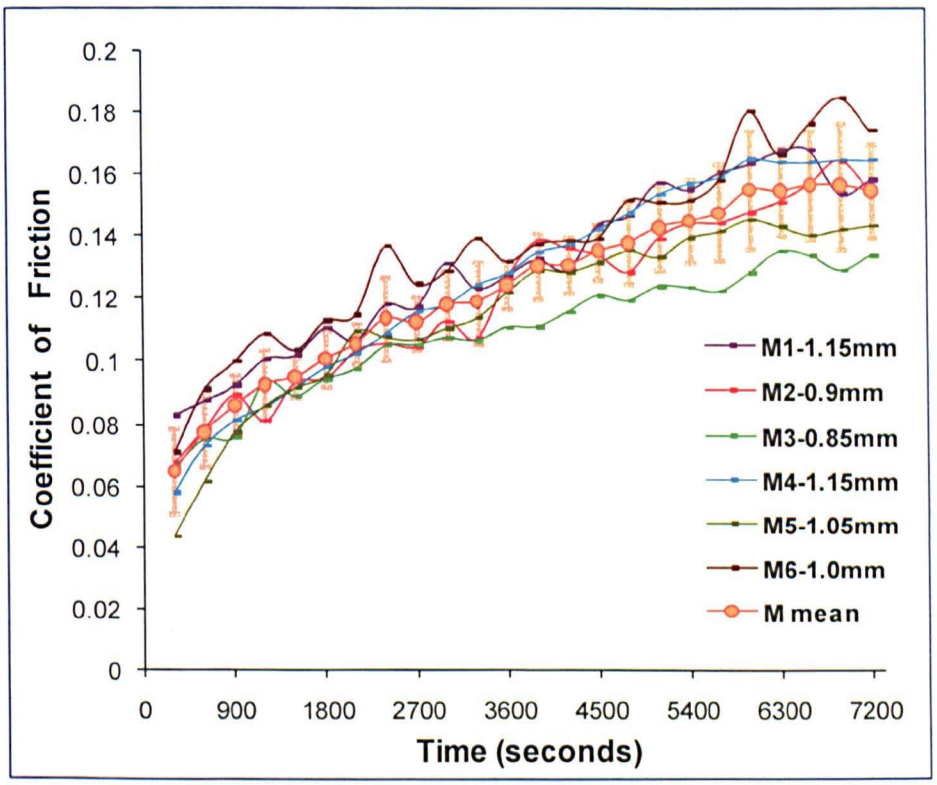

Figure 5.9 The coefficient of friction for specimens with medium clearances (0.6mm ≤ FE radial clearance < 1.2 mm) under dynamic loading (n=6, mean ± 95% confidence limits) (*M_n-x.xx: M-Medium clearance, n-specimen number, x.xx-FE radial clearance*).

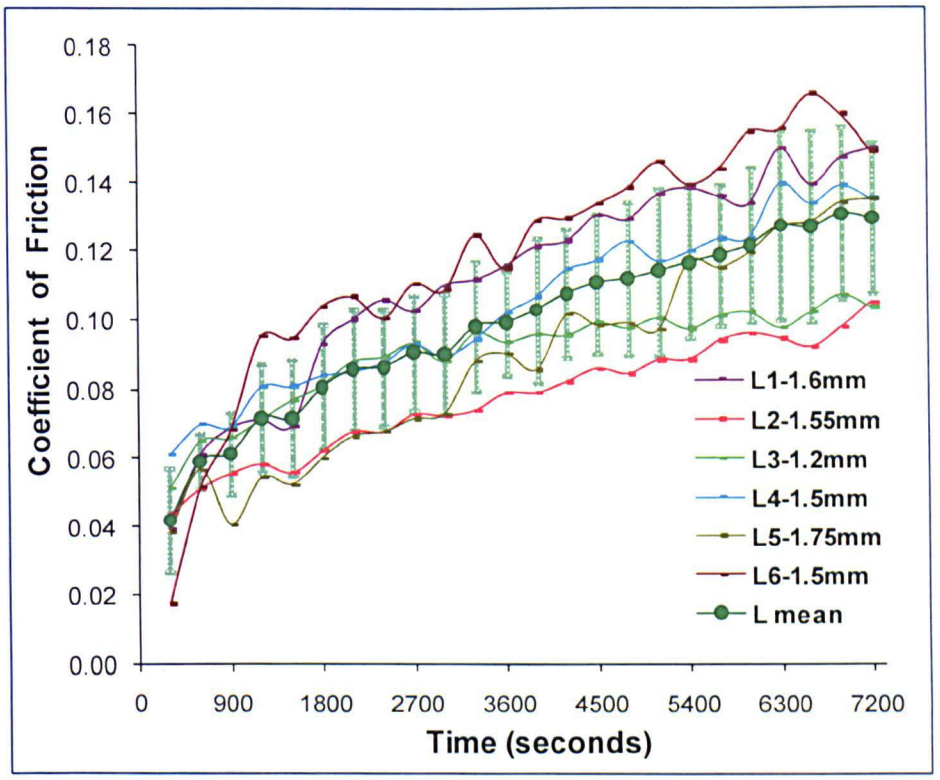

Figure 5.10 The coefficient of friction for specimens with large clearances (1.2mm ≤ FE radial clearance < 1.8 mm) under dynamic loading (n=6, mean ± 95% confidence limits) (*L_n-x.xx: L-Large clearance, n-specimen number, x.xx-FE radial clearance*).

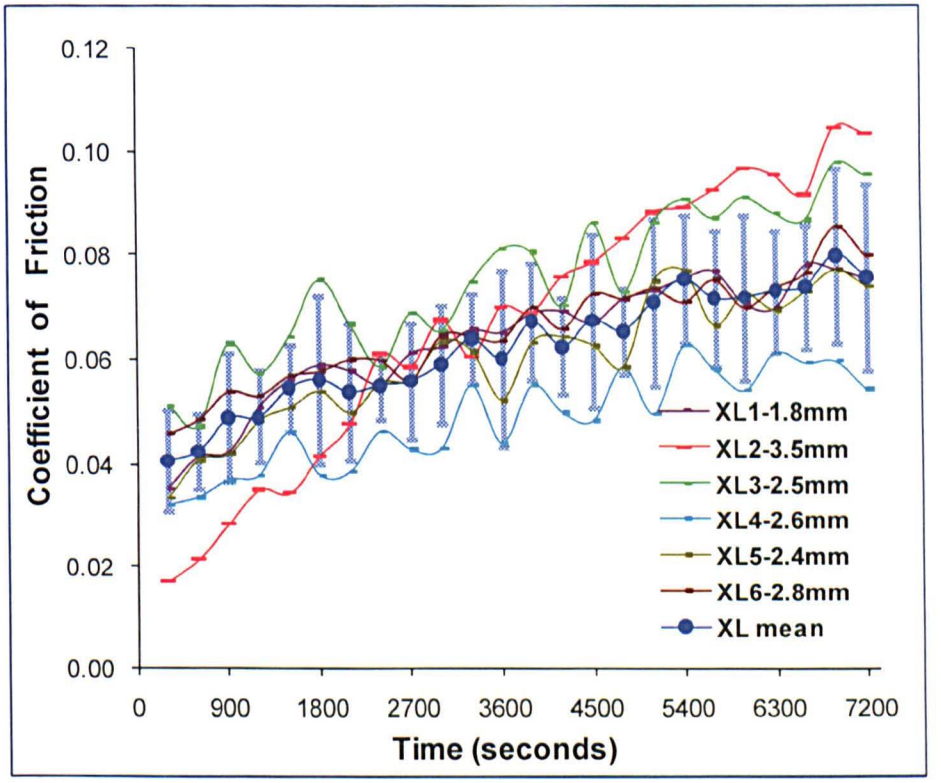

Figure 5.11 The coefficient of friction for specimens with extra large clearances (1.8mm ≤ FE radial clearance < 2.4 mm) under dynamic loading (n=6, mean ± 95% confidence limits) (*XL_n-x.xx: XL-Extra large clearance, n-specimen number, x.xx-FE radial clearance*).

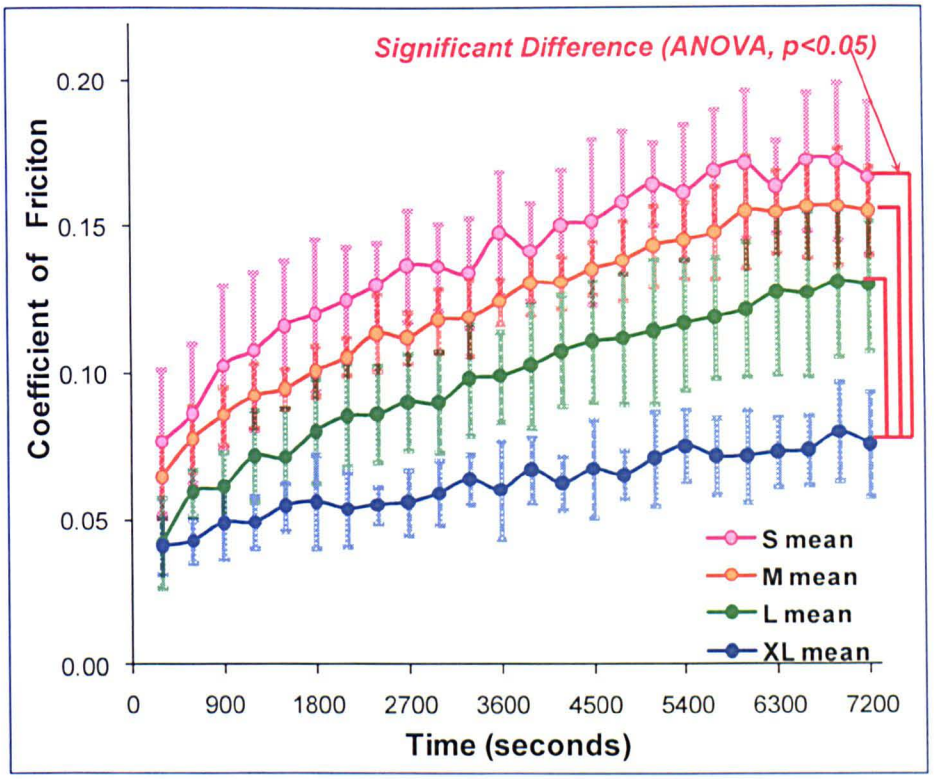

Figure 5.12 The mean coefficient of friction for specimens with small, medium, large, and extra large clearances under dynamic loading, (n=6, mean ± 95% confidence limits) (*S: small, M: medium, L: large, and XL: extra large clearance).*

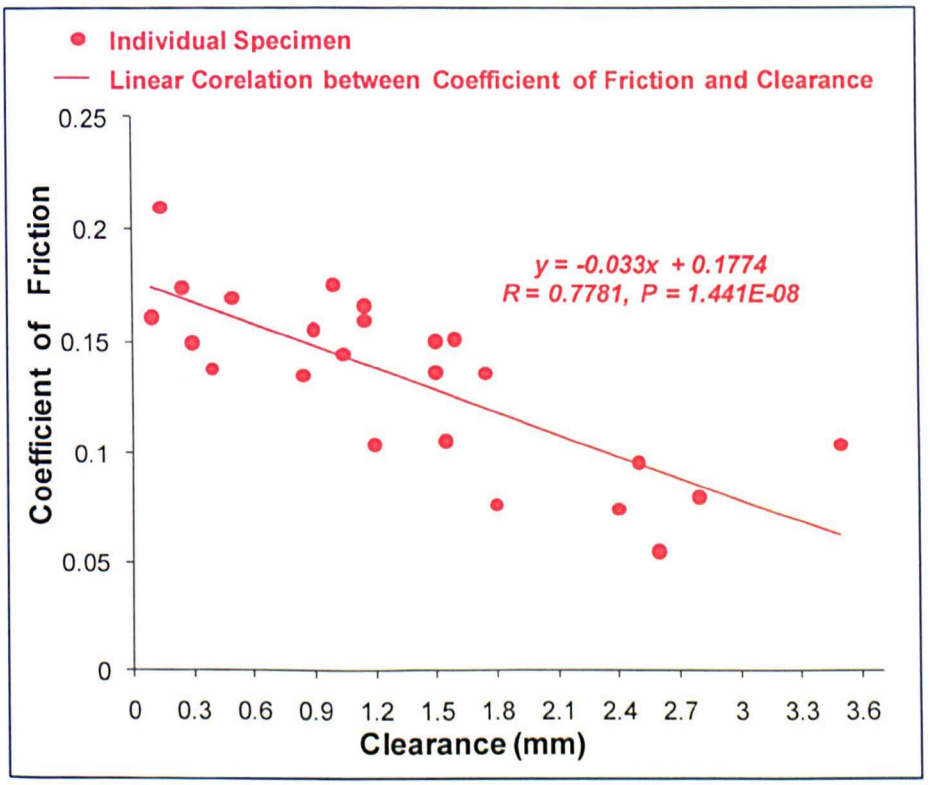

Figure 5.13 Correlation (R=0.78) between the coefficient of friction and FE radial clearance following 2 hours of dynamic load testing. R and P values were obtained using a regression analysis in Microsoft Excel 2007 (Microsoft Corporation, Redmond, USA).

The mean value of the coefficient of friction in specimens with different clearances is compared in Figure 5.12. A trend of decreasing coefficient of friction in specimens with increasing clearance (from small to extra large) is shown. The coefficient of friction was significantly lower in specimens with extra large clearances compared to specimens with small, medium, and large clearances (n=6, ANOVA, $p<0.05$).

The correlation of the coefficient of friction at 2 hours and FE radial clearance is shown in Figure 5.13. The coefficient of friction decreased in specimens with increasing clearances with a correlation of R=0.78.

5.5.2.2 Frictional Shear Stress

The calculated average frictional shear stress and the calculated peak frictional shear stress in specimens with different clearance groups are shown in Figure 5.14.

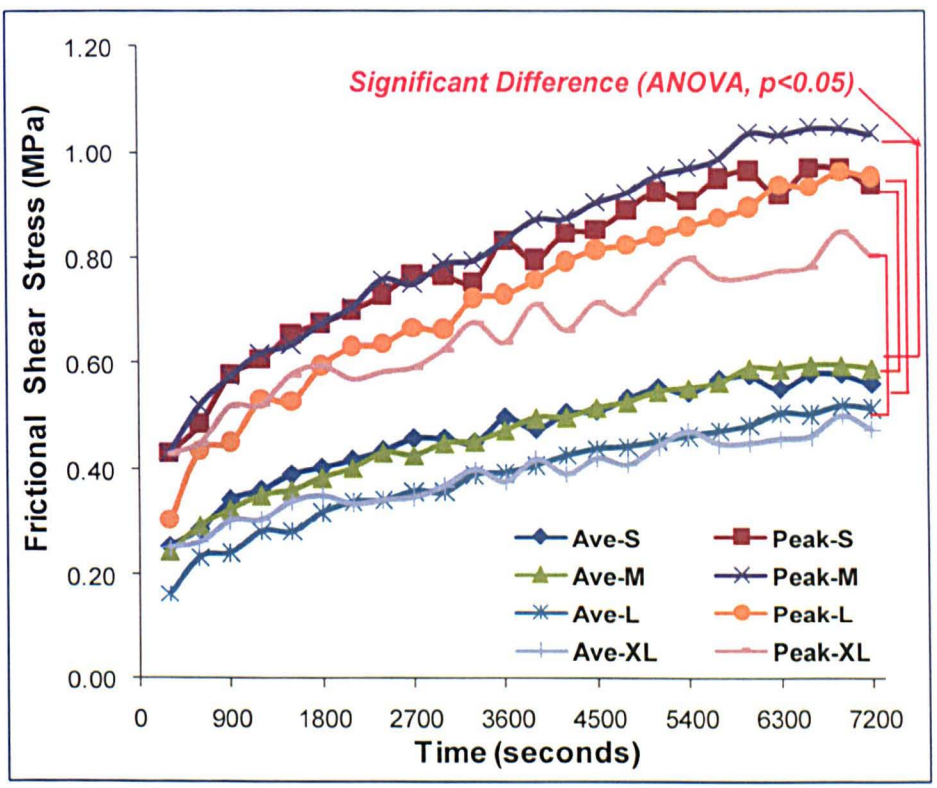

Figure 5.14. Comparison of calculated average frictional shear stress and the calculated peak frictional shear stress in specimens with small, medium, large, and extra large clearances under dynamic loading (mean, n=6) ***(Ave: average value, Peak: peak value, S: small, M: medium, L: large, and XL: extra large).***

Both the average and the peak frictional shear stress continued to increase with time during 2 hours of dynamic loading in specimens with small, medium,

large, and extra large clearances. No significant difference of both the average and the peak frictional shear stress was found between specimens with small, medium, large, and extra large clearances (n=6, ANOVA, $p>0.05$). However, the peak frictional shear stress was significantly higher in specimens at each clearance level compared to the average frictional shear stress (n=6, T test, $p<0.05$).

5.5.3 Effect of Clearance on Cartilage Surface Roughness and Wear

5.5.3.1 Surface Roughness

Comparison of the surface roughness (R_a) of cartilage (using acetabular replicas) from specimens with different clearances is shown in Figure 5.15. The surface roughness of the replicas in different clearances groups was 5.84 (± 3.25) – 10.31 (±2.40) μm. No significant difference in the surface roughness was observed between the different clearances groups (n=3, ANOVA, $p>0.05$).

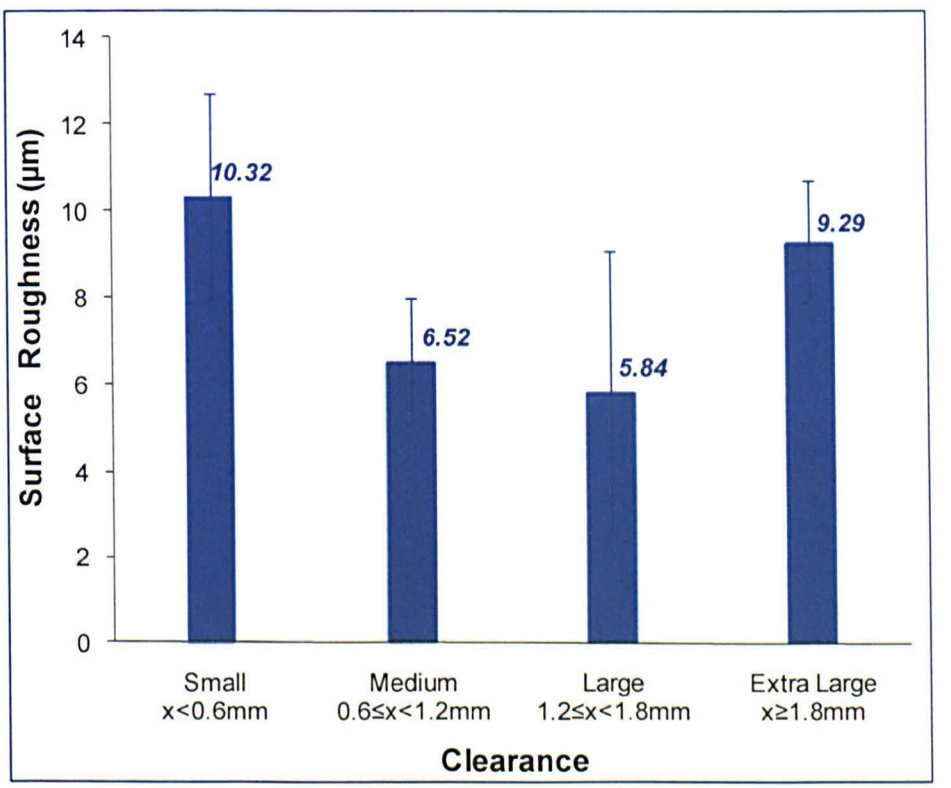

Figure 5.15. The mean acetabular replica surface roughness (R_a) in specimens with small, medium, large, and extra large clearances following testing with a dynamic load for 2 hours (n=3, mean ± 95% confidence limits).

5.5.3.2 Cartilage Wear Grade

The percentage of the different wear grade areas are shown in Figure 5.16. Wear grades 1, 2, and 3 were observed in specimens of all clearance levels. In specimens tested with both large and extra large clearances wear areas graded as 1 were significantly smaller compared to the wear areas graded as 1 in specimens with both small and medium clearances (ANOVA arcsine, $p<0.05$, $n=6$). No significant differences in the size of wear grade 1 areas were found between specimens with small and medium clearances, or between specimens with large and extra large clearances (T-test, arcsine, $p>0.05$, $n=6$). No significant differences in the area of wear graded as 2 and graded as 3 were observed among specimens with small, medium, large, and extra large clearances (ANOVA arcsine, $p>0.05$, $n=6$).

The unworn area in specimens with extra large clearances was significantly higher compared to specimens with small, medium, and large clearances (Figure 5.17, ANOVA arcsine, $p<0.05$, $n=6$). The unworn area in specimens with large clearances was significantly higher compared to specimens with small clearances (T-test, arcsine, $p<0.05$, $n=6$).

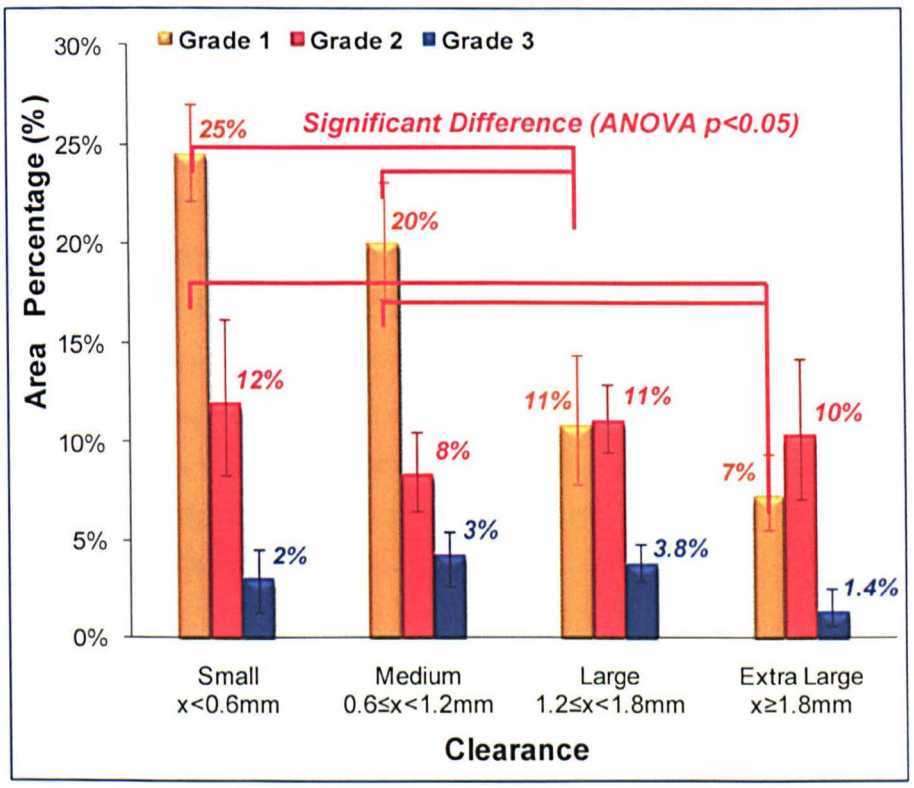

Figure 5.16 The acetabular replica surface wear grade area percentage for specimens with small, medium, large, and extra large clearances following dynamic load testing for 2 hours (n=6, mean ± 95% confidence limits).

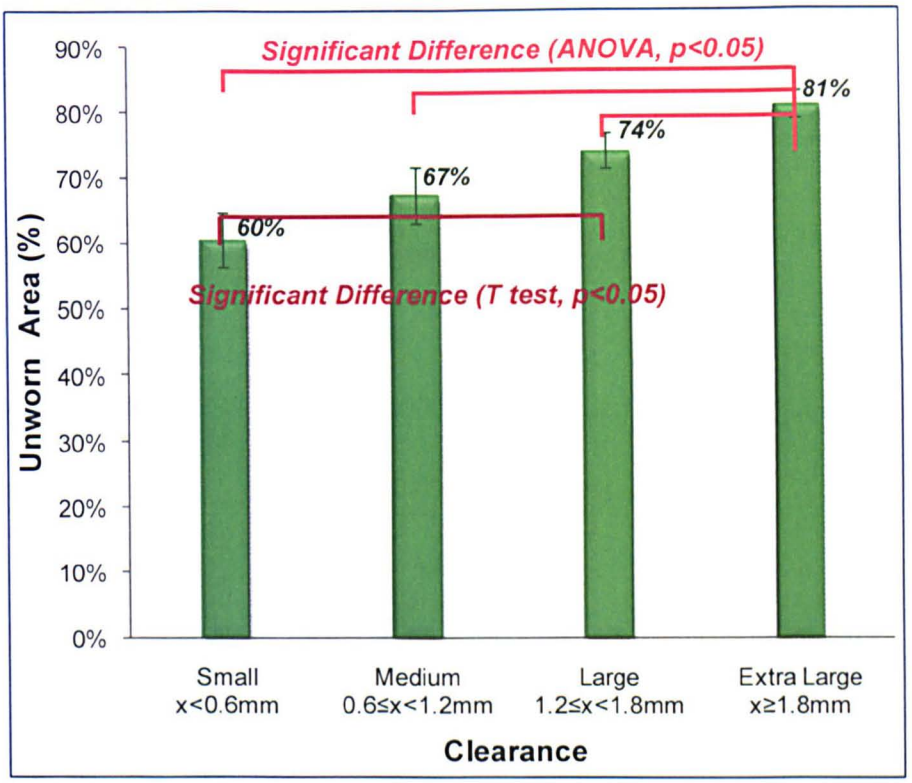

Figure 5.17. The wear grade 0 area (unworn area) percentage in specimens with small, medium, large, and extra large clearances following 2 hours of dynamic load testing (n=6, mean ± 95% confidence limits).

5.5.4 Effect of Clearance on Cartilage Surface Deformation

5.5.4.1 Cartilage Deformation Volume

The deformation volume of acetabular cartilage following 2 hours of dynamic load testing is compared for specimens with small, medium, large and extra large clearances in Figure 5.18. It was found that the deformation volume in specimens with small and extra large clearances was significantly higher compared to specimens with medium and large clearances (ANOVA, $p<0.05$, $n=3$). In specimens with large clearances the deformation volume was found to be significantly smaller compared to in specimens with small, medium, and extra large clearances (ANOVA, $p<0.05$, $n=3$).

5.5.4.2 Cartilage Deformation Depth

The average deformation depth of acetabular cartilage is compared in specimens with small, medium, large and extra large clearances following 2 hours of dynamic load testing in Figure 5.19. It was found that the average deformed depth was significantly higher in specimens with extra large clearances compared to specimens with medium and large clearances (ANOVA, $p<0.05$, $n=3$).

Specimens with small clearances the average deformed depth was significantly higher than specimens with medium clearances (T-test, $p<0.05$, $n=3$).

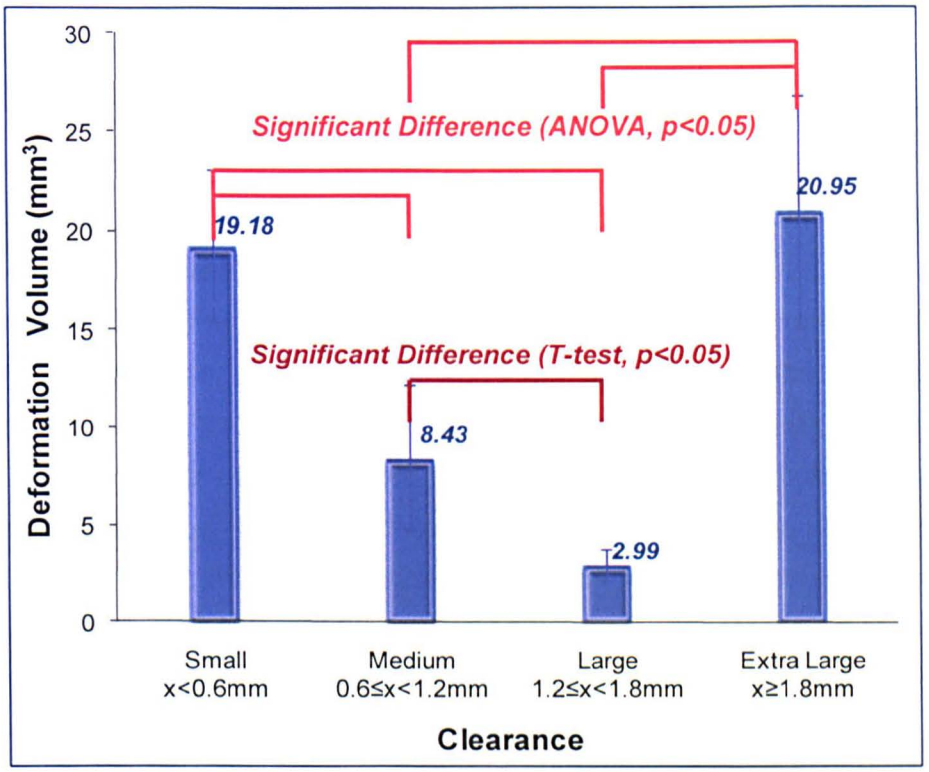

Figure 5.18. Comparison of deformation volume of acetabular cartilage in specimens with small, medium, large, and extra large clearances following 2 hours of testing with dynamic load (n=3, mean ± 95% confidence limits).

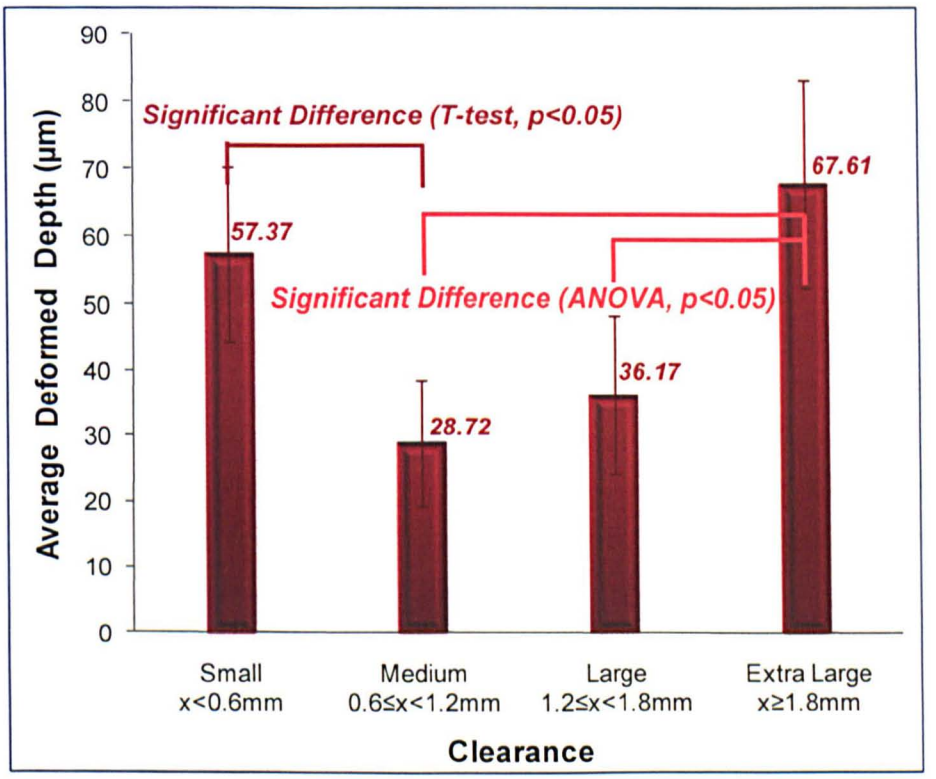

Figure 5.19. Comparison of average deformation depth in acetabular cartilage in specimens with small, medium, large, and extra large clearances following 2 hours testing with dynamic load (n=3, mean ± 95% confidence limits).

5.5.5 Comparison of Different Parameters Measured under Constant and Dynamic Loading

5.5.5.1 Contact Area and Contact Stress

A comparison of the contact area in specimens with different clearances when loaded with 400 N or 800 N **static** loading was applied for 30 seconds is shown in Figure 5.20. $R_{800\ N}=0.86$ *and* $R_{400\ N}=0.79$ correlations of the contact area to the clearance was observed under a load of 800 N or 400 N.

Comparison of the mean value of the contact area in specimens with different clearance levels (small, medium, large, and extra large) when loaded with 400 N or 800 N **static** loading for 30 seconds is shown in Figure 5.21. It was found that the contact areas in specimens subjected to 800 N were significantly larger compared to the contact areas in specimens following 400 N loading at the same clearance level (T test, $p<0.05$, $n=6$). The mean contact area in specimens with extra large clearance was significantly smaller compared to in specimens with small, medium, and large clearances under both 400 N or 800 N static loading (ANOVA, $p<0.05$, $n=6$).

Comparison of the calculated average contact stresses and the measured peak contact stresses in specimens with different clearances when loaded with 400 N or 800 N **static** loading for 30 seconds is shown in Figure 5.22. Similar correlation between the peak contact stress and the clearance was observed under 400 N or 800 N static loading ($R_{400N}=0.87$, $R_{800N}=0.88$). Better correlation between the average contact stress and the clearance was found under 800 N static loading compared to 400 N static loading ($R_{400N}=0.79$, $R_{800N}=0.85$).

Comparison of the mean value of the calculated average and measured peak contact stresses in specimens with different clearance levels (small, medium, large, and extra large) is shown in Figure 5.23. Significantly higher contact areas were observed in specimens under 800 N loading compared to under 400 N loading with the same clearance level ($n=6$, T test, $p<0.05$). Under both 400 N and 800 N static loading the average and peak contact stresses in specimens with extra large clearance were found significantly higher compared to small, medium, and large clearances ($n=6$, ANOVA, $p<0.05$).

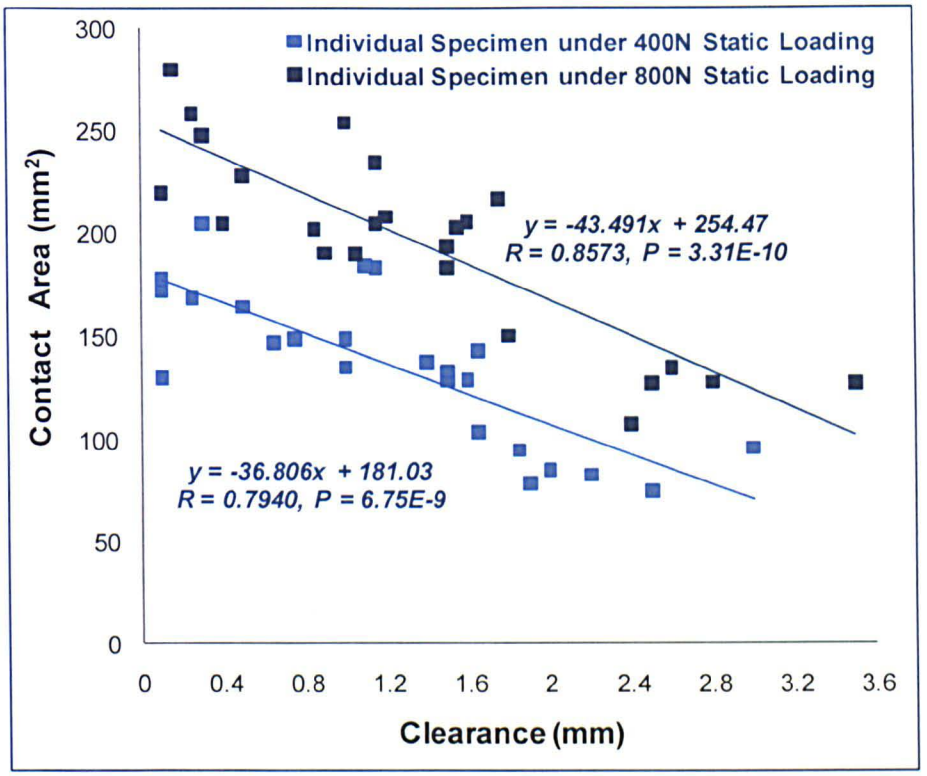

Figure 5.20 Comparison of the contact areas in specimens with different clearances when 400 N or 800 N static loading was applied for 30 seconds. R and P values were obtained using a regression analysis in Microsoft Excel 2007 (Microsoft Corporation, Redmond, USA).

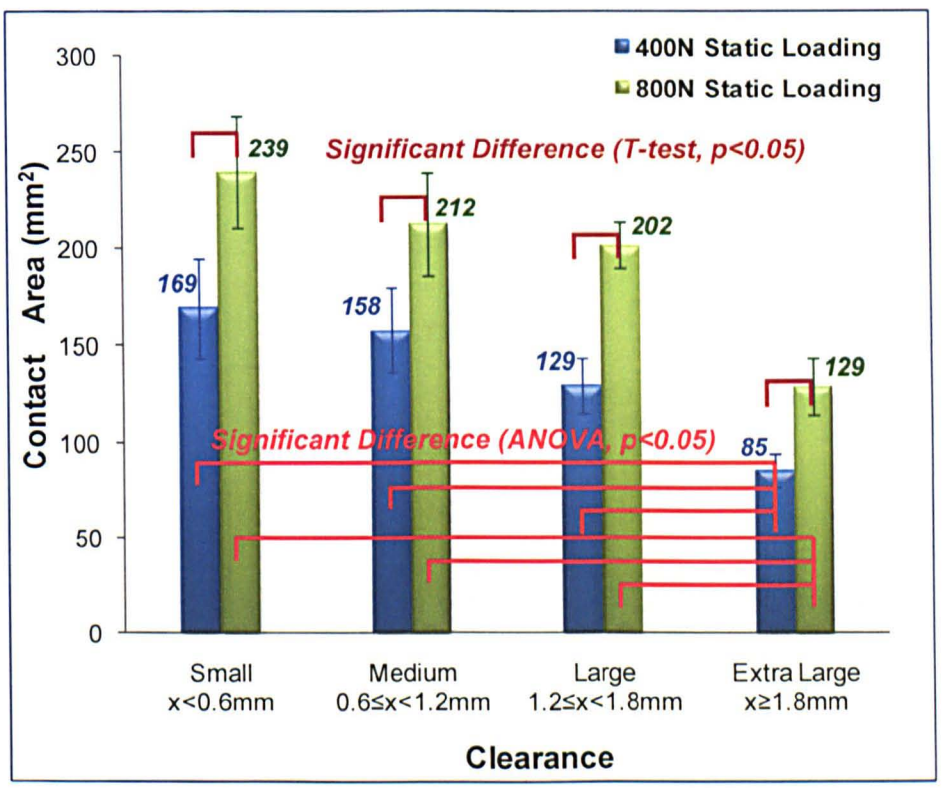

Figure 5.21 Comparison of the mean contact area in specimens with different clearance levels when 400 N or 800 N static loading was applied for 30 seconds (n=6, mean ± 95% confidence limits).

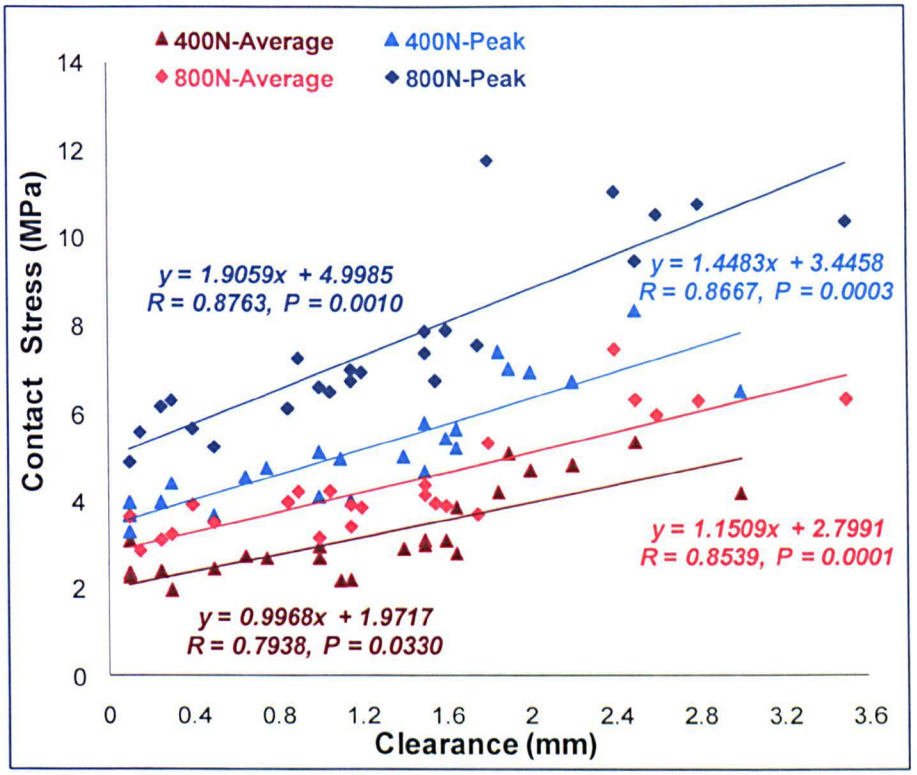

Figure 5.22 Comparison of the calculated average and the measured peak contact stress when under 400 N or 800 N static load was applied for 30 seconds (n=6, mean ± 95% confidence limits). R and P values were obtained using a regression analysis in Microsoft Excel 2007 (Microsoft Corporation, Redmond, USA).

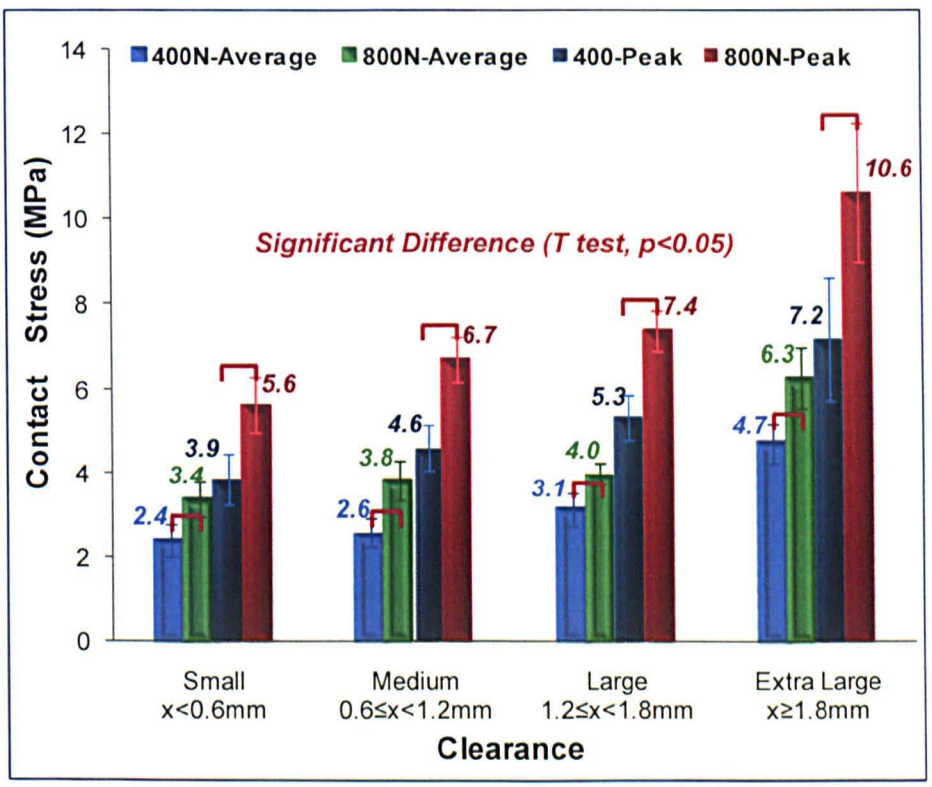

Figure 5.23 Comparison of the mean contact area for specimens with different clearance levels when 400 N or 800 N static loading was applied for 30 seconds (n=6, mean ± 95% confidence limits).

5.5.5.2 Coefficient of Friction and Frictional Shear Stress

A comparison of the coefficient of friction in specimens with different clearances tested with 400 N constant or 25~800 N dynamic loading for 2 hours is shown in Figure 5.24. The coefficient of friction was significantly lower in specimens tested under dynamic loading compared to constant loading within each clearance level (n=6, ANOVA, $p<0.05$).

A similar correlation of the FE radial clearance and coefficient of friction following 2 hours testing was observed in specimens tested under 400 N constant or 25~800 N dynamic loading (Figure 5.25, $R_{dynamic}=R_{constant}=0.78$)

A comparison of the mean value of the average frictional shear stress in specimens tested under 400 N constant or 25~800 N dynamic loading is shown in Figure 5.26.

The average frictional shear stress was observed to be significantly lower in specimens with large and extra large clearances following 2 hours testing under dynamic load compared to specimens tested under constant load at all different clearance levels (ANOVA, $p<0.05$, n=6).

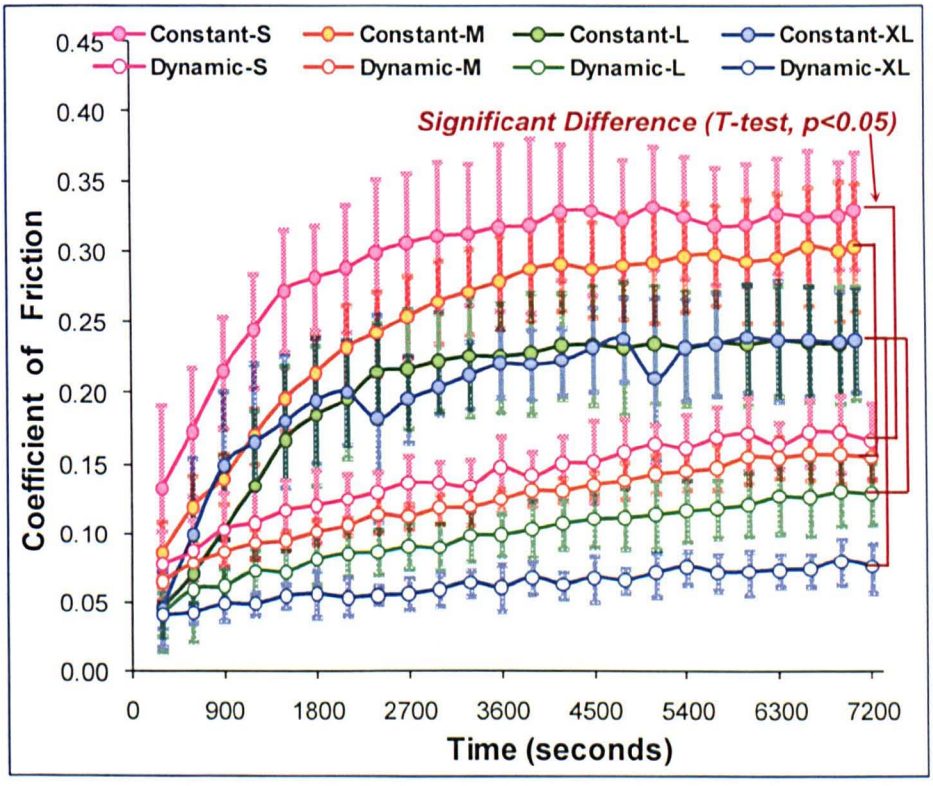

Figure 5.24 Comparison of the coefficient of friction in specimens with small, medium, large, and extra large clearances in testing with 400 N constant or 25~800 N dynamic loading (n=6, mean ± 95% confidence limits).

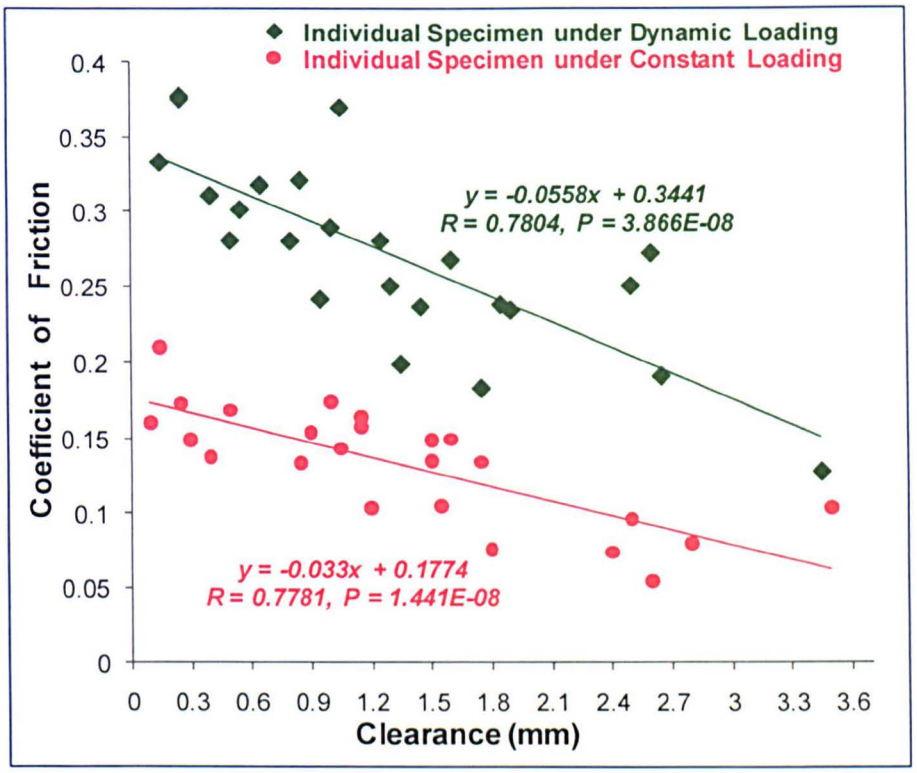

Figure 5.25 Correlation comparison (R^2=0.61) between coefficient of friction and FE radial clearance after 2 hours of testing under 400 N constant or 25~800 N dynamic loading. R and P values were obtained using a regression analysis in Microsoft Excel 2007 (Microsoft Corporation, Redmond, USA).

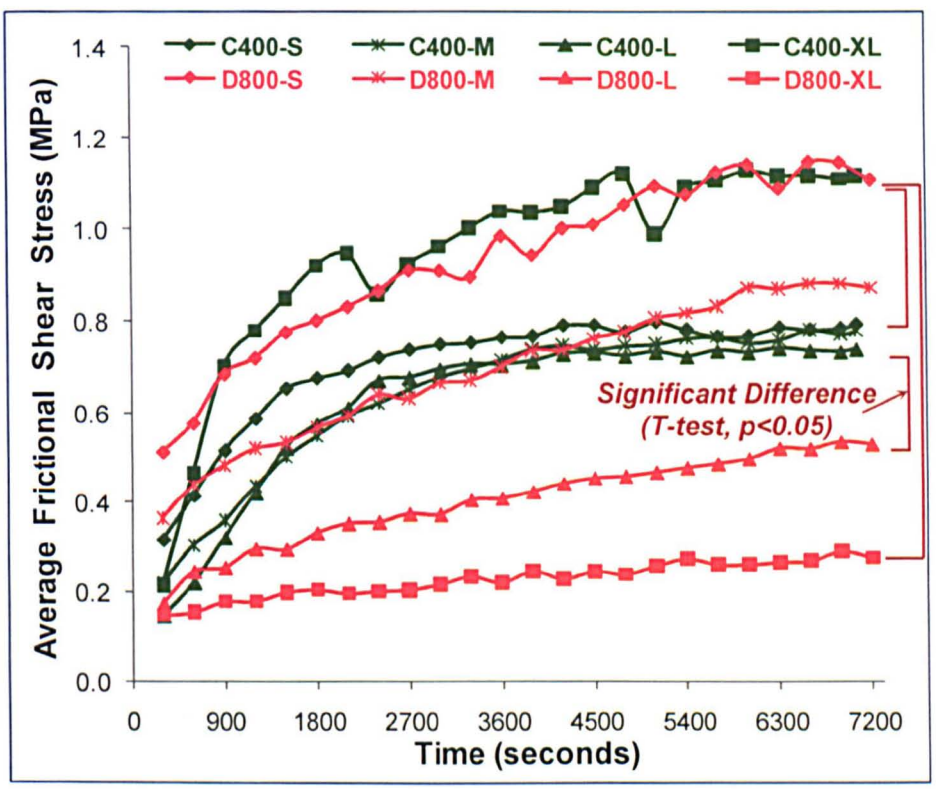

Figure 5.26. Comparison of the average frictional shear stress in specimens with small, medium, large, and extra large clearances tested under constant and dynamic loading (n=6, mean), *(C400: 400 N constant loading, D: 25~800 N dynamic loading).*

Comparison of the mean value of the peak frictional shear stress in specimens tested under 400 N constant or 25~800 N dynamic loading is shown in Figure 5.27. The mean peak frictional shear stress was observed to be significantly higher in specimens under 400 N constant loading compared to under 25~800 N dynamic loading in specimens at each different clearance level (ANOVA, $p<0.05$, $n=6$).

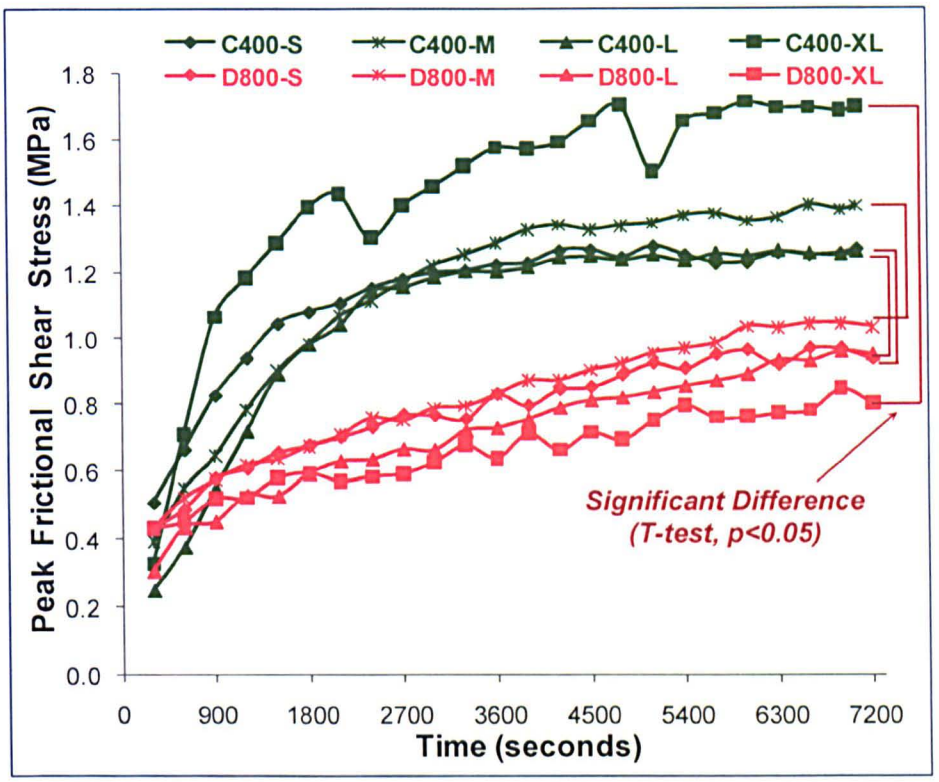

Figure 5.27. Comparison of the peak frictional shear stress in specimens with small, medium, large, and extra large clearances tested under 400 N constant or 25~800 N dynamic loading (n=6, mean), *(C400: 400 N constant loading, D: 25~800 N dynamic loading).*

5.5.5.3 Cartilage Surface Roughness and Cartilage Wear Grades

Comparison of cartilage surface roughness, cartilage wear grade percentage and percentage of acetabular cartilage unworn area in specimens with different clearance levels following testing under 400 N constant or 25~800 N dynamic loading are shown in Figure 5.28-30.

No significant difference of the cartilage surface roughness was observed in specimens tested under 400 N constant or 25~800 N dynamic loading at each different clearance levels (T test, $p>0.05$, $n=3$, Figure 5.28).

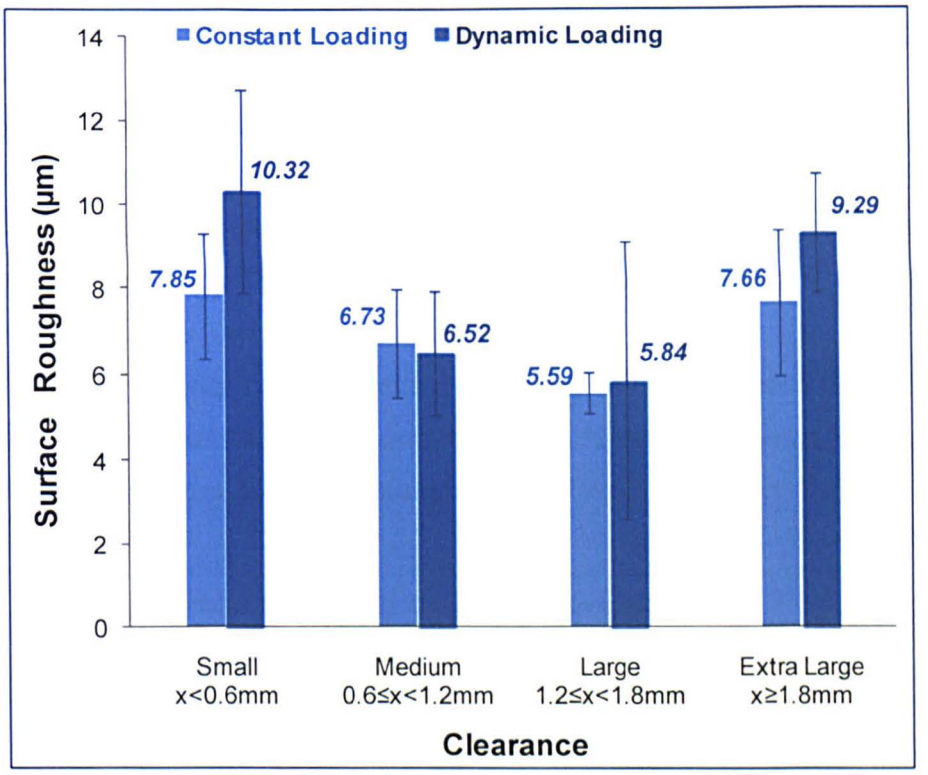

Figure 5.28. Comparison of the acetabular replica surface roughness in specimens with small, medium, large, and extra large clearances tested under 400 N constant or 25~800 N dynamic loading (n=3, mean ± 95% confidence limits).

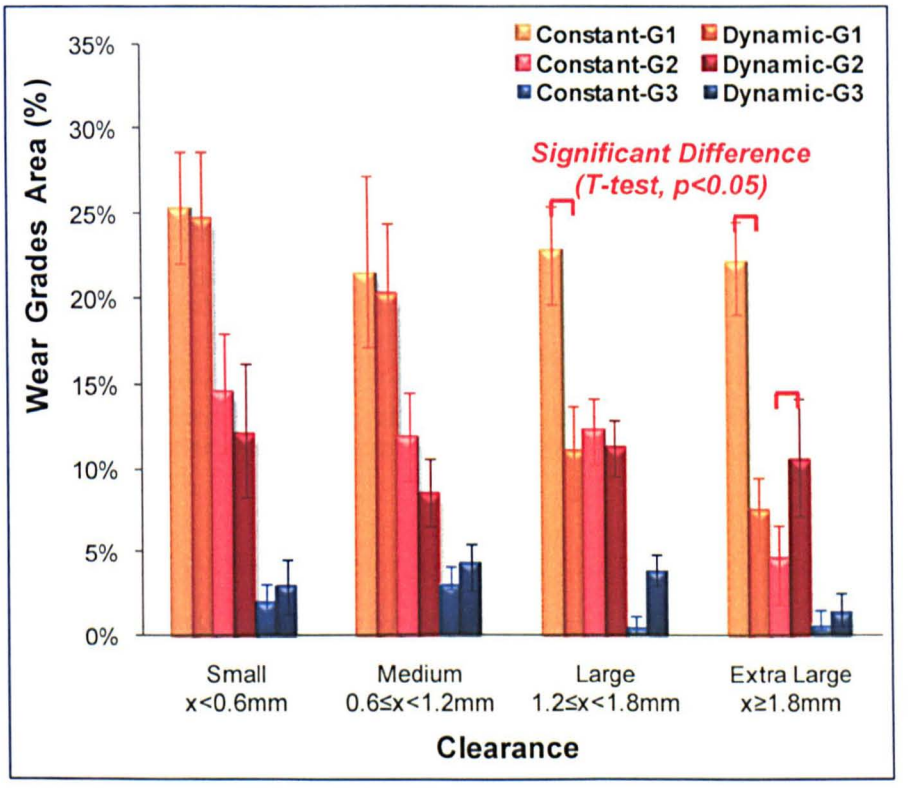

Figure 5.29 Comparison of acetabular wear grades in specimens with different clearances tested under 400 N constant or 25~800 N dynamic loading (n=3, mean ± 95% confidence limits, G1, 2, 3: wear grade 1, 2, 3).

Significantly higher grade 1 wear area percentages were found in specimens with large and extra large clearances tested under 400 N constant loading compared to those tested under 25~800 N dynamic loading (n=6, T test, $p<0.05$, Figure 5.29). The wear area percentage graded 2 in specimens with extra large clearances was observed to be significantly lower in specimens tested under 400 N constant loading compared to those tested under 25~800 N dynamic loading (n=6, T test, $p<0.05$, Figure 5.29).

Significantly higher unworn areas were observed in specimens with both large and extra large clearances tested under 25~800 N dynamic loading compared to specimens tested under 400 N constant loading (T-test, $p<0.05$, n=3, Figure 5.30).

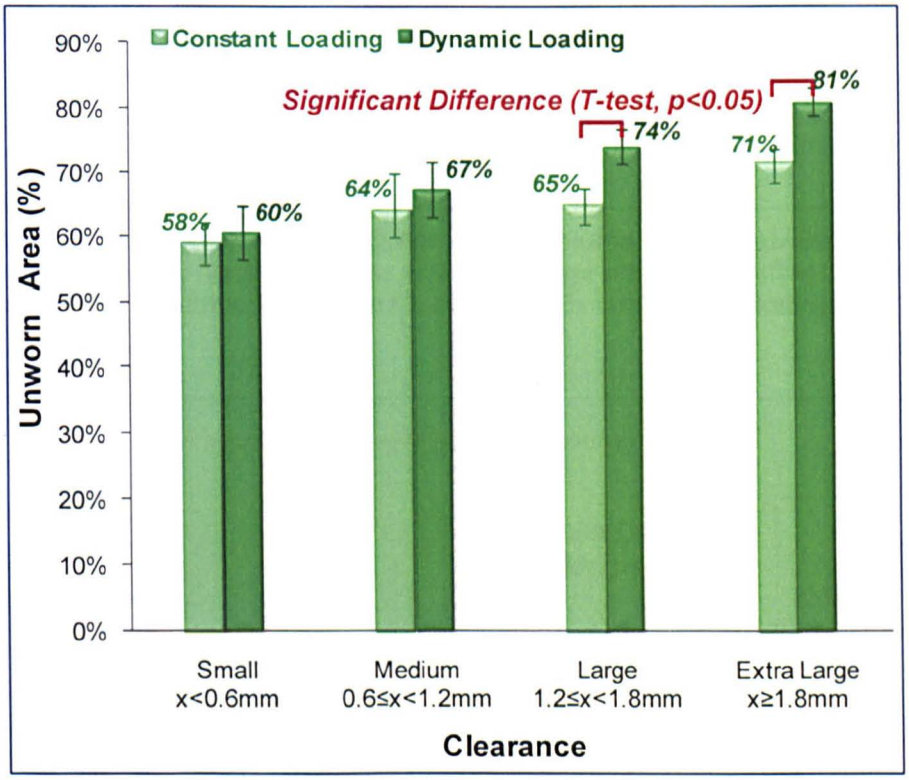

Figure 5.30 Comparison of acetabular unworn area in specimens with different clearances tested under 400 N constant or 25~800 N dynamic loading, (n=3, mean ± 95% confidence limits).

5.5.5.4 Cartilage Surface Deformation Volume and Depth

Comparison of the mean value (n=3) of the deformation volume, and the average deformation depth between specimens tested under 400 N constant or 25~800 N dynamic loading with different clearance levels are shown in Figures 5.31, and 32 respectively.

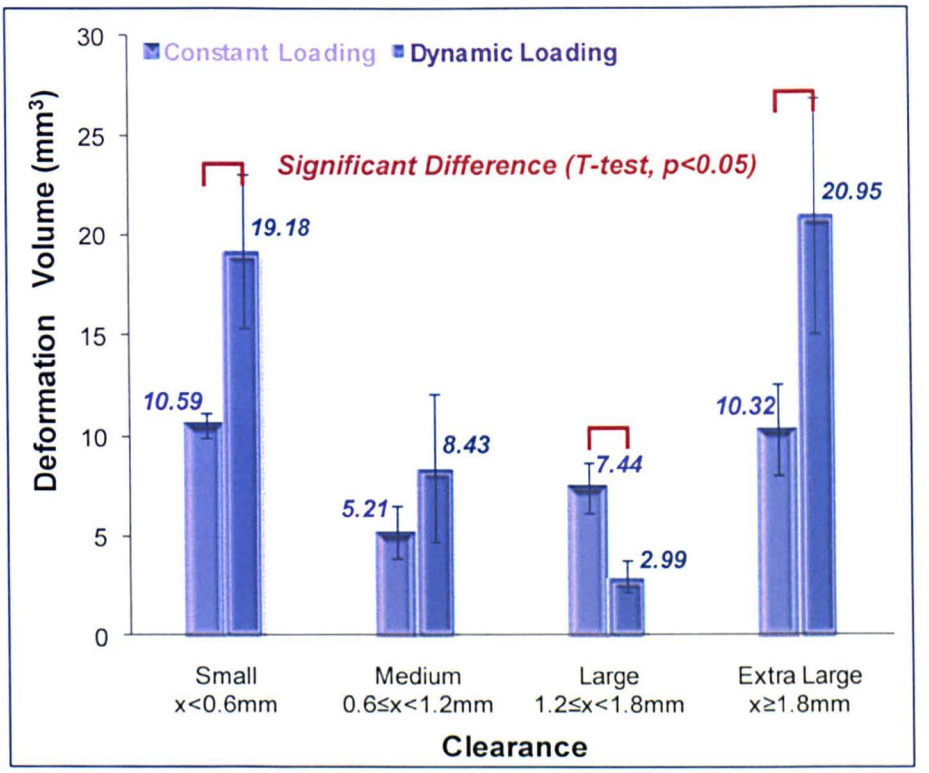

Figure 5.31. Comparison of acetabular wear volume of acetabular cartilage in specimens with small, medium, large, and extra large clearances after 2 hours tested under constant or dynamic loading (n=3, mean ± 95% confidence limits).

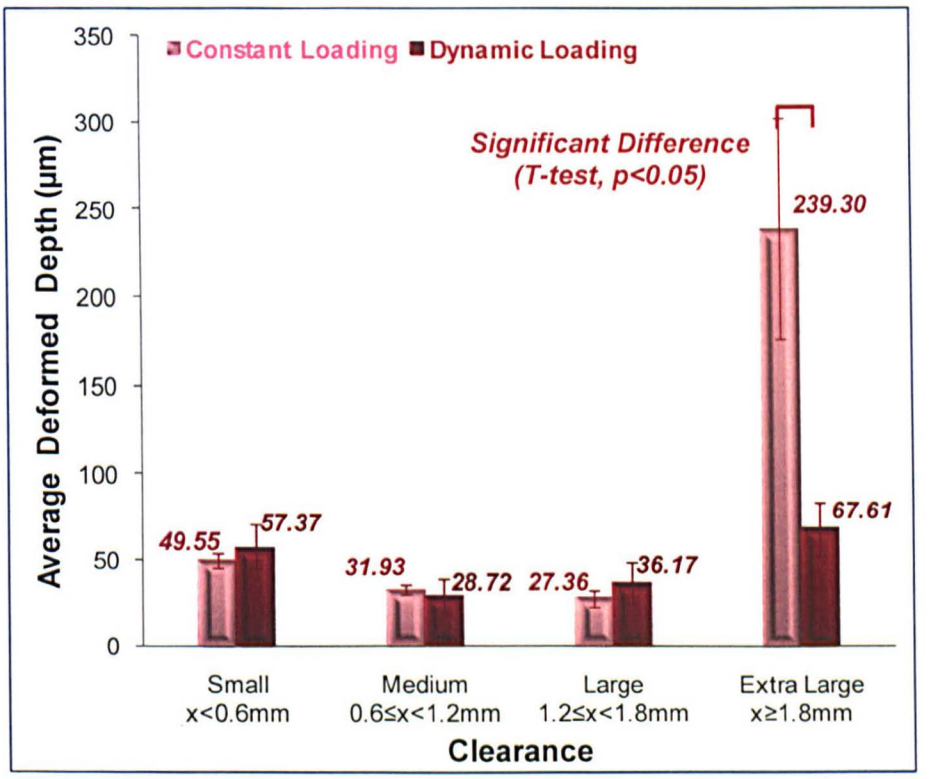

Figure 5.32. Comparison of average deformation depth of acetabular cartilage in specimens with small, medium, large, and extra large clearances after 2 hours testing under constant or dynamic loading (n=3, mean ± 95% confidence limits).

In specimens with small and extra large clearances, the mean deformation volume was significantly lower following testing under 400 N constant loading than following 25~800 N dynamic loading (Figure 5.31, T test, $p<0.05$, $n=3$). For specimens with large clearances, the deformation volume was found to be significantly higher following testing under 400 N constant loading compared to following testing under 25~800 N dynamic loading (Figure 5.31, T test, $p<0.05$, $n=3$).

In specimens with extra large clearance, the average deformation depth was significantly higher following testing under 400 N constant loading compared to under 25~800 N dynamic loading (Figure 5.32, T test, $p<0.05$, $n=3$).

5.6 Discussion

5.6.1 Effect of Clearance on Contact Stress and Contact Area

Contact stress in the hip has been shown as one of the most important factors influences the friction, deformation, degradation and degeneration of acetabular cartilage in the hemiarthroplasty hip model under constant loading (Chapter 4). In this dynamic loading study, the entire porcine body weight was applied statically to the metal heads in the acetabula with a range of FE radial clearances (0.1~3.5mm), the average contact stress on the acetabulum was between 3.4 and 6.3 MPa, and the peak contact stress was approximately 5.6 to 10.6 MPa. This peak contact stress range is close to those in the literature for human hip joints, where the hip peak contact stress measured *in-vitro* in humans by pressure-sensitive films was between 2.90 and 9 MPa (Afoke *et al.*, 1987; Bay *et al.*, 1997; Hak *et al.*, 1998; von Eisenhart *et al.*, 1999).

In this hemiarthroplasty hip model under 800 N static loading for 30 seconds, the contact stress increased with increasing clearance due to the decreasing contact area in specimens. In specimens with extra large clearances the contact stress (both average and peak) was significantly higher compared to specimens with small, medium, and large clearances (ANOVA, $p<0.05$, $n=6$). This was due to the significantly reduced contact area in specimens with extra large clearance (ANOVA, $p<0.05$, $n=6$). However, similarly to when 400 N static loading was applied for 30 seconds, there were some errors due to the sensitivity of super-low pressure film, this was when the load was initially applied onto the porcine acetabulum as the metal head slid to fit inside the acetabulum due to the narrow clearance.

The significantly decreased contact area may cause severe damage to the articular cartilage when it articulates against a metal counterface. To avoid higher contact stress on the articular acetabulum after hip hemiarthroplasty, extra large FE radial clearances (≥1.8 mm) are not recommended.

5.6.2 Effect of Clearance on Friction and Frictional Shear Stress

The coefficient of friction for metal (cobalt chrome alloy) heads articulating with cartilage was shown as a time-dependent response due to the continued dynamic loading applied on the tissue and ensuing loss of fluid load support.

In this hemiarthroplasty hip model, fluid flow in the cartilage during the pendulum motion and dynamic loading was controlled by the contact area and contact stress. Hence, the change in the dynamic loading during the cycle and motion were important to understand the changes to friction. In the hemiarthroplasty hip model, the fluid in the loaded area of cartilage was transferred towards to unloaded areas. For example, in each cycle, the metal head moved from 0° through -15°, 0°, +15°, back to 0°, with the load increasing from 25 N to 800 N and then decreasing to 25 N (Figure 5.33). When the load first was applied from 25 N to 800 N, a large proportion of it was carried by the fluid phase of the cartilage, and the increasing load increased the proportion of the load carried by the fluid (from the loading centre to the edge of loading area, Figure 5.33, blue arrows). When the load decreased from 800 N to 25 N, an increasing area of acetabular cartilage was "recharged" with fluid and therefore more fluid exuded back to the loading area (from the edge of loading area to the centre of loading area, Figure 5.33, green arrows) and was ready for the fluid support in the next cycle of loading. Hence, the fluid load support phase was "recharged" in each cycle when the load was reduced from the peak load to the minimum load, and this increased the fluid transaction during the pendulum motion of the femoral head.

The coefficient of friction under pendulum dynamic loading decreased with the increasing clearances from small, medium, large, to extra large which is contrary to the hypothesis. Increasing clearances reduced the contact area, and therefore the contact stress was increased, the fluid support increased following the contact area migration in the whole articular acetabulum; hence the coefficient of friction was reduced. When the pendulum reciprocating motion was applied the contact area migrated and smaller contact area had more fluid support phase following the migration of contact area, and the coefficient of friction decreased (similar to the explanation in Chapter 4, Figure 4.24).

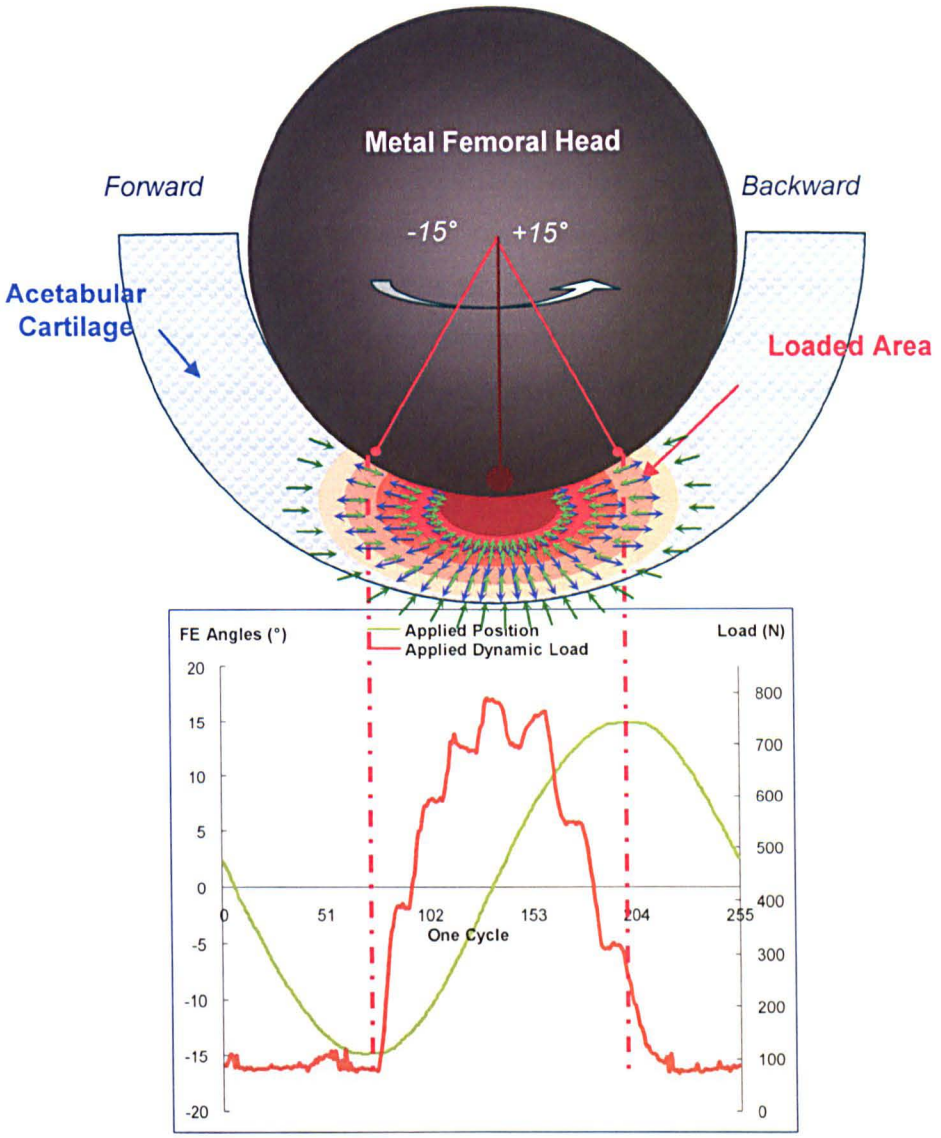

Figure 5.33 Loading area and fluid movements of the acetabular cartilage during the pendulum motion under dynamic loading.

5.6.3 Effect of Clearance on Cartilage Surface Roughness and Wear

No significant differences in cartilage surface roughness (R_a=6.52~10.32μm) was observed between specimens with different clearance levels (ANOVA, $p>0.05$, n=3). However, the roughness value only partially presents the cartilage surface damage texture, deformation, and wear.

Significantly higher cartilage wear graded as 1 was observed in specimens with small and medium clearances, compared with specimens with large and extra large clearances (ANOVA, $p<0.05$, n=6). Wear grade 1 was the lowest level of damage in porcine acetabular cartilage in this study, and it occupied over 50% of the total worn area. The reduced proportion of wear grade 1 was related to the

reduced contact area due to the increasing FE radial clearance. Similarly, significant lower total unworn area percentage was found in specimens with extra large clearances and this was due to the reduced contact area with significant increased clearances.

Different cartilage wear grades 1, 2, and 3 were seen in specimens with small, medium, large, and extra large clearances, and this was caused by the pendulum sliding motion of the metal head contacting the articular acetabulum. When the motion occurred between hard and soft (metal head on acetabular cartilage) counterfaces, the cartilage deformed and lost material in the contact area. However, due to the individual geometry of each porcine acetabulum, the different contact areas were subjected to different contact stress. Hence, the difference of wear grade 1, 2, and 3 percentages was not clear and obvious between each different clearance level.

5.6.4 Effect of Clearance on Cartilage Deformation

The deformation volume and the average deformation depth was found to be affected by clearance in this hemiarthroplasty hip model under dynamic loading. The cartilage deformation volume is a combination of the cartilage deformation area on the lunate surface, and the cartilage deformation depth. In this hemiarthroplasty hip model, after 2 hours of pendulum dynamic loading, significantly higher deformation volume was observed in specimens with small and extra large FE radial clearances compared to specimens with medium and large clearances (ANOVA, $p<0.05$, $n=3$).

It is postulated that the increase of the deformation volume in specimens with small and extra large clearances was caused by different factors:

For specimens with small clearances, although the cartilage deformation depth was not significantly increased compared to specimens with other clearances, the contact area between the metal head and the articular cartilage was increased. This enlarged the deformation area, hence the deformation volume increased.

For specimens with extra large clearances, the increased clearance decreased the contact area between the metal head and the articular cartilage, and this increased the contact stress. This increased the acetabular cartilage deformation depth which increased the deformation volume. Hence, the deformation volume changes depending on the greater increase of these two factors (surface deformation area, and deformation depth). In this hemiarthroplasty

hip dynamic loading model, the increase of the deformation depth was more significant than the decrease of the contact area ($p_{deformation\text{-}depth} = 0.037 < p_{contact\text{-}area} = 0.045$), hence, the deformation volume increased.

Significantly higher average deformation depths were observed in specimens with extra large clearances, due to the increased contact stress. As previous metal on cartilage indentation tests have demonstrated: increased contact stress increases the deformation of articular cartilage (Forster and Fisher, 1996; Northwood and Fisher, 2007; Northwood *et al.*, 2007; Pawaskar *et al.*, 2007; Katta *et al.*, 2008b; McCann *et al.*, 2008).

5.6.5 Effect of Loading on Cartilage Tribological Properties

5.6.5.1 Contact Area and Contact Stress

After hip hemiarthroplasty, information regarding the hip joint contact area and contact stress distribution during the patients' daily activities is essential in predicting the acetabular cartilage degeneration mechanism, friction, and wear. In this hemiarthroplasty hip model, good correlation between the clearance and the contact area, average contact stress and peak contact stress was observed under both 400 N and 800 N static loading for 30 seconds. When the load was increased from 400 N to 800 N, the contact area, average contact stress, and the peak contact stress were increased by about 40%. This result demonstrates the biphasic properties of articular cartilage, the increased load increases both contact area and the deformation of the articular cartilage.

5.6.5.2 Friction and Frictional Shear Stress

The coefficient of friction was significantly lower under 25~800 N dynamic load compared to 400 N constant load within each different clearance group. This is due to the different proportion of load carried by the fluid phase and solid phase of the total or aggregate friction force during the pendulum motion. The overall friction and friction coefficient has been simply expressed by Forster and Fisher (1996), as Equation 1-2 described in Chapter 1

In the pin on plate simple geometry model, when the constant loading time was increased the load carried by the fluid phase decreased and the load carried by the solid phase increased. This was due to the articular cartilage pin remaining loaded, therefore a large amount of load was carried by the fluid phase of the

cartilage (Ateshian *et al.*, 1994). Hence, following Equation 1-2, for $\mu_f << \mu_s$, the coefficient of friction μ_T increased as the proportion of load carried by the solid phase increases with time.

However, in this hemiarthroplasty hip model, under the dynamic loading regime the fluid support phase support decreased slowly. Hence, the proportion of load carried by the solid phase contributed less to the total (aggregate) friction force of the two phases due to the replacement of fluid support when the load moved to a different area of the acetabular cartilage. This caused the proportion of load carried by the solid phase to increase slowly, as the ability of the cartilage to "recharge" the fluid phase support under motion was diminished. Following Equation 1-2, for $\mu_f << \mu_s$ the coefficient of friction increased slowly as the proportion of load carried by the solid phase increased with time. Interstitial fluid pressurization of articular cartilage has been measured experimentally (Oloyede and Broom, 1991; Soltz and Ateshian, 1998; Park *et al.*, 2003; Basalo *et al.*, 2004), these results have demonstrated that the load supported by interstitial fluid can be in excess of 90% of the total applied load immediately upon loading, but this subsides to zero under prolonged static loading. The theoretical predictions in the late 90's have confirmed the above experimental measurement results (Ateshian *et al.*, 1994; Macirowski *et al.*, 1994; Ateshian and Wang, 1995; Kelkar and Ateshian, 1999).

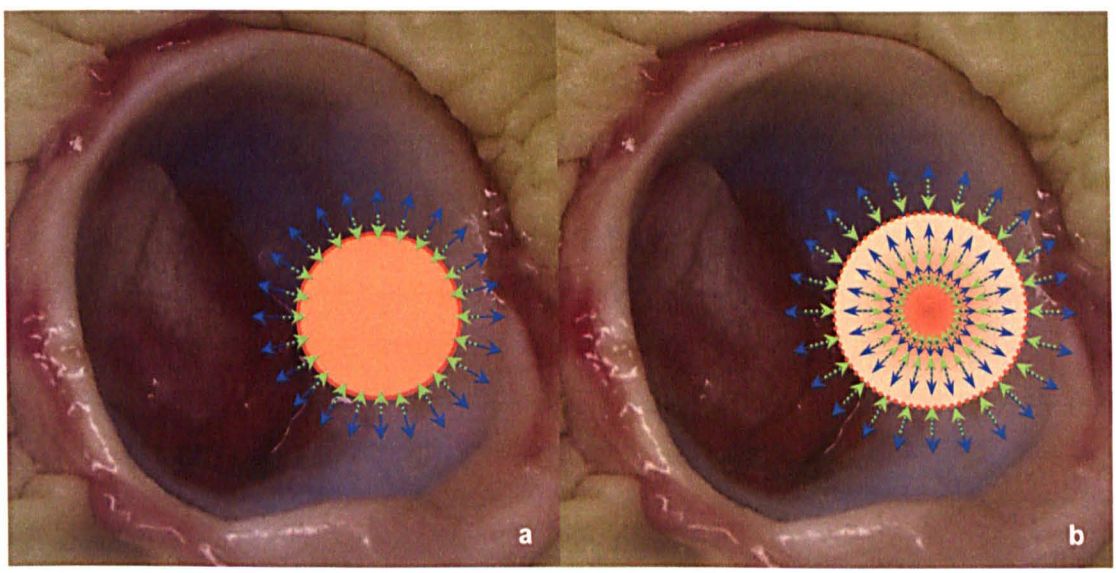

Figure 5.34 Fluid movements in the acetabular cartilage loading area: a. under constant loading, and b. under dynamic loading, green arrows: fluid moves from the centre to the edge of loading area, blue arrows: fluid moves from the edge to the centre of loading area.

When dynamic loading fluid movements were compared to the movements generated by constant loading in the hemiarthroplasty hip model, there was an

additional influence due to the variation in the dynamic load cycle (Figure 5.34.a, green arrows). When the load is applied there is greater opportunity for fluid phase support to be maintained. For example, for the same porcine acetabulum, under constant loading the fluid moves from the centre of loaded area of cartilage to the edge (Figure 5.34.a, blue arrows). However, under dynamic loading, the fluid moves out and in from the centre of the contact area when the load applied increased and reduced (Figure 5.34.b, blue and green arrows. Hence, the loading area was rehydrated partially under dynamic loading, and more fluid support carried the applied load, this led to the significantly lower of coefficient of friction. It has been reported that when compared to static loading, dynamic loading reduced the coefficient of friction of articular cartilage and maintained this reduction over a wider range of normal stresses (Malcom, 1976).

5.6.5.3 Surface Roughness and Wear Grades

As discussed in the previous chapter, the surface roughness changes partially present the cartilage surface texture, and from the microscopic point of view it presents the fissures levels of articular cartilage surfaces. Surface fissures may be created by the relatively stiff tangential layer of cartilage when it is being stretched by radial movements of the softer underlying cartilage as it attempted to move away from the loaded region (Adams *et al.*, 1998; Flachsmann *et al.*, 2001; Korhonen *et al.*, 2002b; Kerin *et al.*, 2003). Hence, cyclic loading does not cause significant differences in surface roughness following testing under constant and dynamic loading.

In this hemiarthroplasty hip model, different wear grades 1, 2, and 3 were shown in specimens with different clearance levels under both constant and dynamic loading cycles. It is postulated that during the pendulum reciprocation, the cartilage surface roughness was created and due to the geometry of individual porcine acetabulum between the metal on cartilage hard-soft bearing counterfaces. The fissures possibly propagate across the surface when the cartilage is subjected to cyclic loading.

Previous impact loading studies of cartilage-on-bone have found that cartilage fissures that extended down into the intermediate zone were produced when the cartilage-on-bone specimens were repeatedly impacted with a pendulum device (Silyn-roberts and Broom, 1990). Zimmerman et al. (1988) found that 250 cycles of a 6.89 MPa contact stress caused surface abrasions, 500 cycles produced primary fissures penetrating to the calcified cartilage, and 1000 cycles

produced secondary fissures extending from the primary fissures. After 25~8000 cycles the fissures coalesced and undermined cartilage fragments (Zimmerman *et al.*, 1988). Histological studies have shown cartilage fissures can propagate mechanically under cyclic compressive loading *in-vitro,* and cyclic loading caused cartilage fissures to increase in length and width, but not depth (Kerin *et al.*, 2003). In this study after 2 hours pendulum reciprocation, cartilage surface fissures were produced to varying extents generating different wear grades on the acetabular cartilage surface in FE direction unevenly.

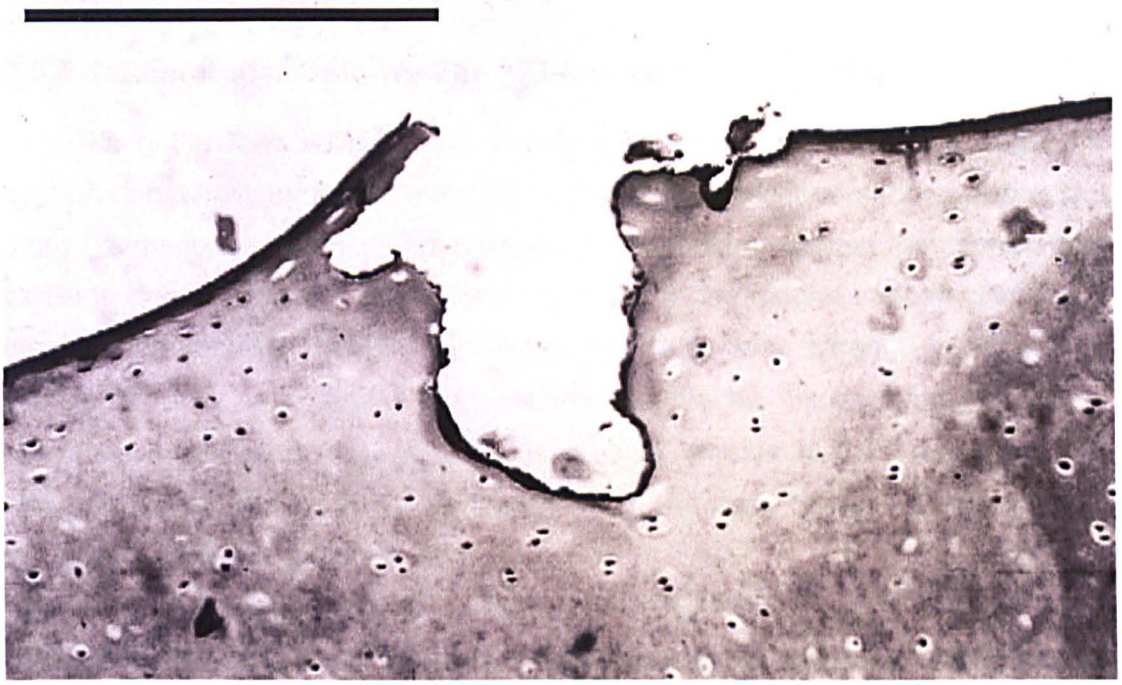

Figure 5.35 Histological Section of cartilage stained with Masson's blue trichrome showing a fissure that has opened up in width as a result of cyclic loading. Note the blunt crack tip, and the manner in which the surface layer has fractured. (Bar length = 200 μm.) (Kerin *et al.*, 2003)

Wear grade 4 is the damage down to the Tide Mark of the cartilage, which means the cartilage surface fissures have been developed to a greater extent leading to cartilage fracture. Wear grade 4 was only seen in specimens with extra large clearances under constant loading. It is postulated that this was due to the increased average and peak frictional shear stress within the loading time in specimens with extra large clearances causing fracture of articular cartilage. A histological image of a typical cartilage fracture is shown in Figure 5.35 (Kerin *et al.*, 2003). In this study when the acetabular cartilage surface was loaded constantly in 2 hours pendulum reciprocating motion with extra large clearances, it is postulated that this kind of cartilage fractures were created. Hence, after the fracture depth

reached to the deepest (radial) zone of articular cartilage, with the pendulum reciprocation friction force with higher frictional shear stress, the piece of cartilage was delaminated and removed. Although the extra large clearance affected the contact area and contact stress similarly under dynamic loading compared to under constant load, the "fluid recharged" loading area on cartilage reduced the coefficient of friction significantly under dynamic loading. Hence the cartilage fracture did not occur due to the frictional shear stress not reaching the cartilage threshold level, and no wear of grade 4 was observed after 2 hours pendulum dynamic loading friction test.

5.6.5.4 Acetabular Deformation Volume and Average Depth

When the load was applied to the acetabulum, the loaded cartilage was supported naturally by the surrounding cartilage and subchondral bone. A previous study (Korhonen *et al.*, 2002a) has shown that the lateral support from surrounding cartilage greatly affects cartilage deformation, and the natural support provided in hip hemiarthroplasty model lies in-between the two extreme conditions of "confined" and "unconfined" compression. In this hip hemiarthroplasty model, specimens with extra large clearances created smaller contact areas and this reduced the lateral support from surrounding cartilage. Hence, the deformation volume and depth was increased.

Differences of deformation volume and depth between specimens tested under constant and dynamic loading were due to the difference of worn area. Additionally, different characterised and types of deformation traces may result in similar deformation volumes with different average deformation depth. For example, with extra large clearances the deformation area and volume of one specimen under constant loading, and one specimen with dynamic loading is shown in Figure 5.36.

With extra large clearance one trace of deformation in a specimen under constant loading (Figure 5.36.a) shows approximately 0.6 mm of cartilage deformation (equal to the deformed cartilage thickness) and evenly distributed. However, under dynamic loading (Figure 5.36.b) the maximum deformation depth was approximate 0.42 mm, and the deformation depth was not evenly distributed - it was deeper in the middle and shallower on both sides. However, the deformation areas in both traces were similar, (2.45 mm^2 in specimen under constant loading and 2.16 mm^2 in specimen under dynamic loading).

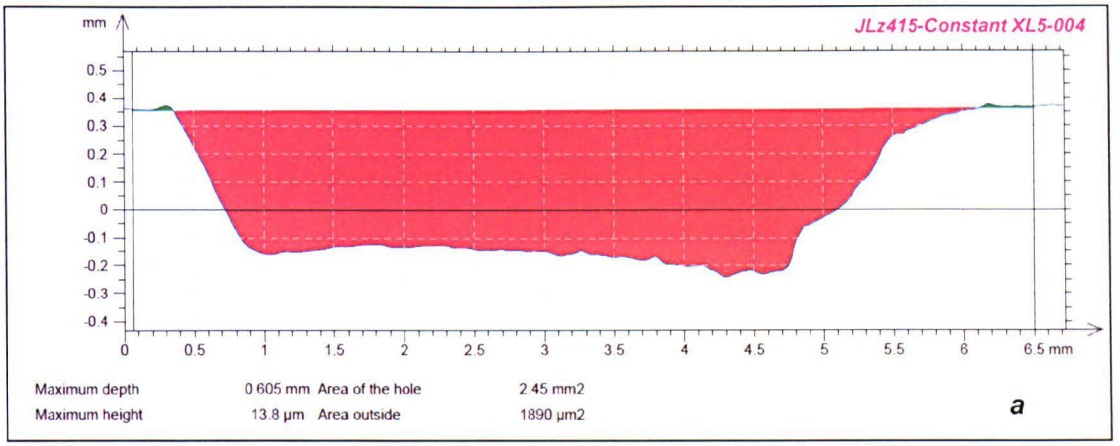

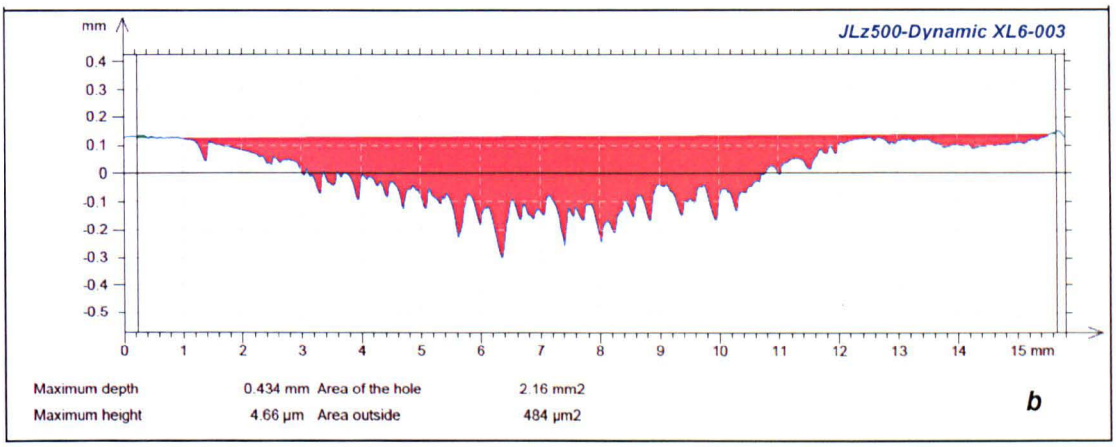

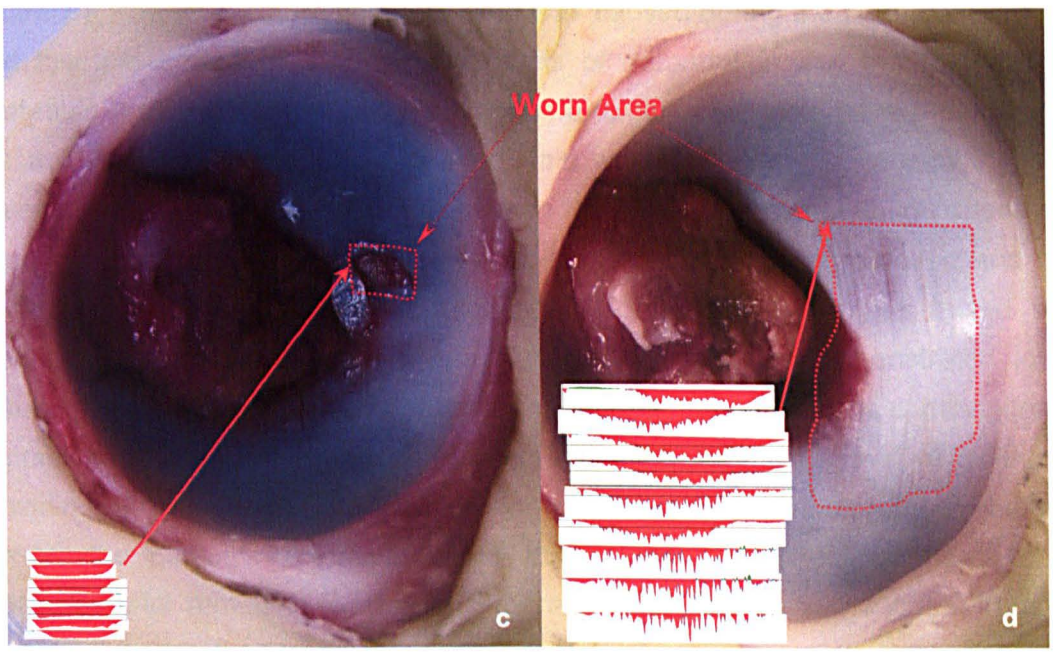

Figure 5.36 A typical trace analysis result of the specimens with extra large clearances, a. under constant loading; b. under dynamic loading; c. one specimen tested under constant loading; d one specimen tested under dynamic loading.

The different worn area (studied) and characters of deformation trace led to the significantly smaller deformation volume of specimens under constant loading or dynamic loading with extra large clearances (Figure 5.36.c: one typical specimen tested after 2 hours under constant loading, d: one typical specimen tested after 2

hours under dynamic loading). Although the average deformation depth was deeper in specimen c (under constant loading) compared to specimen d (under dynamic loading), the deformation area of specimen c and d was similar, and the deformation volume in specimen c was smaller than in specimen d. Hence, the cartilage deformation volume is a complex parameter which presents the combined effects of deformation area, deformation depth, and total worn area.

5.6.6 Clearance Recommendation in Clinical Practice

In this hip joint hemiarthroplasty dynamic loading model, four categories of clearances were chosen. The clearance was calculated from two parameters (femoral head size and acetabulum size). This type of categorisation was selected because clinically, patients have different sizes of acetabula, and it is realistic for different femoral head sizes could to be selected to provide a specific clearance. The results have shown that small clearances limited the space between the femoral head and acetabular cartilage especially in ML direction as in general the dimension in FE direction was greater than the dimension in ML direction. When the clearance was small, more cartilage wear was caused during the pendulum motion, and the metal head caused deeper levels of deformation into the cartilage. In acetabula tested with heads to produce extra large clearances, severe damage to the acetabular cartilage was observed, this was due to the increased frictional shear stress. The greater space between the head and acetabulum caused the head motion to delaminate the cartilage, it then became fully removed and this cartilage segment could be repositioned. Compared to samples tested with medium clearances, samples tested with large clearances demonstrated lower results in friction and cartilage deformation, and this may due to the combination of contact area, frictional shear stress and lubrication within this level of clearance providing a more suitable condition for better cartilage tribological properties. Hence, the patient's acetabulum size in FE direction is recommended to be measured after removing the natural femoral head during the surgery, and from the 2 hours dynamic loading cartilage friction and deformation results large clearance (1.2-1.8 mm) is ideally recommended clinically.

5.7 Conclusion

In conclusion, this study assessed the effect of clearance on cartilage friction, and deformation in hip hemiarthroplasty under dynamic loading. The findings were as follows:

1. With increasing clearance, the contact area decreased, and both average contact stress and peak contact stress increased. Good correlations of contact area (R^2=0.73), contact stress (average and peak, R^2=0.73 and R^2=0.77), with the FE radial clearance were observed.
2. A trend of decreasing coefficient of friction with increasing clearance under dynamic loading conditions was observed. Good correlations of coefficient of friction (R^2=0.61) with the FE radial clearance were observed.
3. Low levels of friction (less than 0.17±0.03) and short term (2 hours) durability were seen for a range of FE radial clearances (up to 3.5mm) under dynamic loading.
4. Cartilage deformation volumes and depths were similar in specimens with small and extra large clearances, and in specimens with medium and large clearances, this was due to the clearance effects to the contact area and deformed surface area.
5. The contact area and contact stress increased by 50% when the applied load increased by 100%, and this improved the cartilage biphasic load support.
6. Significantly lower coefficients of friction were observed under dynamic loading compared to under constant loading in specimens at each clearance levels. This was due to a greater proportion of load being carried by the fluid phase and the loading area of cartilage being partially rehydrated under dynamic loading.
7. A trend of increased unworn area with increased clearance was observed under both constant and dynamic pendulum reciprocation; and this was due to the reduced contact area with increased clearance.
8. Significantly greater deformation volume and deformation depth were observed for specimens with extra large clearances after 2 hours under both constant and dynamic loading cycles.
9. Metallic heads and porcine acetabula with the FE radial clearances in a range of 1.2~1.8mm (large clearance group) *in-vitro* showed lower wear volume (2.99±0.84 mm^3) and lower coefficient of friction (0.13±0.02) compared to other clearance groups, and the choice of head size in this range is possibly recommended for clinical practice.

Chapter 6 The Effect of Head Material on Cartilage in Hemiarthroplasty

6.1 Introduction

Previous chapters have discussed the effect of FE radial clearance on acetabular cartilage contact stress, friction, surface roughness, wear, and deformation under both constant and dynamic loading in a hip hemiarthroplasty model *in-vitro*. In addition to the effect of clearance in hip hemiarthroplasty the acetabular cartilage tribological properties will be affected by the direct contact with the articulating counterfaces of the implant (femoral head). Hence, the material used for the femoral head in hip hemiarthroplasty may play a very important role on the acetabulum friction and wear.

Clinically Biolox delta ceramic material is highly recommended and widely used, particularly as the femoral heads in ceramic-on-ceramic articulations. This is due to the material having excellent wear performance, good wettability, good biocompatibility, high hardness (1925 HV) and being highly polished (BIOLOX, 2008). The excellent wettability of the ceramic material is due to the hydrophilic atomic structure which attracts molecules such as water. The Biolox delta ceramic consists of Alumina (Al_2O_3) and Zirconia (ZrO_2) and other additives. Its microstructure is shown in Figure 6.1.

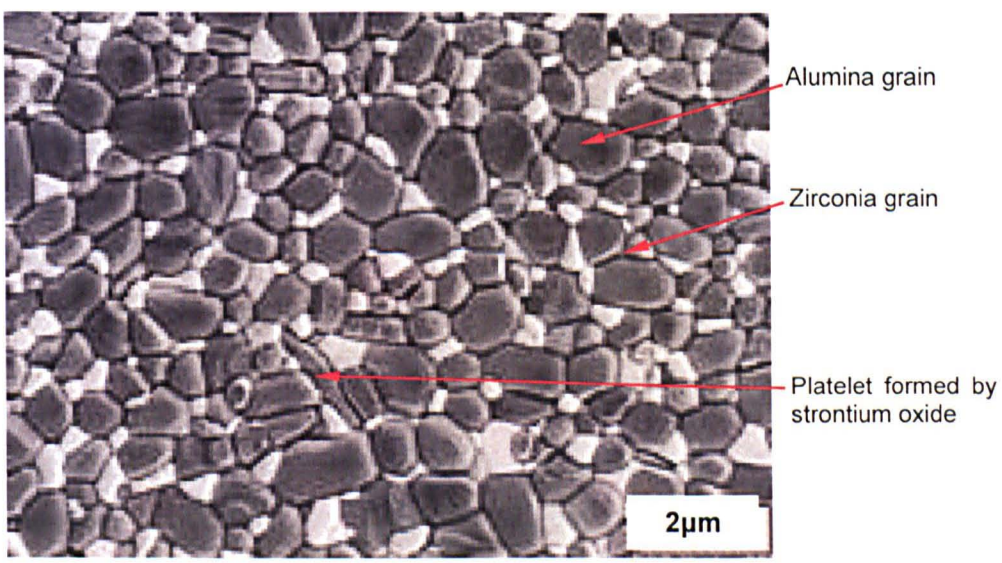

Figure 6.1 Microstructure of Biolox delta ceramic (BIOLOX®* delta OPTION Ceramic Femoral Head - Data sheet / surgical technique, 2008) (BIOLOX, 2008)

Although little is known about the clinical outcome and benefit of various materials used for hip hemiarthroplasty, a few studies *in-vivo* have discussed the effect of different implant materials on the cartilage degeneration, and wear.

One of the earliest reports of ceramic heads as endoprostheses found erosion of cartilage down to the bone, however, despite articulation with bone no scratching of the ceramic head was observed in 20 dogs after 2 years *in-vivo* (Lade *et al.*, 1983). Later a study compared hip hemiprostheses made of ceramic or cobalt chromium that were implanted in 30 dogs (Yoshinaga, 1987). The dogs were examined after 1, 3, and 6 months postoperatively, and progressive destruction of cartilage was observed with almost full thickness wear of the acetabular cartilage at 6 months. Somewhat more favourable results for the ceramic group were shown at 6 months. The long-term effects of cobalt-chromium or ceramic heads articulating with acetabular cartilage was compared in 20 dogs (Maistrelli *et al.*, 1991). After 5 months implantation, less severe degenerative changes were observed in the cartilage articulating with the ceramic implants compared to the cartilage articulating with the metal implants, although equal cartilage damage was evident in both groups at 8 months postoperatively. Recently a retrospective review of 471 patients with an average age 81.5 years, who were treated with hip hemiarthroplasties using Biolox Delta ceramic heads for head fractures was conducted. There were 140 surviving patients with a mean prosthesis longevity of 55.8 months and with a mean Harris hip scores of 70.6 (Müller *et al.*, 2000).

Generally, *in-vivo* studies comparing cobalt chromium to ceramic hemiarthroplasties have shown advantages in reducing the degeneration of acetabular cartilage in the hip joint after 6~56 months of articulation. However, the benefits of ceramic shown in hip hemiarthroplasty were not observed in knee hemiarthroplasty, this may be due to the different geometry and contact of the implants. A study reported an *in-vivo* knee hemiarthroplasty study of rabbits implanted with cobalt chrome implants on the femoral condyle side. Knees were examined after 3 months, less damage to the articulating cartilage surface was observed in the cobalt chromium group compared with the ceramic group ($p<0.03$) of rabbits (Jung *et al.*, 2007).

It has been demonstrated that aluminium oxide ceramics have better lubricating properties due to their better wettability compared to steel, and therefore ceramic head prostheses exhibit less frictional resistance (Dawihl *et al.*, 1979; Dawihl and Dörre, 1980; Maistrelli *et al.*, 1991; Willmann, 1993). However, the real friction values between ceramic femoral head and natural acetabular cartilage compared to cobalt chrome alloy heads have not been commonly reported. The

only reports of consistent findings regarding friction were observed in an *in-vitro* study using a pendulum (HEPF1Ex) hip simulator (Müller *et al.*, 2004). The friction tests were conducted with a dynamic load (double peak, 2.5 kN peak load) in new born calf serum mixed with Ringer's lactate solution lubricant (in a ratio of 1:3), and had a swivel range of +30/-18° with a 45° angle set-up of the apparatus at 37°C temperature-controlled condition in 900 cycles. The mean coefficient of friction against porcine acetabula (n=20) was μ=0.065 for ceramic and μ=0.081 for metal; against human cadaveric acetabula (n=10) μ=0.066 for ceramic and μ=0.099 for metal. The authors concluded that the lower coefficient of friction of ceramic (Al_2O_3) against fresh cadaveric acetabulum may have a clinical impact on the process of the protrusion of the femoral head through the acetabulum compared with metal.

Some studies have shown that advantages of ceramic hip implants compared to metal hip implants when articulated against soft bearing like Polyethylene. It was evaluated the differences of polyethylene wear *in-vivo* between metal and ceramic on polyethylene hip prosthesis in a biopsy post-mortem study (Bos *et al.*, 1991). It was demonstrated that three times fewer polyethylene wear particles (wear debris analysis) were revealed in the ceramic on polyethylene prostheses group compared to the metal on polyethylene group. Hence, in this study when articulating against soft tissue cartilage, it was hypothesed that the ceramic heads would reduce the cartilage wear compared to metallic (cobalt chrome) heads.

Although several experimental studies assessing *in-vivo* hip hemiarthroplasty have demonstrated superior tribological properties of ceramic implants compared to metallic implants, the tribological properties of the tested specimens may be influenced other variables, such as activities (loads) and movements (motions) of each sample. Hence, examining the tribological properties *in-vitro* is essential. However, the evidence *in-vitro* is limited. This study limited all the other variable factors that may affect cartilage tribology, and focused on the effect of the femoral head material on the acetabular cartilage friction, surface roughness, wear, deformation area, deformation volume, and deformation depth. The purpose of this study was to determine whether hip hemiarthroplasty *in-vitro* using a ceramic head provides better tribological performances compared to a cobalt chrome head under constant or dynamic loading. Ceramic heads articulated against porcine acetabular cartilage with small clearances (<0.6mm) for 2 hours in a reciprocating pendulum simulator with constant or dynamic loading to answer the following questions:

- Will the coefficient of friction with a ceramic head be lower compared with a cobalt chrome head (Chapters 4 and 5) as shown in *in-vivo* studies?

- What is the acetabular cartilage surface roughness after 2 hours pendulum reciprocation? What is the difference of roughness compared to previous studies with cobalt chrome heads?
- What kind of cartilage damage will be observed after 2 hours pendulum reciprocation with ceramic heads? What are the wear grade levels and the wear area of the lunate acetabular cartilage? How does this compare to cartilage that has articulated against metal heads?
- What is the difference in acetabular cartilage deformation area, volume, and depth when cartilage that articulated against ceramic heads is compared to cobalt chrome heads?

6.2 Objectives

The objectives of this study were to use a hip joint model of the acetabular cartilage cup reciprocating against a ceramic head to consider the effect of head material on cartilage tribological properties under constant or dynamic load. The clearance was considered in the flexion-extension direction and small clearances (<0.6 mm) only were studied. Tribological properties studied were: (1) contact area and contact stress, (2) coefficient of friction and frictional shear stress, (3) surface roughness, (4) cartilage wear grade, and (5) surface deformation volume and depth after the 2 hours ±15° motion and 400 N constant or 25~800 N dynamic loading in a pendulum friction study. An overview of this study is shown in Figure 6.2.

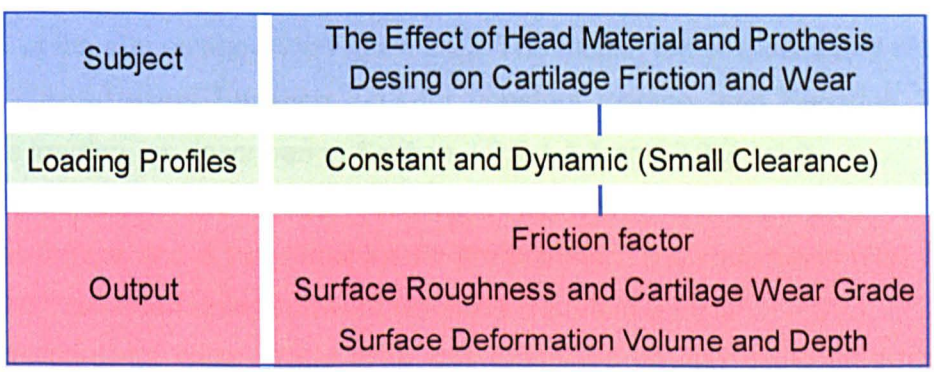

Figure 6.2 Summary of studied tribological properties in pendulum constant loading study in hip joint

6.3 Materials

Test materials used were ceramic heads Biolox Delta, (supplied by DePuy International Ltd, UK, 36 mm in diameter, surface roughness R_a=0.004 ±0.001μm) and six-month old porcine acetabula, and the lubricant was 25% bovine serum, as described in Section 2.3.1.2, 4, 5, and 8 respectively. The 12 porcine acetabula were chosen as FE direction diameter from 36.1 to 37.1 mm, and set in PMMA cement 45 degrees as described in Section 2.3.2.2. The friction tests were conducted on the pendulum friction simulator as described in Section 2.3.2.1. Microset silicon replicas were taken from the porcine acetabulum after the friction test for the wear study described as Section 2.3.2.3. The cartilage wear grade measurements were taken as described in Section 2.3.2.5, and the surface deformation measurement were taken as described in Section 2.3.2.6.

6.4 Methods

The constant load was chosen as half porcine body weight approximate 400 N (as described in Chapter 4), and the dynamic peak load was selected as the whole porcine body weight approximately 800 N (as described in Chapter 5), with a loading time of 2 hours (n=6) (explained in Section 2.3.2.1.1). This protocol was the same as previous studies (Chapters 4 and 5). The **constant** and **dynamic loading profile** was set as shown in Figure 2.24.

The **friction factor** was analysed as the coefficient of friction at the 0 degree position where the head was vertically loaded and in contact with the lowest position of the cup as shown in Figure 2.25. The friction factor (coefficient of friction) was calculated using Equation 2-13 for constant loading, and Equation 2-15 for dynamic loading, as described in Section 2.3.2.1.1.1 and 2.3.2.1.1.2.

The acetabular cartilage **surface roughness** was measured using the microset replica and a two-dimensional profilometer. The roughness (Ra) of each trace was calculated using software following Equation 2-19.

The cartilage **wear grade area** was examined visually using an adaption of the International Cartilage Repair Wear Grading System (Section 2.3.2.6). The area of the different wear grades were measured through marking a transparent cling film covering the microset replica of the acetabulum, as described in Section 2.3.2.6. Then the wear area of the different wear grades and the whole acetabular lunate surface area were calculated using Image Pro Plus, and presented as the percentage of the acetabular lunate surface area. The mean value of each wear

grade area percentage (six specimens) in both constant and dynamic loading groups were calculated and compared (ANOVA arcsine, $p<0.05$).

The acetabular replicas were selected based on the records of the original surface on the replicas (described in Section 2.3.2.7.1, Figure 2.36). Three most measurable replicas of each group were measured using a two-dimensional profilometer across the wear scar as described in Section 2.3.2.6.1, Figure 2.40. The acetabular surface **deformation volume** and the **average deformation depth** were calculated using the Equation 2-20, and 2-21. The mean value of deformation volume and average deformation depth of each group was calculated and compared (T-test, $p<0.05$).

6.5 Results

6.5.1 Effect of Head Material on Cartilage Friction

6.5.1.1 Coefficient of Friction under Constant Loading

The coefficients of friction measured under constant loading for specimens with small clearances (from 0.05 to 0.55 mm) articulating with ceramic heads for 2 hours are shown in Figure 6.3 (n=6). The mean coefficient of friction in specimens continued to increase from 0.08±0.03 to 0.32±0.03 during the 2-hour test (n=6).

A comparison of the mean coefficient of friction in specimens that articulated against different femoral heads (ceramic or cobalt chrome) under constant loading for 2 hours is shown in Figure 6.4. No significant difference of the coefficient of friction was observed in specimens that articulated with different materials at all time points (T-test, $p>0.05$, n=6).

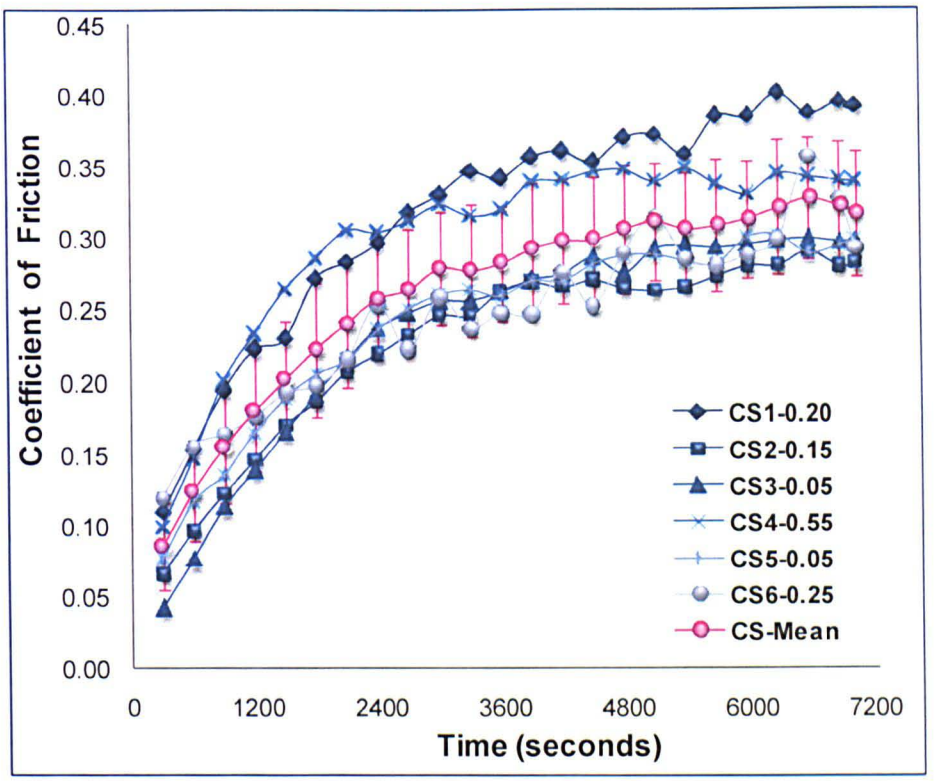

Figure 6.3 The coefficient of friction for specimens articulated against a ceramic head (n=6, mean ± 95% confidence limits), (*CS_n-x.xx: C- Constant loading, S-Small clearance, n-specimen number, x.xx- FE radial clearance*).

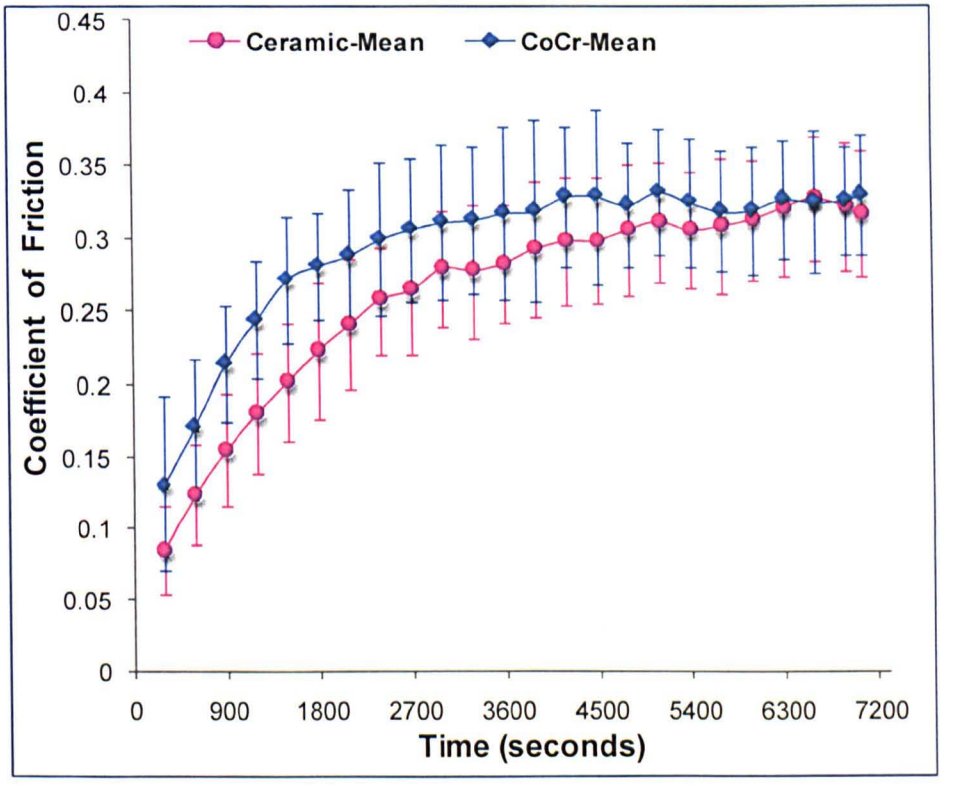

Figure 6.4 A comparison of the mean coefficient of friction in specimens with small clearances articulated against a ceramic head (Ceramic-Mean) and a cobalt chrome head (CoCr-Mean) under constant loading (n=6, mean ± 95% confidence limits).

6.5.1.2 Coefficient of Friction under Dynamic Loading

The coefficients of friction under dynamic loading of specimens articulating with ceramic heads are shown in Figure 6.5. The coefficient of friction in specimens increased from 0.05±0.02 to 0.13±0.03 during the 2-hour test.

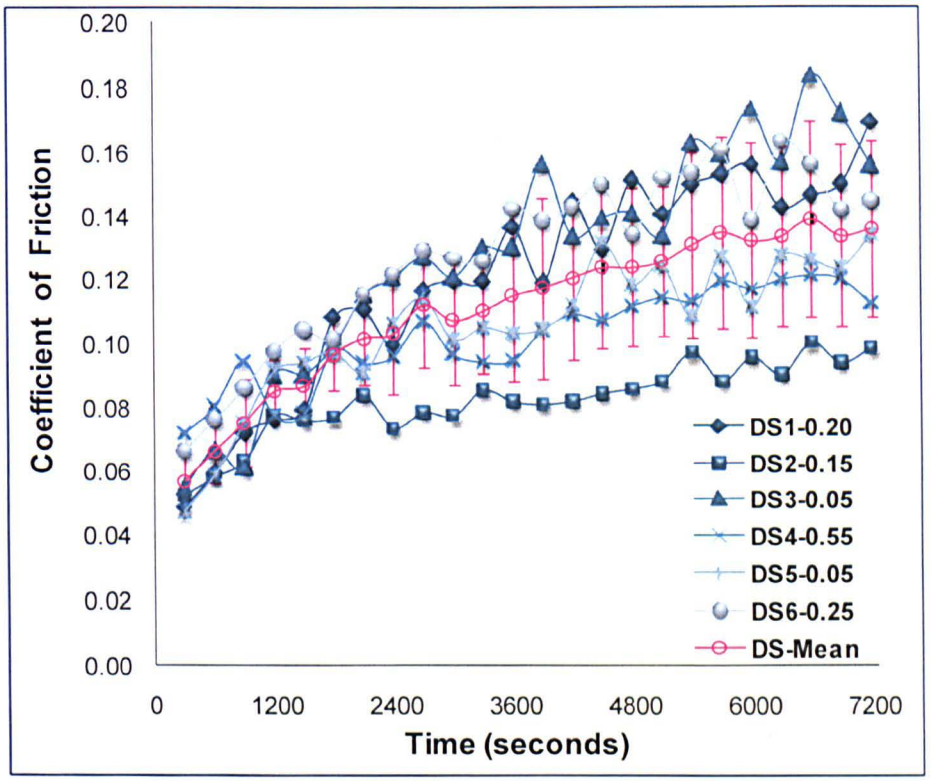

Figure 6.5 The coefficient of friction for specimens articulated against a ceramic head (n=6, mean ± 95% confidence limits), (*DS_n-x.xx: Dynamic loading with Small clearance, specimen number – FE radial clearance*).

A comparison of the mean coefficient of friction for specimens articulating against ceramic or cobalt chrome heads under dynamic loading is shown in Figure 6.6. No significant difference of the coefficient of friction was observed for specimens articulated against different materials (T-test, $p>0.05$, $n=6$).

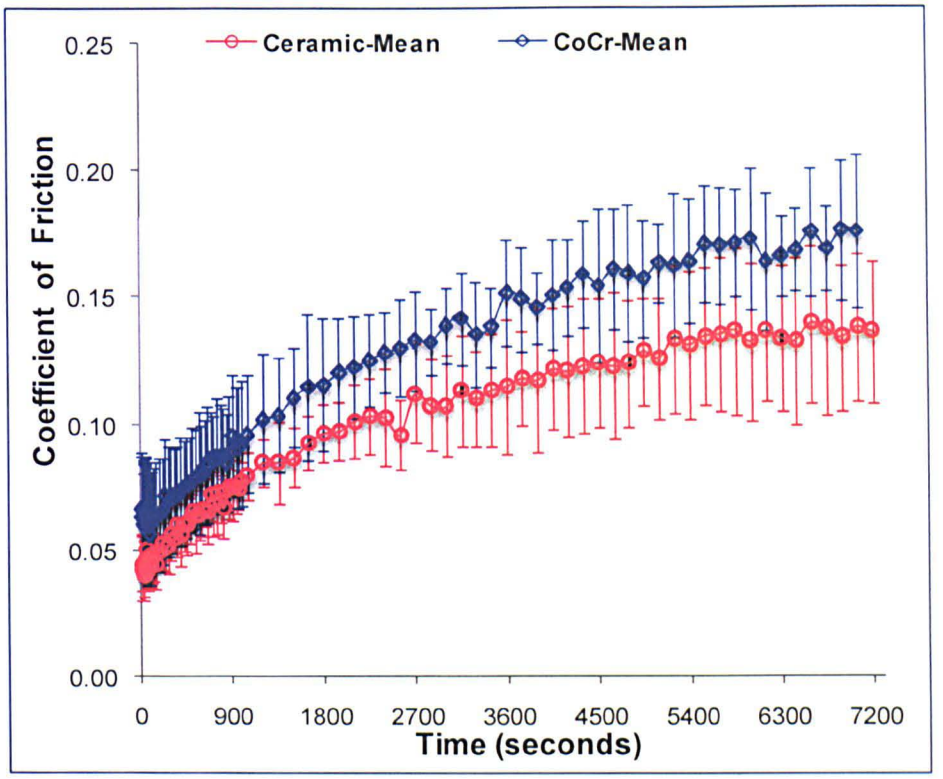

Figure 6.6 A comparison of the mean coefficient of friction for specimens with small clearances articulated against a ceramic head (Ceramic-Mean) and a cobalt chrome head (CoCr-Mean) under dynamic loading (n=6, mean ± 95% confidence limits).

6.5.1.3 Coefficient of Friction Comparison

A comparison of the mean coefficients of friction in specimens with small clearances that articulated against a ceramic head or a cobalt chrome head under constant or dynamic loading is shown in Figure 6.7 (n=6). Significantly higher coefficients of friction were observed in specimens under constant loading compared to under dynamic loading when articulating against a ceramic head. A similar result was shown for cobalt chrome in Section 5.5.5.2) (T-test, $p<0.05$, n=6). However, as previously described there was no significant difference in samples that articulated against metal or ceramic heads.

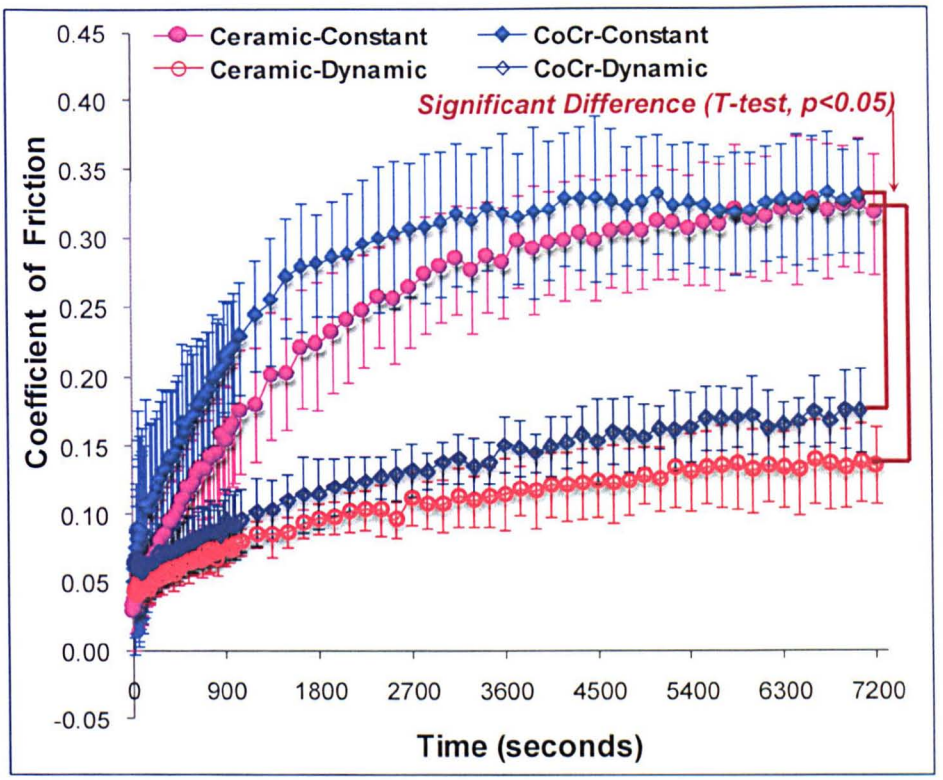

Figure 6.7 A comparison of the mean coefficients of friction in specimens with small clearances articulated against a ceramic head (Ceramic-Mean) or a cobalt chrome head (CoCr-Mean) under constant or dynamic loading (n=6, mean ± 95% confidence limits).

6.5.2 Effect of Head Material on Cartilage Surface Roughness and Wear

6.5.2.1 Cartilage Surface Roughness

A comparison of the surface roughness (R_a) of cartilage in replicas of samples following 2 hours articulation against different femoral head materials under constant or dynamic loading is shown in Figure 6.8. No significant difference was found in the surface roughness of cartilage in replicas that articulated against ceramic head under dynamic loading compared to under constant loading (T-test, $p>0.05$, $n=3$). The surface roughness replicas from acetabula that articulated against ceramic heads were significantly lower compared to samples that articulated against cobalt chrome heads under constant loading and under dynamic loading (T-test, $p<0.05$, $n=3$).

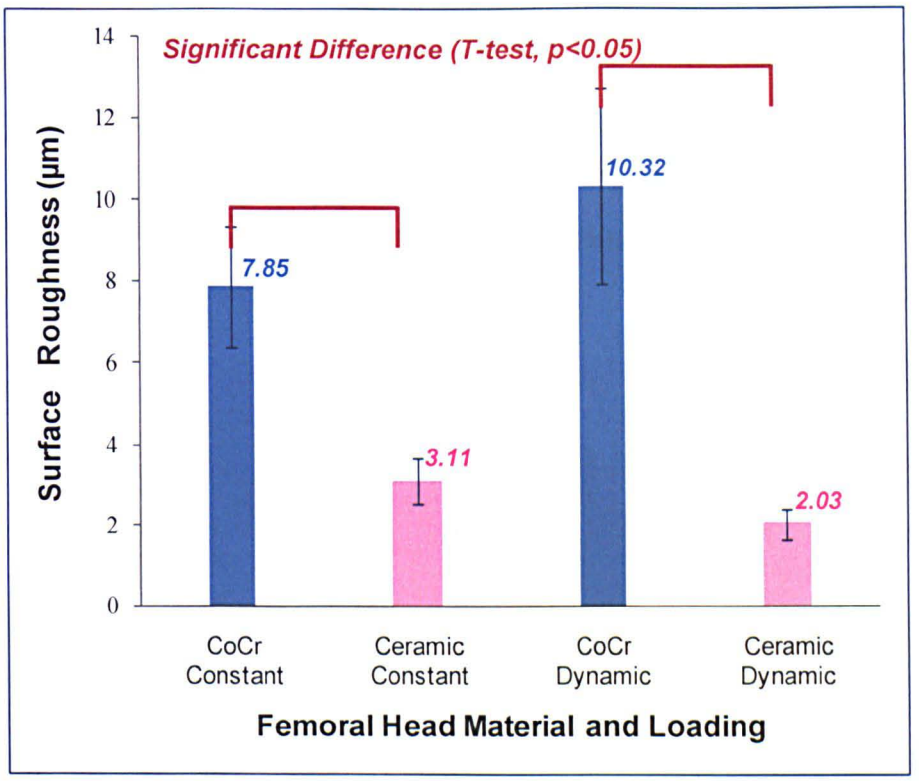

Figure 6.8. Comparison of the mean acetabular replica surface roughness in specimens with small clearances articulating against cobalt chrome and ceramic heads under both 400N constant and 25~800N dynamic loading (n=3, mean ± 95% confidence limits).

6.5.2.2 Cartilage Wear Grade

A comparison of the percentages of the different wear grade areas of specimens after 2 hours articulation against ceramic and cobalt chrome heads are shown in Figure 6.9.

For specimens tested with a ceramic head:

1) Wear grades 1, and 2 were observed in all the specimens used in tests under both constant load and dynamic load;
2) Wear grade 3 was only seen in specimens tested under constant load;
3) Wear grade 1 area percentage was significantly smaller under constant loading compared to the wear grade 1 area in specimens tested under dynamic loading (T-test, $p<0.05$, $n=6$).

Compared to specimens tested with cobalt chrome heads:

1) Under constant loading: wear grade 1 percentage in specimens tested against ceramic heads was significantly smaller compared to wear grade 1 in specimens articulated against cobalt chrome heads (T-test, $p<0.05$, $n=6$);
2) Under dynamic loading: Wear grade 3 was only seen in specimens used in tests against cobalt chrome heads.

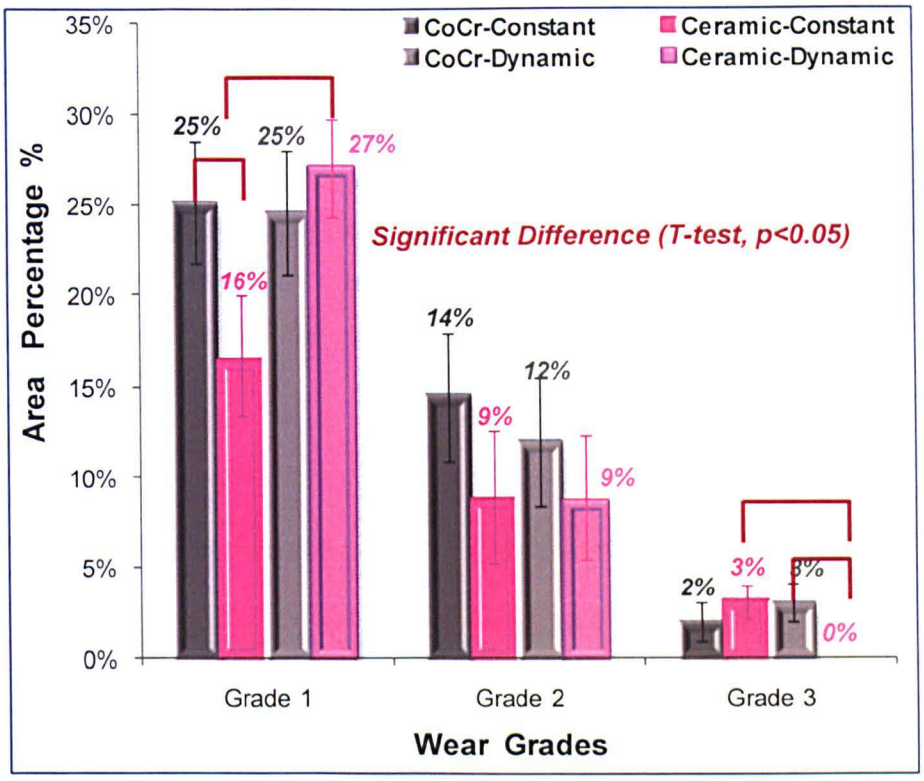

Figure 6.9 Comparison of acetabular replica surface wear grade areas for specimens with small clearances articulated against a cobalt chrome (CoCr) or a ceramic head under constant or dynamic loading (n=6, mean ± 95% confidence limits).

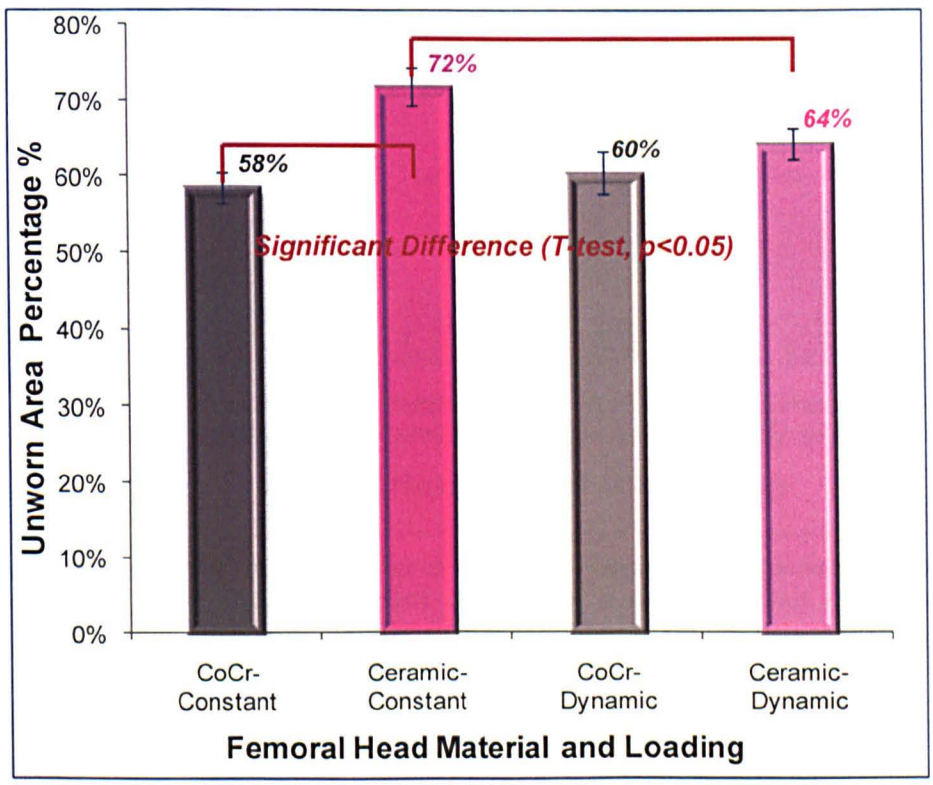

Figure 6.10. Comparison of unworn areas (wear grade 0) in specimens with small clearances articulated against a cobalt chrome (CoCr) or a ceramic head after 2 hours constant or dynamic loading (n=6, mean ± 95% confidence limits).

The comparison of total unworn area (wear grade 0) percentage for acetabular specimens after 2 hours articulating with ceramic or cobalt chrome femoral heads is shown in Figure 6.10.

The unworn area in specimens tested with a ceramic head under constant loading was significantly larger compared to specimens under dynamic loading (T-test, $p<0.05$, $n=6$). The unworn area in specimens articulating against ceramic head were significantly larger compared to specimens that articulated with cobalt chrome heads (T-test, $p<0.05$, $n=6$).

6.5.3 Effect of Head Materials on Cartilage Surface Deformation

6.5.3.1 Cartilage Deformation Volume

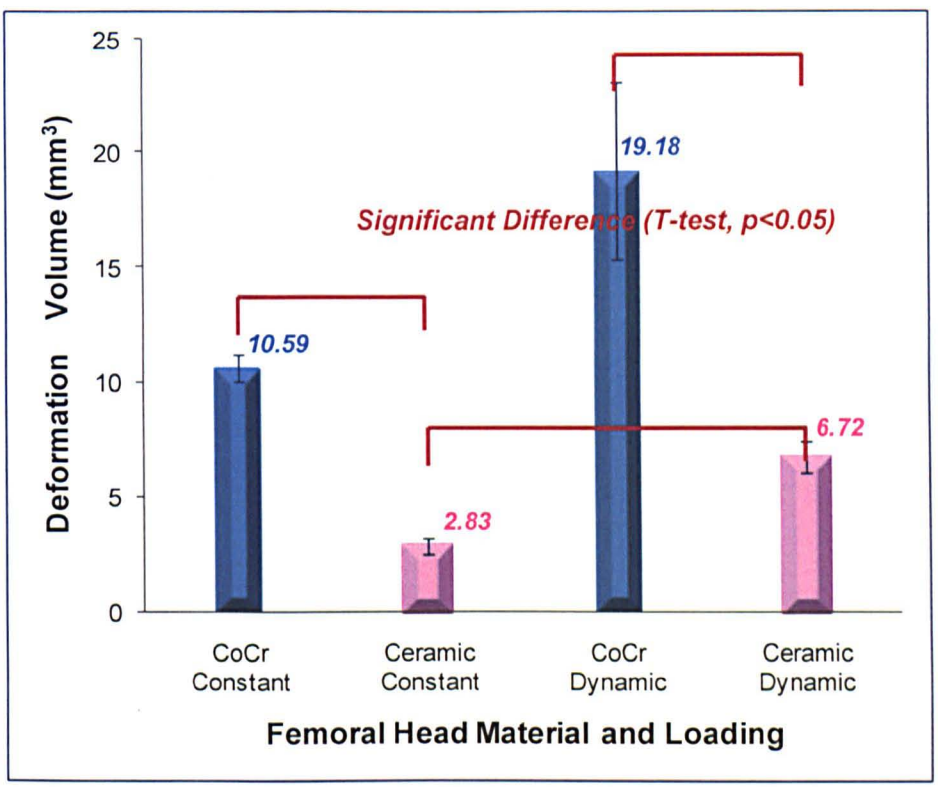

Figure 6.11. Comparison of acetabular deformation volume for specimens with small clearances articulated against a cobalt chrome or a ceramic head under constant loading or dynamic loading (n=3, mean ± 95% confidence limits).

The deformation volume is compared in specimens after 2 hours of articulation against ceramic or cobalt chrome femoral heads under constant or dynamic loading in Figure 6.11.

In specimens tested against ceramic femoral heads, it was found that the deformation volume following constant load testing was significantly smaller compared to under dynamic loading (T-test, $p<0.05$, $n=3$).

In specimens that articulated with cobalt chrome femoral heads, it was observed that the deformation volume was significantly greater compared with specimens that articulated against a ceramic head under constant loading or under dynamic loading (T-test, $p<0.05$, $n=3$).

6.5.3.2 Cartilage Deformation Depth

The average deformed depth of acetabular cartilage in specimens that articulated against a ceramic femoral head or a cobalt chrome femoral head under constant or dynamic loading is shown in Figure 6.12.

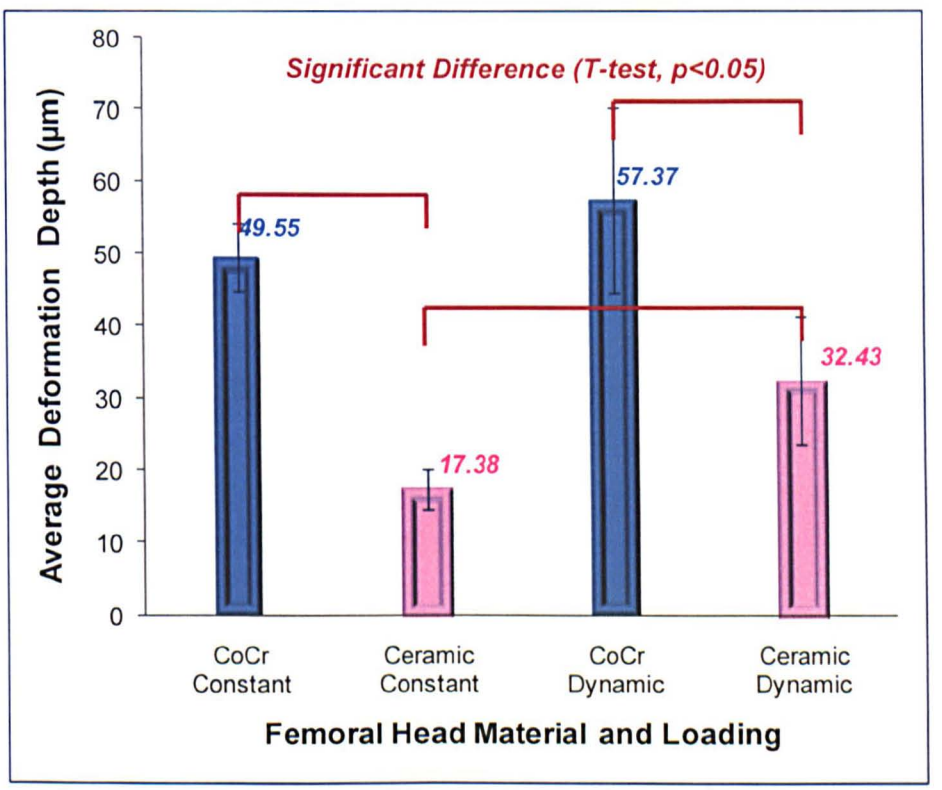

Figure 6.12. Comparison of average deformation depth of acetabular cartilage in specimens with small clearances articulated against a cobalt chrome head or a ceramic head under constant loading or dynamic loading (n=3, mean ± 95% confidence limits).

In specimens tested against ceramic femoral heads, significantly smaller average deformation depth was observed in those tested under constant loading compared to under dynamic loading (T-test, $p<0.05$, $n=3$).

In specimens tested against a cobalt chrome femoral head, it was found that the average deformation depth was significantly greater compared to those that articulated against ceramic heads under constant loading or under dynamic loading (T-test, $p<0.05$, $n=3$).

6.6 Discussion

This study conducted the tribological tests on porcine acetabula with ceramic femoral heads with small radial clearances (FE direction), to examine the effect of femoral head material on cartilage tribological properties under constant or dynamic loading.

6.6.1 Effect of Head Materials on Cartilage Friction

No significant difference was observed in the coefficient of friction in specimens that articulated against ceramic and cobalt chrome heads either under constant loading or under dynamic loading. However, the mean value of the coefficient of friction (Figure 6.7) of the ceramic group was lower compared to the cobalt chrome group under both constant and dynamic loading. This may indicate improved friction properties created between a ceramic on cartilage counterface compared to a cobalt chrome alloy on cartilage counterface. This result is possibly due to the better wettability of ceramic compared with cobalt chrome (Dawihl *et al.*, 1979; Dawihl and Dörre, 1980; Maistrelli *et al.*, 1991; Willmann, 1993). This better wettability of ceramic may also be the main factor that results in significant lower surface roughness compared to cobalt chrome.

Similar findings have been reported in a previous *in-vitro* study, the coefficient of friction was significantly lower (Figure 6.13.a) when testing was conducted with a ceramic head compared to with a metal head when 2.5 KN double-peak dynamic loading was applied for 900 cycles (Müller *et al.*, 2004). A greater coefficient of friction for metal heads compared to ceramic heads was observed in both human cadaver acetabulum specimens ($n=10$) and porcine acetabulum specimens ($n=20$). A greater difference of coefficients of friction between two different materials (ceramic and metal) was observed in human acetabulum samples compared to porcine acetabulum samples.

The test variables and results between Müller et al (2004) study and this study are shown as Tables 6-1 and 6-2 respectively.

Table 6.1.Differences of the tests variables between the study by Müller *et al.* (2004), and this study.

Tests Variables	Müller *et al.*, 2004	This Study
Dynamic Loading	Double Peak	Single Peak
Peak Load (N)	2500	800
Lubricant	New born calf serum mixed with Ringer's lactate solution (1:3)	New born bovine serum mixed with PBS (1:3)
Temperature (°C)	37	21 ± 1
Swivel Angle (°)	+30 / -18	+15 / -15
Sample Number	20 (porcine); 10 (human cadaver)	6x2 (porcine)
Calculation of μ_{eff}	$\mu = \frac{\sum_{j=1}^{3} \mu_{AH_{ij}}}{3}$	$f_d = f_p - \frac{f_{de,-2m} + f_{de,+2m}}{2}$
Measurements	Against each acetabulum three measurements (j) of one material of each cycle (i), same porcine acetabulum was tested by both ceramic head and metal head.	f_p was calculated form friction torque at peak load, and the f_d was taken off the transducer drift and off-set of the setting; different specimens with same clearance control.

When Müller et al (2004) study is compared to this study, differences test variables are observed e.g. numbers of peak load each cycle, peak load value, test temperature, lubricant, range of swivel angle, and calculation method for the coefficient of friction. However, in both studies similar findings have been observed when porcine acetabula articulated against ceramic or metal heads (see Table 6-2):

Table 6.2.Similarities of tests results at 900 cycles of dynamic loading between the study by Müller *et al.*, (2004) and this study.

Tests Results		Müller *et al.*, 2004	This Study
$\overline{\mu}$ (900 cycles)	Porcine	Ceramic: 0.082; Metal: 0.101	Ceramic: 0.075; Metal: 0.096
	Human	Ceramic: 0.083; Metal: 0.118	N/A
$\Delta\overline{\mu}$ (metal-ceramic)	Porcine	0.019	0.021
	Human	0.035	N/A

1. Lower mean coefficient of friction ($\overline{\mu}$) when porcine or cadaveric acetabula articulated with ceramic material compared to metal;

2. The difference of mean coefficient of friction between the two materials ($\Delta\overline{\mu}$) after 900 cycles of dynamic loading was 0.02.

The coefficient of friction was slightly higher in Müller et al. (2004) study. The reasons for this may be higher peak load increasing the frictional shear stress, and also the double-peak reducing the proportion of fluid transferring back to the loading areas. In this study, the difference of coefficient of friction between ceramic and metal materials was not found to be significant, this may due to the small number of samples (n=6).

6.6.2 Effect of Head Materials on Cartilage Surface Roughness and Wear

The acetabular surface was significantly smoother in specimens following articulation against ceramic heads compared to specimens tested with cobalt chrome heads for 2 hours pendulum reciprocation under constant or dynamic loading (R_a, T-test, $p<0.05$, $n=3$). For specimens that articulated against cobalt chrome heads compared to specimens tested with ceramic heads, the surface of lunate acetabular cartilage (measured areas) was 250% rougher under constant loading, and approximate 500% rougher under dynamic loading (Figure 6.8).

It is postulated that the significant difference of the acetabular cartilage surface roughness is due to the different material properties of the articulating surfaces. Ceramic has an improved wettability and much higher hardness compared to metal (cobalt chrome), and this enhances the lubricating properties when articulating with cartilage, hence the damage of cartilage was reduced. The better hardness of the femoral head reduced the damage of the head during friction, and this provided a smoother contact surface onto the acetabular cartilage which reduce the cartilage damage and wear.

Similar to the previous results in Chapter 4 and 5, no significant difference of the acetabular cartilage surface roughness was seen between samples selected under constant loading or under dynamic loading when articulated against ceramic heads. Hence, it is concluded that the surface roughness of acetabular cartilage is mainly dependent on the femoral head material which it articulates against, but not the loading.

In specimens tested under constant loading, significantly lower proportions of wear grade 1 area were observed in specimens after 2 hours of articulation against ceramic femoral heads compared to against cobalt chrome heads (Figure 6.9); Under dynamic loading, significantly lower wear grades were seen in specimens

tested against ceramic femoral heads compared to against cobalt chrome heads. This is due to the improved wettability of the ceramic material causing less cartilage damage compared to the cobalt chrome material. With the same load applied to the different heads, the total contact area and contact stress was similar, the less wear grade 1 areas (demonstrating less wear) led to the smaller total unworn area in ceramic group under constant loading, and lower wear grades observed overall under dynamic loading (wear grade 3 was not seen in ceramic group, Figure 6.9). Hence, the wear grade level and wear area depends on the articulating surface material properties under constant loading and dynamic loading. The different reduction of wear grade area, and wear grade level in the ceramic group when constant and dynamic loading are compared is possibly due to the type of loading.

6.6.3 Effect of Head Material on Cartilage Surface Deformation

Significantly smaller deformation volume, and average deformation depth was observed in specimens that articulated against ceramic head compared to in specimens that articulated against metallic (cobalt chrome) heads under both constant and dynamic loading (Figure 6.11~12).

This difference was 1.7~3.3 times greater in deformation area, 2.9~3.7 times greater in deformation volume, and 1.8~2.9 times greater in average deformation depth created by a metallic cobalt chrome head compared to a ceramic head following articulation against acetabular cartilage under constant or dynamic loading.

Typical deformation traces generated following articulation against ceramic or cobalt chrome heads under constant or dynamic loading are shown in Figure 6.13. Smoother surface (significantly smaller R_a) and reduced wear areas are seen in ceramic constant and dynamic groups (Figure 6.13. a, and c) compared to in cobalt chrome constant and dynamic groups (Figure 6.13. b and d). Hence, the ceramic material makes an improved bearing surface due to the increased hardness, and high wettability compared with metallic material (e.g. cobalt chrome alloy). When ceramic compared to metal on soft bearing surfaces (hard-on-soft counterfaces), similar observations have been reported. For example, ceramic and metal on polyethylene *in-vivo*; the polyethylene wear with ceramic was three times fewer compared to metal hip prostheses (Bos *et al.*, 1991).

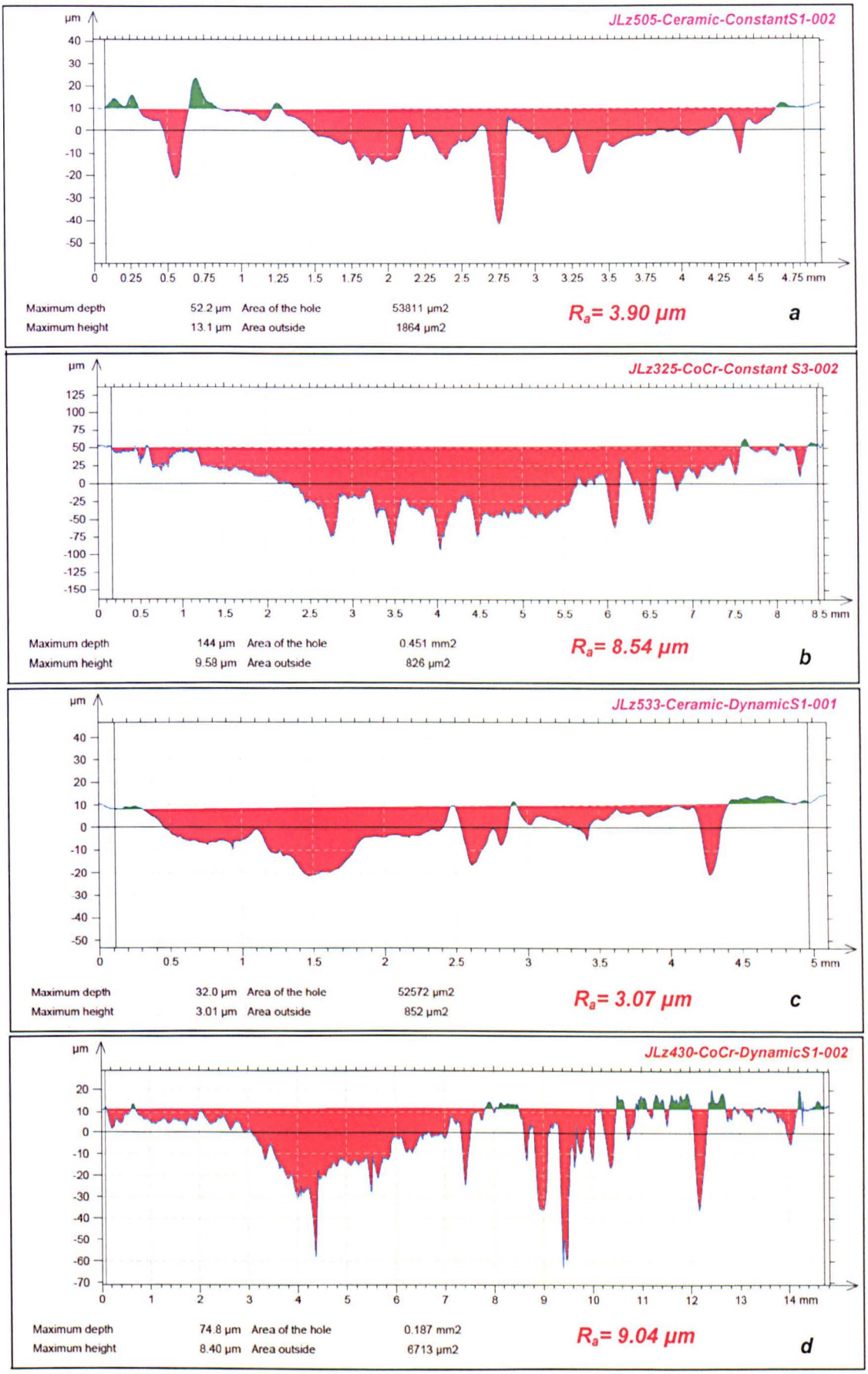

Figure 6.13 Comparison of wear trace analysis in specimens with small clearances articulated against: a. a ceramic head under constant loading; b. a cobalt chrome head under constant loading; c. a ceramic head under dynamic loading; d. a cobalt chrome head under dynamic loading.

6.6.4 Other Factors

In this study, biological specimens were used and clearances were matched. However, some differences between samples remould including the precise acetabulum geometry, the lunate acetabular cartilage thickness, variation in the size of the fat pad, and difference the removing portion of the ligament size following dissection. These factors would also affect cartilage friction, surface roughness, cartilage wear, and cartilage deformation during the pendulum reciprocation. Additionally, the femoral head and the acetabulum sizes used in this study should be considered. All specimens were matched in regard to clearance, however, the ceramic head used for both constant and dynamic loading tests was a 36mm in diameter ceramic head, and porcine acetabula in the range of 36.1~37.1 mm in the FE direction were chosen. However, cobalt chrome heads were available in three different sizes; 35, 36, and 37mm in diameter, and therefore the porcine acetabulum specimens were in a larger range of 35.1~38.2mm in diameter in the FE direction. The different sizes of femoral heads and acetabula may also have some effect on the tribological properties during the pendulum reciprocation. For example, the different sizes of metal heads may affect slightly the contact area, contact stress, and wear area percentages on the lunate surface cartilage.

6.7 Conclusion

In hip hemiarthroplasty, the material of the femoral head affects the tribological properties of cartilage. The effects of head material on cartilage friction, deformation, degradation, and degeneration during 2 hours pendulum reciprocation were as follows:

1. When articulated against acetabular cartilage, compared to metallic femoral heads, ceramic femoral heads caused significantly less increase of cartilage surface roughness, less cartilage wear, lower cartilage wear grade levels, less acetabular cartilage surface deformation volume and deformation depth.
2. Ceramic material may be recommended for the femoral head in hip hemiarthroplasty due to the lower coefficient of friction examined *in-vitro*, and less acetabular cartilage degeneration reported clinically.

Chapter 7 The Effect of Prosthesis Design on Hemiarthroplasty Function

7.1 Introduction

In Chapter 4, 5, and 6 the effects of clearance in FE direction, loading regimes, and femoral head materials on the cartilage friction and deformation in a hemiarthroplasty hip simulation have been discussed. The lowest coefficient of friction, least surface damage of the acetabular cartilage, and the minimum cartilage deformation was observed with large FE radial clearance level (≥1.2 mm and <1.8 mm) with cobalt chrome heads under dynamic loading in this hip hemiarthroplasty model (Chapter 4 and 5). Additionally, it was observed that ceramic heads generated significantly less cartilage surface damage and deformation compared to cobalt chrome heads within the same level of clearance (Chapter 6). Hence, it is hypothesised that ceramic heads with large FE radial clearances level would provide the optimum cartilage tribological properties with unipolar heads in this *in-vitro* hip hemiarthroplasty model.

However, these studies all investigated a unipolar prosthesis design, and there is interest to investigate the tribological properties of acetabular cartilage versus a novel design of a bipolar prosthesis. Hence, this chapter focuses on the effect of prosthesis design, and investigates the effect of a novel bipolar hemiarthroplasty on cartilage tribological properties.

Unipolar prostheses have generally been satisfactory in the short-term clinically. Problems occur with increasing time, for example: pain, femoral head loosening, and on occasions progressive protrusion of the acetabuli. Bipolar hemiarthroplasty prostheses (also called bipolar endoprostheses) were first used in the 1970's. The development of bipolar femoral-head prostheses have been reported by Bateman (1974, Figure 7.1) and Giliberty (1974), with a monoblock femoral head and stem, and a polyethylene bearing insert covered with a metal bearing surface (Bateman, 1974; Gilberty, 1974). The polyethylene bearing insert articulates with the femoral head (22 mm in diameter in the Bateman prosthesis and 32 mm in diameter in the Gilberty prosthesis), and the insert is covered with a metal bearing surface which articulates with the acetabulum.

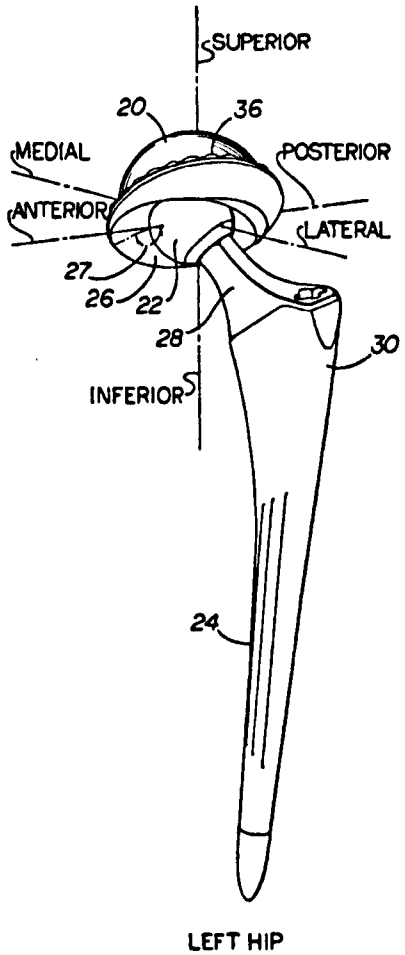

Figure 7.1 Bipolar Bateman prosthesis (http://www.freepatentsonline.com/)

The bipolar design is intended to distribute the friction force at both the inner and the outer articulation surfaces, and to diminish the motion and therefore wear at the acetabular cartilage interface. This type of prosthesis also reduces the dislocation risk, the advantages of the bipolar design have been reported in different clinical studies:

1) The bipolar design diminishes friction and impact forces of the prosthetic head on cartilage without compromising hip stability, and can be easily converted to a total hip joint replacement by cementing in an acetabular component (Bhuller, 1982).
2) Patients with bipolar hemiarthroplasties received pain relief and early mobilisation and restoration of function compared to patients receiving unipolar hemiarthroplasties, loosening and acetabular bone loss were not major problems due to less motion occurring on the outer surfaces (Bochner *et al.*, 1988).
3) When a bipolar prosthesis was compared to a unipolar prosthesis, they provided better stability, permitted earlier weight bearing and ambulation,

shortened hospital stays, increased rehabilitation, and decreased subsequent operations (Lestrange, 1990).

4) Patients with a bipolar hemiarthroplasty had an increased satisfaction in terms of postoperative pain, more rapid return to unassisted activity, greater range of movement, no acetabular erosion and fewer unsatisfactory results compared to patients with an Austin-Moore unipolar hemiarthroplasty in 4 years follow-up (Malhotra *et al.*, 1995).
5) Superior long-term results of the bipolar prosthesis have been reported compared to unipolar bearings in the treatment of femoral neck fracture. This was due to the delayed acetabular wear which reduced motion, and shear forces at the prosthetic–bone interface (Gaine *et al.*, 2000b).

Over the last 30 years, indications for using a bipolar component have broadened to include femoral head avascular necrosis, and degenerative osteoarthrosis (Calton *et al.*, 1998). This is due to the perceived advantages of bipolar prostheses compared to unipolar bearings, including wear and protrusion of the acetabular component and pain relief, different designs have been developed (for example, Charnley-Hastings prosthesis) and used as an effective treatment for femoral neck fracture and femoral head necrosis. However, problems with polyethylene wear are associated with fixed acetabular components and subsequent osteolysis can also occur in bipolar implants. The linear rate of polyethylene wear has been reported as 0.07~0.6 mm per year in patients who received a hip arthroplasty in 2~15 year follow-up after a THR (Charnley and Halley, 1975; Griffith *et al.*, 1978; Collier *et al.*, 1990). It was reported that with a bipolar implant, a decrease in the thickness of polyethylene bearing to less than 6~8 mm was associated with a rapid increase in stress within the polyethylene (Bartel *et al.*, 1985; Bartel *et al.*, 1986). The minimum acceptable polyethylene thickness was estimated to be 6 mm (Wright *et al.*, 1989; Calton *et al.*, 1998), or 8 mm (Calton *et al.*, 1998). However, the greater thickness of the polyethylene bearing may increase the possibility of the metal head dislocation due to the decreased inner friction torque, but also produce higher volumes of polyethylene wear debris which may develop osteolysis. Limited range of motion and neck impingement on the rim of existing bipolar have also been reported as one major problem with small diameter heads in polyethylene bearings (Schaffer *et al.*, 1991; McGrory and Lawhead, 2005). These impingements may result in polyethylene and / or metal wear debris, leading to early femoral stem loosening (Messieh *et al.*, 1994; Nohuhiro *et al.*, 2001).

This novel design of bipolar prosthesis used in this study is very different compared to normal bipolar designs (e.g. Bateman prosthesis, Giliberty prosthesis, etc), it excludes a polyethylene bearing and hence avoids polyethylene wear. However, it may still provide reduced motion and therefore cartilage degeneration at the acetabular interface. The large metal head with thin metal cup of this bipolar design allows improvement of the range of motion and rotation of hip joint. Clinically, this bipolar design reduces the requirement of surgical preparation of the acetabulum as in this design, the cup is expected to set naturally into the acetabular cartilage compared to THR and surface replacement.

Few studies have investigated the tribological characteristics of articular cartilage *in-vitro* with a bipolar prosthesis under physiological walking condition due to the complicated analysis of the frictional properties. For example, the coefficient of friction between the cadaver acetabular cartilage and the metal cup in a bipolar prosthesis under a pendulum trial has been reported as 0.014-0.07 at 100-600 N for a Batemann UPF II Bipolar prosthesis (Tsukamoto *et al.*, 1992); 0.02-0.06 at 2 kN for a Hasting bipolar prosthesis (Wetherell *et al.*, 1992).

This chapter focuses on a novel bipolar prosthesis (Figure 7.2) with a metal femoral head and a metal cup to understand the following research questions:

- What are the frictional properties *in-vitro* with this novel design of bipolar prosthesis?
- Where does motion occur when a dynamic load and motion is applied?
- What is the difference between this bipolar prosthesis and the previously reported unipolar prostheses on cartilage friction, deformation and wear?

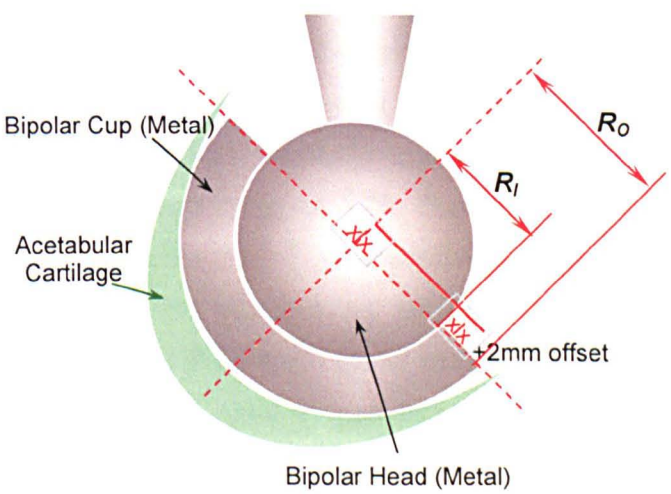

Figure 7.2 The biomechanics of the bipolar prosthesis

7.2 Objectives

The objectives of this study were to use a hip joint model of the acetabular cartilage cup reciprocating against a novel bipolar prosthesis to consider the effect of the different prosthesis design by comparing to the friction, and cartilage deformation due to articulation against a unipolar bearing when tested under dynamic load.

7.3 Materials

Tests materials used were six-month old porcine acetabula and a bipolar prosthesis which consists of a 28 mm in diameter cobalt chrome head and a 28/36 cobalt chrome cup (shell) (inner diameter 28 mm, and outer diameter 36 mm, described in Section 2.3.1.3, Figure 2.19 and Figure 7.2). Small radial clearance (<0.6 mm) in FE direction between the porcine acetabulum and the bipolar cup outer surface was chosen for this test, and six specimens were used at the range of FE direction diameter 36.2~37.1 mm, and the lubricant was 25% bovine serum. The porcine acetabulum was set in PMMA cement at 45 degrees as described in Section 2.3.2.2, and friction tests were conducted on the pendulum friction simulator as described in Section 2.3.2.1.

7.4 Methods

The peak dynamic load was chosen as the entire porcine body weight (800N) with a loading time of 2 hours (described in Section 2.3.2.1.1). The **dynamic loading profile** was set as shown in Figure 2.24.

The **friction factor** was analysed as the coefficient of friction at the 0 degree position where the head was vertically loaded and in contact with the lowest position of the cup as shown in Figure 2.25. The friction factor (coefficient of friction) was calculated using Equation 2-12, as described in Section 2.3.2.1.1.

However, due to the two bearing surfaces of the bipolar prosthesis, the biomechanical analysis of the friction factor in bipolar prosthesis was calculated in two bearing surfaces – the inner friction factor and the outer friction factor. The pendulum friction test was recorded by video to examine the motion surfaces, and the true friction torque (T_t) was measured through the piezoelectric sensor followed the same equation (Equation 2-12). The motion might occur at the two bearing interfaces during the pendulum friction test (Table 7.1 and Figure 7.3):

1. When the motion occurred at the inner bearing: $T_I = T_t < T_O$
2. When the motion occurred at the outer bearing: $T_I > T_O = T_t$
3. When the motion occurred at both inner and outer bearings: $T_I = T_O = T_t$

Where, T_I is the friction torque at inner bearing (Nm), T_O is the friction torque at outer bearing (Nm), and T_t is the true friction torque measured through the pendulum friction simulator (Nm).

Table 7.1 Friction torque analysis of bipolar prosthesis in three types of motions

Friction Torque Analysis	$T_I < T_O$	$T_I > T_O$	$T_I = T_O$
Motion Surface(s)	Inner Bearing	Outer bearing	Inner Bearing & Outer Bearing
Combined as one Object	Metal Cup & Acetabulum	Metal Head & Metal Cup	None
Measured Friction Torque (T_t)	T_I	T_O	T_I

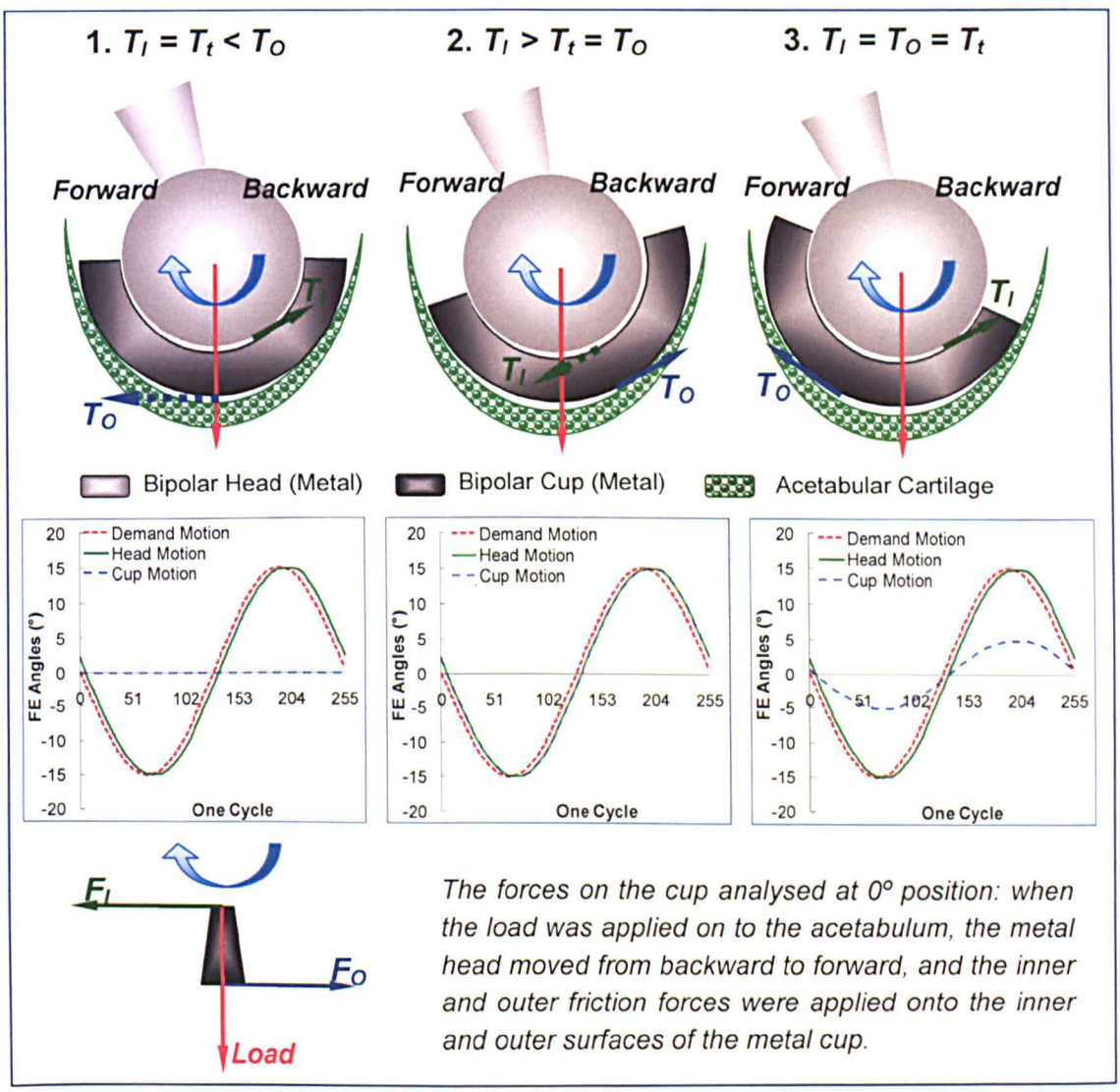

Figure 7.3 Schematic diagrams of the bipolar prosthesis demonstrating how three different types of motion can occur

The inner friction factor and the outer friction factor was calculated by Equations 7-1 and 7-2

$$f_I = \frac{T_I}{R_I \times L}$$ **Equation 7-1**

$$f_O = \frac{T_O}{R_O \times L}$$ **Equation 7-2**

Where, f_I is the inner bearing friction factor, R_I is the inner surface radius (m), f_O is the inner bearing friction factor, R_O is the inner surface radius (m), L is the load (N).

During the dynamic load bipolar friction study, the off-set and transducer drift were ignored due to the unstable motion interface. Motions occurred at both interfaces and varied during the pendulum reciprocation; hence a video was recorded of each test to examine where the motion occurred. However, when the metal cup was pushed to one side of the acetabulum, it became 'locked' in that position and the test needed to be stopped due to the friction was not occurred on the outer surfaces between the metal cup and the porcine acetabulum.

7.5 Results

7.5.1 Motion Bearing Surface

From observations during testing and reviewing the recorded video clips of the pendulum friction test, motions were found to occur at both the inner and outer bearing surfaces in the first 5~20 minutes of testing. Images of the bearing surface motion were taken during the test, and a typical motion pattern is shown in Figure 7.4.

During the dynamic pendulum reciprocation, the metal cup was pushed by the metal head forward (Figure 7.4.c) and backward (Figure 7.4.d) in the FE direction of each cycle. However, following between 5 and 20 minutes of testing, the metal cup was always pushed further to an extreme forward or backward position, and was locked at that extreme position in the porcine acetabulum, then the test was manually stopped.

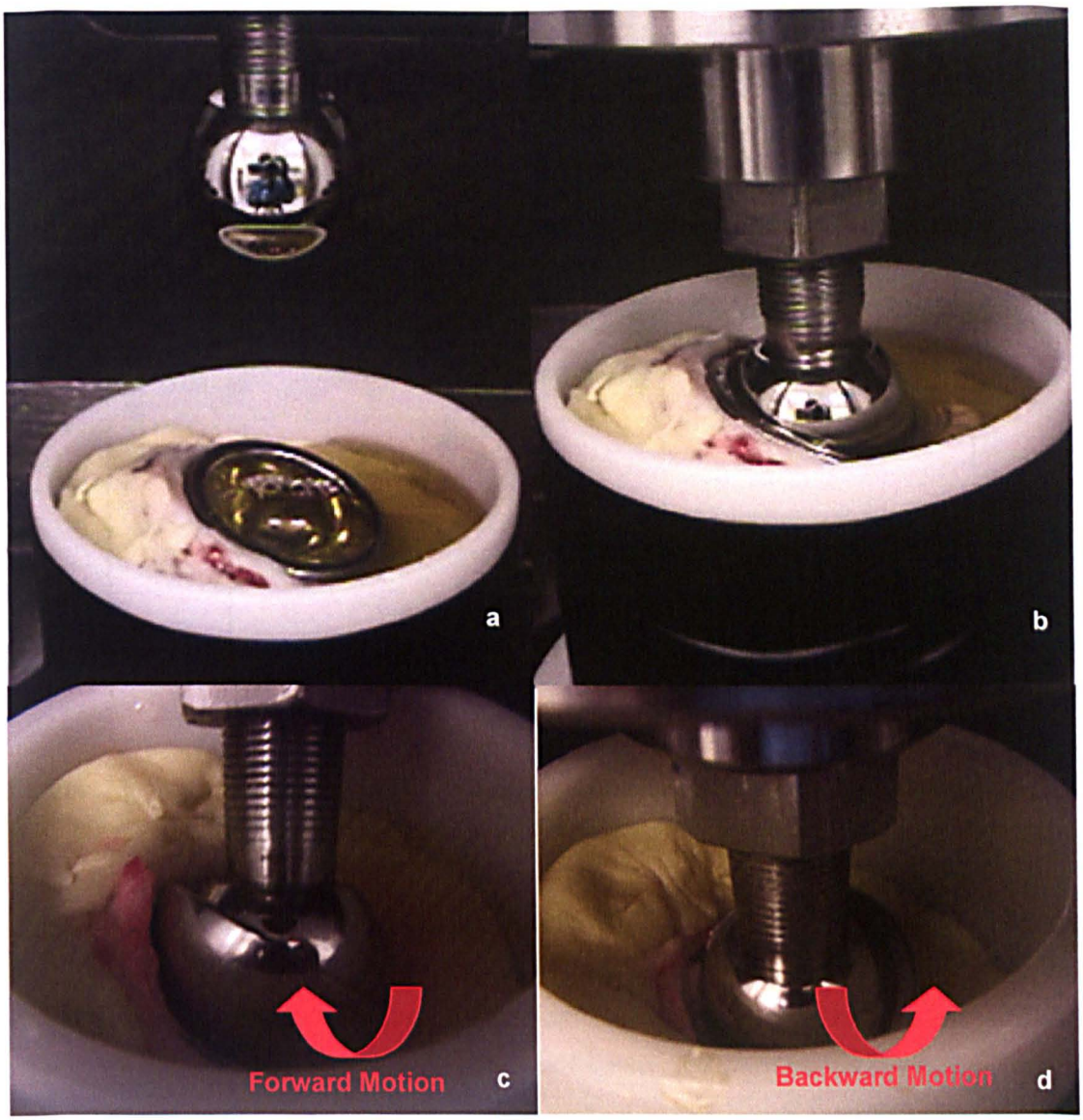

Figure 7.4 A typical motion process of a bipolar prosthesis during dynamic pendulum reciprocation: a. metal cup was positioned inside the porcine acetabulum at 45° in lubricant; b. metal head set inside the metal cup before starting the test; c and d. the cup was pushed forwards / backwards with motion of the head.

7.5.2 Coefficient of Friction on Both Bearing Surfaces

During the friction testing, motion was observed at both bearing surfaces, and following the principles described in Section 7.4; the outer friction torque was speculated to be equal to the inner friction torque. The longest dynamic pendulum reciprocation prior to locking was 22.5 minutes of one specimen, and inner and outer coefficients of friction of this specimen are shown in Figure 7.5.

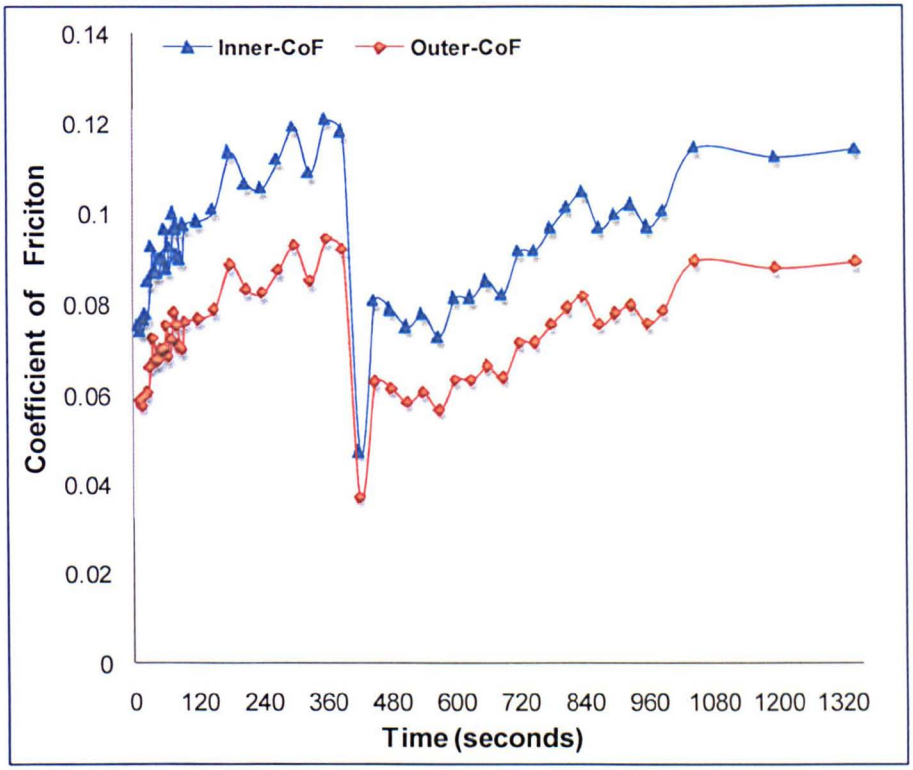

Figure 7.5 Inner and outer coefficients of friction with a bipolar prosthesis in 22.5 minutes dynamic pendulum reciprocation on one porcine acetabulum specimen.

The coefficient of friction at the inner bearing was found to be 1.3 times the outer coefficient of friction at the outer bearing in the same specimen due to the same frictional torque being created at both bearing surfaces (with 14 mm and 18 mm in radiuses). The drop of coefficient of friction at 7 minutes (421 cycles, Figure 7.6) was due to the metal cup becoming locked in the porcine acetabulum for one cycle (as observed on video). After that, the metal cup was released and continued to move forward and backward following the metal head.

The dynamic pendulum reciprocation lasted approximately 6 minutes on average prior to the metal cup becoming locked, hence, the coefficient of friction was recorded and analysed in 360 cycles. The inner and outer coefficients of friction of six specimens (from 0.1 to 0.5 mm) in six minutes dynamic pendulum reciprocation are shown in Figure 7.7, and 7.8.

Both mean coefficients of friction on the inner and outer bearing surfaces increased 20% in the first six minutes of dynamic loading: the coefficient of friction between the metal head and metal cup bearing surface was from 0.08 ± 0.02 to 0.1 ± 0.02, and between the metal cup and the porcine acetabular cartilage bearing surface the coefficient of friction was from 0.07 ± 0.02 to 0.08 ± 0.01 (Figure 7.9). The coefficient of friction on the inner bearing between the metal head and metal cup is 1.29 times of the coefficient of friction on the outer bearing between the metal cup and acetabular cartilage.

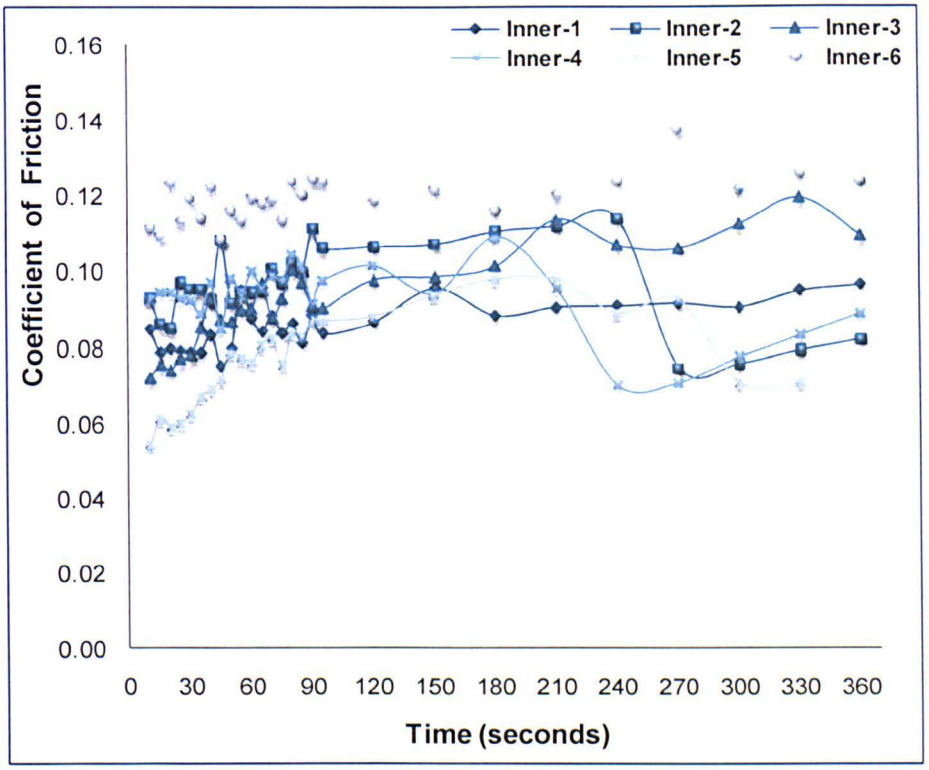

Figure 7.6 Coefficient of friction on the inner surfaces with a bipolar prosthesis in 6 minutes dynamic pendulum reciprocation.

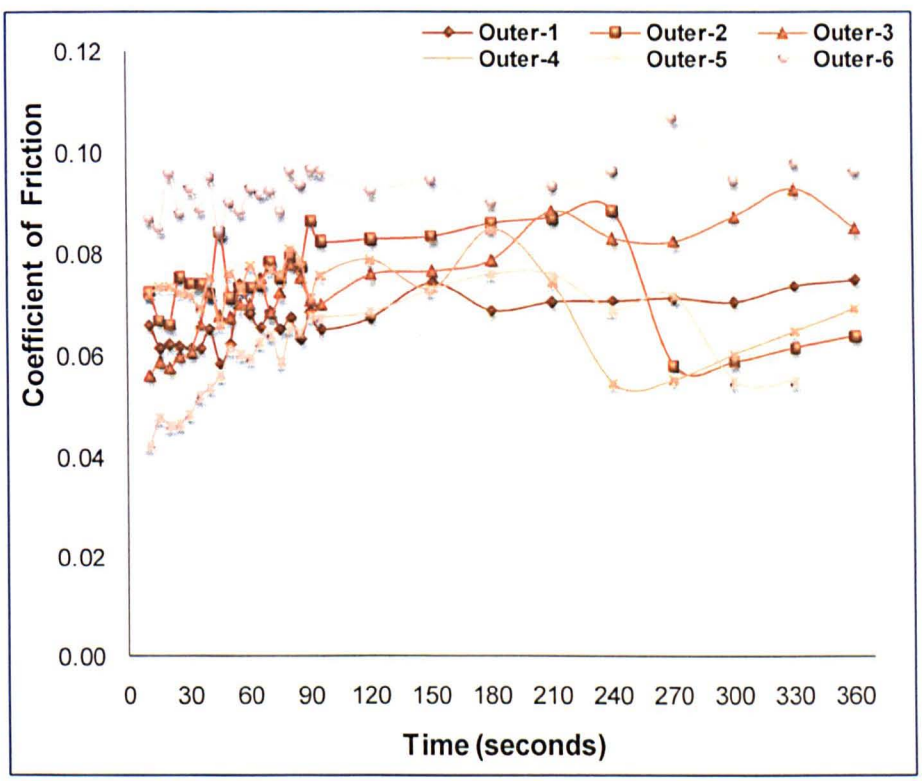

Figure 7.7 Coefficient of friction on the outer surfaces with a bipolar prosthesis in 6 minutes dynamic pendulum reciprocation.

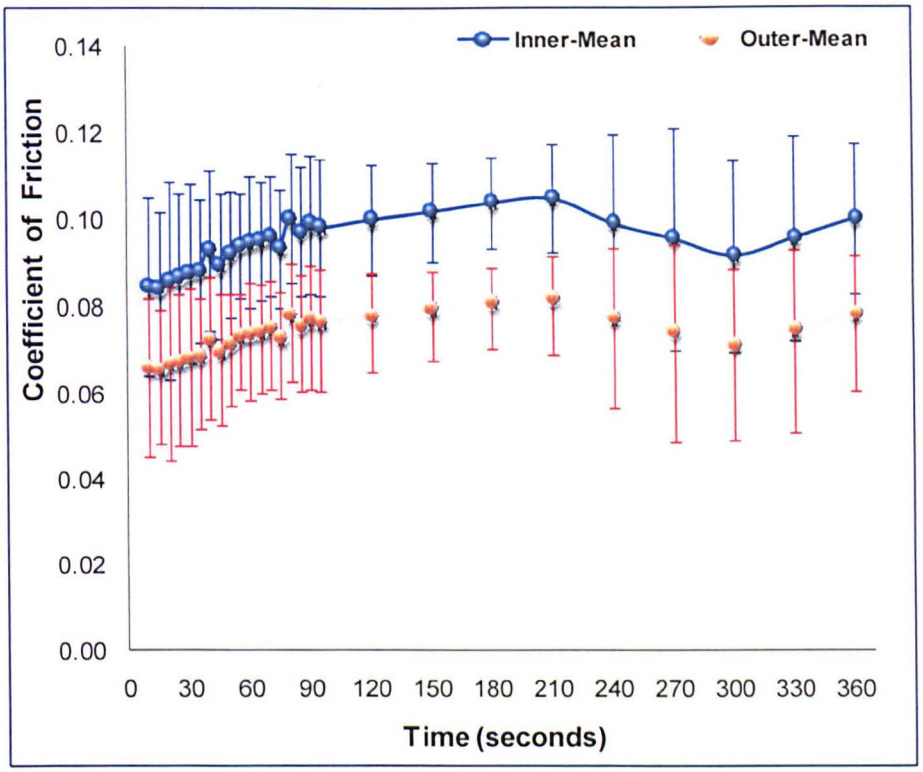

Figure 7.8 Mean coefficients of friction on inner and outer surfaces (± 95% confidence limits, n=6).

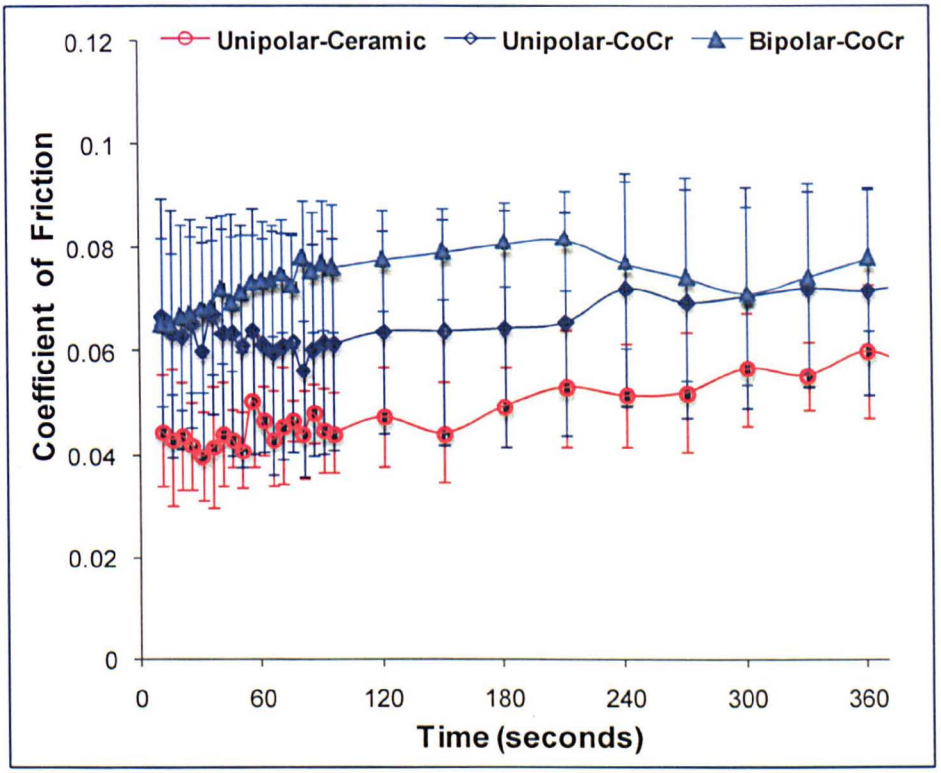

Figure 7.9 Comparison of the mean coefficients of friction between the metal and acetabular cartilage counterfaces in the first 6 minutes among specimens with a unipolar ceramic head, a unipolar cobalt chrome head, and a bipolar cobalt chrome prosthesis, (mean ± 95% confidence limits, n=6).

On the porcine acetabular cartilage surface, the mean outer coefficient of friction in specimens with a bipolar prosthesis is compared with the mean coefficient of friction in specimens with a unipolar cobalt chrome head (Chapter 5) and a unipolar ceramic head (Chapter 6) (Figure 7.9). No significant difference was found between the mean coefficient of friction with a metal unipolar head and a metal bipolar head in six minutes dynamic loading. However, the coefficient of friction was significantly lower in specimens articulated with a unipolar ceramic head compared to in specimens with a bipolar metal prosthesis in the first 4 minutes dynamic pendulum reciprocation.

7.5.3 Cartilage Surface Deformation

No wear scars (wear grade 1~4) were seen on the acetabular cartilage surfaces in five specimens tested in 6 minutes dynamic pendulum loading with the bipolar prosthesis. Cartilage surface deformation was seen in the specimen tested for 22.5 minutes after removing the load, shown in two circled red areas in Figure 7.10. The acetabular cartilage was deformed into two red circled pink areas and damaged in the two blue circled areas.

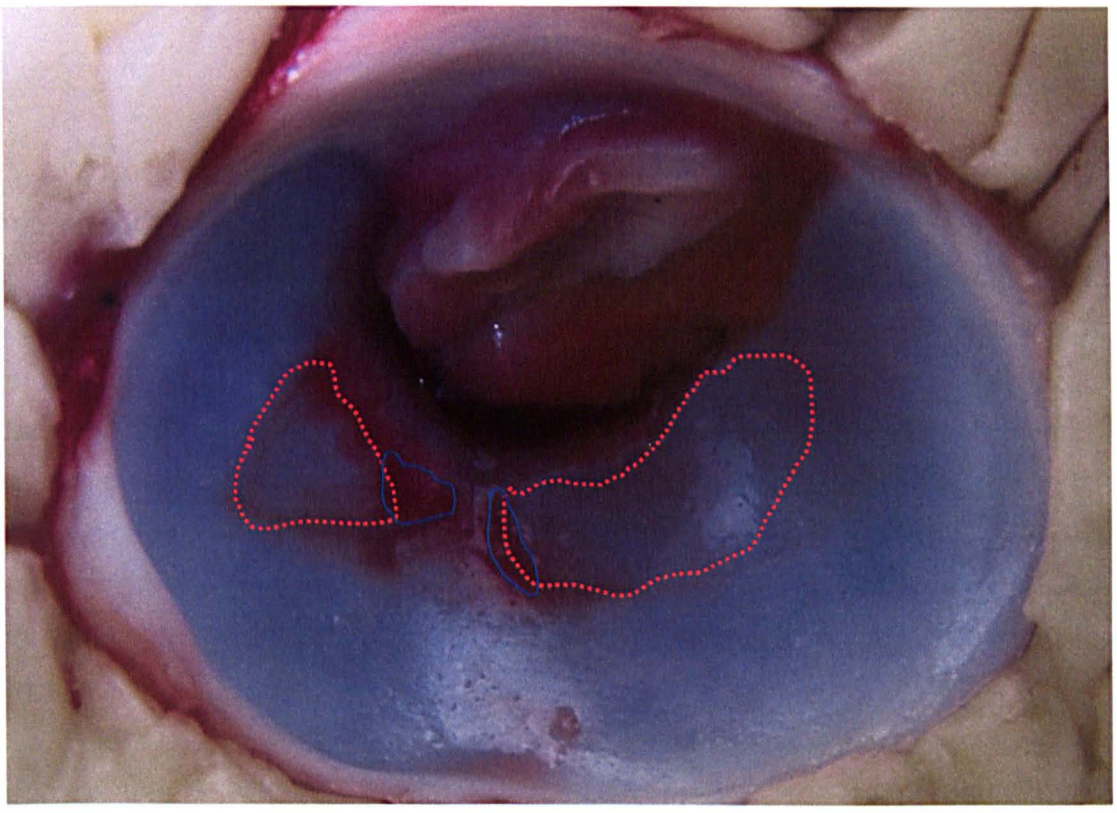

Figure 7.10 Deformation areas (red circled areas) and damaged areas (blue circled areas) of cartilage on the acetabular lunate surface after in 22.5 minutes dynamic loading with a bipolar prosthesis.

7.6 Discussion

7.6.1 Tribological Properties of Bipolar Prosthesis

This design of bipolar endoprosthesis is expected to achieve low-friction metal-on-metal inner bearing motion while decreasing shear stress across the acetabular cartilage, and increase the range of motion. This design provides a greater range of rotation and motion of hip joint movement, and also avoids polyethylene wear, and hence, reduces the likelihood of dislocation and loosening due to osteolysis.

The result of this bipolar hip hemiarthroplasty study is that the motion unexpectedly occurred on both inner and outer bearing surfaces. During the dynamic pendulum reciprocation, similar frictional torques at both the inner and outer surfaces occurred, and the coefficient of friction on the inner surface (metal-on-metal) was 1.3 times of the coefficient of friction on the outer surface (metal-on-cartilage) due to the outer radius of the metal cup being 1.3 times that of the metal head radius when the equal load and the equal friction torque was applied as Equation 7-3.

$$\because \frac{T_I}{T_O} = \frac{f_I \times R_I \times L}{f_O \times R_O \times L} = 1$$

$$\therefore \frac{f_I}{f_O} = \frac{R_O}{R_I} \qquad \textbf{Equation 7-3}$$

Hence, this design of bipolar prosthesis cannot achieve a bearing where most motion occurs at the inner bearing.

Compared to the previous unipolar studies, the coefficient of friction results (Chapter 5) between the metal head and the porcine acetabulum, this novel bipolar prosthesis was shown to demonstrate no advantages when the outer friction between the metal cup on the porcine acetabular cartilage in short period 6 minutes dynamic loading are compared. Furthermore, the outer coefficient of friction in this novel bipolar prosthesis was found to be significantly higher compared to a unipolar ceramic prosthesis in the first 4 minutes of dynamic pendulum reciprocation. Hence, in terms of the coefficient of friction, this bipolar design was not ideal to reduce the friction.

Although no wear scars were observed on the acetabular cartilage surface in approximate 6 minutes dynamic reciprocation, the cartilage surface deformation was more severe when the dynamic loading was applied for approximately 25 minutes. Compared to the deformation of specimens which articulated with a

unipolar head (metal or ceramic), this novel bipolar design may cause more damage of the acetabular cartilage if reciprocation continued for 2 hours. It is concluded that this novel bipolar prosthesis increased the cartilage surface deformation (by visual observation) in over 25 minutes dynamic loading compared to a unipolar prosthesis.

This novel bipolar design has not delivered lower friction or reduced cartilage deformation compared to a unipolar prosthesis in this *in-vitro* study. However, this bipolar prosthesis design may still achieve the expectation of a larger range of motion and function in the hip joint.

7.6.2 Advantages of Bipolar Prosthesis:

To summaries this novel bipolar design provides:

1. This bearing successfully avoided using polyethylene inner bearing, and hence it reduced the risk of osteolysis as no polyethylene wear debris;
2. This bipolar delivered better mechanical function compared to a unipolar prosthesis, by providing a larger range of motion and rotation of the femoral head due to the large femoral head size and the thin metal cup.
3. This bipolar mainly reduced the amount of motion between the outer metal cup sphere and the acetabular cartilage after on average 6 minutes of dynamic loading and motion.
4. When motion mainly occurred in the inner surfaces, low friction, less wearing was expected for metal on metal contacts (Williams *et al.*, 2004; Williams *et al.*, 2006; Brockett, 2007).

7.6.3 Disadvantages of Bipolar Prosthesis:

The disadvantages in this bipolar design were mainly due to the larger range of motion:

1. The cup angle kept changing during the dynamic loading. This may cause more cartilage degeneration, pain, and impingement clinically.
2. The instability of the metal cup as it was only temporarily 'locked' in the acetabula; it may be repositioned following the metal head's movements. This reposition of the metal cup may cause pain in patients clinically.
3. The migration of the cup may also cause dislocation of the metal femoral head in some extreme movements *in-vivo.*

4. No benefit of lower coefficient of friction between the metal cup and cartilage compared to unipolar (metal or ceramic) prosthesis in short-term *in-vitro*.
5. If in the long-term the metal cup would be settled firmly inside the acetabulum and most motion occurs at the inner bearing (metal on metal), the metal wear ion levels may be similar to the metal wear in THR (Williams *et al.*, 2004; Brockett *et al.*, 2008; Ogunwale *et al.*, 2009) of hip resurfacing (Brockett, 2007; Mont *et al.*, 2008; Afolaranmi *et al.*, 2010) in long-term clinically which is of increasing concern.

7.7 Conclusion

The tribological properties study of this bipolar prosthesis was limited due to the failure of free-moving under dynamic pendulum reciprocation in long-term. However, compared to the unipolar prosthesis, this bipolar prosthesis design has not shown any advantages on the acetabular cartilage frictional properties. The findings of this bipolar prosthesis were as follows:

1. Motions occurred at both inner and outer bearing surfaces in the short-term (6 minutes of dynamic reciprocation on average).
2. The metal cup was repositioned by the metal head during the pendulum reciprocation, and it was easily locked or repositioned by the acetabulum.
3. With the same radial clearance in FE direction, the coefficient of friction with this bipolar metal prosthesis was similar to with a unipolar metal prosthesis.
4. With the same radial clearance in FE direction, the coefficient of friction with this bipolar metal prosthesis was higher compared to specimens with a unipolar ceramic head.
5. This bipolar prosthesis design was not a better option on cartilage friction and deformation compared to unipolar prosthesis (metal and ceramic).

Chapter 8 Overall Discussion and Conclusions

Due to the several reasons such as increased life expectancy, patient demands, and social influences, (e.g. alcohol, smoking, medications, obesity, and extreme sports, etc), there is an increase in the population suffering from musculoskeletal conditions. Hence, there are increasing demands for investigations into the efficacy of existing treatments (e.g. hip hemiarthroplasty) to ensure they are used optimally. There is also a desire to design and validate *in-vitro* simulation systems for pre-clinical investigations.

This research has investigated the tribology of hemiarthroplasty, when articular cartilage has articulated against biomaterial (metal or ceramic) counterfaces. The main factors that affect cartilage tribological properties have been examined *in-vitro* in both unconfined plug specimens (bovine articular cartilage plugs) and whole joint confined specimens (entire porcine acetabula). The factors investigated include: contact stress, contact areas, sliding distance and velocity, clearances between the femoral head and the acetabular cartilage, types of loading, different implant materials, and design of prostheses. Cartilage friction, deformation, wear in the unconfined pin-on-plate (PoP) model, cartilage friction, wear, surface damage, deformation in the confined hip joint hemiarthroplasty model have been studied and compared to both the simulation studies *in-vitro* and clinical studies *in-vivo.*

8.1 Cartilage Tribological Properties in a Plug Model

The contact problem between cartilage and metals is very complex when addressed from a bioengineering perspective. The biomechanical and tribological properties of articular cartilage has been investigated over the past 20 years *in-vitro* through pin-on-plate or sphere-on-disk (Lipshitz *et al.*, 1975; Zimmerman *et al.*, 1988; Forster *et al.*, 1995; Forster and Fisher, 1996; Pickard *et al.*, 1998a; Pickard *et al.*, 1998b; Forster and Fisher, 1999; Freeman *et al.*, 2000; Basalo *et al.*, 2004; Krishnan *et al.*, 2004b; Basalo *et al.*, 2005; Basalo *et al.*, 2006; Bell *et al.*, 2006b; Katta *et al.*, 2007b; Northwood and Fisher, 2007; Northwood *et al.*, 2007; Katta *et al.*, 2008b; Katta *et al.*, 2008a), and computer modelling (Armstrong and Mow, 1983; Ateshian *et al.*, 1994; Ateshian *et al.*, 1997; Wu and Herzog, 2000; DiSilvestro and Suh, 2002; Ateshian *et al.*, 2003a; Park *et al.*, 2003; Krishnan *et al.*, 2004a; Krishnan *et al.*, 2005; Pawaskar *et al.*, 2007). More recently some

investigations of articular cartilage have moved to the tribological properties study in the entire joint simulation *in-vitro* and *in-vivo*: the friction and cartilage wear has been reported in a few *in-vitro* studies in hemiarthroplasty model in knee (McCann *et al.*, 2008; McCann *et al.*, 2009), in hip (Müller *et al.*, 2004; Démarteau *et al.*, 2006), in modelling studies (Boschetti *et al.*, 2004; Cilingir *et al.*, 2008). and *in-vivo* studies (Cook *et al.*, 1982; Cruess *et al.*, 1984; McGibbon *et al.*, 1999; van der Meulen *et al.*, 2002; Kyoung Ho *et al.*, 2008). In all cases the measured coefficient of friction was shown to be time-dependent, however, friction and cartilage wear under higher contact stress (over 4 MPa) for longer loading times (over 8 hours) conditions have not been reported.

The study of friction of cartilage against metal counterfaces in these conditions was essential in consideration of hemiarthroplasty applications. The study in Chapter 3 replicated an *in-vitro* hemiarthroplasty condition in order to focus on the mechanical effects on cartilage friction and wear, although it did not consider the compounding effects of biological factors and cartilage degeneration in PBS at 20±2°C. It expanded previous investigations of friction and wear properties of cartilage under low (0.5, 1, and 2 MPa), medium (4, and 8 MPa), and high (12, and 16 MPa) levels of contact stress for longer loading times (over 8 hours) in cartilage-on-metal configurations in consideration of hemiarthroplasty applications. Importantly, this study is the first to quantify such parameters, and so provides a unique understanding of the wear characteristics in a *in-vitro* hemiarthroplasty.

In short-term (one hour) loading, the contact stress affected the coefficient of friction: the coefficient of friction was shown to be time- and load-dependent due to the biphasic properties of articular cartilage. The coefficient of friction increased with time under loading, and different contact stress, it decreased from 0.38 to 0.22 with increasing contact stress from 0,5 to 2 MPa, but remained at 0.35 when contact stress increased from 4 MPa to 16 MPa.

In long-term studies, the comparison of the coefficient of friction and cartilage linear wear, and the coefficient of friction and frictional shear stress with increasing contact stress are shown in Figures 8.1 and 8.2. Both the cartilage linear wear and frictional shear stress increased proportional to the contact stress, but the coefficient of friction showed no significant difference under a range of contact stresses (0.5-8 MPa).

Severe cartilage damage and catastrophic wear occurred, when high levels of contact stresses (≥12 MPa) were reached with over one hour static loading and reciprocation, or when frictional shear stress approached over 4 MPa in long-term static loading and reciprocation.

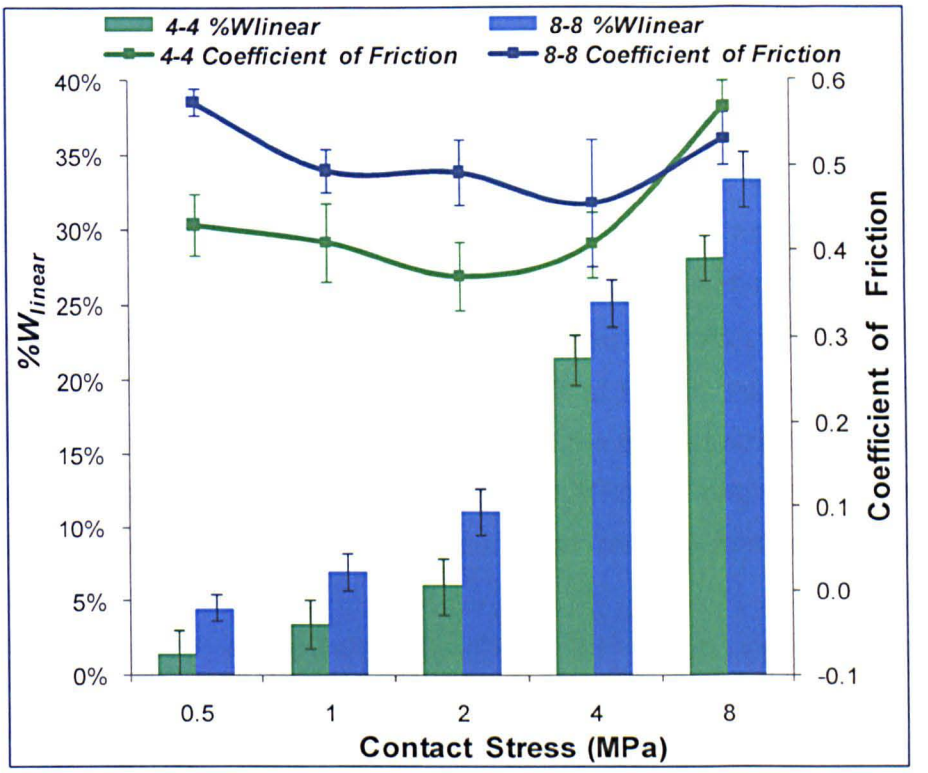

Figure 8.1 Long-term studies in the plug model: coefficient of friction and cartilage % W_{linear} correlates to contact stress under 4-4 and 8-8 conditions.

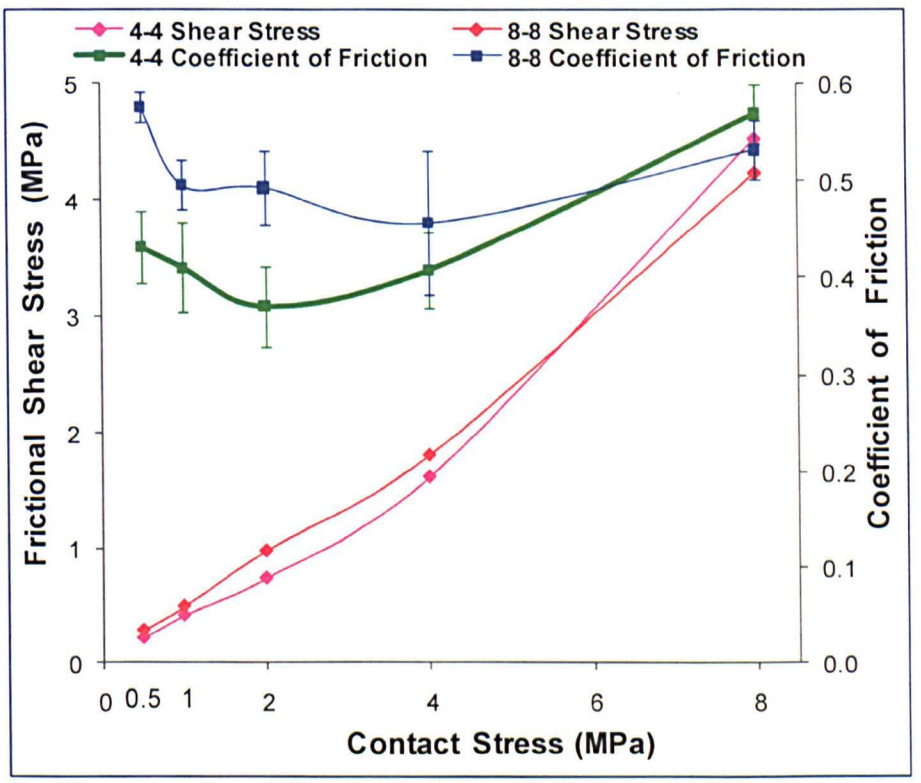

Figure 8.2 Long-term studies in the plug model: coefficient of friction and frictional shear stress correlates to contact stress under 4-4 and 8-8 conditions.

In terms of the effect of contact area on the coefficient of friction under the same contact stress (e.g. 3.5 MPa): in short-term loading, the smaller contact area

increased the coefficient of friction due to the lower aspect radio. However, in long-term loading, there was no significant difference in the coefficient of friction due to the load supported by the cartilage fluid phase being completely transferred to the solid and fluid phase in equilibrium support of the cartilage. It is concluded that under the same contact stress (≤4 MPa), the coefficient of friction with a smaller contact area is higher compared to the larger contact area in short-term loading due to the lower aspect ratio, but in long-term loading, the different contact areas do not cause any significant difference in the coefficient of friction. However, the contact area effects on the friction may be different when the contact stress is higher than 4 MPa due to the cartilage severe damage (8 MPa in long-term loading) and catastrophic wear (12 and 16 MPa in short-term loading) that were observed at higher contact stresses.

Sliding distance and velocity only affects the friction coefficient under low contact stress (0.5 to 2 MPa), and this finding was similar to the recently reported studies which have shown how that a shorter stroke length increased friction and due to the decreased fluid film (Bell *et al.*, 2006a; Caligaris and Ateshian, 2008). However, cartilage linear wear increased significantly with sliding distance and sliding velocity under the same contact stresses after long-term (24 hours) constant loading due to the longer friction distance causing more material loss.

8.2 Cartilage Tribological Properties in a Joint Model

Studies using a joint hemiarthroplasty model of the entire porcine acetabulum have enhanced the understanding of the tribological characteristics of articular cartilage under different contact stresses due to varying clearances in this model. Tribological properties in this simulation were compared to other hemiarthroplasty experimental and clinical hemiarthroplasty studies *in-vitro* and *in-vivo.*

Chapters 4 and 5 considered the tribological properties of articular cartilage that were studied in a joint model of hemiarthroplasty in an entire hip joint *in-vitro* with pendulum motion under both constant and dynamic loading with different levels of clearances. With increasing clearance, the contact area decreased, and both average contact stress and peak contact stress increased under both constant and dynamic loading.

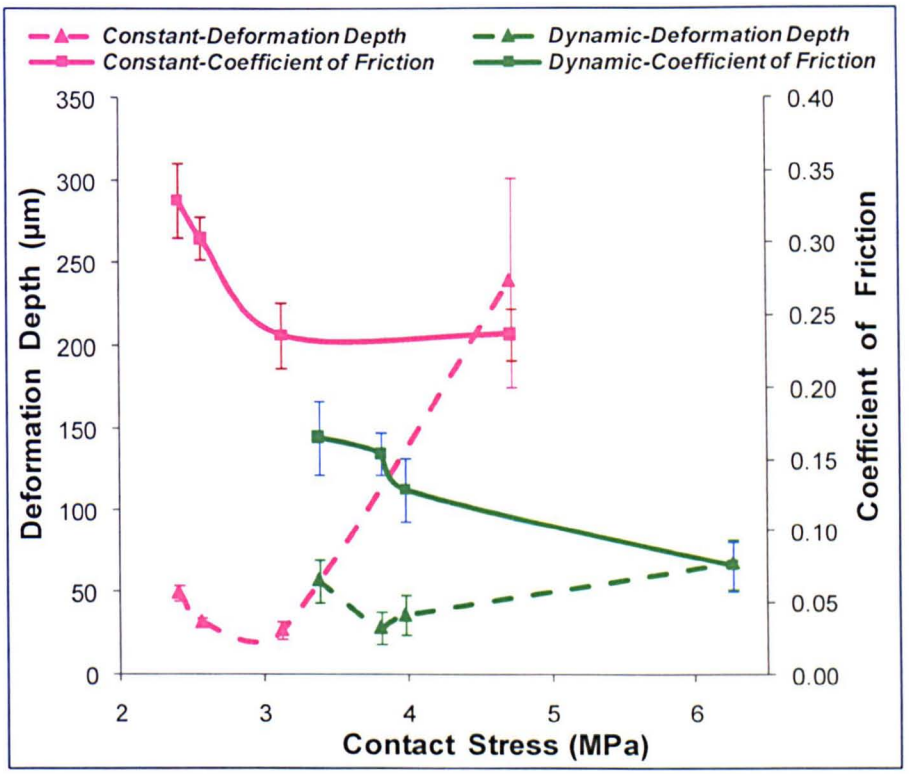

Figure 8.3 Short-term (2 hours) studies in the joint hemiarthroplasty model: coefficient of friction and cartilage deformation depth correlates to contact stress under constant loading (C) or dynamic loading (D).

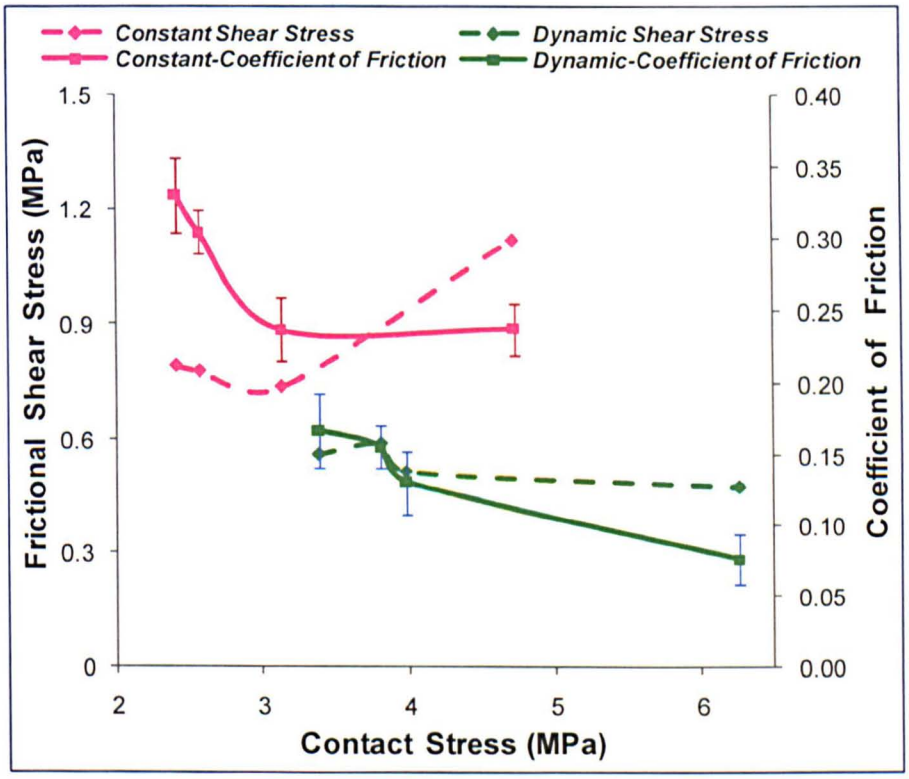

Figure 8.4 Short-term (2 hours) studies in the joint hemiarthroplasty model: coefficient of friction and frictional shear stress correlates to contact stress under constant loading (C) or dynamic loading (D).

Good correlations of contact area ($R_{constant}^2$=0.63, $R_{dynamic}^2$=0.73), contact stress (average: $R_{constant}^2$=0.73, $R_{dynamic}^2$=0.73; and peak: $R_{constant}^2$=0.75 $R_{dynamic}^2$=0.77), with the clearance were observed. Hence, clearance, contact area, and contact stress can be considered simultaneously and this relationship to cartilage deformation and the coefficient of friction, and frictional shear stress and coefficient of friction which are shown in Figures 8.3 and 8.4 respectively. The conclusions are:

1. A trend of decreasing coefficient of friction with increasing contact stress under both constant and dynamic loading conditions was observed (Figure 8.3). Significantly lower coefficients of friction were observed under dynamic loading compared to under constant loading when similar range of contact stress was applied due to a greater proportion of load being carried by the fluid phase under dynamic loading.
2. After 2 hours of pendulum reciprocation, the deformation depth increased significantly when the contact stress increased to a certain level under either constant (>4.7 MPa) or dynamic (>6.3 MPa) loading cycles (Figure 8.3).
3. The frictional shear stress increased with the decreasing coefficient of friction under constant loading (Figure 8.4), but it decreased with the decreasing coefficient of friction under dynamic loading (Figure 8.4). Some evidence has shown that when the frictional shear stress limit of the cartilage was exceeded (above the critical threshold) under constant loading, severe damage / degradation of the acetabular cartilage occurred.
4. Metallic heads and porcine acetabula with contact stress level at 3.98 MPa (in a range of 1.2-1.8mm radial clearances) *in-vitro* showed lower deformation depth 37μm, deformation volume 2.99 mm^3, and lower coefficient of friction 0.13 compared to other contact stress levels, and this range of clearance is possibly recommended for clinical practice.

The counterface material was another key factor which affected the cartilage tribological properties, and was investigated in Chapter 6. Compared to metallic femoral heads, ceramic femoral heads caused significantly lower increases in cartilage surface roughness, less cartilage wear, lower cartilage wear grade levels, and less acetabular cartilage surface deformation when articulated against acetabular cartilage. However, there was no significant difference in the coefficient of friction with ceramic material heads compared to metal heads when articulating against the acetabular cartilage with the same clearance. This finding is consistent with the limited clinical follow-up studies conducted (Dawihl *et al.*, 1979; Knahr *et*

al., 1981; Yoshinaga, 1987; Trabelsi *et al.*, 1989). This is also similar to the comparison studies *in-vitro* reported by Müller *et al.* (2004) which compared human and porcine acetabular cartilage friction when articulating against ceramic or cobalt chrome alloy femoral heads. Hence, ceramic material demonstrated some advantages and may be recommended as the first choice of femoral head material in hip hemiarthroplasty due to less acetabular cartilage degeneration reported clinically. This result is possibly due to the better wettability of ceramic compared with cobalt chrome (Dawihl *et al.*, 1979; Dawihl and Dörre, 1980; Maistrelli *et al.*, 1991; Willmann, 1993; Motta *et al.*, 2004).

Over the last 30 years, indications for using a bipolar component have broadened (Calton *et al.*, 1998) and compared to unipolar prosthesis, superior long-term results of bipolar hemiarthroplasty have been reported in many clinical studies. This includes reduced friction (Bhuller, 1982); increased pain relief, early mobilisation and restoration of function (Lestrange, 1990; Malhotra *et al.*, 1995). This was possibly due to the delayed acetabular wear because the motions are decoupled by the bipolar prosthesis (Gaine *et al.*, 2000b). Therefore, a novel design of bipolar prosthesis which included a thin metal shell with a metal head was examined in chapter 7. However, this novel bipolar prosthesis did not succeed due to the failure of the free-moving cup under dynamic pendulum reciprocation. The metal cup was repositioned by the metal head during the pendulum reciprocation, and it was then locked in an inappropriate position in the acetabulum. With the same radial clearance, the coefficient of friction with this bipolar metal prosthesis was similar to with a unipolar metal prosthesis and higher compared to specimens with a unipolar ceramic head in the first 6 minutes dynamic loading.

8.3 Differences *in-vitro* and *in-vivo*

Cartilage tribological properties *in-vitro* studies have demonstrated to be affected by the mechanical factors (such as contact stress, contact area, the geometry of articulating surfaces, materials, and sliding speed), biological factors (such as matrix changes), chemical factors (such as temperature, lubricant), and other time-dependent factors may influence the cartilage tribological properties.

However, the exact physiological circumstances are very difficult to obtain with simulators *in-vitro* due to the effects of different variables (e.g. lack of soft tissue around the joint, dynamic biological processes, clinical techniques, the medication of patients, soft tissue biological response and environment, the diet and life style of the patients, etc) *in-vivo* cannot be displayed. Hence, the cartilage

tribological properties *in-vivo* need to be considered both the test results in mimicked *in-vitro* conditions and the influences of the different variables (i.e. the level of activity of the patients and the aging of materials, surrounding tissues supporting, and the biological environment in the body, etc) *in-vivo* conditions. These differences of variables *in-vivo* and *in-vitro* may sometimes cause the different results which may lead to different conclusion and resolution.

However, for most studies in *in-vitro* and *in-vivo* which have investigated in similar conditions, the results are consistent. The author believes that the results concerning the performance of different contact stress, contact area, sliding distance and velocity, contact surface geometry, implant clearance, loading type, contact materials, prosthesis design, articulating against cartilage must be evaluated as the essential key factors that affect the cartilage tribological properties in hemiarthroplasty. Hence, the findings in this study are valuable for both the clinical practice and the development of hip hemiarthroplasty from the mechanical and tribological point of view.

8.4 Discussion

8.4.1 Key Methods in Hemiarthroplasty Tribology Study

The essential model of hemiarthroplasty tribology study was in the whole hip joint confined model in pendulum articulation simulation, which was based on the extended understanding and foundation examination of articular cartilage on the simple geometry pin-on-plate unconfined model.

A study of the tribology of hemiarthroplasty has been conducted, and examined such as coefficient of friction, cartilage deformation and wear volume/depth. The principal novel methodologies in this study were: 1) the calculation of the coefficient of friction under dynamic loading, 2) the wear grade assessment and acetabula measurement techniques and 3) the developed statistical analysis of cartilage surface deformation and wear. In the future the methods of calculation on wear grade areas may be improved using some software which can pick up colour automatically (e.g. MatLab 7.8 (Mathworks, Natick, USA), Stradwin 4.0 (Stradwin, Cambridge, UK) instead of Image Pro plus which needs highlighting the areas manually.

Cartilage surface roughness was found to be somewhat insensitive to test conditions. Contact stress, contact area, and cartilage wear grades were examined through FUJI Pressure film, but critically speaking, due to the sensitivity and flat

texture of the FUJI film which limited its measurements on the curved acetabular counterfaces, this area would benefit from the development of a new measurement method in the future.

For the study hip hemiarthroplasty *in-vitro*, friction, cartilage deformation and wear are considered essential parameters to examine, and contact stress, contact area, and wear grade areas may provide compatible information when more developed methods are used.

8.4.2 Clinical Implications

For patients who have a hip hemiarthroplasty, it is recommended to avoid high contact stress and long static loading time due to the cartilage severe damage and wear which has been demonstrated in both the unconfined model (observed as the as 'mushroom effect') and confined model (seen as 'delaminated or broken or severe wear' cartilage). The radial clearance between the metal head and the natural acetabulum FE direction has been demonstrated to have a significant effect on the tribological properties in hip hemiarthroplasty, and it is suggested that the FE direction dimension of the acetabulum be measured when selecting a suitable femoral head size – a radial clearance of 1.2-1.8 mm is recommended from the in vitro studies undertaken. For unipolar hip hemiarthroplasty, ceramic heads have better wettability and hardness (and are therefore more resistant to third body damage) compared to CoCr heads and should therefore be considered favourably.

8.4.3 Future Work

In the future, the hemiarthroplasty tribological studies could be developed to further investigate ceramic materials and different bipolar design in long-term (e.g. 8 hours, 24 hours, 3 days, etc) in-vitro, deformation, wear, surface changes can be examined based using the developed hemiarthroplasty system. Better wear resistance and reduced surface roughness are believed to be possible with ceramic femoral head compared to metal heads. In further tests of unipolar hemiarthroplasty head roughness measurements should be also be completed.

Although the particular design of bipolar in this study (Chapter 7) has shown poor stability, locking, and no significant difference of friction in short-term (6 minutes), most clinical reports have shown that bipolar hemiarthroplasty presents better clinical results (e.g. wider motion range, better stability, longevity, and less impingements) compared to unipolar devices(Vǎzquez-Vela and Vǎzquez-Vela, 1990; Vazquez-Vela *et al.*, 1990; Marcus *et al.*, 1992; Gaine *et al.*, 2000a; Ong *et al.*, 2002; Cantu, 2004; Bhattacharyya and Koval, 2009). Due to the cartilage wear

and the developed techniques in hip replacements, unipolar hemiarthroplasty is no longer used in the United States. The advantages of bipolar designs are due to the double (triple) bearing surfaces which increase the hip functional activities, reduce the friction and wear of acetabular cartilage, and prolong the duration of implants. Hence, further cartilage tribological studies *in-vitro* on different designs of bipolar and tripolar hemiarthroplasty could be important to clinical practice.

This simulation system and developed methodology used in this study can also be expanded in the future to include tribological studies of the natural hip (ie femoral head cartilage articulating against acetabular cartilage) to consider ostechrondral replacements and minimally invasive interventions.

8.5 Conclusions

1. In both plug and joint hemiarthroplasty models, the cartilage coefficient of friction has time-dependent property in short-term (2 hours) static loading due to the biphasic supporting phases of cartilage. The coefficient of friction is shown an inverse proportional correlation to the contact stress: in a range of 0.5 to 4 MPa in the plug model; and 2.4–4.7 MPa under constant loading, 3.4-6.3 MPa under dynamic loading in the joint model.
2. In the plug model, the coefficient of friction remains after the cartilage fluid phase support is fully transferred into the equilibrium state of solid and fluid phase support of the loading from 2-24 hours' constant loading in the plug model with a less than 8 MPa contact stress.
3. The frictional shear stress is proportional to the contact stress in the plug model, when it is over 4 MPa with over one hour loading, catastrophic wear of cartilage occurs; in the joint model under constant loading due to the geometry characterises of the specimen, the cartilage is broken and delaminated when the frictional shear stress reaches 1.2 MPa.
4. The cartilage deformation is shown proportional to the contact stress in the plug model, but in the joint model it increases only when contact stress reaches a certain level (3 MPa under constant loading, and 4 MPa under dynamic loading).
5. In the joint model dynamic loading leads to lower friction and less deformation compared to constant loading due to the rehydration of cartilage in the loading area when the peak load is removed.

6. Ceramic (Biolox Delta) material is a superior material for femoral head in hip unipolar hemiarthroplasty due to the reduced surface roughness, and deformation of cartilage may caused by the better wettability of the material compared to metallic materials, although the friction is not shown significant difference in 6 minutes testing.

7. The novel design of bipolar prosthesis with larger metal head and thin metal cup failed due to the 'locking' of the metal cup giving poor stability.

Appendices

Appendix-1. Mechanical drawings of the porcine acetabulum setting device designs

Cup holder

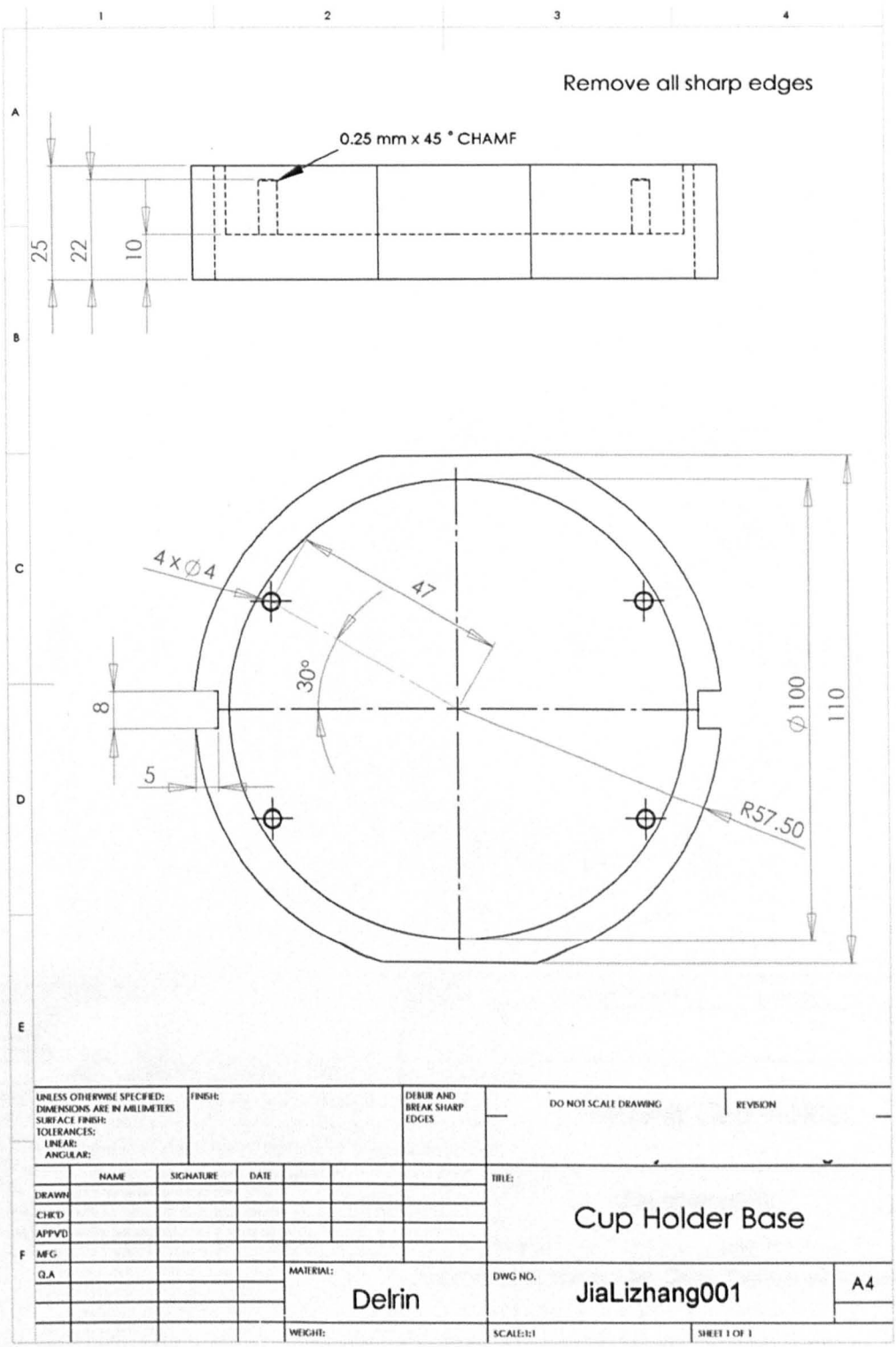

Technical assistant from Mr. Simon Taylor is acknowledged

Porcine cup holder

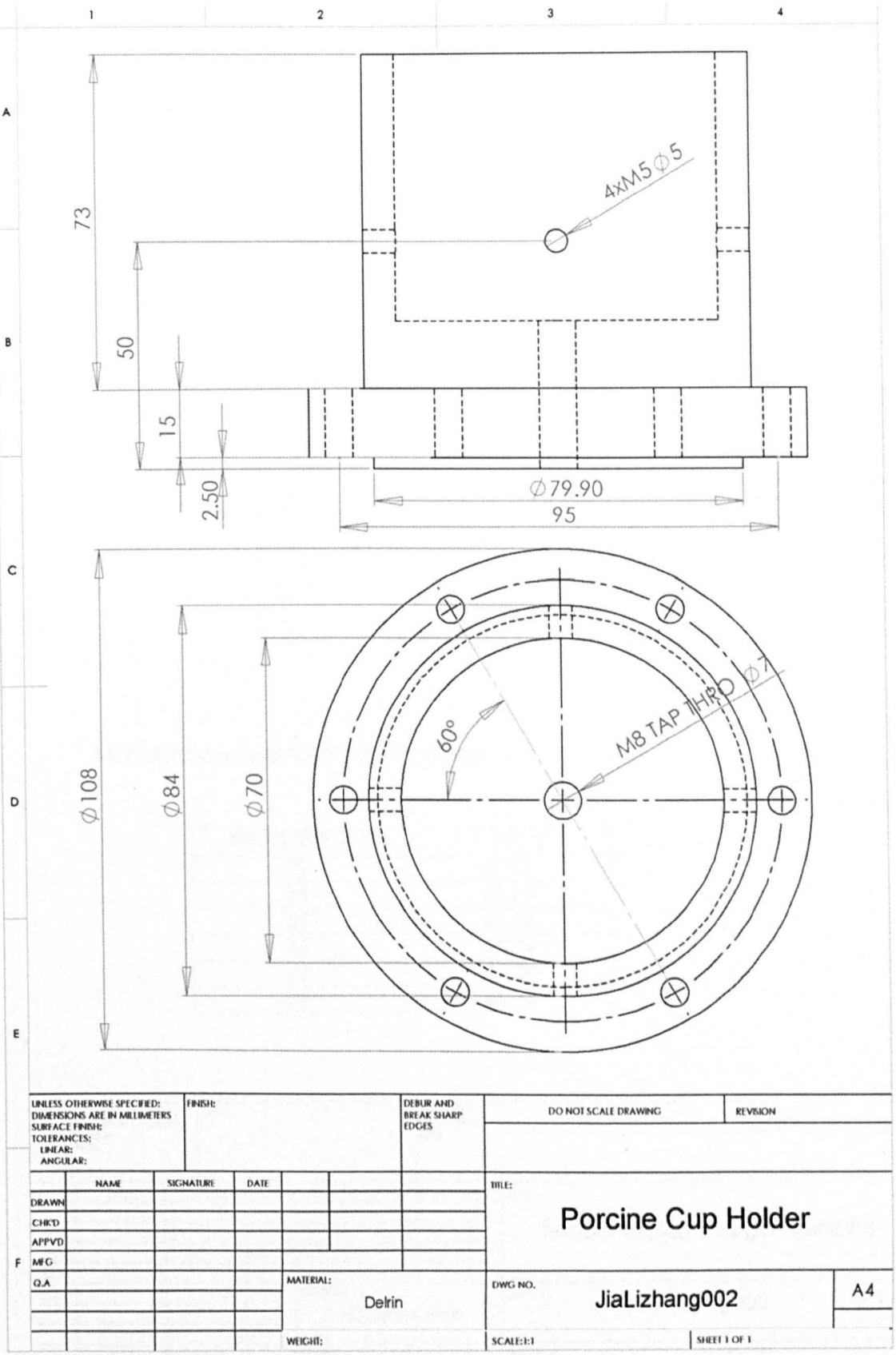

Technical assistant from Mr. Simon Taylor is acknowledged

Metal head height blocks

Remove all sharp edges

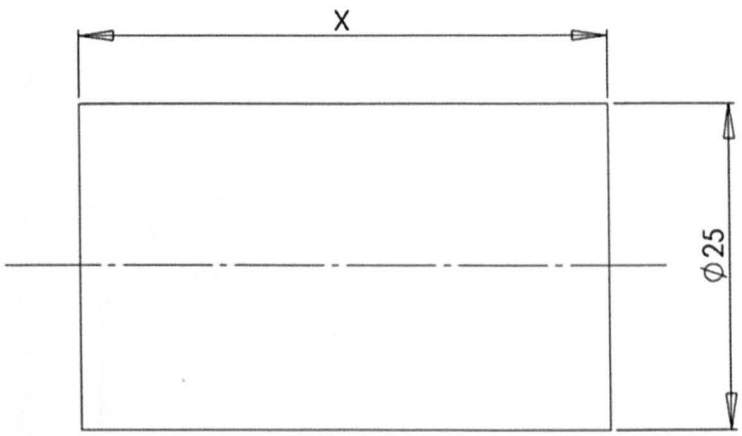

Manufacture one for each head size

Head Size (mm)	X (mm)
32	47.74
34	48.74
35	48.24
36	47.74
37	47.24
38	46.74

UNLESS OTHERWISE SPECIFIED: DIMENSIONS ARE IN MILLIMETERS SURFACE FINISH: TOLERANCES: LINEAR: ANGULAR:		FINISH:			DEBUR AND BREAK SHARP EDGES	DO NOT SCALE DRAWING	REVISION
	NAME	SIGNATURE	DATE			TITLE: Metal Head Height Blocks	
DRAWN							
CHK'D							
APP'VD							
MFG							
Q.A				MATERIAL: 303 Stainless Steel		DWG NO. JiaLizhang003	A4
				WEIGHT:		SCALE:1:1	SHEET 1 OF 1

Technical assistant from Mr. Simon Taylor is acknowledged

Metal head position arm

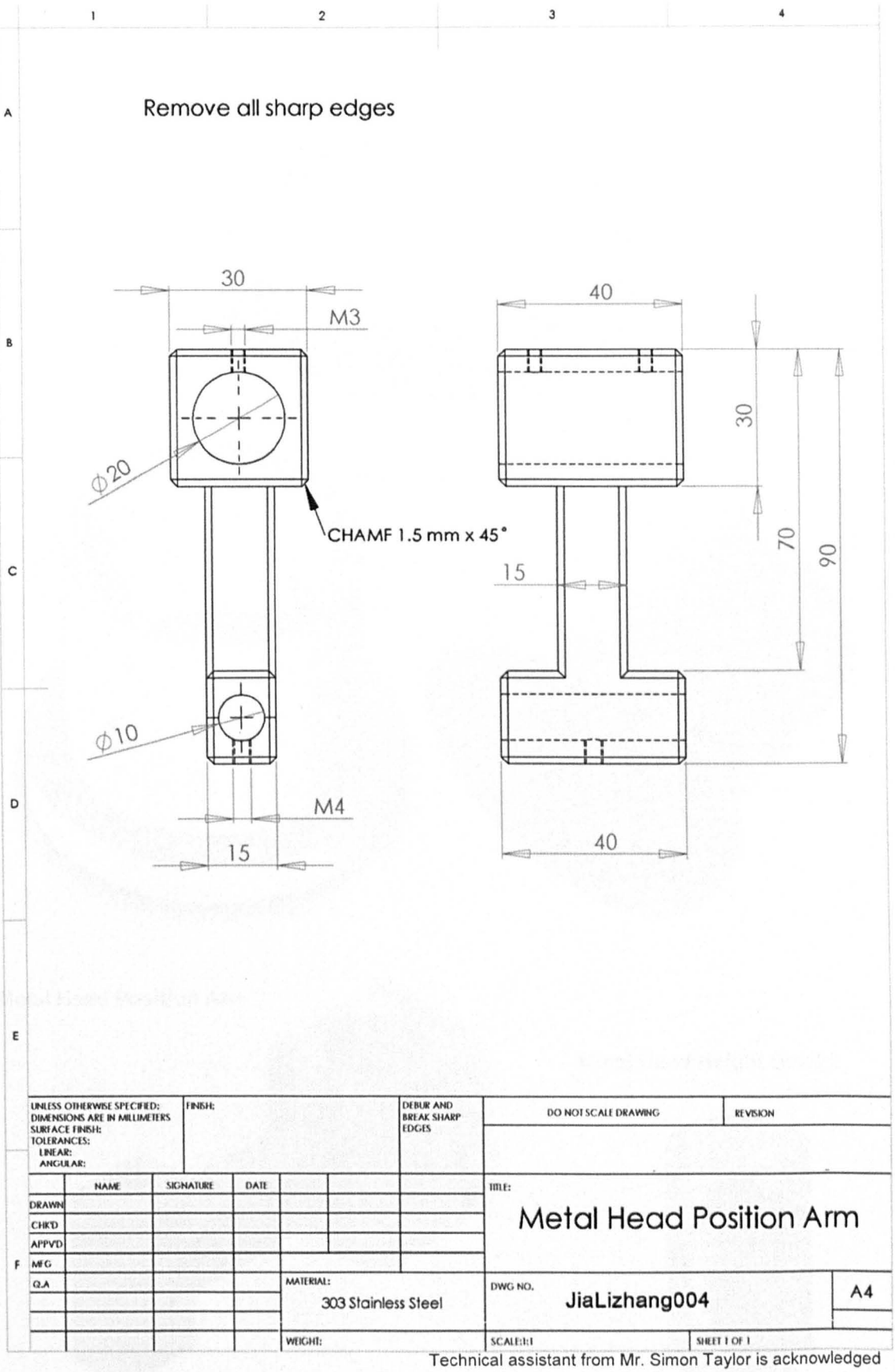

Technical assistant from Mr. Simon Taylor is acknowledged

3D images of porcine setting devices

Cup holder base

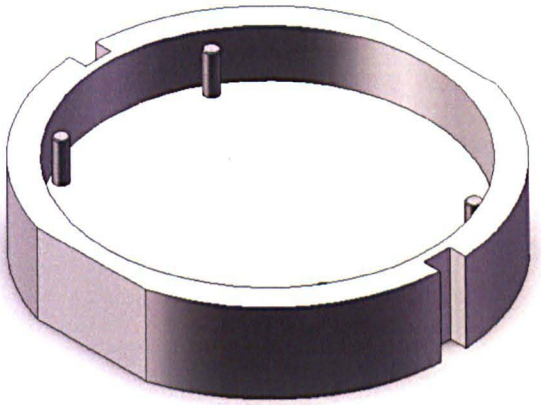

Porcine cup holder

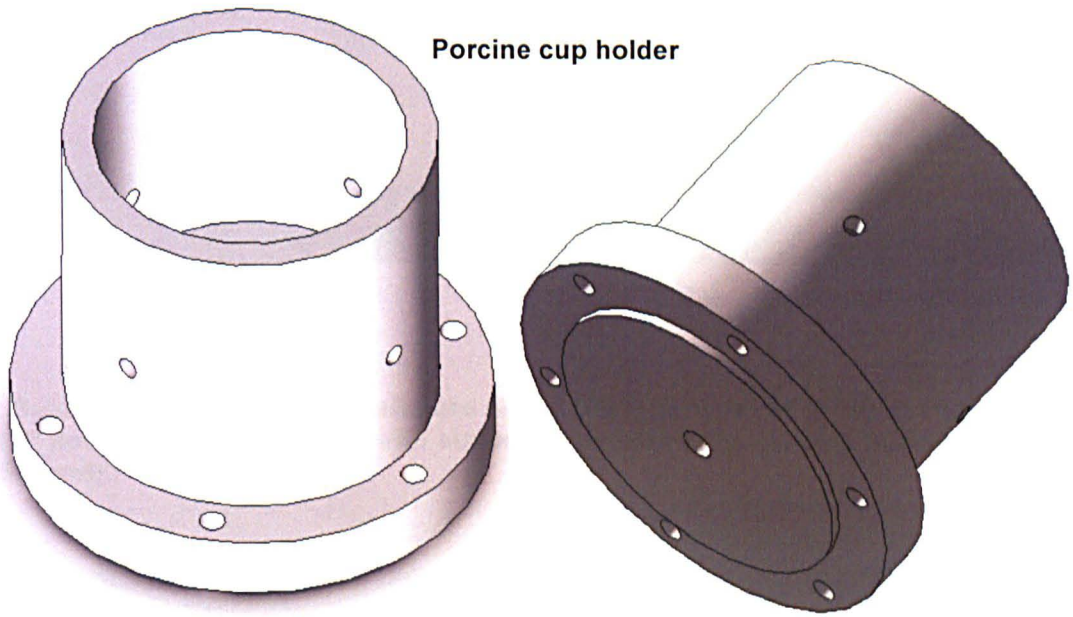

Metal Head Position Arm

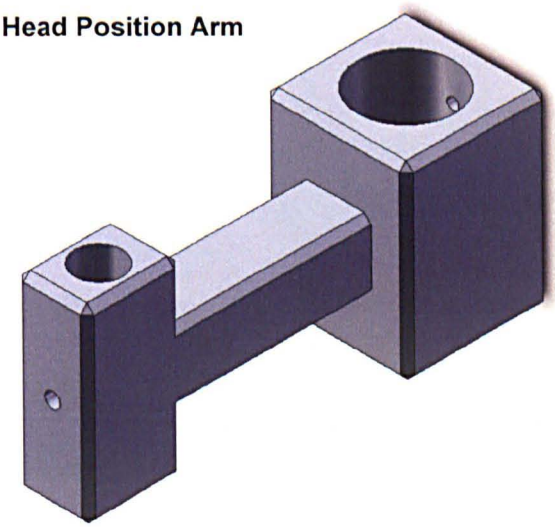

Metal Head Height Blocks

Appendix-2. Images of FUJI pressure film measurements of contact area and contact stress

1. Specimens with small clearances under 400 N (left) or 800 N (right) static loading at 0° position for 30 seconds, with super-low pressure film (upper), and low pressure film (n=6).

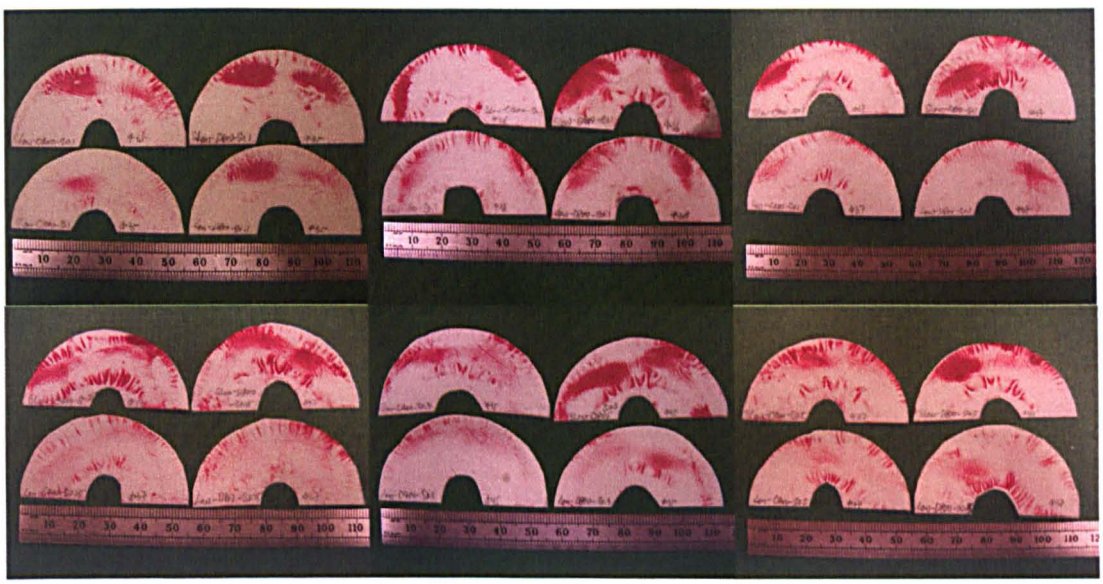

2. Specimens with medium clearances under 400 N (left) or 800 N (right) static loading at 0° position for 30 seconds, with super-low pressure film (upper), and low pressure film (n=6).

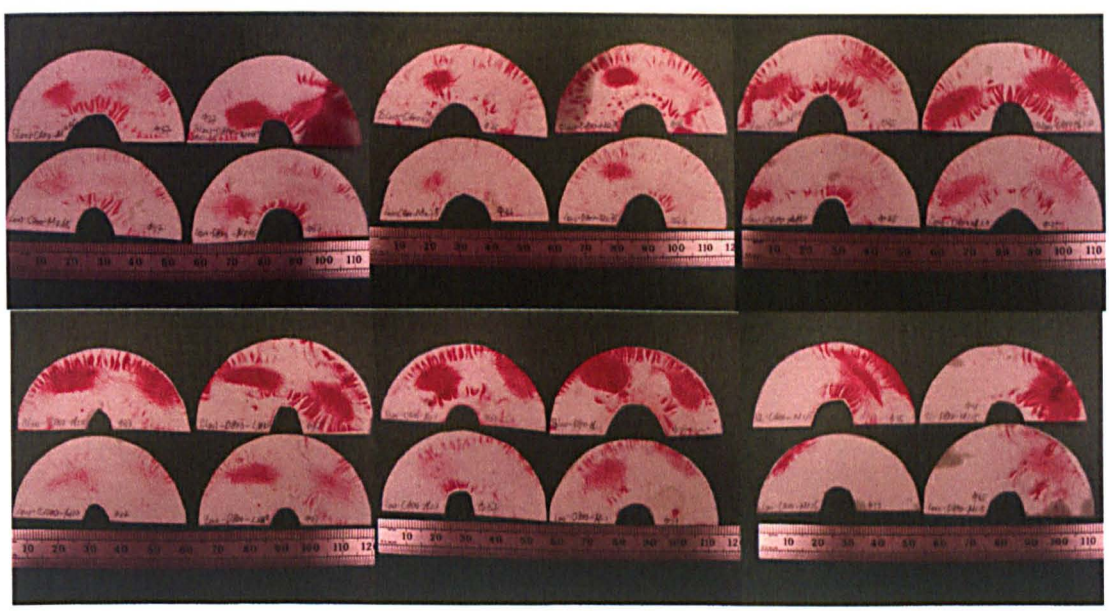

3. Specimens with large clearances under 400 N (left) or 800 N (right) static loading at 0° position for 30 seconds, with super-low pressure film (upper), and low pressure film (n=6).

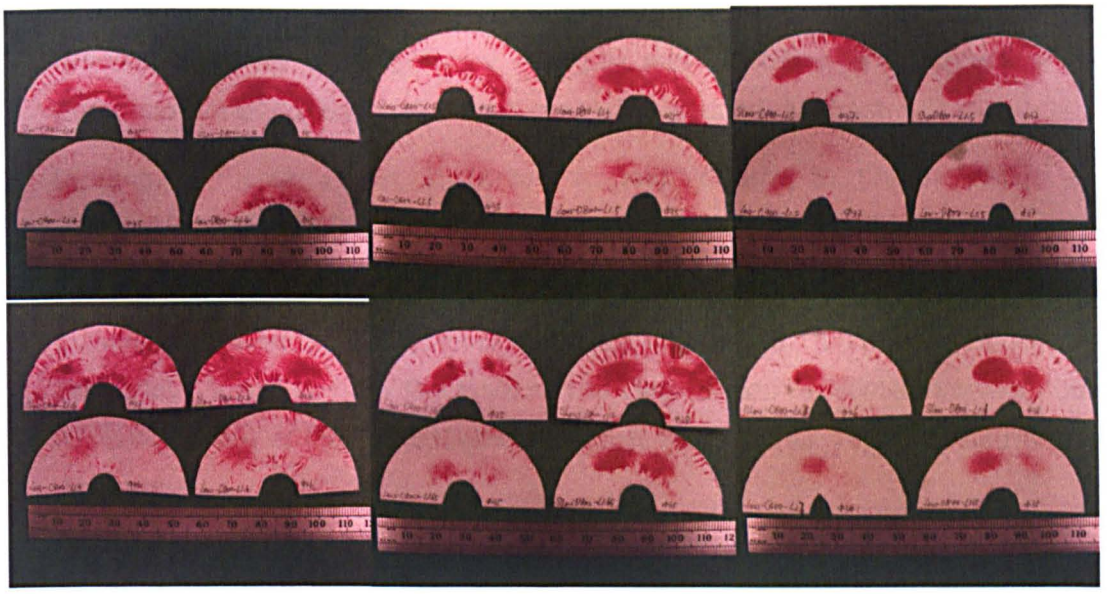

4. Specimens with extra large clearances under 400 N (left) or 800 N (right) static loading at 0° position for 30 seconds, with super-low pressure film (upper), and low pressure film (n=6).

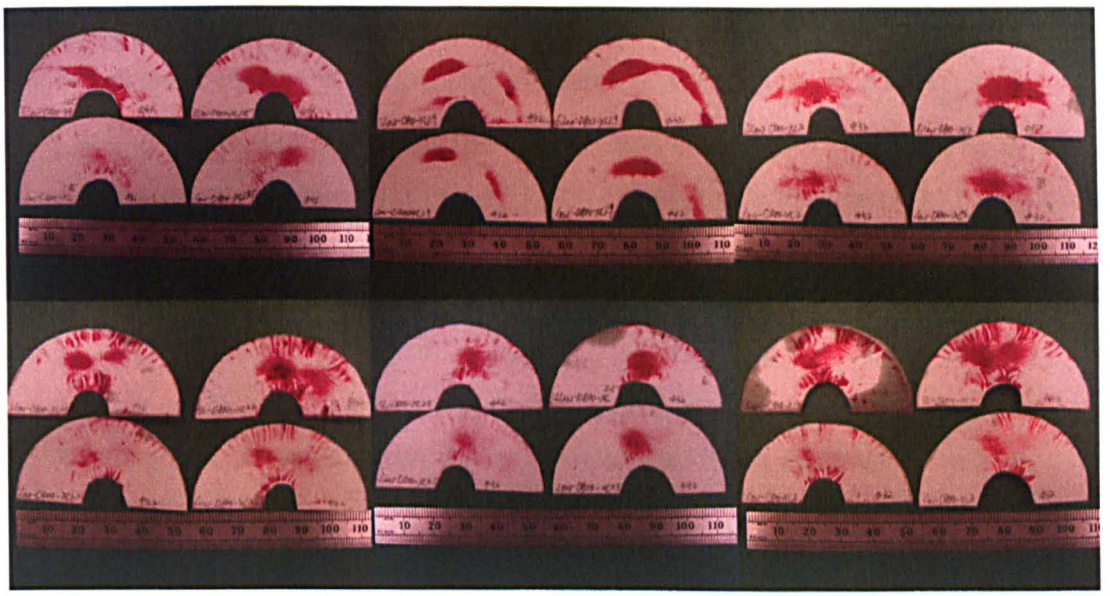

Appendix-3. Publication List

1. Lizhang, J., Fisher, J., Jin, Z., Burton, A., and Williams, S., (2008) *Friction of Articular Cartilage under Different Pressure and Velocities* 16th congress of the European Society of Biomechanics, Luzern, Switzerland, Abstract.
2. Lizhang, J., Fisher, J., Jin, Z., Burton, A., and Williams, S., (2008) *Friction and Wear of Biomaterial Head against Cartilage Hip Acetabulum* 5th China International Symposium on Tribology, Beijing, China, Abstract.
3. Lizhang, J., Fisher, J., Jin, Z., Burton, A., and Williams, S., (2009) *The Influence of Frictional Shear Stress to the Friction and Degradation of Hemiarthroplasty* 55th Annual Meeting of the Orthopaedic Research Society, Las Vegas, United States, Abstract.
4. Lizhang, J., Fisher, J., Jin, Z., Burton, A., and Williams, S., (2009) *Friction and Wear of Hip Hemiarthroplasty under Constant Load* 8th World Congress of the International Cartilage Repair Society, Miami, United States, Abstract.
5. Lizhang, J., Fisher, J., Jin, Z., Burton, A., and Williams, S., (2009) *How does Clearance and Wear Affect Acetabular Cartilage Friction in Hip Hemiarthroplasty* Annual Meeting British Orthopaedic Research Society, Newcastle, United Kingdom, Abstract.
6. Lizhang, J., Fisher, J., Jin, Z., Burton, A., and Williams, S., (2010) *The effect of contact stress on cartilage friction deformation and wear* 56th Annual Meeting of the Orthopaedic Research Society, New Orleans, United States, Abstract.
7. Lizhang, J., Fisher, J., Jin, Z., Burton, A., and Williams, S., (2010) *The effect of clearance on cartilage friction and wear in hip hemiarthroplasty* 11th European Federation of National Associations of Orthopaedics and Traumatology Congress, Mildred, Spain, Abstract.
8. Lizhang, J., Fisher, J., Jin, Z., Burton, A., and Williams, S., (2010) *The effect of contact stress on cartilage friction deformation and wear* 9th World Congress of the International Cartilage Repair Society, Barcelona, Spain, Abstract.
9. Lizhang, J., Fisher, J., Jin, Z., Burton, A., and Williams, S., (2010) *The biotribology of hip hemiarthroplasty* 6th World Congress on Biomechanics, Singapore, Abstract.
10. Lizhang, J., Fisher, J., Jin, Z., Burton, A., and Williams, S., (2010) *The effect of contact stress on cartilage friction deformation and wear* Journal of Engineering in Medicine, paper, (In press).

1. 16th congress of the European Society of Biomechanics, Luzern, Switzerland, Jul, 2008. Abstracts – presented as a 15 minutes oral presentation.

FRICTION OF ARTICULAR CARTILAGE UNDER DIFFERENT PRESSURES AND SLIDING VELOCITIES

J L Zhang, A. P. Burton, Z M Jin, J Fisher and S Williams

School of Mechanical Engineering, University of Leeds, Leeds UK, LS2 9JT

Background

The More conservative tissue substitution therapies such as hemiarthroplasty of the hip would maintain the healthy bone and cartilage tissue and avoid the immediate need for total joint replacement surgery. However, development of these treatment options is hindered by the lack of in vitro pre-clinical experimental simulation systems.

Purpose

The aim of this study was to assess the tribological properties and functional response of cartilage against cobalt chromium during long term (24hours) multi-directional sliding friction tests, in particular to assess the effect of different pressures and different sliding velocities on the friction coefficient and cartilage deformation.

Method and materials

Cartilage/bone plugs (diameters of 9 and 4 mm) from 18 months old bovine patello-femoral groove were used to articulate against a cobalt chromium plate (Ra=0.006μm) under different loads (define loads). The friction test was conducted on a reciprocating motion pin-on-plate apparatus, and friction assessed by means of a piezoelectric transducer. Samples were lubricated with 25% bovine serum. The deformation of the cartilage pin was assessed using a Nikon Profile Projector and a height gauge.

Result

It was found that as the contact pressure increased, both the coefficient of friction and the cartilage deformation increased. The effect of sliding velocity had little effect on the cartilage deformation. The higher sliding speed increased the surface damage of the cartilage during the movement, but did not alter the friction coefficient. These studies indicate the importance of contact stress on the tribological performance of articular cartilage in hemi arthroplasty.

Equations

$$FrictionCoefficient = \frac{Friction}{Load} \qquad (1)$$

Figure and Tables

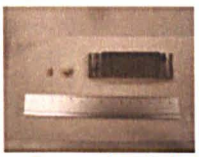

Figure 1: Cartilage Pins and Cobalt Chromium Plate

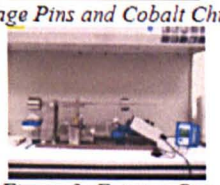

Figure 2: Friction Rig

Group	Stroke Length (mm)	Side Speed (mm/sec)	Rate (cycles/second)	Pressure (MPa) Load (N)					
				0.5MPa	1MPa	2MPa	4MPa	8MPa	16MPa
				32N	64N	127N	509N	1000N	2000N
				Pin Radius = 4.5mm			Pin Radius = 2mm		
1	4	4	0.5	n=6	n=6	n=6	n=6	n=6	n=6
2	8	4	1	n=6	n=6	n=6	n=6	n=6	n=6
3	8	8	0.5	n=6	n=6	n=6	n=6	n=6	n=6

Table 1: Different Test Groups Settings.

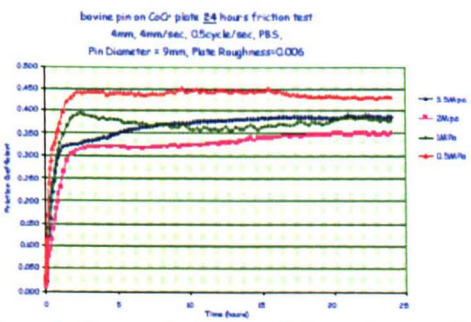

Figure 3: Friction Coefficient of Group 1 test result

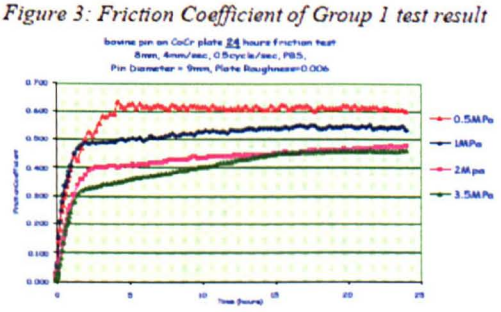

Figure 4: Friction Coefficient of Group 2 test result

2. 5th China International Symposium on Tribology, Beijing, China, Sep, 2008. Abstracts - presented as a 20 minutes oral presentation.

Friction and Wear of Biomaterial Head against Cartilage Hip Acetabulum

Jia Zhang, John Fisher, Zhongmin Jin, Andrew Burton*, Gemma John*, Sophie Williams
Institute of Mechanical Engineering, University of Leeds, Leeds, UK, LS2 9JT
*DePuy International Ltd., Leeds, UK

Keywords: Tribology, Cartilage, Friction, Lubrication, Wear

ABSTRACT

Hemi-arthroplasty may offer a conservative option to total hip replacements in the early stages of osteoarthritis. However, the conditions required for a successful hemi-arthroplasty are not fully understood. This study has investigated a hemi-arthroplasty in vitro model, to assess the friction and wear of acetabulum cartilage against a metal head. It has demonstrated that loading has an effect on the friction, additionally, the clearance between the head and cup and the contact area affected friction.

INTRODUCTION

Currently osteoarthritis of the hip is treated with a total hip replacement, which removes the healthy tissue as well as the diseased and degenerated cartilage. A more conservative option, that can be used for elderly patients who have suffered neck of femur fractures or in some cases osteonecrosis of the femoral head which replaces only the head of the femur is hemi-arthroplasty. However, for young active patients with higher physical demands, the incidence of early hemi-arthroplasty failure is substantial. This has been attributed to prosthesis loosening and acetabular cartilage degeneration, due to the friction between the metal head and acetabular cartilage [1].

In Japan, over 50% of hip replacements are bi-polar hemi-arthroplasty. This has a spherical bearing, onto which a UHMWPE bearing is locked, this is capped with a metallic cup [2]. A low friction inner articulation is produced and the potential for acetabular erosion [3,4] is reduced. However clinical results remain variable. There is little understanding of the tribology of hemiarthroplasty in the hip

Previous simple geometry pin on plate testing [5] has demonstrated that if cartilage stress is maintained between approximately 1 and 5MPa the friction is reduced, compared to stresses >5MPa. It is postulated that if the stress applied to cartilage in a hemi-arthroplasty is reduced by alternative designs, and minimising clearances between the metallic femoral head and cartilage acetabulum, friction (and therefore cartilage degradation) could be reduced. If the conditions required for a successful hemi-arthroplasty could be better understood then this may offer a conservative option in the early stages of osteoarthritis in some patients.

AIM

The aim of this study was to develop an in vitro system to investigate the tribology (cartilage friction, degradation and wear) and functional response to a metallic femoral head. The parameters investigated in this initial study included the clearance between the head and cup; loading (dynamic and constant), different levels of flexion-extension motion (±15° and ±25°) and lubricants (25% bovine serum and PBS).

MATERIALS AND METHODS

Porcine hip joints were dissected within 36 hours of slaughter from 12 month old animals. The acetabulum was mounted at an angle of 45 degrees in PMMA cement (Figure 1). A silicon rubber mould (Synthetic Rubber Replicating Compound, Microset Product Ltd, UK) was made of the acetabulum and the dimensions shown in Figure 1 measured were in the flexion-extension [F-E] and medial – lateral [M-L] directions.

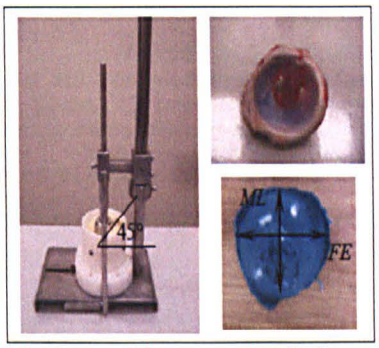

Figure 1 Porcine acetabulum mounted at 45 degrees in bone cement for friction testing, mould measurement: *F-E* direction (flexion-extension) acetabulum dimension, *M-L direction* (medial-lateral) acetabulum dimension

Cobalt chrome alloy heads, 34, 35, 36 and 37mm in diameter were supplied by DePuy International Ltd., The surface roughness (Ra) of the untested heads was 0.008μm (measured using a contact profilometer, Talysurf, Taylor Hobson, Leciester, UK).

The friction test was conducted using a pendulum motion friction simulator (Simulator Solutions, Stickport, UK) (Figure 3). Components were mounted in an inverted configuration compared to the anatomical position (i.e. the head superior to the cup). A flexion-extension motion of ±15 degrees was applied to the head. A constant load test with a 400N load and dynamic load regime (Figure 2) were carried out. The lubricant was 25% bovine serum (18g/l protein) or PBS. Detailed sizes of the acetabulums tested and clearance variables as measured from the moulds taken are shown in Table 1.

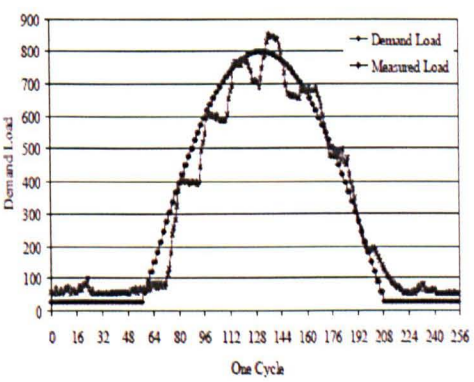

Figure 2 Demand load and measured load in each cycle of dynamic load regime

Tests were conducted for 2 hours and data recorded at the peak load / high velocity part of the cycle, data was logged every 5 cycles in the first 100 cycles, every 30 cycles from 101 cycles to 1000 cycles, and every 150 cycles from 1001 cycles to 7200 cycles). The coefficient of friction was calculated using Equation 1.

Group	No.	Load	FE diameter	ML diameter	FE clearance	ML clearance
1	1	400N constant	36.8	33.9	0.40	-1.05
	2		40.2	38.6	2.10	1.30
	3		37.2	36.3	0.60	0.15
	4		36.2	34.0	0.10	-1.00
	5		40.6	38.4	2.30	1.20
	6		37.0	34.7	0.50	-0.65
2	1	25N ~ 800N dynamic	40.3	38.0	2.15	1.00
	2		35.3	34.0	-0.35	-1.00
	3		36.2	34.4	0.10	-0.80
	4		36.4	35.3	0.20	-0.35
	5		36.7	34.8	0.35	-0.60
	6		37.6	35.6	0.80	-0.20

Table 1 Detailed sizes tested and clearance variables

$$f = \frac{T_t}{RL_p} \qquad \text{Equation 1}$$

The friction factor (f, Equation 1) is similar in magnitude to the co-efficient of friction, but variable with the finite contact area, (R) is the bearing radius (m), and (L_p) is the peak load (N).

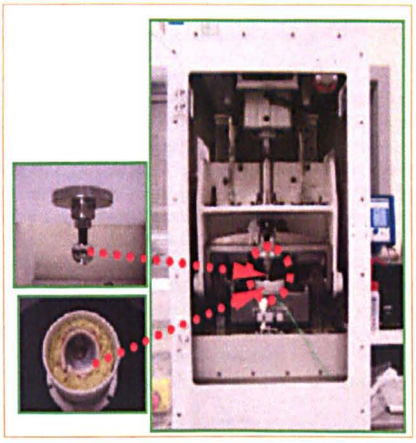

Figure 3 A Pendulum Friction Simulator

RESULTS

Six porcine acetabulum specimens were tested against 36mm diameter metal head under 400N constant load for two hours and the friction coefficient was measured over time (Figure 4).

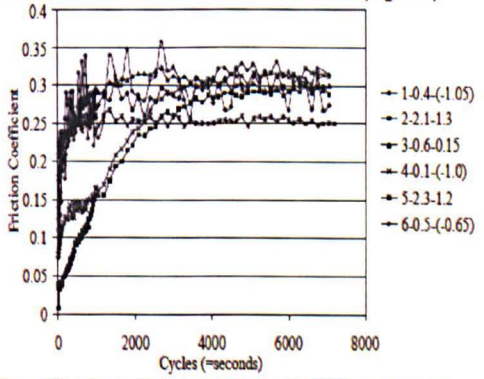

Figure 4 Two hours friction coefficient under 400N constant load friction test, lubricant: 25% bovine serum, angle: ±15°, head size: 36mm. Legend: case number-*FE* clearance-*ML* clearance.

As the number of cycles increased so did the coefficient of friction. There was no obvious variation in friction over time compared to clearance.

A second study was conducted, where six porcine acetabulum specimens were tested against a 36mm diameter metal head under 800N peak dynamic load for two hours. The friction coefficient against time was recorded (Figure 5). As in testing with a constant load the friction increased with time, however, the rate of this increase was less under dynamic loading compared to the testing under constant loading.

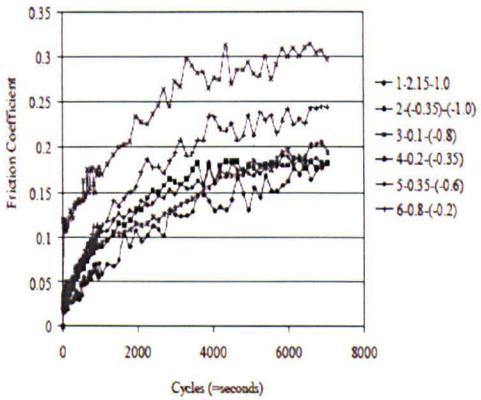

Figure 5 Two hours friction coefficient under 800N dynamic load friction test, lubricant: 25% bovine serum, angle: ±15°, head size: 36mm. Labels: case number-*FE* clearance-*ML* clearance.

The wear area of the tested porcine acetabulum specimens is shown in Figure 6.

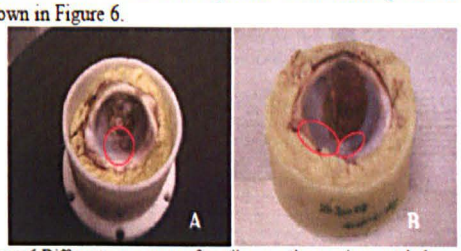

Figure 6 Different wear areas of cartilage on the porcine acetabulum surface after two hours friction test

An acetabulum with a clearance of FE-0.6mm and ML-0.15mm tested for 2 hours with a 400N constant load is shown in Figure 6A the cartilage was degraded to bone in the area shown. Following a 2 hour 800N dynamic load friction test with FE-2.15mm and ML-1.0mm clearance, two areas of cartilage were degraded as shown (Figure 6B).

DISCUSSION

This study has investigated wear of cartilage in an in vitro hemi-arthroplasty simulation. Friction increased with time in the constant and dynamic load test. This was due to biphasic nature of cartilage, with increasing time the fluid phase support decreases and the solid-phase support increases. This effect was less in the dynamic testing; the dynamic load allows some recovery of the cartilage fluid-phase during the unloaded period of the cycle. The radial clearances had a marked effect on the contact mechanics and tribology.

This initial study forms part of an on-going study to continue to develop this method to test the parameters *in vitro* that effect cartilage degeneration.

ACKNOWLEDGMENTS

The authors would like to acknowledge the financial support of the EPSRC & DePuy International Ltd., UK.

REFERENCES

[1] Yamagata. J Arthroplasty 2 327 1987
[2] Phillips T. JBJS 69B 761 1987
[3] Bateman J et al CORR 54-60 1990
[4] LaBelle L et al. CORR 251 20 1990
[5] Zhang et al., Euro Soc Biomect., Lucerne 2008

3. 55th Annual Meeting of the Orthopaedic Research Society, Las Vegas, United States, Feb, 2009. Abstracts – presented as a poster

THE INFLUENCE OF FRICTIONAL SHEAR STRESS ON CARTILAGE TO HEMI-ARTHROPLASTY

+[1]Zhang JL; [1]Fisher J; [1]Jin ZM; [2]Burton AP, [1]Williams S
+[1]iMBE, School of Mechanical Engineering, University of Leeds, Leeds, UK, [2]DePuy International Ltd., Leeds, UK
Senior author: s.d.williams@leeds.ac.uk

INTRODUCTION:

Currently osteoarthritis of the hip is treated with a total hip replacement which removes the diseased and healthy tissue. A more conservative option that can be used for elderly patients who have suffered osteonecrosis of the head or neck of femur fractures is hemi-arthroplasty, a procedure which replaces only the femoral head. However, for young active patients with higher physical demands, the incidence of early hemi-arthroplasty failure has increased. This has been attributed to prosthesis loosening and acetabular cartilage degeneration, due to the loading and friction between the metal head and cartilage.

It is postulated that if the stress applied to the cartilage was reduced by alternative designs of hemi-arthroplasty, and optimising clearances between the metallic femoral head and cartilage acetabulum, friction, frictional shear stress (product of contact stress and friction coefficient) and therefore cartilage degradation would be reduced. If the conditions required for a successful hemi-arthroplasty could be better understood then this could be a feasible conservative option in the early stages of osteoarthritis in some patients. The aim of this study was to assess the effect of contact area, contact stress, sliding distance and velocity of a cartilage pin against a metal plate in this simple model to mimic the hemi-arthroplasty model and better understand the effect of these parameters on friction and degradation of cartilage.

METHODS:

Cartilage/bone plugs (diameters of 4 and 9 mm) from 18 months old bovine patella femoral grooves were used to articulate against a cobalt chromium plate (R_a=0.006μm) under different contact stresses (between 0.5 and 16MPa). This simple geometry friction test was conducted on a reciprocating motion pin-on-plate apparatus, and friction assessed by means of a piezoelectric transducer. Samples were lubricated with PBS (Phosphate Buffered Solution).

The effect of the following parameters on friction was studied:

1. Same constant contact stress (3.5MPa) due to different loads and pin diameters (44N and 4mm pin compared with 220N and 9mm pin) for 24 hours long-term studies.
2. Varying constant contact stress conditions:
   - Low contact stress: 0.5, 1, and 2MPa for long-term 24 hours studies;
   - Medium contact stress: 4 and 8MPa for long-term 24 hour studies;
   - High contact stress: 12 and 16MPa for short-term one hour studies.
3. Stroke length and velocity:
   - 4mm stroke length with 4mm per second velocity (4-4)
   - 8mm stroke length with 8mm per second velocity (8-8)

To calculate the friction coefficient (μ_{eff}) and frictional shear stress, the following equations were used (r is the radius of the cartilage pin).

$$\mu_{eff} = \frac{Friction}{Load} \quad (1)$$

$$Frictional\ Shear\ Stress = \frac{\mu_{eff} \times Load}{\pi \times r^2} \quad (2)$$

RESULTS:

1. **Effect of different contact load and area with same contact stress:** In the 4-4 condition, the μ_{eff} of 4mm diameter pin was significantly higher than 9mm pin during the first 2 hours study as the stress at the center of the pin was higher for the smaller diameter. No significant differences were observed between the 2 and 24 hours friction studies as the load was gradually transferred to the solid phase (Figure 1).

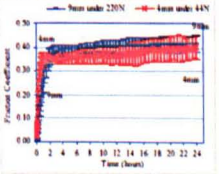

Figure 1. 24 hours friction test at 4-4 setting μ_{eff} vs. time different contact area with same contact stress (3.5MPa), n=6

2. **Effect of contact stress conditions:**
   a. For low and medium contact stress in 24 hour studies: in both the 4-4 and 8-8 conditions, the μ_{eff} increased quickly during the first 40 minutes of testing, then remained stable under low contact stress but continued to increase under medium stress over 24 hours study. The μ_{eff} decreased from very low stress (0.5MPa) to approximately 2-4MPa (Figure 2), then increased with increasing contact stress.

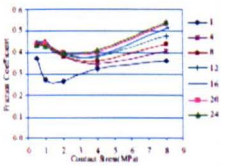

Figure 2. 1 to 24 hours friction study at 4-4 setting friction coefficient vs. contact stress (0.5~8MPa), n=6

   b. High contact stress: In both the 4-4 and 8-8 conditions, no significant difference in friction coefficient was observed. When the contact stress exceeded 8MPa and loading time exceeded one hour, cartilage damage was observed.
   c. Frictional shear stress increased with both contact stress and loading time (μ_{eff}): in both the 4-4 and 8-8 conditions, high frictional shear stress (over 4MPa) also caused the cartilage damage (Figures 3).

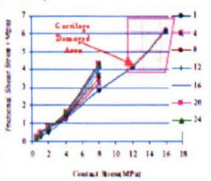

Figure 3. 1 to 24 hours friction study at 4-4 setting frictional shear stress vs. contact stress (0.5~8MPa), n=6

3. **The influence of sliding distance (stroke length) and velocity:** under low contact stress (0.5 and 2MPa) the μ_{eff} was significantly higher for 4-4 conditions than 8-8 conditions as the cartilage was under the biphasic and boundary lubrication condition; under medium contact stress (4 and 8MPa) the μ_{eff} was not significantly different (P_{max}=0.005) during the first 9 hours friction study as the cartilage surface transferred to solid phase, (μ_{eff} followed equation1), but after 9 hours the surface wear and degradation due to the 8-8 conditions caused higher friction, thus μ_{eff} increased more rapidly than when tested under the 4-4 conditions.

DISCUSSION:

Friction coefficient and friction force have been used to describe the tribological properties of hyaline cartilage in articular joints[1]. It was concluded that for the same contact stress different contact loads and areas had little effect on friction coefficient after the cartilage loses a certain amount of water (following 2 hours of loading), as the contact surface transfers into solid phase.

However, contact stress influenced friction with higher friction coefficient at both low and high contact stress levels. Degradation and wear only occurred under high contact stress conditions and it was shown that increased values of frictional shear stress were related to degradation and wear, thus providing a better understanding of the tribology response of the cartilage. High frictional shear stress was largely responsible for cartilage damage and degradation. It was found in this model that when the frictional shear stresses 4MPa, damage and wear of cartilage surface resulted. This study was undertaken for constant load only and other work under dynamic loading in the knee indicates degradation at lower levels of frictional shear stress. This will be pursued in further work in a hemi arthroplasty model in hip.

REFERENCE

[1] Zhang et al., Euro Soc Biomech., Lucerne 2008

4. 8th World Congress of the International Cartilage Repair Society, Miami, United States, Mar, 2009. Presented as a poster.

Title: Cartilage Wear and Degradation of Hip Hemi-arthroplasty under Dynamic Load

Topic: Clinical Research/Hip (Chondra and Osteochondral defects)

Authors: J. LIZHANG, J. Fisher, Z. Jin, S. Williams; Leeds/UK

Introduction

One of the main issues of hip hemiarthroplasty main is the cartilage wear and degradation after the surgery. This study investigated the cartilage wear and degradation in the natural acetabulum articulating against a metallic femoral head under two hours dynamic loading with different clearances. We hypothesise that the outcome of hemiarthroplasty could be improved if the clearance is optimised.

Methods and Materials

Cartilage wear and degradation was measured after 2 hours dynamic pendulum friction test on the – month old porcine acetabulums. The Microset silicon rubber replica was made from the porcine acetabulum immediately after the friction test. Then the mould surface was covered by the cling film and marked different wear grades with different colours followed the ICRS cartilage wear grading system. The picture of the cling film was take with a ruler and analysed through Image Pro Plus software, the cartilage lunate area and different wear grade areas were calculated. Porcine acetabulums were dissected from 12-month old animal's hip joints and mounted in PMMA at 45° with respect to the loading, and then a silicon rubber replica was made to assess dimensions. The cobalt chrome alloy head diameters were 34, 35, 36, or 37mm with 0.008μm roughness (Ra). Clearances were small (≤0.7mm), medium (>0.7 & ≤1.4mm), and large (>1.4mm).

Two-hour 400 N constant load friction tests were conducted using a pendulum motion friction simulator with a flexion-extension motion of ±15° in 25% bovine serum. The friction coefficient (μ_{eff}) was measured throughout testing and wear damaged assessed visually at the end of the test and classed as zero, mild and severe.

Result

The friction coefficient (the friction factor at 0° position) was not significantly different in testing with different clearances, and it was approximately 0.27 following 7200 cycles (range±0.025). However, if wear and friction were correlated: the friction coefficient of zero-wear group (μ_{eff}=0.20) was significantly lower (T test p=0.0037) than both mild and severe wear groups (μ_{eff} =0.28).

Conclusions

The friction of hemi-arthroplasty under constant load was dependent on both the clearance and the acetabulum geometry, cartilage is damage led to elevated friction.

Acknowledgements

The authors would like to acknowledge the financial support of the EPSRC & DePuy International Ltd., UK.

5. Annual Meeting British Orthopaedic Research Society, Newcastle, United Kingdom, July, 2009. Poster.

How does Clearance and Wear Affect Acetabular Cartilage Friction in Hip Hemiarthroplasty

+[1]Lizhang J; [1]Fisher J; [1]Jin ZM; [2]Burton AP, [1]Williams S
+[1]iMBE, School of Mechanical Engineering, University of Leeds, Leeds, UK;
[2]DePuy International Ltd., Leeds, UK
menjzha@leeds.ac.uk

Key words: Tribology, Cartilage, Friction, Wear, Lubrication.

Introduction:

Hemi-arthroplasty (replacement of the femoral head only) can be used to treat fractured neck of femurs. For patients with high activity levels however, the incidence of early failure is high. Failure is attributed to acetabular cartilage degeneration and has been reported as resulting from high friction levels between the metal head and acetabular cartilage [Yamagata, 1987].
This in vitro study investigated hemi-arthroplasty tribology (friction, degradation and wear) and functional response of acetabular cartilage to metallic femoral heads.

Methods:

The diameter of 12-month old porcine acetabulum were measured in the flexion-extension direction and mounted at 45 degrees to loading axis in the pendulum friction simulator. Cobalt chrome heads (34-mm diameter, Ra=0.008 μm) were assembled with the acetabuli, in an inverted configuration compared to anatomical position. This was lubricated with 25% bovine serum. Flexion-extension (±15 degrees) and constant load (400N) were applied to the head and friction measured for 2hrs. Head/acetabular diametral clearances were chosen as follows: large (≥1.4 mm); medium (between 0.7 mm and 1.4 mm) and small (<0.7 mm). Following testing, acetabulum cartilage was visually assessed for wear/damage (zero, mild and severe).

Results and Discussion:

1. Effect of clearance on friction and wear

Clearance did not have a significant effect on friction coefficient. Larger clearances allowed the contact area to translate, thus maintaining fluid-phase support in the cartilage through rehydration. However, clearance affected the levels of wear.

2. Effect of friction and clearance on cartilage wear

Increased friction caused mild or severe cartilage wear while low friction showed no visual signs of damage (zero wear). Smaller clearances reduced wear: due to reduced contact pressures.

Clearances and sizing of the femoral head appear to be a significant factor in biotribological performance of hemi arthroplasty.

Acknowledgements:

EPSRC, and DePuy International Ltd

6. 56th Annual Meeting of the Orthopaedic Research Society, New Orleans, United States, Mar, 2010. Abstract – presented as a 5 minutes short talk.

EFFECT OF CLEARANCE ON FRICTION AND CARTILAGE DAMAGE IN HIP HEMI-ARTHROPLASTY

+[1]Zhang JL; [1]Fisher J; [1]Jin ZM; [2]Burton AP, [1]Williams S
+[1]iMBE, School of Mechanical Engineering, University of Leeds, Leeds, UK, [2]DePuy International Ltd., Leeds, UK
Senior author: s.d.williams@leeds.ac.uk

INTRODUCTION:

Hemi-arthroplasty offers a more conservative option compared to total hip replacement in cases of fractured neck of femur as it replaces only the femoral side. However, the incidence of early hemi-arthroplasty failure is substantial and has been attributed to acetabular cartilage degeneration due to the friction between the metal head and acetabular cartilage [1]. It is hypothesized that an increase in clearance between the head and natural acetabulum and resulting increase in cartilage contact stress will increase cartilage degradation.

This study investigated the biotribology of hemi-arthroplasty in an *in vitro* model to assess cartilage tribology (friction, degradation and wear) as a function of clearance between head and cup under constant and dynamic loading cycles.

METHODS:

Porcine acetabulums were dissected within 36 hours of slaughter from 12 month old animals, mounted at an angle of 45 degrees inclination in PMMA cement and measured in the flexion-extension (*FE*) and medial–lateral (*ML*) directions. The diameters of the Cobalt Chrome alloy heads were 32, 34, 35, 36 and 37mm each having a surface roughness (Ra) of 0.008μm prior to testing (measured using a contact profilometer, Talysurf, Taylor Hobson, Leciester, UK).

The tribological simulation was conducted using a pendulum motion simulator (Simulator Solutions, Stockport, UK; Figure 1). Components were mounted in an inverted configuration compared to the anatomical position (i.e. the head superior to the cup). A FE motion of ±15 degrees was applied to the head. A constant load test with a 400N load regime or a dynamic load test with a 75~800N load regime was applied at a frequency of 1 Hertz. The lubricant was 25% bovine serum.

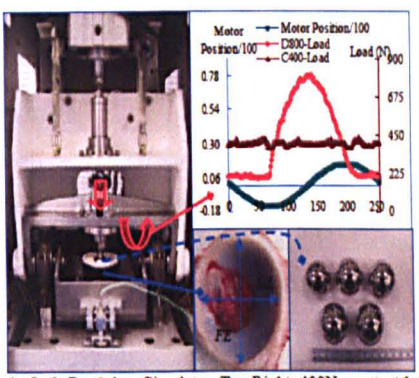

Figure 1 - Left: Pendulum Simulator; Top Right: 400N constant load and 75~800N dynamic load regime profile; Bottom Right: porcine acetabulum and Cobalt Chrome heads

The radial *FE* clearance 'x' was defined as Small (S: x<0.6mm), Medium (M: 0.6≤x<1.2mm), Large (L: 1.2≤x<1.8mm), and Extra Large (XL: x≥1.8mm). The friction factor (*f*, Equation 1) was calculated using R (the bearing radius [meters]), L_p (peak load [N]) and T (friction torque [Nm]). Friction factor magnitude is similar to the coefficient of friction (μ_{eff}), but varies with the finite contact area. The coefficient of friction (μ_{eff}) was calculated when the head was passing the lowest position of the acetabulum (i.e. at 0 degree *FE*).

$$f = \frac{T}{RL_p} \qquad \textit{(Equation 1)}$$

Porcine acetabulum specimens (8 variables studied, n=6 per group) were tested with different clearances under constant load or dynamic load for two hours and coefficient of friction was measured over time.

RESULTS:

The coefficient of friction was significantly lower with increased clearance (ANOVA single factor, 0.005; be tested at 10, 20, 120 minutes time points), contrary to the hypothesis. The coefficient of friction decreased as the clearance was increased under both dynamic loading (Figure 2) and constant loading. The coefficient of friction was higher under constant load and showed a trend of decreasing with increasing clearance.

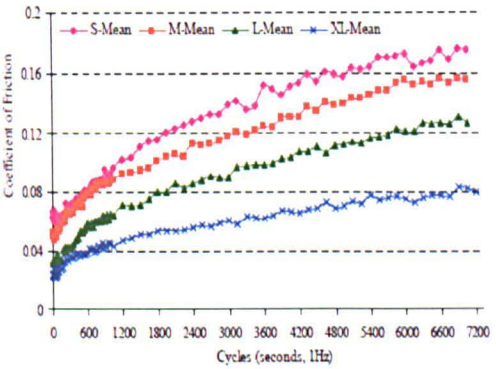

Figure 2 - Mean (n=6) coefficient of friction of different clearances under dynamic loading, ±15 degrees *FE*, 25% bovine serum

Under constant loading with XL clearance, cartilage was damaged/ removed from bone and cartilage friction was reduced. It is postulated that this was when the cartilage damage occurred (Figure 3).

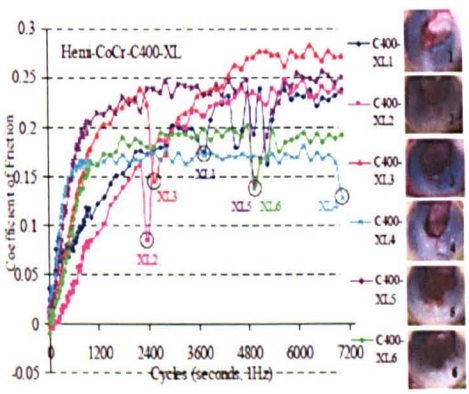

Figure 3 - Coefficient of friction under 400N constant loading with XL clearance (reduced friction due to cartilage damage relating to circled points)

DISCUSSION:

Friction coefficient under constant load was higher than under dynamic load due to the biphasic properties of cartilage. The coefficient of friction did not, however, increase with clearance as hypothesized but instead reduced as the clearance increased (over the range of <0.6 to >2mm). This was due to an increase in translation of the contact point over the surface of the cartilage in the cup allowing for fluid to re-imbibe into the cartilage when unloaded, such that the fluid phase supported the load when reapplied. For extra large clearances under constant load this was not the case and cartilage was disrupted and damaged. This was due to contact pressures and frictional shear stress exceeding the durability limit for articular cartilage (as reported for in the knee following meniscectomy [2]). This study indicates that low levels of friction and short term durability is achievable for a range of clearances in hemi-arthroplasty of the hip (up to 1.8mm), whereas extra large clearances (>1.8mm) should be avoided.

REFERENCE

[1] Yamagata. J Arthroplasty 2 327 1987
[2] McCann et al., Osteoarthritis and Cartilage, ICRS 2009

Acknowledgements

This work was supported by LMBRU (Leeds Musculoskeletal Biomedical Research Unit), EPSRC, and DePuy International Ltd., UK.

7. 11th European Federation of National Associations of Orthopaedics and Traumatology Congress, Mildred, Spain, Jun, 2010. E-poster

Effect of clearance on friction and cartilage damage in hip hemi-arthroplasty

+[1]Zhang JL; [1]Fisher J; [1]Jin ZM; [2]Burton AP, [1]Williams S

+[1]iMBE, School of Mechanical Engineering, University of Leeds, Leeds, UK.

[2]DePuy International Ltd., Leeds, UK

INTRODUCTION:

Hemi-arthroplasty offers a conservative treatment option for femoral neck fractures. Early hemi-arthroplasty failure has been attributed to acetabular cartilage degeneration due to friction between the metal head and acetabular cartilage. It was hypothesised that an increase in clearance between the head and acetabulum and resulting cartilage contact stress increase, will accelerate cartilage degradation. The biotribology of hemi-arthroplasty in an *in vitro* model was assessed in terms of cartilage friction, degradation and wear, as a function of clearance under constant and dynamic loading.

METHODS:

Porcine acetabulums were dissected, mounted at an angle of 45° and measured in the flexion-extension (*FE*) direction. These were paired with CoCr heads (diameters 32, 34, 35, 36, 37mm), to give radial *FE* clearance clearances (x): Small ($x<0.6$mm), Medium ($0.6\leq x<1.2$mm), Large ($1.2\leq x<1.8$mm), Extra Large ($x\geq 1.8$mm). A pendulum simulator was used and components were mounted in an inverted configuration (compared to anatomic). A *FE* motion of ±15° was applied. A constant 400N or a dynamic 75~800N load regime was applied at 1 Hz in 25% bovine serum. Head and acetabular samples were tested in each clearance range and friction coefficient (FC) measured over time.

RESULTS:

The FC was significantly lower with increased clearance (contrary to hypothesis). The FC decreased as the clearance increased under both dynamic and constant loading. The FC was higher under constant load and decreased with increasing clearance. Under constant loading with XL clearance, cartilage was damaged/ removed, however, cartilage friction was reduced.

DISCUSSION:

The FC under constant load was higher than under dynamic load due to the biphasic properties of cartilage. The FC did not increase with clearance as hypothesised but reduced as clearance increased (over the range of <0.6 to >2mm). This was due to an increase in translation of the contact point over the surface of the cartilage in the cup allowing for fluid to re-imbibe into the cartilage when unloaded, such that the fluid phase supported the load when reapplied. For extra large clearances under constant load this was not so, and cartilage was disrupted/damaged. This was due to contact pressures and frictional shear stress exceeding the durability limit for cartilage (as reported in knee meniscectomy). This study indicates that low levels of friction and short term durability is achievable for a range of clearances in hemi-arthroplasty of the hip (up to 1.8mm), whereas extra large clearances (>1.8mm) should be avoided.

Acknowledgements

This work was supported by LMBRU (Leeds Musculoskeletal Biomedical Research Unit), EPSRC, and DePuy International Ltd., UK.

8. 6th World Congress on Biomechanics Singapore, Aug, 2010. Oral presentation.

Biotribology of hip hemi-arthroplasty

Jia Lizhang, John Fisher, Zhongmin Jin and Sophie Williams
Institute of Medical and Biological Engineering, School of Mechanical Engineering, University of Leeds, Leeds, UK,

Introduction

Hemi-arthroplasty of the hip provides a more conservative treatment option for femoral neck fractures, compared to a total hip replacement. However, hemi-arthroplasty failure has been attributed to acetabular cartilage degeneration and wear due to friction between the metal head and acetabular cartilage. It was hypothesised that an increase in clearance between the metallic head and acetabulum and the resulting increase in cartilage contact stress and frictional shear stress will accelerate cartilage degradation. The biotribology of hemi-arthroplasty in an in vitro model was assessed in terms of cartilage friction, degradation and wear, as a function of clearance under constant and dynamic loading.

Methods

Porcine acetabulums from 12-month old animals were obtained from a commercial abattoir and dissected, mounted using PMMA at an angle of 45° and dimensions measured in the flexion-extension (FE) direction. These acetabulums were paired with CoCr heads (diameters 32, 34, 35, 36, 37mm; supplied by DePuy International Ltd.), to give radial FE clearances (x) as follows (n=6): small ($x<0.6$mm), medium ($0.6\leq x<1.2$mm), large ($1.2\leq x<1.8$mm), extra large ($x\geq 1.8$mm). These pairs were mounted in an inverted configuration in a pendulum simulator (Simulation Solutions, UK). A FE motion of ±15° was applied to the head, tests were conducted using two different loading regimes; a constant 400N or dynamic (between 75-800N) cycle was applied at 1 Hz in 25% bovine serum for 2 hours. The coefficient of friction was measured throughout testing and cups were assessed for cartilage damage post-test.

Results

Higher friction was always observed for the same clearance when constant loading was compared to dynamic loading. The friction coefficient was significantly lower with increased clearance (contrary to hypothesis) under constant and dynamic load regimes. However, under constant loading with XL clearance, cartilage was significantly damaged.

Discussion

The friction observed in testing with a constant load was higher than dynamic loading due to the biphasic fluid load supporting properties of cartilage. Friction did not increase with clearance as hypothesised; but reduced as clearance increased (between <0.6 to >2mm). Increased clearances caused an increase in the translation of the contact point over the surface of the cartilage in the cup allowing for fluid to re-imbibe into the cartilage when unloaded, this mitigated for the effect of the increased contact stress. However, with extra large clearances under constant load a threshold limit of the cartilage was reached (in terms of frictional shear stress) and cartilage was permanently damaged. Similar effects in terms of cartilage damage are seen following knee meniscectomy (McCann et al., 2008). This study indicates that low levels of friction and short term durability is achievable for a range of clearances in hemi-arthroplasty of the hip (up to 1.8mm), whereas extra large clearances (>1.8mm) should be avoided.

Acknowledgements

This work was supported by LMBRU (Leeds Musculoskeletal Biomedical Research Unit), EPSRC, and DePuy International Ltd., UK.

9. 9th World Congress of the International Cartilage Repair Society, Barcelona, Spain, Sep, 2010. E-poster.

Title: The effect of clearance on cartilage wear in hip hemiarthroplasty

Topic: Basic Science / Biomechanics

Authors: J. Lizhang, J. Fisher, Z. Jin, S. Williams; Leeds/UK

Purpose

Hip hemiarthroplasty is used in elderly patients following femoral neck fracture. However, longevity of this treatment is limited by the metal or composite prosthesis degrading the cartilage over time. Inappropriate sizes of implant in hip hemiarthroplasty may cause early cartilage wear (Beksaç et al, 2008). This study investigated the effect of clearance (between acetabular cartilage and metal head) on cartilage wear area and volume. We hypothesised that the outcome of hemiarthroplasty could be improved if the clearance is optimised.

Methods and Materials

Acetabulums (from 6-month old porcine hips) were dissected and mounted at 45° in a pendulum friction simulator, Cobalt Chrome heads were set homocentric to the acetabulums and applied a dynamic (75~800N) load and a flexion-extension motion (±15°) in 25% bovine serum for 2 hours. Components were set up to allow the different radial clearances: Small (≤0.6mm), Medium (>0.6 & ≤1.2mm), Large (>1.2 & ≤1.8mm), Extra Large (>1.8mm), n=3 per group.

A silicon rubber replicate was made of the acetabular surface after testing to investigate wear. The wear area was traced onto flexible film and the area of different cartilage damage grades (followed ICRS wear grades) measured. Additionally, the replica surface was measured by a two-dimensional profilometry across the wear area with approximately 20 traces, and this was multiplied by the wear area length to provide a volume (Figure 1).

Results

Different cartilage wear grades (1~3) were seen in different clearances, and when clearance increased contact area decreased, hence the percentage of unworn cartilage area increased (Figure 2.a). Wear volume increased significantly with XL due to the increase in contact stress above a critical threshold and the increase of cartilage wear depth clearance (Figure 2.b).

Conclusions

Cartilage wear in hip hemiarthroplasty is affected by clearance which influences both wear area and wear grade, and significantly higher wear is produced with extra large clearance.

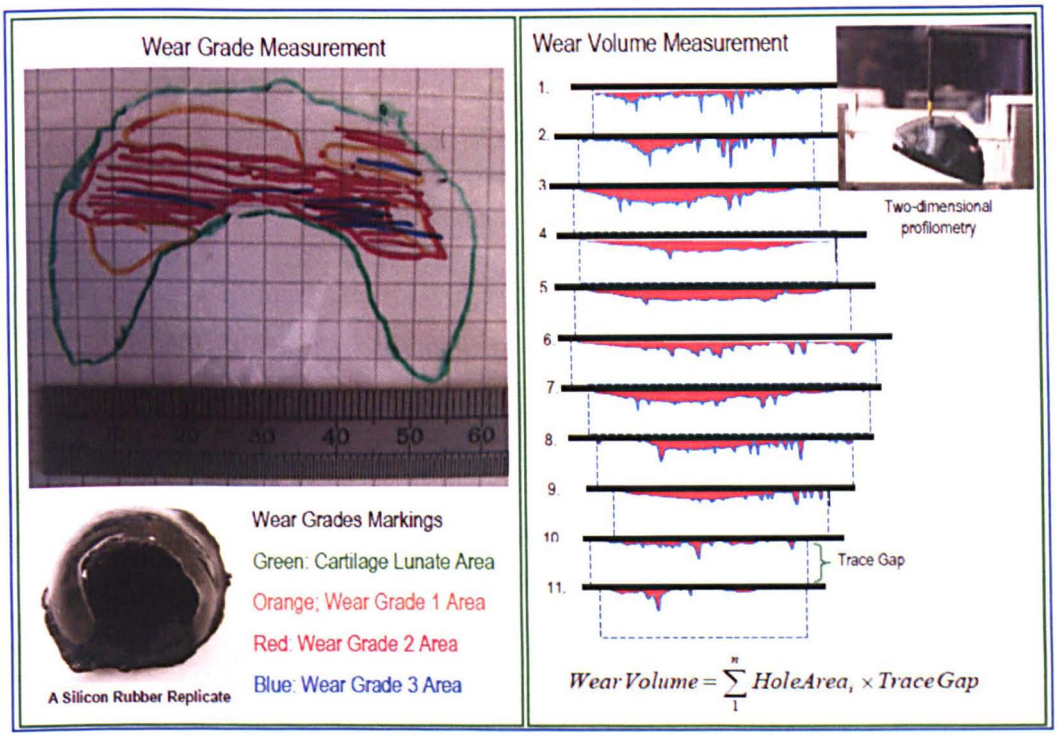

Figure1. Acetabular Cartilage Wear Grade and Wear Volume Measurements

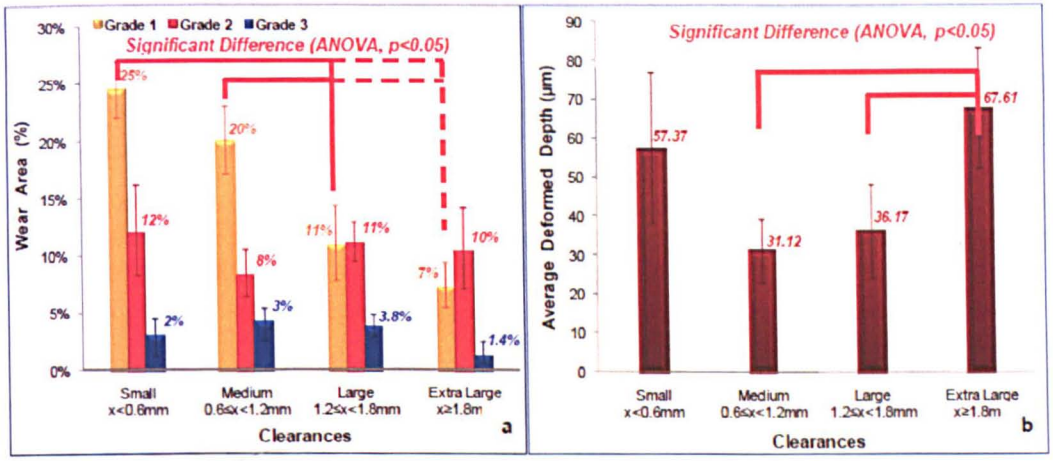

Figure2. a. Wear Grade Area (%), and b. Wear Volume (mm^3) with Different Clearances (n=3)

Disclosures

John Fisher receives a Senior Investigator Award from the NIHR. Sophie Williams and John Fisher are paid consultants to DePuy International Ltd. Andrew Burton is an employee of DePuy International Ltd. Jia Lizhang is a PhD research student and received a studentship from EPSRC and DePuy International Ltd.

This work was supported by the NIHR (National Institute for Health Research) as part of collaboration with the LMBRU (Leeds Musculoskeletal Biomedical Research Unit), EPSRC, and DePuy International Ltd., UK.

References

ADAMS, D. & SWANSON, S. A. V. 1985. Direct measurement of local pressures in the cadaveric human hip joint during simulated level walking. *Annals of the Rheumatic Diseases,* 44, 658-666.

ADAMS, M. A., KERIN, A. J. & WISNOM, M. R. 1998. Sustained Loading Increases the Compressive Strength of Articular Cartilage. *Connective Tissue Research,* 39, 245-256.

AFOKE, N., BYERS, P. & HUTTON, W. 1987. Contact pressures in the human hip joint. *J Bone Joint Surg Br,* 69-B, 536-541.

AFOLARANMI, G. A., TETTEY, J. N. A., MURRAY, H. M., MEEK, R. M. D. & GRANT, M. H. 2010. The Effect of Anticoagulants on the Distribution of Chromium VI in Blood Fractions. *The Journal of Arthroplasty,* 25, 118-120.

AHN, J., MAN, L.-X., PARK, S., SODL, J. & ESTERHAI, J. 2008. Systematic Review of Cemented and Uncemented Hemiarthroplasty Outcomes for Femoral Neck Fractures. *Clinical Orthopaedics and Related Research®,* 466, 2513-2518.

AMSTUTZ, H. & SMITH, R. 1979. Total hip replacement following failed femoral hemiarthroplasty. *J Bone Joint Surg Am,* 61, 1161-1166.

ANDERSON, L., HAMSA, W. & WARING, T. 1964. Femoral-Head Prostheses: A REVIEW OF THREE HUNDRED AND FIFTY-SIX OPERATIONS AND THEIR RESULTS. *J Bone Joint Surg Am,* 46, 1049-1065.

ANDERSON, P. R. & MILGRAM, J. W. 1978. Dislocation and Component Separation of the Bateman Hip Endoprosthesis. *Journal of the American Medical Association,* 240, 2079-2080.

ANISSIAN, H. L., STARK, A., GUSTAFSON, A., GOOD, V. & CLARKE, I. C. 1999. Metal-on-metal bearing in hip prosthesis generates 100-fold less wear debris than metal-on-polyethylene. *Acta orthopaedica Scandinavica,* 70, 578 - 582.

ARCAM, E. S. 2007. ASTM F75 CoCr Alloy.

ARMSTRONG, C. G. & MOW, V. C. 1982. Variations in the intrinsic mechanical properties of human articular cartilage with age, degeneration, and water content. *J Bone Joint Surg Am,* 64, 88-94.

ARMSTRONG, C. G. & MOW, V. C. 1983. The mechanical properties of articular cartilage. *Bull Hosp Jt Dis Orthop Inst,* 43, 109-17.

ATESHIAN, G. A. 1997. A Theoretical Formulation for Boundary Friction in Articular Cartilage. *Journal of Biomechanical Engineering,* 119, 81-86.

ATESHIAN, G. A., CHAHINE, N. O., BASALO, I. M. & HUNG, C. T. 2004. The correspondence between equilibrium biphasic and triphasic material properties in mixture models of articular cartilage. *Journal of Biomechanics,* 37, 391-400.

ATESHIAN, G. A., LAI, W. M., ZHU, W. B. & MOW, V. C. 1994. An asymptotic solution for the contact of two biphasic cartilage layers. *Journal of Biomechanics,* 27, 1347-1360.

ATESHIAN, G. A., SOLTZ, M. A., MAUCK, R. L., BASALO, I. M., HUNG, C. T. & LAI, W. M. 2003a. The role of osmotic pressure and tension-compression nonlinearity in the frictional response of articular cartilage. *Transport in Porous Media,* 50, 5-33.

ATESHIAN, G. A., SOLTZ, M. A., MAUCK, R. L., BASALO, I. M., HUNG, C. T. &

MICHAEL LAI, W. 2003b. The Role of Osmotic Pressure and Tension-Compression Nonlinearity in the Frictional Response of Articular Cartilage. *Transport in Porous Media,* 50, 5-33.

ATESHIAN, G. A. & WANG, H. 1995. A theoretical solution for the frictionless rolling contact of cylindrical biphasic articular cartilage layers. *Journal of Biomechanics,* 28, 1341-1355.

ATESHIAN, G. A., WANG, H. Q. & LAI, W. M. 1998. The role of interstitial fluid pressurization and surface porosities on the boundary friction of articular cartilage. *Journal of Tribology-Transactions of the Asme,* 120, 241-248.

ATESHIAN, G. A., WARDEN, W. H., KIM, J. J., GRELSAMER, R. P. & MOW, V. C. 1997. Finite deformation biphasic material properties of bovine articular cartilage from confined compression experiments. *J Biomech,* 30, 1157-64.

BARTEL, D., BICKNELL, V. & WRIGHT, T. 1986. The effect of conformity, thickness, and material on stresses in ultra-high molecular weight components for total joint replacement. *J Bone Joint Surg Am,* 68, 1041-1051.

BARTEL, D. L., BURSTEIN, A. H., TODA, M. D. & EDWARDS, D. L. 1985. The Effect of Conformity and Plastic Thickness on Contact Stresses in Metal-Backed Plastic Implants. *Journal of Biomechanical Engineering,* 107, 193-199.

BARTONÍCEK, J. 2001. Pauwels' Classification of Femoral Neck Fractures: Correct Interpretation of the Original. *Journal of Orthopaedic Trauma,* 15, 358-360.

BASALO, I. M., CHEN, F. H., HUNG, C. T. & ATESHIAN, G. A. 2006. Frictional response of bovine articular cartilage under creep loading following proteoglycan digestion with chondroitinase ABC. *J Biomech Eng,* 128, 131-4.

BASALO, I. M., MAUCK, R. L., KELLY, T. A., NICOLL, S. B., CHEN, F. H., HUNG, C. T. & ATESHIAN, G. A. 2004. Cartilage interstitial fluid load support in unconfined compression following enzymatic digestion. *J Biomech Eng,* 126, 779-86.

BASALO, I. M., RAJ, D., KRISHNAN, R., CHEN, F. H., HUNG, C. T. & ATESHIAN, G. A. 2005. Effects of enzymatic degradation on the frictional response of articular cartilage in stress relaxation. *J Biomech,* 38, 1343-9.

BATEMAN, J. E. 1974. Single-assembly total hip-prosthesis - preliminary report. *Orthop. Dig.,* 2, 15-22.

BATEMAN, J. E. 1977. Experience with a multi-bearing implant in reconstruction for hip deformities. *journal of orthopaedic transactions,* 1, 242.

BAUDOIN, C., FARDELLONE, P., BEAN, K., OSTERTAG-EZEMBE, A. & HERVY, F. 1996. Clinical outcomes and mortality after hip fracture: A 2-year follow-up study. *Bone,* 18, S149-S157.

BAY, B. K., HAMEL, A. J., OLSON, S. A. & SHARKEY, N. A. 1997. Statically equivalent load and support conditions produce different hip joint contact pressures and periacetabular strains. *Journal of Biomechanics,* 30, 193-196.

BECKENBAUGH, R., TRESSELER, H. & JOHNSON, E. J. 1977. Results after hemiarthroplasty of the hip using a cemented femoral prosthesis. A review of 109 cases with an average follow-up of 36 months. *Mayo Clinic Proceedings, Mayo Clinic,* 52, 349-53.

BELL, C. J., CARRICK, L. M., KATTA, J., JIN, Z., INGHAM, E., AGGELI, A., BODEN, N., WAIGH, T. A. & FISHER, J. 2006a. Self-assembling peptides as injectable lubricants for osteoarthritis. *Journal of Biomedical Materials Research Part A,* 78A, 236-246.

BELL, C. J., INGHAM, E. & FISHER, J. 2006b. Influence of hyaluronic acid on

the time-dependent friction response of articular cartilage under different conditions. *Proc Inst Mech Eng [H],* 220, 23-31.

BENYA, P. D., QIAO, B. & PADILLA, S. R. Year. Synthesis of superficial zone protein/lubricin is synergistically stimulated by TGF-ß and adenoviral expression of TAK1A in rabbit articular chondrocytes. *In:* 49th annual meeting of the ORS, 2002. 0135.

BERGLUND-RÖDÉN, M., SWIERSTRA, B. A., WINGSTRAND, H. & THORNGREN, K.-G. 1994. Prospective comparison of hip fracture treatment: 856 cases followed for 4 months in The Netherlands and Sweden. *Acta Orthopaedica,* 65, 287-294.

BERGMANN, G., DEURETZBACHER, G., HELLER, M., GRAICHEN, F., ROHLMANN, A., STRAUSS, J. & DUDA, G. N. 2001. Hip contact forces and gait patterns from routine activities. *Journal of Biomechanics,* 34, 859-871.

BERGMANN, G., GRAICHEN, F. & ROHLMANN, A. 1993. Hip joint loading during walking and running, measured in two patients. *Journal of Biomechanics,* 26, 969-990.

BHATTACHARYYA, T. & KOVAL, K. J. 2009. Unipolar Versus Bipolar Hemiarthroplasty for Femoral Neck Fractures: Is There a Difference? *Journal of Orthopaedic Trauma,* 23, 426-427 10.1097/BOT.0b013e3181adb057.

BHULLER, G. S. 1982. Use of the Giliberty Bipolar Endoprosthesis in Femoral Neck Fractures. *Clinical Orthopaedics and Related Research,* 162, 165-169.

BILGEN, F., KARAEMINOGULLARI, O., LEK & IOGLU, A. 2000. Results of Conversion Total Hip Prosthesis Performed Following Painful Hemiarthroplasty. *The Journal of International Medical Research,* 28, 307-312.

BIOLOX, D. 2008. BIOLOX®* delta OPTION Ceramic Femoral Head - Data sheet / surgical techanique.

BOCHNER, R., PELLICCI, P. & LYDEN, J. 1988. Bipolar hemiarthroplasty for fracture of the femoral neck. *the journal of bone and joint surgery,* 70-A, 1001-1010.

BOS, I., MEUWSSEN, E., HENßGE, E. & LÖHRS, U. 1991. Unterschiede des Polyäthylenabriebs bei Hüftgelenkprothesen mit Keramikund Metall-Polyäthylenpaarung der Gleitflächen. *Z Orthop,* 129, 507-515.

BOSCHETTI, F., PENNATI, G., GERVASO, F., PERETTI, G. M. & DUBINI, G. 2004. Biomechanical properties of human articular cartilage under compressive loads. *Biorheology,* 41, 159-66.

BOWDEN, F. T., D 1964. *The friction and lubrication of solids*, Oxford University Press.

BROCKETT, C. 2007. Tribology of large diameter metal-on-metal hip resurfacing replacements. PhD, Leeds.

BROCKETT, C., HARPER, P., WILLIAMS, S., ISAAC, G., DWYER-JOYCE, R., JIN, Z. & FISHER, J. 2008. The influence of clearance on friction, lubrication and squeaking in large diameter metal-on-metal hip replacements. *Journal of Materials Science: Materials in Medicine,* 19, 1575-1579.

BROOM, N. D., OLOYEDE, A., FLACHSMANN, R. & HOWS, M. 1996. Dynamic fracture characteristics of the osteochondral junction undergoing shear deformation. *Medical Engineering & Physics,* 18, 396-404.

BRUETON, R. N., CRAIG, J. S. J. & HINVES, B. L. 1987. A study of 75 two-component hemi-arthroplasties. Do they behave as Thompson's, total hips or true bi-polar prostheses? *Journal of Bone Joint Surgery,* 69, 488.

BRUETON, R. N., CRAIG, J. S. J., HINVES, B. L. & HEATLEY, F. W. 1993. Effect of femoral component head size on movement of the two-component hemi-arthroplasty. *Injury,* 24, 231-235.

CALIGARIS, M. & ATESHIAN, G. A. 2008. Effects of sustained interstitial fluid pressurization under migrating contact area, and boundary lubrication by synovial fluid, on cartilage friction. *Osteoarthritis and Cartilage,* 16, 1220-1227.

CALLAGHA, J. J., ROSENBERG, A. G. & RUBASH, H. E. 2004. *The Adult Hip,* Lippincott Williams & Wilkins.

CALTON, T. F., FEHRING, T. K., GRIFFIN, W. L. & MCCOY, T. H. 1998. Failure of the Polyethylene after Bipolar Hemiarthroplasty of the Hip. A Report of Five Cases. *J Bone Joint Surg Am,* 80, 420-3.

CAMERON, H. 1991. Ceramic head implantation failures. *Journal of Arthroplasty,* 6, 185-8.

CANTU, R. V. 2004. Unipolar versus Bipolar Arthroplasty. *Techniques in Orthopaedics,* 19, 138-142.

CAREY-BETH, J. & TIMOTHY, L. 2001. A Review of Articular Cartilage Pathology and the Use of Glucosamine Sulfate. *Journal of Athletic Training,* 36, 413-419.

CARTER, M. J., BASALO, I. M. & ATESHIAN, G. A. 2007. The temporal response of the friction coefficient of articular cartilage depends on the contact area. *Journal of Biomechanics,* 40, 3257-3260.

CHAKRAVARTHY, J., MANGAT, K., QURESHI, A. & PORTER, K. 2007. Postoperative radiographs following hip fracture surgery. Do they influence patient management? *International Journal of Clinical Practice,* 61, 421-424.

CHAPPIUS, J., SHERMAN, I. A. & NEUMANN, A. W. 1983. Surface tension of animal cartilage as it relates to friction in joints. *Annals of Biomed. Eng.,* 11, 435-449.

CHARNLEY, J. & HALLEY, D. K. 1975. Rate of wear in total hip replacement. *Clin Orthop,* 112, 170-179.

CHARNLEY, J. 1959. The lubrication of animal joints. *Inst. Mech. Eng. London,,* Proc. Symp. Biomech.,, pp.12-22.

CHEN, S. C., SARKAR, S. & PELL, L. H. 1980. A radiological study of the movements of the two components of the Monk prosthesis (hard-top [']duo-pleet') in patients. *Injury,* 12, 243-249.

CHIANG, E. H., LAING, T. J., MEYER, C. R., BOES, J. L., RUBIN, J. M. & ADLER, R. S. 1997. Ultrasonic characterization of in vitro osteoarthritic articular cartilage with validation by confocal microscopy. *Ultrasound Med Biol,* 23, 205-13.

CHRISTIANSEN, T. 1969. Christiansen, A new hip prosthesis with trunnion-bearing. *Acta Chri Scand,* 135, 43.

CHRISTIE, J., BURNETT, R., POTTS, H. & PELL, A. 1994. Echocardiography of transatrial embolism during cemented and uncemented hemiarthroplasty of the hip. *J Bone Joint Surg Br,* 76-B, 409-412.

CILINGIR, A. C., UCAR, V., UDOFIA, I. J. & JIN, Z. M. 2008. Biphasic Finite Element Modelling of Contact Mechanics of Hemi-arthroplasty of Human Hip Joint. Part II: Polycarbonate Urethane on Cartilage Contact. *Trends Biomater. Artif. Organs, ,* 22, 65-72 (2).

CLARKE, I. C., CONTINI, R. & KENEDI, R. M. 1975. Friction and wear studies of articular cartilage: a scanning electron microscope study. *J. Lub. Tech,* 97, 358-368.

COLLIER, J. P., MAYOR, M. B., SURPRENANT, V. A., SURPRENANT, H. P., DAUPHINAIS, L. A. & JENSEN, R. E. 1990. The Biomechanical Problems of Polyethylene as a Bearing Surface. *Clinical Orthopaedics and Related Research,* 261, 107-113.

COOK, S. D., SKINNER, H. B., WEINSTEIN, A. M., LAVERNIA, C. J. & MIDGETT, R. J. 1982. The Mechanical Behavior of Normal and Osteoporotic Canine Femora before and after Hemiarthroplasty. *Clinical Orthopaedics and Related Research,* 170, 303-312.

COOK, S. D., THOMAS, K. A. & KESTER, M. A. 1989. Wear characteristics of the canine acetabulum against different femoral prostheses. *J Bone Joint Surg Br,* 71-B, 189-197.

COOPER, C., CAMPION, G. & MELTON, L. J. 1992. Hip fractures in the elderly: A world-wide projection. *Osteoporosis International,* 2, 285-289.

COSSEY, A. J. & GOODWIN, M. I. 2002. Failure of Austin Moore hemiarthroplasty: total hip replacement as a treatment strategy. *Injury,* 33, 19-21.

CRUESS, R., KWOK, D., DUC, P., LECAVALIER, M. & DANG, G. 1984. The response of articular cartilage to weight-bearing against metal. A study of hemiarthroplasty of the hip in the dog. *J Bone Joint Surg Br,* 66-B, 592-597.

CUMMINGS, S. R., BLACK, D. M. & RUBIN, S. M. 1989. Lifetime Risks of Hip, Colles', or Vertebral Fracture and Coronary Heart Disease Among White Postmenopausal Women. *Arch Intern Med,* 149, 2445-2448.

D'ARCY, J. & DEVAS, M. 1976. Treatment of fractures of the femoral neck by replacement with the Thompson prosthesis. *J Bone Joint Surg Br,* 58-B, 279-286.

DAWIHL, W. & DÖRRE, E. 1980. The adsorption behavior of high purity alumina ceramics exposed to fluids. *Biomedizinische Technik. Biomedical engineering,* 25, 315-319.

DAWIHL, W., MITTELMEIER, H., DÖRRE, E. & AL, E. 1979. Tribology of aluminium oxide ceramic hip joint endoprostheses. *MOT* 99, 114-118.

DÉMARTEAU, O., PILLET, L., INAEBNIT, A., BORENS, O. & QUINN, T. M. 2006. Biomechanical characterization and in vitro mechanical injury of elderly human femoral head cartilage: comparison to adult bovine humeral head cartilage. *Osteoarthritis and Cartilage,* 14, 589-596.

DEVAS, M. & HINVES, B. 1983. Prevention of acetabular erosion after hemiarthroplasty for fractured neck of femur. *J Bone Joint Surg Br,* 65-B, 548-551.

DISILVESTRO, M. R. & SUH, J. K. 2002. Biphasic poroviscoelastic characteristics of proteoglycan-depleted articular cartilage: simulation of degeneration. *Ann Biomed Eng,* 30, 792-800.

DOWSON, D. 2001. New joints for the Millennium: wear control in total replacement hip joints. *Proceedings of the Institution of Mechanical Engineers, Part H: Journal of Engineering in Medicine,* 215, 335-358.

DOWSON, D. & JIN, Z. M. 1986. Micro-elastohydrodynamic lubrication of synovial joints. *Eng Med,* 15, 63-5.

DOWSON, D., WRIGHT, V. & LONGFIELD, M. 1969. Human joint lubrication. *Biomed Eng,* 4, 160-5.

EL-ABED, K., MCGUINNESS, A., BRUNNER, J., DALLOVEDOVA, P., O'CONNOR, P. & KENNEDY, J. G. 2005. Comparison of outcomes following uncemented hemiarthroplasty and dynamic hip screw in the treatment of displaced subcapital hip fractures in patients aged greater than 70 years. *Acta Orthop. Belg.,* ,

71, 48-54.

FAGERSON, T. L., KREBS, D. E., HARRIS, B. A. & MANN, R. W. 1995. Examining Shibboleths of Hip Rehabilitation Protocols Using in vivo Contact Pressures from an Instrumented Hemiarthroplasty. *Physiotherapy,* 81, 533-540.

FERRANDEZ, W., GRAINDORGE, S. L., FISHER, J., JIN, Z. M., TWIGG, P., GRANT, C. A. & INGHAM, E. Year. Biphasic surface layer lubrication of cartilage, surface characterization. *In:* 50th Annual meeting of ORS, 2004 San Francisco. 0526.

FIGVED, W., OPLAND, V., FRIHAGEN, F., JERVIDALO, T., MADSEN, J. & NORDSLETTEN, L. 2009. Cemented versus Uncemented Hemiarthroplasty for Displaced Femoral Neck Fractures. *Clinical Orthopaedics and Related Research®,* 467, 2426-2435.

FIRKINS, P. J., TIPPER, J. L., INGHAM, E., STONE, M. H., FARRAR, R. & FISHER, J. 2001. A novel low wearing differential hardness, ceramic-on-metal hip joint prosthesis. *Journal of Biomechanics,* 34, 1291-1298.

FISHER, J. 2001. *Modern Tribology Handbook,* Coca Roton, London, New York, Washington, D.C., CRC Press.

FLACHSMANN, R., BROOM, N. D. & HARDY, A. E. 2001. Deformation and rupture of the articular surface under dynamic and static compression. *Journal of Orthopaedic Research,* 19, 1131-1139.

FORSTER, H. & FISHER, J. 1996. The influence of loading time and lubricant on the friction of articular cartilage. *Proc Inst Mech Eng [H],* 210, 109-19.

FORSTER, H. & FISHER, J. 1999. The influence of continuous sliding and subsequent surface wear on the friction of articular cartilage. *Proc Inst Mech Eng [H],* 213, 329-45.

FORSTER, H., FISHER, J., DOWSON, D. & WRIGHT, V. 1995. The effect of stationary loading on the friction and boundary lubrication of articular cartilage in the mixed lubrication regime. *In:* D. DOWSON, C. M. T. T. H. C. C. & DALMAZ, G. (eds.) *Tribology Series.* Elsevier.

FOSTER, A. P., THOMPSON, N. W., WONG, J. & CHARLWOOD, A. P. 2005. Periprosthetic femoral fractures - a comparison between cemented and uncemented hemiarthroplasties. *Injury,* 36, 424-429.

FRANKLIN, A. & GALLANNAUGH, S. C. 1983. The bi-articular hip prosthesis for fractures of the femoral neck--a preliminary report. *Injury,* 15, 159-162.

FREEMAN, M. A. R. 1979. *Adult Articular Cartilage,* Kent, Pitman Medical Publishing Co Ltd.

FREEMAN, M. E., FUREY, M. J., LOVE, B. J. & HAMPTON, J. M. 2000. Friction, wear, and lubrication of hydrogels as synthetic articular cartilage. *Wear,* 241, 129-135.

GAINE, W. J., SANVILLE, P. R. & BAMFORD, D. J. 2000a. The Charnley-Hastings bipolar prosthesis in femoral neck fractures --: a study of dynamic motion. *Injury,* 31, 257-263.

GAINE, W. J., SANVILLE, P. R. & BAMFORD, D. J. 2000b. The Charnley–Hastings bipolar prosthesis in femoral neck fractures —: a study of dynamic motion. *Injury,* 31, 257-263.

GARDEN, R. S. 1964. STABILITY AND UNION IN SUBCAPITAL FRACTURES OF THE FEMUR. *J Bone Joint Surg Br,* 46-B, 630-647.

GEIGER, F., ZIMMERMANN-STENZEL, M., HEISEL, C., LEHNER, B. &

DAECKE, W. 2007. Trochanteric fractures in the elderly: the influence of primary hip arthroplasty on 1-year mortality. *Archives of Orthopaedic and Trauma Surgery,* 127, 959-966.

GILBERTY, R. P. 1974. A new concept of bipolar endoprosthesis. *Orthopaedic Review,* 3, 40-45.

GILIBERTY, R. 1977. Low friction bipolar hip endoprosthesis. *International Surgery,* 62, 38-41.

GILIBERTY, R. P. 1983. Hemiarthroplasty of the Hip Using a Low-friction Bipolar Endoprosthesis. *Clinical Orthopaedics and Related Research,* 175, 86-92.

GINGRAS, M., CLARKE, J. & MCCOLLISTE ERVARTS, C. 1980. Prosthetic Replacement in Femoral Neck Fractures. *Clinical Orthopaedics & Related Research,* 152, 147-57.

GONG, J. P. & OSADA, Y. 2002. Surface friction of polymer gels. *Progress in Polymer Science,* 27, 3-38.

GPS ISO 11562 - 1996. Surface texture: Profile method Metrological characteristics of phase correct filters. Geometric Product Specifications

GRAINDORGE, S. 2006. Unicondylar Hemiarthroplasty Friction Simulator.

GRAINDORGE, S., FERRANDEZ, W., INGHAM, E., JIN, Z., TWIGG, P. & FISHER, J. 2006. The role of the surface amorphous layer of articular cartilage in joint lubrication. *Proc Inst Mech Eng [H],* 220, 597-607.

GRAINDORGE, S., FERRANDEZ, W., JIN, Z., INGHAM, E., GRANT, C., TWIGG, P. & FISHER, J. 2005. Biphasic surface amorphous layer lubrication of articular cartilage. *Medical Engineering & Physics,* 27, 836-844.

GRAINDORGE, S. L., JIN, Z. M., FISHER, J., FERRANDEZ, W., TWIGG, P., GRANT, C. A. & INGHAM, E. Year. Biphasic amorphous surface layer lubrication of articular cartilage under dynamic loading condtions. *In:* 50th annual meeting of the ORS, 2004 san francisco.

GRIFFITH, M. J., SEIDENSTEIN, M. K., WILLIAMS, D. & CHARNLEY, J. 1978. Socket Wear in Charnley Low Friction Arthroplasty of the Hip. *Clin Orthop,* 137, 37-47.

GU, W. Y., LAI, W. M. & MOW, V. C. 1997. A triphasic analysis of negative osmotic flows through charged hydrated soft tissues. *Journal of Biomechanics,* 30, 71-78.

GU, W. Y., LAI, W. M. & MOW, V. C. 1998. A Mixture Theory for Charged-Hydrated Soft Tissues Containing Multi-electrolytes: Passive Transport and Swelling Behaviors. *Journal of Biomechanical Engineering,* 120, 169-180.

GUILAK, F., RATCLIFFE, A., LANE, N., ROSENWASSER, M. P. & MOW, V. C. 1994. Mechanical and biochemical changes in the superficial zone of articular cartilage in canine experimental osteoarthritis. *Journal of Orthopaedic Research,* 12, 474-484.

GULLBERG, B., JOHNELL, O. & KANIS, J. A. 1997. World-wide Projections for Hip Fracture. *Osteoporosis International,* 7, 407-413.

HAK, D. J., HAMEL, A. J., BAY, B. K., SHARKEY, N. A. & OLSON, S. A. 1998. Consequences of Transverse Acetabular Fracture Malreduction on Load Transmission Across the Hip Joint. *Journal of Orthopaedic Trauma,* 12, 90-100.

HARJEET, S., SUHAIL, A., SHAHRIL, Y., MASBAH, O. & SUBANESH, S. 2009. Outcome of Traumatic Intracapsular Neck of Femur Fractures in Patients Aged Above 60 Years Treated by Hemiarthroplasty. *Malaysian Orthopaedic Journal,* 3,

24-7.

HARRIS, W., RUSHFELDT, P., CARLSON, C., SCHOLLER, J. & MANN, R. 1975. Pressure distribution in the hip and selection of hemi-arthroplasty; The Hip. *Proceedings of the Third Open Scientific Meeting of the Hip Society St. Louis: CV Mosby.*

HEYSE-MOORE, H., MACEACHERN, A. G. & EVANS, D. C. J. 1983. Treatment of intertrochanteric fractures of the femur: a comparison of the Richard's screw-plate with the Jewett nail-plate. *Journal of Bone and Joint Surgery America,* 65, 262.

HINCHEY, J. & DAY, P. 1964. Primary Prosthetic Replacement in Fresh Femoral-Neck Fractures: A REVIEW OF 294 CONSECUTIVE CASES. *J Bone Joint Surg Am,* 46, 223-334.

HIPP, J., SUGANO, N., MILLIS, M. & MURPHY, S. 1999. Planning acetabular redirection osteotomies based on joint contact pressures. *Clin Orthop Relat Res,* 364, 134-43.

HODGE, W. A., FIJAN, R. S., CARLSON, K. L., BURGESS, R. G., HARRIS, W. H. & MANN, R. W. 1985. Contact pressures in the human hip joint measured in vivo. *Biophysics,* 83, 2879-2883.

HUNTER, G. 1974. A further comparison of the use of internal fixation and prosthetic replacement for fresh fractures of the neck of the femur. *British Journal of Surgery,* 61, 382-384.

IKEUCHI, K., OKA, M. & KUBO, S. 1994. The relation between friction and creep deformation in articular cartilage, Elsevier Science B.V.

IPAVEC, M., BRAND, R. A., PEDERSEN, D. R., MAVCIC, B., KRALJ-IGLIC, V. & IGLIC, A. 1999. Mathematical modelling of stress in the hip during gait. *Journal of Biomechanics,* 32, 1229-1235.

JALOVAARA, P., BERGLUND-RÖDÉN, M., WINGSTRAND, H. & THORNGREN, K.-G. 1992. Treatment of hip fracture in Finland and Sweden -- Prospective comparison of 788 cases in three hospitals. *Acta orthopaedica Scandinavica,* 63, 531 - 535.

JAY, G. D., HABERSTROH, K. & CHA, C. J. 1998. Comparison of the boundary-lubricating ability of bovine synovial fluid, lubricin, and Healon. *J Biomed Mater Res,* 40, 414-8.

JENSEN, J. S., TØNDEVOLD, E. & MOSSING, N. 1978. Unstable Trochanteric Fractures Treated with the Sliding Screw-Plate System: A Biomechanical Study of Unstable Trochanteric Fractures III. *Acta orthopaedica Scandinavica,* 49, 392 - 397.

JIN, Z. M., PICKARD, J. E., FORSTER, H., INGHAM, E. & FISHER, J. 2000. Frictional behaviour of bovine articular cartilage. *Biorheology,* 37, 57-63.

JONES, E. S. 1934. *Joint Lubrication*, The Lancet.

JORDAN, K. M. & COOPER, C. 2002. Epidemiology of osteoporosis. *Best Practice & Research Clinical Rheumatology,* 16, 795-806.

JUNG, M., WIELOCH, P., LORENZ, H., GOTTERBARM, T., VEYEL, K., DANIELS, M., MARTINI, A. K. & DAECKE, W. 2007. Comparison of Cobalt Chromium, Ceramic and Pyrocarbon Hemiprostheses in a Rabbit Model: Ceramic Leads to More Cartilage Damage Than Cobalt Chromium. *Journal of Biomedical Materials Research.*

KACZMAREK, M., WALKE, W. & KAJZER, W. 2007. Chemical composition of passive layers formed on metallic biomaterials. *Archives of Materials Science and*

Engineering, 28, 273-276.

KALTSAS, D. S. & KLUGMAN, D. J. 1986. Acetabular erosion: a comparison between the Austin Moore and Monk hard top prostheses. *Injury,* 17, 230-236.

KANIS, J. A. & MCCLOSKEY, E. V. 1996. Evaluation of the risk of hip fracture. *Bone,* 18, S127-S132.

KATTA, J. 2007. Self-assembling Peptide Networks for Treatment of Cartilage Degenerative Diseases. PhD, Leeds.

KATTA, J., JIN, Z., INGHAM, E. & FISHER, J. 2007a. P163 Chondroitin sulfate: An effective joint lubricant for articular cartilage. *Osteoarthritis and Cartilage,* 15, B129-B129.

KATTA, J., JIN, Z., INGHAM, E. & FISHER, J. 2008a. Biotribology of articular cartilage--A review of the recent advances. *Medical Engineering & Physics,* 30, 1349-1363.

KATTA, J., JIN, Z., INGHAM, E. & FISHER, J. 2008b. Effect of nominal stress on the long term friction, deformation and wear of native and glycosaminoglycan deficient articular cartilage. *Osteoarthritis and Cartilage,* In Press, Corrected Proof.

KATTA, J., PAWASKAR, S., JIN, Z., INGHAM, E. & FISHER, J. 2007b. Effect of load variation on the friction properties of articular cartilage. *Proceedings of the Institution of Mechanical Engineers, Part J: Journal of Engineering Tribology,* 221, 175-181.

KEENE, G. S., PARKER, M. J. & PRYOR, G. A. 1993. Mortality and morbidity after hip fractures. *British Medical Journal,* 307, 1248-1250.

KELKAR, R. & ATESHIAN, G. A. 1999. Contact Creep of Biphasic Cartilage Layers. *Journal of Applied Mechanics,* 66, 137-145.

KENZORA, J. E., MAGAZINER, J., HUDSON, J., HEBEL, J. R., YOUNG, Y., HAWKES, W., FELSENTHAL, G., ZIMMERMAN, S. I. & PROVENZANO, G. 1998. Outcome After Hemiarthroplasty for Femoral Neck Fractures in the Elderly. . *Clinical Orthopaedics & Related Research,* 348, 51-58.

KERIN, A. J., COLEMAN, A., WISNOM, M. R. & ADAMS, M. A. 2003. Propagation of surface fissures in articular cartilage in response to cyclic loading in vitro. *Clinical Biomechanics,* 18, 960-968.

KHAN, R. J. K., MACDOWELL, A., CROSSMAN, P. & KEENE, G. S. 2002. Cemented or uncemented hemiarthroplasty for displaced intracapsular fractures of the hip--a systematic review. *Injury,* 33, 13-17.

KIM, S.-Y., KIM, Y.-G. & HWANG, J.-K. 2005. Cementless Calcar-Replacement Hemiarthroplasty Compared with Intramedullary Fixation of Unstable Intertrochanteric Fractures. A Prospective, Randomized Study. *J Bone Joint Surg Am,* 87, 2186-2192.

KNAHR, K., SALZER, M., PLENK JR, H., GRUNDSCHOBER, F. & RAMACH, W. 1981. Experience with bioceramic implants in orthopaedic surgery. *Biomaterials,* 2, 98-104.

KOBAYASHI, M., TOGUCHIDA, J. & OKA, M. 2001. Study on the lubrication mechanism of natural joints by confocal laser scanning microscopy. *J Biomed Mater Res,* 55, 645-51.

KOFOED, H. & KOFOD, J. 1983. Moore prosthesis in the treatment of fresh femoral neck fractures. A critical review with special attention to secondary acetabular degeneration. *Injury,* 14, 531-40.

KORHONEN, R. K., LAASANEN, M. S., TÖYRÄS, J., RIEPPO, J., HIRVONEN,

J., HELMINEN, H. J. & JURVELIN, J. S. 2002a. Comparison of the equilibrium response of articular cartilage in unconfined compression, confined compression and indentation. *Journal of Biomechanics,* 35, 903-909.

KORHONEN, R. K., WONG, M., AROKOSKI, J., LINDGREN, R., HELMINEN, H. J., HUNZIKER, E. B. & JURVELIN, J. S. 2002b. Importance of the superficial tissue layer for the indentation stiffness of articular cartilage. *Medical Engineering & Physics,* 24, 99-108.

KRIKLER, S. & SCHATZKER, J. 1995. Ceramic head failure. *The Journal of Arthroplasty,* 10, 860-862.

KRISHNAN, H., YOON, T. & PARK, K. 2010. Bipolar Hemiarthroplasty in Elderly Patients Presenting With Displaced Intracapsular Femoral Neck Fractures - A Comparison of Cemented and Uncemented Prosthesis Placement. *Malaysian Orthopaedic Journal,* 4, 26-31.

KRISHNAN, R., CALIGARIS, M., MAUCK, R. L., HUNG, C. T., COSTA, K. D. & ATESHIAN, G. A. 2004a. Removal of the superficial zone of bovine articular cartilage does not increase its frictional coefficient. *Osteoarthritis and Cartilage,* 12, 947.

KRISHNAN, R., KOPACZ M & GA., A. 2004b. Experimental verification of the role of interstitial fluid pressurization in cartilage lubrication. *Journal of Orthopaedic Research,* 22, 565-570.

KRISHNAN, R., MARINER, E. N. & ATESHIAN, G. A. 2005. Effect of dynamic loading on the frictional response of bovine articular cartilage. *Journal of Biomechanics,* 38, 1665-1673.

KYOUNG HO, M., JUN SOON, K., TONG JOO, L., SANG HYEOP, L., SUNG WOOK, C. & MAN HEE, W. 2008. Degeneration of Acetabular Articular Cartilage to Bipolar Hemiarthroplasty. *Yonsei Med J,* 49, 719-724.

LADE, R., SAUER, B. & DOERRE, E. 1983. Long term performance of hig purity aluminium oxide ceramic heads in canine endoprothetic hip replacement. *In:* P, V. (ed.) *Ceramic in Surgery, Processding of the 2nd International Symposium on Bioceramics (2nd BIOSIMP) - Special session of the 5th International Meeting on Modern Ceramics Technologies.* Lignano Sabbiadoro, Italy: Elviser Science Publ, Amsterdam, Neth.

LAI, W. M., HOU, J. S. & MOW, V. C. 1991. A Triphasic Theory for the Swelling and Deformation Behaviors of Articular Cartilage. *Journal of Biomechanical Engineering,* 113, 245-258.

LANYON, P., MUIR, K., DOHERTY, S. & DOHERTY, M. 2003. Age and sex differences in hip joint space among asymptomatic subjects without structural change: Implications for epidemiologic studies. *Arthritis & Rheumatism,* 48, 1041-1046.

LESTRANGE, N. R. M. D. 1990. Bipolar Arthroplasty for 496 Hip Fractures. *Clinical Orthopaedics & Related Research February,* 251, 7-19.

LEVICK, J. R. 1979. The influence of hydrostatic pressure on trans-synovial fluid movement and on capsular expansion in the rabbit knee. *J Physiol,* 289, 69-82.

LEWIS, P. R. & MCCUTCHEN, C. W. 1959. Experimental evidence for weeping lubrication in mammalian joints. *Nature,* 184, 1285.

LINN, F. C. 1968. Lubrication of animal joints II. The mechanism. *J. Biomechanics,* 1, 193-205.

LIPSHITZ, H., ETHEREDGE, R., 3RD & GLIMCHER, M. J. 1975. In vitro wear of articular cartilage. *J Bone Joint Surg Am,* 57, 527-34.

LITTLE, T., FREEMAN, M. A. R. & SWANSON, S. A. R. 1969. *Experiments on friction in the human hip joint* London, Wright, V. (ed.). Sector.

LU-YAO, G., KELLER, R., LITTENBERG, B. & WENNBERG, J. 1994. Outcomes after displaced fractures of the femoral neck. A meta-analysis of one hundred and six published reports. *J Bone Joint Surg Am,* 76, 15-25.

MABUCHI, K., TSUKAMOTO, Y., OBARA, T. & YAMAGUCHI, T. 1994. The effect of additive hyaluronic acid on animal joints with experimentally reduced lubricating ability. *J Biomed Mater Res,* 28, 865-70.

MACCONAILL, M. 1932. The function of inter-articular fibrocartilages, with special references to the knee and inferior radio-ulnar joints. *J Anat,* 66, 210-27.

MACIROWSKI, T., TEPIC, S. & MANN, R. W. 1994. Cartilage Stresses in the Human Hip Joint. *Journal of Biomechanical Engineering,* 116, 10-18.

MAINDS, C. C. & NEWMAN, R. J. 1989. Implant failures in patients with proximal fractures of the femur treated with a sliding screw device. *Injury,* 20, 98-100.

MAISTRELLI, G., SESSA, V. & FORNASIER, V. 1991. Response of the articular cartilage to weight-bearing: comparison of hemiarthroplasty with ceramic and cobalt-chromium head in dogs. *Italian journal of orthopaedics and trumatology,* 17, 387-93.

MALCOM, L. L. 1976. An experimental investigation of the frictional and deformational response of articular cartilage interfaces to static and dynamic loading. PhD, University of California,.

MALHOTRA, R., ARYA, R. & BHAN, S. 1995. Bipolar hemiarthroplasty in femoral neck fractures. *Archives of Orthopaedic and Trauma Surgery,* 114, 79-82.

MANKIN, H. J. 1974. The Reaction of Articular Cartilage to Injury and Osteoarthritis. *New England Journal of Medicine,* 291, 1285-1292.

MARCUS, R. E., HEINTZ, J. J. & PATTEE, G. A. 1992. Don't throw away the austin moore. *The Journal of Arthroplasty,* 7, 31-36.

MATS, B., PAOLO, A., RALPH, G., LASZLO, H., HANS, J. H., ROLAND, P. J., DAVID, L., STEFAN, L., BERT, R. M., LARS, P. & HANS-ULRICH, S. 2000. ICRS Cartilage Injury Evaluation Package.

MAUTALEN, C. A., VEGA, E. M. & EINHORN, T. A. 1996. Are the etiologies of cervical and trochanteric hip fractures different? *Bone,* 18, S133-S137.

MAXIAN, T. A., BROWN, T. D. & WEINSTEIN, S. L. 1995. Chronic stress tolerance levels for human articular cartilage: Two nonuniform contact models applied to long-term follow-up of CDH. *Journal of Biomechanics,* 28, 159-166.

MCCANN, L. 2009. Tribological Investigation of Articular Cartilage Substitution in the Medial Compartmental Knee. PhD, Leeds.

MCCANN, L., INGHAM, E., JIN, Z. & FISHER, J. 2009. An investigation of the effect of conformity of knee hemiarthroplasty designs on contact stress, friction and degeneration of articular cartilage: A tribological study. *Journal of Biomechanics,* 42, 1326-1331.

MCCANN, L., UDOFIA, I., GRAINDORGE, S., INGHAM, E., JIN, Z. & FISHER, J. 2008. Tribological testing of articular cartilage of the medial compartment of the knee using a friction simulator. *Tribology International,* 41, 1126-1133.

MCCUTCHEN, C. W. 1959. Mechanism of Animal Joints: Sponge-hydrostatic and Weeping Bearings. *Nature,* 184, 1284-1285.

MCCUTCHEN, C. W. 1962. The frictional properties of animal joints. *Wear,* 5, 1-17.

MCGIBBON, C. A., KREBS, D. E., TRAHAN, C. A., TRIPPEL, S. B. & MANN, R. W. 1999. Cartilage degeneration in relation to repetitive pressure: Case study of a unilateral hip hemiarthroplasty patient. *The Journal of Arthroplasty,* 14, 52-58.

MCGRORY, B. & LAWHEAD, B. 2005. Bipolar femoral neck-cup impingement observed on radiographic examination: report of a case. *Journal of Surgical Orthopaedics Advances,* 14, 96-8.

MCLEISH, R. D. & CHARNLEY, J. 1970. Abduction forces in the one-legged stance. *Journal of Biomechanics,* 3, 191-194, IN7-IN9, 195-209.

MESSIEH, M., MATTINGLY, D. A., TURNER, R. H., SCOTT, R., FOX, J. & SLATER, J. 1994. Wear debris from bipolar femoral neck-cup impingement: A cause of femoral stem loosening. *The Journal of Arthroplasty,* 9, 89-93.

MOLLER, B. N., LUCHT, U., GRYMER, F. & BARTHOLDY, N. J. 1984. Instability of trochanteric hip fractures following internal fixation: A radiographic comparison of the Richards sliding screw-plate and the McLaughlin nail-plate. *Acta orthopaedica Scandinavica,* 55, 517 - 520.

MONK, C. J. E. Year. Treatment of subcapital fractures of the neck of the femur by replacement of the femoral head. *In:* International Congress Series, 1976. 65.

MONT, M. A., MCGRATH, M. S., ULRICH, S. D., SEYLER, T. M., MARKER, D. R. & DELANOIS, R. E. 2008. Metal-on-Metal Total Hip Resurfacing Arthroplasty in the Presence of Extra-Articular Deformities or Implants. *J Bone Joint Surg Am,* 90, 45-51.

MOORE, A. T. 1952. Metal Hip Joint: A New Self-Locking Vitallium Prosthesis. *Southern Medical Journal,* 45, 1015-1019.

MOORE, A. T. 1957. The Self-Locking Metal Hip Prosthesis. *J Bone Joint Surg Am,* 39, 811-827.

MORONI, A., FALDINI, C., PEGREFFI, F., HOANG-KIM, A., VANNINI, F. & GIANNINI, S. 2005. Dynamic Hip Screw Compared with External Fixation for Treatment of Osteoporotic Pertrochanteric Fractures. A Prospective, Randomized Study. *J Bone Joint Surg Am,* 87, 753-759.

MOTTA, F. V., BALESTRA, R. M., RIBEIRO, S. & TAGUCHI, S. P. 2004. Wetting behaviour of SiC ceramics: Part I. E2O3/Al2O3 additive system. *Materials Letters,* 58, 2805-2809.

MOW, V., PROCTOR, C. & KELLY, M. 1989. *Biomechanics of articular cartilage,* Philadelphia, Lea and Febiger.

MOW, V. C., HOLMES, M. H. & LAI, W. M. 1984. Fluid transport and mechanical properties of articular cartilage: a review. *J Biomech,* 17, 377-94.

MOW, V. C. & HUISKES, R. 2005. *Basic orthopaedic biomechanics and mechano-biology,* Philadephia, Lippincott Williams & Eilkins.

MOW, V. C. & LAI, W. M. 1980. Recent developments in synovial joint biomechanics. *SIAM Review,* 22, 275-317.

MÜLLER, L. P., DEGREIF, J., BASTEN, K., ZÖPHEL, O. & ROMMENS, P. M. 2000. Is there still an indication for operative treatment of femoral neck fractures with a ceramic hemiprosthesis? *Archives of Orthopaedic and Trauma Surgery,* 120, 299-303.

MÜLLER, L. P., DEGREIF, J., RUDIG, L., MEHLER, D., HELY, H. & ROMMENS, P. M. 2004. Friction of ceramic and metal hip hemi-endoprostheses against

cadaveric acetabula. *Archives of Orthopaedic and Trauma Surgery,* 124, 681-687.

MÜLLER, M. 1990. The AO-classification of fracture of long bones. *Springer-Verlag.* Berlin.

MÜLLER, M. E., ALLGÖWER, M., SCHENEIDER, R. & WILLENEGGER, H. 2003. *manual of internal fixation: techniques recommended by the AO-ASIF group,* Spring-Verlag.

MURAKAMI, T., OHTSUKI, N. & HIGAKI, H. 1995. *The adaptive multimode lubrication in biotribological system,* Uokohama, Japan, Tribology Conf.

NARMONEVA, D. A., WANG, J. Y. & SETTON, L. A. 1999. Nonuniform swelling-induced residual strains in articular cartilage. *Journal of Biomechanics,* 32, 401-408.

NIZARD, R., SEDEL, L., CHRISTEL, P., MEUNIER, A., SOUDRY, M. & WITVOET, J. 1992. Ten-year survivorship of cemented ceramic-ceramic total hip prosthesis. *Clinical Orthopaedics and Related Research,* 282, 53-63.

NOHUHIRO, K., HIROSHI, T. & TAKEHIKO, T. 2001. Qualitative analysis of polyethylene wear in a bipolar femoral prosthesis: A case report. *Journal of Orthopaedic Surgery,* 9, 71-76.

NORTHWOOD, E. 2007. Cartilage Wear Simulation Models for Surface and Spacer Hemiarthroplasty and Tissue Engineering. PhD, Leeds.

NORTHWOOD, E. & FISHER, J. 2007. A multi-directional in vitro investigation into friction, damage and wear of innovative chondroplasty materials against articular cartilage. *Clinical Biomechanics,* 22, 834-842.

NORTHWOOD, E., FISHER, J. & KOWALSKI, R. 2007. Investigation of the friction and surface degradation of innovative chondroplasty materials against articular cartilage. *Proceedings of the I MECH E Part H Journal of Engineering in Medicine,* 221, 263-279.

O'KELLY, F. & MCNULTY, C. 1978. Survey of patients seen in their own homes and in nursing homes in a group practive population. *Ir Med J,* 71, 621-4.

ODDING, E., VALKENBURG, H. A., ALGRA, D., VANDENOUWELAND, F. A., GROBBEE, D. E. & HOFMAN, A. 1998. Associations of radiological osteoarthritis of the hip and knee with locomotor disability in the Rotterdam Study. *Annals of the Rheumatic Diseases,* 57, 203-208.

OGUNWALE, B., SCHMIDT-OTT, A., MEEK, R. & BREWER, J. 2009. Investigating the Immunologic Effects of CoCr Nanoparticles. *Clinical Orthopaedics and Related Research®,* 467, 3010-3016.

OLOYEDE, A. & BROOM, N. D. 1991. Is classical consolidation theory applicable to articular cartilage deformation? *Clinical Biomechanics,* 6, 206-212.

ONG, B. C., MAURER, S. G., AHARONOFF, G. B., ZUCKERMAN, J. D. & KOVAL, K. J. 2002. Unipolar Versus Bipolar Hemiarthroplasty: Functional Outcome After Femoral Neck Fracture at a Minimum of Thirty-six Months of Follow-up. *Journal of Orthopaedic Trauma,* 16, 317-322.

OZTURKMEN, Y., KARAMEHMETOGLU, M., CANIKLIOGLU, M., INCE, Y. & AZBOY, I. 2008. Cementless hemiarthroplasty for femoral neck fractures in elderly patients. *Indian Journal of Orthopaedics,* 42, 866-875-2262.

PARK, S., COSTA, K. D. & ATESHIAN, G. A. 2004. Microscale frictional response of bovine articular cartilage from atomic force microscopy. *Journal of Biomechanics,* 37, 1679-1687.

PARK, S., KRISHNAN, R., NICOLL, S. B. & ATESHIAN, G. A. 2003. Cartilage Interstitial Fluid Load Support in Unconfined Compression. *journal of biomechanics,*

36, 1785-1796.

PARKER, M. 1992. Internal fixation or arthroplasty for displaced subcapital fractures in the elderly? *Injury,* 23, 521-4.

PARKER, M. I., PRYOR, G. & GURUSAMY, K. 2010. Cemented versus uncemented hemiarthroplasty for intracapsular hip fractures: A RANDOMISED CONTROLLED TRIAL IN 400 PATIENTS. *J Bone Joint Surg Br,* 92-B, 116-122.

PARKER, M. J. & PRYOR, G. A. 2000. Internal fixation or arthroplasty for displaced cervical hip fractures in the elderly: A randomised controlled trial of 208 patients. *Acta Orthopaedica,* 71, 440-446.

PARKER, M. J., PRYOR, G. A. & THORNGREN, K. 1997. *Handbook of Hip Fracture Surgery,* United Kingdom, Butterworth-Heinemann.

PARTANEN, J., JALOVAARA, P., HIRVENSALO, D. E. & SVENSSON, O. 2003. *ETIOPATHOLOGY AND TREATMENT-RELATED ASPECTS OF HIP FRACTURE.* University of Oulu.

PASZENDA, Z., TYRLIK-HELD, J. & JURKIEWICZ, W. 2008. Physical properties and haemocompatibility of passive-carbon layer. *Journal of achievements in Materials and Manufacturing Engineering,* 31, 348-355.

PAUL, J. P. 1966. Forces transmitted by joints in the human body. ARCHIVE: Proceedings of the Institution of Mechanical Engineers, Conference Proceedings 1964-1970 (vols 178-184), Various titles labelled Volumes A to S, 181, 8-15.

PAUL, J. P. 1999. Strength requirements for internal and external prostheses. *Journal of Biomechanics,* 32, 381-393.

PAWASKAR, S., JIN, Z. & FISHER, J. 2007. Modelling of fluid support inside articular cartilage during sliding. *Proceedings of the Institution of Mechanical Engineers, Part J: Journal of Engineering Tribology,* 221, 165-174.

PHILLIPS, T. W. 1989. Thompson hemiarthroplasty and acetabular erosion. *J Bone Joint Surg Am,* 71, 913-917.

PICKARD, J., INGHAM, E., EGAN, J. & FISHER, J. 1998a. Investigation into the effect of proteoglycan molecules on the tribological properties of cartilage joint tissues. *Proc Inst Mech Eng [H],* 212, 177-82.

PICKARD, J. E., FISHER, J., INGHAM, E. & EGAN, J. 1998b. Investigation into the effects of proteins and lipids on the frictional properties of articular cartilage. *Biomaterials,* 19, 1807-1812.

PUOLAKKA, T., LAINE, H., TARVAINEN, T. & AHO, H. 2001. Thompson hemiarthroplasty is superior to Ullevaal screws in treating displaced femoral neck fractures in patients over 75 years. A prospective randomized study with two-year follow-up. *Annales chirurgiae et gynaecologiae,* 90, 225-8.

RADIN, E. L., SWANN, D. A. & WEISSER, P. A. 1970. Separation of a Hyaluronate-free Lubricating Fraction from Synovial Fluid. *Nature,* 228, 377-378.

RATNER, B., HOFFMAN, A., SCHOEN, F. & LEMONS, J. (eds.) 2004. *Biomaterials Science - An Introduction to Materials in Medicine* ADEMIC PRESS

RAVIKUMAR, K. J. & MARSH, G. 2000. Internal fixation versus hemiarthroplasty versus total hip arthroplasty for displaced subcapital fractures of femur -- 13 year results of a prospective randomised study. *Injury,* 31, 793-797.

REPO, R. & FINLAY, J. 1977. Survival of articular cartilage after controlled impact. *J Bone Joint Surg Am,* 59, 1068-1076.

ROBERTS, B. J., UNSWORTH, A. & MIAN, N. 1982. Modes of lubrication in

human hip joints. *Ann Rheum Dis,* 41, 217-24.

ROBERTS, S., WEIGHTMAN, B., URBAN, J. & CHAPPELL, D. 1986a. Mechanical and biochemical properties of human articular cartilage from the femoral head after subcapital fracture. *J Bone Joint Surg Br,* 68-B, 418-422.

ROBERTS, S., WEIGHTMAN, B., URBAN, J. & CHAPPELL, D. 1986b. Mechanical and biochemical properties of human articular cartilage in osteoarthritic femoral heads and in autopsy specimens. *J Bone Joint Surg Br,* 68-B, 278-288.

RÖHRLE, H., SCHOLTEN, R., SIGOLOTTO, C., SOLLBACH, W. & KELLNER, H. 1984. Joint forces in the human pelvis-leg skeleton during walking. *Journal of Biomechanics,* 17, 409-424.

SALVATI, E. A. & WILSON, P. D. 1973. Long-Term Results of Femoral-Head Replacement. *J Bone Joint Surg Am,* 55, 516-524.

SCHAFFER, J., WILSON, M. & SCOTT, R. 1991. Capsular impingement as a source of pain following bipolar hip arthroplasty. *Journal of Arthroplasty,* 1991, 163-8.

SCHWARZ, I. M. & HILLS, B. A. 1998. Surface-active phospholipid as the lubricating component of lubricin. *Br J Rheumatol,* 37, 21-6.

SEINSHEIMER, F. 1978. Subtrochanteric fractures of the femur. *J Bone Joint Surg Am,* 60, 300-306.

SHARIF, K. M. & PARKER, M. J. 2002. Austin Moore hemiarthroplasty: technical aspects and their effects on outcome, in patients with fractures of the neck of femur. *Injury,* 33, 419-422.

SHARKEY, P. F., RAO, R., HOZACK, W. J., ROTHMAN, R. H. & CAREY, C. 1998. Conversion of hemiarthroplasty to total hip arthroplasty: Can groin pain be eliminated? *The Journal of Arthroplasty,* 13, 627-630.

SIKORSKI, J. & BARRINGTON, R. 1981. Internal fixation versus hemiarthroplasty for the displaced subcapital fracture of the femur. A prospective randomised study. *J Bone Joint Surg Br,* 63-B, 357-361.

SILYN-ROBERTS, H. & BROOM, N. D. 1990. Fracture Behaviour of Cartilage-On-Bone in Response to Repeated Impact Loading. *Connective Tissue Research,* 24, 143 - 156.

SIM, R. 1983. Displaced femoral neck fractures: the rationale for primary total hip replacement. *Proceedings of Eleventh Open Scientific Meeting for Hip Society.* St Louis: CV Mosby.

SIMON, S. 1977. New concepts in femoral head replacement: The place of the Bateman prosthesis in hip surgery. *Bulliten of the Hospital for Joint Diseases,* 38, 59-61.

SOLTZ, M. A. & ATESHIAN, G. A. 1998. Experimental verification and theoretical prediction of cartilage interstitial fluid pressurization at an impermeable contact interface in confined compression. *Journal of Biomechanics,* 31, 927-934.

SÖREIDE, O., ALHO, A. & RIETTI, D. 1980. Internal fixation versus endoprosthesis in the treatment of femoral head fractures in elderly. A prospective analysis of the comparative costs and the consumption of hospital resources. *Acta Orthop Scand,* 51, 827-831.

SØREIDE, O., LERNER, A. P. & THUNOLD, J. 1975. Primary prosthetic replacement in acute femoral neck fractures. *Injury,* 6, 286-293.

SÖREIDE, O., MÖLSTER, A. & RAUGSTAD, T. 1979. Internal fixation versus primary prosthetic replacement in acute femoral neck fractures: a prospective,

randomized clinical study. *The British Journal of Surgery,* 66, 56-60.

STACHOWIAK, G. W., BATCHELOR, A. W. & GRIFFITHS, L. J. 1994. Friction and wear changes in synovial joints. *Wear,* 171, 135-142.

STANDARD, B. 2002. Implants for surgery - Wear of total hip-joint prostheses.

SUN, D. N., GU, W. Y., GUO, X. E., LAI, W. M. & MOW, V. C. 1999. A mixed finite element formulation of triphasic mechano-electrochemical theory for charged, hydrated biological soft tissues. *International Journal for Numerical Methods in Engineering,* 45, 1375-1402.

SVESNSSON, N. L., VALLIAPPAN, S. & WOOD, R. D. 1977. Stress analysis of human femur with implanted Charnley prosthesis. *Journal of Biomechanics,* 10, 581-588.

SWANN, D. A., HENDREN, R. B., RADIN, E. L., SOTMAN, S. L. & DUDA, E. A. 1981. The lubricating activity of synovial fluid glycoproteins. *Arthritis Rheum,* 24, 22-30.

SWANN, D. A., SILVER, F. H., SLAYTER, H. S., STAFFORD, W. & SHORE, E. 1985. The molecular structure and lubricating activity of lubricin isolated from bovine and human synovial fluids. *Biochem J,* 225, 195-201.

TALYOR-HOBSON 2005. A guide to Surface Texture Parameters. *A division of Ametek.*

THOMPSON, F. R. 1954. TWO AND A HALF YEARS' EXPERIENCE WITH A VITALLIUM INTRAMEDULLARY HIP PROSTHESIS. *J Bone Joint Surg Am,* 36, 489-500.

TIMOUR, E.-H. 1999. Replacement Options in Femoral Neck Fracture. *In:* FRACTURE, R. O. I. F. N. (ed.). Cairo.

TRABELSI, R., TREHEUX, D., ORANGE, G., FANTOZZI, G., HOMERIN, P. & THEVENOT, F. 1989. Relationship Between Mechanical Properties and Wear Resistance of Alumina-Zirconia Ceramic Composites. *Tribology Transactions,* 32, 77 - 84.

TSUKAMOTO, Y., MABUCHI, K., FUTAMI, T. & KUBOTERA, D. 1992. Motion of bipolar hip prosthesis components - Friction studies in cadavers. *Acta orthopaedica Scandinavica,* 63, 648-652.

UNSWORTH, A., DOWSON, D. & WRIGHT, V. 1975. Some new evidence on human joint lubrication. *Ann Rheum Dis,* 34, 277-85.

VAN DER MEULEN, M. C. H., BEAUPRÉ, G. S., LANE SMITH, R., GIDDINGS, V. L., ALLEN, W. A., ATHANASIOU, K. A., FANG ZHU, C., MANDELL, J. A., SONG, Y., POSER, R. D. & GOODMAN, S. B. 2002. Factors influencing changes in articular cartilage following hemiarthroplasty in sheep. *Journal of Orthopaedic Research,* 20, 669-675.

VĂZQUEZ-VELA & VĂZQUEZ-VELA, G. 1990. Acetabular Reaction to the Bateman Bipolar Prosthesis. *Clinical Orthopaedics and Related Research,* 251, 87-91.

VAZQUEZ-VELA, G. M. D., VAZQUEZ-VELA, E. M. D. & DOBARGANES, F. G. M. D. 1990. The Bateman Bipolar Prosthesis in Osteoarthritis and Rheumatoid Arthritis A Review of 400 Cases. *Clinical Orthopaedics & Related Research February,* 251, 82-86.

VERBERNE, G. 1983. A femoral head prosthesis with a built-in joint. A radiological study of the movements of the two components. *J Bone Joint Surg Br,* 65-B, 544-547.

VON EISENHART, R., ADAM, C., STEINLECHNER, M., MÜLLER-GERBL, M. & ECKSTEIN, F. 1999. Quantitative determination of joint incongruity and pressure distribution during simulated gait and cartilage thickness in the human hip joint. *Journal of Orthopaedic Research,* 17, 532-539.

WALKE, W., PASZENDA, Z. & TYRLIK-HELD, J. 2006. Corrosion resistance and chemical composition investigations of passive layer on the implants surface of Co-Cr-W-Ni alloy. *Journal of achievements in Materials and Manufacturing Engineering,* 16, 74-79.

WALKE, W., PASZENDA, Z. & ZIÊBOWICZ, A. 2007. Corrosion behaviour of Co-Cr-W-Ni alloy in diverse body fluids. *Archives of Materials Science and Engineering,* 28, 293-296.

WALKER, P. S., DOWSON, D., LONGFIELD, M. D. & WRIGHT, V. 1968. "Boosted lubrication" in synovial joints by fluid entrapment and enrichment. *Ann Rheum Dis,* 27, 512-20.

WALKER, P. S., UNSWORTH, A., DOWSON, D., SIKORSKI, J. & WRIGHT, V. 1970. Mode of aggregation of hyaluronic acid protein complex on the surface of articular cartilage. *Annals of Rheum. Dis.,,* 29, 174-179.

WARMAN, M. 2003. Delineating biologic pathways involved in skeletal growth and homeostasis through the study of rare Mendelian diseases that affect bones and joints. *Arthritis Res Ther,* 5, 5.

WEI, L., SVENSSON, O. & HJERPE, A. 1997. Correlation of morphologic and biochemical changes in the natural history of spontaneous osteoarthrosis in guinea pigs. *Arthritis & Rheumatism,* 40, 2075-2083.

WEST, W. & MANN, R. 1979. Evaluation of the Bateman self-articulating femoral prosthesis. *Orthopaedic Transactions,* 3, 17.

WETHERELL, R. G., UNSWORTH, A. & AMIS, A. A. 1992. The function of bipolar hip prostheses—a laboratory study using cadaveric acetabula. *ARCHIVE: Proceedings of the Institution of Mechanical Engineers, Part H: Journal of Engineering in Medicine 1989-1996 (vols 203-210),* 206, 37-42.

WHITTAKER, R., ABESHAUS, M., SCHOLL, H. & CHUNG, S. 1972. Fifteen years' experience with metallic endoprosthetic replacement of the femoral head for femoral neck fractures. *Journal of Trauma,* 12, 799-806.

WILLIAMS, J. F. & SVENSSON, O. 1968. A force analysis of the hip joint, *Biomed. Engng.* 3 (1968. *biomed eng*, 366-370.

WILLIAMS, S., GRAHAM ISAAC, PETER HATTO, MARTIN H. STONE, EILEEN INGHAM & FISHER, J. 2004. Comparative Wear Under Different Conditions of Surface-Engineered Metal-on-Metal Bearings for Total Hip Arthroplasty.

WILLIAMS, S., JALALI-VAHID, D., BROCKETT, C., JIN, Z., STONE, M. H., INGHAM, E. & FISHER, J. 2006. Effect of swing phase load on metal-on-metal hip lubrication, friction and wear. *Journal of Biomechanics,* 39, 2274-2281.

WILLIAMS, S., LESLIE, I., ISAAC, G., JIN, Z., INGHAM, E. & FISHER, J. 2008. Tribology and Wear of Metal-on-Metal Hip Prostheses: Influence of Cup Angle and Head Position. *J Bone Joint Surg Am,* 90, 111-117.

WILLIAMS, S., SCHEPERS, A., ISAAC, G., HARDAKER, C., INGHAM, E., VAN DER JAGT, D., BRECKON, A. & FISHER, J. 2007. THE 2007 OTTO AUFRANC AWARD: Ceramic-on-Metal Hip Arthroplasties A Comparative In Vitro and In Vivo Study. *Clinical Orthopaedics & Related Research,* 465, 23-32.

WILLMANN, G. 1993. Fretting bei modular aufgebauten Implantatsystemen - Fretting of Modular Implant Systems. *Biomedizinische Technik/Biomedical*

Engineering, 38, 48-52.

WRIGHT, T. M., BARTEL, D. L. & RIMNAC, C. M. 1989. Surface damage in polyethylene total joint components. *Proceedings of the Institution of Mechanical Engineers - Part C,* C384, 187-192.

WU, J. Z. & HERZOG, W. 2000. Finite element simulation of location- and time-dependent mechanical behavior of chondrocytes in unconfined compression tests. *Annals of Biomedical Engineering,* 28, 318-330.

YAMAGATA, M., CHAO, E. Y., ILSTRUP, D. M., MELTON III, L. J., COVENTRY, M. B. & STAUFFER, R. N. 1987. Fixed-head and bipolar hip endoprostheses: A retrospective clinical and roentgenographic study. *The Journal of Arthroplasty,* 2, 327-341.

YAU, W. P. & CHIU, K. Y. 2004. Critical radiological analysis after Austin Moore hemiarthroplasty. *Injury,* 35, 1020-1024.

YOSHIDA, H., FAUST, A., WILCKENS, J., KITAGAWA, M., FETTO, J. & CHAO, E. Y. S. 2006. Three-dimensional dynamic hip contact area and pressure distribution during activities of daily living. *Journal of Biomechanics,* 39, 1996-2004.

YOSHINAGA, K. 1987. Replacement of femoral head using endoprosthesis (alumina ceramics vs metal)--an experimental study of canine articular cartilage. *Japanese Orthopaedic Association,* 61, 521-30.

YUEHUEI H. AN & MARTIN, K. L. (eds.) 2003. *Handbook of Histology Methods for Bone and Cartilage*: The Human Press: Totowa, New Jersey, USA.

ZIMMERMAN, N., SMITH, D., POTTENGER, L. & COOPERMAN, D. 1988. Mechanical disruption of human patellar cartilage by repetitive loading in vitro. *Clinical Orthopaedics and Related Research,* 229, 302-7.